Università Politecnica delle Marche
Scuola di Dottorato di Ricerca in Scienze dell'Ingegneria
Curriculum in Ingegneria Civile, Edile e Architettura
XV edition - New series

---

# Multiscale Rheological and Mechanical characterization of Cold Mixtures

Ph.D. Dissertation of:

**Carlotta Godenzoni**

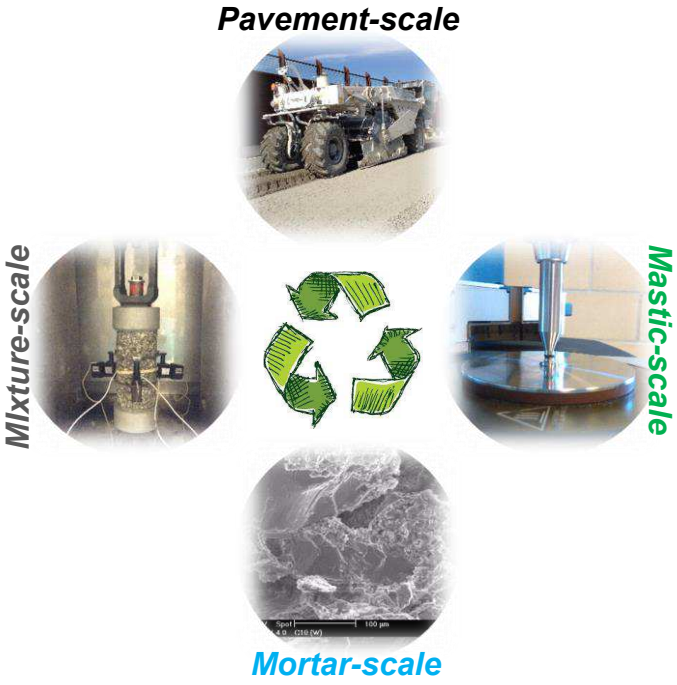


Advisor:

**Prof. Maurizio Bocci**

Co-Advisor:

**Dr. Ph. D. Andrea Graziani**

Curriculum Supervisor:

**Prof. Stefano Lenci**

Università Politecnica delle Marche
Scuola di Dottorato di Ricerca in Scienze dell'Ingegneria
Curriculum in Ingegneria Civile, Edile e Architettura

---

# Multiscale Rheological and Mechanical characterization of Cold Mixtures

Ph.D. Dissertation of:

**Carlotta Godenzoni**

Advisor:
**Prof. Maurizio Bocci**

Co-Advisor:
**Dr. Ph. D. Andrea Graziani**

Curriculum Supervisor:
**Prof. Stefano Lenci**

XV edition - New series

Università Politecnica delle Marche
*Dipartimento di Ingegneria Civile, Edile e Architettura*
Via Brecce Bianche — 60131 - Ancona, Italy

*To my Family*

*"…Experience is not what happens to you...*
*it's what you do with what happens to you…"*

(Aldous Huxley: An Anthology With Commentaries)

# Acknowledgements

*Desidero ricordare tutti coloro che mi hanno sostenuto durante questi tre anni di dottorato: a loro va la mia gratitudine, anche se a me spetta la responsabilità per ogni imperfezione contenuta in questa tesi.*

*Ringrazio anzitutto il Professor Maurizio Bocci, Relatore, e l'Ing. Andrea Graziani, Co-relatore della presente tesi di dottorato: senza il loro supporto e la loro guida sapiente questa tesi non esisterebbe. Proseguo con il Professor Francesco Canestrari, professionista instancabile della ricerca da cui si può trarre solo esempio, fuori e dentro l'ambiente accademico. Un ringraziamento particolare lo voglio rivolgere al Professor Daniel Perraton e al Dottor Emmanuel Chailleux responsabili scientifici delle mie esperienze di ricerca internazionali, rispettivamente presso l'"École de technologie supérieure" (Montréal, Canada) e l'"Institut français des sciences et technologies des transports, de l'aménagement et des réseaux" (Nantes, Francia).*
*Un grazie di cuore lo dedico ai colleghi del Dipartimento DICEA-Area Strade, ricercatori, tecnici e dottorandi che prima di essere compagni di lavoro sono stati compagni di vita ma soprattutto amiche inestimabili e insostituibili. Grazie Arianna, Francesca e Giorgia!*

*Vorrei infine ringraziare le persone a me più care: i miei genitori Mauro e Rosanna che mi hanno supportato ma soprattutto sopportato in questo lungo percorso, mia nonna Maria sempre al mio fianco e infine il mio compagno e collega Emiliano.*

Ancona, 10 Febbraio 2017

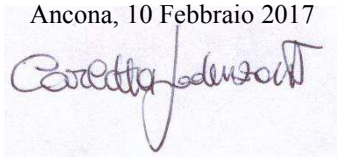

# Abstract

Nowadays, the growing social and political awareness about environmental issues is moving towards the development of low-energy and low-emission technologies. In this context, cold technologies as cold mixtures may represent a valid alternative to traditional hot mix asphalt for road pavements. Cold mixture combines both economic and environmental benefits related to the reduction of energy necessary for heating both bitumen and aggregates. Moreover, when cold mixtures are adopted for pavement recycling, the consumption of virgin aggregate can be significantly reduced.

In the past, the use of cold mixture for structural layers has attracted relatively little attention largely because of problems related to the time required for full strength to be achieved after paving and its susceptibility to early life damage by rainfall.

Currently, the profound lack of technical guidelines and adequate standardized procedures, forces technicians and professionals to refer exclusively to previous experiences.

The PhD research aimed at scientifically verifying advantages and disadvantages of cold mixtures. To this aim an extensive experimental study was carried out involving advanced characterizations in order to identify the physical, mechanical and rheological behavior of cold mixtures.

Besides the traditional laboratory investigations, an original research methodology based on the multiscale analysis was applied. In fact, cold mixture can be considered as an evolutive material because its physical state evolves over time according to moisture loss. In this context, the characterization of cold mixture should be developed at different time during the in-service life of the material (time-scale) and at different level of investigation (size-scale).

Optimum correlation was found between the results collected from different levels of investigation (size and time-scales); hence demonstrating the scientific validity of the adopted research approach. A detailed description of specific results carried out in these investigations can be found in the “Summary” section of each chapter.

Based on the overall findings, no elements discourage the use of cold mixture as support layers for pavement structure. Therefore, materials should be properly designed in terms of aggregate blend, water content and binding agents (type and dosage).

According to this observation, it can be concluded that using specific precautions, the adoption of cold mixture may contribute to improve and preserve the performance of road pavements.

# Sommario

Oggigiorno, la crescente consapevolezza sociale e politica riguardante le questioni ambientali si sta orientando verso lo sviluppo di tecnologie a basso consumo e basse emissioni. In questo contesto, le tecnologie a freddo come le miscele bituminose a freddo possono rappresentare una valida alternativa ai tradizionali conglomerati bituminosi a caldo, per le pavimentazioni stradali. L'adozione di miscele bituminose a freddo combina benefici sia economici che ambientali legati alla riduzione dell'energia necessaria per il riscaldamento sia il bitume che di aggregati. Inoltre, quando questi materiali vengono utilizzati per il riciclaggio di pavimentazioni stradali ammalorate, il consumo di aggregati vergini può essere considerevolmente ridotto.
In passato, l'uso di miscele bituminose a freddo per strati di pavimentazione ha attirato relativamente poca attenzione soprattutto a causa dei problemi legati al tempo richiesto per il completo sviluppo di resistenza e la sua suscettibilità all'infiltrazione di acque meteoriche, nei primi mesi di vita.
Attualmente, la profonda mancanza di linee guida e di adeguate procedure standardizzate, costringe i tecnici e professionisti che voglio confrontarsi con l'utilizzo di queste nuove tecnologie, a riferirsi esclusivamente a esperienze precedenti.
Il presente dottorato di ricerca è volto a verificare scientificamente i vantaggi e gli svantaggi dell'adozione di miscele bituminose a freddo. A tale scopo, è stato condotto un vasto studio sperimentale servendosi di caratterizzazioni avanzate per identificare il comportamento fisico, meccanico e reologico di questo materiale.
Oltre alle tradizionali indagini di laboratorio, è stata applicata una metodologia di ricerca originale basata sull'analisi multiscala. Infatti, la miscela bituminosa a freddo può essere considerata come un materiale evolutivo poiché il suo stato fisico evolve nel tempo a causa della continua perdita di umidità. In questo contesto, la caratterizzazione delle miscele bituminose a freddo deve essere sviluppata su scale temporali differenti durante la vita in servizio del materiale e a diversi livelli di indagine (scala dimensionale).
I risultati raccolti ai diversi livelli di indagine (scale temporali e dimensionali) hanno mostrato una correlazione ottimale tra loro; a dimostrazione del fatto che il metodo di ricerca adottato può ritenersi scientificamente valido. Una descrizione dettagliata dei risultati ottenuti in queste indagini sperimentali sono stati riportati nella sezione "Sommario" di ciascun capitolo.
Sulla base dei risultati complessivamente ottenuti, nessun elemento scoraggia l'uso delle miscele bituminose a freddo come strati di supporto per la sovrastruttura stradale. Ad ogni modo, i materiali impiegati devono essere adeguatamente progettati in termini di assortimento granulometrico, contenuto d'acqua e di leganti (tipo e dosaggio).
In conclusione si può affermare che, seguendo particolari accorgimenti, l'adozione di miscele bituminose a freddo può contribuire a migliorare e preservare le prestazioni delle pavimentazioni stradali.

# Contents

# List of Figure

# List of Tables

# List of Standard Specifications


- AASHO T-99/T-180, Standard method of test for moisture-density relations of soils, ASHTO Materials , Part II, Tests, 1986.
- AASHTO T342 (2011). Standard Method of Test for Determining Dynamic Modulus of Hot Mix Asphalt (HMA)
- AASHTO, Pavement Management Guide. Washington, D.C., 2001.
- AASHO Road Test, Flexible Pavement Research. Special Report 52, (1972). Washington, DC: American Association of State Highway and Transportation Officials.
- AC 150/5370-11B. Use of nondestructive testing in the evaluation of Airport Pavements (2011) FAA, Federal Aviation Administration. Washington D.C.: U.S. Government Printing Office.
- ASTM D1559-89, Test Method for Resistance of Plastic Flow of Bituminous Mixtures Using Marshall Apparatus (Withdrawn 1998).
- ASTM-D2488, Standard Practice for Description and Identification of Soils (Visual-Manual Procedure), (2000).
- ASTM C295, Petrographic Examination of Aggregates for Concrete, 2012.
- EN 197-1: Cement – Part 1: Composition, specifications and conformity criteria for common cements, 2011.
- EN 933-1: Test for geometrical properties of aggregates - Part 1: determination of particle size distribution - Sieving method, 2009.
- EN 933-2: Test for geometrical properties of aggregates - Part 1: determination of particle size distribution – Test sieves and nominal size of apertures, 2007.
- EN 1097-6 (2013). Test for mechanical and physical properties of aggregates – Part 6: Determination of particle density and water absorption.
- EN 12697-1 (2001). Bituminous mixtures - Test methods for hot mix asphalt - Part 1: Soluble binder content.
- EN 12697-5: Test methods for hot mix asphalt - Part 5: Determination of the maximum density, 2009.
- EN 12697-6: Bituminous mixtures - Test methods for hot mix asphalt - Part 6: Determination of bulk density of bituminous specimen, 2009.
- EN 12697-8: Bituminous mixtures - Test methods for hot mix asphalt - Part 8: Determination of void characteristics of bituminous specimens, 2009.
- EN 12697-23: Bituminous mixtures - Test methods for hot mix asphalt – Part 23: Determination of indirect tensile strenght of bituminous specimen, 2006.
- EN 12697-26: Bituminous mixtures - Test methods for hot mix asphalt - Part 26: Stiffness, 2012.

- EN 12697-31: Bituminous mixtures - Test methods for hot mix asphalt - Part 31: Specimen preparation, by gyratory compactor, 2009.
- EN 12697-44: Bituminous mixtures - Test methods for hot mix asphalt - Part 44: Crack propagation by semi-circular bending test, 2010
- EN 13043: Aggregates for bituminous mixtures and surface treatments for roads, airfields and other trafficked areas, 2013.
- EN 13108-1: Bituminous mixtures: Material specifications - Part 1: Asphalt Concrete, 2006.
- EN 13108-7, Bituminous mixtures: Material specifications - Part 7: Porous asphalt, 2006.
- EN 13108-8: Bituminous mixtures: Material specifications - Part 8: Reclaimed asphalt, 2006.
- EN 13242: Aggregates for unbound and hydraulically bound materials for use in civil engineering work and road construction, 2008.
- EN 13286-2: Unbound and hydraulically bound mixtures - Part 2: Test methods for the determination of the laboratory reference density and water content - Proctor compaction, 2005.
- EN 13808: Bitumen and bituminous binders - Framework for specifying cationic bituminous emulsions, 2013.
- SHRP-P-654, Strategic Highway Research Program National Research Council (1993). SHRP Procedure for Temperature Correction of Maximum Deflections[R]
- SN 630 317b. Essai de plaque $E_v$ et $M_E$, (1998).

# Introduction

# CHAPTER 1.

## Background and problem statement

Nowadays, construction sector plays an important role in the European economy. It generates almost 10% of the Gross Domestic Product (GDP) and provides 20 million jobs, mainly in micro and small enterprises. Construction is also a major consumer of intermediate products (raw materials, chemicals, electrical and electronic equipment, etc.) and related services. Because of its economic importance, the performance of the construction sector can significantly influences the development of the overall economy [COM (2012) 433].
The quality of construction works also has a direct impact on the quality of life of Europeans. Not least, the energy performance of constructions and resource efficiency in manufacturing, transport and the use of products for the construction of structures and infrastructures have an important impact on energy, climate changes and environment.
In addition, the construction sector is fundamental in the delivery of the Europe 2020 Strategy on smart, sustainable and inclusive growth. Furthermore, the Commission's Communication on the "Energy Roadmap 2050" points out that higher energy efficiency in new and existing structures and infrastructures is the key for the transformation of the EU's energy system. In particular, transport infrastructure has an enormous environmental impact as well as substantial energy, raw materials consumption and waste generation. Infrastructure networks must make the greater contribution towards a more sustainable Europe.
In order to allow the concept of sustainable construction to be better understood and more widely used, harmonized indicators, codes and methods for assessments of environmental performances should be developed for construction products, processes and works.
"Sustainability" is one of the world's most talked about but least understood words. Its meaning is often clouded by differing interpretations and by a tendency for the subject to be treated superficially. For most companies, countries and individuals who do take the subject seriously, the concept of sustainability embraces the preservation of the environment as well as critical development-related issues such as the efficient use of resources, continual social progress, stable economic growth, and the eradication of poverty. In the world of construction, structures and infrastructures have the capacity to make a major contribution to a more sustainable future for our planet. The Organization for Economic Cooperation and Development (OECD), for instance, estimates that buildings in developed countries account for more than forty percent of energy consumption over their lifetime (incorporating raw material production, construction, operation, maintenance and decommissioning). Add to this the fact that for the first time in human history over a half of the world's population now lives in urban environments and it's clear that sustainable structures/infrastructures have become vital cornerstones for securing long-term environmental, economic and social viability. Sustainable construction aims to meet present day needs for housing, working environments and infrastructure without compromising the ability of future generations to meet their own needs in times to come. It incorporates elements of economic efficiency, environmental performance and social responsibility.

Although the concept related to sustainability appears already well-established in many productive fields, it is not completed developed in its entirety with regard to the civil engineering in general, and to road infrastructure specifically.
The sustainability of a structure/infrastructure is determined by the combination of three fundamental elements:

- economic sustainability, is the ability to support a defined level of economic production indefinitely;
- social sustainability, is the ability of a social system, such as a country, to function at a defined level of social well being indefinitely;
- environmental sustainability, is the ability to maintain rates of renewable resource harvest, pollution creation, and non-renewable resource depletion that can be continued indefinitely.

A more complete definition of sustainability is thus environmental, economic, and social sustainability; this forms the goal of *The Three Pillars of Sustainability*. The three pillars of sustainability are a powerful tool for defining the complete sustainability problem. This consists of at least the economic, social, and environmental pillars. If any one pillar is weak then the system as a whole is unsustainable. Two popular ways to visualize the three pillars are shown in **Figure 1. 1**.

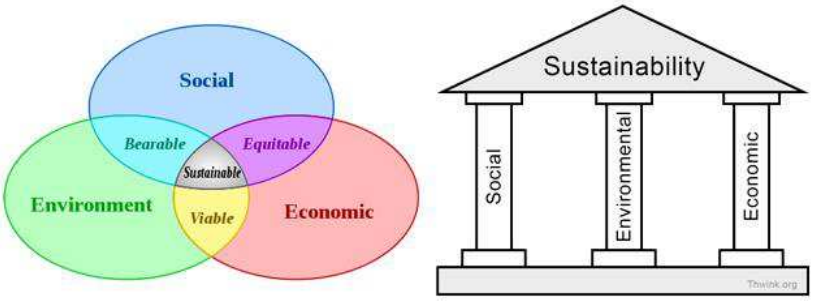


**Figure 1. 1** Three Pillars of Sustainability.

Most national and international problem solving efforts focus on only one pillar at a time. For example, the United Nations Environmental Programme (UNEP), the environmental protection agencies (EPA) of many nations, and environmental Non-governmental organizations (NGOs) focus on the environmental pillar. The World Trade Organization (WTO) and the OECD focus mostly on economic growth, thought the OECD gives some attention to social sustainability, like war reduction and justice. The United Nations attempts to strengthen all three pillars, but due to its consensual decision making process and small budget has minor impact. The United Nations focuses mostly on the economic pillar, since economic growth is what most of its members want most, especially developing nations. This leaves a void; no powerful international organization is working on the sustainability problem as a whole, which would include all three pillars. However, as the Great Recession of 2008 demonstrated, weakness in the other pillars can directly weaken the environmental pillar. Many nations and states are cutting back or postponing stricter environmental laws or

investment, since their budgets are running deficits. Many environmental NGOs are seeing their income fall. If the Great Recession grew substantially worse and morphed into another Great Depression, you would expect the environmental pillar would get severely less attention, since eating now is a priority over saving the environment.
The social pillar is critical too; once a war breaks out environmental sustainability has zero priority. If a nation lives in dire poverty, the environment is pillaged with little thought for the future. Therefore, solutions to sustainability problem must include making all three pillars sustainable.
The above definition of sustainability goes against the norm. The most popular definition of sustainability is that from the Brundtland Report of 1987, which said:
"*Sustainable development is development that meets the needs of the present without compromising the ability of future generations to meet their own needs*". It contains within it two key concepts:

- the concept of 'needs', in particular the essential needs of the world's poor, to which overriding priority should be given; and
- the idea of limitations imposed by the state of technology and social organization on the environment's ability to meet present and future needs.

Already in the Nineties, as a result of the affirmation and diffusion of the sustainable development concept, specific guidelines have been elaborated to guarantee economic growth without compromising a valid structure ecosystem and preserve, restore and enhance the quality of the territory. Moreover, the main social and economic policies and the new national and European guidelines are moving more and more towards the encouragement of all those practices useful to achieve sustainability goals, for example involving the re-use of secondary and waste materials, hence allowing the simultaneous minimization of raw resources.
In particular, nowadays economic and environmental sustainability are key words also for the design of new road infrastructures and for the maintenance activities of old pavements that need rehabilitation efforts. Aspects to be taken into account both for the definition of the road layout (e.g. size, length, location, landscape impact) and for the design of the pavement structure (e.g. layers thickness, materials, manufacturing techniques).
In that sense, over the last few years the pavement industry have tried to adopt sustainable practices to align itself with the global notion of habitable environments. To this aim, there has been growing the use of Life-Cycle Analysis (LCA) as powerful tool to quantify the environmental performance of sustainability.
LCA is a structured methodology that quantifies environmental impacts over the full life cycle of a product or system, including impacts that occur throughout the supply chain [Thomas et al., 2013]. The precursors to LCA were originally developed in the late 1960s to analyze air, land, and water emissions from solid wastes. The principles were later broadened to include energy, resource use, and chemical emissions, with a focus on consumer products and product packaging rather than complex infrastructure systems [Hunt and Franklin 1996; Guinée 2012]. In the transportation area, LCA topics have included assessing bituminous binder and cement production, evaluating low carbon fuel standards for on-road vehicles, examination of transportation networks, and examination of interactions between transportation infrastructure, vehicles, and human behavior. LCA provides a comprehensive

approach to evaluating the total environmental burden of a particular product (such as a ton of aggregate) or more complex systems of products or processes (such as a transportation facility or network), examining all the inputs and outputs over its life cycle, from raw material production to the end of the product's life. A generic model of the life cycle of a product for LCA is shown in **Figure 1. 2**. As can be seen, the life cycle begins at the acquisition of raw materials, proceeds through several distinct stages including material processing, manufacturing, use, and terminates at the end-of-life (EOL).

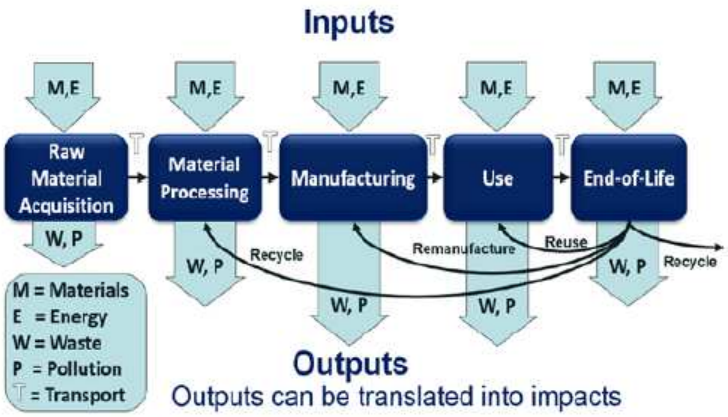


**Figure 1. 2** Generic life cycle of a production system for LCA [Kendall, 2012].

LCA can be used for a variety of purposes, including:

- Identifying opportunities to improve the environmental performance of products and production systems at various points in their life cycle.
- Informing and guiding decision makers in industry, government, and non-governmental organizations as part of strategic planning, priority setting, product or process design selection, and redesign.
- Developing appropriate indicators of environmental performance of a product or production system; for example, to implement an eco-labeling scheme [EPA 2014; EC 2011], to make an environmental claim, or to produce an environmental product declaration (EPD).

In the field of road constructions, LCAs can be adopted to evaluate the environmental footprint of a new infrastructure or rehabilitation action. The analysis should consider a lot of aspects (e.g. materials, construction, maintenance and rehabilitation, visual impacts, transportation costs traffic issues) but the supply of raw materials has a fundamental role that strongly affects each single step of the LCA cycle and of course the final decision.
For example, aggregates used in construction should comply with all the requirements of the relevant European Standards. These standards include comprehensive and specific requirements for natural aggregates, iron and steel making slag and recycled aggregates, dealing with, for example, the stability of certain basalts, the expansion of certain slags and the constitution of recycled aggregates [EN 13043]. In particular, from the quality point of

view, the selected aggregates should satisfy structural requirements in order to avoid lack of performance in the final layers of the road pavements.
Moreover, the use of secondary (recycled), instead of primary (virgin), materials helps easing landfill pressures and reducing demand of extraction. This is one way of getting the road construction industry on track towards sustainable construction practices. Current research and practice tends to concentrate on the use of waste materials in the lower courses (base, subbase, etc.) of the road as these absorb materials in larger quantities than the upper courses. However, highway authorities are dealing more with the maintenance and repair works rather than new construction of roads. Such works are affecting the upper pavement layers as well as the lower part of road structure. In addition, it can be argued that the cost of transporting and processing waste materials into desired properties can only be justified by using the recycled materials, in value added applications such as bituminous surface layers. Thus, the property requirements for these applications need to be understood to ensure that materials intended for recycling are able to meet relevant specifications, by using available technologies and facilities, at a reasonable cost [Huang et al., 2007].
Secondary aggregates can be defined as by-products from industrial processes or other human activities. Of those waste materials a large fraction might have the potential to be used in road or building construction projects: the same materials that compose pavements, defined as road byproducts (usually referred as reclaimed asphalt, RA) can be employed, as well as old materials coming from other activities, such as those from Construction and Demolition (C&D, demolition byproducts) or the recovery of rubber tires (PFU), steel slag and coal fly ash (referred as industrial byproducts). The final goal of re-using, recycling and/or recovering 70% of construction and demolition waste by 2020 according to the Waste Framework Directive [COM (2012) 433] represents a valuable business opportunity for the construction value chain.
The modern trend of using the intrinsic values of the material within the existing pavement combined with several recycling techniques, such as hot mix recycling, hot in-place recycling, cold in-place recycling and full depth reclamation, have evolved over the past forty years. In-place recycling and, in particular, cold in-place recycling and full depth reclamation reduce the use of new materials but, at the same time, reduces emissions, traffic and energy associated with the transport and production of these materials.
Currently, the use of materials in civil engineering is lacking a systematic approach not allowing an adequate comparison of performance measured with well established criteria and international standards.
In Europe, the lack of a common European law related to such a topic makes the need to deeply analyze the effect of including recycled materials in new pavement mixtures a major issue which must be properly addressed through a comprehensive study that can provide useful information related to each performance-related property.
The pavement industry, recognizing the need to move toward a sustainable pavement system, has also been promoting sustainable practices for many years achieving good results.
Anyway, a scientific and rigorous support is needed to prove the efficiency of such practices in order to establish worldwide recognized standards and make sustainable technology as cold recycling, a well-established production technique, with fundamental rules that allow the same performance of a traditional production technique to be reached.
Obviously, the combined adoption of cold technologies and recycled aggregates is able to maximize both economic and environmental benefits. However, it is necessary to corroborate

such claims in a quantified way, scientifically verifying if the performance of the final mixture are penalized or not.

Finally, on the basis of the abovementioned discussions, the work presented in this thesis aims at providing a rheological and mechanical characterization of cold mixtures (CMs).An extensive experimental study was carried out to scientifically verify the possibility to adopt cold mixtures such a valid alternative for support layers (subbase layers) in new road pavements without penalize the corresponding in-service performance.

# CHAPTER 2.

# Literature review

Over the last decades, the study of cold bituminous materials and the evaluation of the corresponding performance has been a challenging topic for researchers [Terrel et al., 1971; Brennen et al. 1983; Maccarone et al., 1995; Needham, 1996; Jenkins, 2000; ARRA, 2001; Santagata e Chiappinelli, 2003; James, 2006; Asphalt Academy, 2009; Bocci et al., 2010; Stroup-Gardiner, 2011]. Although the experimental studies carried out were not sufficient to fully characterize this complex topic such as cold materials, they constitute an important reference point to identify the main issues related to the use of this relative *young* technology. Thus, an extensive literature review on the state of the art regarding the use of cold-recycling and in particular, of cold bituminous materials, was conducted and it is described in this chapter.

First, the main aspects related to the recycling of bituminous pavements are reported. Then, the major issues derived from cold technologies and from the use of reclaimed asphalt are summarized. Finally, an overview of cold mixtures, their constituents and corresponding performance is presented.

## 2.1 Background

In the last 50 to 70 years, population growth and economic development have resulted in an extensive network of bituminous paved roadways. Many thousands of kilometers were constructed to meet the demands of increased traffic and the majority of these roads are near/at/or past the end of their original design life.
When the roadway network was rapidly expanding, the initial construction cost was the most important issue, with little or no attention being paid to the ongoing maintenance costs. However, as the roadway network has matured, as the traffic volume and gross vehicle weights have increased, and as funds have become more tightly budgeted, increased emphasis has been focused on preventive maintenance and preservation of the existing roadways. In many jurisdictions, the funds available have not been able to keep pace with the increased preventive maintenance and preservation costs as the roadway network aged. This has resulted in a significant reduction in the condition and the service level provided by the roadways, within the network. This has in turn resulted in increasing overall preventive maintenance and more expensive rehabilitation/reconstruction costs.

There was growing necessity to quantify the extent to which the pavement is serving its purpose, or its "*performance*". Such a quantification can be done with respect to distress conditions exhibited by the pavement at any time after its construction.

Nowadays, road authorities often employ a data-base system, known as a Pavement Management System (PMS) [AASHTO 2001], to continuously monitor condition and the service level of road pavements within their network.
PMS have been designed and implemented in order to assist an agency in its planning, programming, construction, preventative maintenance and rehabilitation functions.
PMS are also used to evaluate and quantify the roadway conditions, as a function of age and/or traffic.
**Figure 2. 1** provides a typical PMS plot that illustrates the effectiveness of timely maintenance and rehabilitation measures and highlights the importance of taking timeout action to maintain as high the pavement condition as possible.

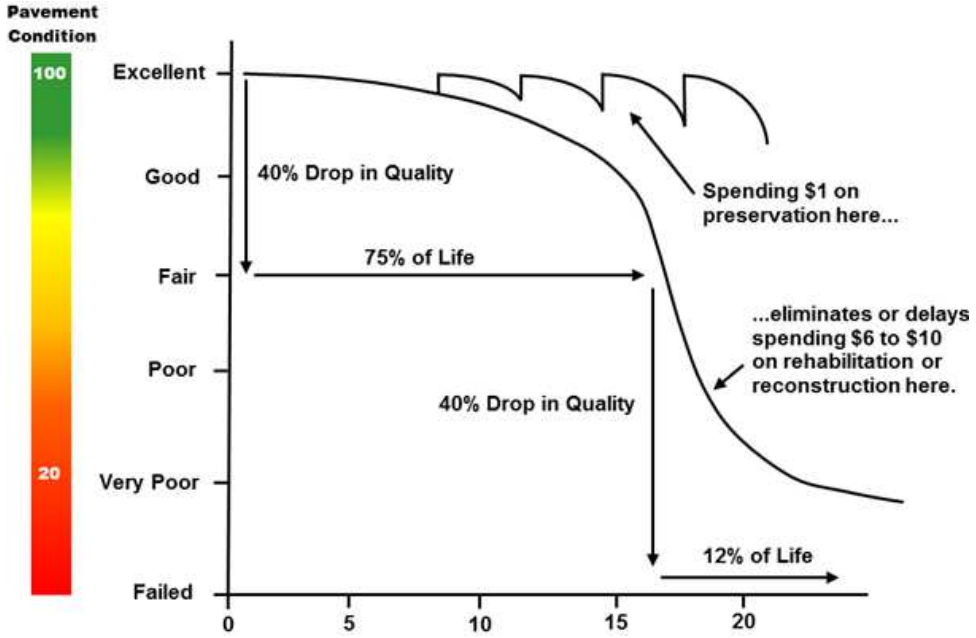


**Figure 2. 1** Pavement maintenance and rehabilitation.

The rate of deterioration is indicated by the pavement condition: poorer pavement condition encourages faster rates of deterioration through dynamic loading. As the pavement condition reduces, the scale of remedial activities becomes greater, as does the cost of such activities.
Since funding for preventive maintenance, preservation, rehabilitation. For this reason, innovation is required in order to do more with less. *Pavement recycling* is one way of increasing the effectiveness of existing budgets in order to maintain, preserve, rehabilitate and reconstruct more kilometers of roadway for each euro spent.

## 2.2 Recycling of bituminous pavements

Recycling of bituminous pavement is not a new concept. Recycling/rehabilitation of roadways with bituminous binders dates to the early 1900's. The first documented case of pavement recycling, in the form of *hot in-place recycling* (HIR), was reported in the literature of the 1930's. However, only moderate advancements in bituminous pavement recycling technology and equipment occurred until the mid 1970's.
Two events of the 1970's rekindled the interest in bituminous pavement recycling which has resulted in its worldwide use today. The petroleum crisis of the early 1970's and the development and the introduction in 1975 of large scale cold planing equipment, complete with easily replaceable tungsten carbide milling tools, were the catalyst for renewed interest in bituminous pavement recycling. During that period, many productive fields, among which also the transport sector, tried to find alternative energy supplies and new technologies to limit the use of oil. In the road market, this necessity arose again in the last two decades, when the companies had to deal with a big increment of the oil price along with a low availability of aggregates characterized by good quality. In that sense, the need to decrease the use of virgin aggregates had as direct consequence the re-use of the material coming from the milling of old pavements (reclaimed asphalt, RA, or reclaimed aggregate, RAg), allowing recycling to become a good alternative [ARRA, 2001; Stroup-Gardiner, 2011].

Current pavement recycling and reclamation methods are the following:

- *Hot in-place recycling*, HIR (resurfacing, repaving and remixing).
- *Cold in-place recycling*, CIR.
- *Full-depth reclamation*, FDR.

Different methods of recycling are applicable to different types, levels, and severity of distresses, and hence different periods during the pavement life (**Figure 2. 2**). Typically, *HIR* is used when the majority of the pavement distresses are minimal and limited to the upper few centimeters of the surface layer with no evidence of structural problems (i.e. longitudinal cracking in wheel path, alligator cracking, and edge cracking). *CIR* is used when there is a higher number, type, and severity of non-load-related distresses that may extend farther down from the surface. *CIR* with an overlay can be used to address some load-related distresses. *FDR* is an in-place rehabilitation process that can be used for reconstruction, lane widening, minor profile improvements, and increasing structural capacity by addressing the full range of pavement distresses.

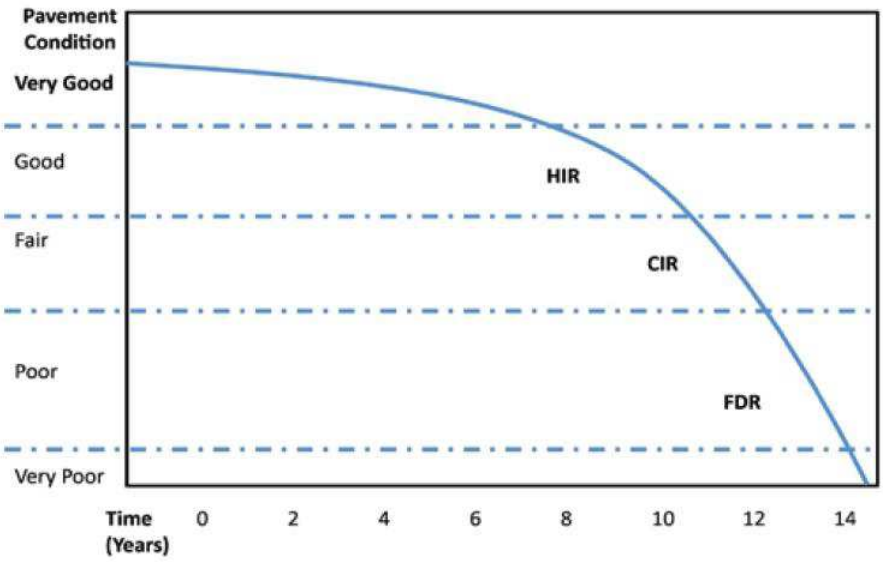


**Figure 2. 2** Pavement condition and type of in-place recycling method [Fisher, 2008].

## 2.3 Major issues related to cold recycling technique

The material coming from the demolition and milling of old bituminous pavements is commonly referred as RA and can be re-added in the production process of new ones. In order to obtain a recycled bituminous mixture that guarantees appropriate characteristics needed to consider the material acceptable according to the current technical specifications, several studies highlighted the necessity to address the following issues [ARRA, 2001; Asphalt Academy, 2009; Stroup-Gardiner, 2011]:

- quality control of the material and the production process adopted.
- characterization of RA, according to the European standard EN 13108-8 (amount and type of external materials eventually included in the RA, type and age of the bituminous component, average bitumen content, type and grading distribution of the original aggregates, nominal maximum aggregate size, homogeneity, type and percentage of the virgin bitumen added.

The recycling technique selected and the properties of the materials that compose RA are of fundamental importance to obtain good recycled mixtures that can guarantee suitable performance in field. In particular, recycling techniques can be divided in two main categories: *hot and cold recycling*.
In this literature review, only the *cold recycling technique* is addressed describing the main experiences collected on this subject, in order to provide a comprehensive picture of the current state of the art.

Cold recycling can be achieved either "*in-plant*" (**Figure 2. 3**a) by hauling material recovered from an existing road to a central depot where it is fed through a mixing unit, or "*in-place*" (**Figure 2. 3**b) using a recycling machine.
Plant processing (i.e. *cold central plant recycling*, CCPR) is generally the most expensive option, primarily due to haulage costs that are absent in in-place recycling but, at the same time, it allows materials from an existing pavement to be selected and pre-treated, thereby increasing the level of confidence that can be achieved in the final product. In general, the milled material is moved from the old pavement location to the plant site where it is processed through crushing and screening to discard foreign matters and clumps too large. Then, it is usually sieved and divided in more fractions prior to be re-used. Thanks to the higher possibility to monitor and control the milled material prior to be re-introduced in the production process, this method avoids high variability of RA and ensures a better quality and a more uniform homogeneity in the final mixture. Moreover, it allows the advantage of having higher flexibility in the production sequences that can be adapted according to several requirements and different types of mixture. At the same time, this method has few drawbacks mainly related to the higher transport and the stocking costs of the milled material in the plant where it is necessary to ensure a big amount of appropriate spaces.

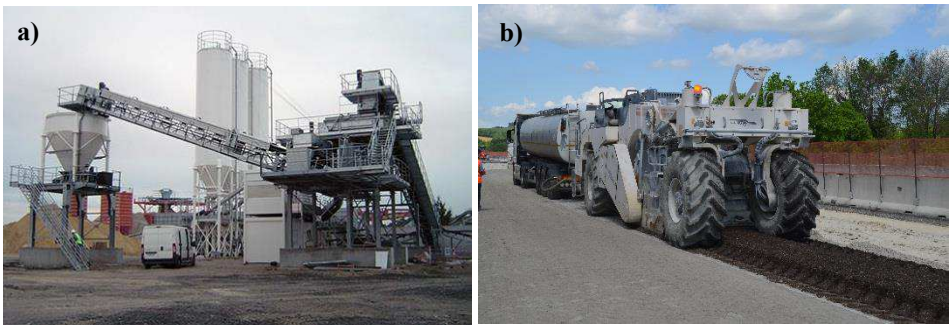


**Figure 2. 3** Cold recycling process: a) in-plant and b) in-place.

In-place recycling is characterized by all production activities (milling, mixing and compaction) realized directly in field by means of specific equipment. Lower control of the milled materials and quality of the production process have to be accounted for. However, these drawbacks are balanced by higher economic benefits and shorter production time. The so produced mixtures are usually employed to build binder or base layers, depending on type and volume of traffic [Tebaldi et al., 2014].
Focusing on the *in-place recycling*, construction operations are undertaken by coupling bulk supply tankers to the recycler. The recycler pushes or pulls the tankers supplying additives required in the mix (e.g. bitumen emulsion or foamed bitumen).
The combination of tankers coupled to the recycler is configured in accordance with the particular recycling application and the type of stabilizing agent that is applied.
The simplest combination consists of a recycler coupled to a single tanker containing water. As the machine advances, the in situ pavement material is recovered and mixed with water drawn from the tanker. The micro-processor ensures that the required amount of water is injected into the mixing chamber through the spraybar that is mounted on the leading face of

the drum housing. The rotating drum mixes the water with the recovered material to achieve a uniform consistency.
The rate of water addition is controlled to achieve the moisture content that will allow an adequate level of density to be achieved when the material is compacted. As the recycler advances, the mixed material falls back into the void created by the cutting drum and is struck off by a sturdy door fitted to the rear of the drum housing. Subsequently, a roller follows behind the recycler to compact the material before a grader that is used to reach the final level.
Compaction and finishing process are usually performed using both vibratory and pneumatic-tyred rollers that work together with a water tanker.
Powdered stabilizing agents (e.g. cement or hydrated lime) are normally spread on the surface of the existing road ahead of the recycling operation. As the recycler advances, the powder is lifted and mixed together with the recovered material and water, all in a single operation. Alternatively, the powder can be mixed with water forming a slurry suspension that is subsequently injected into the mixing chamber. When this method is adopted, a special mixing unit is coupled to the recycler. This "*slurry mixing unit*" manufactures the slurry by combining the precise amounts of both cement and water required to treat the volume of material being recycled. The slurry is then pumped across to the recycler by means of a flexible hose and injected through the spraybar.
At the current state-of-the-practice, two main cold in-place procedures can be categorized: the *cold in-place recycling* (CIR) and the *full-depth reclamation* (FDR).

*Cold in-place recycling*
The term *CIR* is used to identify procedures where only bituminous layers are milled and incorporated in the recycled mixture. In CIR, RA, containing high-quality aggregates and bitumen, is actually re-used adding a bitumen emulsion or foamed bitumen and chemical or mineral additives. Virgin aggregates (VAs) can also be included to obtain an optimal gradation.
CIR is undertaken on site and generally uses 100 percent of the RA generated during the process. The CIR treatment depth is typically within the 50 to 100 mm range when the recycling agent is only a bitumen emulsion or an emulsified recycling agent. Treatment depths of 125 to 150 mm are possible when chemical additives, such as Portland cement, lime, kiln dust or fly ash are used to improve the early strength gain and resistance to moisture damage. If lime or Portland cement is added to the recycled mix, they can be added in dry form or as slurry. The slurry method eliminates potential dust problems and permits greater control of the amount of recycling modifier being added.
There are different types of CIR trains with different equipment configurations, a typical configuration is reported in **Figure 2. 4**. The trains differ from one another in how the RA is removed and sized, how the recycling additives and modifiers are added, how they are mixed and controlled and how the resultant mix is placed. Densification of these materials requires more compaction energy than conventional hot mix asphalt (HMA). This feature is due to the high internal friction developed between the mixture particles, the higher viscosity of the binder due to aging and colder compaction temperatures.

CIR mixtures are compacted and the bitumen emulsion begins to "*break*," mixture turning from brown to black. When bitumen emulsions or emulsified recycling additives are used,

this could take from 30 minutes to 2 hours, depending on the characteristics of the bitumen emulsion, thickness of the CIR mixture and environmental conditions. The compacted CIR material must be adequately cured before the wearing surface is placed. The rate of curing is quite variable and depends on several factors including environmental conditions, drainage and moisture characteristics of the mixture. Typical curing periods range from several days to 2 weeks, depending on the above mentioned factors, recycling additive and any modifiers used [ARRA, 2001; EAPA, 2008; Thompson et al., 2009; Stroup-Gardiner, 2011].

Cold in-place recycling *advantages* include:

- conservation of non-renewable resources;
- energy conservation compared to other reconstruction methods;
- eliminates the disposal problems inherent in conventional methods;
- surface irregularities and cracks are interrupted and filled;
- rutting, potholes, and raveling are eliminated;
- base and subgrade materials are not disturbed;
- pavement cross-slope and profile can be improved.

*Full depth reclamation*

The term *FDR* is used to identify procedures where recycling machines mill the entire thickness of the distressed bituminous layers together with a predetermined amount of the underlying unbounded or cement-treated courses [Thompson et al., 2009; Bocci et al.,2011; 2014]. Reclamation of the existing bituminous bound (RA) and unbound (reclaimed aggregates, RAg) layers provides a granular blend, which can also be combined with additional granular materials for improving its gradation (usually up to 15-20%). The granular mixture is enhanced by mixing stabilizing agents, such as lime, cement, fly ash, bitumen emulsion and foamed bitumen [Lewis and Collings, 1999; ARRA, 2001; Asphalt Academy, 2009]. The addition of a sole additive or a combination of two or more additives is usually required to cover mechanical deficiencies related to reclaimed material, and thereby, to increase the structural characteristics of new base or subbase layers.

Due to the development of innovative and powerful equipment, treatment depth can vary from 10 to 30 cm depending on the thickness of the existing pavement layers and design requirements. In fact, FDR technologies allow a larger amount of material to be recycled (up to 100%), with considerable environmental advantages over CIR. However, lower quality mixtures are generally produced and must be protected from heavy-load-induced stress by thicker bituminous layers.

For heavily trafficked highway and even for rural roadways, where dips, cracking, potholes and depression seriously compromise the ride ability and safety driving, FDR can be a viable, long-term and often preferable option with respect to conventional maintenance works (i.e. overlay or milling and overlay). In fact, by removing deep pavement crack pattern, FDR eliminates the potential of reflective cracking and improves the structure-bearing capacity, allowing the reduction of future maintenance costs.

Over the years, a number of reclamation methods were tried, including the use of rippers, scarifiers, pulvi-mixers, milling machines, stabilizing additives to reclaim the existing

surface and underlying materials. A typical configuration for FDR operations is reported in **Figure 2. 4**.

In the last few years, the evident advantages and cost-effectiveness of the FDR process have also been recognized by local public administrations as an appropriate strategy for the rehabilitation of their local roadway network [Smith, 1999; Collings et al., 2004; Overby et al., 2004; Eller and Olson, 2009; Bocci et al., 2010 and 2014].
FDR advantages include:

- conservation of non-renewable resources;
- energy conservation compared to other reconstruction methods;
- few pieces of equipment are required;
- elimination of bumps and dips, rutting, potholes, patches, and cracks;
- subgrade deficiencies can be corrected by stabilization;
- problems with existing aggregate gradation can be corrected with proper selection of new granular materials;
- deteriorated base can be reshaped to restore surface profile and drainage;
- significant structural improvement with the addition of stabilizing additive(s);
- produces thick, bound layers that are homogeneous;
- permits more flexibility in the choice(s) of wearing surface type and thickness;
- in-place construction and high production rates improve safety by reducing traffic disruptions and users inconvenience;
- economic savings are realized.

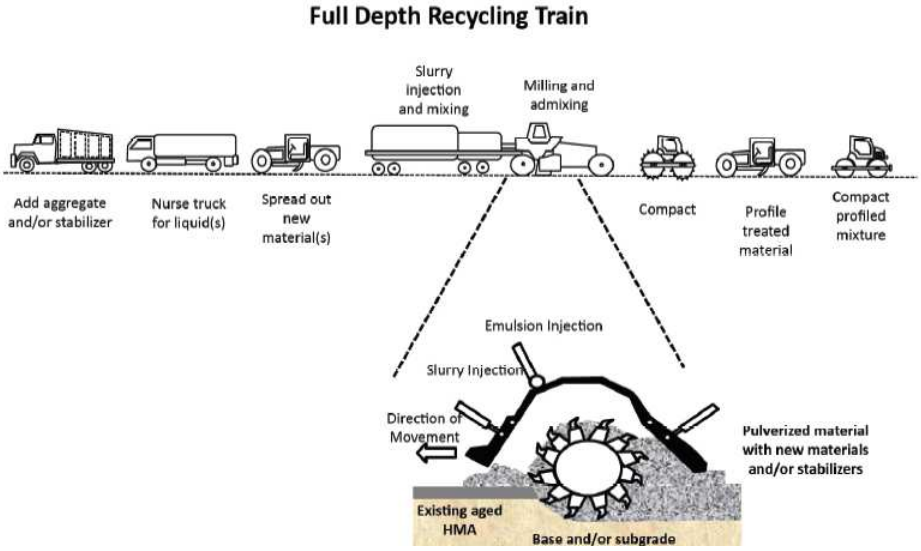


**Figure 2. 4** Typical equipment used for CIR recycling and FDR reclamation trains [Thompson et al., 2009].

## 2.4 State of the art in Europe

The adoption of cold mixtures in Europe is mostly related to the production of cold recycled mixtures (CRMs) using bitumen emulsion or foamed bitumen and cement. In fact, recycling techniques applied to the pavement industries are a common practice in most of the European countries. In that sense, the statistical data available highlighted that the production of new bituminous mixtures in 2008 allowed the recycling of 57% of all produced RA [EAPA, 2014]. In **Table 2. 1**, the European background about the use of cold techniques are reported [De la Roche et al., 2013].

| Countries | Cold techniques |
|---|---|
| BE (F+W) | 20% in base layer |
| CZ | Foamed bitumen, emulsions and cement |
| FR | Emulsions or foamed bitumen |
| DE | Emulsions or foams<br>Recommended for tar contaminated RA |
| IT | Mainly emulsions but foam increases. Higher %RA allowed |
| NL | - |
| NO | Emulsions and foamed bitumen |
| DK | Almost none |
| ES | 100% RA in base layer. Emulsions |

**Table 2. 1** European cold techniques.

As it can be observed from **Table 2. 1**, European practices are more oriented to the adoption of bitumen emulsions for cold mixtures (CMs) production. Different types of CMs based on aggregate grading (see Section 2.7) are used for repair and maintenance operations. In addition, CMs are also used for wearing course. They are layable in thicknesses varying from 3 to 22 cm and are designed to have high surface rugosity and allow drainage which can reduce aquaplaning.
For small jobs, laying is carried out by hand and compacted using small vibrating roller. Reshaping work usually employs a grader but pavers are also used. As the grading used in these mixtures is typically open, layers normally require the application of a sealing coat.
Currently, the increasing in the use of recycled aggregates for the production of new bituminous mixtures is a key point of the European policies, above all for the construction and maintenance of the highway system. Many European countries has established the use of 100% of RA as one of the main long-term objectives to achieve without compromising the performance of the material. Nowadays, RA is mostly employed for the deeper layers (unbound layers or base layer), but the tendency is pushing towards the ordinary use of such material also for the production of the upper bituminous layers.

### 2.4.1 European projects

*OPTEL Project*
Over the last years, the development of cold mixtures has certainly been one of the major challenges for the road building industry. The European project entitled OPTEL: "*Slow-Setting Cationic Bituminous Emulsions for Construction and Maintenance of Roads*" has been run by seven industrial partners or research organizations and represented an overall effort close to 300 man pour months over a period of more than 3 years (June 1996 to December 1999). Its prime objective was to improve the fundamental understanding of the various phenomena controlling the behavior of cold mixtures.
This understanding was to be used for the development of a more rational cold mix design and optimization methodology [Eckmann et al., 2001].
The OPTEL work has been directed towards two main topics:

- The fundamental understanding of key factors and phenomena (exchanges between aggregates, water-phase and emulsifier; characteristics of bitumen emulsions and how to control them; simulation and understanding of breaking and coalescence mechanisms).
- A global approach of the main performance requirements for cold mixtures (coating and workability; ability for compaction and maturation and final mechanical properties).

*DIRECT-MAT Project*
The research project DIRECT-MAT represents an important program in the European background for the promotion and development of recycling techniques [Bocci et al., 2010]. It is aimed at shearing and spreading the knowledge and the practices of each European country about recycling. The main goal of the program is to establish guidelines useful for the construction of long lasting pavements produced through secondary materials. To this aim, an on-line database was created to make the current state of the art about the research

on recycling and the corresponding experimental data always available. Downhill of the comparative evaluation of all the documents and the several national experiences collected over time, specific guidelines about the recycling techniques will be defined. Such a database should constitute a reference point constantly updated according to a continuous and accurate standard methodology.
Thus, the final goal of the project DIRECT-MAT is to improve the cooperation and coordination between the several European research groups through the implementation of a sheared scientific vision and research methodology. Within the scope of this project, also the collaboration between theoretical research and practical application has a fundamental importance. Therefore, the research activities are always carried out in accordance with pavement construction companies in order to find a good balance between the theoretical aspects and the everyday issues.

*CoRePaSoL - Characterization of Advanced Cold-Recycled Bitumen Stabilized Pavement Solutions*
This project was developed amongst four partners such as Czech Republic, Germany, Ireland and Denmark and it focuses mainly on harmonizing mix design of cold-recycled bitumen stabilized materials following the existing scientific and engineering experience and approaches. The key objective is to develop and recommend comprehensive mix design and characterization by studying compaction methods, curing procedures and performance tests. The output should be applicable to all variants of cold-recycled mixtures containing bituminous binders or combination with other binders or alternative fines. Aspects considerable for defining durability of cold-recycled mixtures will be evaluated and specified as well. Existing practice focuses only on water immersion and stiffness. Both characteristics are not a standard part in all mix designs known in Europe. Nevertheless, to vindicate and promote cold recycling as an equivalent solution for hot mix asphalt the durability must be predictable. For this reason, the project focuses on assessing stiffness, fatigue behavior, resistance to cracking and on long-term moisture effects. Different test procedures will be evaluated and most suitable approach recommended including proposed threshold limits. This will make performance-based mix design possible. Further gained results will be used for formulating preferable inclusion of cold-recycled mixture in existing pavement design manuals. It is primarily not expected to modify the mechanistic calculation of pavement design, more important seems to be the definition of typical structures where cold-recycled bitumen stabilized materials are used for base or binder courses and critical parameters are defined. This should allow to road administrators and designer to use cold-recycled mixtures as a standard component of a pavement structure.
Multiple recycling should present one of the key advantages of cold recycling techniques. The activation of reclaimed asphalt, impact of material ageing and range of applicability (for cold recycled mixtures and for the partial substitute of aggregates in hot mix asphalts) will be specified and the most suitable practice recommended. The final part of the project focuses on environmental stability/compactability which becomes an integral part of building materials' use and modern civil engineering. Leaching of cold-recycled mixtures will be specified with recommendations for threshold limits. At the same time, some hazardous or problematic materials in existing pavements will be assessed in relation to their immobilization and most suitable reuse by cold recycling (tar, asbestos, crumb-rubber modified asphalt). Part of this environmental assessment will be devoted to technically

correct assessment of cold-recycled mixtures with respect to their carbon footprint. It is believed, that in the near future, such energy equivalent will be considered in decision about most appropriate technical solutions in pavement construction or rehabilitation and energy savings achievable by recycling should be considered as a benefit [Valentin et al., 2014].

## 2.5 State of the art in Southern Africa

Treatment of granular material with bitumen emulsion has been used in pavement construction in Southern Africa since the 1960's. The initial development of foamed bitumen took place during the same period (late 1950's by Csanyi), but because of patent rights, the use of the foamed bitumen was limited to a small group of countries. After the expiration of the patent rights in the 1990's, the use and further development of foamed bitumen technology accelerated [Jenkins, 2000].
Throughout the years a number of guidelines have been developed by various institutions in South Africa. The publishing of these guidelines was generally prompted by pioneer work and developments that took place in the pavement construction industry. An overview of bitumen stabilized material (BSM) guidelines as published in South Africa is provided in **Table 2. 2**. As it can be observed, because of the limited application of foamed bitumen prior to the 1990's, no guidelines for the use of foamed bitumen were developed earlier on.

| Published | Bitumen Emulsion | Foamed bitumen |
|---|---|---|
| 1972 | TRH 7: The use of bitumen emulsions in construction and maintenance of roads | |
| 1993 | SABITA manual 14: GEMS - The design and use of granular emulsion mixes | |
| 1999 | SABITA manual 21: ETB, the design and use of emulsion-treated bases | |
| 2002 | | TG 2: The design and use of foamed bitumen treated materials |
| 2009 | | TG 2: Bitumen stabilized materials (2nd ed.) |

**Table 2. 2** Overview of BSM guidelines published.

The first document, THR7: The Use of Bitumen Emulsion in Construction and Maintenance of Roads [Department of Transport, 1972], provided little guidance in terms of stabilization and/or cold-mix design. It incorporated general aspects of the use of bitumen emulsions in all fields of pavement construction, including seals, tack and prime coats, bitumen treatment and recycling. For the possible use of bitumen emulsion in soil stabilization (reduction of plasticity index and increase of shear strength), reference was made to the knowledge and experience that existed in the industry at the time. The THR7 did, however, provide some general practical guidelines for the reuse of existing base layers treated with bitumen emulsion.
During the 1970's and 1980's, the popularity of bitumen emulsion treatment of granular pavement layers increased and the term ETB's was established. SABITA published the GEMS manual in 1993 that dealt with the design and use of granular emulsion mixes. It made

a clear distinction between stabilization and modification. Stabilization was defined as addition of bitumen emulsion with the residual binder content exceeding 1.5% by mass with the purpose to produce a structural layer with an 'asphalt type' of material. Modification was defined as generally less than 1.5% residual binder content by mass being added with the objective to improve the properties of substandard material [SABITA, 1993]. The latter was the more popular application in Southern Africa during that period.
The SABITA GEMS manual was the first of its kind to introduce laboratory test procedures, mix design procedures, evaluation criteria and structural design guidelines for granular bitumen emulsion mixes in South Africa.
While the GEMS manual was still fairly new, SABITA embarked on a follow-up research program to address certain shortcomings that were already identified in the GEMS manual. The main objective was to provide updated and extended guidelines on structural design, mix design, constructability and economic guidelines to broaden the range of the application of ETB's. An ETB would typically have a residual binder content of 1.5% by mass or less. Therefore it would, according to the GEMS manual, be classified as a modified granular emulsion mix. The mix design and structural design guidelines for such a modified granular emulsion mix were not appropriate for an ETB material. This resulted in the publishing of SABITA's ETB manual [SABITA, 1999] in 1999.
Prior to the publishing of the Asphalt Academy's TG2 Interim Guideline for foamed bitumen treatment in 2002 [Asphalt Academy, 2002], designers in Southern Africa mainly 'borrowed' from the available guidelines for bitumen emulsions, international foamed bitumen guidelines, as well as hot-mix asphalt design guidelines. TG2 introduced laboratory test procedures, mix design procedures, evaluation criteria and structural design guidelines for foamed bitumen treated materials in South Africa. The guideline was launched as an interim guideline with the intention to update the manual once further research results (on different types and qualities of parent material and more bitumen/cement ratios) became available. The second updated edition of the Asphalt Academy's TG2 Interim Guideline for foamed bitumen treatment was published in 2009 [Asphalt Academy, 2009].

## 2.6 State of the art in Northern America

Cold mixtures were used in United States of America since the 1960's. Due to the remoteness of some areas of the country, CM is an essential part of the road construction industry. Information on US practice is easily available in technical manuals compiled by various organizations [Schramm, 1994; ARRA 2001; Stroup-Gardiner, 2011] to advise on all aspects of production and laying of CM as well as cold recycling. Two classifications of CM are identified according to mixing method. There are plant-mixed and mix-in-place (road mix). The environmental, economic and versatility benefits are recognized as are the limitations such as sensitivity to wet weather and slow build up of strength. Two types of bituminous binder are prescribed for CM, namely *cutback* and *bitumen emulsion*. Differently, foamed bitumen was limited used for CMs production in the past as well as in the present.
Due to environmental concerns, cutback is becoming restricted in many areas. Thirteen grades of bitumen emulsion are used with a range of setting rates and binder types. It should be stressed that in most cases, American emulsions almost contain solvent. Different grades of cutback are also used. This cold applied binder is produced by diluting bitumen with solvent to liquefy the binder at low temperatures. Medium curing cutback (MC) use kerosene

as solvent, which is relative volatile, whereas slow curing (SC) cutbacks use heavy flux oils or are made by distilling the crude directly to the desired grade. The setting rate is dependent upon the rate of solvent evaporation. In **Table 2. 3** are reported the suitable emulsions or cutbacks for each particular operation.

| | Emulsified asphalt | | | | | | | | | Cut-back asphalts | | | | | | |
|---|---|---|---|---|---|---|---|---|---|---|---|---|---|---|---|---|
| | Anionic | | | | | Cationic | | | | Medium curing | | | | slow curing | | |
| Type of construction | MS2 | MS2h | HFMS2S | SS1 | SS1h | CMS2 | CMS2h | CSS1 | CSS1h | 70 | 250 | 800 | 3000 | 250 | 800 | 3000 |
| **Cold-laid plant mix pavement base and surfaces** | | | | | | | | | | | | | | | | |
| Open-graded aggregate | X | X | | | | X | X | | | | | | | | | |
| Well-graded aggregate | | | X | X | X | | | X | X | | X | X | X | X | X | X |
| Patching, immediate use | | | | X | X | | | X | X | | X | X | | | X | |
| Patching, Stockpile | | | | | | | | | | | X | X | | X | X | |
| **Mixed in place(Road mix) Pavement base and surfaces** | | | | | | | | | | | | | | | | |
| Open-graded aggregate | X | X | | | | X | X | | | | | X | X | | X | X |
| Well graded aggregate | | | X | X | X | | | X | X | | X | X | | X | X | |
| Sand | | | X | X | X | | | X | X | X | X | X | | | | |
| Sandy soil | | | X | X | X | | | X | X | | X | X | | | | |
| Patching, immediate use | | | X | X | X | | | X | X | | X | X | | | X | |
| **Cold mix recycling** | | | | | | | | | | | | | | | | |
| All mixtures | X | X | X | X | X | X | X | X | X | | | | | | | |

**Table 2. 3** Guide for bituminous binder use in cold mixture.

There is no national accepted cold mixture design method. However, either Marshall [ASTM D1559-89] or Hveem methods [Asphalt Institute, 1997], or modified versions, are nearly always used.

## 2.7 Cold mixtures

In the framework of promoting environmental friendly technologies for the construction of new bituminous pavements and their corresponding maintenance, *cold materials* (CMs) play

a fundamental rule. In fact, comparing different processes for road construction (hot, warm, half-warm and cold), cold technologies as well as CMs are characterized by the lower energy consumption for heating (**Figure 2. 5**) and consequently, combined with the adoption of recycled materials, they can maximized all benefits related to the conservation of non-renewable resources.

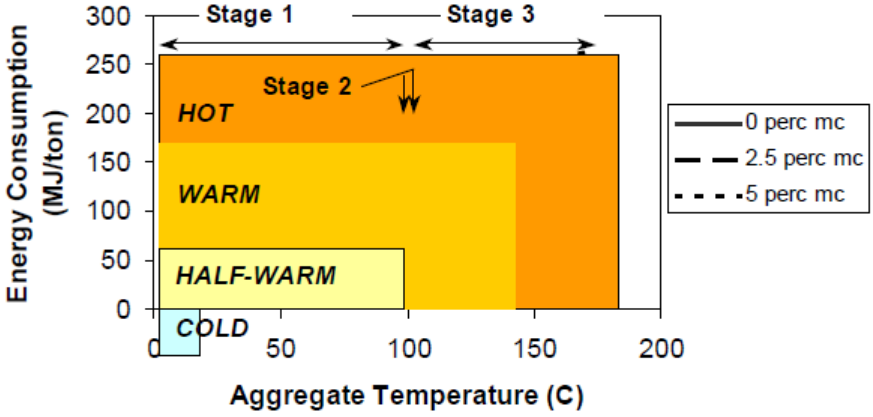


**Figure 2. 5** Classification of bituminous mixtures in terms of aggregate mixing temperature and energy consumption for heating, Reference material at 20 °C and varying moisture content (mc).

In current practices, the term CMs indicates a mixture consisting of an aggregate blend (composed by virgin or reclaimed aggregates) mixed with bitumen in form of bitumen emulsion or foamed bitumen, cement and other additional stabilizing agents such as lime or fly ash. In addition, it is important to highlight that, although the simultaneous presence of bitumen and other *active or inactive fillers* (e.g. cement, calcium carbonate, hydrated lime, ecc…), they do not produce a new binder.

The addition of these binding agents (bituminous and/or active fillers) guarantees suitable structural and durability properties [Bocci et al., 2012; Santagata et al., 2009; Stroup-Gardiner, 2011]. Water instead of heating is used in order to allow CM laydown and compaction**.** In particular, when RA is adopted replacing VA within CM, it is usually referred to a cold recycled mixture (CRM).

Generally, there are three types of CMs: dense graded (DG), sand (S) and open-graded (OG). Aggregate gradations for each of these mixture types are reported in the Section 2.6.1.

The emulsion types used are the slow-setting or medium-setting grades.

*Dense-graded mixtures* consist of aggregates that are graded from the maximum size down to and including material passing the No 200 (75 µm, ASTM). They include a wide variety of aggregate types and gradations can be used for all types of pavement applications. A wide range of emulsion grades are used based on environmental and traffic conditions. *Sand bitumen mixtures* are produced by treating bank-run sands and poorly graded sand-gravels. Sand mixtures are generally restricted to fine granular sands and silty sands low in clay content. Sand mixtures have provided good performance as subbase and base layers when produced using the proper bitumen emulsion grades. *Open-graded mixtures* provide high air voids with the aim to drain water through the mixture but they are also characterized by the

lack of fines. These materials were used successfully for both base and surface courses. These mixtures have shown good resistance to fatigue, reflection cracking, rutting and shoving.
In general, DG and S mixtures require a surface seal for waterproofing and to provide a more durable wearing surface. Chip seals are typically used for DG mixtures. For OG mixtures, a surface seal is not usually required [AEMA, 2008].
Through CMs, a wide range of mixtures, characterized by different mechanical behaviors, can be classified according to type and dosage of binding agents adopted (bitumen and cement).
At least four CM families can be distinguished:

- Cement-treated materials (CTMs);
- Bitumen-stabilized materials (BSMs);
- Cement-bitumen treated materials (CBTMs);
- Cold-mix Asphalt (CMA).

In **Figure 2. 6**, they are compared with traditional pavement materials using the representation proposed by Asphalt Academy (2009) and readapted by Grilli (2012).

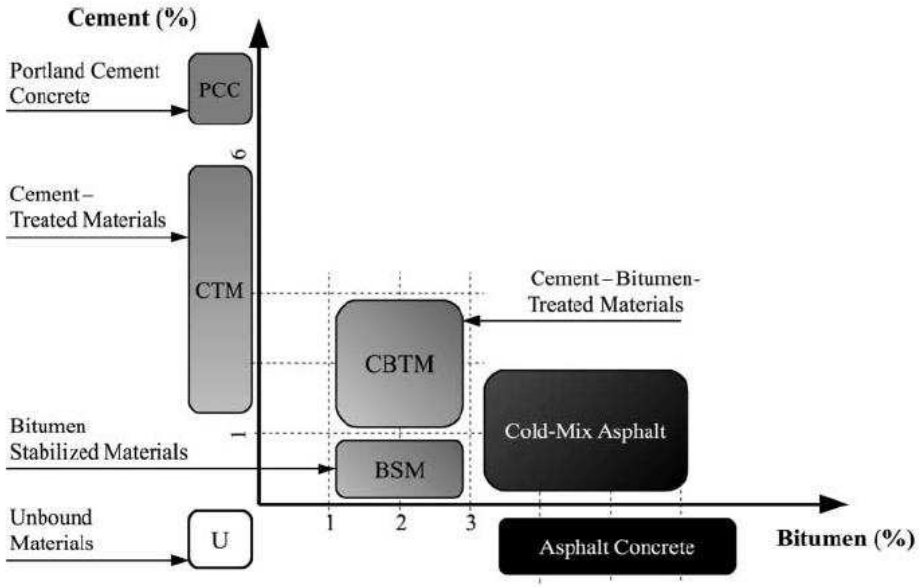


**Figure 2. 6** Conceptual composition of pavement mixtures [Asphalt Academy, 2009; Grilli et al., 2012].

## 2.7.1 Cement treated materials

If only cement is added as the binding agent, conventional cement-treated materials (CTMs) can be obtained [Paige-Green and Ware, 2006; Ramzi Taha et al., 2002; White and

Gnanendran, 2002]. CTMs are generally produced in plants and they consist of selected aggregates, cement, ranging from 2 to 5% by dry aggregate weight [Siripun et al., 2009, Guthrie et al., 2002], and a defined percentage of water, which plays an important role in both compaction and cement hydration [White et al., 2005]. CTM is preferred in the production of base courses rather than in-situ cement stabilised soil, in order to enhance the bearing capacity of pavements and to improve the distribution of traffic-induced stresses through the underlying layers. CTMs were originally produced using natural or crushed aggregates but nowadays, the term CTM is increasingly associated with recycling. In order to preserve natural resources and to reduce the disposal of materials coming from the demolition of civil constructions, recycled aggregates such as crushed concrete [Molenaar et al., 2011; Marradi et. al, 2008], crushed masonry [Xuan et al., 2012, Molenaar et al., 2011], foundry sand [Gupta et al., 2009], reclaimed asphalt [Taha et al., 2002; Rupnow et. al., 2002; Gupta et al., 2009; Yuan et al., 2011] and reclaimed aggregates [White et al., 2005; Paige-Green et al., 2006] are being used in CTM. Moreover, considering the scarce availability of high quality VA, the cement treatment of recycled materials proves to be one of the most viable recycling techniques for road construction and maintenance [White et al., 2002; Tam et al., 2006; Yuan et al., 2011]. Cement treatment can really maximize the amount of RA to be recycled without penalizing the mechanical characteristics of the final product while at the same time exploiting the intrinsic properties of RA [Grilli et al., 2013].
From the mechanical point of view, CTMs including recycled aggregates typically show high stiffness and tendency to premature cracking (brittle behavior, i.e. cement-like behavior). Although the bitumen contained in RA appeared to be very stiff and the cement bond tended to inhibit any thermo-dependent or time-dependent response of the mixtures, both temperature and load frequency influence the stiffness of CTM produced using RA.

### 2.7.2 Bitumen stabilized materials

*Bitumen-stabilized materials* (BSMs) are produced using a bitumen emulsion or foamed bitumen as binding agent. The residual bitumen usually does not exceed 3% by dry aggregate weight, and up to 1% of cement can be added as an "*active*" filler. Small amounts of active filler can significantly increase the retained strength without affecting the flexibility of the layer. Cement content should also not exceed the percentage of the bitumen stabilizer, (i.e. the ratio between bitumen percentage and cement percentage, B/C, should always be greater than 1). If this ratio is less than one (high cement content), then the material should be considered such a cement treated material [Asphalt Academy, 2009].
The aggregate gradation of BSM is usually referred to that of S type for CMs (see Section 2.6.1).
When bitumen emulsion is added (*BSM-emulsion*), the charged bitumen droplets are attracted to the smaller aggregate particles with the opposite charge. Active filler assists the extraction of the water phase from bitumen emulsion, causing the breaking (see Section 2.5.3). Differently, when foamed bitumen is adopted (*BSM-foam*), the tiny bitumen particles that are produced when the foamed bitumen bubbles burst have only enough energy to warm the smaller aggregate particles sufficiently to permit adhesion (**Figure 2. 7**). Active filler acts as a catalyst in dispersing the bitumen particles (see Section 2.5.2).

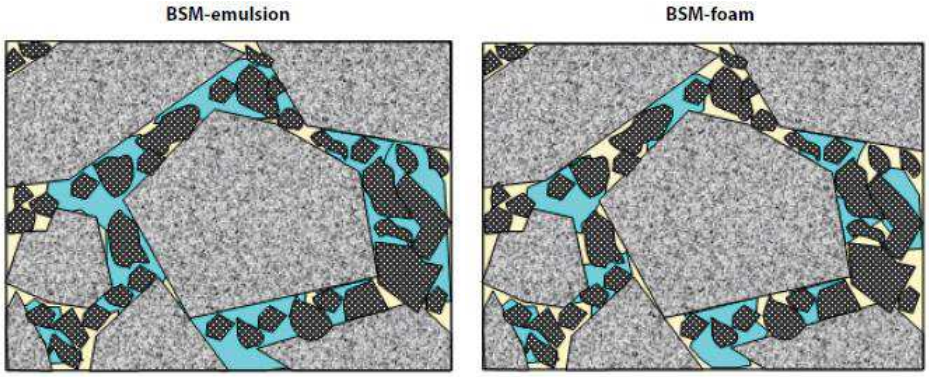


**Figure 2. 7** BSM structure: with bitumen emulsion, BSM-emulsion; with foamed bitumen BSM-foam.

BSMs, unlike HMA, are not black in appearance and do not have a sticky feel. Considering BSMs, the larger aggregate particles are not totally coated with bitumen. The bitumen disperses only amongst the finest particles, resulting in a bitumen-rich mortar between the coarse particles.
Current practice prefers to treat BSMs produced with bitumen emulsion or foamed bitumen equally in terms of their performance properties. However, the addition of foamed bitumen or bitumen emulsion does not change the nature of the material; it does not become a cold mixture but BSMs remain granular in nature and must be processed as such during construction. A layer constructed using BSMs is relatively more flexible compared with a layer of the same material treated with cement. BSMs may be trafficked immediately after construction due to the substantial increase in cohesion that is realized when the material is compacted. This cohesion prevents the material ravelling under the traffic [Wirgten, 2010].
BSMs show a stress-dependent mechanical behavior that is similar to that of granular materials (failure by permanent deformation or shear stress). In addition, the bitumen dispersed among the fine aggregate fraction creates “non-continuous” bonds between coarser particles, increasing resistance to fracture, cohesive strength, shear properties and reducing moisture sensitivity [Fu and Harvey, 2007; Jenkins et al., 2007; Khosravifar et al., 2015].

The main features of BSMs are:

- BSMs exhibit a significant increase in cohesion in comparison to the untreated material. The friction angle of the treated material is typically similar to the untreated material.
- BSMs acquire flexural strength from the combined effect of the linear viscoelastic properties of the dispersed bitumen droplets. Since the individual bitumen droplets are not linked and the coarser aggregate particles remain uncoated, BSMs retain the granular characteristics of the untreated material. Therefore, it is stress dependent and not prone to cracking when subjected to tensile stresses.
- BSMs perform well when cohesive strength is improved through proper mix design protocol (in order to determine the optimal bitumen and active filler contents).

- Since the bitumen is dispersed only amongst the finer aggregate particles, fines are encapsulated and blocked. This improves the moisture sensitivity and durability of the treated materials. In addition, providing sufficient bitumen, the tendency for BSM to pump under loading, in saturated conditions, is also significantly reduced because fines are bound.

Similar to unbound granular materials, the stiffness of BSM is dependent on:

- stiffness of the untreated material;
- density of the material used in the layer;
- quantities of binder and active filler added, and their dispersion degree throughout the mixed material;
- local climate, particularly ambient temperature and rainfall;
- stiffness of the subgrade.

However, it is important to understand that there are two ways in which the optimal shear strength of a BSM can be compromised, both resulting from the inclusion of too much active filler:

- Excessive amounts of active filler will transform the material from a flexible to a brittle state. In this state, the cohesive strength will dominate but it will significantly reduce once fracture occurs. This is usually associated with deformation and cracking, and will result in a material affected by large fractured clumps and with a low frictional resistance.
- Poorly graded or non-durable source materials (soft weathered natural gravel or material with excessive fines) will compromise the frictional resistance of the material. Such fine grained, brittle materials will be highly susceptible to crushing and fatigue failure [Jenkins, 2000].

### 2.7.3 Cement-bitumen treated materials

In Italian current practices, CRMs characterized by higher cement contents (up to 2.5% by dry aggregate weight) are usually adopted as subbase layer for road pavement. These mixtures, referred to *cement–bitumen-treated materials* (CBTMs), are characterized by considerably higher cohesion and stiffness with respect to BSMs. The basic idea while preparing CBTMs, is to start from a CTM and, adding bitumen emulsion or foamed bitumen, reduce cracking susceptibility and the overall structural stiffness of the recycled layer. However, the ratio between bitumen percentage and cement percentage (B/C) should always be about or slightly higher than 1.This results in a mechanical behavior closer to that of an *asphalt concrete* (AC) as thermal dependency and fatigue issues appear [Grilli et al., 2012].
The dosages of residual bitumen and cement control the stiffness and thermal sensitivity of CBTMs; these factors must be addressed both in the design and in the construction control phase [Bocci et al., 2010].
A more representative explanation can be put forward considering the physical structure of CBTM mixtures (produced with bitumen emulsion or foamed bitumen). This type of mixture

can be represented as a skeleton of coarse aggregates bounded by bituminous and hydraulic mortars, formed by the finer aggregate particles. The coarse aggregate skeleton is formed by virgin aggregate and/or reclaimed aggregate (considered as "*black rock*", see Section 2.5.1). In addition, coarse aggregates are coated by bituminous mortar, formed by the fresh bitumen after emulsion breaking [Asphalt Academy, 2009] or foamed bitumen collapse, whereas hydraulic mortar, formed by the hydrated cement (**Figure 2. 8**).

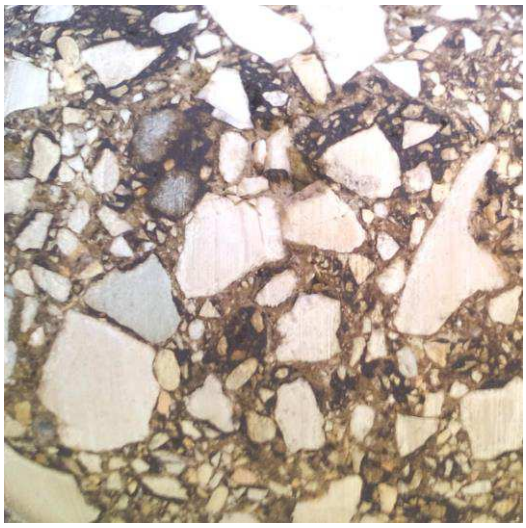

**Figure 2. 8** Cement-bitumen treated material (CBTM) composed by: VA, RA, cement, bitumen emulsion and voids.

The use of CBTMs has been documented by various authors [Santagata et al.,2009; Thompson et al., 2009; Grilli et al., 2012; Cardone et al., 2015] and although CBTMs are significantly different from traditional HMA, their mechanical behavior can be analyzed following similar approaches [Montepara and Giuliani, 2002; Santagata and Chiappinelli, 2003].

According to the proportions in which bitumen and cement are mixed, the mechanical response of a CBTM is extremely variable. In general, the addition of cement increases strength, stiffness and permanent deformation resistance but, at high cement content, mixture could be affected by premature cracking (brittle behavior, i.e. cement-like behavior) [Grilli et al., 2012; Du, 2014]. Whereas, the presence of bitumen amongst the recycled aggregate increases cohesion, durability, fatigue cracking resistance and reduced moisture sensitivity of the mixture but, if high bitumen content is adopted, mixture could be more prone to failure by permanent deformation (or shear stress) [Bocci et al., 2011]. In addition, the viscoelastic behavior and temperature dependency of bituminous binder confers to CBTM, asphalt-like properties (i.e. frequency-dependent and thermo-dependent) [Cardone et al., 2014; Grilli et al., 2012].

## 2.7.4 Cold-mix asphalt

Cold-mix asphalt (CMA) is produced using bitumen emulsion or foamed bitumen as bituminous binding agent.
Aggregate blend can include both virgin and reclaimed aggregates; in general, the bitumen content (derived from bitumen emulsion or foamed bitumen) is similar to the bitumen content adopted for traditional *asphalt concrete* (AC), it can vary from 3% up to 6% by dry aggregate weight, and up to 2% of cement can be added as "*active*" filler. Consequently, CMA is characterized by higher bitumen/cement ratio ranging from 1.5 to 3 and this indicates that mechanical properties closer to those of an AC, such as thermal dependency and flexibility, are more marked.
The most known CMA is *Grave emulsion* (G-E) that firstly appeared in France, sixty years ago [Sferb; 1991]. It is used extensively as base course and for reprofiling, overlaying and strengthening old pavements and construction/rehabilitation of lightly trafficked roads. G-E mixture is also adopted for overlaying cement stabilized base course in order to prevent crack propagation.
Aggregate mixture used in G-E is densely graded and the optimum design is characterized by high sand content to improve high internal friction in the curing period and good surface texture. The latter consideration is often an interim requirement because G-E layers are always overlaid with a surface dressing to seal the pavement surface [Needham, 1996]. A low filler content is also preferred to minimize the susceptibility to rutting which can occour if voids are overfilled with a bituminous/filler mastic [Brown and Snaith M. S., 1974].
The most notable feature of G-E mixtures is the partial coating of aggregates. The bitumen amount, added to the mixture (about 3% by dry aggregate weight) confers a very lean appearance and leaves the mixture potentially susceptible to water which is the typical reason of surface dressing. In the past, low binder contents were originally used in order to promote a high level of aggregate contact and to improve the internal friction. In recent years, there was a trend to move towards higher binder contents, about 4% by dry aggregate weight. Bitumen emulsion used during G-E mixtures production, is designed to have a medium setting rate in order to guarantee the coating of fine aggregates before that partial coalescence takes place [Needham, 1996]. The produced fine coated mastic acts as a binder that bind discontinuously the larger aggregate particles.
The compaction of G-E is a fundamental aspect in fact, an effective densification prevents future settlement or rutting and improves internal friction and cohesion.
Heavy pneumatic tyred rollers (PTR) are often advised for compaction because their kneading action is very efficient for achieving good densification and bitumen redistribution but care must be taken in order to avoid over-compaction that can lead to surface cracking. As the binder approaches the state of full break, it becomes somewhat dry and crumbly (usually referred to "*cheesy*" state). From this moment, the binder is lacking in cohesion and the application of heavy loads can cause cracks on the material surface.
G-E can be trafficked immediately after compaction and this is due to the high internal friction and cohesion which characterize the early life of the mixture. The potential full strength is achieved as a result of water evaporation that is a slow process and it is dependent on climatic conditions and partly improved by the action of traffic [Needham, 1996].
The mentioned phenomenon is known as *curing* and it will be explained more in details for all CMs in Section 2.7.

# 2.8 Constituents of cold mixtures

As previously described, cold materials (CMs) can be schematized as a multi-phase material and their composition combines:
- solid particles (virgin or reclaimed aggregates and bitumen in the cured state of the mixture);
- fluids (bitumen emulsion and foamed bitumen in the fresh state of the mixture and water);
- air voids.

Both volumetric properties and mechanical behavior of CMs can be evaluated according to water content used in the mixture and to the proportions (bitumen/cement B/C ratio) in which bitumen and cement (stabilizing agents) are mixed.

## 2.8.1 Aggregates (virgin or recycled)

Aggregate is defined as *processed soil*. Virgin aggregates (VA) are obtained from quarries or riverbeds. The process of obtaining aggregates consists of blasting or dredging; large-size particles are crushed to obtain usable sizes that range from 50 mm to less than 0.075 mm for most pavement mixes. Since aggregates are derived from parent rocks, their characteristics depend on their properties. Parent rocks can be classified in terms of their geologic origins, which dictate their chemical composition and hence many of the other key properties that affect their corresponding behavior and performance [Mallick and El-Korchi 2013].
In most cases, pavement engineers are obliged to use locally available aggregates. There are certain characteristics of different types of aggregates that must be considered during the mix and structural design of pavements. For example, petrographic examination [ASTM C-295] of aggregates can be conducted to identify different parent rock materials and minerals in an aggregate sample. Such examinations can provide valuable information regarding the suitability of aggregates for bituminous and concrete mixtures, particularly with respect to their durability, such as resistance against breakdown under freeze–thaw or moisture actions. Petrographic examination may include tests ranging from detailed visual examination to investigation using a polarizing microscope, differential thermal analysis and x-ray diffraction. **Figure 2. 9** shows an example of results carried out with petrographic test performed on an aggregate sample.

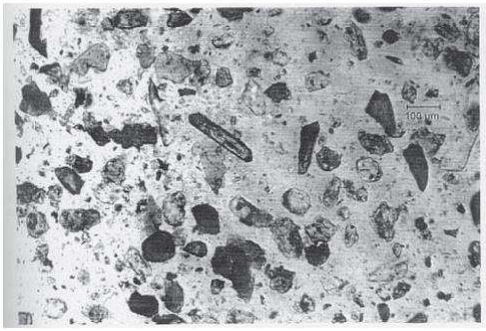


**Figure 2. 9** Example of petrographic examination result of a sand. particle dimensions less than 0.075 mm under plane polarized light.

The European Standard EN 13043 specifies each property of aggregates and filler obtained by processing natural, manufactured or recycled materials and mixtures composed by these aggregates in order to adopt them in bituminous mixtures and surface treatments for roads, airfields and other trafficked areas.
Using the term "recycled aggregates", it is possible to identify by-products obtained from industrial processes or other human activities:

- Construction and demolition (C&D) defined as solid wastes from the construction, re-modelling and repairing of individual residences, commercial buildings, and other civil engineering structures [Spencer, 1989; Kalin, 1991];
- Waste glass derived from building/automobile windows and doors, glassware and bottles [Chang et al., 2000; Su and Chen, 2002];
- Steel slag, the molten by-product of many metallurgical operations [Farrand and Emery, 1995; Asi et al., 2007];
- Tyres rubber and plastics [Presti, 2013; Partl et al., 2010].

The EN 13043 does not cover the use of reclaimed bituminous mixtures but the increasing use of recycling in the production of road pavements makes it necessary to identify reclaimed asphalt (RA) as a construction material (**Figure 2. 10**). In fact, RA have important residual properties which must not be underestimated. RA should not be demoted to a waste material but it should be adequately reused [Grilli ISAP, 2012].
Few years ago, the European specification EN 13242 has considered the use of RA as aggregate for unbound and hydraulically bound layers (road embankment, subgrade and foundation) and EN 13108-1 up to and including EN 13108-7 permitted the addition of RA in asphalt products (asphalt concrete, asphalt concrete for very thin layers, soft asphalt, hot-rolled asphalt, stone mastic asphalt, mastic asphalt, porous asphalt).
Recently, the European Standard EN 13108-8 has introduced RA as possible constituent material that can be included in the mixture during the production of bituminous materials manufactured in a hot mix asphalt plant.
It defines RA as asphalt, reclaimed by milling of bituminous road layers, by crushing of slabs ripped up from bituminous pavements, lumps from slabs, asphalt from reject and surplus production. This European Standard contains requirements for RA with respect to binder and aggregate properties and foreign matter that apply in all cases of RA usage. Since the requirements for bituminous mixtures are the same for mixtures with and without RA, the level of homogeneity of the material practically determines the maximum amount of reclaimed asphalt that can be used. Technical difficulties or environmental issues limit the use of RA in both applications, i.e. for bound and unbound layers [McDaniel et al., 2002].For this reason, national regulations establish the maximum RA content. In this context, both in-plant or in-place cold recycling can really maximize the amount of RA to be recycled without penalizing the mechanical characteristics of the final product while at the same time exploiting the intrinsic properties of RA [Kandhal and Mallick, 1997].
Cold in-place or in-plant recycling allow the use of highest amount of RA (up to 100%) [Paige-Green and Ware, 2006; Santagata et al., 2009; Bocci et al., 2010] although, currently,

there is no European standard which specifies the requirements of RA as a constituent material for CRMs.

**Figure 2. 10** Reclaimed asphalt (RA).

However, EN 13108-8 gives important guidelines and principles for the classification and description of RA which should also be followed or adapted when RA is used in cold recycling process.
On the one hand, the particle size and grading of RA, the presence, content and type, of any foreign matter, the identification of RA source from which the stockpile is derived and the homogeneity of the feedstock should be determined when RA is used in cold mixtures. On the other hand, binder type and content could be less important when there is no melting of RA in the mixture and it can be supposed that RA behaves as a "*black rock*". If RA is a black rock, the aged bitumen content in RA has no effect on the total bitumen content and consequently no significant blending ensues [Soleymani et al., 2000].

The growing use of RA requires the definition of appropriate specifications, comparable to ones adopted for hot in-plant asphalt recycling in order to allow quality control to be performed and thus high performance materials to be produced.
The aggregate blend for CMs as well as CRMs production can combine VA and RA in different proportions depending and the type of pavement layer to be manufactured (subbase or foundation layers). In addition, gradation is generally specified (in specifications) by pavement project owners (such as state departments of transportation) and determined in accordance with EN 933-1 and EN 933-2.
Aggregates may comprise single sizes, all-in aggregates or combinations of two or more than two sizes. Aggregates supplied as a mixture of different sizes or types should be uniformly blended. When aggregates of significantly different density are blended, caution is necessary to avoid segregation.
The main aim of the aggregate blend design is to remain close as much as possible to the maximum density gradation in order to avoid too high voids content in the mixture, provide a stable structure but also retain enough space for accommodating adequate bitumen binder for material durability [Mallick and El-Korchi 2013].
The maximum density lines are based on the concept proposed by Fuller and Thompson (1907, also known as *Fuller's curve* equation), which is as follows:

$$P = 100 \cdot \left(\frac{d}{D}\right)^n \quad (1)$$

where

*P* is the percentage passing;
*d* is the diameter of sieve;
*D* is the maximum size of the aggregate;
*n* is the coefficient, first proposed as 0.5 and then modified to 0.45.

A wide variety of aggregate blends may be used successfully for CMs. From **Table 2. 4** to **Table 2. 6**, some of the most common gradations adopted for DG, S and OG cold mixtures are shown [AEMA, 2008].

| | **Percent passing by weight** | | | | |
|---|---|---|---|---|---|
| **Sieve size** | **Processed Dense-graded cold mixtures** | | | | |
| 50 mm | 100 | - | - | - | - |
| 37.5 mm | 90-100 | 100 | - | - | - |
| 25 mm | - | 90-100 | 100 | - | - |
| 19 mm | 60-80 | - | 90-100 | 100 | - |
| 12.5 mm | - | 60-80 | - | 90-100 | 100 |
| 9.5 mm | - | - | 60-80 | - | 90-100 |
| 4.75 mm | 20-55 | 25-60 | 35-65 | 45-70 | 60-80 |
| 2.36 mm | 10-40 | 14-45 | 20-50 | 25-55 | 35-65 |
| 1.18 mm | - | - | - | - | - |
| 600 µm | - | - | - | - | - |
| 300 µm | 2-16 | 3-18 | 3-20 | 5-20 | 6-25 |
| 150 µm | - | - | - | - | - |
| 75 µm | 0-5 | 1-7 | 2-8 | 2-9 | 2-10 |

**Table 2. 4** Aggregate blend for dense-graded cold mixtures.

| **Sieve size** | **Total percent passing** | | |
|---|---|---|---|
| | **Poorly-graded** | **Well-graded** | **Silty Sands** |
| 12.5 mm | 100 | 100 | 100 |
| 4.75 mm | 75-100 | 75-100 | 75-100 |
| 300 µm | - | 15-30 | - |
| 150 µm | - | - | 15-65 |
| 75 µm | 0-12 | 5-12 | 12-20 |

**Table 2. 5** Aggregate blend for sand cold mixtures.

| Sieve size | Base | | | Surface coarse |
|---|---|---|---|---|
| | Coarse | Medium | Fine | |
| 37.5 mm | 100 | - | - | - |
| 25 mm | 95-100 | 100 | - | - |
| 19 mm | - | 90-100 | - | - |
| 12.5 mm | 25-60 | - | 100 | - |
| 9.5 mm | - | 20-55 | 85-100 | 100 |
| 4.75 mm | 0-10 | 0-10 | - | 30-50 |
| 2.36 mm | 0-5 | 0-5 | 0-10 | 5-15 |
| 1.18 mm | - | - | 0-5 | - |
| 75 µm | 0-2 | 0-2 | 0-2 | 0-2 |

**Table 2. 6** Aggregate blend for open-graded cold mixtures.

## 2.8.2 Cement

Lime, cement and blends of these products with fly ash, ground blast furnace slag and other such pozzolanic materials, are the most commonly used stabilizing agents in the production of CMs. The primary function of these agents is to increase bearing strength. This feature is achieved either by significantly increasing tensile and compressive strength of the material or by reducing plasticity. *Cement* is the stabilizer that provides most enhancement of strength. Free lime released during the hydration process reacts with any clay particles that may be present, thereby reducing plasticity. Lime, however, is comprised predominantly of free lime and therefore it is the most appropriate stabilizing agent for plastic materials (Plasticity Index, $PI > 10\%$).

The use of cement and cement blends should be limited to treat materials characterized by a *PI* lower than 10. The strength achieved is governed by the amount of stabilizing agent added and the type of material to be treated. However, it must be recognized that adding more cement in order to obtain higher strengths can be detrimental for the performance of the layer. The addition of cementitious stabilizing agents produces *semi-brittle* materials (**Figure 2. 11**). An increase in strength detected for the stabilized layer results in an increase in brittleness as well as a consequential reduction in flexibility (i.e. cement-like behavior) [Little and Petersen, 2005; Grilli et al., 2013].

Higher strength concentrated in a cement treated layer attract more stresses from the wheel loading. As a consequence, this phenomenon leads to accelerated crack propagation under repeated heavy traffic loading, thereby reducing structural performance. Therefore, it is important that the performance requirements of the stabilized layer are perfectly understood and that a proper mix design is conducted on representative samples in order to determine the suitable cement content.

According to Italian current practices, Portland limestone cement type II/A-LL, strength class 32.5 R is the most used type of cement adopted during cold recycling operations.

The European Standard EN 197-1 defines the composition, specifications and conformity criteria for common cements and it can be helpful during the mix design procedure.

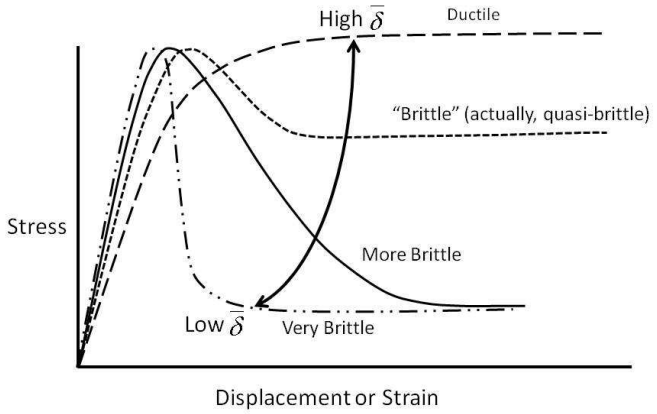


**Figure 2. 11** Semi-brittle behavior of material stabilized with cementitious agents.

## 2.8.3 Bitumen emulsion

First bitumen emulsions used in road construction were prepared in the early part of the 20th century. Currently, more than 8 million tons of emulsions are produced worldwide and the products vary greatly among countries [SFERB, 2002].

With viscosities ranged from 0.5 to 10 Poise at 60°C, bitumen emulsion is characterized by considerably lower viscosity than plain bitumen (100 – 4,000 Poise), allowing it to be used at ambient and low temperature. Low temperature techniques (e.g. cold recycled process) for construction and maintenance reduce emissions, energy consumption, avoid oxidation of the bitumen, and are less dangerous than techniques using HMA.

Bitumen emulsions are water-based and in many cases can be diluted further with water for applications such as dust control and priming. They are also compatible with hydraulic binders like cement and lime as well as water-based polymer dispersions like natural and synthetic latex [James, 2006].

*Emulsion definition*

An emulsion is a dispersion of small droplets of one liquid in another liquid. Emulsions can be formed by any two immiscible liquids, but in most emulsions one of the phases is water. *Oil-in-water* (O/W) emulsions are those in which the continuous phase is water and the disperse (droplet) phase is an "oily" liquid. *Water-in-oil* (W/O) or "inverted" emulsions are those in which the continuous phase is an oil and the disperse phase is water. In addition, emulsions can have more complex structures. Such as *multiple emulsions* (W/O/W), the disperse phase contains another phase which may not have the same composition as the continuous phase (**Figure 2. 12**) [AzkoNobel, 2000; James, 2006; Tadros, 2011].

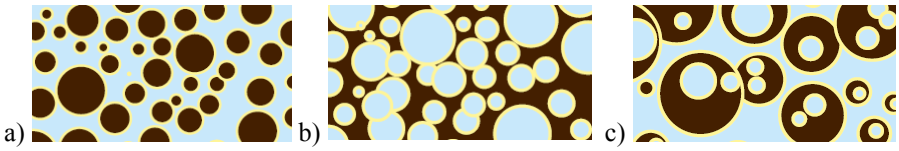


**Figure 2. 12** Types of emulsions: a) O/W emulsion; b) W/O emulsion and c) multiple W/O/W emulsion**.**

Standard bitumen emulsions are normally considered to be of the O/W type but they can invert to W/O (inverted emulsion) during the setting process [Needham, 1996]. Standard bitumen emulsions usually contain from 40% to 75% bitumen, 0.1% to 2.5% emulsifier, 25% to 60% water plus some minor components. The most part of commercial emulsions contain about 28% droplets smaller than 1 microns in size, 5% droplets 1-5 microns in size and the rest 5-10 microns in size. Emulsions with particle sizes in this range are sometimes referred to as *macro-emulsions*. Bitumen emulsions are brown liquids with consistencies from that of milk to double cream, which depend mostly on the bitumen content and the particle size. Some bitumen droplets may contain smaller water droplets within them; a better description of bitumen emulsion could be a *W/O/W multiple emulsion*. The viscosity of the emulsion and especially changes in the viscosity of the emulsion during storage are strongly influenced by this internal water phase [Furlong et al., 1999; Poirier et al, 2000].
The distribution of droplets in the emulsion is influenced by the emulsion recipe, the mechanics and operating conditions of the emulsion manufacturing plant (**Figure 2. 13**).

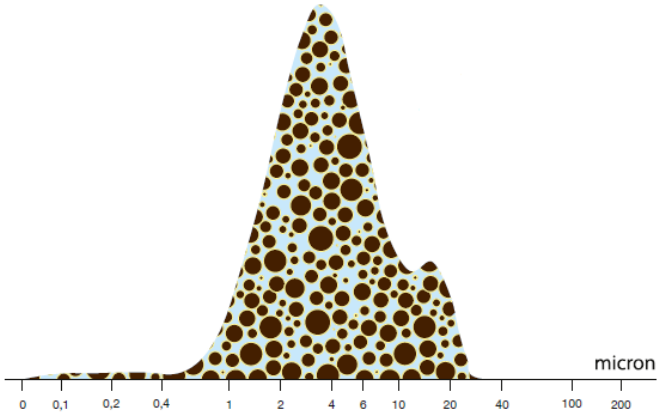


**Figure 2. 13** Typical particle size distribution of bitumen emulsion droplets.

Moreover, droplets size and its corresponding distribution of the emulsion droplets strongly influence the physical properties of the emulsion, such as viscosity and storage stability; larger average droplets size leads to lower emulsion viscosity [Holleran et al., 2002]. In general, smaller droplets size leads to an improvement in emulsion performance [Yuan, 2011]. Macro-emulsions are inherently unstable. Over a period of time, which may be hours or years, the bitumen phase will eventually separate from the water. Bitumen is insoluble in

water, and breakdown of the emulsion involves the fusion of droplets (*coalescence*) (**Figure 2. 14**).
The bitumen droplets in the emulsion have a small charge. The source of the charge is the emulsifier, as well as ionisable components in the bitumen itself. These small charges on the droplets normally provide an electrostatic barrier to their close approach to each other (like charges repel). However, when two droplets achieve enough energy to overcome this barrier and approach closely, then they adhere to each other (*flocculate*) (**Figure 2. 14**). This flocculation may sometimes be reversed by agitation, dilution, or addition of more emulsifier. Consequently, the water layer between droplets in a floccule will be thin and the droplets will coalesce. The coalescence cannot be reversed. Factors which force the droplets together such as settlement under gravity, evaporation of the water, shear or freezing will accelerate the flocculation and coalescence process, as does anything which reduces the charge on the droplets. Bitumen characterized by lower viscosity coalesces more rapidly than high viscosity bitumen.

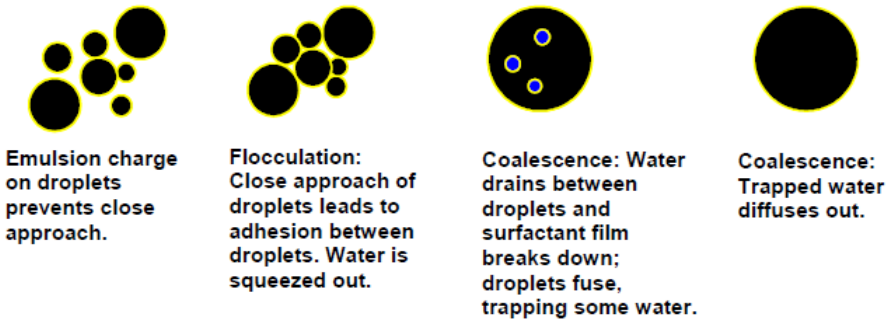


**Figure 2. 14** Stages in the breakdown of emulsions.

*Manufacture of bitumen emulsions*
Emulsions are made by mixing hot bitumen with water containing emulsifying agents (*soap*) and applying mechanical energy sufficient to break up the bitumen into droplets. The emulsifying agent(s) and other additives, if needed, provide the electrical charges to the droplets of bitumen so they are able to repel each other and remain dispersed in water.
Emulsifier is usually added via the waterphase; there are two methods of doing this:

- preparing batches of waterphase by dissolving the emulsifier in water along with acid or base (*batch manufacture*) (**Figure 2. 15**);
- Dosing the emulsifier and acid or base to the water directly into the mill (*inline manufacture*) (**Figure 2. 15**).

Emulsions are produced in a colloid mill, containing a high-speed (1000–6000 revolutions/min) rotor, through which hot bitumen and emulsifier solutions are passed at specific temperatures (**Figure 2. 16**).
Emulsification is opposed by the internal cohesion, viscosity of the bitumen and the surface tension of the droplet which resists to the creation of new interface. Smaller droplets are favored by a high energy input, a low bitumen viscosity at the emulsification temperature

and by the choice and concentration of emulsifier (which reduces the interfacial tension) [AzkoNobel, 2000; James, 2006].

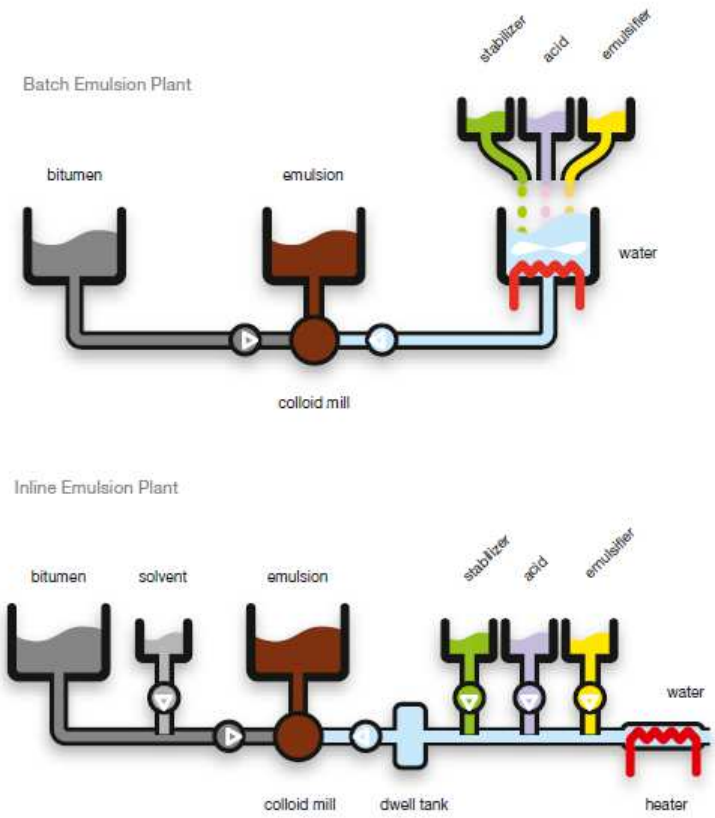


**Figure 2. 15** Manufacture of bitumen emulsion: in batch and inline emulsion production.

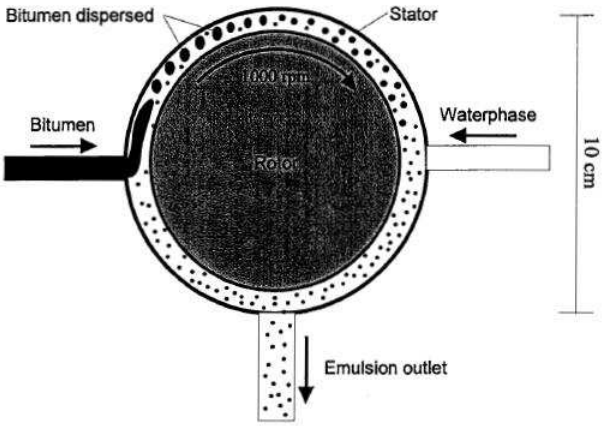


**Figure 2. 16** Diagram of emulsification process.

*Chemical nature and function of the emulsifier*

Water molecules at the interface between oil and water have higher energy than those in bulk water. The result is an interfacial energy or tension which acts to minimize the interfacial area. The production of emulsion involves the creation of a large interfacial area between the bitumen and water.

Emulsifiers are surface active agents (surfactants) characterized by nonpolar lipophilic (*oil-loving*) and polar hydrophilic (*water-loving*) portions in the same molecule (**Figure 2. 17**). Both reduce the energy required to emulsify the bitumen and prevents coalescence of the droplets once formed. The choice and concentration of emulsifier also largely determines the charge on the bitumen droplet and the reactivity of the emulsion produced. Emulsifiers can be classified into *anionic*, *cationic* and *nonionic* types depending on the charge of their head groups adopted in water, although this charge may depend on pH.

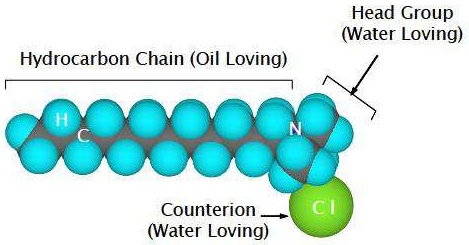


**Figure 2. 17** Cationic emulsifier molecule.

Common anionic emulsifiers, which impart negative charges, are made from the saponification of fatty acid–type materials, such as rosins and lignins (wood by-products) with sodium or potassium hydroxide. Cationic emulsifiers are generally made from fatty amines (such as diamines) and hydrochloric acids, as well as from fatty quaternary ammonium salts.

In the case of bitumen emulsions, the bitumen itself contains surface active species which can also concentrate at the interface [Rabio et al., 1999]. The size and sign of the charge on

the bitumen droplets can be measured and it is expressed as the "*zeta potential*" of the droplet. The zeta potential is strongly pH-dependent both because of the pH dependence of the charge on the emulsifier and also because polar components of the bitumen itself may ionize. Zeta potential measurements show that the charge on the bitumen droplets becomes more negative as the pH rises. Generally, more emulsifier is required to provide good stability and the right performance properties to the emulsion, necessary to fill the interface. In particular, this bitumen emulsions will contain some "*free*" emulsifier in the water phase, presents partly in micellar form, which acts as a reservoir helping to prevent coalescence after emulsification, storage and transport. This free emulsifier also plays an important role in the *breaking process* (see below) [Boussad and Martin, 1996; Verlhac et al., 2002].

*Bitumen emulsion stability and breaking process*

Emulsion stability refers to the ability to keep the bitumen droplets well dispersed throughout the emulsion. Because of the density of bitumen slightly higher than the aqueous phase of the emulsion at ambient temperature, the droplets would tend to settle down over time, forming clumps by agglomeration, and ultimately forming larger globules by coalescing [Mallick and El-Korchi 2013]. In fact, an emulsion is defined to be *stable* when droplets retain their individuality as opposed to an *unstable* emulsion where the droplets tend to coalesce forming a final film of bitumen [Lesueur and Potti, 2004].

On a physicochemical standpoint, emulsion stability is obtained thanks to the repulsive forces between bitumen droplets. These interparticle forces can be described by the so-called DLVO theory, named after its founders Derjaguin- Landau-Verwey-Overbeek [Israelachvili, 2011]. According to this theory, inter-droplet interactions are the sum of an electrostatic repulsion and a Van-der-Waals attraction.

When the repulsion overcomes the attraction, the droplets are prevented from approaching each other and the emulsion is stable, i.e. no breaking occurs. On the contrary, when the attraction overcomes the repulsion, the droplets tend to contact and then coalesce. Even so the detailed mathematical treatment of these phenomena fall outside of the scope of this thesis, an example of a typical DLVO interaction between bitumen droplets is given in **Figure 2. 18**.

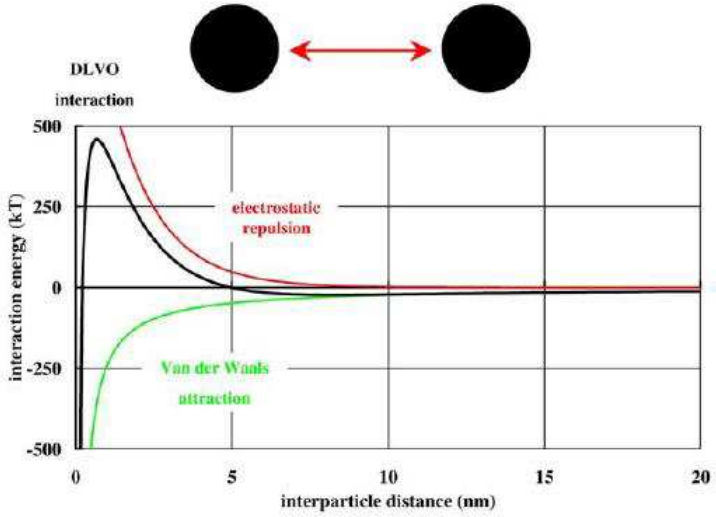


**Figure 2. 18** Typical DLVO interaction between two bitumen droplets and its two main electrostatic and Van der Waals components: interaction energy (in units of thermal energy kT) versus interparticle distance.

The Van der Waals attraction is a macroscopic manifestation of the intermolecular attraction between molecules [Israelachvili, 2011]. A typical energy versus interparticle distance for this attraction, in the case of bitumen droplets, is also pictured in **Figure 2. 18**.
On the other hand, the electrostatic repulsive interaction comes from the presence of electrical charges on the droplet surfaces and arises because charges repel each other. In our case, these charges are essentially those coming from the polar heads of the emulsifiers [Takamura et al., 1987; Rodrıguez-Valverde et al., 2003]. Given this context, the breaking of the emulsion is a consequence of the diminution of the surface charge up to a point where it can not overcome the Van der Waals attraction anymore.
**Figure 2. 19**b represents the case where a bitumen emulsion is brought into contact with some species (cement, aggregate,...) modifying directly or indirectly the surface charge of the droplets and/or their ionic environment, therefore inducing breaking. However, another manner to cause emulsion breaking consists in removing the water from the emulsion **Figure 2. 19**a (e.g. through evaporation), as a consequence only the bitumen remains [Boussad and Martin, 1996]. In this case, breaking occurs when bitumen concentration becomes so high that the droplets are pushed against one another, the crowding finally overcoming all repulsive forces.

Hence, the emulsion breaking can now be described in rational terms as a consequence of two causes:

- Disappearance of the electrostatic repulsion between droplets (*gel contraction*),
- Very high bitumen concentration (*film forming*) (**Figure 2. 19**).

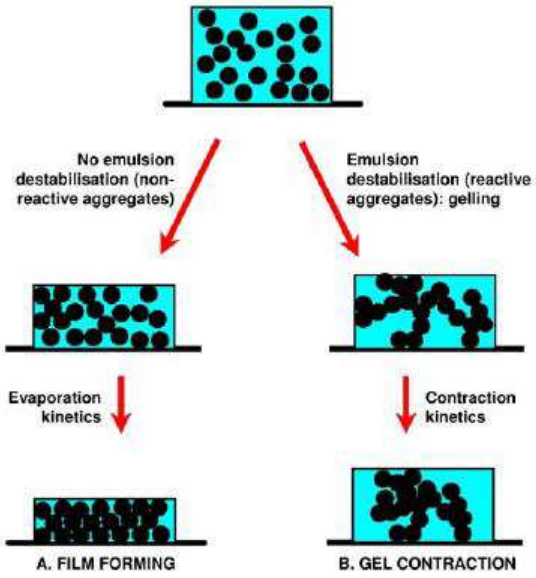


**Figure 2. 19** The two possible breaking scenarios for the bitumen emulsion: a) film forming and b) gel contraction.

The breaking characteristics of an emulsion can be affected by the bitumen content, composition of the aqueous phase, droplet size distribution, environmental conditions, types of aggregate and use of breaking agents. Evaporation and absorption of water by aggregates may be the main breaking mechanism for very slow-setting emulsions, but in most cases, chemical reactions between aggregate and emulsion contribute to the emulsion setting and it is not necessary that all the water evaporates before curing takes place. The strength of the emulsion/aggregate reaction is in many cases sufficient to remove water from the system.
The speed of these setting and curing processes depends on the reactivity of the emulsion, the reactivity of the aggregate and environmental factors, such as temperature, humidity, wind speed, and mechanical action. Important factors are pH changes caused by the reaction of the aggregate with acids in the emulsion, adsorption of free emulsifier onto the aggregate surface and flocculation of the emulsion droplets with the fines.
The relative timescale of *flocculation* (setting) and *coalescence* (curing) depends on the system but in general, flocculation is the most rapid process in which some water can be expelled from the system and initial cohesive strength develops, followed by a slower coalescence process which results in a continuous bitumen phase. This bitumen phase must also adhere to the aggregate. Coalescence is an inversion process where the O/W emulsion is transformed into a W/O emulsion type which then slowly loses its internal water phase. This inverted process is favored as the ratio of bitumen to water in the system increases.
In field, too early coalescence of the bitumen droplets can hinder final curing by skin formation [Lesueur et al., 2002; Walter and Day, 2002] reducing the water evaporation.

*Bitumen emulsion/Aggregate adhesion*

In parallel to emulsion breaking, part of the droplets will cover the aggregate surface providing appropriate aggregate/droplet interactions.

This process controls the *coating quality*; droplet attraction by the aggregate surface is generally thought to be of electrostatic origin and therefore depends on the aggregate surface charge, and consequently related to its *petrography* and droplet surface charge [SFERB, 2002; Bourrel and Verzaro, 1998]. For example, siliceous aggregates usually bear negative charges and therefore attract all positively charged droplets. In particular, the adsorption of the free emulsifier is shared between emulsion and bitumen droplets. Due to their much bigger micron size, the droplets are however much slower and therefore surfactant adsorption is the fastest process. It's important to remark that droplet size will influence the process since the larger the droplets, the slower they diffuse.

In addition, the "free", "no adsorbed" or "residual" emulsifier is that part of the emulsifying agent which is not located at the bitumen-water interface and therefore remains in the continuous aqueous phase of the emulsion [Lesueur and Potti, 2004].

On the one hand, an excess of surfactant is dangerous not only because it will not leave any surface available for the droplets, but also because it can form a repulsive double layer on the aggregate surface when in excess [Boussad and Martin, 1996]. On the other hand, if the emulsifier is absorbed from the solution into the aggregates at the desired rate (such as through a rough-textured porous surface), the lowering of charge on droplets causes rapid coalescence and good adhesion of the bituminous binder to the aggregate surface.

**Table 2. 7** summaries the compatibility between bitumen emulsion and aggregate type.

| Bitumen emulsion type/aggregate type compatibility | | | |
|---|---|---|---|
| Emulsion Type | Aggregate (Rock) Type | Trends | |
| | | Breaking rate | Adhesion |
| Anionic | Acidic | Slow | Poor |
| Anionic | Alkaline | Medium | Good |
| Cationic | Acidic | Fast | Excellent |
| Cationic | Alkaline | Fast | Good |

**Table 2. 7** Compatibility between bitumen emulsion and aggregate type [Wirtgen, 2010].

*Designation of bitumen emulsions*

The European Standards EN 13808 (or ASTM-D977 and D2397/D2397M) specifies the requirements in terms of performance characteristics of bitumen emulsions that are suitable for road construction and maintenance activities, airfields and other paved areas.

Considering European standards, bitumen emulsion is classified according to their:

- Charge, cationic [C] and anionic [no symbol];
- percentage of residual bitumen (e.g. 60 indicates a bitumen emulsion characterized by 60% of bitumen content);
- type of bitumen, plain [B] or modified [symbol selected according to the type of additive adopted];
- rate of breaking or setting, number from [2] for rapid setting emulsions up to [12] for over stabilized bitumen emulsions (very slow setting).

Each application requires the correct type of bitumen emulsion (**Table 2. 8**).

| | ANIONIC | | | CATIONIC | | | |
|---|---|---|---|---|---|---|---|
| | RAPID SETTING | MEDIUM | SLOW | RAPID SETTING | MEDIUM | SLOW | SUPER-STABLE |
| **SPRAY APPLICATIONS** | | | | | | | |
| Surface Dressing (Chip Seal) | • | | | • | | | |
| Fog Seal | | • | • | | • | • | • |
| Tack Coat | | •[a] | • | • | •[a] | • | |
| Prime Coat | | | • | • | | • | • |
| Penetration Macadam | | | | • | | | |
| **SLURRY SURFACING** | | | | | | | |
| Slurry Seal | | | • | | | •[b] | • |
| Cape Seal | | | • | | | •[b] | • |
| Microsurfacing | | | | | | •[b] | |
| **PLANT MIXES** | | | | | | | |
| Open Graded/Semi Dense | | •[a] | | | • | | |
| Dense Graded | | | • | | | • | • |
| RAP | | • | | | | • | • |
| Stockpile Mix | | •[a] | | | •[a] | | • |
| Pre-coated Chips | | | | | • | • | |
| **MIX PAVING** | | | | | | | |
| Open Graded | | | | | •[a] | | |
| **IN PLACE MIXES** | | | | | | | |
| RAP | | •[a] | | | •[a] | • | • |
| Soil Stabilization | | | • | | | | • |
| Dense Graded | | | • | | | • | • |

a) May contain solvent. b) Need to pass cement mix test.

**Table 2. 8** Applications of bitumen emulsion [AzkoNobel, 2000].

## 2.8.4 Foamed bitumen

More than fifty years ago, Dr Ladis Csanyi at the Bituminous Research Laboratory of the engineering Experiment station at Iowa state University successfully injected steam into bitumen to create a *temporary* foaming mass that could be mixed with wet mineral aggregates at ambient temperatures for the first time [Csanyi, 1957 and 1959]. The most part of the literature has been published from Australia where Mobil Oil held the patent rights from Dr Ladis Csanyi and they modified the system using cold foamant water instead of steam. As the use of foamed bitumen involved many countries (USA, UK, Canada and the North of Africa), so the criteria selection for the optimum foam production varied, basing on different formulations and interpretation. However, mix design procedures for foamed mixes have not been formalized and this lack of standard specifications is mainly due to the limited application and often to secret approaches to the process by operators. This resulted in an absolute absence of fundamental and rational guidelines for the use of foamed bitumen.

*Foamed bitumen definition and manufacture*

Foamed bitumen is a foaming mass of bitumen that can be produced through the injection of small quantities of cold moleculized water (typically 2% by mass), as a fine mist, into hot bitumen located in the expansion chamber. Water, turned into vapor, is trapped in thousands of tiny bitumen bubbles. This phenomenon is also known as *foaming process* and it is reported in **Figure 2. 20**.

Key points of the foaming process require that first considerations on factors affecting the characteristics of foamed bitumen have been analyzed. The laws governing the behavior of the bitumen during foaming are primarily physical, although chemistry does also play an important role.

At the moment, when cold water droplets (at ambient temperature) make contact with the bitumen at 170°C to 180°C, the following chain of events occur:

- bitumen exchanges energy with the surface of the water droplet heating droplets to a temperature of 100°C and cooling the bitumen.
- The transferred energy of the bitumen exceeds the latent heat of steam resulting in explosive expansion and in steam generation. Steam bubbles are forced into the continuous phase of bitumen under pressure, in the expansion chamber.
- With emission from the spray nozzle, the encapsulated steam expands until a thin film of slightly cooler bitumen holds the bubble intact through its surface tension.
- During expansion, the surface tension of the bitumen film counteracts the ever-diminishing steam pressure until a state of equilibrium is reached.
- Due to the low thermal conductivity of bitumen and water, bubbles can remain stable for a period of time, usually measurable in seconds [Jenkins, 1999; Jenkins, 2000].

This process occurs for a multitude of bitumen bubbles that live contemporary metastable lives, providing foamed bitumen. Foamed bitumen can be classified as *bubble-form* foam in the group of polyederschaum that consisting of non-spherical bubbles separated by surfactant-stabilized, thin liquid films called *lamelle* [Schramm, 1994] (**Figure 2. 21**). As the colloidal mass cools at ambient temperature, the steam in the bubbles condenses causing bubbles to collapse and the foam to "decay".
In foamed state, which is a temporary state characterized by low viscosity (foam dissipates in less than one minute), bitumen can be added and mixed with wet aggregates at ambient temperatures.

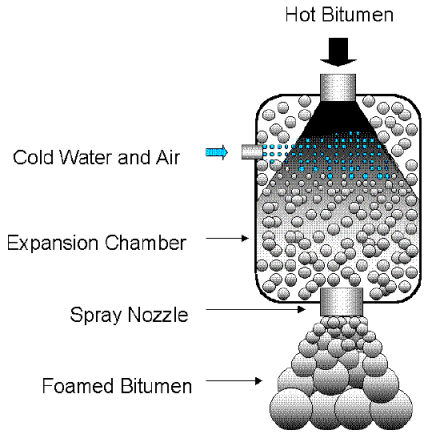

**Figure 2. 20** Production of foamed bitumen in an expansion chamber.

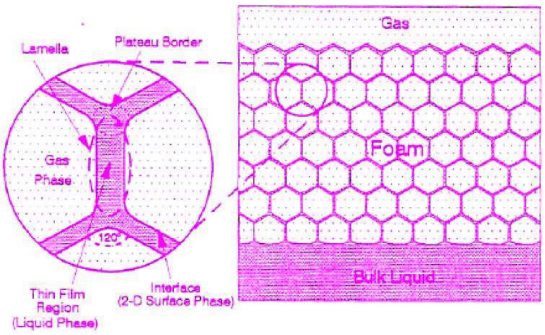


**Figure 2. 21** Generalized foam with non-spherical bubbles [Schramm, 1994].

During the mixing process, foamed bitumen is *selective* in its dispersion throughout the mineral aggregate. In fact, the bitumen bubbles burst, producing tiny bitumen splinters that disperse by adhering to the finer particles (fine sand and smaller) forming a bitumen rich mastic. As shown in **Figure 2. 22**, foamed bitumen collapses during mixing, only a limited number of bitumen droplets are attached to the larger aggregate particles resulting in *partial coating* and in localized non- continuous bonds ("*spot welding*") [Jenkins, 2000]. On the contrary, the adoption of bitumen emulsion during CMs production can improve more homogeneous and continuous particles coating.

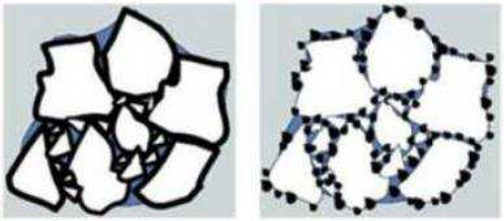

**Figure 2. 22** Continuously and non-continuously bounds for bitumen emulsion and foamed bitumen, respectively.

Moisture in the mixture prior to the addition of foamed bitumen plays an important role in dispersing the bitumen during mixing.
Generally, bitumen with penetration values between 80 and 250 are generally selected for foaming, although softer and harder bitumen have been successfully used in the past and may be used when available. For practical reasons, very hard bitumen is generally avoided because of the poorer quality of foam, that leads to poorer dispersion of the bitumen in the mix [Asphalt Academy, 2009; Wirgten, 2010].

*Bitumen foamability*
The term foamability explains the ability to produce foam from a given substance.

Two properties form the basis of bitumen's suitability for foaming process, namely the *Expansion Ratio* (ER) and *Half-life* ($\tau_{1/2}$):

- The *expansion ratio* is a measure of viscosity of the foam and determines how well bitumen will disperse in the mix. It is calculated as the ratio of the maximum volume of foam with respect to the original volume of bitumen.
- The *half-life* is a measure of the stability of the foam and provides an indication of the rate of collapse of the foam. It is calculated as the time taken in seconds for foam to collapse reaching one half of its maximum volume.

*Foaming properties* or *foamability* of each bitumen type needs to be tested. However, standard specifications for expansion ratio and half-life do not exist, although recommended values have been collected in literature. For example, Ruckel et al. (1983) and Acott and Myburgh (1983) recommended limits from 8 to 15 for ER and 20 seconds (minimum) for half-life, CSIR (1998) recommends an ER of at least 10 and a half-life of at least 12 seconds and Asphalt Academy (2009) suggests an ER of at least 8 and a half-life of at least 6 seconds. A lot of factors influence these properties of bitumen [Brennen et al., 1983], the most important are: the amount of foam produced; the foamant water addition, the foaming temperature of the bitumen and type of mineral aggregate. Although these four factors are fundamental to improve the foamability of bitumen, they do not completely explain the fluctuations in foamability of bitumen [Jenkins, 2000]. It is important to highlight that the penetration value alone does not qualify bitumen for use; anyway, bitumen composition can provide additional information to better understand foaming phenomena.

Focusing the attention on foamant water, by varying its application rate a graph such that reported in **Figure 2. 23** may be obtained. From this plot, foam characterization system can provide the selection of foamant water rate to be applied.
It is evident that these two parameters and the method used to determine them are not enough to characterize adequately the foam properties. Improved or additional parameters that take into account other aspects able to characterize the foaming process such as the foam decay (**Figure 2. 24**) are necessary to better understand the process and predict the performance of foamed bitumen during the mixing phase.

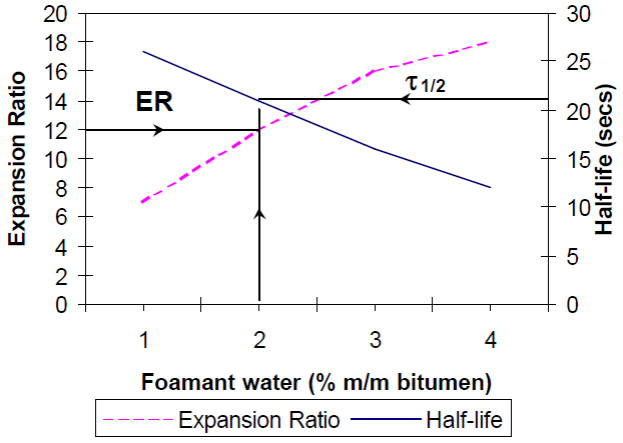


**Figure 2. 23** Foam characteristics for typical bitumen.

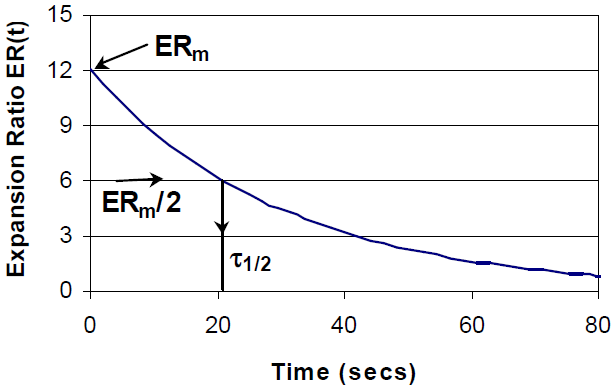


**Figure 2. 24** Foam decay curve for selected bitumen with 2% of foamant water.

*Determination of the optimum foamant water content (OFWC) and foaming temperature – Laboratory procedure provided by Wirgten and Jenkins KJ.*

One of the dominant factors influencing the foam properties is the water that is injected into the expansion chamber to produce the foam (foamant water), as illustrated in **Figure 2. 20**. A higher application rate of foamant water causes greater expansion (*higher ER*) but leads to more rapid subsidence or decay, i.e. a shorter half-life (*lower* $\tau_{1/2}$).

In addition, higher bitumen temperature usually creates better foam. An experimental analysis is recommended with the aim to identify a target of bitumen temperatures for foaming.

The variability of foam characteristics measured in laboratory and in field, both in terms of repeatability and reproducibility, are significant. At least three tests are recommended for each set of conditions (foamant water rate and foaming temperature), to obtain an acceptable level of statistical reliability.

At the moment, a unique laboratory procedure provided by Wirgten and Jenkins KJ. [Jenkins, 2000; Wirgten, 2010] is available to determine the temperature and percentage of water addition (foamant water) that is required to produce the best foam properties (maximum expansion ratio and half-life) for a particular source of bitumen. This is performed using *Wirgten WLB 10S laboratory unit*, considering three different bitumen temperatures (not exceeding 195° C) with the following procedure:

- Step 1, heat the bitumen in the kettle of the Wirtgen *WLB 10 S laboratory unit* with the pump circulating the bitumen through the system until the required temperature is achieved (normally starting with 160° C). Maintain the required temperature for at least 5 minutes prior to start the test.
- Step 2, calibrate the discharge rate of the bitumen and set the timer on the *Wirtgen WLB 10 S* to discharge 500 g of bitumen ($Q_{bitumen}$).
- Step 3, set the water flow-meter achieving the required water injection rate (normally starting with 2% by mass of the bitumen).
- Step 4, discharge foamed bitumen into a preheated (± 75° C) steel drum in order to calculate spray time related to 500 g of bitumen. Immediately after the foam discharge stops, start the stopwatch.
- Step 5, using the dipstick supplied with the *Wirtgen WLB 10 S* (which is calibrated for a steel drum of 275 mm in diameter and 500 g of bitumen) to measure the maximum height that the foamed bitumen achieves in the drum. This is recorded as the maximum volume (*ER*).
- Step 6, using the stopwatch to measure the time in seconds that the foam takes to dissipate to one half of its maximum volume. This is recorded as the foamed bitumen's half-life ($\tau_{1/2}$).
- Step 7, repeat the above procedure three times or until similar readings are achieved.
- Step 8, repeat steps from 3 to 7 for a range of at least three water injection rates. Typically, values of 2%, 3% and 4% by mass of bitumen are selected.
- Step 9, plot each result in a graph where the expansion ratio versus half-life is reported, at different water injection rates on the same set of axes (**Figure 2. 25**). The optimum foamant water content is selected as an average of the two water contents required to meet these *minimum criteria*.

Repeat Steps from 1 to 9 for two other bitumen temperatures (normally 170° C and 180° C) in order to select the best one (*foaming temperature*).

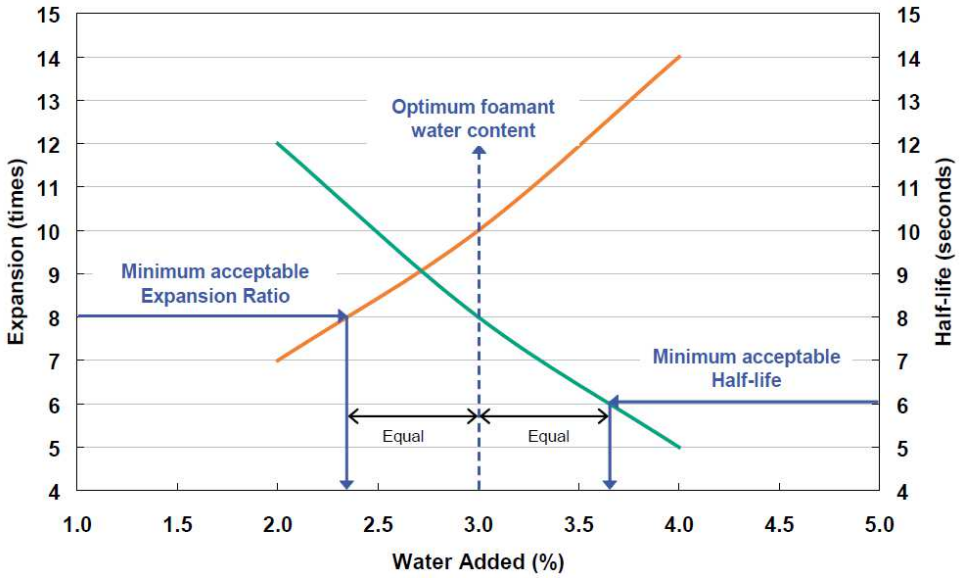


**Figure 2. 25.** Determining the optimum foamant water content (*OFWC*).

## 2.8.5 Fluid content

The role of moisture in mineral aggregate is similar for both CMs prepared using bitumen emulsion (CM-emulsion) or foamed bitumen (CM-foam) in many aspects, but there are some differences.

For a conscientious evaluation, the entire fluid content in the mixture (moisture and bitumen) needs to be considered. The role of moisture for both CM-emulsion and CM-foam is summarized in **Table 2. 9**.

| Component | CM-emulsion | CM-foam |
|---|---|---|
| Bitumen | Contributes to fluids for compaction | Negligible contribution to fluids for compaction |
| Moisture in aggregate | Reduces absorption of bitumen emulsion water into aggregate | Separates and suspends fines making them available to bitumen during mixing |
| | Prevents premature breaking | Acts as carrier for bitumen droplets during mixing |
| | Extends curing time and reduces early strength | Reduces early strength |
| | Provides workability of CM at ambient temperatures | |
| | Reduces friction angle and lubricates for compaction | |
| | Provides shell-life for mixtures | |

**Table 2. 9** Role of fluids in CMs.

Considering CM-emulsion, changes in moisture content occur in two distinct phases, namely:

- *Breaking*, is the separation of bitumen from the water phase through flocculation and coalescence of bitumen droplets to produce films of bitumen on aggregates (see Section 2.5.3). The breaking process with anionic bitumen emulsions is a *mechanical process* (evaporation), whereas cationic bitumen emulsions produce a *chemical break*.
- *Curing*, is the loss of water and resultant increase in stiffness and tensile strength of bitumen.

Differently for CM-foam, changes in moisture content occur exclusively as a result of *curing*. For both CM-emulsion and CM-foam, *curing* is an important aspect because mixtures need time to acquire sufficient stiffness and cohesion between particles before carrying traffic [Asphalt Academy, 2009]. Insufficient water reduces the workability of the mix and results in an inadequate dispersion of the binder, while too much water requires longer curing times, reduces the strength and density of the compacted mix and may reduce the coating of the aggregates. Fluids content in the mixture is identify as the *optimum moisture content* (*OMC*); this amount can vary and should be optimized during mixing and compaction phase in order to improve strength, density, water absorption and swelling.
In literature, a unique standard procedure developed to determine the *OMC* for both CM-emulsion and CM-foam is not available yet. Actually, this value is estimated according to standard specifications for granular unbound materials such as mod AASHTO T180 OMC, modified Proctor compaction EN 13286-2 or to limited technical guidelines [ARRA, 2001; Asphalt Academy, 2009; Wirgten, 2010].
For example, investigations carried out by Mobil Oil on BSM-foam suggested that the optimum moisture content for mixing lies at the "*fluff point*" of the aggregate, i.e. the moisture content at which the aggregates have a maximum loose bulk volume (70 % - 80 % mod AASHTO T180 OMC, or modified Proctor compaction EN 13286-2). However, the fluff point may be too low to ensure adequate mixing (foam dispersion) and compaction, especially for finer materials.
Bowering (1970) observed that where inadequate foam dispersion occurred as a result of insufficient mixing moisture, the compacted densities were low and no benefit was gained from the bitumen treatment.
Lee (1981) found that the optimum mixing moisture content occurs in the range of 65 - 85% of the modified AASHTO T-180 OMC (or modified Proctor compaction EN 13286-2) for the aggregates. Lee also suggested that moisture should be added to the mix before the injection of foamed bitumen, otherwise the moisture would have no beneficial. This optimum range of moisture contents for mixing was confirmed by Bissada (1987).

The concept of *optimum fluid content* (*OFC*) is relevant for BSM-foam and it considers the binder (foamed bitumen) as additional lubricating contribution to that of the moisture. Thus, the actual moisture content of the mix for optimum compaction (*OMC*) is reduced in proportion to the amount of binder incorporated. Castedo Franco and Wood (1983) also agree with this consideration: the best compaction moisture condition occurs when the total fluid content (moisture + bitumen) is approximately equal to the *OMC*.
Sakr and Manke (1985) developed a relationship (Equation 2) to calculate the mixing moisture content (*MMC*) in order to achieve the maximum density of foamed bituminous

mixes, which considers the modified AASHTO T180 OMC (modified Proctor compaction EN 13286-2), percentage of fines (*PF*) of the aggregate and the bitumen content (*BC*). As suggested by the equation, the higher the bitumen content the lower the mixing moisture content.

$$MMC = 8.92 + 1.48 \cdot OMC + 0.4 \cdot PF - 0.39 \cdot BC \quad (2)$$

The optimum moisture content for mixing (*OMMC*) is approximately 10 to 20 per cent higher than the mixing moisture content (*MMC*), as predicted by Equation 2. In order to prevent the time consuming task of drying the mix after mixing (to reach the *MMC*), Sakr and Manke (1985) suggested that the *MMC* can be used and no significant differences in mix properties can be observed when this procedure has been adopted.
Australia Wirgten company was the first that provides a practical and useful laboratory procedure to determine the *optimum moisture content* (*OMC*) including BSM-emulsion and not exclusively dedicated to BSM-foam.
Regarding BSM-foam, Wirtgen company [Wirgten, 2010] suggested the *OMMC* should be determined using the Equation 3:

$$W_{\text{add}}[\%] = 0.75 \cdot W_{\text{OMC}} - W_{\text{air-dry}} \quad (3)$$

in which $W_{\text{add}}$ is the moisture to be added during the mixing of BSM-foam, $W_{\text{OMC}}$ is the *OMC* determined by modified AASHTO T180 (or modified Proctor compaction EN 13286-2) and $W_{\text{air-dry}}$ represents the initial moisture of granular materials.
Differently, for BSM-emulsion the amount of water to be added for mixing purposes $M_{\text{water}}$ (Equation 4) is calculated in terms of mass, considering the bitumen emulsion adopted in the mixture as a fluid component.

$$M_{\text{water}}[g] = \left(\frac{W_{\text{OMC}} - W_{\text{air-dry}}}{100}\right) \cdot M_{\text{sample}} - M_{\text{emul}} \quad (4)$$

in which $W_{\text{OMC}}$ represents the *OMC* determined by modified AASHTO T180 (modified Proctor compaction EN 13286-2), $W_{\text{air-dry}}$ is the initial moisture of granular materials, $M_{\text{sample}}$ represents the dry mass of the sample and $M_{\text{emul}}$ is the mass of bitumen emulsion to be added.
In recent years, European researchers [Santagata and Chiappinelli, 2004; Grilli et al. 2012] have focused their studies on the influence of liquid content (emulsion and water) on CBTM compactability. The topic can be investigated using both modified Proctor [EN 13286-2] and Shear Gyratory Compactor SGC [EN 12697-31] as references because they represent current European standards for compaction of granular and bituminous materials.
Considering the experimental activities carried out by Grilli et al. (2012) using modified Proctor as compaction method for CBTM, **Figure 2. 26** reports results in terms of dry density plotted as a function of *free water* $W_F$ (water) and *free liquids* $L_F$ (water + emulsion). As it can be observed, the typical "*bell-shaped*" curves were obtained for all samples and an optimum *free water* content, about 6% by dry aggregate weight, can be identified for all mixtures. Obviously, a unique value of optimum *free liquid* content was not found because the compaction curves appear to be horizontally shifted by the difference in amount of

residual bitumen that characterizes each investigated mixture (bitumen emulsion content ranging from 1.5 to 3.0% by dry aggregate weight).

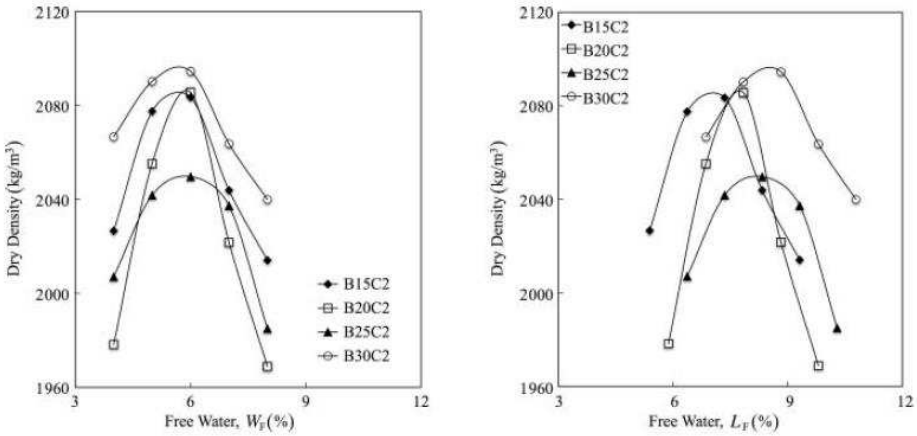


**Figure 2. 26** Proctor compaction test results [Grilli et al., 2012].

This indicates that even before emulsion breaking, the effective bitumen did not contribute to the compaction process.
This behavior is significantly different from the one assumed for BSMs [Asphalt Academy, 2009] where the Proctor optimum liquid content (water + bitumen) is determined using only water, implicitly assuming that bitumen will behave exactly like water during compaction. The fluidity of the emulsified bitumen can be represented by using the interesting model proposed for the mix design of CRMs [Santagata and Chiappinelli, 2004]:

$$L_{\text{opt}} = \%W + (a + K \cdot b) \cdot \%E \tag{5}$$

where $\%L_{\text{opt}}$ is the optimal liquid dosage, $\%W$ is the added water dosage and $\%E$ is the emulsion dosage. Coefficients $a$ and $b$ correspond to the weight ratios of the water and bitumen phases, respectively, to the total emulsion, while $K$ is a "*fluidity index*" ranging between 0 and 1. For $K = 1$, the bitumen contained in the emulsion has an effect that is equivalent to that of water; for $K = 0$, the liquids that control compaction are the sum of water added to the mixture and of that contained in the emulsion (bitumen is not taken into account). Results carried out by Grilli et al. (2012) showed that is possible to consider $K = 0$; the effective bitumen added with the emulsion can be treated as a *solid phase* and should not be considered a substitute of water during compaction phase.
The hypothesis that bitumen added in the mixture through bitumen emulsion behaves as *solid* has been considered during each experimental activity of the present thesis.

## 2.9 Compaction

Special attention needs to be paid to compaction issue, because it is fundamental for improving particle contacts and reducing voids. The density achieved is critical for the ultimate performance of the mixture.
A laboratory compaction technique that not exclusively achieves the density expected in the field, but also emulates the particle orientation after rolling, can be performed using different compaction methods besides the standard Marshall compaction (**Table 2. 10**).

| Compaction method | Settings/Temperature | Binder | Reference |
|---|---|---|---|
| Kneading compactor | Ambient temperature | Foamed bitumen | Shackel, 1974 |
| Kneading compactor | Ambient temperature | Foamed bitumen | Bowering and Martin, 1976 |
| Gyratory compactor | Angle = 1°<br>Pressure = 1.38 MPa | Foamed bitumen<br>Bitumen emulsion | Tia and Wood, 1982 |
| Texas gyratory compactor | 25°C | Foamed bitumen | Little et al., 1983 |
| Gyratory | 20 revolutions<br>Pressure = 1.38 MPa | Foamed bitumen | Brennen et al., 1983 |
| Gyratory compactor | 150 revs, Angle = 2°,<br>Pressure = 0.24 MPa<br>(100 mm diameter)<br>150 revs, Angle = 3°,<br>Pressure = 0.54 MPa<br>(150 mm diameter) | Foamed bitumen<br>Bitumen emulsion | Maccarrone et al., 1995 |
| PCG (French gyratory compactor) | 200 cycles with LCPC carousel | Bitumen emulsion | Brosseaud et al., 1997 |
| Vibratory hammer compaction. | Power rating 1500 W<br>Freq. 15 – 31.5Hz<br>Point Energy 25 J | Foamed bitumen<br>Bitumen emulsion | Asphalt Academy, 2009 |
| Shear gyratory compactor | EN 12697 -31 | Bitumen emulsion | Brayton et al., 2000; Oke, 2011; Grilli et al., 2012 |
| Static compaction | Compaction force of 25 kN for 3 mins | Bitumen emulsion | Miljković and Radenberg, 2016 |

**Table 2. 10** Summary of laboratory compaction techniques.

It is evident from the reported literature, that an ideal laboratory compaction for specimens preparation is not completely verified yet. Both volumetrics and engineering properties of each investigated mixture require consideration in the selection of an appropriate compaction technique, in order to recreate field densification as much as possible.

## 2.10 Volumetric properties of cold mixtures

Volumetric characteristics are important for bituminous mixtures both in mix design and in quality control phases, as they significantly influence the mixture mechanical performance and its durability [Cominsky, 1994].
Van de Yen in 2003 referred to volumetric properties in terms of "*spatial approach*": the 3-D volumetric structure of a material or its surface at *micro-*, *meso-* and *macro-level* in order

to develop spatial model that can be used to explain material behavior and assist in the performance prediction. This observation is particularly valid for mix design of cold mixtures where the structure of the material evolves over time during its life, i.e. production (*fresh state*), laydown and compaction (*initial curing*) and in-service life (*cured state*).
The heterogeneity of the constituent materials and the specific interaction among them make cold mixtures different from traditional ones [Bocci et al., 2011; Stimilli et al., 2013]. In particular, they are characterized by a composition (and consequently a mechanical behavior) that shares properties of both HMA and unbounded granular mixtures [Khosravifar et al., 2015]. The typical approach used to evaluate the volumetric properties and compactability of granular mixtures and cold mixtures is based on dry bulk density $\rho_d$.
However, such method does not provide the presence of bituminous component (emulsion or foam) in a satisfactory manner, so it needs to be adequately reformulated to be used with CM. Moreover, since the dry bulk density is closely related to the particle density of each component (which is significantly different between RA and virgin aggregate), it is not convenient to use it when comparing the compactability of mixtures containing different constituent materials or different proportion between them [Kuna et al.,2014].
Therefore, the volumetric approach used for HMA, based on voids in mixture ($V_m$), voids in the mineral aggregate (*VMA*) and voids filled with bitumen (*VFB*), seems to be more suitable to analyse the workability of CM [Grilli et al., 2012].
European Standard EN 12697-08 identifies the volumetric quantities considered for HMA and describes the procedure for their calculation. In particular, EN 12697-08 defines:

- air voids content ($V_m$) as the volume of air voids in the HMA sample, in percentage of the total volume;
- void in the mineral aggregate (*VMA*) as the volume of intergranular voids (i.e. the voids between aggregate granules) in the HMA compacted sample, which includes air voids and bitumen volume, as percentage of the total volume;
- void filled with bitumen (*VFB*) as the volume took up by the bituminous binder, in percentage on the VMA.

When CM reaches the end of the curing process ("*hardened*" or "*cured*" state), its volumetric properties can be determined through the same analytical relations used with HMA (no residual water is available in the mixture).
However, in the "*fresh*" state, water plays a key role driving the bitumen into the mixture and acting as lubricant for a better compaction [Garcia et al., 2013; Fang et al., 2015]. In this phase: the void in the aggregates (*VA*) represents the non-solid portion in a unit volume (in this case, the term aggregate includes mineral and active fillers as well as mineral and recycled aggregate) while the void filled with liquid (*VFL*) measures the *level of saturation*.

### 2.10.1 CM – foam

In literature, the analysis of volumetric properties for CM mixtures produced with foamed bitumen was more focused on BSM-foam and in particular, on the importance of the amount of mineral filler added in the mixture during mixing phase [Jenkins, 2000] as well as the traditional mix design method for asphalt concrete [Cominsky et al., 1994].

During its metastable life, foamed bitumen is mixed with cold fine mineral aggregate which is being agitated inside the mixer. The colloidal mass collapses very quickly during this phase, with the erupted bitumen providing globules at low viscosity that prefer the highest surface-to-mass ratio i.e. the finest fraction. The result is a bitumen rich foamed mastic composed by foamed bitumen, filler and water. The importance of *foamed mastic* has been identified for this mentioned reason, values for filler/bitumen ratio have been recommended in order to guarantee a good foamed mastic as well as acceptable volumetric properties [Rukel et al., 1983]. In addition, water addition causes a totally different volumetric composition in the foamed mastic. Cooley (1998) established a composition and a useful phase diagram of the filler mastic for different combinations between filler and bitumen (**Figure 2. 27**). In this diagram, Cooley introduces the idea of "*Percent bulk volume*" which consists in a measure of the ratio between filler volume (including voids) and the total volume of bitumen and filler (voids excluded). As the percent bulk volume increases, so the bitumen in the mastic is located more in filler voids thus reducing the volume of free bitumen. For determining the percent bulk volume, the water phase is supposed to be not displaced from the voids in filler, as the water to be in the filler before the addition of foamed bitumen.

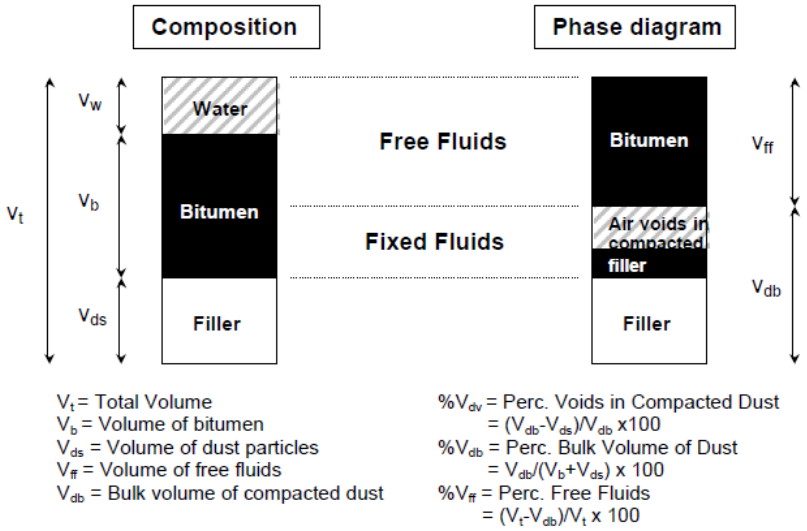


**Figure 2. 27** Volumetric of voids in filler/bitumen mastic for foamed bitumen [Cooley et al., 1998].

Considering the entire mixture, water improved workability during compaction but during curing phase and moisture loss, the volume occupied by water will be replaced with air voids ($V_V$). The fluid component of these mixtures during their early-age of life is therefore *dynamic* and can vary significantly. This evolution may be illustrated using voids in the mineral aggregates *VMA* relative to the fluid content selected for the mixture (water and binder) and according to a given level of compaction. At a fixed fluid content, optimal packing of mineral aggregate may be achieved (**Figure 2. 28**). The volume of water $V_{water}$ in

mineral aggregate is selected to provide the optimal packing at the required bitumen content $V_{binder}$ [Jenkins, 2000].

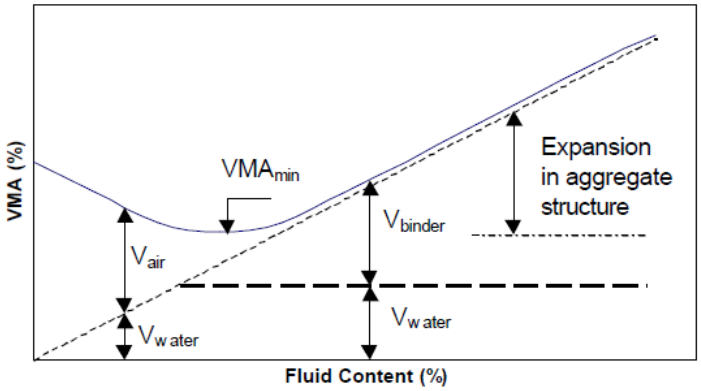


**Figure 2. 28** Volumetric composition of a CM produced with foamed bitumen, considering the influence of fluid content on VMA for a specific compaction level.

## 2.10.2 CM – emulsion

As previously explained, CMs are characterized by physical characteristics that evolve with curing time; thus, the study of volumetric properties is different when the mix is analyzed in its fresh state or in its cured state.
The volumetric characterization procedure defined by current European regulations [EN 12697-5, 6 and 8] for asphalt concrete highlights its limits when barely applied to CMs.
According to a rational approach developed by Grilli (2012) and updated by the same author in 2016 for CBTM, the definitions of the above mentioned volumetric parameters can be easily deduced:

$$V_m = \frac{v_{air}}{v_{ag}+v_{bit}+v_{air}} \cdot 100 = \frac{\rho_m - \rho_b}{\rho_m} \cdot 100 \quad (6)$$

$$VMA = V_m + V_{bit} = V_m + \frac{B \cdot \rho_b}{\rho_B} \quad (7)$$

$$VFB = \frac{V_{bit}}{VMA} \cdot 100 = \frac{B \cdot \rho_b}{\rho_B} \cdot \frac{1}{VMA} \quad (8)$$

where:
$v_{air}$: volume of air voids (cm$^3$);
$v_{ag}$: volume of aggregate (cm$^3$);
$v_{bit}$ : volume of bitumen (cm$^3$);
$V_{bit}$ : volume occupied by the bitumen (% by mix);
$\rho_m$: maximum density (g/cm$^3$);
$\rho_b$: HMA sample bulk density (g/cm$^3$);

$\rho_B$: density of the binder (g/cm$^3$).
$B$: bitumen content in weight (% by mix).

The volumetric analysis for CMs follows the same principles, even if the introduction of different components such as water ($W$), bitumen emulsion (consisting of *water* and *residual bitumen*) and cement ($C$) make some modifications necessary. It's important to highlight that, in the cold recycling process, RA does not experience any heating thus acts as a "*black rock*" [Soleymani et al., 2000; Grilli et al., 2012; Tebaldi et al., 2014] and hence, aged bitumen in the RA does not give any contribution as binder (contrarily from the bitumen in the emulsion) and can be considered as a *solid component*.
**Figure 2. 29** shows the materials typically used for CBTM and defines the abbreviations for their mass and density.

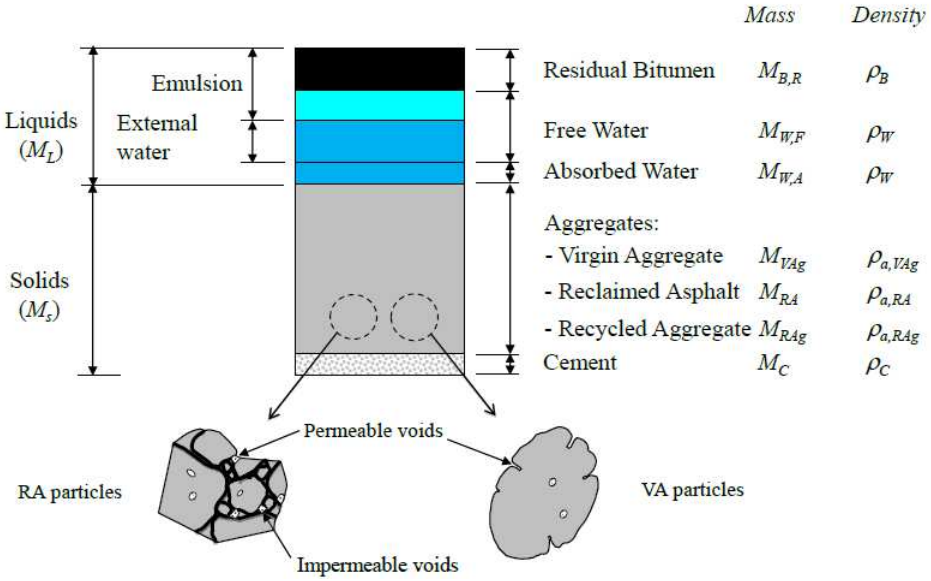


**Figure 2. 29** Typical component materials for CBTM before emulsion breaking [Grilli et al., 2012].

It has to be remarked that bitumen emulsion consists of bitumen powder dispersed in water. Consequently, the bitumen is actually solid and cannot be absorbed by aggregate particles (differently from the hot bitumen in HMA). However, it is convenient to consider the bitumen in the emulsion to act as a liquid during the compaction. In this phase, the emulsion gives its contribution to aggregate lubrication, so it influences the compactability of the granular mixture. On the other hand, after emulsion breaking, there is separation between water and residual bitumen, so they act as different materials. In particular, bitumen coats and bonds aggregates, influencing mixture performance.
Therefore, before the emulsion breaking, the mass of liquids $ML$ consists of the water absorbed by aggregates, emulsion and external water (*intergranular water*). In particular,

the external water includes the water added during the mixing phase and/or water present around granular particles as humidity. On one hand, the free water includes external water and water brought into the mixture by the bitumen emulsion. On the other hand, in terms of volume, the water absorbed has to be considered as part of the aggregate.
For this reason, aggregates are generally used in *wet condition* (it is not heated or dried), the *particle saturated-surface dry density* ($\rho_{ssd}$) should be the most representative density parameter. In this context, from **Figure 2. 30**, it can be noticed that voids in the aggregate ($VA$) consider air voids, the volume of residual bitumen from emulsion and the volume of free water (water from emulsion and external water). After emulsion breaking, bitumen acts as a solid (it is no more dispersed in water) and air voids content ($V_m$) includes volume of air and volume of free water. Obviously, the free water content changes during the in-service life as a function of external conditions (temperature, humidity, rainfall, drainage conditions etc.).

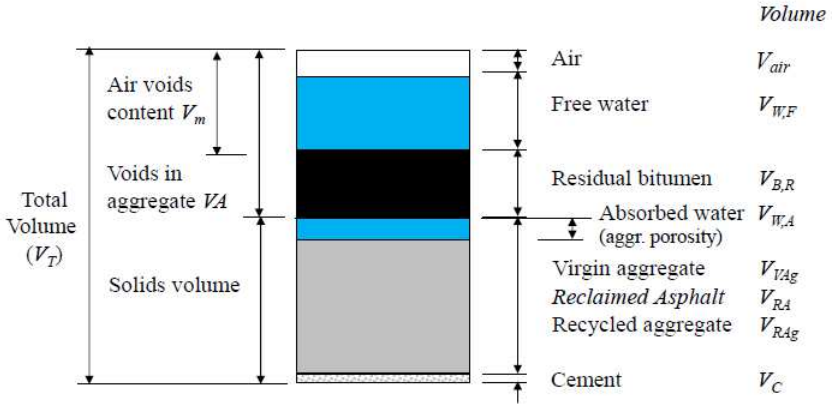


**Figure 2. 30** Volumetric analysis of CM produced with bitumen emulsion [Grilli et al., 2012].

For example, considering CBTM mixtures, the first compaction parameter that can be measured is the wet density
$\rho_b$ (Equation 9):

$$\rho_b = \frac{M_{VAg}+M_{RA}+M_{RAg}+M_C+M_{B,R}+M_W}{V_T} \quad (9)$$

where $M_{VAg}$, $M_{RA}$, $M_{RAg}$, $M_C$, $M_{B;R}$, $M_W$ are the mass of the virgin aggregate, RA, recycled aggregate from unbound mixtures, cement, residual bitumen from emulsion and water respectively, while $V_T$ is the total volume. Note that the mass of aggregates is referred to its dried state and the mass of water considers the total water content.
Wet density is determined considering the water content ($w$, by solid weight) in the mixtures, which is not a constant parameter during pavement life. For this reason, dry density $\rho_d$, which represents the amount of solid material per volume unit, should be considered (Equation 10):

$$\rho_d = \frac{M_{VAg}+M_{RA}+M_{RAg}+M_C+M_{B,R}}{V_T} = \frac{\rho_b}{w+1} \quad (10)$$

In this case, even if, during compaction, the separation between residual bitumen and water from the emulsion has not still occurred, residual bitumen should be considered as a stand-alone solid material, as it is going to be after emulsion breaking.
For CBTM the maximum density ($\rho_m$), that is an intrinsic material property related to constituent materials and mixture composition, follows the same principle and measurement method than for HMA. Obviously, water (external water and water included in the emulsion) shall not be considered. Thus, it can be calculated through Equation 11:

$$\rho_m = \frac{\sum_i M_i}{\sum_i V_i} = \frac{100}{\frac{p_{VAg}}{\rho_{VAg}} + \frac{p_{RA}}{\rho_{RA}} + \frac{p_{RAg}}{\rho_{RAg}} + \frac{p_C}{\rho_C} + \frac{p_{B,R}}{\rho_B}} \tag{11}$$

where $M_i$ is the mass of the i$^{th}$ constituent solid material (including the residual bitumen from the emulsion), $p_i$ is the percentage by mass of the i$^{th}$ constituent material (expressed as percent by weight of solid material) and $\rho_i$ is the density of the i$^{th}$ constituent material (aggregate refer to $\rho_{ssd}$ ). Obviously, $\rho_m$ can also be measured by means of a pycnometer [EN 12697-5].
Once the quantities and the basic concepts have been defined, it is possible to perform the volumetric analysis of CBTM. Considering that water is a variable amount which does not offer any mechanical contribution during the service life, the air void content ($V_m$) is the sum of the volumes of air voids and free water (external water and water from the emulsion) of the sample, in percentage of the total volume. It has to be noticed that moving from volumes to densities, mass of free water has not been adequately considered (Equation 12):

$$V_m = \frac{v_{air} + v_{W_F}}{v_{ag} + v_{bit} + v_{air} + v_{W_F}} \cdot 100 = \frac{\rho_m - \rho_d}{\rho_m} \cdot 100 \tag{12}$$

where $v_{WF}$ is the volume of the free water. Similarly to HMA, the voids in the aggregate (*VA*) is the volume of intergranular voids (i.e. the voids between aggregate granules, both virgin and recycled, mineral and not) in the compacted sample, which includes air voids and free water volume (as defined for $V_m$) and residual bitumen volume, in percentage on the total volume. It can be calculated through Equation 13:

$$VA = V_m + v_{B_R} = V_m + \frac{B_R \cdot \rho_d}{\rho_{B_R}} \tag{13}$$

where $B_R$ is the residual bitumen content expressed as percent by weight of solid and $\rho_{BR}$ is the density of the residual bitumen. For CBTM mixtures, taking into account that the aggregate consists of RA (sealed aggregate) and virgin aggregate that are generally wet, the amount of bitumen from the emulsion which is absorbed by the aggregate (*not-effective* virgin bitumen) is considered negligible. However, as water occupies a relevant volume and bitumen emulsion acts as a liquid during compaction phase, for CBTM mixtures also void filled with liquids (*VFL*), i.e. the volume of emulsion and external water in percentage on VA, has to be considered (Equation 14):

$$VFL = \frac{v_{W_F} + v_{B_R}}{VA} \cdot 100 = \frac{\frac{W_F \cdot \rho_d}{\rho_w} + \frac{B_R \cdot \rho_d}{\rho_{B_R}}}{VA} \cdot 100 \quad (14)$$

where $W_F$ is the free water content expressed as percent by weight of solid. It has to be clarified that, even if aged bitumen from RA influences the mechanical behavior of the mixture in the volumetric analysis, it is considered part of RA (*black rock*).
Currently, the adoption of *Shear Gyratory compaction SGC* [EN 12697-31] instead of Proctor compaction [EN 13286-2] for laboratory specimens production allows to monitor very quickly the evolution of *VA*, $V_m$ and *VFL* parameters, considering the height data recorded during the compaction process and the initial composition of the mixtures.
In particular, it is important to highlight the typical trend registered for *VA* and *VFL* curves as a function of *SGC* gyrations ($N_g$). For example, Grilli (2012) reported two types of compaction curves (**Figure 2. 31**).

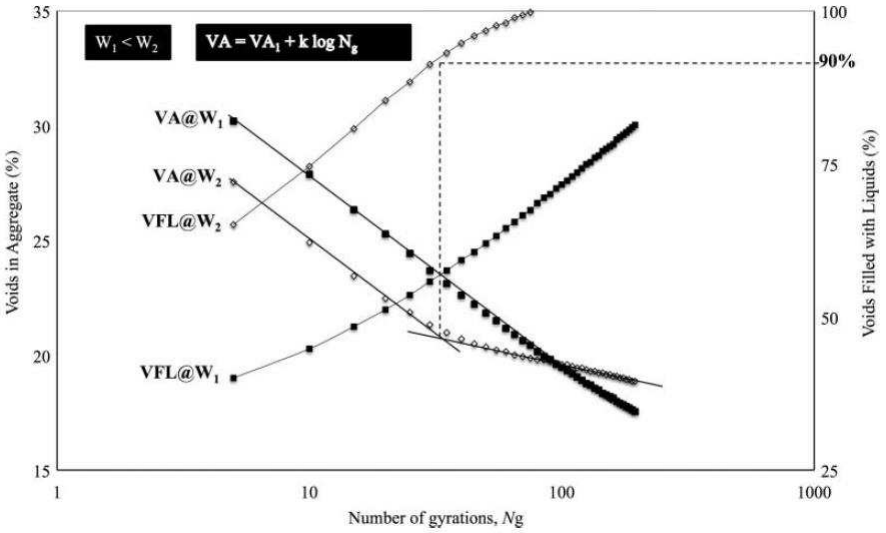


**Figure 2. 31** Evolution of *VA* and *VFL* parameters as a function of SGC gyrations, at different water content $W_1$<$W_2$ [Grilli et al., 2012].

At low water contents ($W_1$), a linear relationship between *VA* and the logarithm of $N_g$ can be assumed up to above 100 gyrations. At higher water contents ($W_2$), the relationship between *VA* and log $N_g$ becomes bi-linear. Observing both *VA* and *VFL* trends, it is possible to locate the point of inflection at the number of gyrations corresponding to a *VFL* of about 90% (*saturated conditions*). This means that as *VAs* are reduced, liquids tend to fill them (mixture approaches saturation), then part of the compaction energy is spent to increase the pore liquid pressure.
The linear portion of the compaction curves related to *VA* parameter, can be modelled as follow:

$$VA = VA_1 + k \cdot \log N_g \quad (15)$$

where $VA_1$ is the voids in aggregate at 1 gyration and $k$ is the slope of the semi-logarithmic plot. The parameter $VA_1$ is a measure of self-compaction of the mixture, while $k$ represents its corresponding workability.
In the present thesis, a similar approach to determine the volumetric properties of CBTM produced with foamed bitumen will be also presented.

## 2.11 The evolutive behavior: key feature of CMs

*Curing* of CMs is the process where the mixed and compacted layer looses moisture through evaporation, particle charge repulsion and pore pressure induced by flow paths.
Moisture content is the main factor controlling the rheological properties of CM in the *fresh state*, in particular their ability to achieve suitable mechanical and volumetric properties [Grilli et al., 2012; Ruckel et al., 1983].
The reduction in moisture content leads to an increase in the tensile and compressive strength, as well as stiffness of cold mixtures.
As compared to hot or warm asphalt mixtures either recycled or not, CM mixtures can be considered as *evolutive* materials because a certain *curing period* is necessary for them to achieve the *long-term* mechanical properties, e.g. strength and stiffness (**Figure 2. 32**).

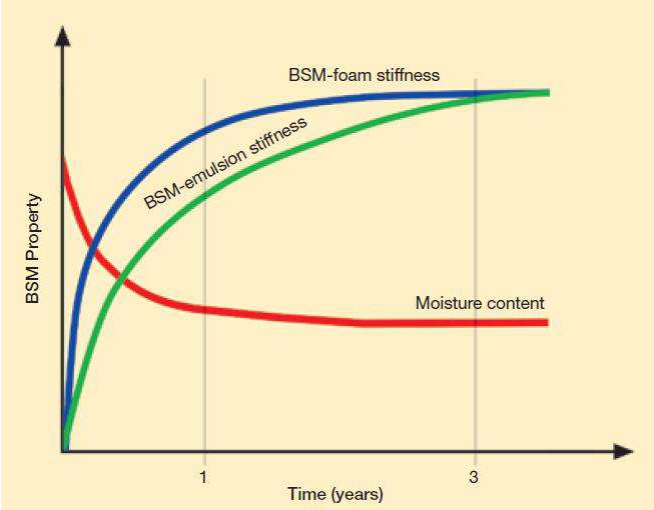


**Figure 2. 32** Concept of Curing and Influence on Mix Stiffness for BSMs [Asphalt Academy, 2009].

Because of the simultaneous presence of both bituminous and hydraulic binders, curing is the result of different time-dependent mechanisms [Du, 2014; Cardone et al., 2015].
When CM mixtures are produced using bitumen emulsion, curing of the bituminous phase is characterized by two phenomena strictly interrelated: *emulsion breaking* and *water expulsion* (see Section 2.5.3). Indeed, flocculation and coalescence of bitumen droplets, that lead to the

formation of continuous bituminous films, are generally due to the increase of the crowding pressure induced by moisture loss [Lesueur and Potti, 2004].
For example, as shown in **Figure 2. 32**, BSMs produced with bitumen emulsion usually requires longer curing times than those produced with foamed bitumen because of the higher moisture contents adopted during mixing [Asphalt Academy, 2009]. Moisture loss, by means of drainage or evaporation, ensures mixture hardening and bonding between bituminous mortar (i.e. fine aggregate particles bonded by the bituminous binder) and coarse aggregate skeleton [Cardone et al., 2015].
Considering CMs produced with foamed bitumen, curing takes place as a result of migration of water during compaction and continues with repulsion of moisture by the bitumen and loss by evaporation [Asphalt Academy, 2009].
The curing process of both CMs produced with bitumen emulsion or foamed bitumen also involves cement hydration since it confers enhanced stiffness and strength to the mixture [Garcia et al., 2013; Bocci et al., 2014]. Moreover, in the early curing stage, cement promotes emulsion breaking or foam collapse and contributes to the bitumen coalescence by reducing the free water within the mixture [Terrel and Wang, 1971; Garcia et al., 2013; Wang et al., 2013]. In the meantime, the presence of bitumen emulsion or foamed bitumen could reduce the rate of hydration of cement and hinder the formation of well-structured cementitious bonds [Muthen, 1998, Jenkins 2000; Pouliot et al., 2003, Weiss et al., 2008]. At low cement content, the hydration products disperse inside the bituminous mortar increasing its viscosity and improving the resistance of the mixture to permanent deformations.
At higher cement content, the volume of hydration products grows forming a stiffer matrix that connects coarser aggregate particles [Garcia et al., 2013].
In particular, it is important to remark that while the curing process of bituminous binders, either emulsion or foam, is strictly linked to moisture loss, the chemical reactions that take place during the hydration of cementitious binders require the presence of water and do not entail any moisture loss [Cardone et al., 2015].
It is imperative that this process should be realistically simulated using laboratory procedures for mixes to be assessed for their expected field performance [Asphalt Academy, 2009; Wirgten, 2010].
Laboratory curing procedures for CMs aim to simulate field curing conditions and try to accelerate the attainment of ultimate properties [Jenkins and Moloto, 2008]. However, the factors that influence field curing are extremely difficult to standardize and reproduce because they are related to *composition* (binder types and dosage) of the mixture, construction features (depth of the layer, degree of compaction, layer thickness, drainage conditions, construction phases) and environmental factors (rainfall, temperature, humidity, wind). Therefore, a rational laboratory curing procedure should: consider the relevant curing mechanisms which arise from mixture composition (emulsion breaking or foam collapse/moisture loss and cement hydration), define specimen shape, dimensions and boundary conditions and control both curing temperature and relative humidity [Muthen, 1998; Jenkins 2000; Asphalt Academy, 2009; Cardone et al., 2015].
Since the curing of CM mixtures in field occurs over several months, it is impractical to reproduce actual field curing conditions in the laboratory. An *accelerated* laboratory curing procedure is required, in which the strength gain characteristics can be correlated with field behavior, especially with the *early*, *intermediate* and *ultimate* strengths attained. This

characterization is especially important when structural capacity analysis, based on laboratory-measured strength values, is required.
In the past, investigations have adopted the laboratory curing procedure proposed by Bowering (1970), i.e. 3 days oven curing at a temperature of 60° C. This procedure results in the moisture content stabilizing at about from 0 to 4 percent, which represents the driest state achievable in the field. The strength characteristics of samples cured in this manner are representative of the in-service state approximately one year after construction [Maccarrone, et al., 1995]. An alternative approach suggested by Muthen (1998) would be to oven dry the mixture until reaching constant mass (*ultimate* state), at temperature of 40° C. The same result may be carried out at ambient temperature but at longer curing time.
Ruckel et al. (1983) proposed that one day of curing in the compaction mold at ambient temperature was enough to simulate the early age of curing. Moreover, ARRA (2001) suggested that short-term (early-age)curing can be carried out by holding the compacted samples at higher temperature (60 °C) for two or four hours while, long-term curing consisted of holding samples at very high temperature (110 °C) until they reach a constant mass.
At the moment, laboratory testing on CMs are usually performed after 72 hours of curing at 40 °C without sealing the specimen (*dry conditions*) or after additional 24 hours with soaked specimen (*wet conditions*) [Asphalt Academy, 2009].
In field, CMs must be adequately cured before laying down of wearing course. The rate of curing is quite variable and depends on several factors such as day and nighttime temperatures, humidity and rainfall after recycling operations, initial moisture content of the mixture before and after recycling, compaction level, in-place voids content, drainage characteristics of the existing subgrade. Sealing the surface prior to an adequate moisture loss could result in a premature failure of CM mixture and/or wearing course. Often curing times ranging from ten days to two weeks represent an acceptable criterion. In any case, it is preferable to overlay a partially cured CM prior to winter shutdown rather than leave it expose to the winter.

## 2.12 Viscoelastic properties

CM materials as well as traditional asphalt concrete exhibit viscoelastic behavior (i.e. time and temperature dependent); it changes its properties accordingly to applied temperature and loading frequency, as well as loading path. This property is strictly related to mixture volumetric properties and properties of the component materials. CMs volumetric composition includes the volume of aggregate and binders (bituminous and hydraulic) and volume of voids [Pellinen et al., 2007]. At higher bitumen contents correspond marked viscoelastic properties and, at the same time, the presence of cementitious component mitigate this attitude.
In this context, four main typical behaviors can be identified according to the strain amplitude ($\varepsilon$) and the number of applied cyclic loadings ($N$) [Olard et al., 2003] (**Figure 2. 33**).

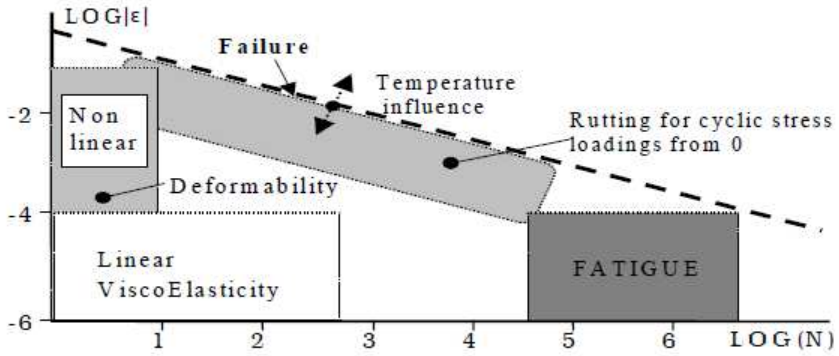


**Figure 2. 33** Typical mix behavior domains [Di Benedetto and De La Roche, 1998; Di Benedetto et al., 2001].

The norm of *complex* (dynamic) *modulus* $|E^*|$ is used as a measure of the elastic stiffness $E$ of a bituminous mixture in the quasi-static flexible pavement analysis. Although $|E^*|$ is dependent upon both temperature and loading rate, $E$ is theoretically dependent only on temperature.

Since the behavior of $E$ is time independent, the development of strain is instantaneous, whereas $|E^*|$ exhibits delayed elastic behavior, which allows the speed of traffic to be incorporated the layered elastic analysis and, as a consequence a more complex viscoelastic analysis of stress and strain can be avoided. The effects of temperature and loading rate are related based on the validity of the *time-temperature* superposition principle.

This concept allows master curve construction in terms of complex modulus as a function of reduced frequency (see Section 5.2.3).

*Complex numbers mathematics* are convenient tools to analyze the viscoelastic behavior of the bituminous mixtures and binders in a forced oscillatory loading. The sinusoidal tension-compression loading can be represented in complex form as $\sigma^* = \sigma_0 \cdot e^{i\omega t}$ and the resulting strain is $\varepsilon^* = \varepsilon_0 \cdot e^{i\cdot(\omega t-\varphi)}$ (**Figure 2. 34**a). The complex modulus $E^*(i\omega)$ is then defined as the complex number:

$$\frac{\sigma^*}{\varepsilon^*} = E^*(i\omega) = \left(\frac{\sigma_0}{\varepsilon_0}\right) \cdot e^{i\varphi} = E_1 + iE_2 \tag{16}$$

in which $\sigma_0$ is the stress amplitude, $\varepsilon_0$ is the strain amplitude, $\omega$ is the angular velocity, which is related to the frequency by $\omega = 2\pi f$, and $i^2 = -1$. In the complex plane, the real part of the complex modulus $E^*(i\omega)$ is called the *storage or elastic modulus* $E_1$ while the imaginary part is the *loss or viscous modulus* $E_2$ (**Figure 2. 34**b). The ratio of the stress and strain amplitudes $\sigma_0/\varepsilon_0$ is the norm of the complex modulus (vector length) defined as the dynamic modulus $|E^*(\omega)|$ or $E_0$, Equation 17. $E_1$ and $E_2$ can be expressed as a function of phase lag or lag angle $\varphi$, Equation 18a and b (**Figure 2. 34**b). For elastic materials $\phi = 0$ (solid-like behavior), and for viscous materials $\phi = 90°$ (liquid-like behavior).

$$|E^*(\omega)| = \sqrt{{E_1}^2 + {E_2}^2} = \frac{\sigma_0}{\varepsilon_0} \tag{17}$$

$$E_1 = \frac{\sigma_0 \cdot \cos\varphi}{\varepsilon_0} \text{ and } E_2 = \frac{\sigma_0 \cdot \sin\varphi}{\varepsilon_0} \quad (18\text{ a, b})$$

$$\tan\varphi = \frac{E_2}{E_1} \quad (19)$$

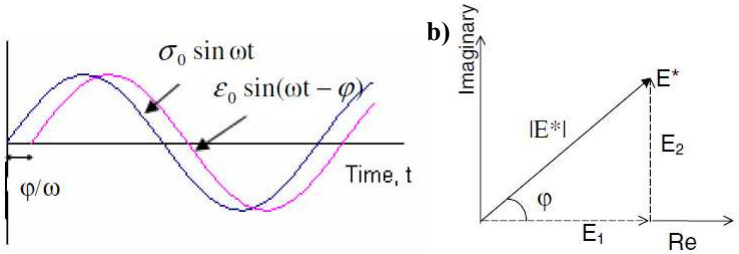


**Figure 2. 34** Sinusoidal Signals solved in Complex Plane.

## 2.12.1 Different test protocols

The oscillatory loading can be applied in several manners as is shown in **Figure 2. 35**. The shear testing is usually conducted in strain control while the axial testing is conducted in stress control. The SST shear testing represents *simple shear loading* and the binder *dynamic shear rheometer* DSR testing represents torsional loading. The dynamic modulus |*E**| has been tested using either haversine tension ($\sigma_t$) or haversine compression ($\sigma_c$) loading, or using combined tension-compression loading ($\sigma_{t/c}$). In DSR testing, SST shear testing, and axial tension-compression testing, the average measured or applied shear stress is zero, whereas in the haversine loading the applied stress (or strain) is comprised of constant creep loading superimposed over sinusoidal loading and the average stress deviates from zero. Subsequently, the type of stress or strain that is introduced or measured in the sinusoidal testing becomes an important variable when comparing test results.

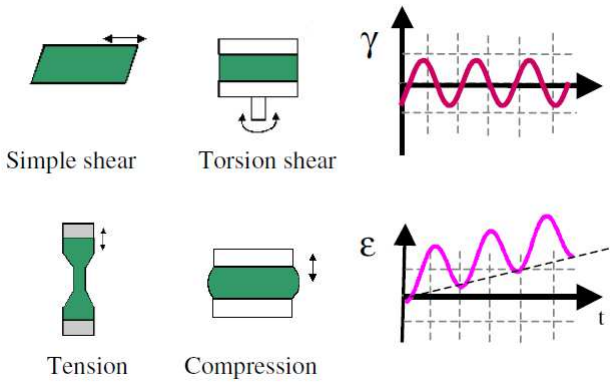


**Figure 2. 35** Methods of applying sinusoidal loading.

In the strain-controlled shear testing, the shear strain amplitude $\gamma_0$ incorporates recoverable ($\gamma_r$) and permanent shear strain ($\gamma_p$). If the material is purely viscoelastic, the permanent strain is caused by *viscous flow*. The phase lag ($\varphi$) in the sinusoidal loading indicates the amount of dissipated and recovered energy; $\varphi = 0°$ corresponds to all straining recovered and $\varphi = 90°$ corresponds to all straining permanent, as the material exhibits viscous flows. However, at higher temperatures, the permanent strain obtained from bituminous mixture may include some plastic (i.e., yield stress dependent) strain.

Similar to the shear strain amplitude ($\gamma_0$), the elongation strain amplitude ($\varepsilon_0$) incorporates recoverable ($\varepsilon_r$) and permanent ($\varepsilon_p$) components, from which the permanent strain may include viscous and plastic components. However, if the strain amplitude in the stress controlled compression or tension testing is obtained from the loading portion of the signal, it incorporates creep strain ($\varepsilon_c$) caused by a nonzero loading stress; but if it is obtained from the unloading portion, it only incorporates the oscillatory straining. The creep strain accumulates as a function of loading cycles as is shown in **Figure 2. 35** and it consists of recoverable and permanent strain components.

If testing is conducted at low and intermediate temperatures, which is the case for the Shell and Asphalt Institute models, the creep strain will be minimal and can be neglected. This was established in the 1979 AASHTO protocol for $|E^*|$, which requires that measurements must be taken from a steady state segment of the strain signal after cessation of the initial creep. However, as higher testing temperatures and lower frequencies are introduced, it is difficult or even impossible to achieve a steady state straining in the haversine testing. As such, the dynamic modulus measurements will be more variable at higher temperatures and there will be more differences between laboratories as the strains are measured and analyzed differently.

As the dynamic modulus testing is conducted in the *linear viscoelastic region* (small stress or strain applied), the specimens should not dilate or develop hardening if loading or straining is applied in tension-compression mode. However, micro-cracks might occur and will grow with the increase in the strain amplitude. This will cause the modulus to drop as the damage progresses in the specimen. When loading is applied in the haversine manner, there is a possibility for strain hardening as the material is creeping continuously. The strain hardening will increase the modulus as aggregates are pushed more tightly together. The situation is slightly different for the SST testing, as any attempt for particle dilatation caused by aggregate movements is confined by applied axial normal force (**Figure 2. 36**). Theoretically, shear straining should not cause volume changes, rather only changes of shape; however, granular materials dilate under simple shear regime [Pellinen, 2007].

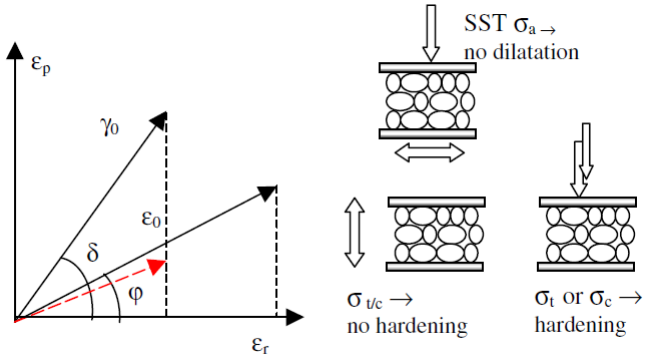


**Figure 2. 36** SST shear and axial dynamic modulus testing.

Finally, it can be stated that the complex modulus $E^*$ (and hence $|E^*|$ and the phase angle $\varphi$) are fundamental information in the performance analysis of bituminous materials. However, as often mentioned, their value depends on the temperature, the stress/strain applied and the loading frequency. Anyway, it is possible to eliminate the stress/strain dependency by verifying that the loads applied (stress or strain) is lower than a limit value, referred as *Linear Viscoelastic limit* (LVE). Below this value, the material behavior is independent on the loading amplitude. Such value can be experimentally determined by applying several stress/strain values at a given temperature and frequency. Then, the stress/strain value which corresponds to a reduction of the initial complex modulus $|E^*|$ equal to 5% is calculated and represents the LVE region. This type of test on binders is usually referred as *strain sweep test*.

# CHAPTER 3.

## Research description and objectives

The research work focuses on the rheological and mechanical characterization of cold mixtures (CMs) as support layers for road pavements, material commonly used in Italian road infrastructures. As previously mentioned in Chapter 2, the disposal and the valorization of material coming from the milling activity of old bituminous pavements represent a priority objective in terms of both economic and environmental benefits. Such an issue is particularly important in the highway network system, where the production of new bituminous mixtures is quantitatively equivalent to the volume of the milled material to substitute, since the paving activities usually carried out are mainly related to maintenance or rehabilitation of existing pavements. In addition, the adoption of low polluting impact technologies such as cold recycling maximizes benefits related to savings in energy and non-renewable natural resources.

Consequently, verifying the possibility to employ CM without penalizing the performance of road pavements, is the main objective to purse in the production of new road pavements.

At the same time, this challenge must be supported by an adequate laboratory investigation in order to identify each criticism related to the use of CMs. Ultimately, it is important to highlight that engineers and technicians in general are obliged to carry out experimental activities on CMs using European standards developed only for traditional hot mix asphalts as references (e.g. EN 12697-23, EN 12697-26, EN 12697-31, etc…). For this reason, each laboratory procedure should be verified gradually in order to evaluate its reliability. Even in field, during construction operations of subbase layers, technicians and operators usually refer to previous experiences or to limited national technical guidelines available instead of relying to adequate standardized procedures.

The whole experimental program aims at characterizing CMs produced with different binding agents (mineral additions and bituminous binders) from the physical and mechanical point of view and at deeply understanding physical and chemical mechanisms that occur within these materials. Experimental activities are carried out targeting testing method at different investigation scales (pavement-, mixture-, mortar- and mastic-scale) where those mechanisms are most noticeable (*multiscale analysis*). Bearing in mind that CMs are evolutive materials at each scale of investigation because its physical state evolves over time according to moisture loss, additional attention should be taken during laboratory testing.

Given the complexity of such a topic, a rational planning of the experimental activities on a multiannual basis is required.

The overall research activities were carried out in the Department of Civil and Building Engineering and Architecture of the *Polytechnic University of Marche*. Part of the experimental program described in this dissertation was carried out in cooperation with *École de technologie supérieure* - ETS (Montréal, Canada) which gave me the opportunity to perform laboratory testing in order to analyze CMs produced with foamed bitumen (First visiting period: from July until October 2014). Additional experimental activities on cold

bituminous mastics prepared with bitumen emulsion were developed during the second visiting period (from February until April 2016) at the *Institut français des sciences et technologies des transports, de l'aménagement et des réseaux* - IFSTTAR (Nantes, France).

# 3.1 Methodological approach

In engineering, mathematics, physics, chemistry, bioinformatics, computational biology, meteorology and computer science, one of the most widespread method adopted in research field is multiscale modeling or multiscale mathematics. This approach represents a powerful tool for solving problems characterized by important features at multiple scales of time and/or space. For example, important topics include multiscale modeling of fluids, solids, polymers, proteins as well as various physical and chemical phenomena (like adsorption, chemical reactions, diffusion, etc…).
In physics and chemistry, multiscale modeling is aimed to material properties calculation or system behavior on a single level using information or models from different levels. On each level, particular approaches are used for describing the system. Moreover, each level addresses a phenomenon over a specific size and time.
Multiscale modeling is especially important in integrated computational materials engineering since it allows the prediction of material properties or system behavior based on knowledge of the *process-structure-property relationships*.

Concerning pavement materials and in particular, bituminous mixtures, these materials can be analyzed as a composite of multiple phase elements.
In the past, many researches focused their attention on the application of multiscale modelling to evaluate physical and mechanical properties of *hot* asphalt mixtures. The main aim was to upscale the studied properties from the lower to the higher level of investigation [Huang and Di Benedetto, 2015].
In general, multiscale modelling in the bituminous mixtures field consists of performing a series of two-phase (matrix and particulate) computational simulations wherein each successive simulation uses the input from the previous one as the matrix phase and increases the characteristic size of the particulate phase by some amount [Underwood and Kim, 2011 and 2013].
The process continues until the full bituminous mixture performance has been predicted; it is important to highlight that the specific level of discretization are dependent upon the degree of accuracy desired.
The multiscale dependencies that characterized an bituminous mixtures (or asphaltic composites) are summarized in **Figure 3. 1**.
According to **Figure 3. 1**, bituminous mixtures can be analyzed at different characteristic times during its service-life (*time-scale*) and at different characteristic sizes (*size-scale*).

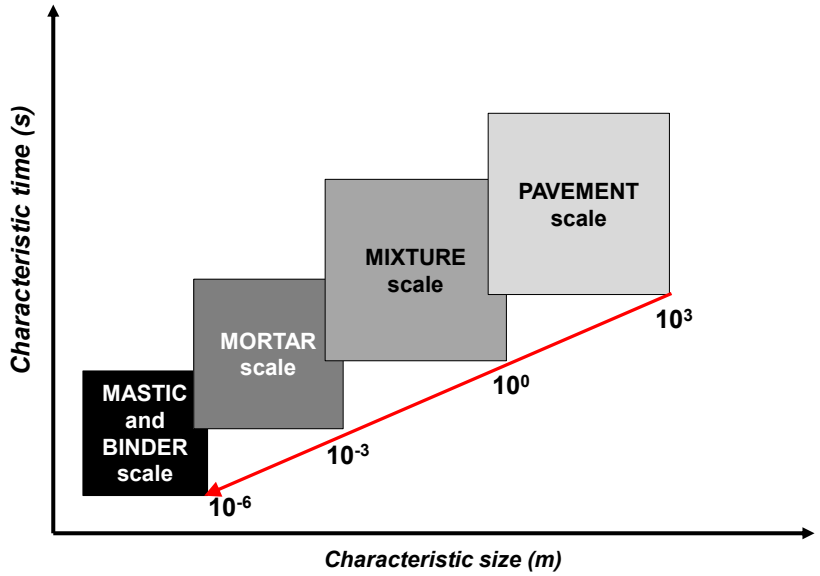


**Figure 3. 1** Multiscale dependencies of bituminous mixtures.

At the smallest scale (size < $10^{-6}$ m), *bituminous binder* can be viewed as a composite of hydrocarbons and other elements in multiple complex structures. In this domain, materials are better understood with respect to the chemical properties of constituent elements. At the next scale (size equal to $10^{-6}$ m), bituminous binder is combined with filler-sized particles and in literature one characteristic scale larger than bituminous binder is usually called as *bituminous mastic*. The importance of this scale in the establishing the connection between bituminous binder and bituminous mixture is the magnification of physicochemical interactions that occur at the interface of binder and aggregate. Here, mechanical behaviors are interpreted primarily in a rheological context either as part of a specification process or as a means to understand the impact of binder compositional factors on mechanical properties.

The next scale of practical interest ($10^{-6}$< size < $10^{-3}$ m) consists in fine aggregate mixture (FAM) and it represents the *mortar scale*. FAM is the combination between bituminous mastic and fine aggregate particles and thus it is synonymous with the mortar phase of Portland cement concrete. As a mortar, FAM forms the material that fills voids between the coarsest aggregate particles in a mixture. It is the FAM phase that deforms under high-temperature loading and shows visible cracking under repeated loading at intermediate temperatures [Huang and Di Benedetto, 2015].

In the right part of **Figure 3. 1**, the two largest scales can be observed: *mixture scale* ($10^{-3}$< size < $10^{0}$ m) that consists in coarse aggregates coated by FAM and *pavement scale* ($10^{0}$< size < $10^{3}$ m). Both scales are more representative in evaluating the performance (by means resistance to distresses) of the investigated material during its in service-life.

In **Figure 3. 2**, a useful scheme regarding the three scale levels (binder/mastic-scale, mortar-scale and mixture-scale) of CM constituents is proposed.

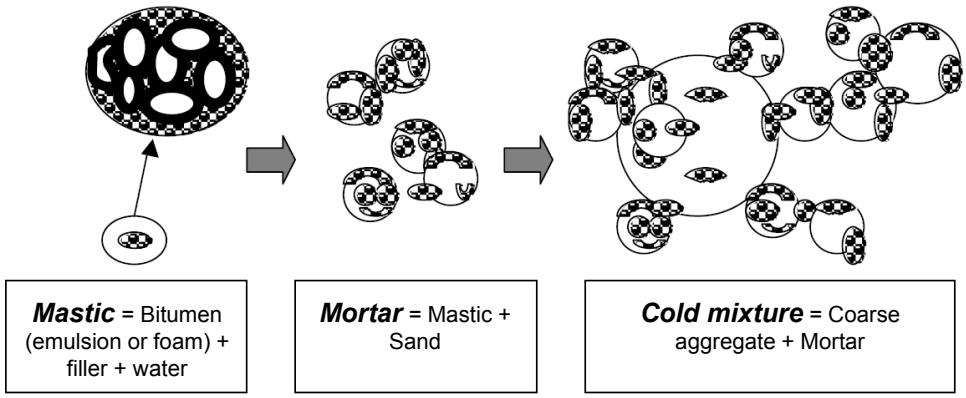


**Figure 3. 2** Multiscale composition of cold mixture.

In the present thesis, the first multiscale approach for the physical and mechanical characterization of cold mixtures properties was developed.
Moreover, the investigation has also taken into account the evolutive behavior of these materials considering different time-scales (**Figure 3. 3**). This additional aspect was fundamental for deeply understand each complex mechanism that characterizes each level of investigation overtime.
In fact, the physical state of CM evolves over time according to moisture content changings due to both evaporation and/or hydration processes. Starting from the early-life of the material, its physical state can be identify as *fresh-state* characterized by the total design water content (%*w*) adopted during mixing and compaction phase (carried out in field or in laboratory), in order to improve the workability of the material. At this moment, the material is saturated, no water losses occur but its mechanical properties (Resistance *Re*, strength or stiffness) are almost null. Over time, its physical state evolves and two opposite phenomena take place: the water content decreases and this induces the development of the material mechanical properties; this phase is also known as *curing*. Finally, at long curing times, the physical state of the material achieves a stationary state (*cured-state*) such as water losses no longer occur and material mechanical properties reach their maximum values ($Re_{max}$=constant). Thus, the long-term behavior of the material is defined with its final mechanical properties that can be taken into account by engineers in order to characterize the material during the design phase.

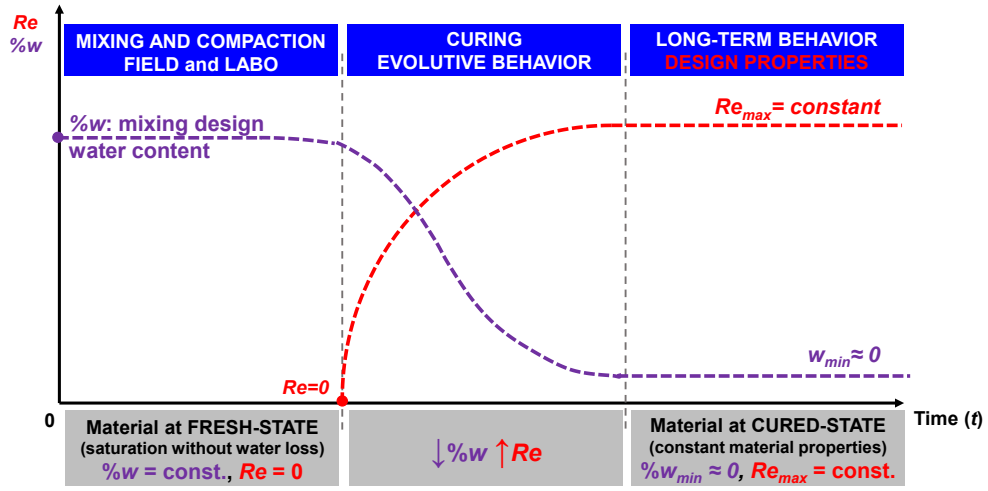


**Figure 3. 3** Evolutive behavior of cold mixtures.

## 3.2 Outline of the dissertation

The research activities aim to achieve the objectives mentioned in the first paragraph.
First, an extensive literature review was conducted in order to allow the assessment of the current state of knowledge on CMs and the identification of the most important related issues to address and investigate.
Afterwards, the study was focused on the interaction effect between the evolutive behavior and the mechanical properties of CMs developing a multiscale approach (described in the previous paragraph) where the testing method is selected according to the:

- *scale of the analysis*,
- *physical state of the sample.*

In this thesis, a multiscale approach was used for the first time in order to characterize the rheological and mechanical behavior of cold mixtures. In particular, experimental activities have been planned and structured in four tasks reported in **Figure 3. 4**, that approximately correspond to each level of investigation analyzed:

- Pavement scale,
- Mixture scale;
- Mortar scale;
- Mastic/binder scale.


**Figure 3. 4** Experimental activities set up.

As it can be observed from the scheme reported in **Figure 3. 4**, the common methodology adopted for a multiscale analysis was completely reversed. In this study, experimental activities started from the bigger size level of investigation (*pavement-scale*) and subtracting particulate by particulate from the matrix, the smaller size level (*mastic/binder-scale*) was achieved (**Figure 3. 1**).
This approach was selected with the aim to deeply understand which and how mechanisms that derive from the smaller scale of investigation, may regulate and affect the in-service behavior of a pavement structure.

In details, the first task is focused on the mechanical characterization of CMs during their in-service life (*Pavement-scale analysis)* and some of these activities are partially superposed on the second task (*Mixture-scale analysis)*. In Task1, the performance of different cold recycled mixtures CRMs produced with bitumen emulsion or foamed bitumen and cement during an experimental pavement section, was directly analyzed in field. The mechanical response of each mixture has been monitored through annual falling weight deflectometer (FWD) surveys. Moreover, cored samples were extracted from the experimental pavement section in order to characterize the stiffness properties of each mixture with laboratory testing (superposed with *Mixture-scale analysis)*. Then an instrumented experimental pavement section was constructed to monitor and evaluate over time both physical (i.e. moisture content evaluated using time domain reflectometer probes) and mechanical (i.e. strength and stiffness) properties of CRMs. In this context, an original approach to the characterization of the curing process of CRMs, based on the evaluation of the rate at which mixture properties evolve over time, was proposed using the application of a mathematical model, called Michaelis-Menten model.
The second task includes the above-mentioned experimental activities related to *Mixture-scale analysis* as well as the volumetric and LVE response characterization of cement-bitumen treated mixtures (CBTM) produced with cement and bitumen emulsion or foamed bitumen at different reclaimed asphalt (RA) content. The influence of water content on the compactability of fresh mixes was also investigated, in order to determine the optimal moisture content for compaction. Moreover, a standardized laboratory procedure that allows to control and measure the curing mechanisms for CBTM was defined. This activities were conducted to evaluate the prevailing mechanism and/or possible interaction between them under specific curing conditions and how they affect the mechanical response of materials. The effect of curing on strength and stiffness was also modelled using two asymptotic regression models and the influence of cement content and curing temperature were considered during this study. In addition, laboratory testing were performed for the first time, in order to characterize CRMs in terms of three-dimensional stress-strain response (*Mixture-scale analysis)*.
The third task is focused on the mechanical characterization of cold bituminous mortars (CBM) (*Mortar-scale analysis*). In this context, the evolution of the failure properties of CBM composed by fine aggregate, bituminous emulsion, water and three different type of mineral additions (Portland cement, hydrated lime and calcium carbonate) was investigated. In particular, the influence of curing conditions on moisture loss and on the development of strength/stiffness was also evaluated.
Finally, the fourth task is addressed to investigate the evolution of consistency and rheological properties of cold bituminous mastic (CBm) prepared with cement or calcium

carbonate during the early age of curing (*Mastic-scale analysis*). The influence of over-stabilized bitumen emulsion on cement setting was evaluated and special attention was also paid to analyze the influence of the mineral addition (type and concentration) on the rheological properties. Different laboratory equipment were adopted to better evaluate the mechanical properties in a wider range of temperatures and frequencies.

This dissertation consists of several chapters, each dealing with a different aspect related to the abovementioned main tasks. The research activities presented in this thesis represent only the first steps towards an overall knowledge of CMs. In addition, another ambitious challenge is the achievement of European standards specifically dedicated to the chacterization/evaluation of CMs performance and as a consequence, the opportunity to "*pave*" the actual gap between practice and theory that affects this topic.

# Part 1
# Pavement-scale analysis: Cold mixtures for subbase layers

# CHAPTER 4.

## Introduction

Nowadays, savings in energy and non-renewable natural resources as well as cost-effectiveness, make the application of cold recycling technologies a strategic solution for the rehabilitation of bituminous pavements [Kandhal and Mallick, 1997; Thompson et al. 2009; Bocci et al., 2010]. In particular, full-depth reclamation (FDR) obtained worldwide success due to the performance quality achieved at lower costs, shorter construction periods and lower environmental impact as compared to in-plant recycling solutions [ARRA, 2001; Stroup-Gardiner, 2011].
As described in previous chapters, the FDR process basically consists in milling the entire thickness of the bituminous layers together with a predetermined amount of the underlying granular or cement-stabilized layer and stabilizing the milled material, i.e. a blend of reclaimed asphalt (RA) and reclaimed aggregates (RAg), with specific binding agents. Thus, FDR potentially allows the production of a 100 % recycled pavement layer, without any transportation or reheating of aggregates [Bocci et al., 2014; Thompson et al. 2009].
Virgin aggregates and water can also be added in order to improve aggregate gradation and enhance laydown and compaction.
A combination of bituminous binder (plain or modified bitumen, either as emulsion or foam) and hydraulic binder (Portland cement, lime and fly ash) is commonly adopted in order to obtain the required mechanical and durability properties of cold recycled layers [Bocci et al., 2011, Eller and Olson, 2009; Loizos, 2007; Stroup-Gardiner, 2011]. Depending on the type and dosage of the binders, the FDR technology allows the production of cold recycled mixtures (CRMs), with different mechanical behavior. In particular, when a combination of bitumen and cement is used, CRM can be considered a cement-bitumen treated material (CBTM). Differently, when only cement is used as binder, the mixture can be identified as a cement treated material (CTM) [Grilli et al, 2013a].

As compared to hot or warm asphalt mixtures either recycled or not, cold mixtures (CMs) can be considered as evolutive materials, where a certain curing period is necessary for them to achieve the long-term mechanical properties, e.g. strength and stiffness. Because of the simultaneous presence of both bituminous and hydraulic binders, curing of CBTMs is the result of different time-dependent mechanisms [Cardone et al., 2015; Du, 2014].
Moreover, the time-dependent physical phenomena leading to influence each other. In the *early curing stage*, cement promotes emulsion breaking or foam collapse and contributes to the bitumen coalescence by reducing the free water within the mixture [Terrel and Wang, 1971; Garcia et al., 2013; Wang et al., 2013]. In the meantime, the presence of bitumen emulsion or foamed bitumen could reduce the rate of hydration of cement and hinder the formation of well-structured cementitious bonds [Pouliot et al., 2003; Weiss et al., 2008]. Finally, it is important to highlight that while the curing process of the bituminous phase is

strictly related to moisture loss, the cement hydration process requires a moist environment and does not entail any mass loss.
Several research studies [Garcia et al., 2013; Bocci et al., 2014; Godenzoni et al., 2016] showed that monitoring the evolution over time of both physical (i.e. moisture content) and mechanical (i.e. strength and stiffness) properties of CRMs is a valid procedure in order to get a quantitative measure of curing. The effect of curing over time is a fundamental aspect for CRMs that can be monitored in field, using advanced instruments installed in the road pavement, or can be simulated using laboratory produced mixtures. However, it should be recognized that laboratory curing procedures can hardly recreate actual field curing conditions, mostly because the factors that influence field curing are extremely variable. Among these factors, one can list mixture composition (aggregate gradation, binder type and dosage), environmental conditions (temperature and relative humidity) as well as construction features (degree of compaction, layer thickness, drainage conditions, construction phases). For this reason, comparing the effects of laboratory and field curing is challenging task that requires the same experimental conditions and modelling approach to be applied.
In this context, an original approach towards the characterization of the curing process of CRMs based on the evaluation of the rate at which mixture properties evolve over time (*curing rate*) and of their *long-term value* was proposed in [Graziani et al., 2016a].
The approach was based on the application of a mathematical model, the Michaelis-Menten model [Michaelis and Menten, 1913] that proved to be effective when applied to laboratory produced mixtures and should be verified also for measurements carried out directly in field.

Further important aspect to be analyzed with CRMs is the evolution of pavement materials properties in field under the effect of traffic, climate and ageing (i.e. the pavement performance during its service life). Distresses can occur and increase over time and, consequently may lead to functional or structural failure of the pavement. .
In this context, monitoring equipment assume extreme importance not only in the evaluation of certain property at *project level* (in little extensions) but mainly at *network level* in association with management systems (e.g. pavement management system, PMS) related to pavement maintenance.
In order to evaluate the bearing capacity and consequently the mechanical behavior of road pavements over time, load tests can be performed. The deflection basins measured on the pavement surface during load tests allow to analyze the pavement structure in field.
Determination of pavement deflections, associated to bearing capacity, can be accomplished using equipment like the Benkelman Beam, Lacroix's Deflectograph, Curviameter, Falling Weight Deflectometer (FWD) and high performance equipment that enable the deflection measurements at traffic speed – *High Speed Deflectometer*.
Limited information are available in international literature [Loizos, 2007 and 2012; Vennapusa et al., 2012] about the field performance of CRMs adopted as subbase layer and more specifically about pavement performance when FDR technique is implemented as rehabilitation method for road pavement [Plati et al., 2010].

The first part of this thesis aims to investigate aspects concerning the assessment of field properties that characterized CMs produced with recycled aggregates (RA and RAg) and adopted as subbase layer (*Task 1*).

Two experimental pavement sections were constructed through FDR technique:

- First experimental pavement section located in the north part of Italy (see Chapter 5 and 6) aims to characterized the evolution of the mechanical behavior for three different types of CRMs. The changings in stiffness were monitored over time by performing annual high performance tests (falling weight deflectometer, FWD);
- Second instrumented pavement section located in the center of Italy (see Chapter 6 and 7) attempts to evaluate the curing process of two different CRMs under different curing conditions measuring the moisture loss that occurs inside subbase layer. Measurements were performed using advanced instruments installed in the subbase layer (time domain reflectometer probes, TDR).

Each measurement carried out in field for both mechanical behavior and evaluation of curing process has been compared with laboratory results obtained according to standard procedures. Laboratory tests have been performed using core samples or specimens directly produced in laboratory for the first and the second experimental pavement section, respectively.

For this reason, the first two tasks (Task 1 and 2) of this thesis are slightly superposed; as described in Chapter 3, the Task 1 combines simultaneously instrumental measurements carried out in field and an additional investigation using laboratory testing.

# CHAPTER 5.

## Evaluation of pavement performance using non-destructive testing and laboratory validation

Road pavements are constructed for the safe and smooth passage of traffic. During their in-service life, there is a need to quantify the extent to which the pavement is serving its purpose, or its "*performance*."
Pavement performance evaluations are conducted to determine functional and structural conditions of a highway section either for purposes of routine monitoring or planned corrective action. Functional condition is primarily concerned with the ride quality or surface texture of a highway section. Structural condition is concerned with the structural capacity of the pavement as measured by deflection, layer thickness and material properties [Mallick and El-Korchi, 2013].
At the *network level*, routine evaluations can be used to develop performance models and prioritize maintenance or rehabilitation efforts and funding. At the *project level*, evaluations are more focused on establishing the root causes of existing distress in order to determine the best rehabilitation strategies.
The performance of road pavements can be monitored using different methods such as visual condition surveys, non-destructive testing or destructive testing, according to distress conditions exhibited by the pavement at any time after its construction.

Focusing on *non-destructive testing NDT*, data collected in field are generally objective in nature, but often subjectivity appears in the data analysis and interpretation. Non-destructive testing is usually performed on an existing pavement structure that do not require subsequent maintenance work. This is generally desirable to minimize disruption to traffic, and is essential as a screening tool to determine road section where selective material sampling should be conducted to evaluate other material properties in the laboratory.
As such, NDT aim is to assess in situ properties that can be used to evaluate the need to perform further "destructive" testing (i.e., coring, boring, trenching).

Various types of NDT equipment are used worldwide for the determination of the structural condition and residual service life of road pavements by means of deflection measurements. NDT equipment ca be classified in deflection and non deflection measurement instruments, in particular NDT deflection measurement equipment can be subsequently divided into six categories [CROW, 1998]:

- Static deflection measurement equipment;
- Automated beam deflection measurement equipment;
- Dynamic deflection measurement equipment;

- Dynamic deflection measurement equipment;
- Deflection instruments with a harmonic load;
- Deflection measuring equipment with an impulse load;
- Wave propagation measurements.

Non deflection measuring equipment that can support deflection testing includes ground-penetrating radar, infrared thermography, dynamic cone penetrometer, and devices that allow to measure surface friction, roughness and surface waves [Texas Department of Transportation, 2011].
In this thesis, *falling weight deflectometer* (FWD) has been selected among nondestructive testing characterized by deflection equipment and an impulse device as dynamic loading equipment, in order to evaluate the pavement performance along an experimental pavement section.

Laboratory testing has been carried out in order to characterize the mechanical behavior of the investigated mixtures and compare results in terms of stiffness moduli, with those obtained from the back-calculation of deflection measurements.

# 5.1 Field equipment: falling weight deflectometer

## 5.1.1 General description

Falling weight deflectometer (FWD) is extensively used NDT deflection equipment for estimating pavement layer moduli and for evaluating the structural condition of pavements. The information obtained from FWD testing can be used in structural analysis to determine capacity, predict expected performance life, and design a rehabilitation plan for pavements.

FWD generates a load pulse by dropping a weight on a damped spring system mounted on a loading plate as shown in
**Figure 5. 1**. The falling mass, the spring system (the rubber buffers) and drop height can each be adjusted to achieve the desired impact loading on the pavement. The peaks of the vertical deflections are measured at the center of the loading plate and at several radial positions by a series of deflection sensors. The impulse load acting on the pavement causes a “wave front” of recoverable deformations, or deflections, spreading out from the load center (**Figure 5. 2**). Both the peak impulse load (force) and the maximum vertical deflections of the “wave front” are measured at several radial distances from the load center. These deflections, considered as a function of the applied impulse load, provide an indication of the structural strength of the pavement.

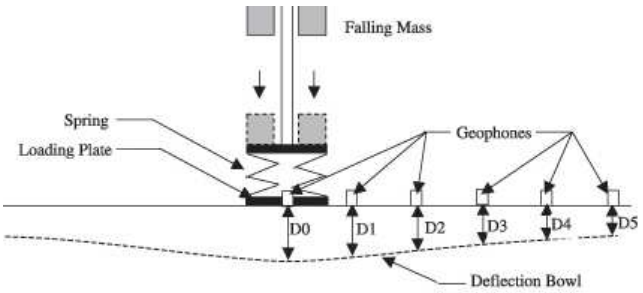


**Figure 5. 1** Schematic diagram of FWD equipment.

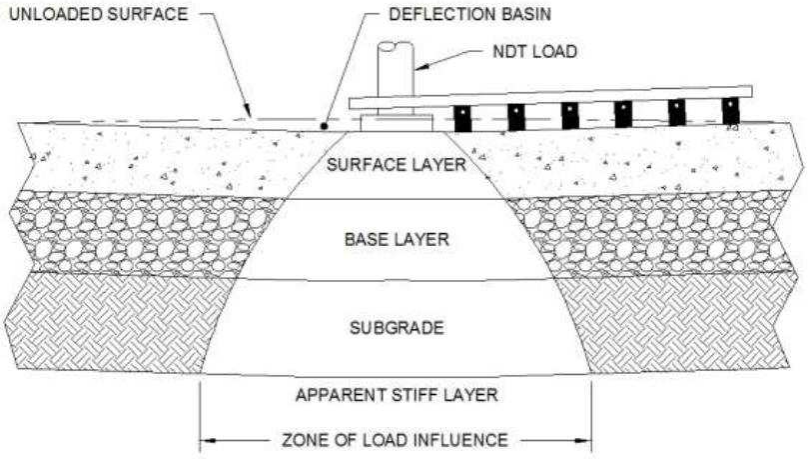


**Figure 5. 2** Scheme of deflection basin.

## 5.1.2 Load pulse

The FWD design may vary in detail depending on the manufacturer. This implies that the configuration of the load pulse can vary from one equipment type to another.
Impulse load devices, such as the FWD or Heavy-Falling Weight Deflectometer (HWD), impart an impulse load to the pavement with a free-falling weight that impacts on a set of rubber springs, as illustrated in **Figure 5. 3**. The time from A to B in this figure is the time required to lift the FWD weight package to the required drop height. The magnitude of the dynamic load depends on the mass of the weight and the height from which the weight is dropped.

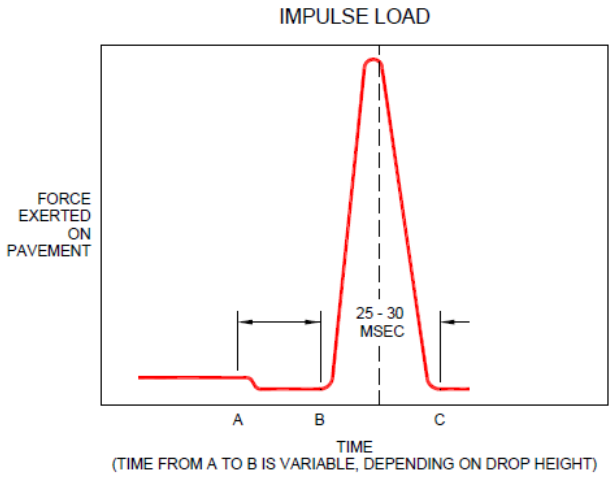


**Figure 5. 3** Time to Peak Load for Impulse-Based on FWD equipment.

If the load pulse simulate a moving vehicle, it should have a rise time, which is approximately equal to the rise time of a moving wheel load.
Most FWDs are characterized by a *load rise time* from start to pulse to peak ranging from 5 ms and 30 ms and a *load pulse base width* in the interval from 20 ms to 60 ms.

### 5.1.2 Deflection sensors

FWD equipment should have a sufficient number of deflection sensors to entirely describe the shape of the deflection bowl. There are two kinds of deflection sensors that are used in FWDs; geophones (**Figure 5. 4**) and seismometers (**Figure 5. 5**). The type that is used depends on FWD design. For the structural evaluation of bituminous pavement, deflections sensors have to be located closer to the load center than the case of a thicker bituminous pavement.
The falling mass impacts on a circular loading plate (**Figure 5. 4**) with a diameter of 300 mm and the deformations must be measured by at least six deflection sensors, which could be positioned at radial offsets from 0 mm to 2500 mm.
In particular, the positions of the deflection sensors should be selected from the following list: 0, 200, 300, 450, 600, 900, 1200, 1500, 1800, 2100 and 2400 mm.

**Figure 5. 4** Deflection sensor: geophone type.


**Figure 5. 5** Deflection sensor: seismometer type.

### 5.1.3 Dynamic analysis of FWD data

In order to obtain the structural condition (in terms of elastic stiffness) of a pavement structure, engineers can use deflection basin data from flexible or rigid pavements obtained though NDT tests, such as FWD tests. The process that is used to conduct this analysis is referred to as *back-calculation* [AC 150/5370-11B].
Basically, back-calculation is an optimization process performed to obtain inverse mapping of a known relation established by discrete or continuous data points.
The back-calculation process in pavement system is the numerical analysis of measured surface deflections performed for the estimation of layer stiffness moduli. In order to accomplish this, measured deflections are matched with calculated deflections. Deflection calculations are conducted using an equivalent pavement response model with synthetic moduli.
Back-calculation analysis is typically conducted using two procedure. The first category allows the engineer to use closed-form procedures that directly compute the elastic modulus of each layer by using the layer thickness and deflections from one or more sensors. The second category uses an iterative mechanistic process to solve for the elastic modulus by using layer thicknesses and deflections from at least four sensors.
The most efficient matching process is the iterative process, in which deflection values are calculated using different set of moduli. Consequently, iterations are continued until a close match between measured and calculated deflection values are satisfied [Lytton, 1989; Uzan,

1994] (**Figure 5. 6**). The estimating initial set of layer elastic moduli (*seed values*) and a reasonable range of moduli for each material type. Modulus and Poisson's ratio values for typical pavement materials are shown in **Table 5. 1**.

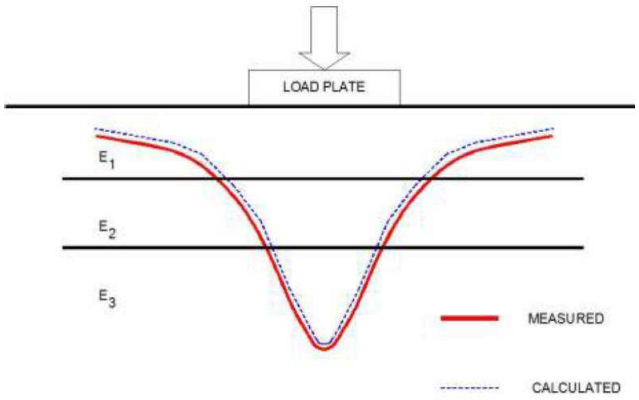


**Figure 5. 6** Comparison of measured and calculated deflection basins.

| Material | Low Value | High Value |
|---|---|---|
| Asphalt concrete or asphalt-treated base | 0.25 | 0.40 |
| Portland cement concrete | 0.10 | 0.20 |
| Lean concrete or cement-treated base | 0.15 | 0.25 |
| Granular base, subbase, or soil | 0.20 | 0.40 |
| Stabilized soil | 0.15 | 0.30 |
| Cohesive soil | 0.30 | 0.45 |

**Table 5. 1** Typical Poisson's Ratios for Paving Materials.

Available sources reveal that numerous backcalculation techniques have been developed for the backcalculation of pavement layer moduli. The discrepancies among these models are related with the type of the pavement (forward) response model and the optimization procedure carried out for the determination of appropriate layer modulus values [Hoffman and Thompson, 1982; Uzan, 1994].
The magnitude of the error and the results that are obtained through iterative back-calculation using elastic layer theory are influenced by many factors, including the following:

- Number of layers;
- Layer thickness;
- Layer interface condition;
- HMA layer temperature;
- Layer "seed" values;
- Adjacent layer modulus ratios;

- Underlying stiff layer;
- Pavement cracks;
- Sensor errors;
- NDT load plate;
- Pulse duration;
- Frequency duration;
- Seasonal effects;
- Material properties variability.

*BAKFAA Software*

BAKFAA (**Figure 5. 7**) is a conventional modulus back-calculation program which considers the pavement as an elastic multi-layered media and assumes that the pavement materials are linear-elastic, homogeneous and isotropic. The BAKFAA was developed under the sponsorship of the FAA Airport Technology Branch and is based on the LEAF layered elastic computation program [Hayhoe, 2002]. In this program, the pavement layer moduli are adjusted to minimize the *root mean square* (rms) of the differences between FWD/HWD sensor measurements and the LEAF-computed deflection basin for a specified pavement structure. A standard multidimensional simplex optimization routine is then used to adjust the moduli values [Marsey and Arze, 2001].

This software was adopted in this thesis to calculate the pavement layer moduli using deflection basin carried out though FWD tests.

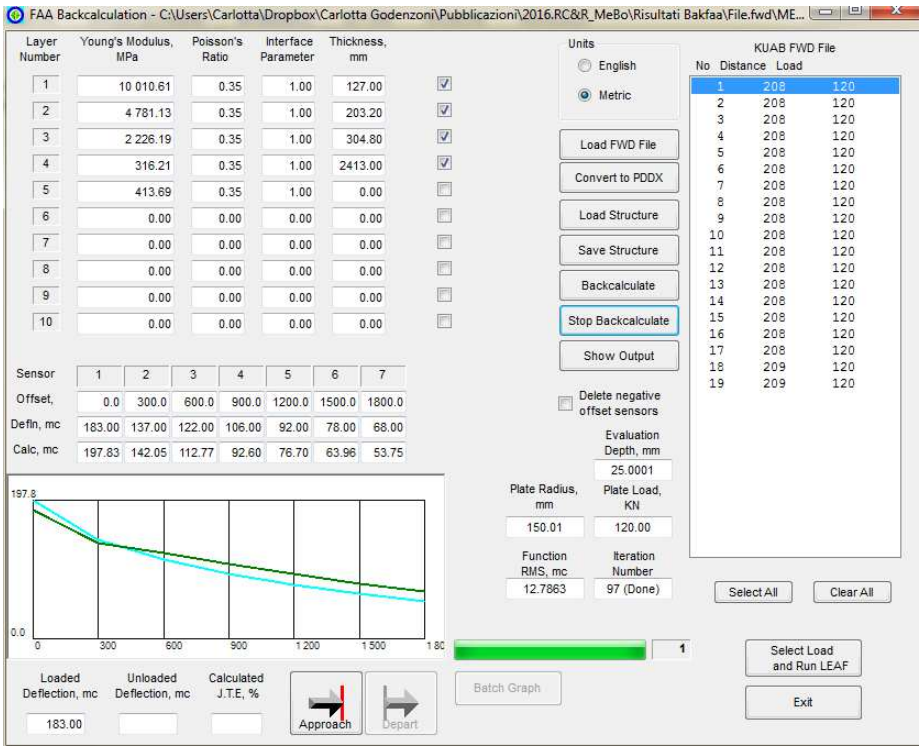


**Figure 5. 7** BAKFAA Software.

*Temperature correction*

When evaluating the structural condition of an road pavement, attention must be paid to the prevailing climatic conditions. To date, no correction of deflections have been carried out in connection with seasonal influences. Very distinct seasonal effects are encountered in zones with severe frost. In any case, the most important climate parameter which must always be taken into account is temperature. Indeed, with regard to bituminous pavements, temperature has a direct influence upon the stiffness of bituminous layers. All survey results must be referred to the weighted average annual air temperature, in order to discount the influence of temperature but, for practical reasons, a reference temperature of 20 °C has been selected for evaluating deflection data [CROW, 1998].

Temperature measured in correspondence of bituminous surface layer (about 25 mm in depth) is very far from the temperature in deeper layers (e.g. base and subbase layer) and in addition, it is well-know that upper layers are more thermos-dependent with respect to those materials used in the lower part of a road pavement structure.

For this reason, temperature correction for deflection measurements should affect more the deformations collected by sensors close to the load plate.

In literature, great confusion and disagreement characterize the temperature correction. In fact, a unique and standard procedure to correct the influence of temperature in deflection basins, is not available yet [SHRP-P-654; CROW, 1998; AC150/5370-11B].

In this thesis, the procedure developed by [Chen et al., 2009] and [Straube and Jansen, 2009] has been considered for correcting the temperature effect on deflection measurements.

The deflection measurement shifted at the reference temperature of 20 °C can be calculated as follow:

$$D_0(20\,°C) = (a - b \cdot T_{\mathrm{FWD}}) \cdot D_0(T_{\mathrm{FWD}}) \tag{20}$$

where $D_0(20\,°C)$ and $D_0(T_{\mathrm{FWD}})$ are the central deflection measured at 20 °C and at the testing temperature $T_{\mathrm{FWD}}$ respectively and $a$ and $b$ are two coefficients depending on geophone position, bituminous layer temperature and type of deflection.

# 5.2 Laboratory equipment, test methods and data analysis

In the following section, the test methods adopted for evaluating the stiffness properties of the selected cored samples are described, along with test protocols and data analysis procedures adopted. A brief description of the test equipment is also provided. The performance-based tests carried out for this investigation phase aim to identify the time and temperature dependence of each mixture.
The results of the laboratory characterization were used to analyze the FWD back-calculated moduli by considering the temperature dependence of the measured deflections. This allowed to compare the stiffness moduli obtained in different years (at different testing temperatures) and evaluate the performance of the CRM over time.

## 5.2.1 Nottingham Asphalt Tester

The *Nottingham Asphalt Tester* (NAT) is one of the most efficient and advanced equipment that allows the measuring and assessment of the mechanical properties of bituminous mixtures. The device is a servo-pneumatic, closed-loop control press developed at the University of Nottingham. It is used to performed several different tests in a number of different configurations (e.g. elastic stiffness modulus using repeated load, indirect tension or cyclic compression, instantaneous and total resilient modulus, resistance to fatigue cracking, resistance to permanent deformation with the uniaxial creep test or the repeated load axial test, dynamic creep with both axial and radial strain measurement). The apparatus consists of a stainless steel load frame fitted with a pneumatic actuator capable of applying vertical loads in the range 0 to 4.3 kN and various load transducers. The device is associated to a temperature controlled chamber capable of controlling the temperature in a range of -10°C to 60°C (**Figure 5. 8**).


**Figure 5. 8** Nottingham Asphalt Tester (NAT)

### 5.2.2 Cyclic uniaxial compression tests

One of the most important parameters that characterize road materials, which is commonly used for pavements design, is the bituminous mixture complex modulus $E^*$ (NCHRP, 2004). Such parameter can be evaluated through dynamic laboratory tests carried out in a suitable range of temperature and loading frequency. The results are then used to build the complex modulus master curve, useful tool to describe the rheological behavior of the material. The test parameters obtained by performing these tests are used in the pavement design for the determination of thicknesses and materials of each layer.
Cyclic uniaxial compression tests to measure the complex modulus ($E^*$) and the phase angle ($\delta$) in accordance with EN 12697-26 were carried out in this study using the NAT equipment and testing cylindrical core samples or laboratory produced specimens.
As previously explained in the Introduction of this thesis, European standard procedures for laboratory testing are mostly developed for asphalt concrete and not for cold mixture yet. For this reason, each test protocol has to be verified systematically in order to avoid any damage of the material during the test.
The specimen is placed between two plan parallel metal platens and positioned under the load actuator (**Figure 5. 9**), paying particular attention to the proper alignment with the vertical load axis in order to avoid eccentricity. The axial deformation was measured by means of two inductive transducers, fixed to the lateral surface of the specimen at 180° apart, with a measurement base of 70 mm.
Tests were run at different temperatures (e.g. from 0 to 50 °C)) by the application of sinusoidal load waves at different frequencies (e.g. from 0.1 to 20 Hz). Tests were carried out in controlled strain mode, setting 30 με as target strain level instead of 50 με, strain level commonly adopted for asphalt concrete.

**Figure 5. 9** Cyclic uniaxial compression tests

### 5.2.3 Data analysis: master curve construction

The cyclic uniaxial compression test performed by applying sinusoidal load waves to a viscoelastic material such as bituminous mixtures allows the construction of the complex modulus $E^*$ identification, intended as the ratio between the sinusoidal stress amplitude and the amplitude of the corresponding sinusoidal strain.
The complex modulus represents the relationship between stress and strain for a linear viscoelastic material submitted to a sinusoidal load wave form at time, *t,* where applying a stress $\sigma_0 \times \sin(\omega t)$ results in a strain $\varepsilon_0 \times \sin(\omega \times (t - \varphi))$ that has a phase angle, $\varphi$, with respect to the stress. The amplitude of strain and the phase angle are functions of the frequency, $\omega$, and the test temperature *T*.
$E^*$ can be determined as follows [Di Benedetto and De La Roche, 1998]:

$$\frac{\sigma^*}{\varepsilon^*} = E^*(i\omega) = \left(\frac{\sigma_0}{\varepsilon_0}\right) \cdot e^{i\varphi} = E_1 + iE_2 \tag{21}$$

in which $\sigma_0$ is the stress amplitude, $\varepsilon_0$ is the strain amplitude, $\omega$ is the angular velocity, which is related to the frequency by $\omega = 2\pi f$, and $i^2 = -1$. The amplitude of the measured stress and strain signals $(\sigma_0, \varepsilon_0)$ and the time lag $(\Delta t)$ between the two signals were calculated performing a sinusoidal regression on the last ten loading cycles (see Section 2.12).

The cyclic uniaxial compression test is carried out at various temperatures to ensure the application of the *time-temperature superposition principle* (TTSP).
In fact, in order to completely characterize the material behavior, the mixture should be tested at very high and low frequencies, too. However, due to laboratory and technical restrictions, some test conditions cannot be performed. For example, tests at very low frequency are too long and not compatible with the laboratory practice, as well as tests at too high frequency cannot be performed due to equipment limitations. These drawbacks can be overcame by applying the TTSP that allows the construction of master curve and the determination of the viscoelastic behavior of the mixture across a wider range of reduced frequencies than the originally tested.
Based on the TTSP, the data measured at each temperature are horizontally shifted and aligned to the data measured at $T_{ref}$ a temperature assumed as reference (**Figure 5. 10**).

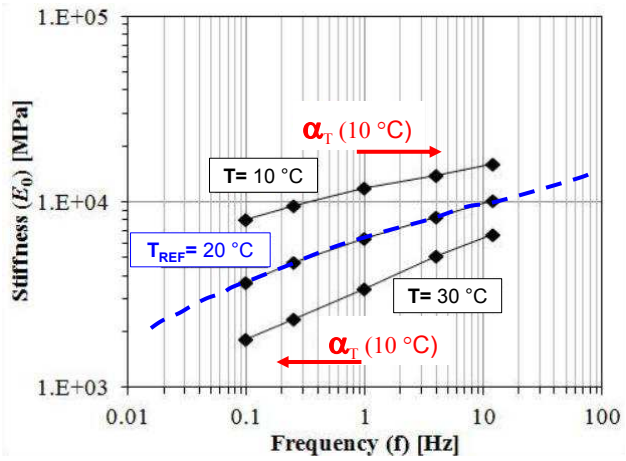


**Figure 5. 10** Time-Temperature Superposition principle: schematic representation.

Thus, master curve describes the rheological behavior of a material at a specific temperature and represents the trend of a rheological property (for mixtures usually the complex Young's modulus or the phase angle) as a function of loading frequency. Therefore, the master curve can be considered as an isothermal representation of the mechanical behavior of viscoelastic materials over a wide range of frequency.
The construction of master curve is realized by exploiting the solver functionality in Microsoft Excel that allows the difference between the measured data and the theoretical model adopted to represent master curve to be minimized. The least-squares regression is performed in order to fit the recorded data (for mixtures usually the complex Young's modulus) to a rheological model that relates that specific rheological property to the loading frequency. The solver functionality allows the simultaneous determination of the model parameters and the horizontal shift factors $a_{\mathrm{Tref}}(T)$ (at each temperature). The shift factors are function of the reference temperature $T_{\mathrm{ref}}$ and the generic test temperature $T$ considered. According to the TTSP, $\tau$ may be written as a function of the test temperature $T$ as follows:

$$\tau(T) = a_{\mathrm{Tref}}(T)\tau_{\mathrm{ref}} \tag{22}$$

where $a_{\mathrm{Tref}}(T)$ are the temperature shift factors used to describe the thermal dependence of $E^*$ and $\tau_{\mathrm{ref}}$ is the characteristic time at the reference temperature $T_{\mathrm{ref}}$. In this study, the reference temperature selected for master curves was $T_{\mathrm{ref}}$ = 20 °C. Next, the Williams–Landel–Ferry (WLF) model was used to fit the temperature dependency of the shift factors [Ferry, 1980]:

$$\log a_{\mathrm{T_{ref}}}(T) = \frac{-C_1 \cdot (T - T_{\mathrm{ref}})}{C_2 + (T - T_{\mathrm{ref}})} \tag{23}$$

where $C_1$ and $C_2$ are experimental coefficients that can be calculated using a linear regression on the experimental values of the shift factors.

A number of different rheological model can be used to construct master curves. In the following section, the Huet-Sayegh (H-S) rheological model [Sayegh, 1967] was employed to fit the experimental data:

$$E^*(\omega) = E_e + \frac{E_g - E_e}{1 + \delta(j\omega\tau)^{-k} + (j\omega\tau)^{-h}} \quad (24)$$

where $\omega = 2\pi f$ is the angular frequency, $E_g$ and $E_e$ are the glass and equilibrium moduli, respectively, $\tau$ is the characteristic time and $\delta$, $k$, $h$ are dimensionless model parameters (**Figure 5. 11**).

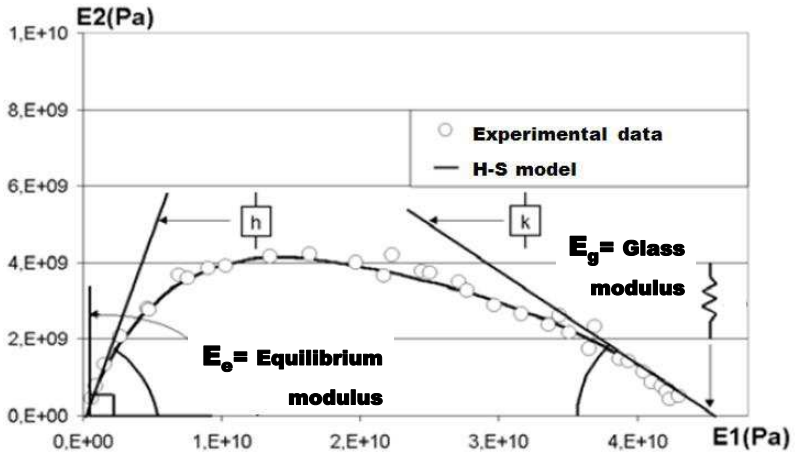


**Figure 5. 11** Huet-Sayegh (H-S) rheological model representation (Cole-Cole plane) [Di Benedetto et al., 2011].

Besides master curve, also the Black diagram ($|E^*|$ Vs. phase angle) and the Cole-Cole plane ($|E_2|$ Vs. $|E_2|$) are useful tools to characterize the viscoelastic material behavior. Combined with the trend of master curve, they provide relevant information about the overall rheological behavior of a bitumen.
Finally, it is important to bear in mind that the applicability of the TTSP provides the determination of identical shift factors for each rheological property (i.e. $|E^*|$ and $\delta$) and can be verified by the determination of a unique continuous curve in the Black diagram and in the Cole-Cole plane. Such a behavior is usually respected for traditional asphalt concrete, but it should be constantly verified with cold mixtures.
For the latter, it is more suitable the application of the *Partial Time-Temperature Superposition Principle* that allows the hypothesis to have different shift factors for the complex modulus and the phase angle [Di Benedetto et al., 2011].

# CHAPTER 6.

## Experimental pavement section: SS38 Highway Merano-Bolzano

In the last decades, the Province of Bolzano started a new sustainable policy to rehabilitate the existing damaged road pavements. In this context, it supported the construction of an experimental pavement section with the aim to evaluate the performance of different FDR techniques.

The experimental pavement section was built up along the *SS38 highway* in May 2007 and interested about 1000 m of road, between km 16+000 to km 17+000 (**Figure 6. 1**). At that time, visual investigations and FWD test campaigns had showed a serious damage (spread and branched cracking) of the pavement in this area, highlighting the necessity to restore the structural properties through a deep rehabilitation.


**Figure 6. 1** Location of the experimental pavement section (source: Google Streetview).

The objective of this research was to measure and compare the field performance of different CRMs produced using FDR techniques. Three mixtures, with the same 100% of reclaimed aggregate composition, were produced and compared:

- CBTM with foamed bitumen and cement (CBTM-FB);
- CBTM with bitumen emulsion and cement (CBTM-BE);
- CTM.

## 6.1 General overview

An experimental pavement section was constructed in 2007 along a two-lane dual carriage highway, the SS38, that links the cities of Bolzano and Merano, in northern Italy. Since then, the field performance of mixtures has been monitored with annual falling weight deflectometer (FWD) surveys.

The experimental pavement section was divided in three sub-sections, where the subbase layer was treated with different binders:

- 400 m with foamed bitumen and cement (CBTM-FB);
- 400 m with bitumen emulsion and cement (CBTM-BE);
- 200 m with cement and no bituminous binder (CTM).

Moreover, in 2014, core samples were extracted from the experimental pavement section in order to characterize the stiffness response of each mixture. Laboratory characterization included complex modulus testing and thermo-rheological modelling in order to identify the time and temperature dependence of each mixture [Cardone et al., 2015; Fu and Harvey, 2007].
The results of the laboratory characterization were used to analyze the FWD back-calculated moduli by considering the temperature dependence of the measured deflections. This allowed to compare the stiffness moduli obtained in different years (at different testing temperatures) and evaluate the performance of the CRM over a period of 8 years.

The site is characterized by a seasonal air temperature ranging from 1.7 °C (winter) to 23.2 °C (summer). The maximum, average and minimum annual temperatures, recorded from 2007 to 2015, are reported in **Figure 6. 2**. Traffic data were recorded on SS38 since 2007 through inductive loop detectors positioned nearby the experimental pavement section. Traffic data, separated for light and heavy vehicles, are summarized in **Figure 6. 3**, with the corresponding passages of 80 kN-weight equivalent single axle loads (ESALs) [AASHO road Road Test, 1972]. Traffic in terms of ESAL, showed a decrease until 2013, when it reached a minimum value of about 900,000 ESAL, and it subsequently started increasing again until 2015.

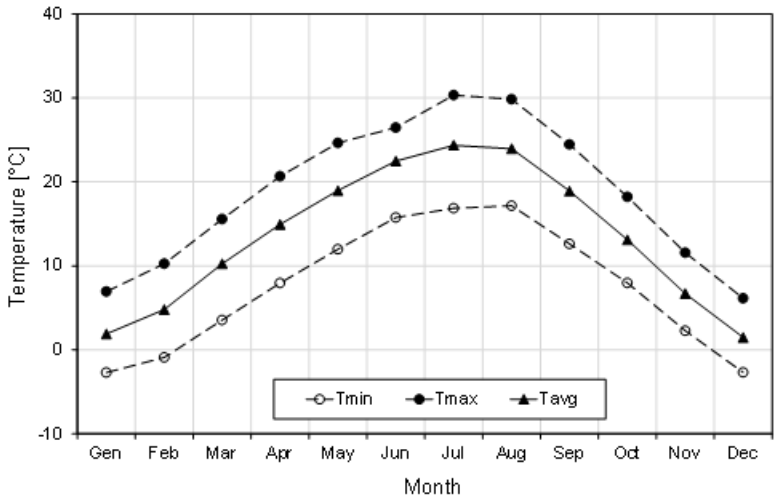


**Figure 6. 2** Maximum, average and minimum annual temperatures, from 2007 to 2015.

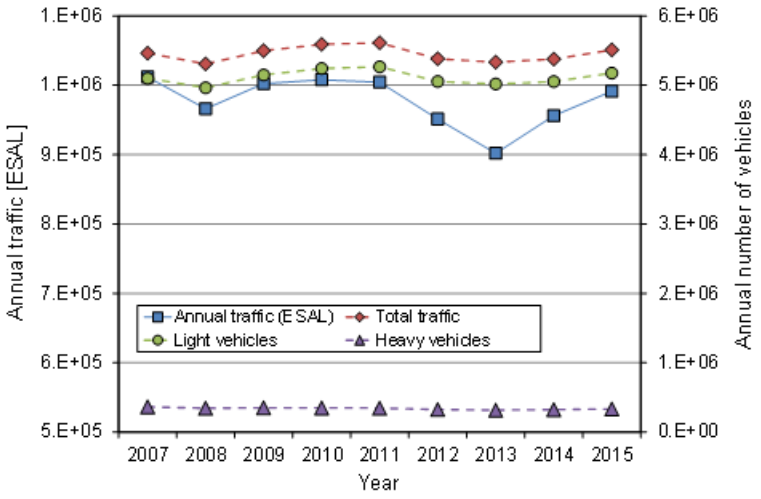


**Figure 6. 3** Traffic data SS38 highway, recorded from 2007 to 2015: annual number of vehicles (light, heavy and total) and annual traffic (ESALs).

## 6.2 Pavement structure

The existing pavement structure on SS38 highway is characterized by 220 mm of HMA (composed of 40 mm of wearing layer, 60 mm of binder layer and 120 mm of base layer), laying on the natural subgrade (**Figure 6. 4**).
The structure of the experimental pavement section consists of 190 mm of HMA (composed of 30 mm of wearing layer, 60 mm of binder layer and 100 mm of base layer), 300 mm of CRM as subbase layer (CBTM-FB, CBTM-BE and CTM) and the natural subgrade (**Figure 6. 4**).

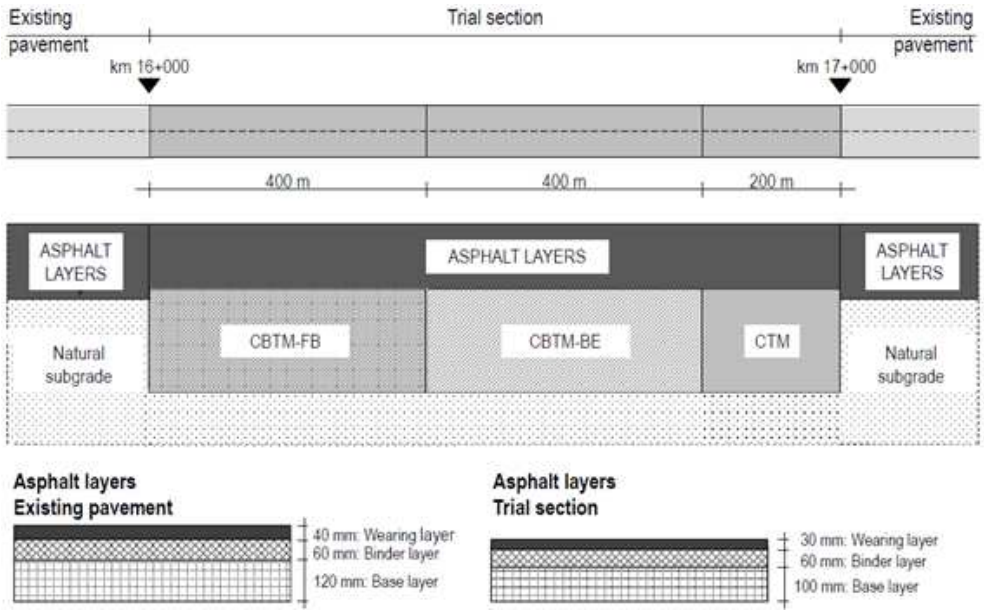


**Figure 6. 4** Configuration of the experimental pavement section.

## 6.3 Materials

Before the construction, the physical characteristics of the natural subgrade were assessed. In particular, two test pits were dug in different locations and samples were taken at three different depths (270 mm, 360 mm and 600 mm below the road surface). Then the soil was characterized in terms of gradation, Atterberg limits (Liquid Limit = 22.3%, Plasticity index = 8.96%) and moisture content (about 5%). The material proved to be homogeneous and, according to the Unified Soil Classification System [ASTM-D2488], was classified as a poorly graded gravel (designated as GP), with a slightly plastic behavior. In addition, static plate loading tests according to Swiss Norm [SN 630-317b] were performed on the top of the existing subgrade (at the depth of 220 mm) and on the new subgrade (at the depth of 490 mm). The deformation moduli calculated after the second loading cycle $E_{v2}$ resulted 157 MPa and 147 MPa and the ratio between the deformation moduli after the second and the first loading cycle $E_{v2}/E_{v1}$ was 2.03 and 2.01, respectively.

The subbase layer (CBTM-FB, CBTM-BE and CTM) was constructed in site according to the construction phases described in Section 5.3.4. The aggregate blend used for CRMs was totally recycled: one third (33%) of the aggregate blend was reclaimed asphalt (RA) from the milling of the HMA layers and the remaining two thirds (67%) was reclaimed unbound aggregate (RAg) from the existing subgrade. The gradation of the aggregate blend (**Figure 6. 5**) was the same for all the CRMs.

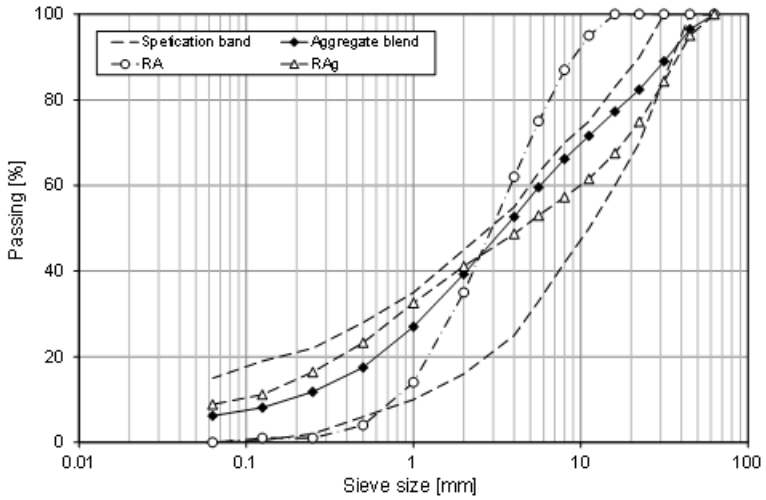


**Figure 6. 5** Grading curves of RA, RAg and the adopted aggregates blend.

A pozzolan-lime cement type IV/A, strength class 32.5 R (EN 197-1), was used. Its composition is clinker (65% - 89%) and a combination of pozzolan and fly ash (11% - 35%). The bitumen emulsion was an over-stabilized cationic type, with designation C 60 B 10, according to EN 13808. Specifically designed for CIR operations, it acts as lubricant during the compaction process and breaks only after the material is compacted. Moreover, the emulsion formulation is intended to delay cement setting as well as to mix high fines content. For these reasons, it is possible to achieve long workability times and the stability of the recycled mixture. The characteristics of the emulsion are shown in **Table 6. 1**.
The foamed bitumen was manufactured in site by using a recycler machine model WR 2000, combining 50/70 penetration bitumen with 3% of foamant water by weight of bitumen. The properties of the base bitumen are summarized in **Table 6. 2**.
The dosage of the different binders was properly determined for each mixture, based on the characteristics of the materials involved and on a preliminary mix design analysis. In particular, CBTM-FB was manufactured with 1.75% of cement and 3% of foamed bitumen by aggregate weight, CBTM-BE was produced with 2% of cement and 3% of bitumen emulsion by aggregate weight (i.e. 1.8% of residual bitumen) and CTM contained 3% of cement by aggregate weight. The binder combinations of the CRMs are shown in **Table 6. 3**.

*Characteristics of the bitumen emulsion*

| Property | Standard | Unit | Value |
|---|---|---|---|
| Water content | EN 1428 | % | 40 |
| pH value | EN 12850 | - | 3 |
| Settling tendency @ 7 days | EN 12847 | % | 8 |
| Breaking value | EN 13075-1 | % | 180 |
| Mixing stability with cement | EN 12848 | G | 0.2 |
| Application temperature | - | °C | 5 - 80 |

| *Characteristics of the residual bitumen* | | | |
|---|---|---|---|
| Property | Standard | Unit | Value |
| Needle penetration at 25 °C | EN 1426 | $mm \cdot 10^{-1}$ | 70 |
| Softening point | EN 1427 | °C | 50 |
| Fraass breaking point | EN 12593 | °C | -10 |

**Table 6. 1** Characteristics of the bitumen emulsion and residual bitumen.

| Property | Standard | Unit | Value |
|---|---|---|---|
| Needle penetration at 25 °C | EN 1426 | $mm \cdot 10^{-1}$ | 62 |
| Softening point | EN 1427 | °C | 50 |
| Dynamic viscosity | EN 13702 | Pa s | 0.18 |
| Flash point (Cleveland) | EN 22592 | °C | 305 |
| Weight loss after RTFOT | EN 12607-1 | % | 0.31 |
| Retained penetration | EN 1426 | % | 68 |
| Increase in softening point | EN 1427 | °C | 8 |

**Table 6. 2** Characteristics of the base bitumen for CBTM-FB.

| Mixture type | Cement content [%] | Bitumen content [%] |
|---|---|---|
| CTM | 3.0 | - |
| CBTM-FB | 1.75 | 3.0 |
| CBTM-BE | 2.0 | 1.8 (3.0% of emulsion) |

**Table 6. 3** Dosage of the different binders in the CRMs.

## 6.4 Construction sequence

In detail, the experimental pavement section was built according to the following program:

- Day 1: first milling of HMA to a depth of 90 mm for a width of 4.70 m and hauling of RA to a storage site (**Figure 6. 6**a);
- Day 1: second milling of HMA for further 100 mm (to a depth of 190 mm) for a width of 4.30 m. The RA was stored on site in order to be reused in the subbase layer (**Figure 6. 6**b);
- Day 2: third milling for further 100 mm (to a depth of 290 mm) for a width of 3.00 m and hauling of RA to a storage site (**Figure 6. 6**c);
- Day 2: replacing the RA from the second milling (phase b) to reach a thickness equal to 100 mm, and levelling with a grader (**Figure 6. 6**d);
- Day 2: first pass of the recycler to mix the subbase layer for a depth of 300 mm. This allowed obtaining an aggregate blend composed by one third of RA and two thirds of RAg (**Figure 6. 6**e and **Figure 6. 7**a). During this operation hydrated lime

was added, with a dosage of 10 kg/m$^2$, in order to reduce the plasticity of RAg. Then, the layer was levelled with a grader and compacted with a vibrating smooth-drum roller, to obtain an adequate support for the wheels of the recycler;

- Day 3: spreading of cement using a vehicle equipped with a volumetric batcher (**Figure 6. 6**f);
- Day 3: second pass of the recycler for stabilizing a thickness of 300 mm. During this operation, the layer was treated with foamed bitumen for the first 400 m in longitudinal direction and bitumen emulsion for the following 400 m. The remaining 200 m of the experimental pavement section were not treated with any bituminous binder (**Figure 6. 6**g and **Figure 6. 7**b). The subbase layer was compacted with a 14-tons vibrating smooth-drum roller and a 25-tons pneumatic tire roller (**Figure 6. 7**c);
- Days 4 and 5: paving with three layers of HMA, i.e. base, binder and wearing courses (**Figure 6. 6**h and **Figure 6. 7**d).

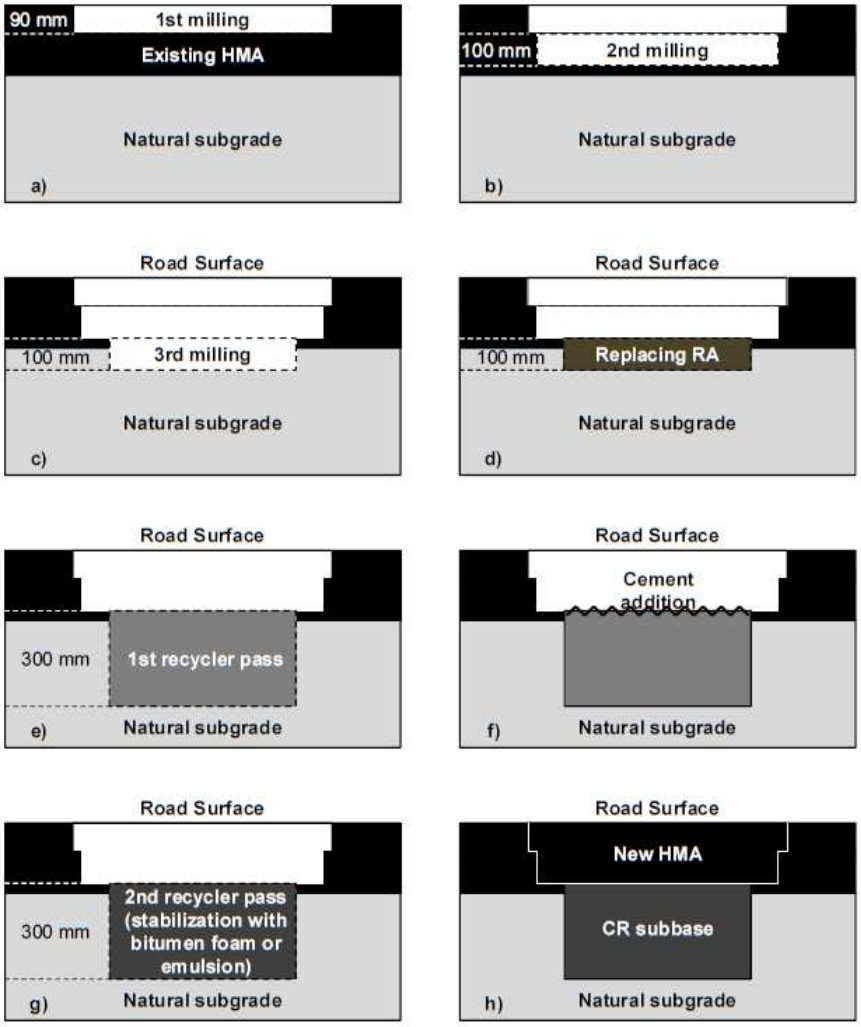


**Figure 6. 6** Construction sequence adopted for the experimental pavement section: a) 1st milling; b) 2nd milling; c) 3rd milling; d) RA replacing e) 1st pass of the recycler; f) Spreading of cement; g) 2nd pass of the recycler for the subbase stabilization; h) Paving with HMA.


**Figure 6. 7** Photos taken during the construction of the experimental pavement section: a) First recycler pass for mixing RA with RAg; b) Subbase stabilization with bitumen emulsion; c) Subbase compaction by means of pneumatic tire roller; d) Laydown of the HMA base layer.

## 6.5 Testing program

### 6.5.1 Laboratory testing

Ten core samples with a nominal diameter of 100 mm were extracted from the experimental pavement section. Specifically, 4 samples were cored from the CBTM-FB sub-section (coded as FB), 3 from the CBTM-BE sub-section (coded as BE) and 3 from the CTM sub-section (coded as CTM).

In the laboratory, each core was sawed in order to obtain two cylindrical specimens: the first specimen included only HMA layers (base course and part of the binder course) whereas the second specimen was obtained from the CRM layer (**Figure 6. 8**). The height of the specimens and their air voids content, measured according to [EN 12697-6], are summarized in **Table 6. 4**. After the volumetric characterization, specimens were air-dried and then capped using a two-component polymer resin. Finally, both specimen sides were polished with a lapping device in order to obtain a perfectly regular and smooth surface.


**Figure 6. 8** Cored samples from the experimental pavement section.

| Mixture type | Specimen ID | Height [cm] | Air voids [%] |
|---|---|---|---|
| CBTM-FB | FB1 | 14.6 | 14.4 |
| | FB2 | 14.5 | 14.7 |
| | FB3 | 14.4 | 9.6 |
| | FB4 | 14.1 | 14.1 |
| CBTM-BE | BE1 | 13.8 | 17.5 |
| | BE2 | 14.0 | 18.9 |
| | BE3 | 14.1 | 18.9 |
| CTM | CTM1 | 14.5 | 13.7 |
| | CTM2 | 14.3 | 14.7 |
| HMA | HMA1 | 11.0 | 7.0 |
| | HMA2 | 11.6 | 9.0 |
| | HMA3 | 11.5 | 7.5 |
| | HMA4 | 12.0 | 7.5 |

**Table 6. 4** Cylindrical specimens for complex modulus testing.

Complex modulus testing was performed on the cylindrical specimens using NAT equipment, in strain controlled mode. A cyclic compression (haversine) axial strain with 30 με amplitude (peak to peak) was applied at six frequencies (20, 10, 3, 1, 0.3, 0.1 and 1 Hz) and four temperatures (0, 15, 35 and 50 °C).
A total of 20 loading cycles were applied at each frequency, and the complex Young's modulus $E^*$ was calculated following the procedure described in Section 5.2.3.

## 6.5.2 FWD testing

The FWD testing protocol adopted throughout this study provided for a loading plate with diameter 300 mm, an impact load of 120 kN and 8 geophones positioned at 0, 200, 300, 600, 900, 1200, 1500 and 1800 mm from the center of the loading plate.
The yearly testing program is summarized in **Table 6. 5** where the average air temperature during the tests and the number of drops for each sub-section (CBTM-FB, CBTM-BE and CTM) are reported. In each survey, the FWD drops were performed approximately every 25 m, on both the right and the left wheelpath (**Figure 6. 9**).

| Inspection date | $T_{air}$ [°C] | FWD drops CTM | FWD drops CBTM-FB | FWD drops CBTM-BE |
|---|---|---|---|---|
| 25/06/2007 | 27 | 10 | 16 | 12 |
| 03/12/2007 | 10 | 14 | 33 | 28 |
| 22/07/2008 | 20 | 14 | 33 | 28 |
| 26/05/2009 | 32 | 22 | 32 | 22 |
| 09/06/2010 | 25 | 12 | 34 | 28 |
| 31/05/2011 | 32 | 12 | 36 | 28 |
| 28/06/2012 | 28 | 12 | 36 | 28 |
| 14/05/2013 | 18 | 12 | 36 | 28 |
| 21/05/2015 | 17 | 6 | 18 | 14 |

**Table 6. 5** FWD – Field investigations program

**Figure 6. 9** Photos taken during the FWD measurements performed on both the right and the left wheelpath.

## 6.6 Experimental findings and analysis

### 6.6.1 Laboratory testing

An example of isothermal curves of the stiffness modulus $E_0$ measured on HMA1, FB2, BE3 and CTM1 is reported in **Figure 6. 10**. For each mixture, stiffness increases when increasing frequency and decreasing temperature. In particular, $E_0$ ranges from 146 MPa to 12856 MPa for HMA1, from 164 MPa to 7700 MPa for FB2, from 1054 MPa to 7770 MPa for BE3 and from 3752 MPa to 9390 MPa for CTM1. Therefore, for all the tested mixtures (HMA, CBTM-FB, CBTM-BE and CTM) frequency (i.e. time) and temperature dependency of $E_0$ is observed.

It can be noticed that the mechanical behavior of the HMA mixtures is very far from that of the CRMs produced with foamed bitumen or bitumen emulsion. This difference is probably due to the higher thermo-dependency of the mixture when the bitumen content increases (bitumen content equal to 4.5% for HMA) and to the presence of cement. Moreover, CTM shows a slightly frequency and temperature dependence, that can be related to both cement

and RA included in the mixture. This behavior of CTM containing RA is also confirmed by previous researches [Grilli et al., 2013a].

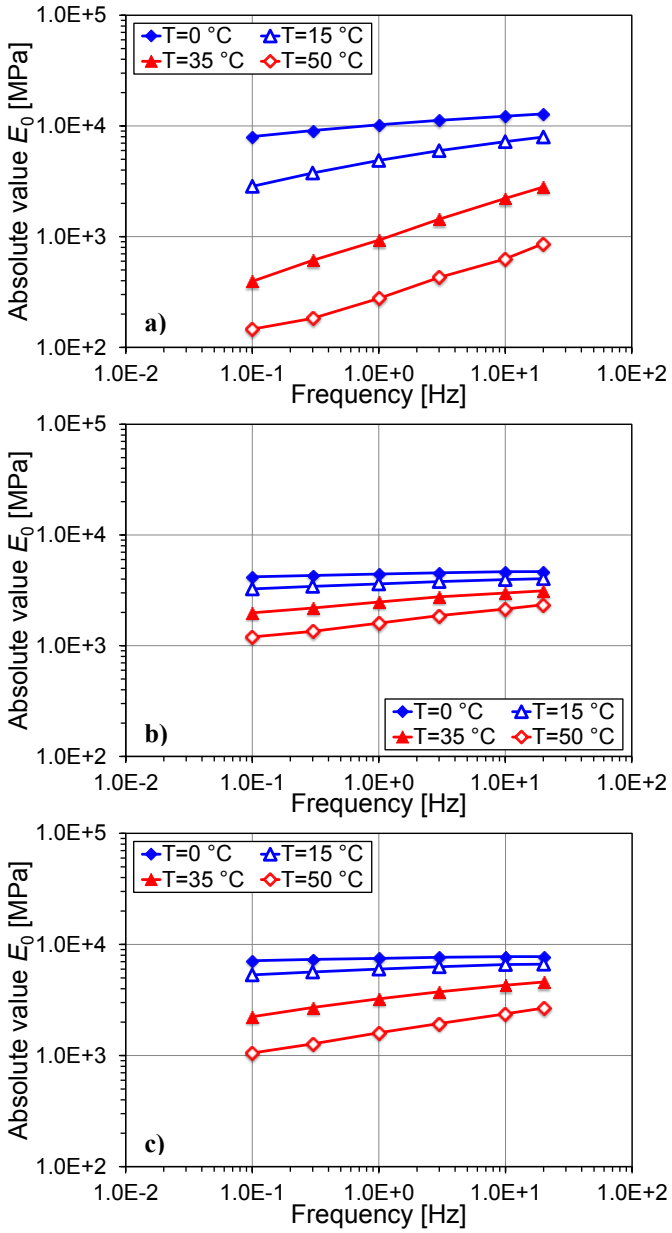

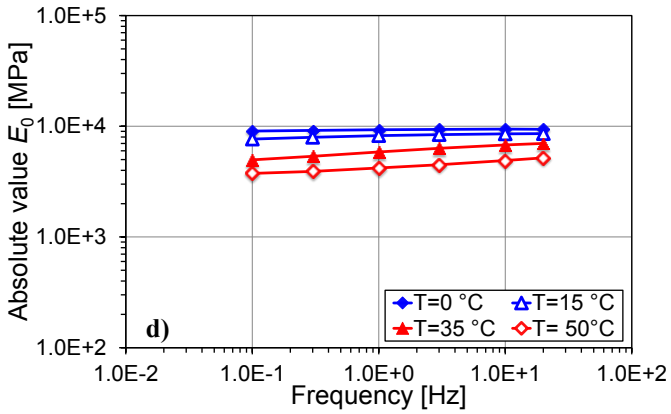


**Figure 6. 10** Isothermal curves of the stiffness modulus ($E_0$) measured on: a) HMA1, b) FB2, c) BE3 and d) CTM1.

For all mixtures, the validity of the time-temperature superposition principle (TTSP) was checked. In addition, the *Huet-Sayegh* (H-S) rheological model [Sayegh, 1967] was employed to fit the experimental data according to the procedure described in Section 5.2.3. In this study, the reference temperature selected for master curves was $T_{ref}$ = 20 °C and the *Williams–Landel–Ferry* (WLF) model was used to fit the temperature dependency of the shift factors [Ferry, 1980] calculated using the fitting procedure also explained in Section 5.2.3. The H-S model parameters obtained from a numerical optimization procedure and WLF model coefficients are summarized in **Table 6. 6**.

**Figure 6. 11** shows master curves of $E_0$ for each tested specimen and it is evident that for both HMA and CRMs, a unique curve could be drawn shifting $E_0$ measurements. This indicates that the TTSP is verified for $E_0$. Moreover, **Figure 6. 11** also confirms a marked difference between the mechanical response of HMA and that recorded for CRMs. In fact, the slope of HMA master curve is higher than the one registered for CRMs highlighting the clear thermo-dependency of HMA mixture.

As it can be observed from **Table 6. 6**, the gap between $E_e$ and $E_g$ estimated for HMA is similar for all the tested specimens and about two orders of magnitude. However, $E_e$ and $E_g$ values exhibit some fluctuations probably related to the volumetric properties of the tested specimens.

Another trend can be noticed for the CTM mixture, where a gap of one order of magnitude, between $E_e$ and $E_g$, is registered (**Table 6. 6**). This result promotes a flat shape of master curves drawn for CTM confirming the slight thermal susceptibility of the material [Grilli et al., 2013a], exclusively due to the RA amount included in the mixture.

The mechanical response of CBTM-FB and CBTM-BE is somewhere between that measured for HMA and CTM (**Table 6. 6** and **Figure 6. 11**). Master curves drawn for these materials are very similar to those obtained for CTM, validating the typical cement-like behavior (i.e. low frequency and thermo-dependent) usually detected for CRMs with bitumen/cement (B/C) ratio around 1 [Grilli et al., 2012]. In particular, the CBTM-FB shows a reduced thermo-dependency even if it is characterized by a higher bitumen content with respect to that adopted for CBTM-BE (3% and 1.8% respectively).

The $h$, $k$ and $\delta$ parameters of H-S model calculated for CRMs are always lower than those identified for HMA. This finding is probably due to the presence of cement in the mixture, even if it is used in small percentages (1.75% for CBTM-FB, 2% for CBTM-BE and 3% for CTM).
The similarity between the mechanical response of FB1 and HMA is the proof of the inhomogeneity that can affect the construction operations of the subbase layer (binder dosage and compaction phase).

| Specimen ID | $E_g$ MPa | $E_e$ MPa | $k$ - | $h$ - | δ - | log $\tau_{Ref}$ - | $C_1$ - | $C_2$ - |
|---|---|---|---|---|---|---|---|---|
| FB1 | 9946 | 100 | 0.227 | 0.488 | 3.275 | 1.47 | 18.2 | 149.8 |
| FB2 | 7010 | 30 | 0.002 | 0.180 | 0.361 | 1.10 | 19.5 | 154.1 |
| FB3 | 20111 | 591 | 0.003 | 0.193 | 0.364 | 1.46 | 32.6 | 224.7 |
| FB4 | 11541 | 37 | 0.033 | 0.227 | 0.359 | 1.36 | 10.1 | 69.8 |
| BE1 | 11829 | 55 | 0.007 | 0.231 | 0.320 | 1.33 | 15.8 | 115.5 |
| BE2 | 12245 | 44 | 0.015 | 0.197 | 0.370 | 1.36 | 17.4 | 117.9 |
| BE3 | 10520 | 120 | 0.009 | 0.251 | 0.358 | 1.37 | 19.0 | 130.6 |
| CTM1 | 9833 | 3104 | 0.086 | 0.298 | 0.418 | 3.45 | 12.9 | 66.2 |
| CTM2 | 9389 | 3819 | 0.099 | 0.261 | 0.482 | 3.07 | 8.6 | 70.4 |
| HMA1 | 15183 | 89 | 0.238 | 0.535 | 1.850 | 0.20 | 16.2 | 130.0 |
| HMA2 | 10620 | 75 | 0.165 | 0.550 | 1.400 | 0.13 | 10.0 | 78.4 |
| HMA3 | 17795 | 114 | 0.127 | 0.472 | 1.153 | 0.24 | 20.8 | 168.3 |
| HMA4 | 18800 | 37 | 0.246 | 0.534 | 1.872 | 0.47 | 16.4 | 119.6 |

**Table 6. 6** Huet-Sayegh and WLF model parameters for the tested specimens ($T_{ref}$ = 20 °C).

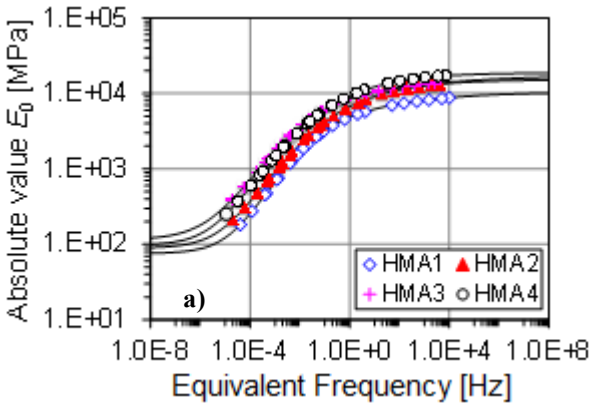

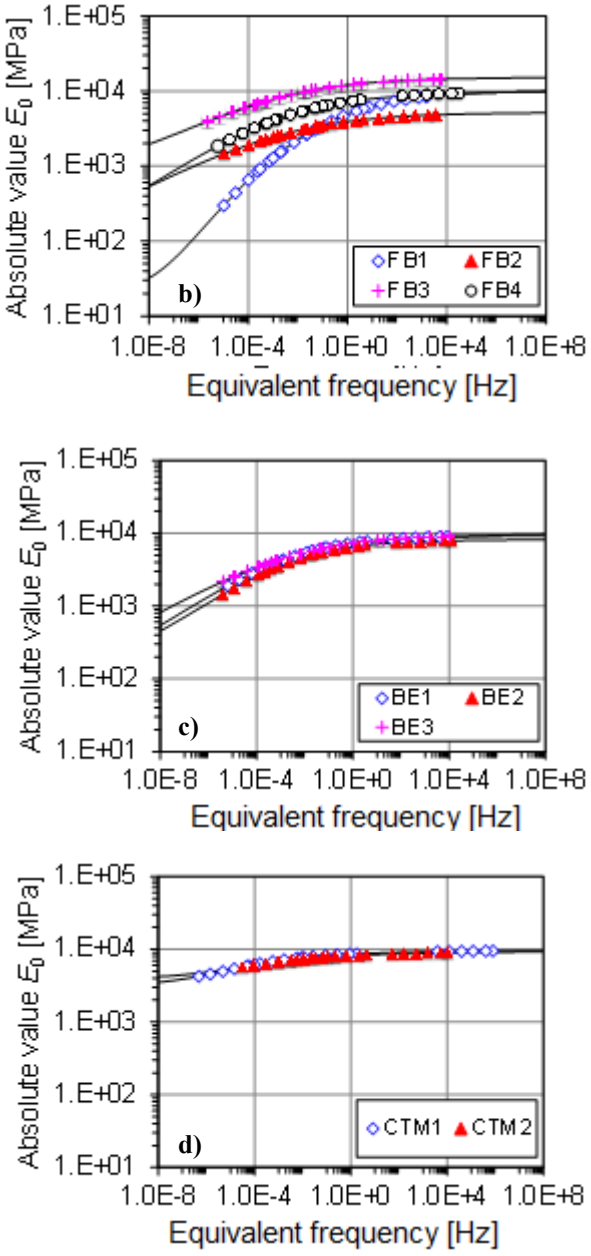


**Figure 6. 11** Master curves of the stiffness modulus E0 at 20 °C: a) HMA specimens, b) FB specimens, c) BE specimens and d) CTM specimens.

In **Figure 6. 12**, $E_0$ values are shifted to the reference frequency of 10 Hz and a second order polynomial regression is drawn in the semi-logarithmic plane. The resulted isochronous curve describes the relationship between the temperature and the logarithm of the stiffness modulus:

$$\log E_0(T) = a \cdot T^2 + b \cdot T + c \tag{25}$$

$$T(f) = a_{\text{fref}}(f) \cdot T_{\text{ref}} \tag{26}$$

where $T$ and $T_{\text{ref}}$ are the FWD test temperature and the reference temperature expressed in degree Celsius respectively, $a_{\text{fref}}(f)$ are the frequency shift factors used to describe the time dependence of $E_0$ at the reference frequency $f_{\text{ref}}$ and $f$ is the testing frequency. The $a$, $b$ and $c$ are the experimental constants estimated using a linear regression procedure, for each type of mixture. The calculated values of the regression parameters are summarized in **Table 6. 7**.

The coefficients of the regression are linked to the *thermal sensitivity* of the investigated mixtures and can be applied to correct back-calculated stiffness moduli obtained from FWD surveys [CROW, 1998]. As it can be observed, the influence of the temperature is higher for HMA and decreases moving from HMA to CBTM-FB and CBTM-BE. In addition, the mechanical response of CTM is only slightly affected by the temperature because of the RA content included in the mixture [Soleymani et al., 2000].

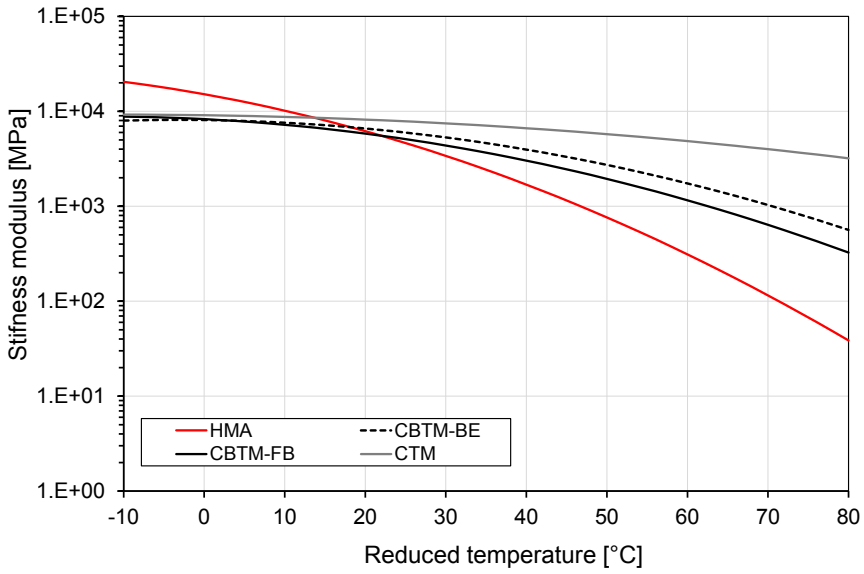


**Figure 6. 12** Isochronous master curves at the reference frequency of 10 Hz for HMA, CBTM-FB, CBTM-BE and CTM.

| | *a* | *b* | *c* |
|---|---|---|---|
| HMA | -0.000216 | -0.015190 | 4.180935 |
| FB | -0.000166 | -0.004270 | 3.918198 |
| BE | -0.000167 | -0.001083 | 3.908451 |
| CTM | -0.000056 | -0.001174 | 3.959360 |

**Table 6. 7** Regression parameters of the isochronous master curves, at the reference frequency of 10 Hz.

## 6.6.2 FWD testing

In this section the results of the FWD test surveys are presented and analyzed. First, raw deflection measurements are considered, because they allow to get a global overview of the pavement response variations, both among the three subsections (i.e. among the three CRMs) and throughout the 8 years of FWD inspections. Then, the back-calculated layer moduli are presented and corrected in order to take into account the effect of the testing temperature. The temperature correction is based on the results obtained from the laboratory tests.

*Deflection measurements*

The first parameter considered in the analysis is the deflection measured at the center of the FWD loading plate $D_0$, i.e. the central deflection. **Figure 6. 13** reports the central deflection profiles measured in June 2007, one month after the rehabilitation operations, and in December 2007, i.e. after 6 months. These surveys were performed to evaluate the mechanical properties of the rehabilitated road section and to verify the quality of the construction operations.

As it can be observed, the central deflections measured in June 2007 ranged from 350 to 500 μm and are consistently higher than those measured in December 2007, which range from 200 to 300 μm. Such a reduction is clearly due to an overall increase in stiffness of the pavement layers that can be attributed to two main causes: the decrease of temperature (the air temperature was 27 °C in June and 10 °C in December) and the curing of CRM. It can be hypothesized that the first cause had an effect mainly on the HMA layers, because of their greater thermal susceptibility with respect to CRM layers (described in Section 6.6.1). On the other hand, curing of CRM was the result of both moisture loss and hydration of cement [Graziani et al., 2016a]. However, since the two causes have similar effects, it is not possible to separate the effect of temperature from the effect of curing.

**Figure 6. 14** reports the central deflection profiles measured throughout the 8 years of inspections. Although these deflection profiles allow to get a global overview of the response variations among the different subsections, and thus among the different CRMs, they do not allow to draw a clear picture of the evolution over time for the pavement behavior. Based on a simple visual classification, three groups of deflection profiles can be identified:

- The first group includes the profiles measured in June 2007 (27 °C), May 2009 (32 °C) and May 2011 (32 °C); for this group the highest deflections were measured;

- The second group includes the profiles measured in December 2007 (10 °C), May 2013 (18 °C) and May 2015 (17 °C); for this group the lowest deflections were measured;
- The third group includes the profiles measured in July 2008 (20 °C), June 2010 (25 °C) and June 2012 (28 °C); for this group the deflection profiles are comprised between the two group of profiles previously identified.

As it can be observed, except for the profile measured in June 2012, the effect of temperature apparently prevails on other possible causes of variation, in particular over the damage due to vehicular traffic and stiffening due to aging of bitumen. In order to remove, at least in part, the effect of temperature, the average deflection measured in each subsection was shifted to a reference temperature of 20 °C, by using the equation proposed in [Chen et al., 2000]:

$$D_0(20\ °C) = (1.3052 - 0.152 \cdot T_{\mathrm{FWD}}) \cdot D_0(T_{\mathrm{FWD}}) \tag{27}$$

where $D_0(20\ °C)$ and $D_0(T_{\mathrm{FWD}})$ are the central deflection measured at 20 °C and at the testing temperature $T_{\mathrm{FWD}}$ respectively.
The average and standard deviation values of the normalized central deflections are reported in **Table 6. 8**. It can be observed that, during the considered 8-years period, the average value shows a decreasing trend, suggesting an overall stiffness increase for all subsections. Whatever the cause of such an increase (bitumen aging, post-compaction due to traffic or curing) it can be stated that it prevails on mechanical damage due to the vehicular traffic. Moreover, on a year-by-year basis, the CBTM-FB subsection is always characterized by lower deflections with respect to both CBTM-BE and CTM subsections. In addition, after 2010 the CBTM-BE subsection always shows the highest deflections.

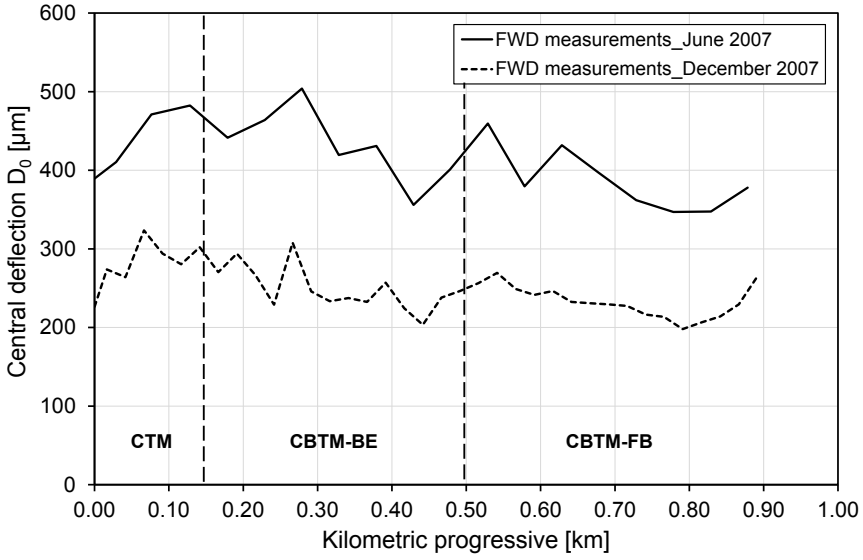

**Figure 6. 13** Central deflections profiles D0 measured in June 2007, one month after the rehabilitation operations, and in December 2007, i.e. after 6 months.

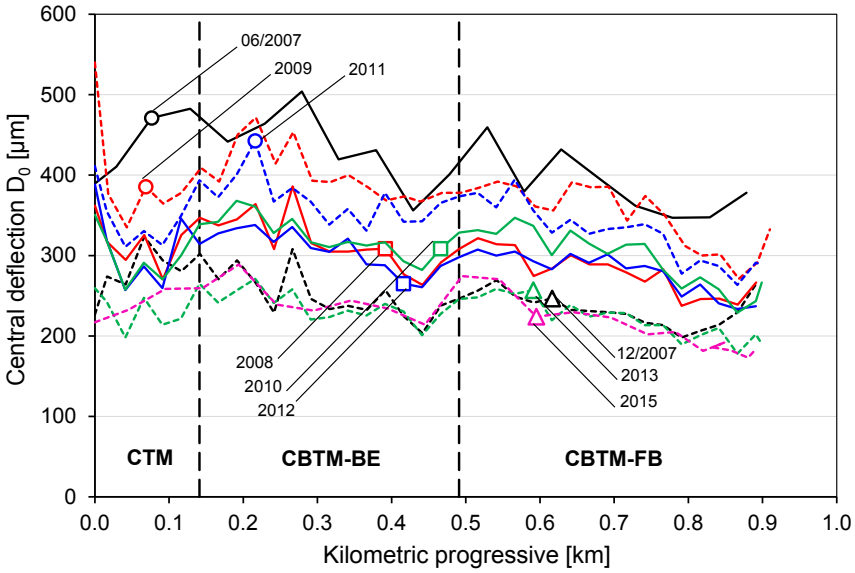


**Figure 6. 14** FWD central deflections recorded during 8 years of FWD inspections, from June 2007 to 2015.

| Inspection date | T | CTM | | CBTM-FB | | CBTM-BE | | RANKING | | |
|---|---|---|---|---|---|---|---|---|---|---|
| - | - | Avg. Value | Std Dev. | Avg. Value | Std Dev. | Avg. Value | Std Dev. | CTM | CBTM -FB | CBTM -BE |
| | [°C] | [µm] | [µm] | [µm] | [µm] | [µm] | [µm] | - | - | - |
| 25/06/2007 | 20 | 426 | 38 | 376 | 39 | 417 | 50 | 3 | 1 | 2 |
| 03/12/2007 | 20 | 320 | 37 | 270 | 23 | 292 | 36 | 3 | 1 | 2 |
| 22/07/2008 | 20 | 316 | 31 | 280 | 27 | 319 | 34 | 2 | 1 | 3 |
| 26/05/2009 | 20 | 325 | 59 | 286 | 33 | 330 | 27 | 2 | 1 | 3 |
| 09/06/2010 | 20 | 286 | 48 | 259 | 23 | 284 | 23 | 3 | 1 | 2 |
| 31/05/2011 | 20 | 282 | 30 | 268 | 31 | 303 | 24 | 2 | 1 | 3 |
| 28/06/2012 | 20 | 262 | 30 | 262 | 31 | 285 | 22 | 2 | 1 | 3 |
| 14/05/2013 | 20 | 238 | 24 | 229 | 25 | 246 | 20 | 2 | 1 | 3 |
| 21/05/2015 | 20 | 247 | 22 | 220 | 35 | 256 | 25 | 2 | 1 | 3 |

**Table 6. 8** Average values and the corresponding standard deviation calculated on the central deflections for 8 years of FWD inspections.

A better overview, focused on the subbase layer, can be drawn using the base damage index (BDI); this parameter is more representative for analysing layers placed at the depth of the

subbase. The BDI parameter is calculated from the difference between the deflections measured at 300 mm and 600 mm from the loading plate.

**Figure 6. 15** shows evolution over time, from 2007 to 2015, of the BDI profiles, without any additional temperature correction. Subbase layers, built in the lower part of a pavement structure, should be characterized by a lower temperature affect but as in this case, some variations could occur depending on the thermal susceptibility of the material used in the subbase layer [Chen et al., 2000; Straube and Jansen, 2009].

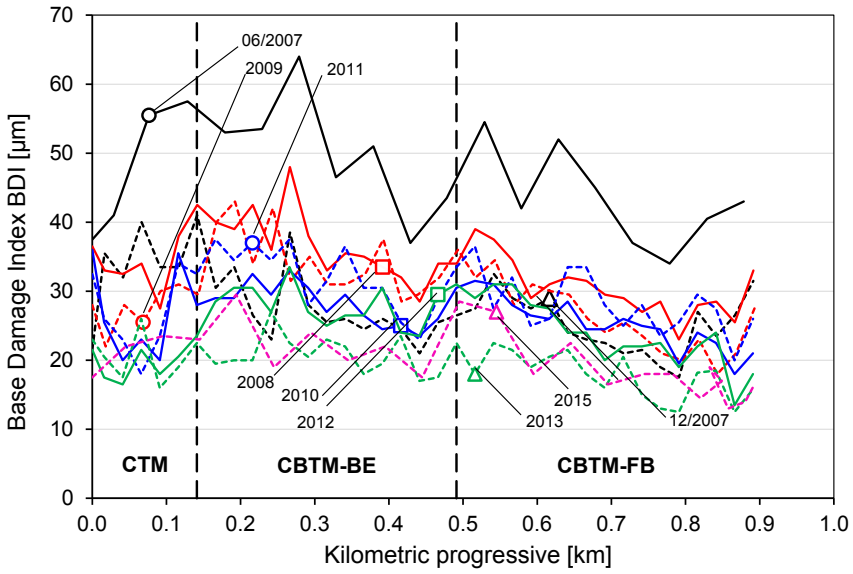


**Figure 6. 15** BDI calculated on $D_{300}$ and $D_{600}$ for 8 years of FWD inspections.

The BDI parameter analysis did not allowed establishing a clear ranking of the three different CRMs in terms of mechanical response. In fact, considering annual records, the BDI parameter ranged from 15 to 58 µm along the field section; this implied that no evident differences can be reported over time and analyzing the three different CRMs. A unique exception was observed with BDI parameters calculated on June 2007 (**Figure 6. 15**), they are characterized by the highest values registered within a period of 8 years. This phenomenon can be due to the curing process of the subbase layer, which was not completely achieved one month after the construction operations.
Both analysis carried out with FWD central deflections $D_0$ (single values and the corresponding average value) and using the BDI parameter proved to be not suitable to accurately evaluate the evolution of the mechanical behavior of the subbase layer over time. In particular, the influence of temperature strongly affects each type of analysis and thus the previous interpretations are useful only to develop a first relative comparison among the different CRMs, but do not allow gaining an absolute judgment of their mechanical performance over time.

*Back-calculation of layer moduli and temperature correction*

The stiffness moduli of the HMA and CRM layers were back-calculated from the measured FWD surface deflections [CROW, 1998] using the BAKFAA software code, developed under the sponsorship of the FAA Airport Technology Branch (see Section 5.1.3) [AC 150/5370-11B]. The pavement structure was modeled as a two-layered system (190 mm of HMA + 300 mm of CRM), resting on the subgrade (infinite depth). The value of the Poisson's ratio was set at 0.35 for all materials except the CTM, for which the value 0.15 was assumed. In addition, full friction was set at all interfaces.

The back-calculation procedure is reported in Section 5.1.3.

It is important to remark that, similar to the measured central deflections, the back-calculated layer moduli are temperature dependent. In fact, when tested in the laboratory, the stiffness of all mixtures showed a variable degree of thermal dependence that is modeled using Equation 28. Therefore, in order to translate all the back-calculated moduli from the temperature of the FWD testing survey ($T_{\mathrm{FWD}}$) to the reference temperature ($T_{\mathrm{ref}} = 20\ °C$), the following correction coefficient $\beta_{\mathrm{i}}$ was employed:

$$\beta_{\mathrm{i}} = \frac{E_{0,i}\,(T_{\mathrm{FWD}})}{E_{0,i}(T_{\mathrm{ref}})} \tag{28}$$

where $E_{0,i}$ are the isochronous master curve moduli (**Table 6. 7**) calculated at the FWD testing temperature $T_{\mathrm{FWD}}$ and at 20 °C (the reference temperature) for each material and $i =$ HMA, CBTM-FB, CBTM-EM, CTM.

The values of the parameters $\beta_{\mathrm{i}}$ calculated for each type of mixture, are reported in **Table 6. 9**. As it can be observed, the higher thermal sensitivity of HMA mixture results in higher values of $\beta_{\mathrm{HMA}}$, with respect to the other mixtures. The values of $\beta_{\mathrm{CBTM-BE}}$ and $\beta_{\mathrm{CBTM-FB}}$ are very similar, whereas the values of $\beta_{\mathrm{CTM}}$ are around 1 since the thermal sensitivity of CTM is very low.

| Inspection Date | Temperature [°C] | $\beta_{\mathrm{HMA}}$ [-] | $\beta_{\mathrm{CBTM-FB}}$ [-] | $\beta_{\mathrm{CBTM-EB}}$ [-] | $\beta_{\mathrm{CTM}}$ [-] |
|---|---|---|---|---|---|
| 25/06/2007 | 27 | 1.504 | 1.210 | 1.155 | 1.063 |
| 03/12/2007 | 10 | 0.607 | 0.808 | 0.869 | 0.936 |
| 22/07/2008 | 20 | 1.000 | 1.000 | 1.000 | 1.000 |
| 26/05/2009 | 31 | 1.941 | 1.381 | 1.276 | 1.108 |
| 09/05/2010 | 24.5 | 1.293 | 1.129 | 1.092 | 1.039 |
| 31/05/2011 | 32 | 2.074 | 1.429 | 1.310 | 1.119 |
| 28/06/2012 | 28 | 1.601 | 1.253 | 1.183 | 1.074 |
| 14/05/2013 | 17.5 | 0.875 | 0.941 | 0.959 | 0.981 |
| 21/05/2015 | 17 | 0.852 | 0.931 | 0.951 | 0.978 |

**Table 6. 9** Coefficients of thermal sensitivity $\beta$ calculated for all mixtures and FWD surveys.

The back-calculated stiffness moduli, obtained analyzing the FWD deflection basins and shifted at the reference temperature of 20 °C are summarized in **Table 6. 10**. As it can be noticed, the back-calculated stiffness moduli of HMA are almost constant from 2007 to 2013 and then increase over time; a completely different trend can be observed for CBTM-FB and CBTM-BE where the back-calculated stiffness moduli increase until 2012 and then decrease very fast over time. The trend of back-calculated stiffness moduli estimated for CTM is similar to that recorded with CBTM-FB and CBTM-BE but in this case, the decreasing is observed after 2011.

| Inspection | | HMA | | CBTM-FB | | CBTM-BE | | CTM | |
|---|---|---|---|---|---|---|---|---|---|
| Date | *T* | *E* (T) | *E*(20 °C) | *E*(T) | *E*(20 °C) | *E*(T) | *E*(20 °C) | *E*(T) | *E*(20 °C) |
| - | [°C] | [MPa] | [MPa] | [MPa] | [MPa] | [MPa] | [MPa] | [MPa] | [MPa] |
| 25/06/2007 | 27 | 1995 | 3001 | 1635 | 1986 | 1330 | 1537 | 1072 | 1140 |
| 03/12/2007 | 10 | 6503 | 3950 | 2962 | 2394 | 3576 | 3107 | 1984 | 1857 |
| 22/07/2008 | 20 | 3043 | 3043 | 4195 | 4195 | 3614 | 3614 | 3516 | 3516 |
| 26/05/2009 | 32 | 1594 | 3094 | 4192 | 5789 | 2750 | 3509 | 5089 | 5637 |
| 09/06/2010 | 25 | 2824 | 3650 | 3722 | 4201 | 3585 | 3916 | 5650 | 5869 |
| 31/05/2011 | 32 | 1664 | 3451 | 3512 | 5019 | 4033 | 5285 | 4388 | 4914 |
| 28/06/2012 | 28 | 2071 | 3314 | 4523 | 5667 | 5036 | 5956 | 4036 | 4334 |
| 14/05/2013 | 18 | 4560 | 3988 | 3992 | 3758 | 3749 | 3594 | 3738 | 3668 |
| 21/05/2015 | 17 | 8153 | 6947 | 2558 | 2380 | 3060 | 2910 | 1897 | 1855 |

**Table 6. 10** FWD back-calculated moduli at FWD test temperature and shifted at $T_{ref}$= 20 °C, test surveys from 2007 to 2015.

## 6.7 Pavement performance

In **Figure 6. 16**, the stiffness modulus $E_0$ normalized with respect to its initial value is reported for each investigated mixture, as a function of the inspection date. The HMA and CRMs behave differently over time. In fact, the performance of HMA is almost constant in the first period (from 2007 to 2012) then the stiffness modulus increases; this finding can be related to the stiffening of the upper bituminous layers promoted by the binder aging and by the over-compaction due to the continuous traffic loads. Otherwise, the performance of CRMs is characterized by a heterogeneous trend over time: the stiffness modulus constantly increases over time in the first period (until 2013) then the performance decreases. This observation can be due to the deterioration of the subgrade (**Figure 6. 16**).
Finally, considering the results carried out on CRMs, the best FDR technique can be identified:

- CTM achieved the higher decreasing rate of the back-calculated moduli during the period of 8 years;

- CBTM-BE is characterized by a fast increase of the mechanical response until 2013 and then decreases as CTM;
- the performance of CBTM-FB increases slowly until 2013 and subsequently decreases but its behavior exhibits more fluctuations over time reaching a lower maximum stiffness modulus with respect to CBTM-BE.

In addition, **Figure 6. 12** highlights that the isochronous master curves, developed using laboratory results, are always above the back-calculated stiffness moduli at the reference temperature of 20°C perhaps because the measurements carried out during FWD surveys could be less accurate with respect to laboratory testing results.

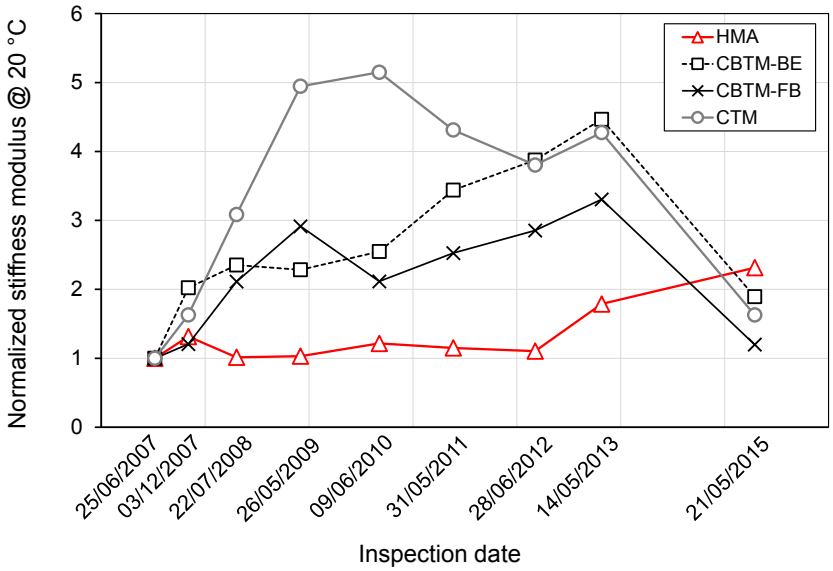


**Figure 6. 16** The mechanical performance of HMA, CBTM-FB, CBTM-BE and CTM during a period of 8 years in terms of stiffness modulus $E_0$, normalized with respect to its initial value.

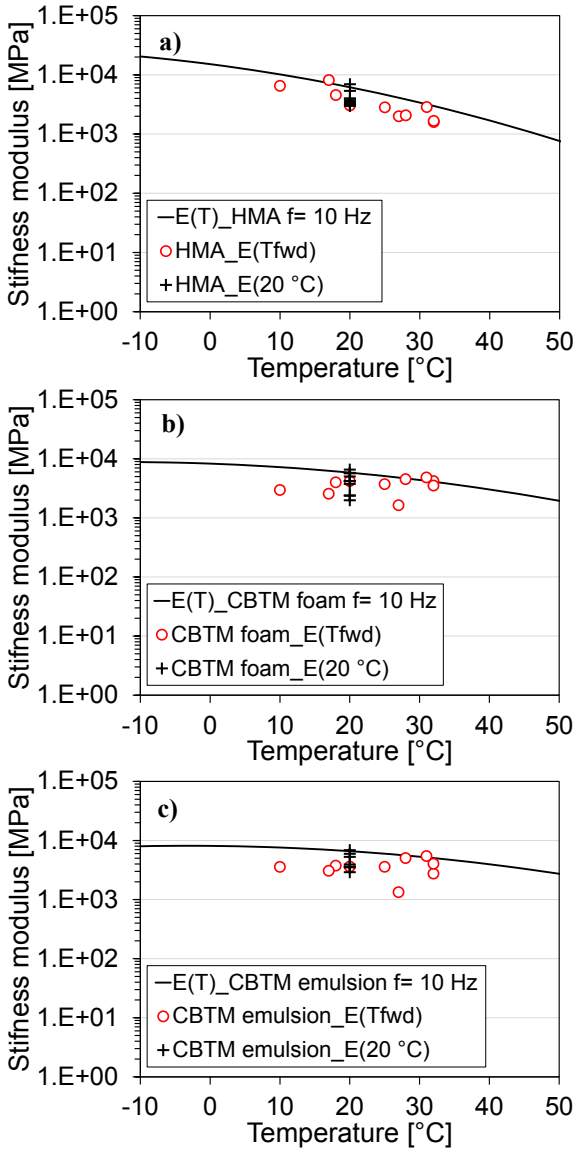
a)
Stifness modulus [MPa]
1.E+05
1.E+04
1.E+03
1.E+02
1.E+01
1.E+00
-10
0
10
20
30
40
50
Temperature [°C]
—E(T)_HMA f= 10 Hz
HMA_E(Tfwd)
+HMA_E(20 °C)
b)
Stifness modulus [MPa]
Temperature [°C]
—E(T)_CBTM foam f= 10 Hz
CBTM foam_E(Tfwd)
+CBTM foam_E(20 °C)
c)
Stifness modulus [MPa]
Temperature [°C]
—E(T)_CBTM emulsion f= 10 Hz
CBTM emulsion_E(Tfwd)
+CBTM emulsion_E(20 °C)

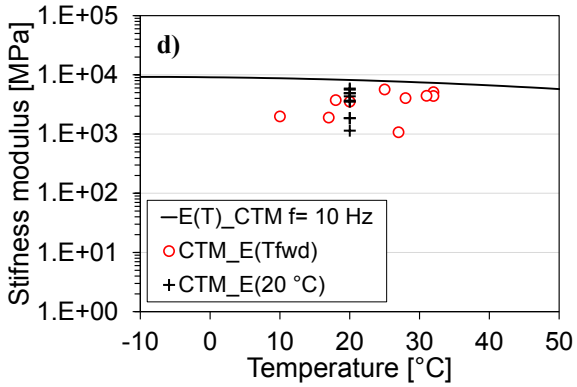


**Figure 6. 17** Isochronous master curves at 10 Hz and back-calculated moduli for a) HMA, b) CBTM-FB, c) CBTM-BE and d) CTM.

Finally, the combination of the monitoring of the mechanical response over time (**Figure 6. 16**) and the isochronous master curves (**Figure 6. 17**) is helpful to predict and evaluate the performance of the investigated materials.

## 6.8 Summary

The experimental study described in this chapter aimed to compare different FDR techniques, as well as different type of CRMs, where the use of cement and bitumen emulsion or foamed bitumen as binding/stabilizing agents is combined.
Annual falling weight deflectometer surveys were performed in order to monitor the application of FDR in an experimental pavement section over time. Moreover, core samples were extracted from the pavement with the aim to characterize the mechanical behavior of each CRM. Basing on complex modulus testing and thermo-rheological modelling, the time-temperature dependency of each mixture was identify.

Concerning non-destructive testing carried out in field, FWD surveys have been inadequate to drawn a precise evaluation on the mechanical behavior of the investigated CRMs because to many factors affect deflection measurements and among them, temperature plays a fundamental role. If the average central deflection shifted at the reference temperature of 20 °C has been analyzed, a practical classification of CRMs performance can be obtained. CBTM-FB shown the lower average central deflection over time but this observation does not provide an absolute judgment yet.
Laboratory testing by means the measurement of stiffness modulus provided a useful procedure to estimate the temperature-dependency of each mixture. In particular, HMA exhibited a marked thermo-dependency (asphalt-like behavior) while CTM showed a mechanical response slightly influenced by temperature (cement-like behavior). In this context, TTSP has been validated for $E_0$. In addition, measurements of stiffness modulus were analyzed to develop isochronous master curves at the reference frequency of 10 Hz, in order to estimate the influence of the temperature on the mechanical behavior and to shift the back-calculated moduli at the reference temperature of 20 °C.

Finally, in order to classify the best FDR technique evaluating the mechanical performance of the investigated CRMs, it is possible to conclude that CBTM-BE mixture better preserves its mechanical properties over time. On the contrary, CTM mixture exhibited the higher level in deterioration rate over time.

# CHAPTER 7.

## Evaluation of *in-situ* performance for road pavements using instrument installation.

*Curing* is the process in which a material (cold mixture) develops strength and stiffness over time though moisture loss (see Section 2.9).
Immediately after mixing and compaction, both in a laboratory or in a field, the strength and stiffness of a cold mixture is relatively low. Curing takes place under certain external conditions (humidity, temperature, compaction level, ecc…) and, in the field, curing continues typically up to 6 – 18 months. With time, moisture content in the mixture decreases and consequently the strength and stiffness increase.
In any case, the field curing times are too long for laboratory mix design purposes. When specimens are to be tested at equilibrium field moisture content, the laboratory curing process needs to be accelerated.
Understanding the curing mechanism of cold mixtures, which is a multi-phase material, entails obtaining insights into the strength development mechanisms of each phase, the interaction between these phases, and the effects of external conditions.

In order to characterize curing mechanism of cold mixtures, is necessary:

- Developing standard laboratory curing procedures to represent field conditions;
- Developing field construction procedures to accelerate early strength development and to optimize for long term (performance at the same time.

The effects of different curing conditions have been documented by many researchers. However, laboratory curing procedures reported in the literature are far from being standardized. At the same time, construction practices are largely empirical and based on common practices, which may not result in optimal performance for cold mixtures.

The research work discussed in Chapter 7 covers a subtask of a comprehensive research program on the in-situ evaluation of curing process on two different cold recycled mixtures (CRMs) produced using full depth reclamation technique.
In particular, cement-treated material (CTM) and cement-bitumen treated material (CBTM) produced with bitumen emulsion were used as subbase layer and advanced instruments (such as time domain reflectometer probes; TDR) were installed inside the layer in order to monitor the moisture loss over time under field curing conditions.

In addition, both CTM and CBTM mixtures were collected from the field and cured in laboratory under fixed curing conditions in order to compare and verify both curing procedures (field and laboratory). Laboratory testing were also performed with the aim to investigate stiffness and strength properties of the investigated CTM and CBTM mixtures.

# 7.1 Field equipment

## 7.1.1 Time domain reflectometer

The measurement of water content in the natural subgrade is a fundamental aspect that should be taken into account not only during road construction operations.
Many hydraulics and mechanical properties are strictly related to the water content in natural subgrade. In addition, water content is not constant bur fluctuates because particularly influenced by seasonal effects and rainfall.
Water content (or moisture content) that characterized the natural subgrade in field or a laboratory specimen, can be described using gravimetric and/or volumetric parameters.

In one hand, the determination of water content $w$ considering the gravimetric approach can be carried out on a subgrade sample and it is the ratio between its wet mass $m_w$ and that in dry conditions $m_d$ ,as follow:

$$w = \frac{m_w}{m_d} \tag{29}$$

In other hand, regarding the volumetric approach the water content $\mu$ can be defined as the ratio between the volume occupied by water $V_w$ in a subgrade/soil sample and the corresponding total volume of the sample $V_s$.

$$\mu = \frac{V_w}{V_s} \tag{30}$$

Both two expressions of water content (in gravimetric and volumetric terms) can be correlated each other using the apparent density of the soil $\rho_s$, that represents the ratio between the wet mass of the sample $m_w$ and its corresponding total volume $V_s$:

$$\rho_s = \frac{m_w}{V_s} \tag{31}$$

Using the apparent density of the soil and the water density $\rho_w$, the water volumetric content $\mu$ is:

$$\mu = w \cdot \frac{\rho_s}{\rho_w} \tag{32}$$

In literature, many technologies are available to measure the water content and can be classified according to the approach adopted as:

- Direct method, using samples collected from the field and then dried in order to determine wet and dry mass of the sample;
- Indirect method, where the water content is estimated using physical and chemical properties of the subgrade/soil. These measurements can continue over the time by means instruments installed inside the pavement layers.

One of the most known indirect methods provide the measurement of water content using the *time domain reflectometry* (TDR) technologies [Topp et al. 1980]: water content is defined determining the characteristics of electrical lines through the observation of reflected waveforms.
In soil field, this technology is enable to measure the elapsed time required by an electromagnetic waveform to propagate along a stainless steel rod placed in the subgrade basing on the dieletric properties of the material.
The dielectric permittivity ($\delta$) is a feature that described how an electric field is influenced by a dielectric medium.
Topp, during his experience, tried to correlate the permittivity and the water content of soils using water content reflectometer (WCR) probes.

WCR methodology guarantees the measurement of water content using the permittivity properties of soil located between the two stainless steel rods and detect changes in moisture by recording changes in the dielectric constant of materials.

Bearing in mind that water is characterized by a high permittivity and that the water content can vary in the subgrade, TDR probes can be adopted in order to estimate the volumetric water content in the subgrade/soil.
A schematic representation of TDR probe is reported in **Figure 7. 1**.

**Figure 7. 1** TDR probe Mod. CS616.

The TDR probes used in this research is CS616 model (provided by Campbell Scientific) and consists of two stainless steel rods connected to a printed circuit board, which is encapsulated in plastic. The rods are 30 mm long and 3.2 mm in diameter. They are parallel and are separated by a distance of approximately 300 mm.

High-speed electronic components on the circuit board are configured as a multi vibrator. Output from the multi vibrator is transmitted to the rods, which then act as vibration wave guides. The travel time for waves along the rods is dependent on the dielectric constant of the materials surrounding the rods. Readings are affected primarily by material that is between the rods; the effective radius of influential materials can be considered as approximately 300 mm. Typical accuracy for these probes is ±2.0 percent moisture by volume if the probes are calibrated for a specific soil [Campbell Scientific, Inc. 2012].

The laboratory calibration procedure is reported in Chapter 8.

## 7.1.2 Temperature probes

Temperature probe is necessary to monitor the temperature after the installation in field. The instrument adopted in this research is a thermistor, Mod. 108 provided by Campbell Scientific (**Figure 7. 2**) .A thermistor is a type of resistor whose resistance is dependent on temperature, more so than in standard resistors. Typical tolerance of these probes is ±0.7 °C in the range from -5 to 95 °C. Generally, temperature probes require a calibration in order to avoid deviation errors but in an experimental pavement section where a temperature accuracy of ±1.0 °C is required, a laboratory calibration is not essential.

**Figure 7. 2** Thermistor Mod.108.

## 7.1.3 Data Acquisition Hardware

The CR1000 Datalogger, AM 16/32 Multiplexer and battery pack are provided by Campbell Scientific in order to collect electrical signals from the TDR and temperature probes and convert them in permittivity and temperature data. A solar panel SP10 recharges the battery pack during daylight hours.
Additionally, a kit CS-GSM/GPS combined with COM110 modem is mounted to transmit the slow speed data wirelessly from the roadside to the research station.

The final configuration for measuring water content and temperature data in field is shown in **Figure 7. 3**.

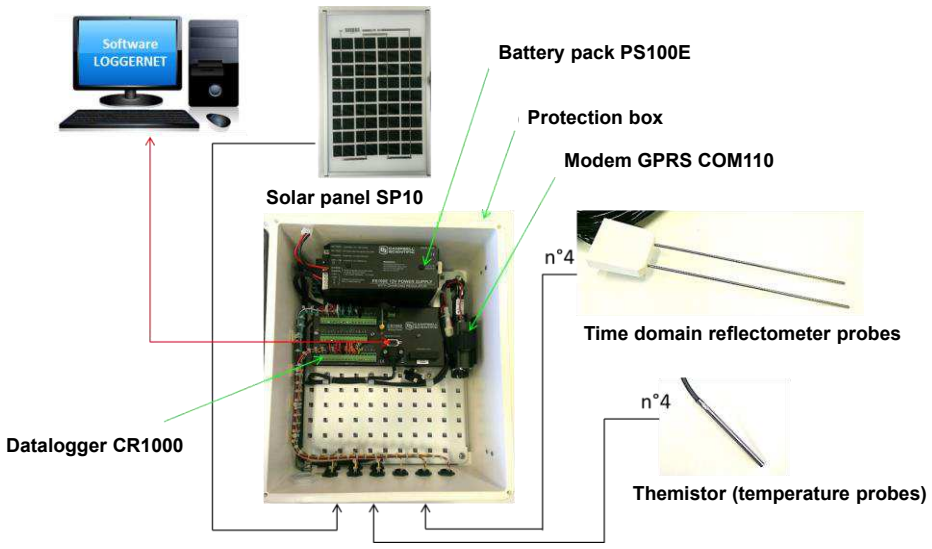


**Figure 7. 3** Configuration for measuring water content and temperature data, Campbell Scientific.

All the information concerning the Software data acquisition is reported in Chapter 8.

### 7.1.4 Earth pressure cell

The role of the earth pressure cell is to measure the dynamic vertical pressures generated under moving loads. As will be explained in next chapter, these gauges were placed at the top of the granular base course and at the top of the subgrade.
The gauges installed in this experiment were Earth Pressure Cells (EPC), Geokon® type 3500, with two different measuring ranges of 0.1 and 1.0 MPa (**Figure 7. 4**). EPCs have a diameter of 230 mm and are equipped with a semiconductor strain gauge transducer. The sensors require an unregulated input of 7–35 VDC and produce a voltage output in the 0–5 V range.

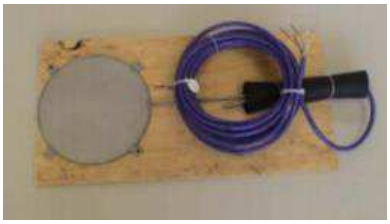

**Figure 7. 4** Geokon Earth Pressure Cell.

### 7.1.5 Asphalt strain gauges

The purpose of asphalt strain gauge installation in the structural experiment is to measure the dynamic strain response at the bottom of the asphalt concrete layer under moving traffic

loads. Asphalt strain gauges Gauges manufactured by Construction Technologies Laboratories (CTL), CTL ASG-152 model, with a measuring base of 200 mm and a range of ±1500 με were installed. The ASG have a full-bridge configuration that requires an excitation up to 10 VDC and produces a full scale output of 2 mV/V. In each subsection two ASG were also equipped with a resistance thermistor for temperature readings. The thermistors have a measuring range from -80°C to 150°C, with an accuracy of 0.5°C. At normal operating temperatures, 0-35°C, the thermistors output is in the 16–33 kOhm range.

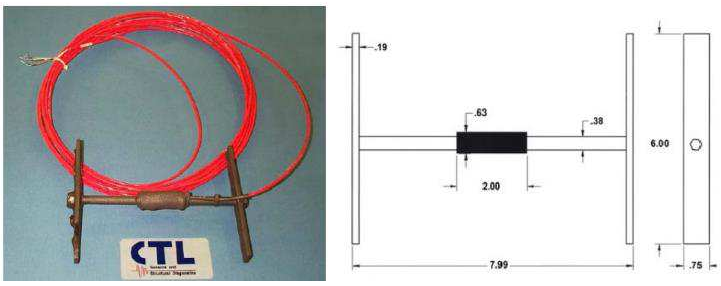


**Figure 7. 5** CTL Asphalt Strain Gauge.

## 7.1.6 Signal conditioning and data acquisition system

For all instruments, signal conditioning, amplification and A/D conversion was carried out using two portable HBM Spider8 units, connected in series to a laptop computer. The HBM Catman Express software was used for data acquisition. Each Spider8 unit is equipped with four digital amplifiers modules (SR55) in 4.8 kHz carrier-frequency technology, suitable for passive transducers, like the ASG, and the DC voltage output of the EPC. The capability of one unit was extended with three DC modules (SR01) suitable for resistance easurements up to 4.0 kOhm.

The data acquisition system was designed to carry out independent measurments in each subsection. Therefore, the Spider8 units are connected to the sensors installed in each subsection in a flexible and efficient manner. For this task, a custom connection board was realized and installed at each subsection, along with custom connection cables. The main system structure in described in **Figure 7. 6**:

- EPC vertical pressure readings were carried out with a SR55 amplifier module, while its excitation was provided by a separate 12 VDC power supply circuit (Spider8 units provide only 1 V excitation voltage);
- the four ASGs were connected to the SR55 modules (4-wires full-bridge circuits).

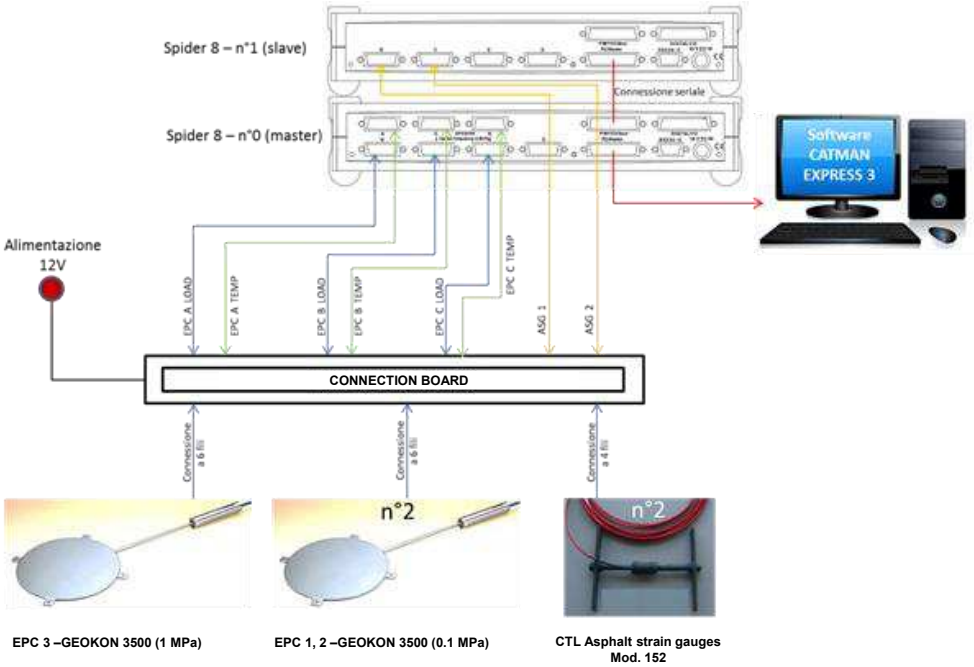


**Figure 7. 6** Data acquisition system layout.

## 7.2 Laboratory equipment, test methods and data analysis

In the following section, the test methods adopted for laboratory specimen compaction and evaluating the physical (moisture content) and mechanical (stiffness and strength) properties of the CTM and CBTM mixtures collected in field are described, along with test protocols and data analysis procedures adopted. A brief description of the test equipment is also provided.

### 7.2.1 Specimens compaction: laboratory procedure using Shear Gyratory Compactor

The Shear Gyratory Compactor (SGC) produces bituminous mixtures specimens simulating the compaction conditions in the field (**Figure 7. 7**).

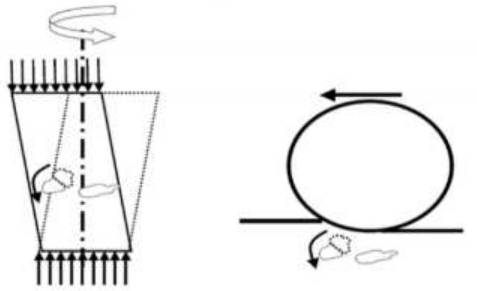

**Figure 7. 7** Comparison between SGC laboratory and field compaction.

According to EN 12697-31, the bituminous mixture specimens are compacted at a constant pressure of 600 kPa, while the upper part of the mould simultaneously rotates around the vertical axis with a constant speed of 30 rpm and a nominal constant angle of 1.25°.
The rotation generates shear stresses in the specimen creating a kneading of the material and facilitating the reorientation of the aggregates.
Knowing the mass and the height of the specimen at each loading cycle, the specimen density can be estimated at each gyration.
The machine is controlled by a specific software which records the vertical pressure, the rotation angle, the specimen height and calculates the corresponding density at each gyration. In this way, an accurate analysis of material compactability and volumetric properties can be evaluated.
The volumetric analysis of compacted specimens (i.e. determination of *VA*, $V_m$ and *VFL*) needs preliminary information achievable through two laboratory tests: theoretical maximum specific gravity (or density) of loose mixtures and bulk specific gravity (or density) of compacted mixtures.
The theoretical maximum specific gravity is the specific gravity of the mixture at zero air voids. Bulk specific gravity gives the specific gravity of the compacted specimen, including air voids within the mixture.
The theoretical maximum specific gravity of a mixture $\rho_m$ was calculated in accordance with the mathematical procedure illustrated in the European standard EN 12697-5 as follows:

$$\rho_m = \frac{100}{P_{agg}/\rho_{agg} + P_B/\rho_B} \quad [\frac{g}{cm^3}] \tag{33}$$

where:
$P_{agg}$ = aggregate percentage by mixture weight [%];
$\rho_{app}$ = aggregate specific gravity, weight average of each single aggregate fractions [g/cm³];
$P_B$ = bitumen percentage by mixture weight [%];
$\rho_B$ = bitumen specific gravity [g/cm³].

Particular attention should be taken with cold mixtures, where the bitumen content comes from bitumen emulsion or foamed bitumen.

The bulk specific gravity $\rho_{app}$ was determined involving weighing the specimen in air and in water in accordance with the European standard EN 12697-6, as described in the procedure "*Saturated Surface-Dry specimens*". The following equation was used:

$$\rho_{app} = \frac{m_1}{(m_3 - m_2)} \times \rho_w \quad (34)$$

where:

$m_1$ = mass of dry specimen in air [g];
$m_2$ = mass of specimen submerged in water [g];
$m_3$ = mass of *Saturated Surface-Dry specimen* in air [g];
$\rho_w$ = water specific gravity at the test temperature [g/cm³].

The bulk specific gravity $\rho_{app}$ , where the aggregate is considered in *saturated surface-dry* condition, is adopted during the calculation of volumetric properties because this situation is more representative of field conditions. In fact, operating with this approach, aggregates are considered saturated with their corresponding value of water absorption (EN 1097-6, see section 2.6.1)

Generally, at each gyration and in the end of compaction process, the volumetric properties (in terms of *VA*, $V_m$ and *VFL*) are evaluated (see section 2.8).
The *VFL* parameter is also adopted to verify the saturation degree achieved by the specimen.

## 7.2.2 Indirect Tensile Stiffness Modulus

After the volumetric analysis, the *Indirect Tensile Stiffness Modulus* (ITSM) was determined in accordance with EN 12697-26 on cylindrical specimens by means of the NAT equipment (see Section 5.2.1). Controlled strain tests were carried out for all the investigated mixtures at 20°C.
The specimen is placed between two stainless steel loading strips. The face in contact with the specimen is concave and shall extend over the full width of the specimen. The edges of the loading strips shall be rounded to avoid cutting the specimen during testing. A means of centralizing the lower platen with the loading axis of the steel load frame is also provided. The upper platen makes contact with the loading system via a spherical seating.
The load actuator applies the stress along the vertical diameter of the specimen via the loading platens. The load has a haversine waveform (**Figure 7. 8**).
The rise-time, measured from when the load pulse commences and which is the time taken for the applied load to increase from zero to maximum value is set up equal to (124 ± 4) ms.

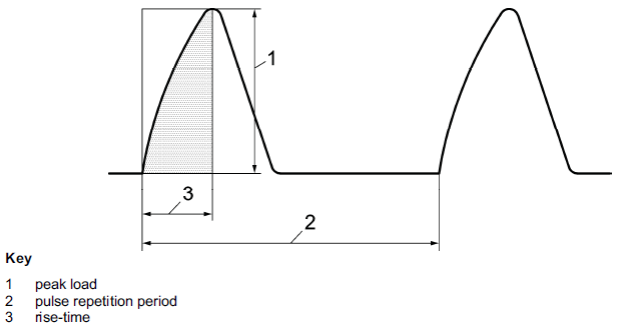


**Figure 7. 8** Form of load pulse, showing the rise-time and the peak (EN 12697-26).

Two Linear Variable Differential Trasducers (LVDTs) are mounted opposite one another in a rigid frame clamped to the specimen. During the test, the frame is only supported by the clamps and it is not in contact with any other part of the equipment They are capable of monitoring the transient horizontal diametral deformation of the specimen during the application of the load pulse. Ten conditioning pulses are applied in order to enable the equipment to adjust the load magnitude and duration to give the specified horizontal diametral deformation and time. After the measurement along a first diameter, the specimen is removed from the test equipment, rotated through (90 ± 10)° about its horizontal axis and replaced in the specimen subframe. The test and calculation are repeated. If the mean value of the stiffness modulus from this test is within +10 % or –20 % of the mean value recorded for the first test, the mean for the two tests is calculated and recorded as the stiffness modulus of the specimen. If the difference between the two values is greater than that specified above, the results are rejected and a third measurement is performed. The measured stiffness modulus is determined for each load pulse using the following formula:

$$S_m = \frac{F \times (\upsilon + 0.27)}{z \times h} \tag{35}$$

where $S_m$ is the measured stiffness modulus, expressed in megapascals (MPa*), F* is the peak value of the applied vertical load, expressed in Newtons (N), $z$ is the amplitude of the horizontal deformation obtained during the load cycle, expressed in millimeters (mm), $h$ is the mean thickness of the specimen, expressed in millimeters (mm); $\upsilon$ is the Poisson's ratio. In this study, the Poisson's ratio was assumed equal to 0,35 for all mixtures. The measured stiffness modulus is then adjusted to a load area factor of 0,60.

## 7.2.3 Indirect Tensile Test

The Indirect Tensile tests were performed on specimens with diameter equal to 150±3 mm (or 50±3 mm) following the European standard EN 12697-23.
The Indirect Tensile test is used to measure the *Indirect Tensile Strength* (ITS) and it is usually performed at 20 °C. A servo-hydraulic testing machine applies a compression force along the two generatrices until the sample reaches the failure. The load was applied with constant rate of deformation of 50 ± 2 mm/min. Assuming a constant distribution of the stress

across the vertical load application plane and considering a continuous load applied, the ITS is calculated as follows:

$$ITS = \frac{2*P_{max}}{\pi*t*d} \quad [MPa] \tag{36}$$

where

$P_{max}$ = maximum force needed to cause failure[N].
$t$ = sample height [mm].
$d$ = specimen diameter [mm].

ITS represents the maximum tensile stress that causes the conventional failure of a cylindrical sample and can be considered as a good indicator of the load transmission capacity of the upper layers (binder and base) to the lower layers (foundation and subbase).

## 7.2.4 Curing process: modelling

In this research, the curing effect on physical (*moisture loss*) and mechanical (*strength and stiffness*) properties of the studied materials, is evaluated using a procedure based on the Michaelis-Menten (MM) model [Michaelis and Menten, 1913]. The MM model is a nonlinear model that describes an asymptotic evolution of the measured response as a function of time (predictor variable), through the evaluation of two parameters:

$$f\left(t,(y_A,K_c)\right) = \frac{y_A \cdot t}{K_c + t} \tag{37}$$

where $y_A > 0$ is the *asymptotic value* of the response (when $t \longrightarrow \infty$, i.e. *long-term* condition) and $K_c > 0$, also known as the *Michaelis constant*, represents the curing time when the response is equal to $y_A/2$ (**Figure 7. 9**). It is underlined that, because of their physical meaning, both $y_A$ and $K_c$ are restricted to positive values and thus Equation 37 defines a concave rectangular hyperbola through the origin.
At the beginning of curing ($t = 0$), the MM model predicts a zero value for the considered curing variables. As curing time increases, the response asymptotically approaches the long-term value $y_A$. The Michaelis constant $K_c$ is used as a measure of the *initial curing rate*: a lower $K_c$ value means a faster increase in the investigated curing variables.

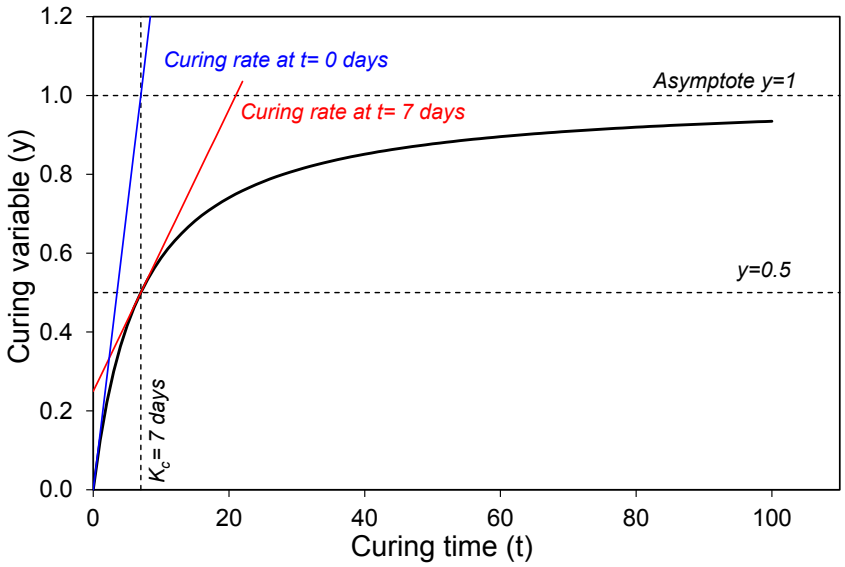


**Figure 7. 9** Michaelis-Menten model**:** an example with $y_A$= 1 and $K_c$ = 7 days.

In addition, the curing rate can be also estimated using the slope of the MM curve, in particular the larger the slope the faster the evolution of the response. The slope is calculated as:

$$f'(t,(y_A,K_c)) = \frac{y_A \cdot K_c}{(K_c+t)^2} \tag{38}$$

In this paper, the slope at the curing time $t = Kc$, $(f'(K_c,(y_A,K_c)) = \frac{y_A}{4 \cdot K_c})$ was evaluated (**Figure 7. 9**, red line).

It is interesting to note that the function described by Equation 37 can also be used to model the relationship between mechanical properties and moisture loss, thus eliminating the explicit influence of curing time.

For example, considering *indirect tensile strength* (ITS) as the investigated mechanical property and *moisture loss* (DW) as physical properties, we have

$$DW = \frac{y_{A,DW} \cdot t}{K_{c,DW}+t} \tag{39}$$

and

$$ITS = \frac{y_{A,ITS} \cdot t}{K_{c,ITS}+t} \tag{40}$$

Obtaining *t* from Equation 39, substituting it into Equation 40 and rearranging the terms, we get

$$ITS = \frac{a_{ITS} \cdot DW}{b_{ITS} + DW} \tag{41}$$

where

$$a_{ITS} = \frac{y_{A,ITS} \cdot K_{c,DW}}{K_{c,DW} - K_{c,ITS}} \tag{42}$$

$$b_{ITS} = \frac{y_{A,DW} \cdot K_{c,ITS}}{K_{c,DW} - K_{c,ITS}} \tag{43}$$

Thus, again, *DW* and *ITS* (or other mechanical properties that are considered) are linked through a MM-type equation, although in this case the regression parameters of $a_{ITS}$ and $b_{ITS}$ are not required to be both positive as in the original MM-model. Indeed, since the parameters $y_A$ and $K_C$ are both positive, the sign of $a_{ITS}$ and $b_{ITS}$ depend on the relative magnitude of $K_{C,DW}$ and $K_{C,ITS}$.
Specifically, if $K_{C,DW} > K_{C,ITS}$, i.e. if the increase in *ITS* up to one half the asymptotic value is faster than the analogous increase of *DW*, both $a_{ITS}$ and $b_{ITS}$ are positive. On the other hand, if $K_{C,DW} < K_{C,ITS}$ the initial moisture loss is faster than the strength increase, and both $a_{ITS}$ and $b_{ITS}$ are negative.
If we consider the curvature of Equation 41:

$$c_{ITS} = \frac{\mathrm{d}^2 ITS}{\mathrm{d}\, DW^2} = \frac{-2 \cdot a_{ITS} \cdot b_{ITS}}{(b_{ITS} + DW)^3} \tag{44}$$

we can also observe that, if $K_{C,DW} > K_{C,ITS}$, i.e. if both $a_{ITS}$ and $b_{ITS}$ are positive, $c_{ITS}$ is negative and thus the curve is concave. On the other hand, if $K_{C,DW} < K_{C,ITS}$, i.e. if both $a_{ITS}$ and $b_{ITS}$ are negative, $c_{ITS}$ is positive and thus the curve is convex, as long as $|b_{ITS}| > DW$. Finally, if $K_{C,DW} \approx K_{C,ITS}$, the curvature is very small and Equation 41 degenerates into a straight line.
Those mathematical considerations lead to an interesting physical interpretation of the curing process of CM mixtures. If the curve *ITS* = *ITS*(*DW*) is concave (**Figure 7. 10**, line "a"), is possible to conclude that the initial development of strength is faster than the initial development of moisture loss. From this it can be inferred that the kinetics of cement hydration is faster with respect to the kinetics of emulsion breaking/setting and hence the initial curing rate is regulated by the cement hydration.
On the other hand, if the curve *ITS* = *ITS*(*DW*) is convex (**Figure 7. 10**, line "b"), is possible to conclude that the initial development of strength is delayed with respect to the initial development of moisture loss. From this it can be inferred that the initial curing process is controlled by the breaking/setting process of the bitumen emulsion: water evaporation leads to an increase in bitumen concentration, which subsequently leads to coalescence of the droplets, emulsion breaking, formation of continuous bitumen films and, ultimately, to an increase in mechanical properties.

The MM models were fitted by minimization of the residual sum of squares (RSS) with respect to the regression parameters (least-squares minimization).
The numerical solution was obtained using *R* [https://www.r-project.org], a free software environment for statistical computing and in particular the model fitting function nls() [Chambers and Hastie, 1991]. Within nls(), RSS minimization is carried out using the default Gauss-Newton algorithm and the self-starter functions SSmicmen() and SSasympOrig() were employed.

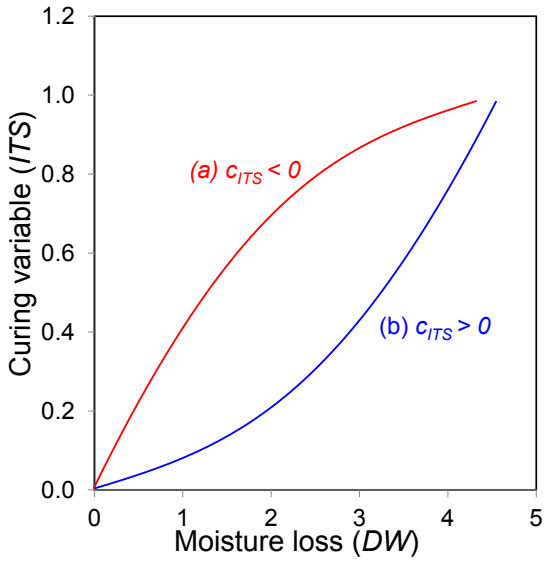


**Figure 7. 10** Relationship between curing rates of *DW* and *ITS* and curvature of *ITS* = *ITS* (*DW*).

# CHAPTER 8.

## Instrumented pavement section: A14 Motorway Bologna-Taranto

Starting from 2011, the Polytechnic University of Marche was involved in a Publicly-founded research project aimed at the characterization of the mechanical performance of cold recycled mixtures. Within this project, a full scale instrumented pavement section was constructed with the aim of: a) characterizing the performance of different CRMs, produced by FDR, in terms of evolution of mixture properties over time (i.e. characterization of the curing effects) and b) monitoring the mechanical response of CRMs under real traffic and environmental conditions.
The instrumented pavement section was constructed in April 2015 near to the city of Ancona (Italy), during the widening of the A14 motorway, which runs along the Adriatic coast of Italy (**Figure 8. 1**).

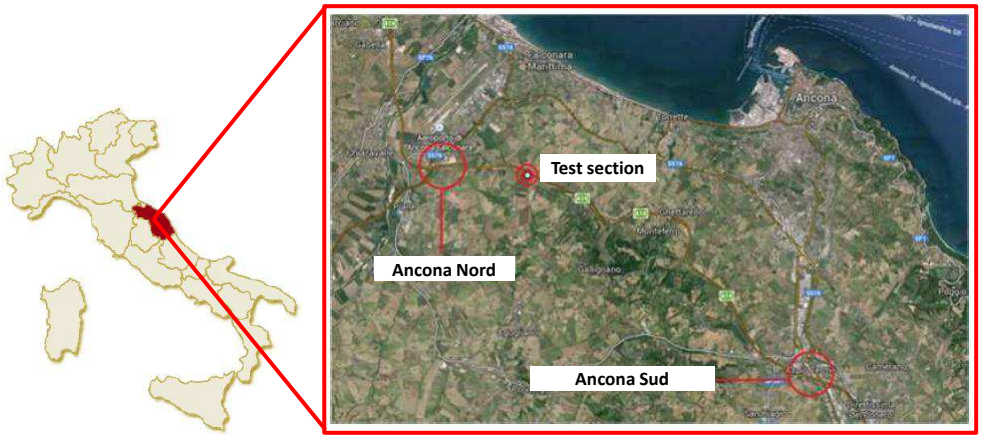


**Figure 8. 1** Location of the test section (source: Google Streetview).

## 8.1 Project description

The standard pavement cross section of the motorway was designed in order to withstand a traffic of 10 Million ESAL/year and consisted of a 300 mm asphalt concrete course (200 mm base course, 60 mm binder course and 40 mm porous wearing course), a 300 mm cement treated subbase course and a 200 mm granular foundation.
The experimental section was 80 m long and 6.75 m wide, interesting the width of both the emergency and the slow lane (**Figure 8. 2**a). Along this section, divided in two contiguous subsections of identical length (40 m + 40 m), the standard 300 mm cement treated layer was

replaced with two different CRMs layers realized on site with a FDR technique (**Figure 8. 2**b):

- cement-treated material, CTM (from 0.0 to +40.0 m);
- cement-bitumen treated material, CBTM (from +40.0 to +80.0 m).

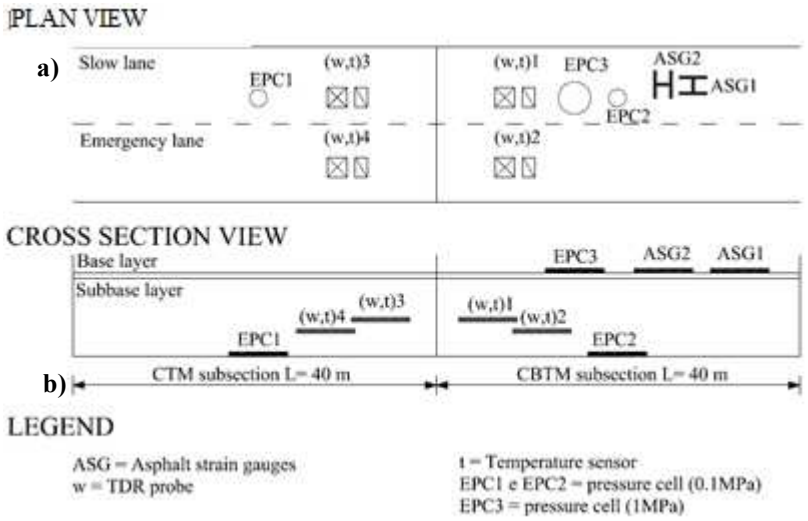


**Figure 8. 2** Experimental pavement section: a) plain and b) cross section view.

Moreover, the pavement section (**Figure 8. 2**) was instrumented with four time domain reflectometer (TDR) probes coupled with four temperature sensors that allow moisture content and temperature data to be recorded over time $(w, t)_i$, three earth pressure cells (EPCs) with different measuring ranges and two H-shaped asphalt strain gauges (ASG).
The instrumentation layout and installation operations are described in details in Section 8.2.3 and 8.24.

## 8.1.1 Objective and methodology

The objective of this research is to analyze the field and laboratory curing process of the CRMs manufactured during the construction of the experimental pavement section, and employed as subbase layer in the pavement structure.
In particular, the effects of different curing conditions (field and laboratory) on moisture loss were evaluated.
To this aim, moisture content and temperature were monitored in field, using time domain reflectomer probes and temperature sensors respectively, and in laboratory carefully weighing each specimen.
In the meantime, experimental tests were carried out on both mixtures directly produced at the jobsite and sampled during the construction operations (CBTM-SITE, CTM-SITE) and mixtures produced in the laboratory (CBTM-LABO, CTM-LABO) using the same aggregates and binders.

The curing process was analyzed by measuring the evolution of moisture loss by evaporation (*DW*) in field and in laboratory, indirect tensile stiffness modulus (*ITSM*) and indirect tensile strength (*ITS*), then, the experimental results were modeled using the Michealis-Menten model [Michaelis and Menten, 1913; Graziani et al., 2016a].
This allowed to characterize the curing process of the investigated mixtures by estimating the rate of evolution and the long-term value of the selected properties. The effects of mixture type (CBTM vs. CTM), mixing procedure (SITE vs. LABO), curing framework (SITE-field vs. SITE) and curing conditions (DRY vs WET) were evaluated.

Within the framework of the project described in Section 8.1, the curing parameters obtained during laboratory activities were compared with those estimated from the sensors installed inside the pavement in order to evaluate, on a parametric basis, the effects of laboratory and the field curing.

# 8.2 Experimental program

## 8.2.1 Materials

The same reclaimed aggregates were used for the CBTM and CTM mixtures. The granular blend was composed of 50% of RA and 50% of RAg; RA was obtained from the milling of the binder and base courses of the existing pavement, whereas the RAg was obtained from the milling of the existing cement-treated subbase.
The aggregates were sampled from the field section, during the construction operations, and characterized in terms of gradation, particle density, water absorption and bitumen content. Results are summarized in **Table 8. 1** and **Figure 8. 3**.
A pozzolanic cement type IV/A (P) with strength class 42.5R (EN 197-1) was used in this project. The dosages were equal to 3% and 2% (by dry aggregate mass) for CTM and CBTM mixtures, respectively.
A cationic overstabilized bituminous emulsion C60B10 (EN 13808) was selected to produce the CBTM mixtures (**Table 6. 1**). This emulsion is specifically formulated for cold in-place recycling, guaranteeing high mixing stability with cement (over-stabilized emulsion) and good workability during the compaction phase. The employed emulsion content was 3% (by dry aggregate mass), corresponding to 1.8% of fresh bitumen.

| **Material** | **Water absorption (%)** (EN 1097-6) | **Particle density (Mg/m$^3$)** (EN 1097-6) | **Bitumen content (%)** (EN 12697-1) |
|---|---|---|---|
| RA | 1.00 | 2.443 | 3.59 |
| RAg | 0.90 | 2.596 | - |
| 50%RA+50%RAg | 0.95 | 2.519 | - |

**Table 8. 1** Physical properties of granular materials.

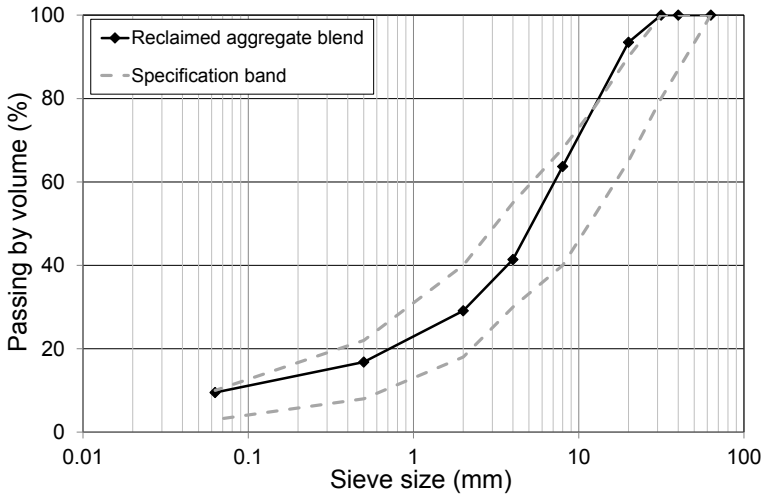


**Figure 8. 3** Gradation of aggregate blend (EN 933-2) and specification limits for A14 motorway construction.

## 8.2.2 Mixtures

The mixtures tested in the present study were produced:

- directly on site during FDR operations, (CBTM-SITE, CTM-SITE);
- in laboratory (CBTM-LABO, CTM-LABO).

A total water content $w_{tot}$ equal to 6% and 5% (by dry aggregate mass), was adopted for mixtures produced on site and for those fabricated in the laboratory, respectively. After field mixing operations, wet mixtures (CBTM-SITE and CTM-SITE) were sampled, transported and compacted in the laboratory.

## 8.2.3 TDR probes: laboratory calibration

TDR probes were calibrated within the same material that was placed around the probes during their installation in field. This material consisted of the selected granular blend (50% of RA and 50% of RAg) (**Figure 8. 3**), with large particles removed. Large particles were removed by passing the soil through a sieve with 4 mm size.
The Campbell Scientific probes were calibrated using soil with four target moisture contents: 1, 3, 5 and 7% by dry aggregate mass. The 4 mm-aggregate blend was mixed at each of the four moisture contents plus the corresponding aggregate water absorption (1% by dry aggregate mass) and was compacted in a polyvinyl chloride (PVC) tube, which was approximately 570 mm tall and had an inside diameter of 100 mm, as shown in **Figure 8. 4**a. The soil was compacted to achieve a density that would be similar to that which would be close to the probes. The soil was compacted in three layers of equal thickness; each layer received 25 blows from a manual standard Proctor hammer.


**Figure 8. 4** Calibration of the CS616 moisture probes: a) PVC tube; b) and C) installation of TDR probe d) sealing of PVC tube with plastic paper.

With the aim to obtain the data necessary for calibration, each Campbell Scientific probe was used to measure moisture content of the aggregate blend that characterizes each PVC tubes (**Figure 8. 4**b). For each probe, the full length of the parallel, stainless steel rods was pushed into the aggregate blend in each PVC tube for three times (**Figure 8. 4**c) following the sequence reported in **Figure 8. 5**. This provided three replicates of raw data readings; measurements were carried out continuously during a period of two weeks.

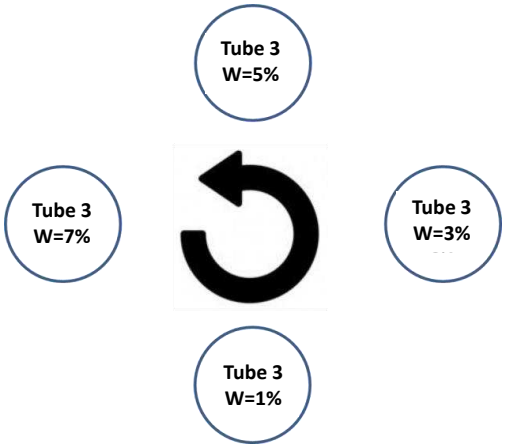


**Figure 8. 5** Rotation scheme of PVC tubes.

Each PVC tube was sealed with a plastic paper (**Figure 8. 4**d) in order to avoid evaporation.
Raw data readings represented the period of electromagnetic wave travel along the rods [μs] consequently converted in volumetric water content (*VWC*).

The *VWC* is calculated as follow:

$$VWC = \frac{V_w}{V_s} \cdot 100 \tag{45}$$

where $V_w$ is the total amount of water added to the sample ($W_{abs}$+$W_{add}$) and $V_s$ is the total volume of the sample ($V_{aggr}$+$V_{water}$).
The absolute average probe measurements obtained during calibrations are shown in **Table 8. 2**. The variability between replicate readings was very small.

| **Absolute average** [μs] | **VWC** [%] |
|---|---|
| 18.497 | 5 |
| 19.331 | 10 |
| 20.188 | 14 |
| 21.431 | 17 |

**Table 8. 2** Absolute average of volumetric water content calculated for four probes and all measurements.

The calibration equation for the Campbell Scientific probes is a quadratic equation as:

$$y = a \cdot x^2 + b \cdot x + c \tag{46}$$

where
$y$ = gravimetric moisture content (as a decimal)

$x$ = measured electromagnetic wave period (μs)

The calibration equation published by Campbell Scientific [Campbell Scientific, Inc. 1996] actually uses volumetric moisture content.
Volumetric water content is proportional to gravimetric water content (*GWC*) and can be calculated by multiplying *GWC* by the specific gravity of the adopted aggregate blend.

Calibration coefficients were obtained for each probe by determining the best-fit curve for a plot of probe measurements versus water contents.
Verified the small variance (**Table 8. 2**) between probes and differences between each replicates, a composite calibration, instead of individual calibration equation, composed by the average of each coefficient is calculated and adopted during the experimental activities (Equation 47).

$$VWC = -0.0094 \cdot x^2 + 0.4136 \cdot x - 4.3972 \quad (47)$$

The calibration equation was set up in the software LoggerNet version 4.0, provided by Campbell scientific (**Figure 8. 6**).
The software unit is connected to the CR1000 datalogger and it allows to:

- monitor the connection network;
- collect, copy end export the data;
- save old records and analyze the data in real time.

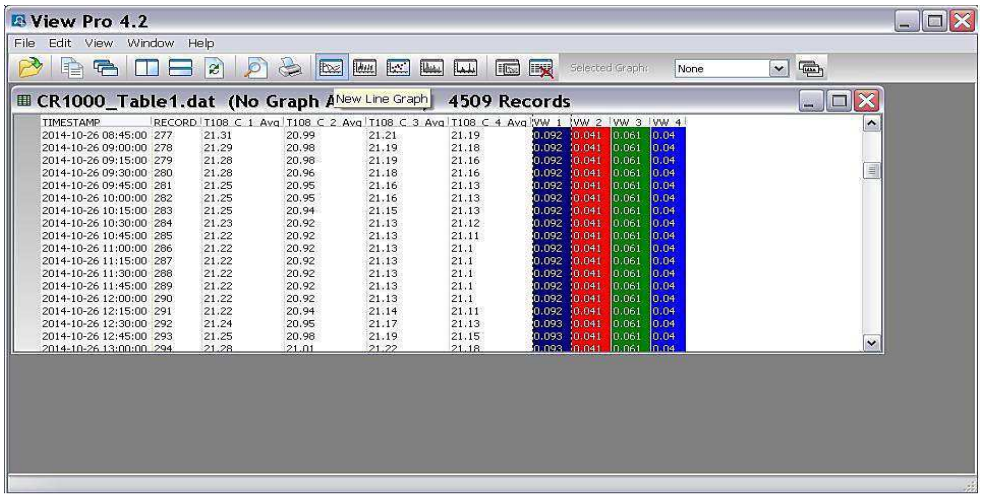


**Figure 8. 6** Software LoggerNet, version 4.0 (Campbell Scientific).

## 8.2.4 On-site construction operations and instruments installation

*On-site construction operations*

Before the construction of the instrumented pavement section, the asphalt concrete and CTM layers were milled without altering the foundation layer.

First, the RA was spread on the prepared foundation and leveled to reach an uncompacted thickness of approximately 200 mm (**Figure 8. 7**a). Subsequently, the RAg was spread on the loose RA material and leveled to the final uncompacted thickness of about 400mm (**Figure 8. 7**b). Finally, RA and RAg were blended with a recycler and levelled (**Figure 8. 7**c). At this moment, the aggregate blend (50% RA +50% RAg) without binders, was sampled to evaluate the moisture content which resulted $w_{site}$= 4.82% (by dry aggregate mass).

The subbase was lightly compacted using a vibrating smooth-drum roller in order to obtain a levelled and stable support for the following operations. On CTM section, around 1% (by dry aggregate mass) of water was added in order to enhance the compactability of the material. On site, $w_{tot}$ was composed of the site moisture content ($w_{site}$= 4.82% by dry aggregate mass) and the water obtained from emulsion for CBTM-SITE ($w_{em}$=1.2% by dry aggregate mass) or added during construction operations for CTM-SITE ($w_{add}$=1.0% by dry aggregate mass).

Different cement dosages (2% and 3% by dry aggregate mass for CBTM and CTM respectively) were spread using a vehicle, equipped with volumetric batchers (**Figure 8. 7**d). Then, the recycler coupled to an emulsion tank was used to stabilize a thickness of 400 mm with bitumen emulsion for a length of 40 m (**Figure 8. 7**e). For the remaining 40 m, the recycler mixed the CTM layer for the same thickness of 400 mm with no emulsion addition. The second sampling was carried out, from the stabilized cold recycled layers (CTM and CBTM) before compacting. Sampled materials, sealed in plastic bags, were immediately transported to the laboratory to start the experimental activities reported in the following sections 8.2.5 and 8.2.6. Then, the treated layers were finally compacted by a 14 ton vibrating smooth drum roller and a 25 ton pneumatic tire roller (**Figure 8. 7**f).


**Figure 8. 7** Construction of CBTM and CTM layers: a) RA material restoring; b) placing of RAg layer; c) mixing of the milled material; d) spreading of cement; e) stabilization with bitumen emulsion and f) final compaction.

*Instruments installation*

In each subsection, following the scheme reported in **Figure 8. 2**, a shallow cavity and cable trench were dug reaching the bottom of the subbase layer to install the earth pressure cells, EPC1 and EPC2 [Timm et al., 2004; Timm, 2009]. The cavity, approximately 300 mm deep, was leveled using a 50 mm layer of clean sand (passing to the 2 mm sieve an retained to the 0.4 mm sieve) to prevent EPC damage from large, sharp base aggregate particles.

The cell and its stem were carefully placed and leveled, avoiding the formation of voids, and a second layer of protection sand was used to fill the cavity (**Figure 8. 8**a). The cabling was also protected using a flexible steel conduit and laid inside the trench that was backfilled with the existing base material (**Figure 8. 8**b).

Select fill was scalped with a No. 4 sieve and the finer fraction was collected. This material and clean sand were put on each EPCs in order to avoid them damage (**Figure 8. 8**c).

In same manner the installation of TDR and temperature probes were carried out. At each designated probe location, a hole was dug through the subbase and 0.125 m into select fill . Shallow trenches, reaching a depth of one-half subbase thickness (150 mm) were also required to run cables to the pavement edge (**Figure 8. 8**d). Placements of Campbell Scientific CS616 and temperature probes required only a single, straight trench (**Figure 8. 8**e). The probes were positioned at the center of the outer traffic lane.

Select fill was scalped with a No. 4 sieve and the finer fraction was collected. The fine fraction of select fill was the same material that was used for probe calibration. This material was placed around probes during installation (**Figure 8. 8**f). Large particles were removing to minimize risk of damaging probes and to improve efficiency of hand-compaction operations.

Care was taken to ensure that the cable had some slack. This practice minimizes the risk of cable damage due to tension. After protecting the cable, trenches were filled with the subbase course material previously removed, the trench was compacted by both foot and portable Marshall hammer, to provide additional protection (**Figure 8. 8**g) [Timm et al., 2004; Timm, 2009]. Then the dug subbase material was replaced and the treated layers were finally compacted by a 14 ton vibrating smooth drum roller and a 25 ton pneumatic tire roller.

An emulsion tack coat was sprayed to guarantee the sealed condition (wet curing in field) in one half of the pavement section (for both CTM and CBTM mixtures) (**Figure 8. 8**h).


**Figure 8. 8** First part of instruments installation: a) placing of EPCs; b) covering with protective material (clean sand and 4 mm-sieved subbase material); c) Placing of cables protected using a flexible steel conduit; d) cavity preparation for TDR and temperature probes; e) placing of TDR and temperature probes; f) Protection of TDR and temperature probes with 4 mm-sieved subbase material; g) trench compaction by portable Marshall hammer; h) partial application of emulsion tack coat.

One month later, the last EPC cell (EPC3) and the two asphalt strain gauges (ASG1 and ASG2) were installed.
The installation of the third EPC cell was carried out in the same manner of the previous ones but on the surface of the compacted subbase layer (**Figure 8. 9**a).
To install the ASGs, shallow small cavities were created on the surface of subbase layer (**Figure 8. 9**b). This position was chosen in order to evaluate the horizontal strains, in both longitudinal (traffic) and transverse direction. The ASGs had a measuring base of 200 mm and are characterized by a range of ±1500 microstrain. A thin layer of sand-asphalt mortar was used to tack the ASG in the correct position and alignment, inside the prepared cavities. The sensors were protected filling and leveling the cavities with a small amount of asphalt concrete, obtained removing larger aggregate particles from the paving mix, with a 8 mm sieve (**Figure 8. 9**c). Compaction was achieved only by static pressure. The cabling was protected by a flexible steel conduit laid inside the trenches and backfilled with the tacking mortar (**Figure 8. 9**b) [Graziani et al., 2011].

Finally, the upper part of the pavement structure were paved with three layers of HMA (i.e. base, binder and wearing courses) (**Figure 8. 9**d) and compacted by a 14 ton vibrating smooth drum roller (**Figure 8. 9**e).


**Figure 8. 9** Second part of instruments installation: a) placing of EPC3; b) installation of ASG1 and ASG2; c) filling and leveling with 8 mm-sieved asphalt concrete in order to protect ASGs; d) HMA layers laydown and e) final compaction.

**Figure 8. 10** shows the connection board and its roadside housing. At the end of construction, a sensor survey revealed the following survival rate:

- TDR probes: 4 out of 4;
- Temperature sensors: 3 out of 4;
- pressure cells: 3 out of 3;
- ASG: 2 out of 2.

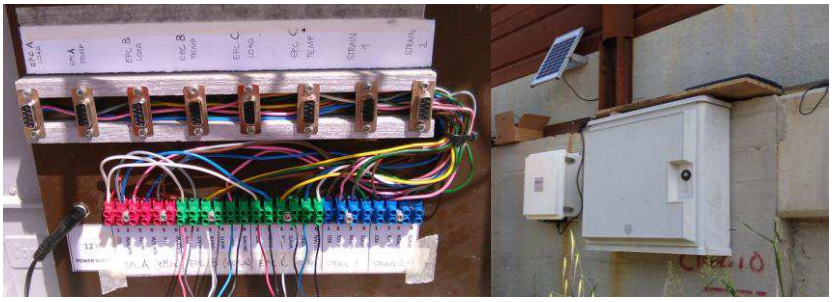

**Figure 8. 10** Cables connection board and roadside housing.

## 8.2.5 Laboratory procedure for specimens production

Concerning to laboratory procedure, the total water content $w_{tot}$ was composed of the water from the emulsion ($w_{em}$) and additional water ($w_{add}$), which is added in two parts. The first part, related to the water absorption ($w_{add\_1} = w_{abs}$) of the constituent aggregates, was added to the dry aggregates blend the day before mixing. Then, the wet mixture (aggregate containing $w_{add\_1}$) was stored in a sealed plastic bag for 12 hours at room temperature, in order to ensure a homogeneous moisture condition and to allow absorption by the aggregates. Subsequently, the aggregate blend was thoroughly mixed, gradually adding the remaining part of the mixing water ($w_{add\_2}$), cement and emulsion in sequence. Samples were mixed using a mechanical mixer at room temperature for at least two minutes, time required to guarantee a good particle coating [Grilli et al., 2012].
All specimens employed for mechanical testing were compacted in a 150 mm diameter mold by means of a SGC (see Section 7.2.1).
For the mixtures produced on site (CBTM-SITE and CTM-SITE), 4500 g of loose mixture were compacted at 180 gyrations obtaining a specimen height of about 110 mm. For the mixtures produced in the laboratory (CBTM-LABO and CTM-LABO), 2800 g of loose material were compacted at 100 gyrations obtaining a specimen height of about 70 mm.

## 8.2.6 Curing

Specimens (CBTM-SITE, CTM-SITE, CBTM-LABO and CTM-LABO) were cured in a climatic chamber at the temperature of 20 ± 2 °C, with a constant relative humidity of 50 ± 5%. In addition, part of the CBTM-LABO specimens were also cured in sealed conditions to avoid free water evaporation. The first procedure was identified as DRY curing, whereas the second procedure was identified as WET curing (**Table 8. 3**).
The moisture loss results, obtained from the above described procedure for laboratory curing, on CBTM-SITE and CTM-SITE were compared with those carried out in field (CBTM-SITE-field and CTM-SITE-field) through TDR probes records. In field, WET curing condition is simulated throught the application of an emulsion tack coat.

| Mixture | | Curing | | Testing (number of specimens) | | |
|---|---|---|---|---|---|---|
| Type | Production | Condition (50% RH, 20 °C) | Times [days] | DW | ITSM | ITS |
| CBTM | LABO | DRY | 1, 3, 7, 28, 90 | 14 | 10 | 14 |
| CBTM | LABO | WET | 1, 3, 7, 28, 90 | 13 | 10 | 13 |
| CBTM | SITE | DRY | 7, 14, 28, 90 | 9 | 0 | 9 |
| CTM | LABO | DRY | 1, 3, 7, 28, 90 | 9 | 0 | 9 |
| CTM | SITE | DRY | 7, 14, 28, 90 | 7 | 0 | 5 |
| CBTM | SITE | DRY-field | During 3 months | | | |
| CBTM | SITE | WET-field | During 3 months | | | |
| CTM | SITE | DRY-field | During 3 months | | | |
| CTM | SITE | WET-field | During 3 months | | | |

**Table 8. 3** Summary of testing program.

### 8.2.7 Testing methods

The curing process was analyzed by measuring moisture loss by evaporation (*DW*), indirect tensile stiffness modulus (*ITSM*) and indirect tensile strength (*ITS*) of compacted specimens at different curing times and conditions. The testing program is summarized in **Table 8. 3**.
*DW* was measured by carefully weighting each specimen before mechanical testing.
In addition, the *DW* results, obtained from the above described procedure for laboratory curing, were compared with those carried out in field though TDR probes records.
The analysis in terms of stiffness properties was carried out measuring *ITSM* according to the procedure described in Section 7.2.2.
*ITSM* test was performed on only CBTM-LABO-DRY and CBTM-LABO-WET specimens because preliminary observations showed that the other mixtures were too brittle and failed during the test. Immediately after *ITSM* tests, cured specimens were tested by means of a mechanical testing machine for the assessment of the *ITS* according to the procedure described in Section 7.2.3.

Concerning the curing effect, it is evaluated on physical (*DW*) and mechanical (*ITSM* and *ITS*) properties of the studied materials, using a procedure based on the Michaelis-Menten (MM) model and explained in Section 7.2.4.

## 8.3 Experimental findings: analysis and modelling

### 8.3.1 Volumetric properties

The volumetric properties of the 52 specimens (36 CBTM specimens and 16 CTM specimens) were first analyzed in order to evaluate their homogeneity and verify the reliability of the compaction procedure.

The mass of each compacted specimen was recorded and compared with the mass of the loose mixture placed in the mold. In **Figure 8. 11**a, the empirical probability density function of the mass loss for CBTM and CTM specimens are compared. The density curves show that the mass loss during compaction was very small (less than 0.5%) and almost identical for CBTM and CTM specimens. Moreover, visual observations performed during extrusion, confirmed that all specimens were homogeneous and stable and that the mass loss was due to emulsion and fine aggregate particles remaining on the inner surface of the mold.
The results of volumetric analysis, in terms of average value and standard deviation of voids in the mixture $V_m$ and voids filled with liquids *VFL* are summarized in **Table 8. 4**. Moreover, in **Figure 8. 11**b, the empirical probability density functions of $V_m$ for the four materials are compared.

| | $V_m$ | | *VFL* | |
|---|---|---|---|---|
| **Materials** | **Avg. value** [%] | **Std. Dev.** [%] | **Avg. value** [%] | **Std. Dev.** [%] |
| CBTM-LABO | 12.47 | 1.283 | 87.28 | 8.397 |
| CBTM-SITE | 13.87 | 1.165 | 78.04 | 6.524 |
| CTM-LABO | 16.60 | 0.907 | 58.29 | 4.266 |
| CTM-SITE | 18.74 | 0.599 | 48.60 | 1.632 |

**Table 8. 4** Volumetric properties of the compacted specimens.

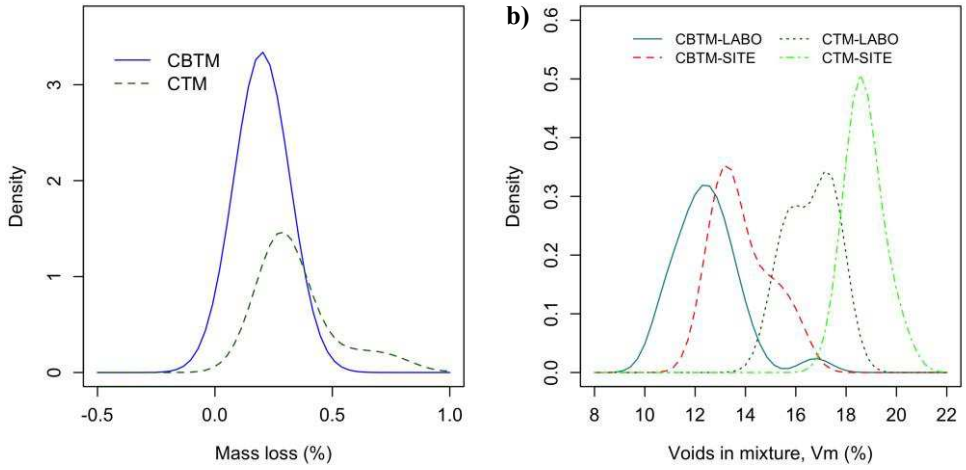


**Figure 8. 11** Empirical probability density function of: a) mass loss and b) voids in the mixture.

It can be observed that CBTM mixtures, fabricated both on site and in laboratory, were characterized by a lower $V_m$ with respect to CTM mixtures. This can be explained by the presence of the bitumen droplets. In fact, inside the CBTM mixture, 1.8% of bitumen (by dry aggregate mass) corresponds to about 3.75% by mixture volume, which is not present

inside CTM mixture. A further contribution to the lower $V_m$ values of CBTM with respect to CTM, may also derive from an improvement of compactability due to the lubricating effect of the bitumen droplets [Grilli et al., 2012].
As far as *VFL* is concerned, it can be noted that all specimens were characterized by values lower than 90%. This means that no specimen approached *saturation* (*VFL* = 100%) and hence, no drainage was likely to occur during the compaction phase (this was also confirmed by the mass loss measurements). In **Table 8. 4**, a significant difference between the average *VFL* values of CBTM and CTM can also be observed. This confirms that in CBTM mixtures a large fraction of $V_m$ is occupied by the bitumen droplets.
Overall, the analysis of mass loss during compaction, $V_m$ and *VFL*, allowed to verify the reliability and the homogeneity of the specimen production procedure.

## 8.3.2 Evolution of material properties and model fitting

The evolution of *DW*, *ITSM* and *ITS* as a function of curing time, is shown from **Figure 8. 12** to **Figure 8. 16**.
Mechanical properties (*ITSM* and *ITS*) were measured and analyzed solely on specimens compacted in laboratory.
The MM model was fitted to the experimental data using R [https://www.r-project.org], a free software environment for statistical computing. The parameters estimates were calculated using the nonlinear fitting function `nls()`, which runs a least-squares estimation [Montgomery and Runger, 2003; Ritz and Streibig, 2008]. The regression curves are superposed to the experimental data, whereas the estimated values of the regression parameters, their standard errors and the standard error of the residuals are summarized in **Table 8. 5**.
The adequacy of the regression model was checked performing an analysis of residuals [Montgomery and Runger, 2003; Ritz and Streibig, 2008]. In **Figure 8. 17**a and **Figure 8. 18**a, the Quantile-Quantile (QQ) plots for the standardized residuals of *DW* and *ITS*, are reported for both materials properties. The points plotted along the equality line confirming that the regression errors may be considered normally distributed. In **Figure 8. 17**b and **Figure 8. 18**b the plots of the standardized residuals versus fitted values of *DW* and *ITS*, are reported. As it can be observed the standardized residuals were in the range from -2 to 2 and no particular patter can be observed in the plots. Thus the adequacy of the model and the absence of outliers are confirmed. This statistical evaluation has been performed only on measurements carried out in laboratory, i.e. on mixtures CBTM-LABO-DRY, CBTM-LABO-WET, CBTM-SITE-DRY, CTM-LABO-DRY and CTM-SITE-WET; records obtained in field from TDR probes are not taken into account for this analysis.

*Moisture loss (site vs laboratory production)*
From **Figure 8. 12** it can be observed that, for mixtures CBTM-LABO-DRY and CBTM-SITE-DRY, *DW* after 7 days of curing was 1.97% and 1.93%, respectively. A small difference can also be noticed between the considered mixtures at longer curing times (90 days), when DW of about 3.8% and 3.5% was measured for mixtures CBTM-LABO-DRY and CBTM-SITE-DRY, respectively. Analogously, for mixtures CTM-LABO-DRY and CTM-SITE-DRY, *DW* after 7 days was 2.35% and 1.4%, respectively. This difference progressively increased and at 90 days *DW* of 3.7% and 2.3% were measured. The results

obtained with mixture CBTM-LABO-WET showed a completely different trend since, in this case, the specimen was sealed and therefore evaporation was virtually impossible.
A parametric evaluation of the *DW* evolution was obtained considering the MM model for all mixtures subjected to DRY curing conditions. Specifically, the estimated value of $K_c$ was used to evaluate the initial curing rate (i.e. the time required to reach one half of the asymptotic value), whereas the estimated value of $y_A$ was used to evaluate the long-term (asymptotic) behavior.
For mixtures CBTM-LABO-DRY and CBTM-SITE-DRY, $K_c$ was 2.4 days and 6.5 days, respectively (**Table 8. 5** Regression parameters of Michealis-Menten model for the time evolution of *DW*, *ITSM* and *ITS*.). Analogously for mixtures CTM-LABO-DRY and CTM-SITE-DRY, $K_c$ was 1.9 days and 5.5 days, respectively. This trend of the initial curing rate, is also confirmed by analyzing the values of the slope $y'(K_c)$ summarized in **Table 8. 5**. In fact, it can be observed that higher $y'(K_c)$ corresponds to lower $K_c$ and consequently faster initial curing rate. Overall, the result highlighted that initial moisture loss by evaporation for mixtures produced on site, was more than 2 times slower with respect to that registered for mixtures produced in the laboratory.
Considering the long-term behavior, it can be observed that for mixtures CBTM-LABO-DRY and CBTM-SITE-DRY the asymptotic value $y_A$ was 3.3% and 3.9%, respectively, whereas, for mixtures CTM-LABO-DRY and CTM-SITE-DRY the value of $y_A$ was 3.4% and 2.5%, respectively. Hence, it can be concluded that the production procedure adopted for the studied mixtures (LABO-DRY or SITE-DRY), influenced the moisture loss of CTM mixture at both short and long curing times. These findings can be related to the different volumetric properties of the mixtures (**Table 8. 4**).

| Mixture | $y_A$ | | $K_c$ | | $y'(K_c)$ | Residual std. error |
|---|---|---|---|---|---|---|
| | Estimate | Std. error | Estimate | Std. error | Estimate | |
| *Moisture loss* vs. *time* | [%] | [%] | [days] | [days] | [%/day] | [%] |
| CBTM-LABO-DRY | 3.30 | 0.24 | 2.40 | 0.62 | 0.34 | 0.4234 |
| CBTM-LABO-WET | | | | | | |
| CBTM-SITE-DRY | 3.88 | 0.19 | 6.54 | 1.41 | 0.15 | 0.2642 |
| CTM-LABO-DRY | 3.40 | 0.22 | 1.94 | 0.45 | 0.44 | 0.3006 |
| CTM-SITE-DRY | 2.47 | 0.07 | 5.51 | 0.56 | 0.11 | 0.0911 |
| CBTM-SITE-DRY-field | 5.22 | 0.15 | 5.86 | 0.35 | 0.22 | 0.2341 |
| CBTM-SITE-WET-field | 5.48 | 0.21 | 10.49 | 0.42 | 0.13 | 0.0822 |
| CTM-SITE-DRY-field | 5.68 | 0.17 | 6.12 | 0.51 | 0.23 | 0.2569 |
| CTM-SITE-WET-field | 5.68 | 0.22 | 10.59 | 0.39 | 0.13 | 0.1215 |
| *ITSM* vs. *time* | [MPa] | [MPa] | [days] | [days] | [MPa/day] | [MPa] |
| CBTM-LABO-DRY | 11060 | 630 | 1.80 | 0.48 | 1536 | 1145 |

| | | | | | | |
|---|---|---|---|---|---|---|
| CBTM-LABO-WET | 13201 | 1146 | 5.86 | 1.85 | 536 | 1564 |
| *ITS* vs. *time* | [MPa] | [MPa] | [days] | [days] | [MPa/day] | [MPa] |
| CBTM-LABO-DRY | 0.54 | 0.04 | 2.23 | 0.60 | 0.06 | 0.0726 |
| CBTM-LABO-WET | 0.54 | 0.06 | 4.89 | 1.71 | 0.03 | 0.0856 |
| CBTM-SITE-DRY | 0.33 | 0.04 | 4.17 | 2.63 | 0.02 | 0.0583 |
| CTM-LABO-DRY | 0.41 | 0.04 | 1.90 | 0.69 | 0.05 | 0.0568 |
| CTM-SITE-DRY | 0.20 | 0.05 | 2.77 | 4.16 | 0.02 | 0.0457 |

**Table 8. 5** Regression parameters of Michealis-Menten model for the time evolution of *DW*, *ITSM* and *ITS*.

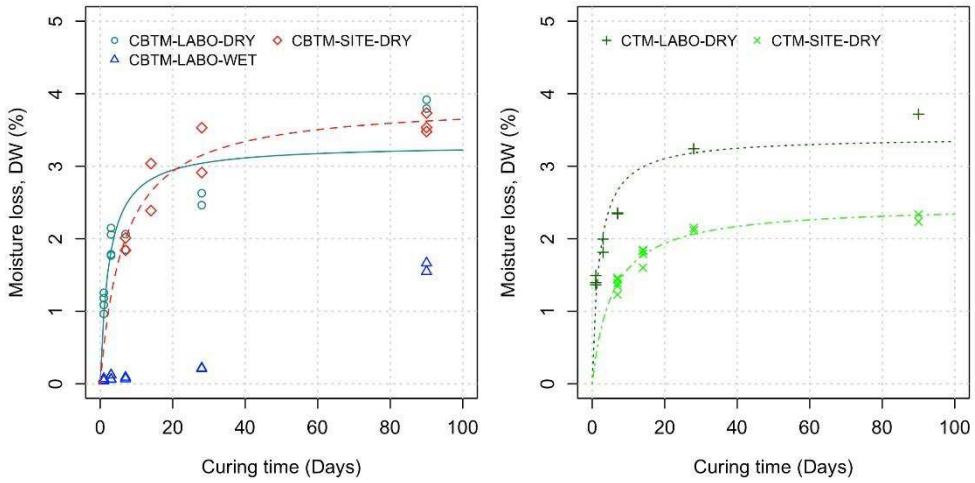


**Figure 8. 12** Evolution of moisture loss (DW) versus curing time.

*Moisture loss (site production, field vs laboratory curing)*
From **Figure 8. 13**, it can be observed that, for mixtures CBTM-SITE-DRY-field and CTM-SITE-DRY-field, *DW* after 7 days of curing was 2.82% and 2.97%, respectively. This difference became more marked at longer curing times (90 days), when *DW* of about 4.91% and 5.31% was measured for mixtures CBTM-SITE-DRY-field and CTM-SITE-DRY-field, respectively.
Analogously, for mixtures CBTM-SITE-WET-field and CTM-SITE-WET-field, *DW* after 7 days was 2.06% and 2.23%, respectively. This difference remain approximatively constant at 90 days, when *DW* of 4.78% and 5.02% were measured.
At longer curing times, CTM-SITE-DRY-field exhibited the maximum value in *DW* (5.31%), among all the mixtures investigated in field.
In **Figure 8. 13**, the fluctuation in terms of temperature values is also reported: temperatures (average values calculated on measurements carried out using temperature probes) ranged from 18.8 to 38 °C, during the observed period of 90 days.

Considering, a parametric evaluation of the *DW* carried out applying MM model on CBTM-SITE-DRY-field, CTM-SITE-DRY-field, CBTM-SITE-WET-field and CTM-SITE-WET-field mixtures, the following considerations can be drawn:

- For mixtures CBTM-SITE-DRY-field and CTM-SITE-DRY-field, $K_c$ was 5.86 days and 6.12 days, respectively (**Table 8. 5**). Analogously for mixtures CBTM-SITE-WET-field and CTM-SITE-WET-field, $K_c$ was 10.49 days and 10.59 days, respectively. This trend of the initial curing rate, is also confirmed by analyzing the values of the slope $y'(K_c)$ summarized in **Table 8. 5**. In fact, the initial curing rate in WET conditions was about twice slower with respect to that registered in DRY conditions. Overall, the result highlighted that initial moisture loss by evaporation for mixtures cured on site in WET conditions (sealed with emulsion tack coat), was about 2 times slower with respect to that registered for mixtures cured in DRY conditions (not sealed).
- At longer curing times, it can be observed that for CBTM-SITE-DRY-field and CTM-SITE-DRY-field mixtures, the asymptotic value $y_A$ was 5.22% and 5.68% respectively, whereas, for mixtures CBTM-SITE-WET-field and CTM-SITE-WET-field the value of $y_A$ was 5.48% and 5.68%, respectively.

Hence, it can be concluded that the curing condition, DRY or WET (i.e. not sealed or sealed with emulsion tack coat), affects the initial curing rate of the mixtures but this influence disappear at longer curing times; this observation is more evident if CTM mixture is considered where the cement content added in the mixture is higher.

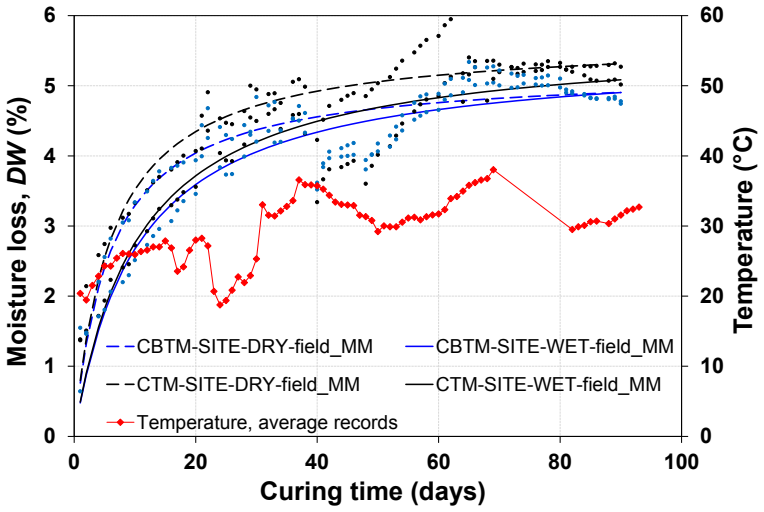


**Figure 8. 13** Evolution of moisture loss (*DW*) and temperature versus curing time, measurements carried out using TDR and temperature probes respectively.

Subsequently the effects of curing procedures, in laboratory (at the temperature of 20 ± 2 °C with a constant relative humidity of 50 ± 5%), and in field (at variable temperatures and exposed to rainfalls) was also evaluated. With this aim, the moisture loss *DW* of CBTM-SITE-DRY, CBTM-SITE-DRY-field, CTM-SITE-DRY and CTM-SITE-DRY-field mixtures was compared.
In **Figure 8. 14**, the moisture loss *DW* normalized according to the estimated asymptotic value of $y_A$, is reported for each mixture.
As it can be observed in **Figure 8. 14**, the difference in terms of *DW* among the selected mixtures is negligible for both the initial and longer curing times.

In conclusion, it is possible to assess that the selected boundary conditions such as temperature and humidity (curing conditions) and type of mixture do not influence the curing process of the subbase layer. In particular, the adopted laboratory curing procedure (temperature of 20 ± 2 °C with a constant relative humidity of 50 ± 5%) well simulates the effect of field curing process if mixtures characterized by the same composition are evaluated.

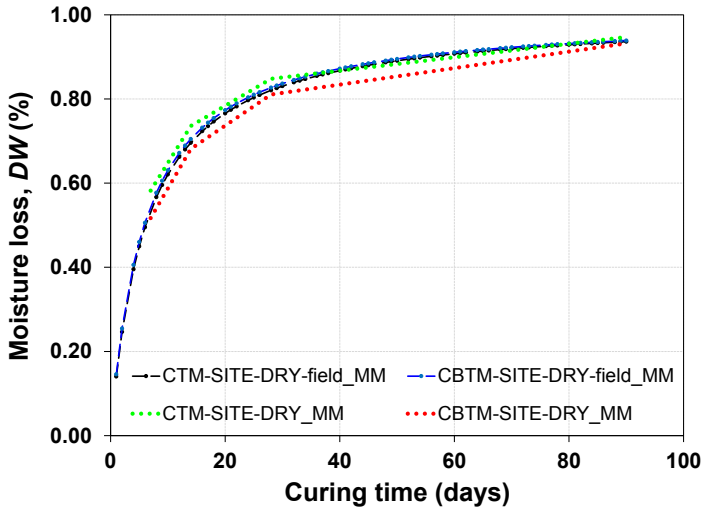


**Figure 8. 14** Evolution of moisture loss (*DW*) versus curing time: comparison between laboratory and field curing process.

*Indirect tensile stiffness modulus*
**Figure 8. 15** reports the *ITSM* results obtained on mixtures CBTM-LABO-DRY and CBTM-LABO-WET at different curing times. The plot highlights the effect of the curing condition (DRY or WET) on *ITSM* evolution. Similar to *DW*, this effect was evaluated by analyzing the parameters of MM model.
As far as the initial curing rate is concerned, the MM model indicates that mixture CBTM-LABO-DRY required 1.8 days to reach one half of the asymptotic *ITSM* value.

Differently for mixture CBTM-LABO-WET, $K_c$ increased up to 5.9 days. Hence, dry curing condition resulted in a higher initial curing rate (**Table 8. 5**). This result is an effect of emulsion breaking due to moisture loss by evaporation in DRY-cured specimens and it is also confirmed by the higher slope $y'(K_c)$ measured on mixture CBTM-LABO-DRY with respect to mixture CBTM-LABO-WET (**Table 8. 5**).
As far as the long-term curing is concerned, the asymptotic *ITSM* value estimated by the MM model for mixtures CBTM-LABO-DRY and CBTM-LABO-WET was 11060 MPa and 13201 MPa, respectively. This highlights the importance of water available inside the specimen, in order to promote the cement hydration process.

*Indirect tensile strength*
The *ITS* evolution (**Figure 8. 16**) showed a trend similar to that observed with *ITSM* (**Figure 8. 15**).
As far as the initial curing is concerned, the MM model indicates that mixtures CBTM-LABO-DRY and CBTM-SITE-DRY reached one half of the asymptotic *ITS* value after 2.2 days and 4.2 days, respectively, whereas, mixture CBTM-LABO-WET required 4.9 days. Analogously, for CTM-DRY specimens the laboratory or site production procedure resulted in a $K_c$ increase from 1.9 days to 2.8 days, respectively.
It is worth noting that $K_c$ values obtained for *ITS* were always lower with respect to those estimated for *DW*, i.e. in the first part of curing, strength development was faster than the moisture loss. The observations carried out analyzing $K_c$ values, are also confirmed by the values of the slope $y'(K_c)$ reported in **Table 8. 5**. Since moisture loss can be directly associated with the curing of bituminous emulsion, this also suggests that the effect of cement hydration was more important at shorter curing times.
As far as the long-term curing performance is analyzed, the asymptotic values of *ITS* for mixtures CBTM-LABO-DRY and CBTM-SITE-DRY was 0.54 MPa and 0.32 MPa, respectively. In addition, mixture CBTM-LABO-WET was characterized by an asymptotic value of 0.53 MPa. This suggests that the curing condition (DRY or WET) did not affect the *ITS* development of CBTM mixtures (produced in laboratory). Regarding CTM specimens, the estimated asymptotic *ITS* for CTM-LABO-DRY and CTM-SITE-DRY was 0.41 MPa and 0.19 MPa, respectively.

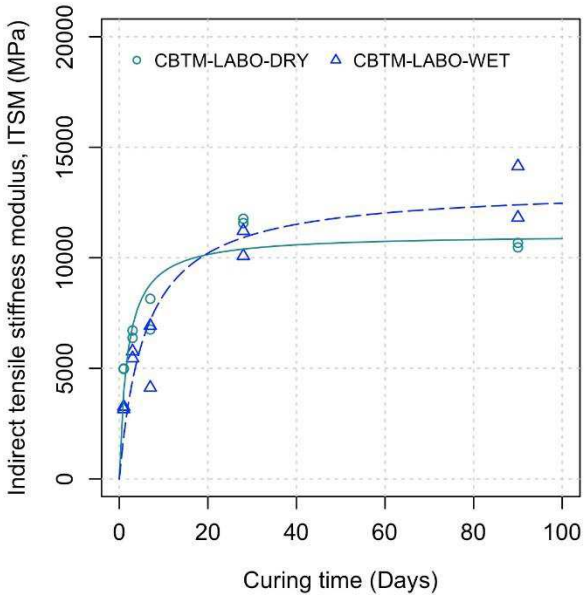


**Figure 8. 15** Evolution of indirect tensile stiffness modulus (*ITSM*) versus curing time.

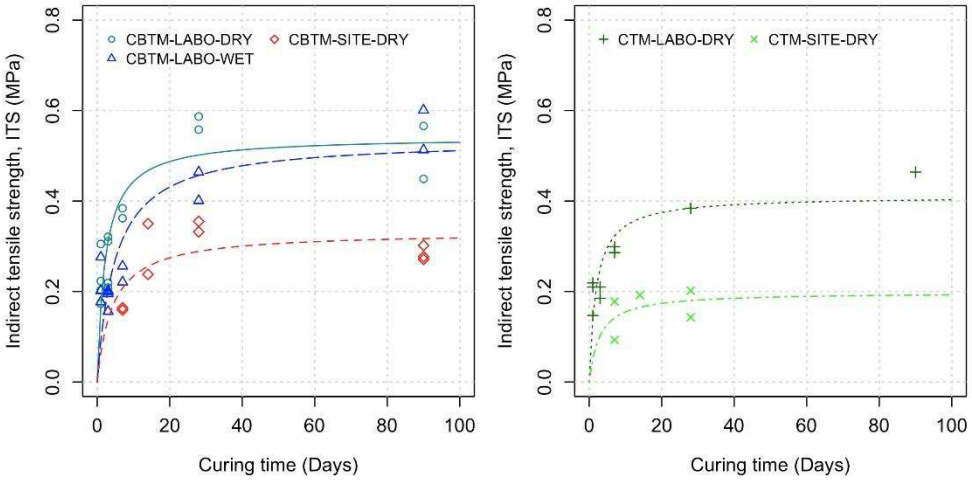


**Figure 8. 16** Evolution of indirect tensile strength (*ITS*) versus curing time.

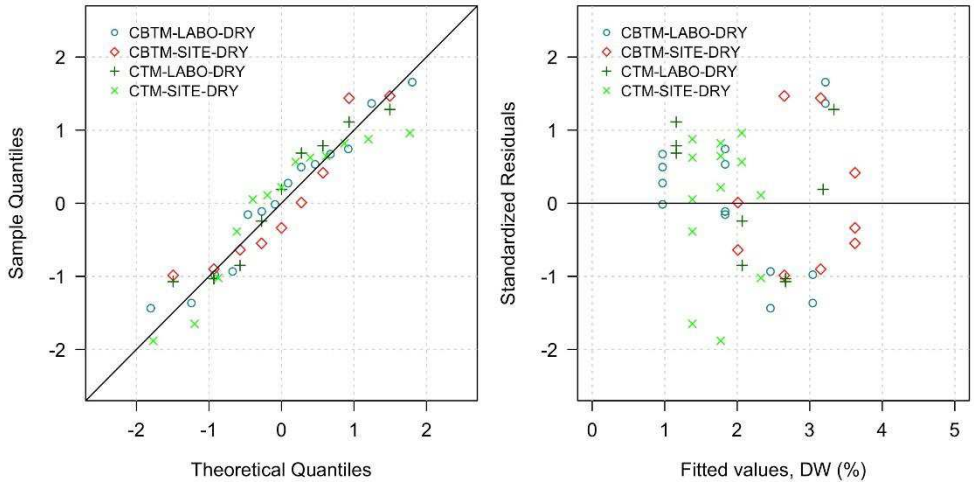


**Figure 8. 17** Residual plots for DW: a) normal QQ plot, and b) standardized residuals versus fitted values.

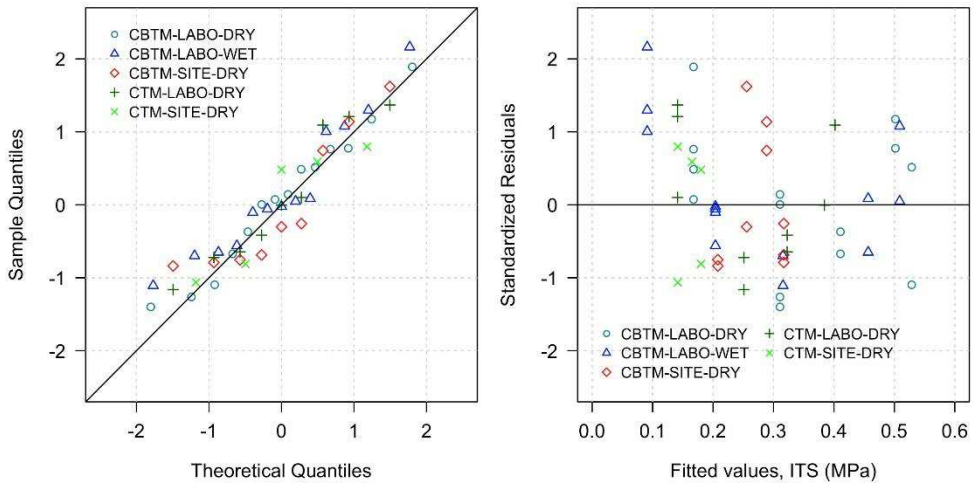


**Figure 8. 18** Residual plots for ITS: a) normal QQ plot, and b) standardized residuals versus fitted values.

### 8.3.3 Relation between moisture loss and mechanical properties

In **Figure 8. 19** the measured values of *ITS* are reported as a function of the corresponding measured values of *DW*. Equation 41 was fitted to the experimental data using the least-squares criterion, then the fitted regression curves are superposed to the experimental data.

The values of the fitted parameters $a_{ITS}$ and $b_{ITS}$ are summarized in **Table 8. 6**.
For CBTM mixtures, $a_{ITS}$ and $b_{ITS}$ are both positive and thus, as predicted by Equation 8, the curvature is negative (concave curve). As explained in Section 3.6, the physical interpretation of the concavity is that the initial curing process of the tested CBTM mixtures was characterized by a faster increase of *ITS* with respect to *DW* and thus in this phase the effect of cement hydration prevailed on the effect of evaporation and emulsion breaking. For mixtures CBTM-LABO-DRY and CBTM-SITE-DRY, the same conclusion could be drawn by comparing the fitted values of the Michaelis constant $K_c$ for both *DW* and *ITS* (**Table 8. 5**). Indeed, the same physical interpretation is clearly valid also for mixture CBTM-LABO-WET (where evaporation is negligible), even though it was not possible to fit the MM model to the *DW* evolution.
For CTM mixtures, the relationship between *DW* and *ITS* was plotted only for the CTM-LABO-DRY (**Figure 8. 18**b) because in the case of CTM-SITE-DRY, the number of *ITS* measurements (5) did not allow to obtain a reliable fitting (only two degrees of freedom).

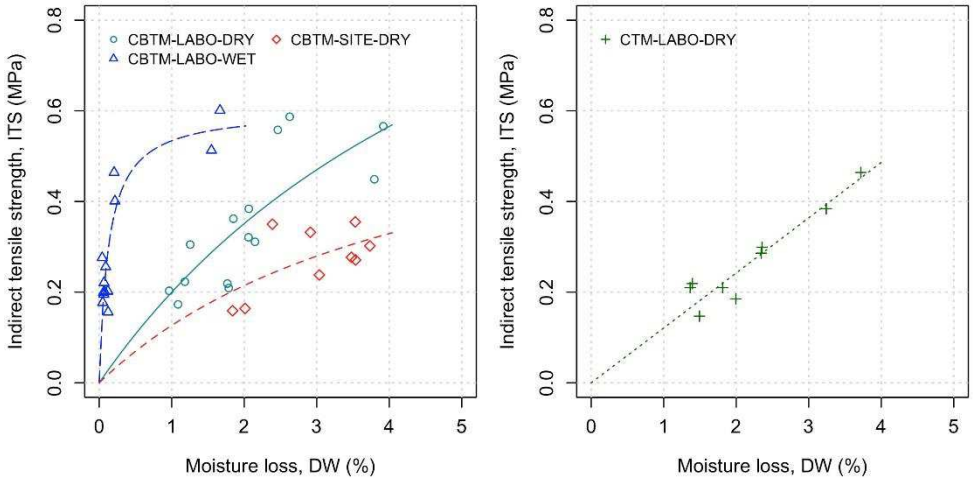


**Figure 8. 19** Relationship between moisture loss (DW) and indirect tensile strength (ITS).

| Mixture | $a_{ITS}$ | $b_{ITS}$ | $c_{ITS}$ | Residual std. error |
|---|---|---|---|---|
| *ITS* vs. *DW* | [MPa] | [%] | [ - ] | [MPa] |
| CBTM-LABO-DRY | 1.45 | 6.26 | -0.074 | 0.087 |
| CBTM-LABO-WET | 0.60 | 0.13 | -71.00 | 0.072 |
| CBTM-SITE-DRY | 0.71 | 4.58 | -0.068 | 0.061 |
| CTM-LABO-DRY | -65.07 | -539.06 | +4.479 | 0.036 |

**Table 8. 6** Regression parameters of the relationship between DW and ITS.

### 8.3.4 Relation between mechanical properties

In **Figure 8. 20**, the measured values of *ITS* are reported as a function of the corresponding measured values of *ITSM*, for the mixtures CBTM-LABO-DRY and CBTM-LABO-WET.
Following the same procedure described in Section 7.2.4, it can be shown that the relation *ITSM = ITSM(DW)* is described by an equation equal to Equation 41 and, consequently, the same nonlinear function can also be used to describe the relationship between *ITS* and *ITSM*:

$$ITS = \frac{a_{ITSM} \cdot ITSM}{b_{ITSM} + ITSM} \tag{48}$$

where $a_{ITSM}$ and $b_{ITSM}$ can be obtained by a nonlinear regression procedure.
First, fitting of the Equation 48 was performed separately for mixtures CBTM-LABO-DRY and CBTM-LABO-WET. The fitted regression curves are superposed to experimental data in **Figure 8. 20** (dashed lines), whereas the values of the fitted parameters $\alpha_{ITSM}$ and $\beta_{ITSM}$ are summarized in **Table 8. 7**. As it can be observed, the fitting appears to be dependent on the curing procedure: DRY vs. WET. Specifically, for the mixture CBTM-LABO-DRY the regression parameters are both negative (convex curve) indicating that *ITSM* increased at faster rate with respect to *ITS.* The same conclusion could be drawn by comparing the fitted values of the Michaelis constant $K_c$ for *ITSM* and *ITS*: 1.80 days and 2.23 days, respectively (**Table 8. 5**). On the other hand, for the mixture CBTM-LABO-WET the regression parameters are both positive (concave curve) indicating that *ITS* increased at faster rate with respect to *ITSM*, in the initial curing stage.
However, since actually the data points of the two mixtures are superposed, a third model was fitted to all the available measurements of *ITSM* and *ITS*, regardless of the curing procedure. The fitted parameters of the "global" model (CBTM-LABO) are summarized in **Table 8. 7**, whereas the fitted regression curve is superposed to the experimental data in **Figure 8. 20** (continuous line). A statistical comparison between the two regression approaches (separate regressions vs. global regression) was performed using the *F*-test, according to the procedure described in [Ritz and Streibig, 2008]. As a result, the value of the *F* statistic was 2.655, corresponding to a *p*-value of 0.101 which suggest that the difference between the two separate fits for WET and DRY conditions is not statistically significant, and therefore the use of the global model is appropriate.

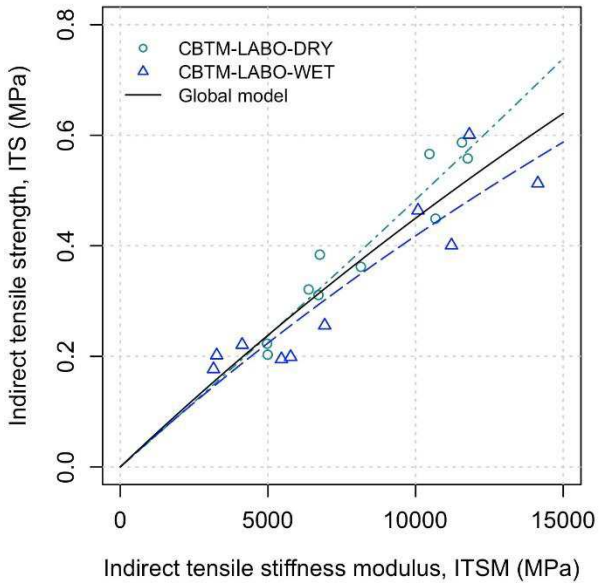


**Figure 8. 20** Relation between indirect tensile stiffness modulus (ITSM) and indirect tensile strength (ITS).

| Mixture | $a_{ITSM}$ | $b_{ITSM}$ | $c_{ITSM}$ | Residual std. error |
|---|---|---|---|---|
| *ITS* vs. *ITSM* | [MPa] | [MPa] | [MPa] | [MPa] |
| CBTM-LABO-DRY | -12.7 | -2.7E+5 | 0.000 | 0.043 |
| CBTM-LABO-WET | 3.11 | 6.45E+4 | -1.495 | 0.065 |
| CBTM-LABO | 4.06 | 8.03E+4 | 0.000 | 0.060 |

**Table 8. 7** Regression parameters of the relationship between *ITS* and *ITSM*.

## 8.4 Summary

The experimental study described in this chapter aimed to investigate the field and laboratory curing process of cold recycled mixtures manufactured during the construction of an instrumented pavement section. Moisture loss by evaporation (*DW*), indirect tensile stiffness modulus (*ITSM*) and indirect tensile strength *(ITS*) were measured and the Michaelis-Menten (MM) model was fitted to the experimental data.

On site, measurements of moisture loss carried out using TDR probes were subsequently compared with those obtained in laboratory weighting specimens of each corresponding mixture.

The adopted curing variables (*DW*, *ITSM* and *ITS*) gave a comparable description of the curing process. Both cement-bitumen treated materials (CBTMs) and cement treated materials (CTMs) are characterized by similar evolutive behavior. Moreover, the trend of

both field and laboratory curing process in terms of evolution of material properties, always exhibited an asymptotic progression that can be appropriately described by the MM model. The MM model also allowed to identify and estimate specific parameters to measure both the initial and the long-term performance.

Concerning the field curing process, the curing condition, DRY or WET (i.e. not sealed or sealed with emulsion tack coat), affects the initial curing rate of the mixtures but this influence disappear at longer curing times. In particular, comparing field and laboratory curing process on the same type of mixtures, it is possible to assess that the different curing conditions, such as temperature and humidity, do not influence the curing process of the subbase layer: the adopted laboratory curing procedure (temperature of 20 ± 2 °C with a constant relative humidity of 50 ± 5%) well simulates the effect of field curing process for cold recycled mixtures.
Focusing on laboratory results, CBTM mixtures cured in sealed conditions exhibited a slower curing rate and a higher long-term performance, in terms of *ITSM*, with respect to CBTM mixtures cured in unsealed conditions. This highlighted the importance of water available inside the specimen in order to promote the cement hydration process. For CBTM mixtures, the *ITS* development in the first part of curing was faster than the *DW*, hence, since *DW* can be directly associated with the curing of bituminous emulsion, this suggests that, in the initial curing stage, the effect of cement hydration prevailed on that of emulsion breaking.

In addition, the relation between *ITS* (or *ITSM*) and *DW* can be described using the same nonlinear equation of the MM model, but without the same constraints on the values of the fitted parameters. Moreover, the curvature of the regression curves shown to have a physical interpretation when CBTM mixtures are analyzed. When applied to the CBTM mixtures tested in this study, the model gave a coherent description of the experimental data and confirmed that their initial curing process was characterized by a faster increase of *ITS* with respect to *DW*. Finally, even the relationship between *ITS* and *ITSM* can be described by the same nonlinear equation of the MM model. When applied to the CBTM mixtures tested in this study, the MM model showed that the effect of the curing condition on the relationship between *ITS* and *ITSM* was not statistically significant.

# Part 2
# Mixture-scale analysis: Laboratory characterization of Cold mixtures

# CHAPTER 9.

## Introduction

The use of cold recycling technologies for pavement maintenance and rehabilitation has constantly increased over the last 20 years. Moreover, the growing use of reclaimed asphalt (RA) allows transportation agencies and contractors to make more efficient use of their resources. Currently, cold mixtures and, in particular, cold recycled mixtures, are mainly used for subbase layers in pavement structures. Moreover, the increasing quantity of RA adopted, which includes aged modified bitumens, and the evolutive behavior of these materials complicate the analysis from both the volumetric and mechanical point of view.
Part 2 describes the several investigations stages planned to address the analysis of physical and mechanical properties of cold mixtures containing high percentage of RA (*Task 2*). A wide experimental program was carried out, involving different cold mixtures, laboratory production procedure and laboratory tests over a wide range of conditions (i.e. temperature, frequency) in order to provide a comprehensive picture of the overall performance. The study has been conducted following three main steps:

- *Step1*: It is focused on the analysis of curing process of cement-bitumen treated materials produced with bitumen emulsion. The evolution of curing was monitored over time using physical and mechanical properties. Moreover, the curing process was all modelled using different asymptotic model;
- *Step2*: it addressed the laboratory characterization in terms of volumetric properties and linear viscoelastic (LVE) response, of cement-bitumen treated materials containing different percentage of RA and produced with bitumen emulsion or foamed bitumen. In addition, the influence of water on the compactability of the fresh mixture was also evaluated.
- *Step3*: Three-dimensional characterization of the stress-strain response of a CRM mixtures. The applicability of both 3D testing protocol and rheological modelling usually adopted for HMA mixtures, was also verified.

## 9.1 Overview

Cold recycling of bituminous pavements is an effective way to preserve our diminishing supply of construction materials, reduce costs of pavement maintenance and limit the carbon footprint of existing road networks [Asphalt Academy, 2009; Stroup-Gardiner, 2011]. Economic and environmental benefits, with respect to both conventional asphalt concrete and hot recycling technologies, derive from the reduction of heating energy, pollutants emission and virgin aggregate (VA) consumption [Stroup-Gardiner, 2011]. In CR process, RA generated from the cold planning of bituminous layers is re-used without heating, producing cold recycled mixtures (CRMs) that are included in new or rehabilitated pavement structures. CRMs show a mechanical behavior strongly dependent on:

- the properties and proportions in which types of aggregate (RA or VA) and binders (bitumen and cement) are mixed. In particular, when the bitumen-cement ratio is less than one and cement content is greater than 1% [Grilli et al. 2012], the mixtures may be considered as cement-bitumen treated materials. Such mixtures generally exhibit asphalt-like properties i.e. time-temperature dependence and cumulative damage failure [Bocci et al. 2011, Stimilli et al. 2013, Thompson et al. 2009].
- curing mechanisms that occur during the early life of CBTM mixtures and at long-term cured state. Curing phenomena depend on the simultaneously presence of water, cement and bitumen phase (in form of bituminous emulsion or foamed bitumen) in the mixture and are related to the interaction of different physical and chemical mechanisms [Brown and Needham, 2000; Giuliani, 2001].

Anyway, when comparing the composition and the behavior of CRM to that of conventional (or recycled) asphalt concrete, two aspects are of the outmost importance. First, water instead of heating is used in order to allow CRM laydown and compaction. Indeed, moisture content is the main factor controlling the rheological properties of CRM in the fresh state, in particular their ability to achieve suitable volumetric properties [Grilli et al. 2012]. Second, the physical structure of CRM evolves over time; the curing process leads to the improvement of the mechanical properties (e.g. stiffness and strength) until reaching long-term cured state [Cardone et al., 2015; Jenkins and Moloto, 2008].
In addition, the curing rate of CRM is extremely important during construction activities because it controls when the upper layers can be constructed and therefore when the new or rehabilitated pavement can be opened to commercial traffic. On the other hand, the long-term material properties are essential for rational pavement design and performance prediction.
Finally, a thorough understanding of the curing process of CBTM requires to define a standardized laboratory procedure that allows to control and measure the current curing mechanisms. This to evaluate the prevailing mechanism and/or possible interaction between them under specific curing conditions and how they affect the mechanical response of materials.

# CHAPTER 10.

# Curing process: analysis and modelling for CBTM

## 10.1 Experimental investigation

### 10.1.1 Materials

The CBTM samples considered in this investigation were produced in the laboratory employing RA, VA, bituminous emulsion, Portland cement and water.
The RA was sampled from a recycling plant and characterized in terms of gradation [EN 933-2], particle density, water absorption [EN 1097-6] and bitumen content [EN 12697-1]. Results are summarized in **Table 10. 1** and **Figure 10. 1**. Before compaction, RA lumps greater than 20 mm were removed to improve the homogeneity of samples (**Figure 10. 2**).
The VA was a crushed limestone sand characterized by maximum dimension of 4 mm . Particle density and absorption are reported in **Table 10. 1**.
Based on grading results, the RA was designated as 40RA 0/12 according to EN 13108-8, whereas the VA was designated as F 0/4 GF85 according to EN 13043. In addition, since for the aggregate blend design the RA was considered as "black rock", it was also designated as 0/32 GA90 according to EN 13043.
A cationic slow-setting bituminous emulsion C60B6 [EN 13808] was selected in this research (**Table 6. 1**). The emulsion is specifically formulated for cold in-place recycling, guaranteeing high mixing stability with cement (over-stabilized emulsion) and good workability during the compaction phase.
A Portland limestone cement type II/A-LL, strength class 32.5 R [EN 197-1] was used. Its composition is a combination of clinker (80 % - 94 %) and limestone dust (20 % - 6 %).
The aggregate blend used in this study was prepared by mixing 80 % RA and 20 % fine VA (**Figure 10. 1**). VA was added to the RA for correcting the fine fraction of the granular blend. As it can be observed, the aggregate gradation fits better the maximum density curve with D = 31.5 mm in the finer fraction of the grading curve. The employed emulsion content was 3.3 % by dry aggregate weight, corresponding to 2 % of fresh bitumen. Two cement dosages, 1 % and 2.5 % by dry aggregate weight, were employed and the corresponding mixtures were coded as C1 and C2.5, respectively.

| Materials | Absorption [%] | Particle density [Mg/m$^3$] | Bitumen content [%] |
|---|---|---|---|
| Reclaimed asphalt | 1.0 | 2.470 | 4.84 |
| Virgin aggregate | 0.9 | 2.712 | - |

**Table 10. 1** Main physical properties of granular materials used for the experimental program

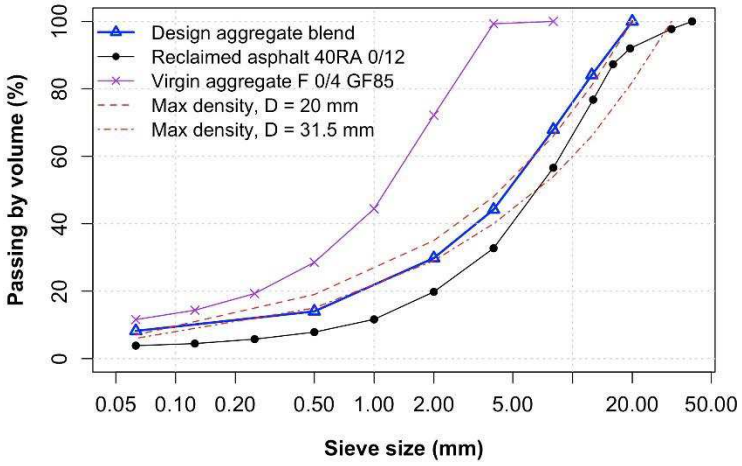


**Figure 10. 1** Grading curves of tested mixture and granular materials.

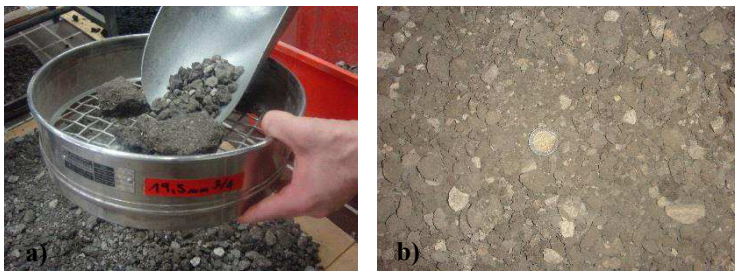


**Figure 10. 2** Reclaimed asphalt used for the experimental program: a) removal of lumps greater than 20 mm; b) RA sieved at 20 mm.

## 10.1.2 CBTM specimens production

In order to facilitate the control of the water content, oven-dried aggregates were employed. The drying temperature was 105 ± 2 °C for VA and 40 ± 2 °C for RA.

The total water content ($w_{tot}$) of each mixture was composed by water from emulsion ($w_{em}$) and additional water ($w_{add}$), which was added in two phases. The first part ($w_{add,1}$), corresponding to the water absorption of the aggregate blend, was added to the dry aggregates the day before mixing. The wet mixture (aggregate containing $w_{add,1}$) was stored in a sealed plastic bag for 24 hours at room temperature in order to ensure a homogeneous moisture condition and to allow absorption by the aggregate. Subsequently, the aggregate blend was thoroughly mixed, gradually adding the remaining part of the additional water ($w_{add,2}$), cement and emulsion, in sequence. Samples were mixed with a mechanical mixer at room temperature for at least two minutes, time required to guarantee a good particle coating (visual evaluation).

Immediately after mixing, specimens were compacted by means of a shear gyratory compactor (SGC) according to EN 12697-31 (Section 7.2.1). After compaction, specimens

were sufficiently stable to allow extrusion and were immediately weighted to check any material loss (**Figure 10. 3**).

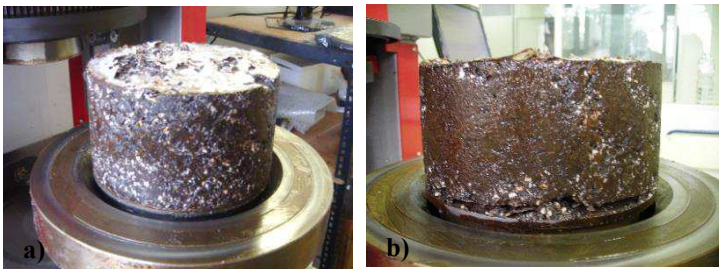


**Figure 10. 3** Specimens compacted by SGC immediately after extrusion produced: a) $w_{tot}$ = 5 % and b) $w_{tot}$ = 7 %.

## 10.1.3 Water content optimization

This preliminary phase was performed in order to establish the total water content $w_{tot}$ of the CBTM mixtures for compaction purpose and optimize the total fluids content of the mixture (Section 2.6.5).
The $w_{tot}$ optimization was based on the volumetric characterization of compacted CBTM specimens, carried out according to the procedure described in [Grilli et al., 2012] and explained in details in Section 2.8.2. The procedure was adapted from that currently adopted for the determination of void characteristics of bituminous specimens [EN 12697-8]. In particular, the following parameters were evaluated:

- Voids in the mixture $V_m$, which designates the percentage of total mixture volume that is occupied by air and free water (water not absorbed by aggregates);
- Voids in the mineral aggregate *VMA*, which designates the percentage of total mixture that is occupied by air, free water and fresh bitumen;
- Voids filled with liquid *VFL*, which designates the percentage of *VMA* that is occupied by water and fresh bitumen.

$V_m$, refers to the volume of the non structural part of the mixture (air voids and water) and was evaluated as:

$$Vm = \frac{\rho_m - \rho_d}{\rho_m} \cdot 100 \quad (49)$$

where $\rho_m$ is the maximum density of the loose mixture whereas $\rho_d$ is the dry bulk density of the compacted mixture (i.e. the ratio of the total mass of solids to the total mixture volume). $\rho_m$ was calculated considering only aggregates, cement and bitumen (not including water), whereas $\rho_d$ was calculated considering the height data recorded during SGC compaction.
*VFL* was evaluated as:

$$VFL = L_F \cdot \frac{\rho_d}{\rho_w} \cdot \frac{100}{VMA} \quad (50)$$

where $L_F$ is the free liquid content, $\rho_w$ is the water density and *VMA* indicates the voids in the aggregate mixture (i.e. the ratio of the volume occupied by air, free water and fresh bitumen to the total mixture volume). $L_F$ is the ratio of the mass of free water (water not absorbed by aggregates, either from the emulsion or added separately) and fresh bitumen to the total mass of solids (aggregate, cement) and free bitumen. Additional details on the calculation procedures are reported in Section 2.8.2.

The CBTM sample employed for the volumetric analysis was characterized by same aggregate blend described for mixtures C1 and C2.5, stabilized with the 3.3 % of emulsion and 1.5 % of cement. Specimens were compacted by means of SGC, according to the previously described procedure, at $w_{tot}$ values of 4 %, 5 %, 6 % and 7 % (two replicate specimens for each $w_{tot}$) up to 180 gyrations.

**Figure 10. 4** reports the average compaction curves obtained for each $w_{tot}$ in terms of $V_m$ and *VFL* as function of number of gyrations, on a logarithmic scale.

The voids in mixture $V_m$ decreased with the increase in gyrations number (**Figure 10. 4**a). Moreover, it can be observed that the increase in water content resulted in a decrease in $V_m$. The mixture with $w_{tot}$ = 7 % showed a different trend, highlighting always a lower $V_m$ during the compaction process.

On the other hand, it can be noticed that *VFL* increased as the number of gyrations and $w_{tot}$ increased (**Figure 10. 4**b). This indicates that during compaction water progressively filled the voids volume available within the mixture. *VFL* computed with Equation 50 is similar to the degree of saturation, hence a value of 100 % represents the saturated condition of the mixture. All mixtures showed a *VFL* below 100 % at the end of compaction, except for the mixture at $w_{tot}$ = 7 % that showed a *VFL* exceeding 100 % already at 100 gyrations (**Figure 10. 4**b). *VFL* values above 100 % can not represent a possible physical condition, hence the results reported in **Figure 10. 4**b can be explained by an excess of water, that was squeezed out from the bottom and the top of the compaction mold. This phenomenon was actually observed at the end of the compaction process (**Figure 10. 3**b). In addition it was also observed that bitumen and fine aggregate particles were also forced out of the mold.

The same situation was also observed in previous experimental studies carried out on both bitumen emulsion [Grilli et al., 2012; Godenzoni et al., 2016], and foamed bitumen mixes. In particular, it has been shown that *VFL* values above 90 % generally imply a visible loss of liquids and fines from the mold, as highlighted in **Figure 10. 3**b. In such case, the actual composition of the compacted sample could be significantly different from the design composition.

These experimental results suggested the following criterion for the selection of compaction energy (number of gyrations) and total water content ($w_{tot}$) to be adopted for compaction purpose. Because increasing $w_{tot}$ helps in reducing $V_m$, its value should be as high as possible. However, drainage of water (mixed with bitumen and fines) should always be avoided. The latter situation, which generally corresponds to *VFL* values above 90 %, leads to establish an upper limit for $w_{tot}$, related to the number of gyrations. In the present study in order to avoid drainage from the compaction mold (*VFL* < 90), a value $w_{tot}$ = 5 % was selected (**Figure 10. 3**a), along with a compaction energy $N$ = 100.

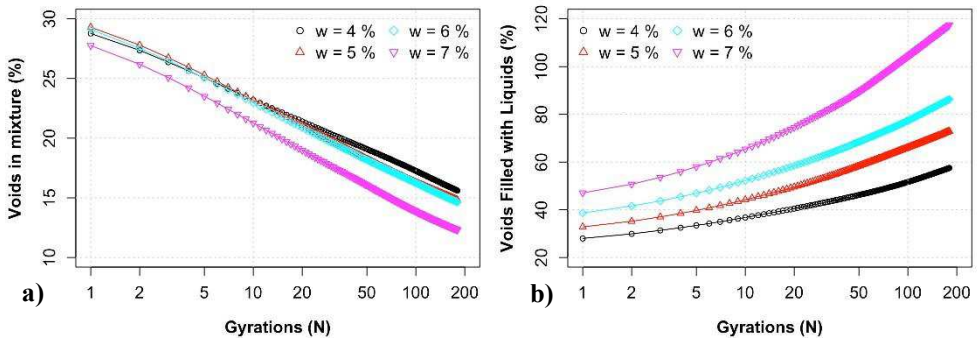


**Figure 10. 4** Influence of water content on the compactability of CBTM: a) void in mixture (Vm); b) voids filled with liquida (VFL).

## 10.1.4 Test program and curing procedure

The curing process was analyzed by monitoring moisture loss by evaporation *(DW),* indirect tensile strength (*ITS*) and indirect tensile stiffness modulus (*ITSM*) of compacted CBTM specimens at six curing times: 1, 3, 7, 14, 28 and 100 days. Two curing temperatures, 25 °C and 40 °C, were selected.

For each mixture (C1 and C2.5), curing time and temperature, two replicate specimens were produced. In particular, 2800 g of wet mixture ($w_{tot}$ = 5 %) were compacted at 100 gyrations obtaining an average specimen height of approximately 70 mm, suitable for mechanical testing. A total of 24 specimens with identical composition were produced for each mixture. After compaction, specimens were weighted and their volumetric properties ($V_m$ and *VFL*) were checked in order to evaluate the repeatability of the sample preparation procedure (i.e. mixing and compaction).

*DW* was measured by carefully weighting each specimen before mechanical testing. *ITS* and *ITSM* were measured according to EN 12697-23 and UNI EN 12697-26-Annex C, respectively. Moreover, both test procedures are explained in detail in Section 7.2.2 and 7.2.3. Both *ITS* and *ITSM* tests were carried out at 20 °C; specimens cured at both 25 °C and 40 °C were conditioned at 20°C for 4 hours before testing. The testing program is summarized in **Table 10. 2**.

| | **Moisture loss** | **ITS & ITSM** |
|---|---|---|
| Mixture code | C1, C2.5 | C1, C2.5 |
| Curing temperature (°C) | 25, 40 | 25, 40 |
| Curing time (days) | 1, 3, 7, 14, 28, 100 | 1, 3, 7, 14, 28, 100 |
| Testing temperature (°C) | 25, 40 | 20 |

**Table 10. 2** Summary of the testing program.

For each mixture (C1 and C2.5), two groups of 12 specimens were cured separately at 25 ± 2 °C and 40 ± 2 °C. A constant relative humidity of 70 ± 5 % was adopted. This value was considered a reasonable compromise to achieve curing of both the bituminous phase (based on emulsion breaking and moisture loss) and the cementitious components (which require a

moist environment). Specimens were not sealed during curing to guarantee free water evaporation.

## 10.1.5 Modelling of curing effects

Modelling of curing effects was carried out using a statistical regression analysis of the evolution of *DW*, *ITS* and *ITSM* (dependent or response variables) versus curing time (independent variable or predictor).
The general form of a statistical regression model is as follows

$$y = E(y|x) + \varepsilon = f(x, \beta_i) + \varepsilon \tag{51}$$

where $y$ is the observed response (a random variable), $x$ is the predictor, $E(y|x)$ is the conditional mean value of $y$ (conditional on the value of the predictor $x$) and $\varepsilon$ is a random error term [Montgomery and Runger, 2003]. According to Equation 51 in this study it was assumed that, given a value of the curing time ($t$), the mean value of *DW*, *ITS* and *ITSM* can be modelled by a function $f(t,\beta_i)$ depending on a set of unknown parameters $\beta_i$.
Two nonlinear models were employed for the regression: the Michaelis-Menten model (MM) (see Chapter 8) and the exponential model (EX).
The Michaelis-Menten model (MM) was already employed in Chapter 8 for modelling the curing process over time of CRMs used as subbase layers.
In this investigation MM model is compared with EX model; both models describe an asymptotic evolution of the measured response as a function of time using two parameters; one representing the asymptotic value of the response and one representing the initial rate of growth.
In the present study, the Michaelis-Menten model is adopted using the following equation:

$$f\big(t, (y_A, K_c)\big) = \frac{y_A \cdot t}{K_c + t} \tag{52}$$

where $y_A$ is the asymptotic value of the response (when $t$ —> ∞, i.e. long-term condition) and $K_c$, also known as the Michaelis constant, represents the curing time when $y = y_A/2$.
The Michaelis-Menten equation defines a rectangular hyperbola through the origin. At the beginning of curing ($t = 0$), the model predicts a zero value for *DW*, *ITS* and *ITSM*. As curing time increases, the response asymptotically approaches the long-term value $y_A$. The Michaelis constant can be viewed as a measure of the initial curing rate: a lower $K_c$ value implies a faster increase of *DW*, *ITS* and *ITSM*.
The asymptotic exponential model is commonly adopted to predict the evolution of a quantity decreasing at a rate proportional to its current value (exponential decay). In the present study the exponential decay model was adapted for the analysis of curing using the simple equation:

$$f\big(t, (A, c)\big) = A \cdot (1 - e^{(-e^c \cdot t)}) \tag{53}$$

where $A$ is the asymptotic value of the response (long-term curing condition) and $e^c$ is the decaying rate.

A more intuitive characteristic of exponential decay the time required for the quantity to become half of its initial value; this time is called the half life and can be written as $t_{1/2} = \ln(2) / e^c$. Here $t_{1/2}$ represents the curing time when $y$ is equal to $A/2$ and therefore its value can be directly compared with the Michaelis constant.
**Figure 10. 5** depicts an example of the MM and EX models with the same asymptotic value ($y_A = A = 1$) and the same initial curing rate ($K_c = t_{1/2} = 7$ days). As it can be observed, the models are almost superposed until one half of the asymptotic value. Afterwards, the MM model predicts a slower evolution of the response, with respect to the EX model.
Both the MM and the EX regression models were fitted by minimization of the residual sum of squares (RSS) with respect to the regression parameters (least-squares minimization):

$$RSS(\beta) = \sum_{i=1}^{n}(y_i - f(t_i, \beta_1, \beta_2))^2 \tag{54}$$

The numerical solution was obtained using R [https://www.r-project.org], a free software environment for statistical computing and in particular the model fitting function `nls()` [Bates and Chambers, 1992]. Within `nls()`, RSS minimization was carried out using the default Gauss-Newton algorithm and the self-starter functions `SSmicmen()` and `SSasympOrig()` were employed.
In order to ensure that the conclusions based upon the analysis of a fitted regression model are correct, the assumptions underlying the nonlinear regression must be validated. In particular the structure of the selected mean function $f(x,\beta_i)$ must be correct and the errors must be uncorrelated, normally distributed random variables with constant variance. In order to verify these assumption graphical procedures based on residuals plots will be used.
The raw residuals $r_i$ are defined as the difference between the measured values of the response and the corresponding fitted values:

$$r_i = y_i - f(t_i, \beta_1, \beta_2) \tag{55}$$

whereas the standardized residuals $e_i$ are defined as the raw residuals divided by their standard error $s$:

$$e_i = r_i / s \tag{56}$$

A plot of the standardized residuals versus fitted values will help in checking if the adopted mean function is adequately capturing the average trend of the data and in detecting deviations from the normal distribution. The latter issue can also be verified using a normal QQ plot comparing the quantiles of the standardized residuals and of the standard normal distribution [Raaijmakers, 1987; Dalgaard, 2002]. If the points in the QQ plot approximately follow a straight line with intercept 0 and slope 1, the two distribution agree.

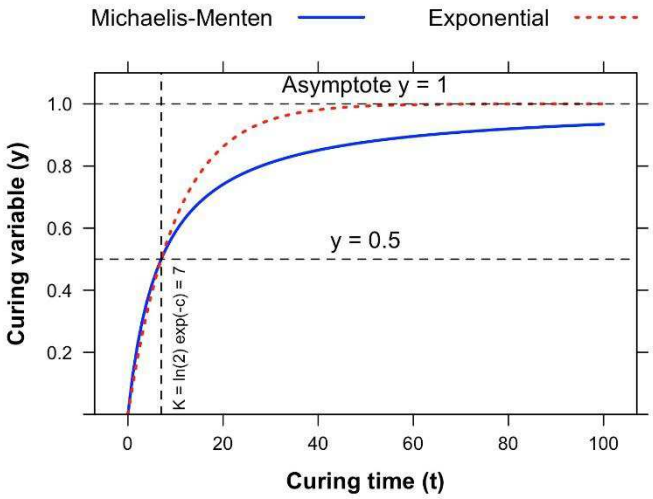


**Figure 10. 5** Comparison of the Michaelis-Menten and Exponential models.

# 10.2 Experimental findings

## 10.2.1 Volumetric properties of the tested specimens

The volumetric properties $V_m$ and *VFL* of the 48 specimens prepared to monitor the evolution of *DW, ITS* and *ITSM* were first analyzed in order to evaluate their homogeneity and the repeatability of the sample preparation procedure.

The weight loss which occurs during compaction is summarized in **Figure 10. 6** in terms of frequency distribution, partial and cumulative. As it can be observed (**Figure 10. 6**) the relative frequency distribution is positively skewed and is characterized by a median value of 0.10 %. Visual observations, performed during specimen extrusion, suggested that such small loss of weight could be assumed to be exclusively a loss of water. Since the specimens are not completely saturated, the water loss can be assumed to occur only from the bottom or the top of the compacted specimens. On the basis of the previous considerations, the 85 % of the specimens had a water loss smaller than 0.3 %, hence their total water content, after compaction and before the curing phase, ranged between 5.0 % (the initial $w_{tot}$) and 4.7 %.

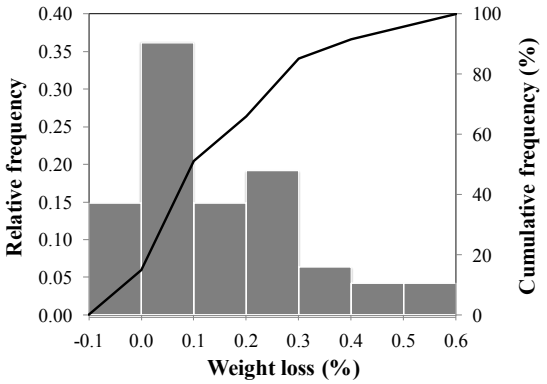


**Figure 10. 6** Relative frequency distribution of the measurements of weight loss during SGC compaction.

The results of volumetric analysis, are summarized in **Figure 10. 7** in terms of relative frequency distribution. Both distributions of the experimental data depict a typical "bell-shaped" trend rather symmetrical. In particular, the $V_m$ distribution is characterized by a mean value of 12.7 % and a standard deviation of 0.7 %, whereas the *VFL* distribution shows a mean value of 73.5 % and standard deviation of 3.4 %.

As far as *VFL* is concerned, it can be noted that all specimens were characterized by values lower than 90% (a maximum of 81% was obtained). This means that no specimen approached saturated condition and hence, the $w_{tot}$ used for specimen production resulted suitable to enhance the workability and partially fill the voids in the specimen.

In both plots, the continuous lines which match the histogram values, describe the normal distribution characterized by the previous parameters (i.e. mean and standard deviation) suggesting that the sample agrees with the normal distribution. The normality of the data allows to conclude that the production of the specimens was carried out under repeatability conditions.

Overall, the analysis of $V_m$ and *VFL* allowed the reliability of the mixing and compaction procedure to be highlighted and therefore the adopted protocol for the production of homogeneous specimens to be validate.

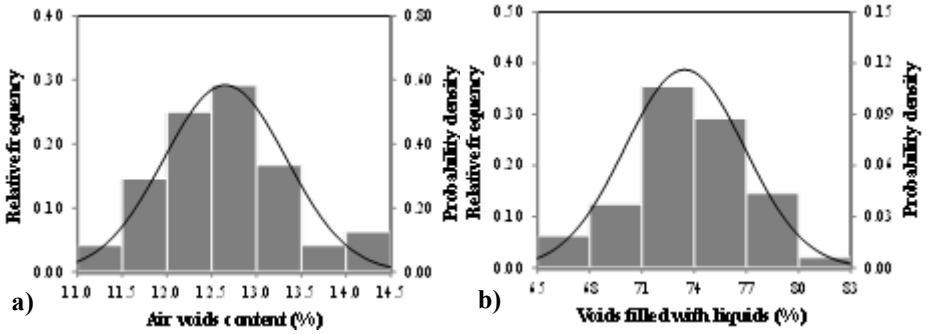


**Figure 10. 7** Frequency distribution of volumetric properties: a) $V_m$ and b) *VFL*.

## 10.2.2 Evolution of material properties

**Figure 10. 8** to **Figure 10. 10** show the evolution of *DW*, *ITSM* and *ITS* as a function of curing time, for mixtures C1 and C2.5 and for both curing temperatures (25 °C and 40 °C). The regression curves obtained with the fitted Michaelis-Menten and Exponential models are superposed to the experimental data. The estimated values of the regression parameters and their standard errors are summarized in **Table 10. 3** and **Table 10. 4** together with the standard error of the residuals.

*Adequacy of the regression models*

The first step in verifying the adequacy of the adopted regression models was to visually check if the measured data of *DW*, *ITSM* and *ITS* actually follow the asymptotic trend described by the Equation 52 and 53. From **Figure 10. 8** to 9 it can be observed that agreement between the measured data and the estimated regression curves is quite good. In addition, from **Table 10. 3** and **Table 10. 4** it can also be noticed that, for all parameters, in all conditions, the values of $y_A$ are higher than the values of $A$. This indicates that the EX model underestimated the asymptotic values of *DW*, *ITSM* and *ITS*, with respect to the MM model.

The plot of the standardized residuals versus the fitted values of *DW* and *ITS* are reported in **Figure 10. 11**a, **Figure 10. 11**b, **Figure 10. 12**a and **Figure 10. 12**b (the plots for *ITSM* are very similar to those for *ITS* and are not shown). A visual examination does not reveal any systematic pattern, for both the MM and the EX models. Moreover, the standardized residuals ranged between -2 and +2 indicating the absence of outliers or heavy tails.

The normal QQ plots for the residuals of *DW* and *ITS* are reported in **Figure 10. 11**c, **Figure 10. 11**d, **Figure 10. 12**c and **Figure 10. 12**d. For both properties the data points plot reasonably well along the equality line. This confirms that for both models the errors may be considered normally distributed.

Overall, the residuals analysis reveals that, from a statistical point of view, both the MM and the EX models appear adequate to describe the curing process. However, checking the values of the standard errors reported in **Table 10. 3** and **Table 10. 4**, it can be observed that, for all mixtures and test conditions, the standard errors of the MM model were lower with respect to those of the EX model.

In conclusion the accuracy of the two models is comparable, however the MM model is characterized by a better precision. Therefore, in the following sections, only the MM model will be used for the analysis of the curing process.

*Moisture loss*

From **Figure 10. 8** it can be observed that, for mixture C1, *DW* after one day curing was 1.8 % and 3.0 % at 25 °C and 40 °C, respectively. This difference reduced at longer times until 100 days, when similar *DW* (approximately 4.4 %) were measured for both curing temperatures. Analogously, for mixture C2.5, *DW* after one day curing was 1.4 % and 2.6 % at 25 °C and 40 °C, respectively. This difference reduced at longer times and at 100 days a similar weight loss (approximately 3.9 %), was measured for both curing temperatures.

In addition, it can be observed that, at 40 °C, the moisture loss did not increase after 14 days anymore, whereas at 25 °C such an “equilibrium” condition was not obtained before 100 days.

Results showed that, for both mixtures, the curing temperature affected the rate of water evaporation but did not modify the water content measured after 100 days $w_{eq}$.
The value of $w_{eq}$ can be measured considering that the initial water content of the compacted specimens is comprised between 5.0 % and 4.7 %. Thus, assuming an average initial value of 4.85 %, $w_{eq}$ = 0.55% and $w_{eq}$ = 0.95% were estimated for mixtures C1 and C2.5, respectively. Therefore, the moisture loss by evaporation decreased with increasing cement content. This evidence is consistent with the fact that cement reduced the evaporable water amount.
It should be considered that $w_{eq}$ contains the water required for the hydration of cement $w_{hydr}$ that is not available for evaporation. Part of $w_{hydr}$, about 23% of cement weight, is required to form the calcium-silicate-hydrate (C-S-H) gel, whereas another part, about 19% of cement weight, is absorbed by the nano-porosity of C-S-H gel and can be removed only at very low relative humidity [Mehta and Monteiro, 1993]. Hence, the amount of water needed for the hydration process can be calculated as:

$$W_{hydr} = (0.23 + 0.19) \cdot \alpha \cdot k \cdot C \tag{57}$$

where $\alpha$ is the degree of hydration of the cement paste, $C$ is the cement content within the mixture and $k$ is the fraction of Portland cement clinker in the cement.
Assuming $k$ = 0.87 (average of the clinker content range) and $\alpha$ = 0.95 at 100 days of curing [Mehta and Monteiro, 1993] Equation 57 yields $w_{hydr}$ = 0.33% and $w_{hydr}$ = 0.82% for mixtures C1 and C2.5, respectively.
The comparison between the $w_{eq}$ and $w_{hydr}$ showed that a small fraction of potentially evaporable water (= $w_{eq}$ - $w_{hydr}$) is still contained inside the mixtures; in particular, 0.22 % and 0.13 % for mixtures C1 and C2.5, respectively. This fraction of potentially evaporable water is probably trapped inside the surface porosity of the aggregate or inside the bituminous mortar [Garcia et al., 2013].
Since, for both mixtures $w_{eq} > w_{hydr}$, it can be hypothesized that moisture evaporation did not hinder the hydration process of cement.

A parametric evaluation of the *DW* evolution can be obtained considering the MM model. In particular, the estimated value of $K_c$ can be used to evaluate the initial curing rate (i.e. the time required to reach one half of the asymptotic value), whereas the estimated value of $y_A$ can be used to estimate the long-term (asymptotic) behavior.
For mixture C1, $K_c$ was 1.54 days and 0.51 days, for curing at 25 °C and 40 °C, respectively (Table 4). Analogously, for mixture C2.5, $K_c$ was 1.88 days and 0.49 days, for curing at 25 °C and 40 °C, respectively. These values indicate that initial curing at 40 °C was more than 3 times faster with respect to curing at 25 °C. Clearly the increase in curing temperature had a dramatic effect on the initial *DW* evolution, whereas the impact of cement dosage was less evident.
Considering the long-term behavior, it can be observed that the asymptotic values of *DW* for mixture C1 (4.16 % for curing at 25 °C and 4.37 % for curing at 40 °C) were higher with respect to those estimated for mixture C2.5 (3.82 % for curing at 25 °C and 4.10 % for curing at 40 °C). It can be concluded that higher cement dosage led to lower moisture loss, at both curing temperatures.

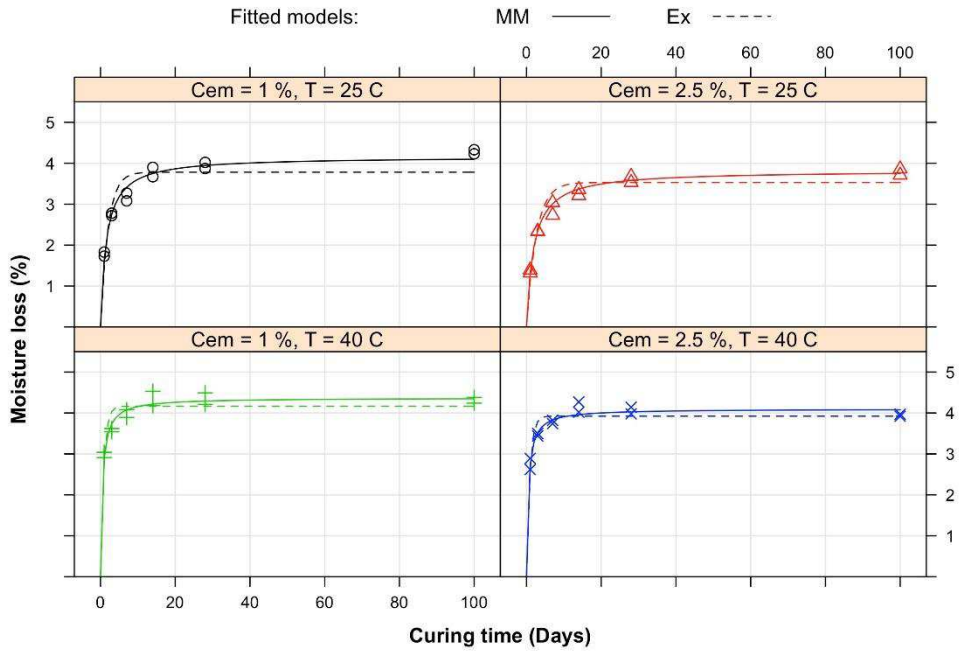


**Figure 10. 8** Evolution of moisture loss (*DW*) versus curing time (1, 3, 7, 14, 28 and 100 days).

*Indirect tensile stiffness modulus*

**Figure 10. 9** highlights the effect of both cement dosage and curing temperature on *ITSM* evolution. Similar to *DW*, this effect can be evaluated by analyzing the parameters of the MM model.

As far as the initial curing rate is concerned, the MM model indicates that C1 specimens cured at 25 °C required 4.48 days to reach one half of the asymptotic ITSM value. Increasing the curing temperature to 40 °C, the initial stiffness development rate was almost 2.5 times higher ($K_c$ = 1.85 days). Analogously, for C2.5 specimens the increase in curing temperature from 25 °C to 40 °C resulted in a $K_c$ reduction from 3.02 days to 1.73 days. In addition, at both curing temperatures, higher cement dosage resulted in higher initial curing rates (**Table 10. 3**). It is highlighted that the $K_c$ values for *ITSM* were always higher with respect to those estimated for *DW*, indicating that, regardless of cement dosage and curing temperature, the initial stiffness increase was slower with respect to the increase of moisture loss. Since moisture loss can be directly associated with the curing of the bituminous emulsion, this also suggests that the effect of cement hydration was more important at longer curing times.

As far as the long-term performance is concerned, the asymptotic *ITSM* values estimated by the MM model for C1 specimens were 3341 MPa and 4154 MPa, for curing at 25 °C and 40 °C, respectively. Increasing the cement dosage, the estimated asymptotic *ITSM* values increased to 6612 MPa and 7726 MPa, for curing at 25 °C and 40 °C, respectively. This highlights the important effect of cement dosage on the long-term performance of the mixtures.

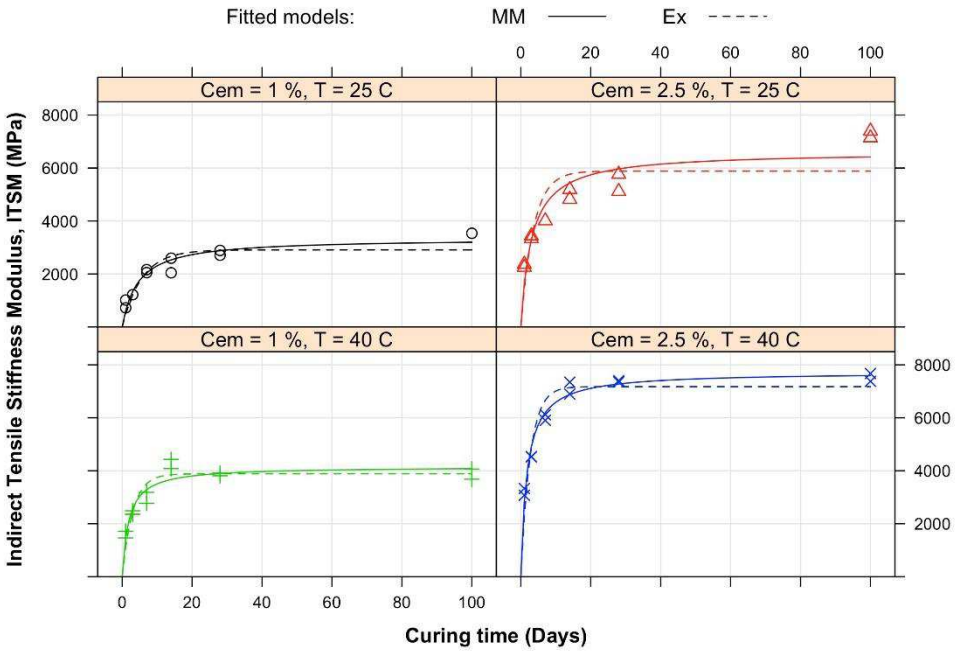


**Figure 10. 9** Evolution of indirect tensile stiffness modulus (ITSM) at 20°C versus curing time (1, 3, 7, 14, 28 and 100 days).

*Indirect tensile strength*

*ITS* evolution (**Figure 10. 10**) showed a trend similar to that of *ITSM* (**Figure 10. 9**).

As far as the initial curing rate is concerned, the MM model indicates that C1 specimens reached one half of the asymptotic performance after 3.24 days and 1.24 days, at curing temperatures of 25 °C and 40 °C, respectively. Analogously, for C2.5 specimens the increase in curing temperature from 25 °C to 40 °C resulted in a $K_c$ reduction from 2.56 days to 1.08 days.

It is highlighted that $K_c$ values estimated for *ITS* were always higher with respect to those estimated for *DW* but lower with respect to those estimated for *ITSM*, i.e. the initial strength development was faster than the stiffness development. This suggests that curing of the bituminous emulsion mainly contributed to the evolution of *ITS*, whereas the evolution of *ITSM* was more linked to the formation of hydration products, which do not entail any moisture loss.

In summary, the experimental results suggest that curing associated with emulsion breaking and evaporation (moisture loss) had a marked impact on strength development, whereas curing associated with cement hydration influenced the delayed development of stiffness.

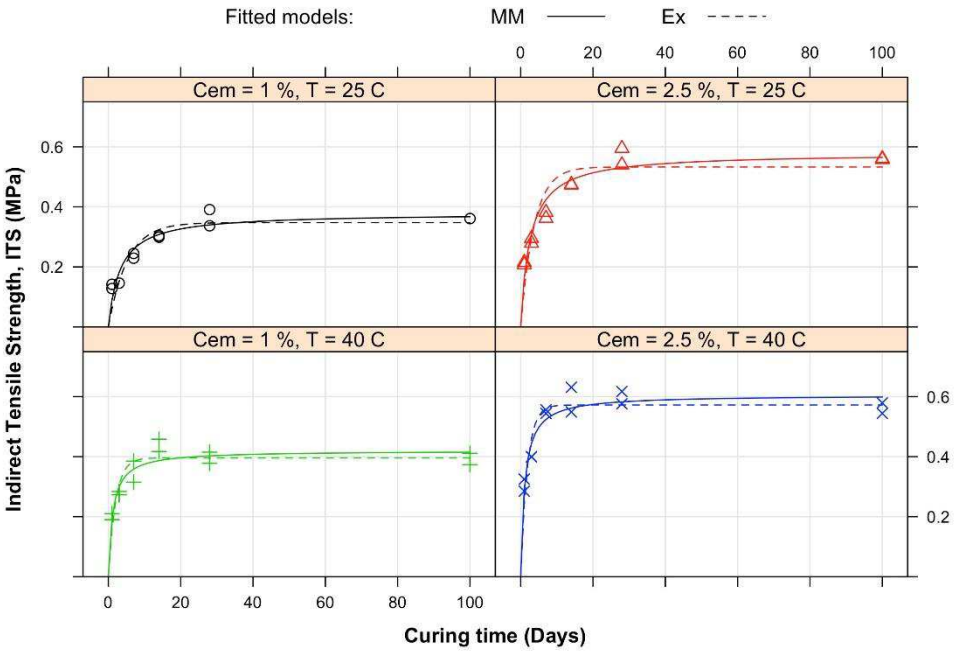


**Figure 10. 10** Evolution of indirect tensile strength (ITS) at 20°C versus curing time (1, 3, 7, 14, 28 and 100 days).

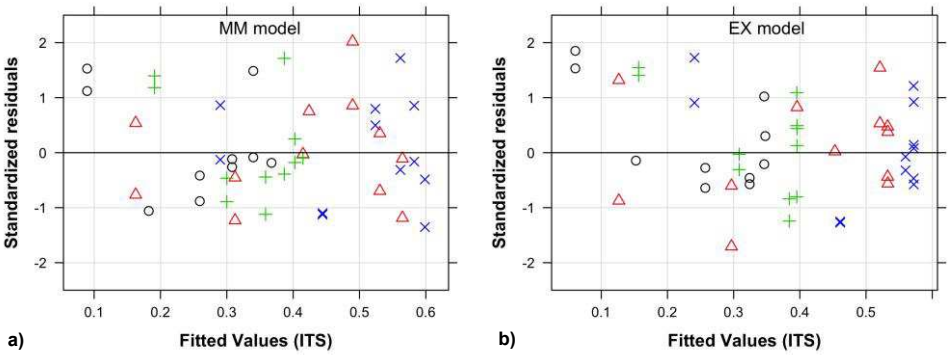

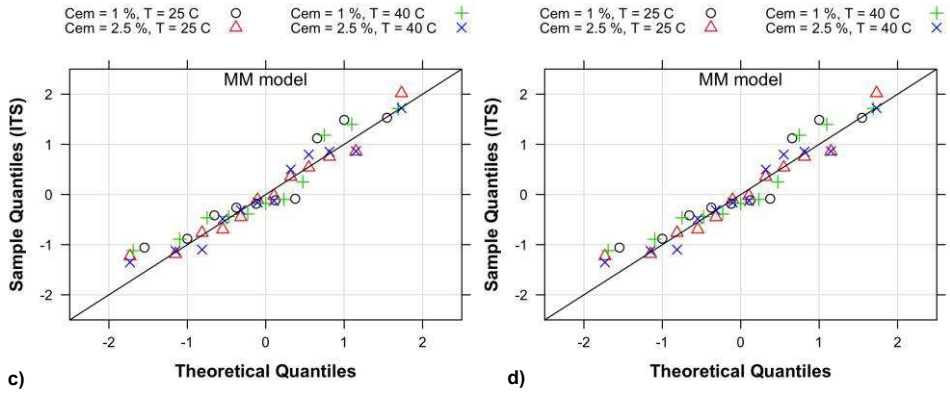


**Figure 10. 11** Residual plots for ITS: a) b) standardized residuals versus fitted values; c) d) normal QQ plot.

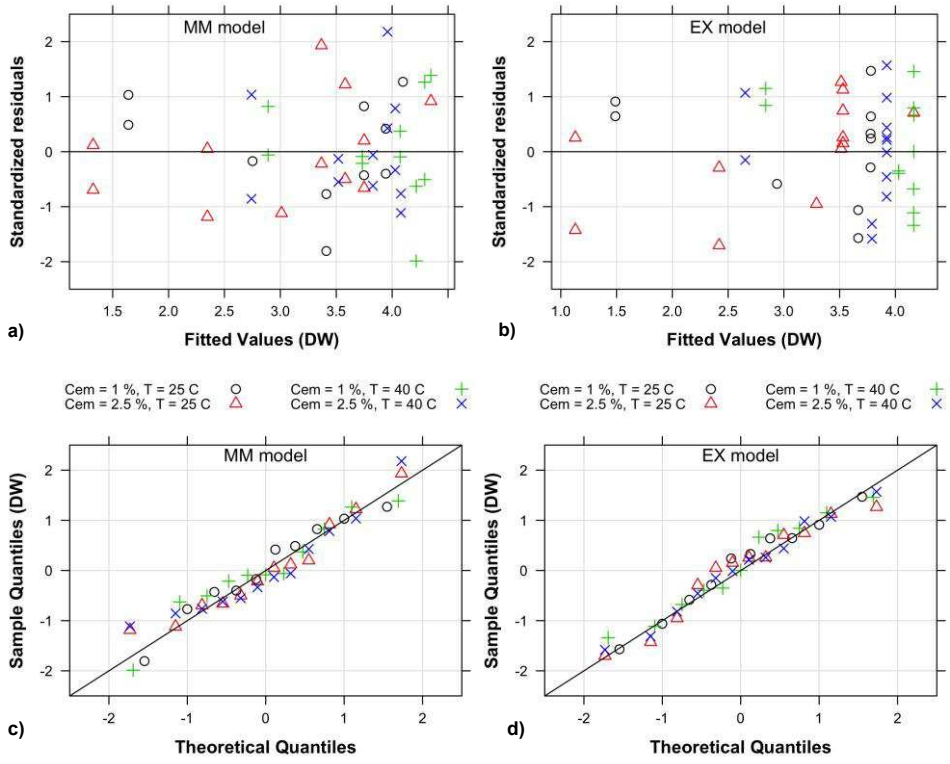


**Figure 10. 12** Residual plots for DW: a) b) standardized residuals versus fitted values; c) d) normal QQ plot.

| Mixture | $y_A$ | | $K_c$ | | Residual Std. Error |
|---|---|---|---|---|---|
| | Estimate | Std. Error | Estimate | Std. Error | |
| **Moisture loss** | | | | | |
| C1T25 | 4.16 | 0.0801 | 1.54 | 0.1574 | 0.1835 |
| C1T40 | 4.37 | 0.0597 | 0.51 | 0.0582 | 0.1627 |
| C2.5T25 | 3.82 | 0.0751 | 1.88 | 0.1857 | 0.0793 |
| C2.5T40 | 4.10 | 0.0595 | 0.49 | 0.0608 | 0.1427 |
| **ITSM** | | | | | |
| C1T25 | 3341 | 345.36 | 4.48 | 1.7613 | 272.7 |
| C1T40 | 4154 | 218.23 | 1.85 | 0.4877 | 361.5 |
| C2.5T25 | 6612 | 248.64 | 3.02 | 0.5084 | 664.9 |
| C2.5T40 | 7726 | 214.81 | 1.73 | 0.2465 | 311.8 |
| **ITS** | | | | | |
| C1T25 | 0.38 | 0.0261 | 3.24 | 0.9459 | 0.0343 |
| C1T40 | 0.42 | 0.0171 | 1.20 | 0.2822 | 0.0353 |
| C2.5T25 | 0.58 | 0.0204 | 2.56 | 0.4209 | 0.0375 |
| C2.5T40 | 0.60 | 0.0168 | 1.08 | 0.1803 | 0.0403 |

**Table 10. 3** Regression parameters of the Michaelis-Menten model for the time evolution of DW, ITSM and ITS.

| Mixture | $A$ | | $C$ | | $t_{1/2}$ | Residual Std. Error |
|---|---|---|---|---|---|---|
| | Estimate | Std. Error | Estimate | Std. Error | | |
| | **Moisture loss** | | | | | |
| C1T25 | 3.78 | 0.1126 | -0.69 | 0.1473 | 1.38 | 0.3738 |
| C1T40 | 4.16 | 0.0932 | 0.13 | 0.1364 | 0.60 | 0.2880 |
| C2.5T25 | 3.53 | 0.1124 | -0.95 | 0.1363 | 1.79 | 0.2267 |
| C2.5T40 | 3.92 | 0.0933 | 0.12 | 0.1443 | 0.61 | 0.2212 |
| | **ITSM** | | | | | |
| C1T25 | 2910 | 348.27 | -1.73 | 0.4162 | 3.91 | 385.0 |
| C1T40 | 3886 | 253.84 | -1.10 | 0.2728 | 2.08 | 404.8 |
| C2.5T25 | 5884 | 266.75 | -1.28 | 0.1859 | 2.49 | 962.3 |
| C2.5T40 | 7175 | 247.17 | -0.97 | 0.1488 | 1.82 | 582.9 |

| | ITS | | | | | |
|---|---|---|---|---|---|---|
| C1T25 | 0.35 | 0.0258 | -1.65 | 0.2666 | 3.61 | 0.0439 |
| C1T40 | 0.40 | 0.0179 | -0.69 | 0.2113 | 1.38 | 0.0405 |
| C2.5T25 | 0.53 | 0.0205 | -1.30 | 0.1572 | 2.54 | 0.0572 |
| C2.5T40 | 0.57 | 0.0176 | -0.60 | 0.1475 | 1.26 | 0.0487 |

**Table 10. 4** Regression parameters of the Exponential model for the time evolution of DW, ITSM and ITS.

### 10.2.3 Relation between moisture loss and mechanical properties

In the previous section a parametric approach to analyse the curing process of CBTM in the laboratory was developed. The evolution of physical and mechanical properties (*DW* and *ITSM*/*ITS*) as a function of curing time was modelled using the Michaelis-Menten asymptotic model and characterized by means of two parameters representing the initial curing rate ($K_c$) and the long-term (asymptotic) behaviour ($y_A$).

Though the conclusions regarding the long-term properties of the tested materials may be considered quite general, their rate of increase is strictly related to the laboratory curing conditions and in particular to shape and dimensions of the specimens. Indeed, it is reasonable to assume that smaller specimen will cure faster than larger specimens. In general, this issue poses some limitations when trying to generalize the laboratory findings to field curing conditions. A possible way to overcome this limitation is to look for a direct correlation between moisture loss and mechanical properties. In such case the assumption is that the same correlation should hold under field curing condition.

In **Figure 10. 13** and **Figure 10. 14** the measured values of *ITS* and *ITSM* were plotted versus their moisture loss. The nonlinear regression lines superposed to the plots were obtained with the Michaelis-Menten equation. Indeed, it can be shown with straightforward algebraic calculations that, if the time evolution of *DW* and *ITS* (or *ITSM*) follows the MM model, than the relationship between *DW* and *ITS* (or *ITSM*) follows the same equation:

$$ITS\ (or\ ITSM) = \frac{a \cdot DW}{b + DW} \tag{58}$$

In this case, contrary to the MM models fitted in the previous section, the regression parameters *a* and *b* found using least-squares minimization were both negative (**Table 10. 5**). From a mathematical point of view, this implies the concave shape of the regression curves (**Figure 10. 13** and **Figure 10. 14**). From a physical point of view this is due to the fact that the *DW* development was faster than the *ITS* and *ITSM* development.

For mixture C1 the correlation between *DW* and *ITS* (or *ITSM*) appears to be influenced by the curing temperature only at long-term curing conditions (**Figure 10. 13** and **Figure 10. 14**). On the other hand, for mixture C2.5 the impact of curing temperature is evident in the initial curing stage and tends to vanish at long-term curing conditions. These results confirm that *DW* can be used to estimate the evolution of *ITS* and *ITSM* due to curing. Although the relationship is not unique, this appears to be a promising approach to estimate the increase of mechanical properties during field curing.

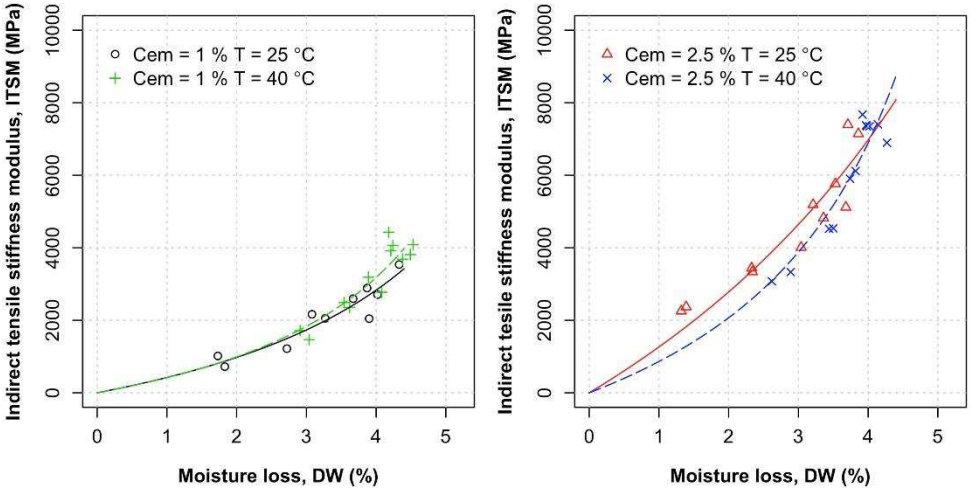


**Figure 10. 13** Relation between Moisture loss and Indirect tensile stiffness modulus: experimental data and fitted MM models.

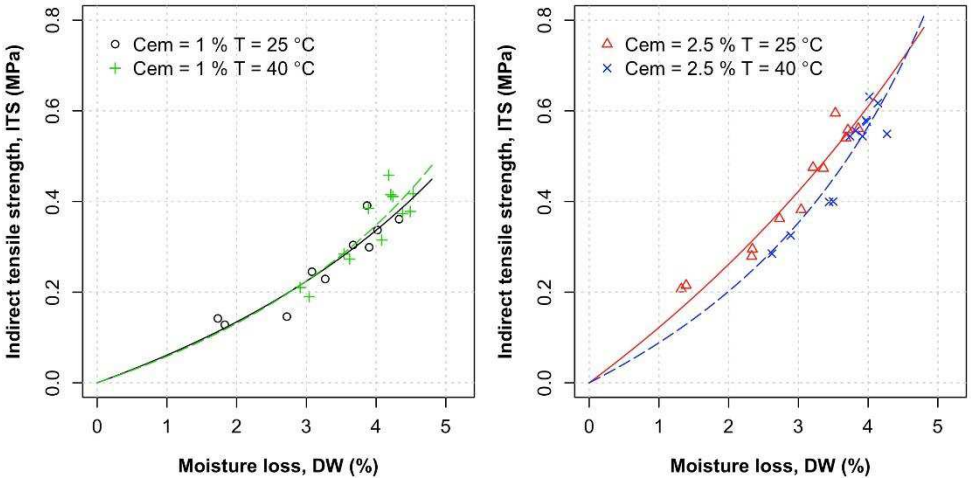


**Figure 10. 14** Relation between Moisture loss and Indirect tensile strength: experimental data and fitted MM models.

| Mixture | *a* | | *b* | | Residual Std. Error |
|---|---|---|---|---|---|
| | Estimate | Std. Error | Estimate | Std. Error | |
| **ITSM** | | | | | |
| C1T25 | -3152 | 1450 | -8.46 | 2.12 | 328 |
| C1T40 | -2636 | 967 | -7.32 | 1.14 | 441 |
| C2.5T25 | -13779 | 10453 | -11.9 | 6.43 | 682 |
| C2.5T40 | -5185 | 1651 | -7.01 | 0.98 | 643 |
| **ITS** | | | | | |
| C1T25 | -0.668 | 0.43 | -11.94 | 5.30 | 0.036 |
| C1T40 | -0.536 | 0.31 | -10.17 | 3.44 | 0.043 |
| C2.5T25 | -1.836 | 1.14 | -16.04 | 7.87 | 0.038 |
| C2.5T40 | -0.704 | 0.28 | -8.98 | 1.97 | 0.044 |

**Table 10. 5** Regression parameters of the Michaelis-Menten model for ITSM and ITS as a function of DW.

## 10.2.4 Relation between mechanical properties

The final step in the study of the curing process, was the analysis of the relation between the and the strength properties. As it can be observed in **Figure 10. 15**, the relation between *ITSM* and *ITS* appears to be independent of both cement dosage and curing temperature.
The regression line superposed to the experimental data (**Figure 10. 15**) follows the Michaelis-Menten equation. Similar to the previous section, it can be shown that, if the relation between *DW* and *ITS* (or *ITSM*) follows the MM model, than also the relation between *ITS* and *ITSM* follows the same equation. Using the least squares method (Section 10.1.5) the following best fit equation was obtained:

$$ITS = \frac{1.333 \cdot ITSM}{9284 + ITSM} \tag{59}$$

with a residual standard error equal 0.036 MPa.
The residual analysis for this regression model is reported in **Figure 10. 16**. No serious deviations from the normal distribution of residuals can be observed, confirming the adequacy of the MM model.
It is highlighted that Equation 59 represents a convex curve (both regression parameters are positive), confirming that *ITSM* increased at a slower rate with respect to *ITS*, regardless of cement dosage and curing conditions.

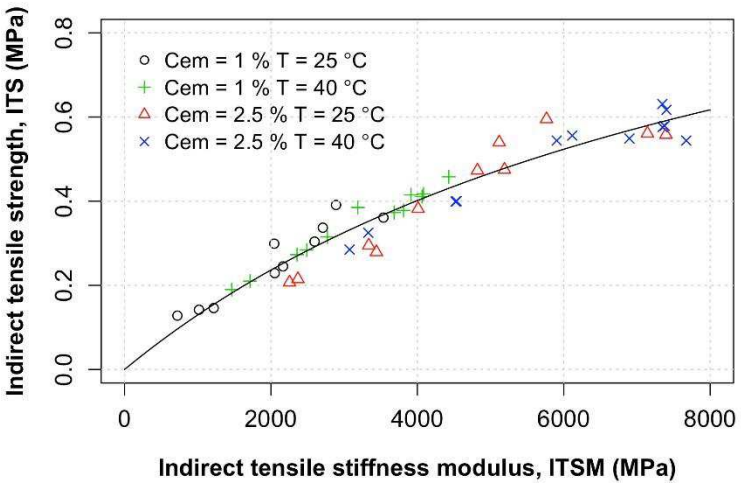


**Figure 10. 15** Relation between indirect tensile stiffness modulus and indirect tensile strength.

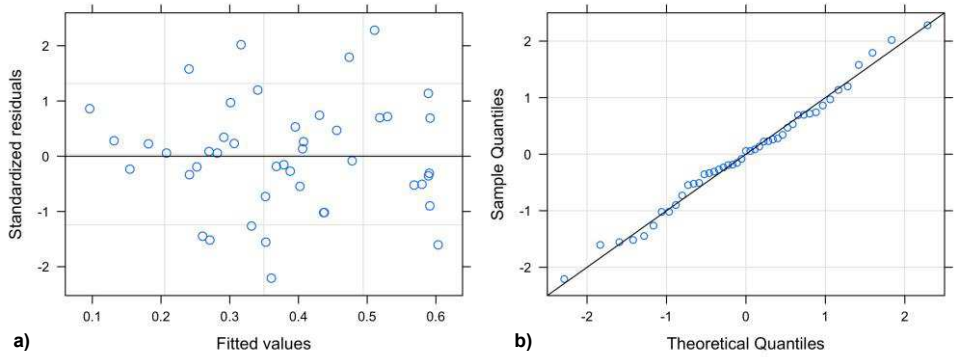


**Figure 10. 16** Residuals plots for ITS vs ITSM: a) standardized residuals versus fitted values and b) normal QQ plot.

## 10.3 Summary

The present Chapter aimed at the characterization of the curing process of cold-recycled mixtures by measuring moisture loss, *ITS* and *ITSM*. The experimental data were analyzed using a statistical regression approach in order to identify by means of suitable parameters the rate at which material properties evolve over time and their long-term value.

A preliminary part of the study was devoted to the selection of the total water content for specimen production. An original approach, based on the evolution of volumetric properties during gyratory compaction, was employed and led to the selection of $w_{tot}$ = 5 %.

The air voids distribution of the compacted specimens was characterized by a standard deviation of 0.7 %. In addition 85 % of the specimens had a moisture loss smaller than 0.3 % during the compaction.

Results showed that the curing temperature affected the rate of water evaporation but did not modify the final water content $w_{eq}$ (i.e. after 100 days of curing). For both mixtures $w_{eq}$ exceeded the water required for the hydration of cement $w_{hydr}$ (water not available for evaporation) and therefore it can be hypothesized that moisture loss by evaporation did not hinder the hydration process of cement.

The Michaelis-Menten and the exponential models were employed and compared to describe the evolution over time of moisture loss, *ITS* and *ITSM*. Both models were accurate in describing the asymptotic trend of material properties, however, the MM model was characterized by a better precision.

In addition, the two parameters of the MM model confirm their straightforward and effective attitude to describe the two main macroscopic aspects of curing: its initial rate (the Michaelis constant $K_c$) and the long term evolution (the asymptotic value $y_A$).

Increasing cement dosage from 1 % to 2.5 % had a clear effect on the long-term values of mechanical properties. In fact, *ITSM* increased from 3341 MPa to 6612 MPa and from 4154 MPa to 7726 MPa, for curing at 25 °C and 40 °C, respectively. Analogously, *ITS* increased from 0.38 MPa to 0.58 MPa and from 0.42 MPa to 0.60 MPa, for curing at 25 °C and 40 °C, respectively.

The increase in curing temperature from 25 °C to 40 °C resulted in a reduction of the Michaelis constant $K_c$, i.e. the time required for a property to reach one half of its long-term value. In particular, when considering moisture loss, $K_c$ decreased from 1.54 days to 0.51 days and from 1.88 days to 0.49 days, for cement dosages of 1 % and 2.5 %, respectively. In addition, regardless of cement dosage and curing temperature, $K_c$ values estimated for moisture loss were lower with respect to those estimated for ITS, which in turn were lower with respect to those estimated for ITSM. This suggests that curing due to moisture loss had an higher impact on the evolution of *ITS*, whereas the evolution of *ITSM* was more linked to cement hydration.

The MM model was also effective in describing the relation between moisture loss and mechanical properties and the relation between *ITSM* and *ITS*. In the first case, although the relationship is not unique, results confirmed that the evolution of *ITS* and *ITSM* can be estimated by measuring moisture loss. In the second case, a unique relationship was found between *ITS* and *ITSM,* regardless of composition and curing temperature.

# CHAPTER 11.

# Influence of reclaimed asphalt on linear viscoelastic properties of cement-bitumen treated materials

This chapter is focused on the characterization of the LVE response of two cement-bitumen treated materials (CBTM), produced with bitumen emulsion (CBTM-BE) or foamed bitumen (CBTM-FB), cement and different RA contents.
The main objective of this investigation is to evaluate the volumetric and the stiffness properties of the CBTM mixtures focusing on the impact of RA content.
In addition, an effort was made to produce CBTM mixtures with the same grading curve (by volume) and the same volumetric properties in order to simplify as much as possible the comparison among the investigated mixtures.

The experimental activities can be organized in two phases:

- A preliminary phase, where the influence of water content on the compactability of the fresh mixtures was investigated. In addition, the foamed bitumen content was optimized for CBTM-FB;
- The LVE response of CBTM-BE and CBTM-FB was evaluated measuring the complex Young's modulus $E^*$ and the thermo-rheological behavior was modelled using the same approach commonly used for bituminous mixtures [Di Benedetto et al., 2001].

The experimental activities on CBTM-FB were carried out in cooperation with *École de technologie supérieure* - ETS (Montreal, Canada).

## 11.1 Experimental program

### 11.1.1 Materials and mixtures

Reclaimed asphalt, virgin aggregate, bituminous emulsion, Portland cement and water were used to prepare both CBTM-BE and CBTM-FB.
Two sources of RA were sample from a cold in-place recycling jobsite, after milling of the aged asphalt surface layers (wearing and binder course): RA (IT) sampled in Italy and RA (CA) sampled in Canada. RA gradations are reported in **Figure 11. 1**, in terms of "black curve" (BC), before binder extraction, and "white curve" (WC), after binder extraction.
Black curves are characterized by 20 mm and 10 mmm of nominal maximum dimension for RA (IT) and RA (CA), respectively. Both curves exhibits a lower content of fines with respect

to the corresponding white curves. This is a typical feature of RA obtained from cold milling, because the finer particles of the original bituminous mixture (sand and filler) are coated and bound by the aged bitumen. In this study, for designing the target gradation of both CBTM-BE and CBTM-FB mixtures, RA particles were regarded as "*black rock*" (the aged bitumen is considered part of the RA particles). The average bitumen content of RA, measured with the ignition method (ASTM D6307), was 4.50 % and 5.15% by dry aggregate weight for RA (IT) and RA (CA), respectively.
The design aggregate blend for CBTM-FB mixture was obtained using one type of mineral filler, one virgin fine size (0/5), and two virgin coarse sizes (5/10 and 10/14); differently for CBTM-BE were used two coarse sizes (4/12, 12/20) one fine size, (0/4) and mineral filler, all having the same mineralogy (limestone). Both fine and coarse sizes were prepared by wet sieving in order to allow a better control on the dust content (passing to the 0.075 mm sieve) of the mixtures. Based on grading curves, RA and virgin aggregate sizes were designated according to the EN 13108-8 and EN 13043 standards, respectively. Density and water absorption, measured according to the EN 1097-6 standard, are reported in **Table 11. 1**.

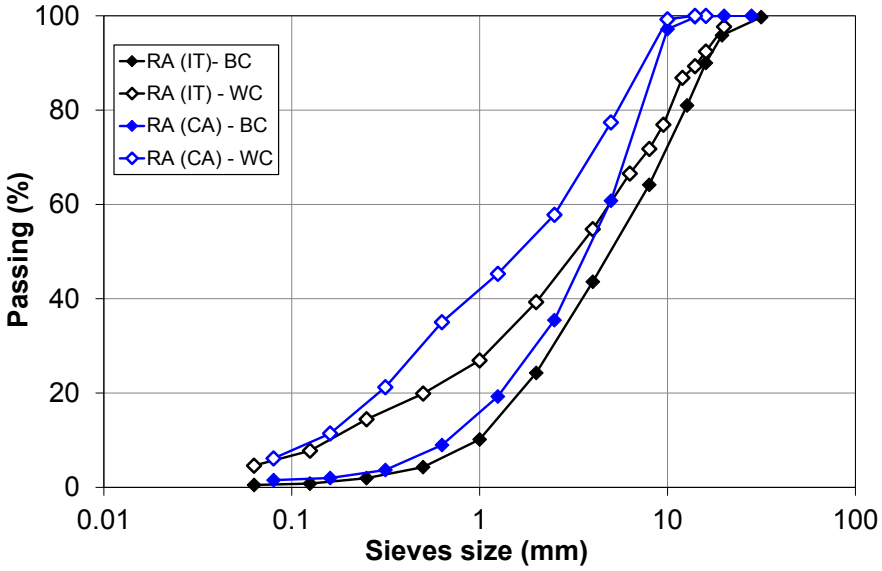


**Figure 11. 1** Grading curves (by volume) of RA sources.

| Type | Source | Designation | Particle Density [g/cm$^3$] | Water absorption [%] |
|---|---|---|---|---|
| RA | IT | 40 RA 0/30 | 2.393 | 1.09 |
| Coarse VA | IT | 12/20 $G_C$ 90/10 | 2.679 | 1.00 |
| Coarse VA | IT | 4/12 $G_C$ 90/10 | 2.675 | 1.10 |
| Fine VA | IT | 0/4 $G_F$ 90 | 2.454 | 0.98 |
| Filler | IT | - | 2.600 | - |
| RA | CA | 20RA 0/10 | 2.559 | 0.99 |
| Coarse VA | CA | 10/14$G_C$ 90/10 | 2.723 | 1.50 |
| Coarse VA | CA | 5/10 $G_C$ 90/10 | 2.723 | 1.50 |
| Fine VA | CA | 0/5 $G_F$ 90 | 2.738 | 1.65 |
| Filler | CA | - | 2.600 | - |

**Table 11. 1** Aggregates properties.

| **Property** | | **Test procedure** | **Value** |
|---|---|---|---|
| Density at 25 °C | g/cm$^3$ | AASHTO T 228 | 1.02 |
| Density at15 °C | g/cm$^3$ | AASHTO T 228 | 1.08 |
| Viscosity Brookfield, 135 °C | Pa s | EN 13702-02 | 0.28 |
| Viscosity Brookfield, 165 °C | Pa s | EN 13702-02 | 0.08 |
| Ta | °C | AASHTO T 315 | 59.4 |
| Tb | °C | AASHTO T 313 | -29 |
| Penetration | $10^{-1}$ mm | EN 1426 | 115 |

**Table 11. 2** Properties of bitumen for foaming process.

A cationic slow-setting bituminous emulsion (**Table 6. 1**) designated as C 60 B 6 (EN 13808) was selected for CBTM-BE mixture production.
The bitumen for the foaming process was a PG 58-28 type, obtained from "Les Industries Mc Asphalt Ltèe-Refinery" in Valleyfield (QC-Canada). The foamed bitumen (FB) is used in the production of CBTM-FB and its main physical properties are summarized in **Table 11. 2**. The FB was produced using a *Wirtgen WLB10 unit*.
Two sources of Portland cement was employed:

- For CBTM-BE, A Portland limestone cement type II/B-LL, strength class 32.5R (EN 197-1) was used. Its com-position is a combination of clinker (65 % - 79 %) and limestone dust (21 % - 35 %);

- For CBTM-FB, A Portland limestone cement type GU (General Use) was employed. Its composition is a combination of clinker (80-94 %) and limestone dust (6-20%) and it is classified according to ASTM C150 and C 1157.

Three different type of mixtures, according to the amount of RA included in the mixture, were analyzed. Three mixtures for each type of material (CBTM-BE and CBTM-FB) were analyzed:

- Mix A, CBTM-BE, 50%RA and 50%VA (50RA-BE);
- Mix B, CBTM-BE, 80%RA and 20%VA (80RA-BE);
- Mix C, CBTM-BE, 0%RA and 100%VA (0RA-BE);
- Mix A, CBTM-FB, 50%RA and 50%VA (50RA-FB);
- Mix B, CBTM-BE,70%RA and 30%VA (70RA-FB);
- Mix C, CBTM-BE, 0%RA and 100%VA (100RA-FB).

Compositions similar to Mix A are often employed in cold in-place recycling projects, where bituminous layers are milled together with the underlying un-bound or cement-bound foundation [Grilli et al. 2012, Bocci et al. 2014]. Mix B was originally intended to be a 100 % RA blend. However, in this research it was decided to prioritize the choice of a unique grading curve for each type of mixture, CBTM-BE and CBTM-FB. Consequently, a correction to the RA gradation ("*black curve*") was necessary. Specifically, 20% and 30 % of fine VA was added to 80RA-BE and 70RA-FB, respectively. Mix C is a cold mixture and it was used as reference, to check the influence of RA on volumetric and mechanical properties in CBTM-BE and CBTM-FB mixtures.
The adopted target gradation for the three mixtures was the classical power curve with exponent 0.45, commonly used for dense-graded asphalt concrete mixtures [Roberts et al., 1996]. It is important to highlight that such gradation considers passing by volume, whereas mixture composition specified above is by weight. The volumetric composition, in terms of aggregate type (RA or VA) and coarse-fine fraction, is summarized in **Table 11. 3**. The design grading curves, for both type of mixtures, are shown in **Figure 11. 2**.
As it can be observed from **Figure 11. 2**, CBTM-FB mixtures result more fine with respect to the corresponding CBTM-BE mixtures because of the different RA sources (RA(IT) and RA(CA)).
For CBTM-BE mixtures, the emulsion content was 3.0 %, by dry aggregate weight, corresponding to 1.8 % of residual bitumen, whereas cement content was 2 %, by dry aggregate weight. Differently, the cement content of 1.5% (by dry aggregate weight) was used for CBTM-FB mixtures, whereas the FB content were established based on results of the mixture design procedure described in Section 11.1.4. The aim is to produce both CBTM-BE and CBTM-FB mixtures at the same bitumen/cement (B/C) ratio in order to better compare the mechanical behavior of these materials.
The water content was optimized for both CBTM-BE and CBTM-FB mixtures but carried out following different methods.

| Mixture ID | Type | Aggregate type | Total composition [%] | Coarse fraction [%] | Fine fraction [%] |
|---|---|---|---|---|---|
| A | CBTM-BE | RA | 52.7 | 65.5 | 34 |
| | | VA | 45.7 | 34.5 | 66 |
| B | CBTM-BE | RA | 77.1 | 100 | 46.6 |
| | | VA | 21.4 | 0 | 53.4 |
| C | CBTM-BE | RA | 0 | 0 | 0 |
| | | VA | 98.3 | 100 | 100 |
| A | CBTM-FB | RA | 52.8 | 69.5 | 46.5 |
| | | VA | 46.1 | 30.5 | 53.5 |
| B | CBTM-FB | RA | 72.1 | 100 | 62.2 |
| | | VA | 26.7 | 0 | 37.2 |
| C | CBTM-FB | RA | 0 | 0 | 0 |
| | | VA | 98 | 100 | 100 |

**Table 11. 3** Volumetric composition of aggregate blends.

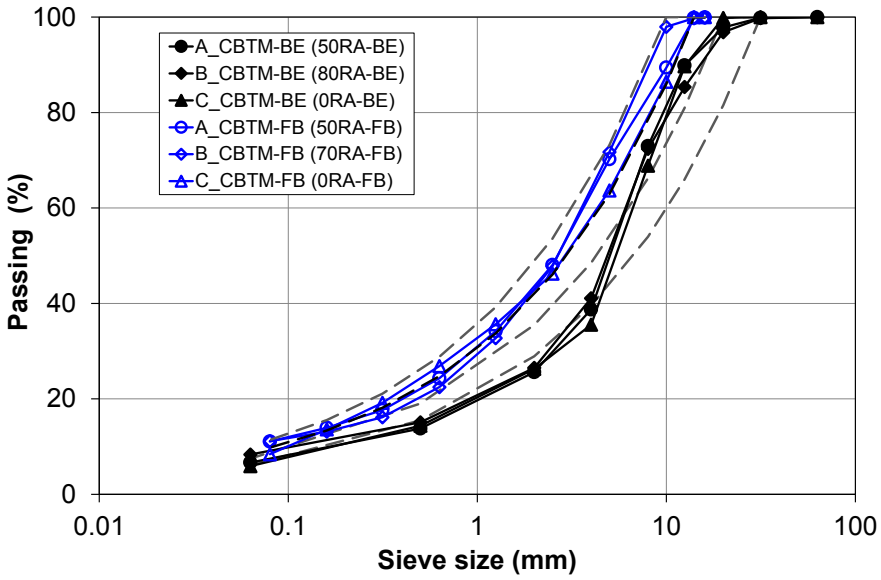


**Figure 11. 2** Grading curves of the tested CBTM-BE and CBTM-FB mixtures.

## 11.1.2 Composition and volumetric properties of CBTM mixtures

*CBTM produced with bitumen emulsion* (CBTM-BE)

The mechanical properties and the durability of CMs are strictly related to their volumetric properties. Therefore, similar to hot mix asphalt (HMA), a thorough assessment of their volumetric properties is essential, particularly in the compaction phase.

In **Figure 11. 3**, the constituent materials of CRMs produced using *bituminous emulsion* and cement, are stated both by mass and by volume. In the common practice, composition is

specified by mass, whereas volume percentages must be calculated using the density of each material. In such a calculation, the aggregate component deserves a special attention. In fact, its composition is extremely variable because it may include RA, reclaimed aggregates from unbounded or cement-bounded layers and VA of various petrographic natures. Therefore, the average density $\rho_A$ of the aggregate shall be calculated using the equation:

$$\rho_A = \frac{100}{\sum_i \frac{p_i}{\rho_i}} \tag{60}$$

where $p_i$ represents the percentage by weight of each aggregate type and $\rho_i$ is its density. In addition, the porosity of aggregate particles must be considered and hence the total water content of the mixture $W_{tot}$ must be split into absorbed water $W_{abs}$ and free water $W_{free}$ i.e. the amount of water that actually enhances compactability by reducing internal friction. As a consequence, the saturated surface-dry density $\rho_{SSD}$ of aggregate particles should be considered in the volumetric analysis.
In **Figure 11. 3**, it is also shown that $W_{tot}$ is the sum of the water coming from the emulsion $W_{em}$ and additional water $W_{add}$ added during mixing.
In the compaction phase of fresh mixtures the evolution of volumetric properties is often evaluated using the dry density $\rho_d$, i.e. the ratio of the total mass of solids to the total mixture volume:

$$\rho_d = \frac{M_S}{V_T} = \frac{M_A + M_C + M_{B_R}}{V_T} \tag{61}$$

where the symbols shown in **Figure 11. 3** have been used. In Equation 61, the mass of residual (fresh) bitumen from emulsion ($M_{B,res}$) is explicitly considered as part of the solids, whereas the mass of the aged binder is implicitly considered inside the aggregate mass $M_A$. The use of $\rho_d$ to evaluate compactability of CBTM mixes can be misleading when different mixture compositions need to be compared, typically for mix design. For example, comparing $\rho_d$ of mixes having different fractions of RA and VA is not appropriate because particle densities may be considerably different. An approach based on volumetric properties, similar to HMA, appears more appropriate (see Section 2.8.2).

Referring to the typical composition depicted in **Figure 11. 3**, voids in the mineral aggregate (*VMA*) of a CBTM mix may be defined as:

$$VMA = \frac{V_V + V_{B,res} + V_{W,free}}{V_T} \cdot 100 \tag{62}$$

*VMA* is the volume percentage of space between solids particles (aggregate and cement); this space includes: air voids, fresh bitumen and free water. *VMA* can be used to evaluate the degree of packing of the aggregate skeleton.
Similarly, the parameter voids in mixture $V_m$ is the volume percentage occupied by air voids and water (i.e. the non-structural component of a CM volume) and is defined as:

$$V_m = \frac{V_V + V_{W,free}}{V_T} \cdot 100 \tag{63}$$

From Equations 62 and 63 we observe that:

$$VMA = V_m + VB_{res} \tag{64}$$

where $VB_{res}$ is the volume percentage of fresh bitumen. In addition, to evaluate the percentage of *VMA* occupied by water and fresh bitumen, the parameter voids filled with liquids *VFL* is defined as:

$$VFL = \frac{V_{B,res} + V_{W,free}}{V_V + V_{B,res} + V_{W,free}} \cdot 100 \tag{65}$$

*VFL* is particularly important in the compaction phase i.e. when fresh bitumen is still dispersed in small droplets inside free water. If *VFL* is less than 100 %, the mixture contains air voids and hence is unsaturated. However, if an excessive compaction effort is applied, *VFL* may reach or exceed 100 %. As a consequence, free water is squeezed out of the mixture together with a fraction of the dispersed fresh bitumen. Such an over-compaction clearly results in an undesirable and uneconomic change of mixture composition.

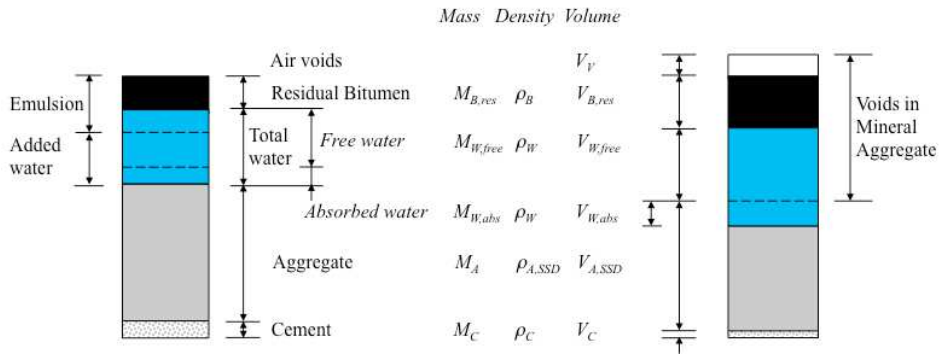


**Figure 11. 3** Constituent materials of CRMs produced using bituminous emulsion and cement stated by mass and by volume.

*CBTM produced with foamed bitumen* (CBTM-FB)
CRMs produced with foamed bitumen, as well as produced with bitumen emulsion, can be considered as four-phase composite materials consisting of solids (aggregates and active filler), foamed bitumen, water and air. These components are depicted in **Figure 11. 4**, which considers a unit volume of fresh CRMs produced with foamed bitumen and highlights the contribution of each component by mass and by volume.
During compaction, foamed bitumen adds its own contribution to the lubricating action of water and therefore considering a single liquid phase (foamed bitumen and water) is useful. On the other hand, the total water in the mixture ($W_{tot}$) is partly absorbed by the aggregate

particles ($W_{abs}$) and does not contribute to the densification process, which is only promoted by the free (inter-granular) water ($W_{free}$).

In literature, the analysis of volumetric properties of CMs produced with foamed bitumen is associated to HMA volumetrics; three main parameters are used: air voids ($V_m$), voids in the mineral aggregate (*VMA*), and voids filled with bitumen (*VFB*).

In this study, the volumetric properties of CMs produced with foamed bitumen are analyzed following the same methodology used above for volumetric properties of CMs produced with bitumen emulsion. The proposed approach was based on a modified definition of the volumetric parameters, taking into account that foamed bitumen does not include water and consequently, free water $V_{W,free}$ (i.e. $W_{free}$) is represented only by the water added in the mixture.

Considering the typical composition and the abbreviations described in **Figure 11. 4**, the following definitions are proposed.

Voids in the mixture $V_m$, refers to the space occupied by air ($V_V$) and free water ($V_{W,free}$):

$$V_m = \frac{V_v + V_{W,free}}{V_T} \times 100 = \left(1 - \frac{V_{RA} + V_{VAg} + V_C + V_B}{V_T}\right) \times 100 \quad (66)$$

Voids in the mineral aggregate *VMA*, refers to the space between aggregate and cement particles in the CRMs produce with foamed bitumen:

$$VMA = \frac{V_v + V_B + V_{W,free}}{V_T} \times 100 = \left(1 - \frac{V_{RA} + V_{VAg} + V_C}{V_T}\right) \times 100 \quad (67)$$

Voids filled with liquid *VFL*, refers to the percentage of *VMA* that is occupied by the liquid phase, i.e. foamed bitumen and water. It represents the corresponding parameter *VFB* in HMA volumetrics:

$$VFL = \frac{V_B + V_{W,free}}{V_V + V_B + V_{W,free}} \times 100 \quad (68)$$

Similar to air voids in HMA and CRMs produced with bitumen emulsion, $V_m$ designates the volume of the non structural part of a CRMs produced with foamed bitumen. It is highlighted that $V_m$ is not affected by water loss due to evaporation, which occurs in the curing phase. *VMA* can be used to evaluate aggregate interlocking, and its evolution due to the compaction process. In this phase, controlling *VMA* is essential because the inter-granular space in the fresh mixture must be able to contain both foamed bitumen and water. In particular, for

CRMs produce with bitumen emulsion, it has been shown that *VFL* values above 90 % generally imply a visible loss of liquids and fines from the mold [Grilli et al., 2012].

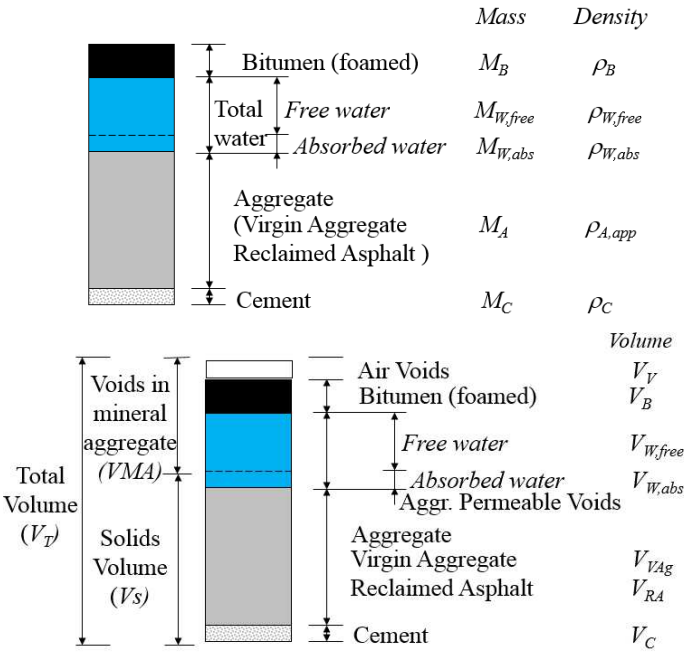


**Figure 11. 4** Gravimetric and volumetric composition of CRMs produced with foamed bitumen.

## 11.1.3 CBTM-BE mixture: specimens preparation and water optimization

CBTM-BE specimens were prepared, mixed and compacted following the procedure described in Section 10.1.2 . In the first part of the experimental program, four total water contents ($W_{tot}$ = 3, 4, 5 and 6 % by dry aggregate weight) were selected to define the optimum water content of each type of mixture. In this phase, about 4500 g of loose mixture were compacted with 180 revolutions. The compaction curves were analyzed using the volumetric approach described in Section 11.1.2.

In the second part of the experimental program, specimens for mechanical tests were prepared at the optimal water content. The mixture weight was adjusted to obtain specimens with height of 150 mm and voids content $V_m$ = 10 %. After compaction, specimens were cured for 7 days at 40 °C and then cored to the diameter D = 94 mm. The curing temperature of 40 °C was selected to obtain accelerated curing and to be sure that the definitive curing has been reached [Bocci et al., 2011].

### 11.1.4 CBTM-FB mixture: mix-design procedure

Since the present research focused on the impact of RA content on complex modulus, an effort was made to test mixtures characterized by the same FB content and similar volumetric properties. Thus, after selecting a unique cement content and target grading curve, a unique FB content was established considering both the mechanical response and the volumetric properties of the mixtures. First, the foaming properties of the bitumen were investigated, in order to determine the optimal foamant water content (*FWC*) for the production of the FB using the Wirgten *WLB10 unit* (**Figure 11. 5**).

**Figure 11. 5** Wirgten WLB 10.

The Wirtgen WLB 10 unit was designed to produce foamed bitumen under laboratory conditions. The foamed bitumen produced by this unit is similar to that produced by the foamed bitumen systems mounted on large recycling machines (such as the Wirtgen WR2500). The Wirtgen WLB10 unit is used to determine the foaming properties of a bitumen sample and to produce the foamed bitumen required for preparing treated samples in order to determine the optimal application rate for stabilisation (known as the mix design procedure

Next, the influence of water on the compactability of the aggregate blends was studied and the optimum water content of each aggregate blend was determined. Finally, the effect of FB content on the mechanical and volumetric properties of the mixtures was studied and the design FB content for the three mixtures was selected.

*Optimization of bitumen foaming properties*

Foamed bitumen consists of bubbles of hot bitumen encapsulating steam. It is produced when a small quantity of cold water (2-3 % by weight of bitumen) under pressure is injected into hot bitumen (150 °C to 180 °C) [Wirgten, 2010]. During this process, exchange of heat energy occurs between bitumen and water leading to steam formation. The steam under pressure is forced into the bitumen forming bubbles that constitute the foamed bitumen.

In order to maximize the foaming properties of the bitumen, two characteristics were measured in this study: the maximum expansion ratio ($ER_m$) and the half life ($HL$). $ER_m$ is the ratio of the maximum volume of FB to the initial volume of bitumen; it is a measure of foam viscosity and indicates how well the bitumen will be dispersed in the mix. $HL$ is the time required by the foam to settle to half of its maximum volume; it is a measure of foam stability and an indicator for its rate of collapse during mixing. When the $FWC$ is increased, $ER_m$ increases, whereas HL decreases. Thus, an optimum $FWC$ can be established specifying minimum values for both parameters (see Section 2.6.4).

In the present research optimization of the FWC was carried out based on the following criteria: $ER_m > 20$ and $HL > 25$ s [Autostrade per l'Italia, 2008]. The bitumen foaming temperature was 170 °C and four $FWC$ (1.5, 2.0, 2.5 and 3.0 % by mass of bitumen) were tested. Results are shown in **Figure 11. 6**, where each point on the graph represents the average value calculated on three repetitions. The optimum $FWC$ was 2.45 % (by mass of bitumen). The corresponding $ER_m$ and $HL$ values were 26 and 27 s, respectively. The coefficient of foamability, defined as the ratio of $ER_m$ to the optimum $FWC$ [Lesueur et al., 2004] was 10.6 s/%.

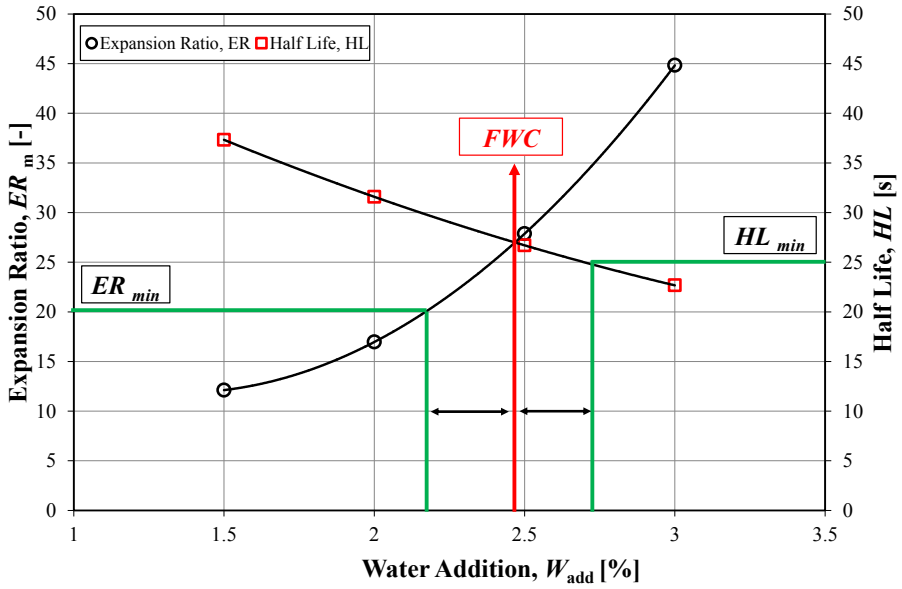


**Figure 11. 6** Optimization of the optimal foamant water content (bitumen temperature: 170°C).

*Compactability of the aggregate blends*

As previously described in Section 2.6.5, in literature [ARRA, 2001; Asphalt Academy, 2009; Wirgten, 2010] CMs produced with foamed bitumen is considered more less than a granular materials. For this reason, the optimum water content was investigated according to the modified Proctor test [EN 13286-2 or AASHTO T-180]. The procedure was performed prior to FB addition, on mixtures 70RA-FB and 0RA-FB. For each batch, the dry aggregate blend was initially hand-mixed adding a water amount corresponding to the absorption value (**Table 11. 1**). To allow water absorption and obtain homogeneous moisture conditions, the wet aggregate blend was sealed in a plastic bag and stored for 12 hours at room temperature. Then, wet aggregates and the additional amount of water for compaction were mixed in order to produce specimens for the modified Proctor test.

The optimum water content was found to be 5.5 % for mixture 70RA-FB and 6.0 % for mixture 0RA-FB. Such a result is consistent with those shown in other studies [Kuna et al. 2014, Grilli et al., 2012] and indicates that mixtures containing RA are characterized by a lower internal friction and thus require less water to achieve their maximum dry density.

*Selection of the design foamed bitumen content*

The effect of FB content on the volumetric and mechanical properties of the FB mixtures was studied analyzing the compaction curves obtained with the gyratory compactor and the indirect tensile strength (ITS) of the cured specimens.

Three FB dosages were selected: 2, 3 and 4 % for mixtures 50RA-FB and 70RA-FB (FB2, FB3 and FB4) and 3, 4 and 5 % for mixture 0RA-FB (FB3, FB4 and FB5) [Wirtgen, 2010]. The FB contents were calculated referring to the dry aggregate weight. The total amount of mixing water was 4.0 % for mixtures 50RA-FB and 70RA-FB, 4.5 % for mixture 0RA-FB, i.e. about 75 % of the optimum water content (see Section 2.6.4). This allowed to take into account the FB contribution to the lubricating action of water [Wirtgen, 2010]. For both FB and water, dosages were calculated with respect to the total mass of solids, i.e. dry aggregates and cement. Mixing water was added in two phases according to the procedure described above during specimens production for modified Proctor test. In addition, during the second water addition, cement was also included in the aggregate blend and then mixing was carried out in a mechanical mixer and until uniformity was reached. Following that, the FB produced by the WLB10 unit was discharged directly into the mixing bowl (**Figure 11. 7**). The mixing time, after FB addition, ranged between 30 s and 60 s. This time was necessary to allow the foam to collapse and to achieve a uniform distribution of the bitumen.

Immediately after mixing, specimens were compacted by means of a gyratory compactor in a 150 mm diameter mold [EN 12697-31] (see Section 7.2.1).

**Figure 11. 7** Mixing and compaction, FB is discharged directly into the mixing bowl.

Nine mixtures (three aggregate blends with three FB dosages) were analyzed. For each mixture, two replicate specimens were produced. 4500 g of material were used for each specimen, and the final height was approximately 110 mm. The evolution of volumetric properties described in Section 11.2.1 was analyzed.
The ITS was used to evaluate the mechanical properties. Before testing, the compacted specimens were cured for 72 h at 40 °C and conditioned for 4 h at 20 °C. ITS tests were carried out at 20 °C, according to the procedure described by the EN 12697-23 standard (see Section 7.2.3).

*Specimens production for complex modulus testing*
CBTM-FB specimens for mechanical testing were produced using a total water content equal to 4.0% for mixtures 50RA-FB and 70RA-FB, 4.5% for mixture 0RA-FB and the designed optimum FB content.
The weight of the mixtures and number of gyrations were adjusted to obtain a unique target value of voids in mixture $V_m = 10$ %. After compaction, specimens were immediately extracted from the mold and cured for 7 days at 40 °C in a climatic chamber. At the end of this first curing phase, specimens were cored to the nominal diameter $D = 80$ mm; moreover, the upper and lower part of the sample were sawed to a nominal height $H = 150$ mm. After coring and sawing, an additional curing period of 7 days at 40 °C was performed before mechanical testing. Based on previous studies carried out on cement-bitumen treated materials with bituminous emulsion [Grilli et al, 2012; Cardone et al. 2015] the adopted curing procedure ensures reaching a reasonable stability of stiffness properties.

# 11.2 Complex modulus testing procedure

## 11.2.1 CBTM-BE specimens

Uniaxial cyclic compression tests were performed using the servo-pneumatic testing equipment, in control strain mode, as described in Section 5.2.1.
A sinusoidal (haversine) axial strain with 50 με amplitude (peak-to-peak) was applied at five frequencies (10, 3, 1, 0.3 and 0.1 Hz) and five temperatures (5, 15, 30, 40 and 55 °C).

A total of 40 load cycles were applied at each frequency in order to measure complex Young's modulus $E^*$.
Test methods and data analysis adopted with $E^*$ measurements are reported in Section 5.2.2 and Section 5.2.3.

## 11.2.2 CBTM-FB specimens

For each CBTM-FB mixture, the complex Young's modulus $E^*$ was evaluated on two cylindrical specimens.
The complex modulus was measured applying haversine compression loading (stress controlled), using a servo-hydraulic testing system (MTS 810, Teststar II) having a maximum load capacity of 100 kN and a ± 50 mm axial stroke. A thermal chamber was used to control the temperature of the specimen. In each test, the temperature was measured with three thermocouples (PT100 surface temperature probe) placed and held against the specimen surface with a rubber band. Axial stress was measured with a load cell, whereas axial strain was measured on the middle part of the specimen using three extensometers, placed 120° apart, with a measuring base of 50 mm (**Figure 11. 8**).

**Figure 11. 8** Complex modulus test setup.

Tests were performed at six different temperatures (25, -20, -5, 10, 25, 40 and 55 °C) and, at each temperature, a frequency sweep of six frequencies (10, 3, 1, 0.3, 0.1 and 0.03 Hz) was carried out. Measurements at 25 °C were repeated two times in order to compare the $E^*$ values obtained before and after loading cycles carried out at low temperature. In this way, it was possible to assess whether damage occurred during the test. For each loading frequency and temperature, the stress level was selected in order to obtain a steady-state strain amplitude ranging from 30 to 50 microstrain. A conditioning period of 6 hours was applied before loading after each temperature change.
$E^*$ measurements were analyzed according to the procedure described in Section 5.2.3 with the aim to obtain the rheological characterization of each CBTM-FB mixture.

# 11.3 Experimental findings: CBTM-BE

## 11.3.1 Volumetric properties and optimal water content

In **Figure 11. 9**, the SGC compaction curves obtained in the first part of the experimental program are reported. In particular, the percentage variation of the voids in mixture $V_m$ and voids filled with liquids *VFL* are plotted as a function of the number of SGC gyrations. As it can be observed, for all CBTM-BE mixtures and all water contents, $V_m$ decreases and *VFL* increases. Results also showed that, increasing the RA content, mixture compactability improved. This is can be explained by the rounded shape and smooth surface texture of the reclaimed aggregate particles. For a fixed number of gyration, an increase of water content produces a $V_m$ decrease, indicating a reduction of the volume occupied by air voids and water. This is due to the larger water films that develop around the aggregate particles, which make it easier for them to be moved and reoriented into a denser configuration. It can also be observed that, at higher water contents, the mixtures tends to reach saturation (*VFL* = 100 %) at lower number of gyrations. It is highlighted that values of *VFL* > 100 % were calculated on the basis of the initial water content of the compacted samples. However, it can be hypothesized that further gyrations after saturation, caused liquids to be squeezed out of the mixture. This hypothesis was confirmed by visual observations of liquids draining from the top and the bottom of the mold, during the compaction process. Visual observations also suggested that the liquid lost was composed by water and fresh bitumen

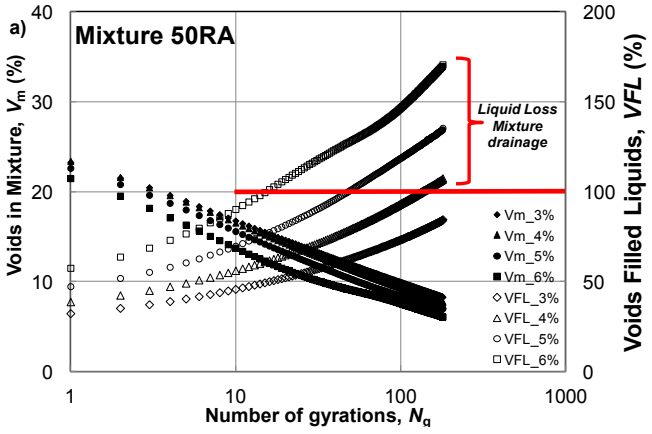

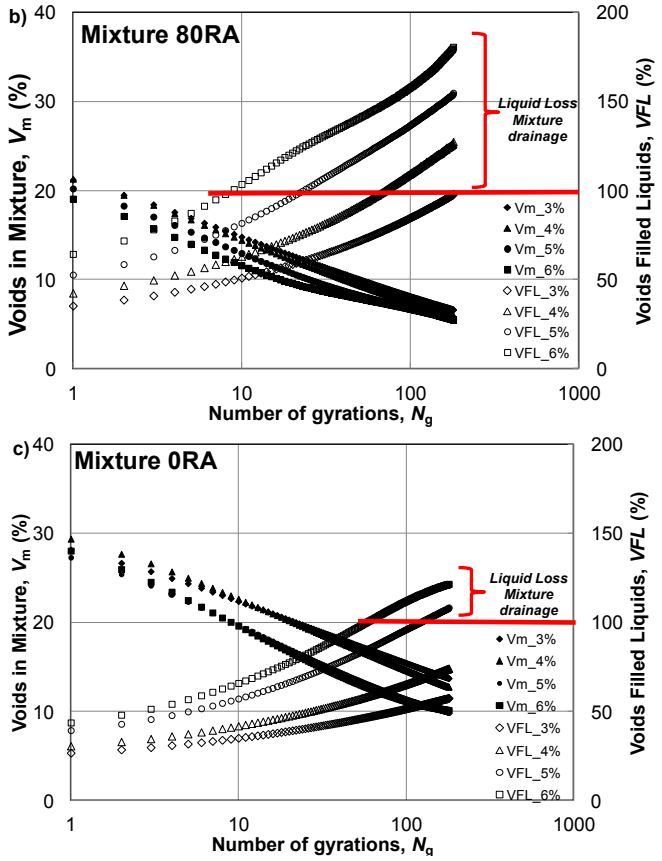


**Figure 11. 9** SGC compaction curves of CBTM-BE mixtures.

To highlight the importance of saturation, the final values of the dry density (i.e. after 180 gyrations) of all compacted specimens are reported in **Figure 11. 10**, as a function of water content. In the same figure, for each mixture, the saturation curve is plotted. These curves are calculated using the equation [Lambe, 1969]:

$$\rho_d = \frac{\rho_w \cdot S_r}{w + \frac{\rho_w \cdot S_r}{\rho_s}} \tag{69}$$

where $\rho_w$ and $\rho_s$ are the water density and the aggregate bulk density, respectively, $w$ is the water content and $S_r$ is the saturation degree, hypothesized equal to one ($S_r = 1$).
As previously observed, increasing water content leads to a voids reduction and hence to an increase of dry density. However, when $VFL > 100$ %, the dry density values plot to the right of the saturation curve, confirming that the initial water content is no more realistic. In these cases, the mixture composition should be corrected by fixing the limit condition $VFL = 100$

%. As shown in **Figure 11. 11**, the correction brings to a reduction of both water content and dry density because both water and fresh bitumen drain from the specimens.
The compaction results were used to establish an optimal value of the total water content, based on the following criteria:

- $W_{tot}$ should be high enough to enhance compaction, and
- $W_{tot}$ should not lead to drainage of water and bi-tumen from the specimens.

According to these criteria, an optimal water content $W_{opt}$ = 4 % was chosen for mixtures A (50RA-BE) and B (80RA-BE), whereas $W_{opt}$ = 5 % was chosen for mixture C (0RA-BE).

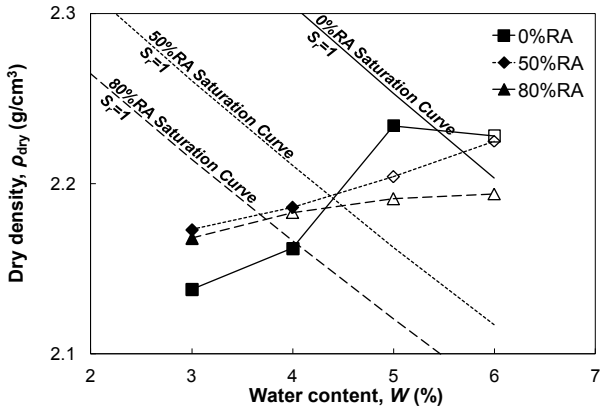


**Figure 11. 10** Dry density at 180 gyrations and saturation curves for chosen for mixtures A (50RA-BE), B (80RA-BE) and C (0RA-BE).

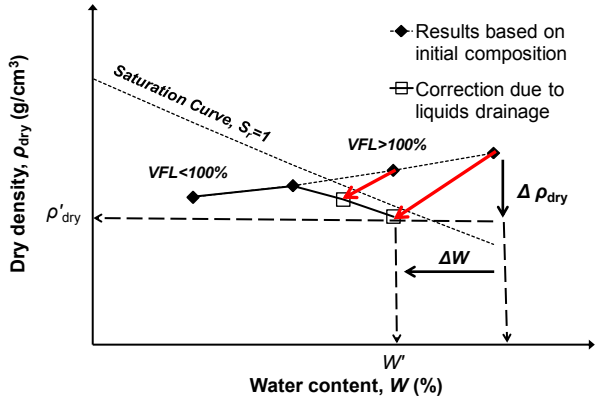


**Figure 11. 11** Dry density at 180 gyrations and saturation curves correction.

## 11.3.2 Complex modulus results

The complex modulus $E^*$ of the studied CBTM-BE mixes, was measured after 7 days of curing at 40°C. The values of the stiffness modulus $E_0$ and phase angle $\varphi$ measured on specimens A1, B1 and C1 are reported in **Figure 11. 12**.

Isothermal curves at 5, 15, 30, 40 and 55 °C showed an increase of $E_0$ with increasing test frequency and decreasing temperature (**Figure 11. 12** a, b, c). The measured values ranged from 1840 MPa to 9800 MPa for specimen A1 (50RA-BE), from 2580 MPa to 9580 MPa for specimen B1 (80RA-BE) and from 6470 MPa to 10650 MPa for specimen C1 (0RA-BE).

Such an asphalt-like behavior (i.e. frequency-dependent and thermo-dependent) was particularly evident for mixes A (50RA-BE) and B (80RA-BE). In addition, different RA contents had a limited effect on the thermo-rheological response. The dependence on temperature and frequency of mixture C (0RA-BE) was less marked.

The isothermal curves of the phase angle $\varphi$ (**Figure 11. 12** d, e, f) did not show a regular trend, suggesting that the viscous component of the thermo-rheological response is probably controlled by the interaction of diverse mechanical phenomena.

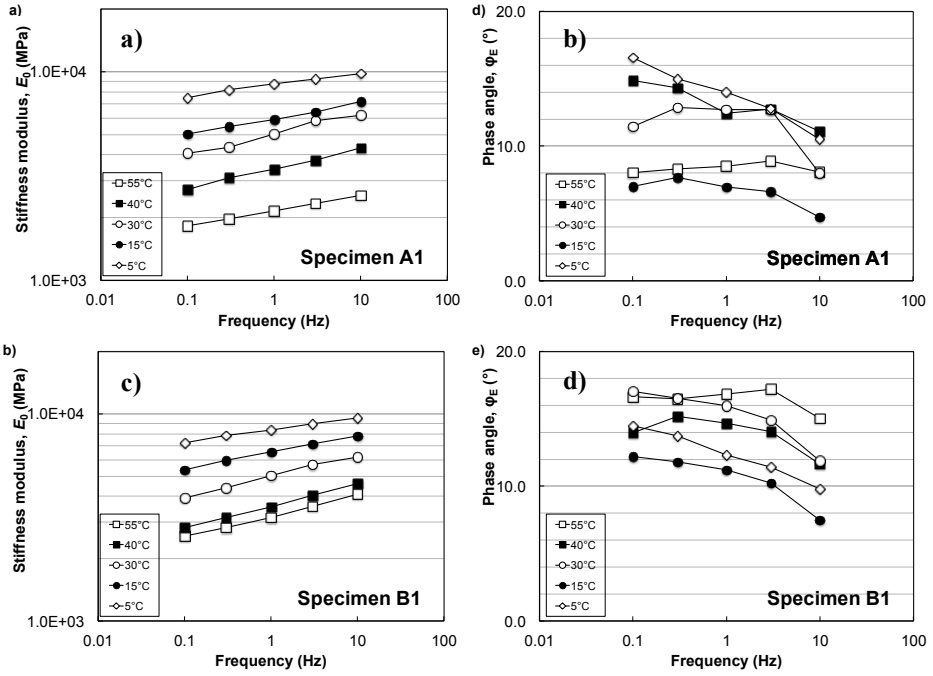

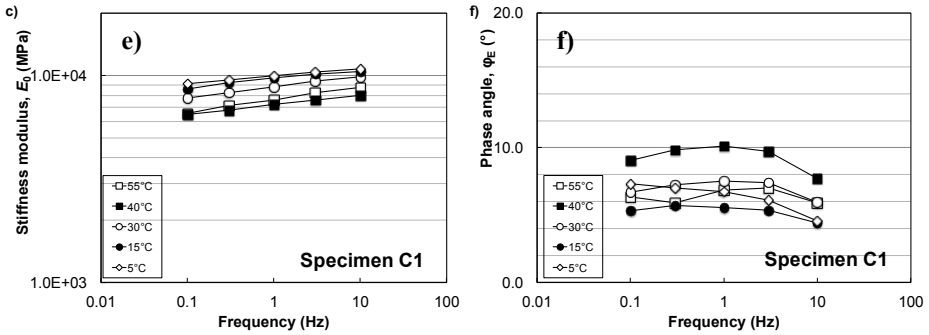


**Figure 11. 12** Isothermal curves of the stiffness modulus $E_0$ (a, b and c) and phase angle $\varphi$ (d, e and f) on specimens A1 (50RA-BE), B1 (80RA-BE) and C1 (0RA-BE) cured for 7 days.

To confirm similarities between the linear viscoelastic response of CBTM and HMA, validity of *the time-temperature superposition* principle (TTSP) was checked. To this aim the Huet-Sayegh rheological model was employed [Sayegh, 1967].
In this study, the reference temperature selected for master curves was $T_{ref}$ = 30 °C.
The Huet-Sayegh model parameters and the temperature shift factors, calculated using a numerical optimization procedure, are summarized in **Table 11. 4**.

| Mixture ID | Specimen ID | $E_g$ [MPa] | $E_e$ [MPa] | $k$ - | $h$ - | $\delta$ - | log $\tau_{ref}$ - |
|---|---|---|---|---|---|---|---|
| 50RA-BE | A1 | 13849 | 1143 | 0.14 | 0.30 | 2.22 | -0.17 |
| 80RA-BE | B1 | 17082 | 1993 | 0.12 | 0.42 | 2.68 | -1.09 |
| 0RA-BE | C1 | 12000 | 4500 | 0.18 | 0.45 | 1.35 | +1.12 |

**Table 11. 4** Shape parameters of the stiffness modulus master curves (reference temperature of 30 °C).

**Figure 11. 13** shows master curves of the stiffness modulus $E_0$ and phase angle $\varphi$, for the tested specimens. It is evident that a unique curve was obtained for $E_0$, but not for $\varphi$. This indicates that the TTSP is verified for the stiffness modulus but not for the phase angle (partial time-temperature superposition principle), confirming previous results on cold-recycled mixtures with similar cement/bitumen ratio [Cardone et al., 2015; Stimilli et al., 2013].
The larger dispersion of the $E_0$ values, which characterizes master curves of mixes A and B (50RA-BE and 80RA-BE) with respect to mixture C (0RA-BE), highlighted the influence of RA content on the thermo-rheological response. In addition, it can be observed that the response of mixtures A and B is almost identical, whereas the response of mixture C (0RA-BE) is similar to that measured on cement-treated materials containing RA [Grilli et al., 2013]. This suggests that the radical change produced by the addition of RA in CBTM mixes may not be explained only by the corresponding addition of aged binder.

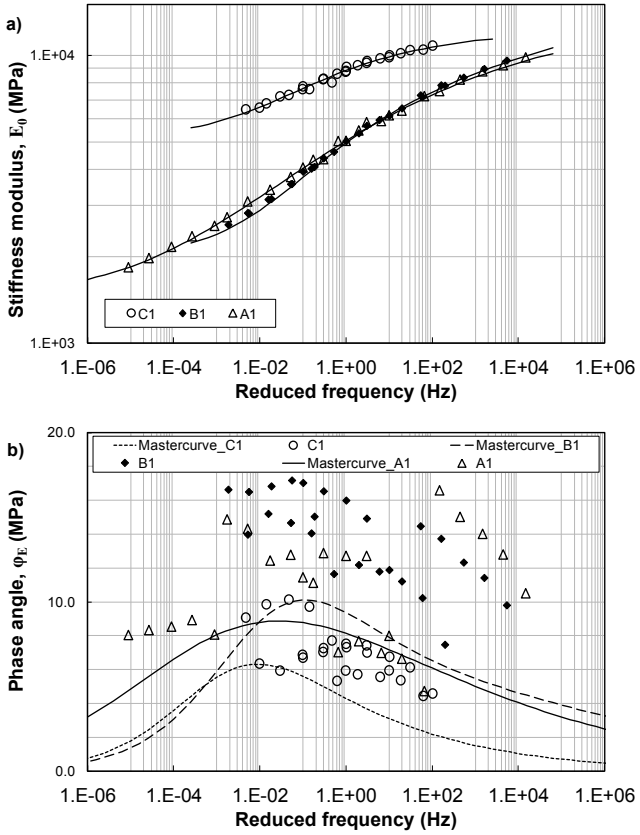


**Figure 11. 13** Master curves at 30 °C of the stiffness modulus $E_0$ and phase angle $\varphi$ for specimens A1 (50RA-BE), B1 (80RA-BE) and C1 (0RA-BE) cured for 7 days.

A more representative explanation can be put forward considering the physical structure of CBTM mixtures. This type of cold-recycled mixes can be represented as a skeleton of coarse aggregates bounded by bituminous and hydraulic mortars, formed by the finer aggregate particles. The coarse aggregate skeleton is formed by virgin aggregate and/or reclaimed aggregate (considered as "*black rock*"). The bituminous mortar is formed by the fresh bitumen, after emulsion breaking [Asphalt Academy, 2009], whereas the hydraulic mortar is formed by the hydrated cement.

In mixture C (0RA-BE), where the skeleton is composed only by virgin aggregates, the hydraulic mortar brings to the formation of a cementitious structure similar to that of cement-treated materials. The bituminous mortar is enclosed in such a rigid structure, and its influence on the mechanical response is negligible (limited frequency and temperature dependence). On the other hand, in mixtures A and B (50RA-BE and 80RA-BE), the coarse aggregate is mainly composed by reclaimed asphalt. Consequently, the coarse particles,

forming the skeleton of the mixture, are almost totally coated with aged bitumen; this hinders the formation of stable bonds with the hydraulic mortar. Therefore, the mechanical behavior of the mixture is controlled by the bituminous mortar, bringing to a clear dependence on temperature and frequency. This also explains the similarity between the response of mixes A and B (50RA-BE and 80RA-BE), which contain nearly the same amount of "*black rock*" and bituminous mortar.

# 11.4 Experimental findings: CBTM-FB

## 11.4.1 Volumetric properties and optimum foamed bitumen content

The effect of compaction energy (number of gyrations) and FB content on the volumetric properties of the CBTM-FB mixtures, is highlighted in **Figure 11. 14**. In particular, the evolution of $V_m$, *VMA* and *VFL* as a function of the number of gyrations, is reported. Volumetric parameters were calculated using Equations 66-68, where the volume of each component was obtained from initial weight and density, whereas the gross volume of the compacted material at each gyration is obtained from the height measurement of the movable pressuring plate of the SGC compactor.

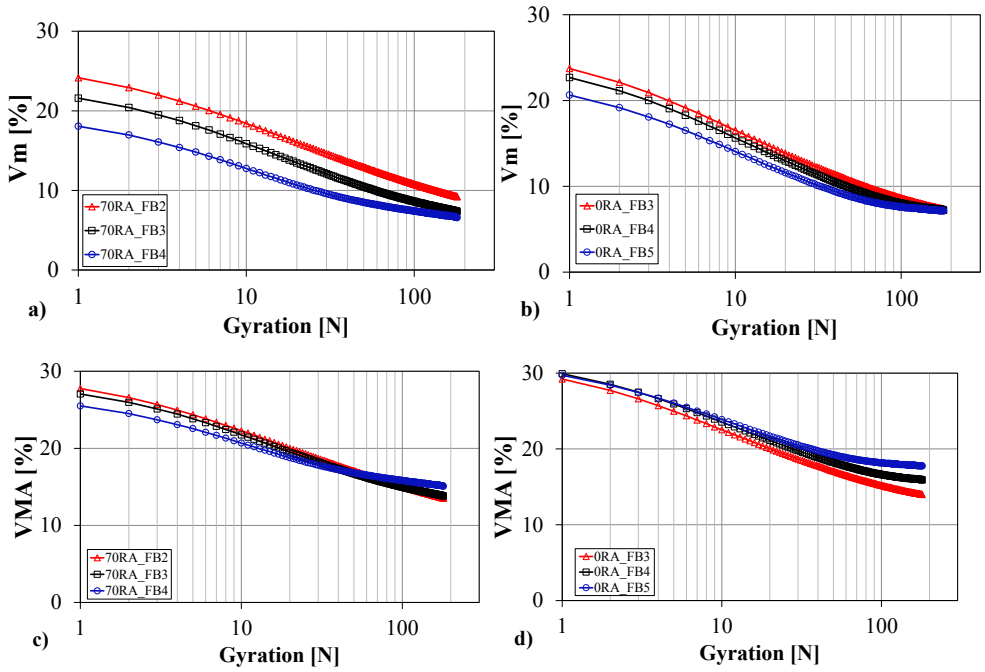

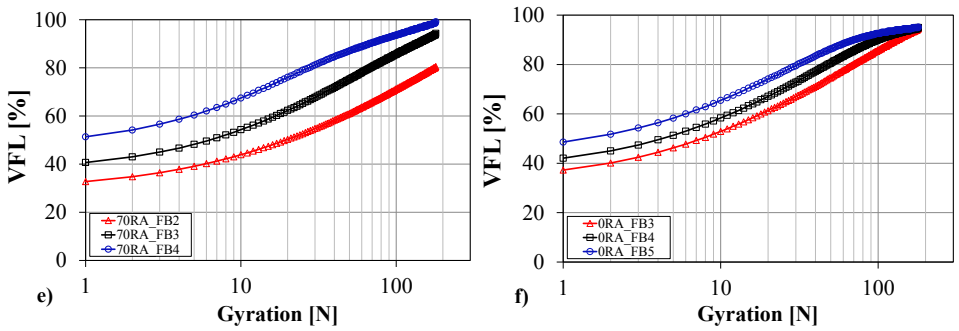


**Figure 11. 14** Evolution of volumetric properties as a function of the number of gyrations; a) $V_m$ for mixture B (70RA-FB); b) $V_m$ for mixture C (0RA-FB); c) *VMA* for mixture B (70RA-FB); d) *VMA* for mixture C (0RA-FB); e) *VFL* for mixture B (70RA-FB); f) *VFL* for mixture C (0RA-FB).

Since the behavior of mixtures A (50RA-FB) and B (70RA-FB) was very similar, only results for mix B are shown and compared with those obtained on mix C (0RA-FB). As it can be observed, for all FB contents, *VMA* (the percentage volume occupied by bitumen, air and water) and $V_m$ (the percentage volume occupied by air and water) decreased, whereas *VFL* (the percentage *VMA* occupied by bitumen and water) increased during compaction. This can be related to the densification of the aggregate skeleton, also leading to the reduction of the volume occupied by air, which is progressively filled by bitumen and water. From **Figure 11. 14** it can also be observed that increasing FB content resulted in a reduction of $V_m$ and an increase of *VFL*. In particular, after 180 gyrations, $V_m$ ranged between 7 % and 10 %, whereas *VFL* exceeded 90 %, indicating an almost complete saturation of the mixtures. In fact, at the end of compaction, a loss of water was observed for mixtures A (50RA-FB) and B (70RA-FB), at FB content above 3 %. However, no material loss was observed for mixture C (0RA-FB). For this reason the actual $V_m$ values of mixtures A (50RA-FB) and B (70RA-FB) may be lower than those calculated. The volumetric properties of the FB mixtures after 180 gyrations are summarized in **Table 11. 5**, whereas the value of $V_m$ and *VMA* as a function of FB content, is reported in **Figure 11. 15**a. As it can be observed, the three CBTM-FB mixtures followed a unique trend: higher FB dosages resulted in a $V_m$ decrease and a *VMA* increase. In particular, the *VMA* increase indicates that higher FB dosages caused lower densification of the aggregate skeleton. The observed behavior is similar to that of HMA at very high bitumen content [Roberts et al., 1996] and suggests that the chosen aggregate gradation was probably too dense and that additional void space was necessary to accommodate the water and FB amount required to achieve a proper compactability.

In **Figure 11. 15**b the *ITS* values at 20 °C, as a function of FB content, are reported. As it can be observed, *ITS* decreased if both FB and RA content increased. *ITS* results confirm the importance of *VMA* and therefore the impact of aggregate interlock on strength of the mixtures.

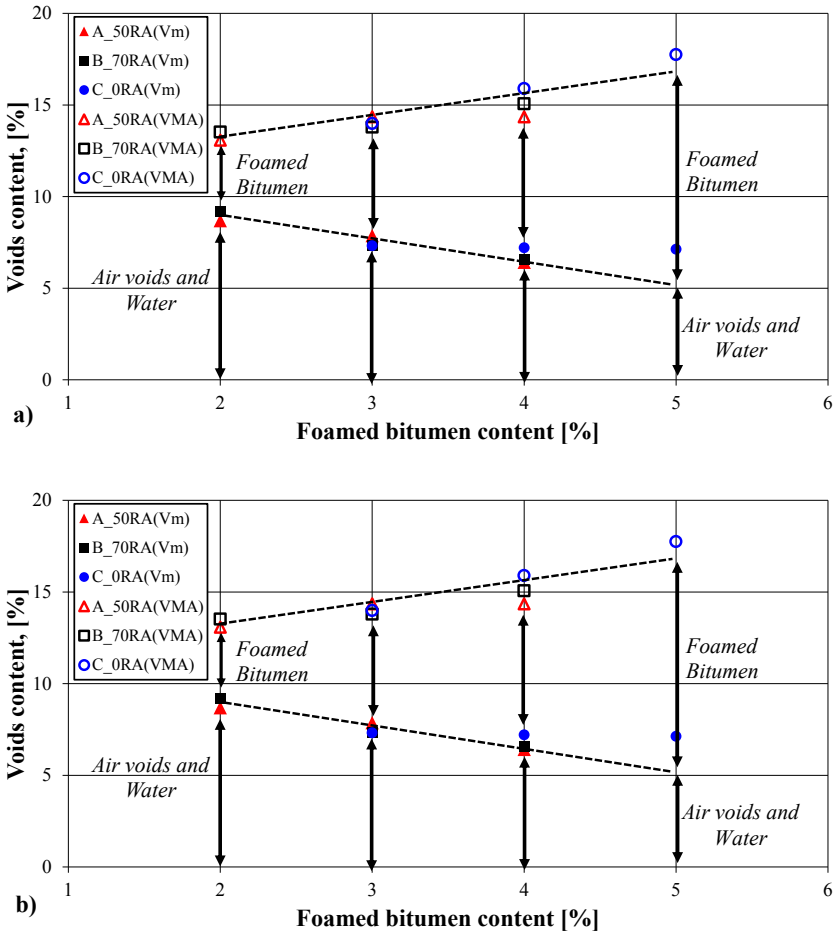


**Figure 11. 15** Volumetric and mechanical properties of the CBTM-FB mixtures as a function of FB content; a) $V_m$ and *VMA* after 180 gyrations; b) *ITS* at 20 °C after 3 days curing at 40 °C for mixtures A (50RA-FB), B (70RA-FB) and C (0RA-FB).

| Mix type | FB | Maximum density g/cm$^3$ | *VMA* % | $V_m$ % | *VFL* % |
|---|---|---|---|---|---|
| A (50RA-FB) | 2 | 2.556 | 13.08 | 8.70 | 82.52 |
| A (50RA-FB) | 3 | 2.519 | 14.37 | 7.89 | 89.12 |
| A (50RA-FB) | 4 | 2.484 | 15.01 | 6.43 | 98.86 |
| B (70RA-FB) | 2 | 2.525 | 13.53 | 9.21 | 80.44 |
| B (70RA-FB) | 3 | 2.489 | 13.79 | 7.33 | 94.32 |
| B (70RA-FB) | 4 | 2.455 | 15.10 | 6.61 | 98.92 |
| C (0RA-FB) | 3 | 2.600 | 14.05 | 7.39 | 94.04 |
| C (0RA-FB) | 4 | 2.561 | 15.96 | 7.28 | 94.54 |
| C (0RA-FB) | 5 | 2.525 | 17.81 | 7.20 | 94.79 |

**Table 11. 5** Volumetric properties of CBTM-FB mixtures (mixtures design phase).

Based on both the volumetric and the strength properties, a FB content equal to 3 % (by dry aggregate weight) was chosen to prepare the CBTM-FB specimens for complex modulus testing. A total of six specimens were compacted with a target air voids content of 10 % and cured according to the procedure described in Section 11.2.2. Before testing the air voids $V_m$ were measured according to the procedure currently adopted for HMA [EN 12697-6 standard]. The measured air voids values ranged from 9.4 % to 10.5 %.

## 11.4.2 Complex modulus results

Isothermal curves of the stiffness modulus ($E_0$) and phase angle ($\phi$) measured on specimens A1, B1 and C1, are reported in **Figure 11. 16**.

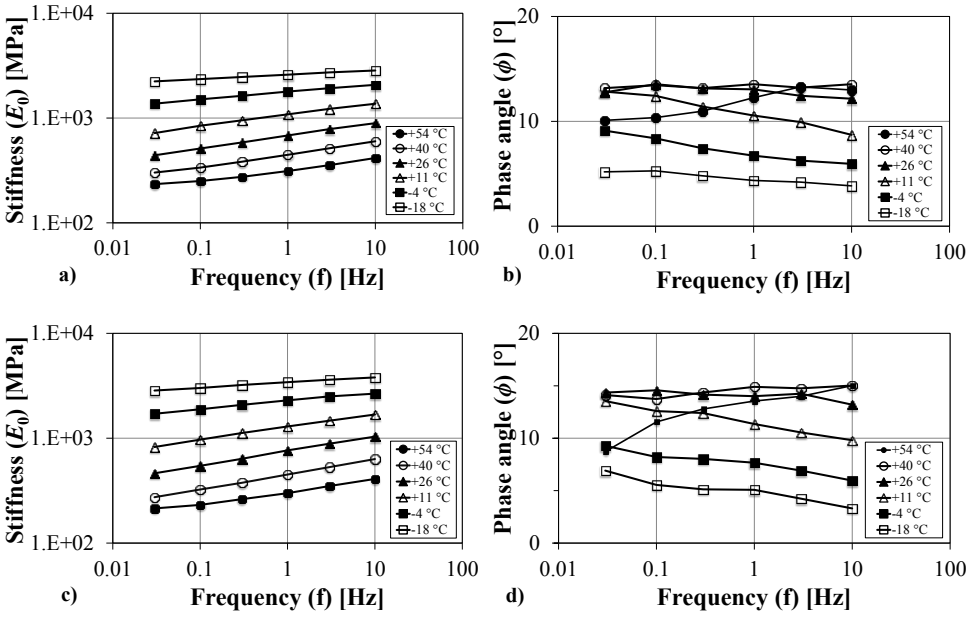

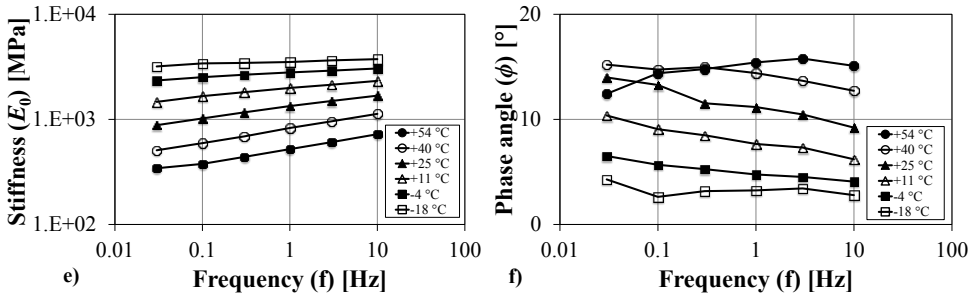


**Figure 11. 16** Isothermal curves of the stiffness modulus $E_0$ (a, c and e) and phase angle $\phi$ (b, d and f) measured on specimens A1 (50RA-FB), B1 (70RA-FB) and C1 (0RA-FB).

Stiffness increased with increasing frequency and decreasing temperature. In particular, $E_0$ ranged from 235 MPa to 2845 MPa for specimen A1 (225 MPa to 2640 MPa for specimen A2), from 214 MPa to 3802 MPa for specimen B1 (171 MPa to 3977 MPa for specimen B2) and from 343 MPa to 3744 MPa for specimen C1 (467 MPa to 4075 MPa for C2). The phase angle ranged from 3° (low temperature/high frequency) to 18° (high temperature/low frequency). Moreover, $\phi$ generally decreased with frequency at the highest test temperature (50 °C).

Although for all the tested mixtures (50RA-FB, 70RA-FB and 0RA-FB) the values of both $E_0$ and $\phi$ are well below those commonly measured on HMA [Di Benedetto et al., 2001], the frequency and temperature variations clearly highlight a typical asphalt-like thermo-rheological behaviour.

In order to verify possible specimen damage during the loading cycles carried out at lower temperatures (-20 °C, -5 °C and 10 °C), the frequency sweep at 25 °C was repeated two times. As shown in **Figure 11. 17**, the $E_0$ values obtained from the second repetition were slightly lower with respect to those obtained from the first repetition. However, from a practical point of view, such variation is not significant. In order to check the validity of the time-temperature superposition principle (TTSP), the complex Young's modulus was represented in the Cole-Cole plane ($E_1$, $E_2$). As it can be observed (**Figure 11. 18**), for all specimens, unique curves appear to identify the mixture responses.

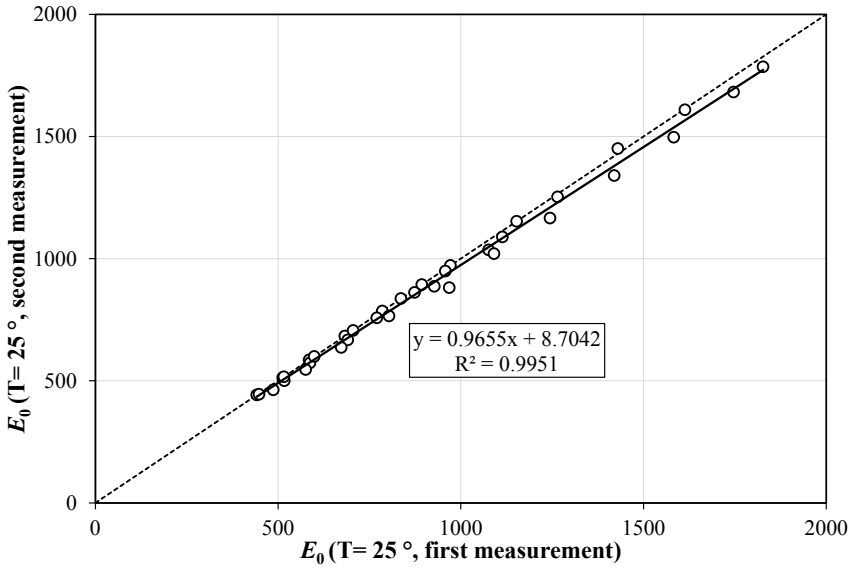


**Figure 11. 17** Correlation plot for E0 values measured at 25 °C.

Therefore, a thermo-rhelogically simple behaviour can be assumed, i.e. the TTSP can be considered valid for $E^*$, regardless of the RA content. Such behaviour is different from that observed on cold recycled mixtures prepared with bituminous emulsion where the TTSP was only verified for the stiffness modulus [Cardone et al., 2015; Stimilli et al., 2013]. This is probably due to the high bitumen content (FB = 3 %) and low cement content (C = 1.5 %) of the CBTM-FB mixtures tested in the present study.
Results plotted in **Figure 11. 18** and **Figure 11. 19** (Black diagram) show a good repeatability between each couple of specimens of the same mixture and thus confirm the reliability of the adopted mixing, compaction and procedures. In addition, results show that the RA content does not have a strong impact on the viscous response. In fact, regardless of the test condition (i.e. frequency and temperature) the range of phase angle variation is around 4°.

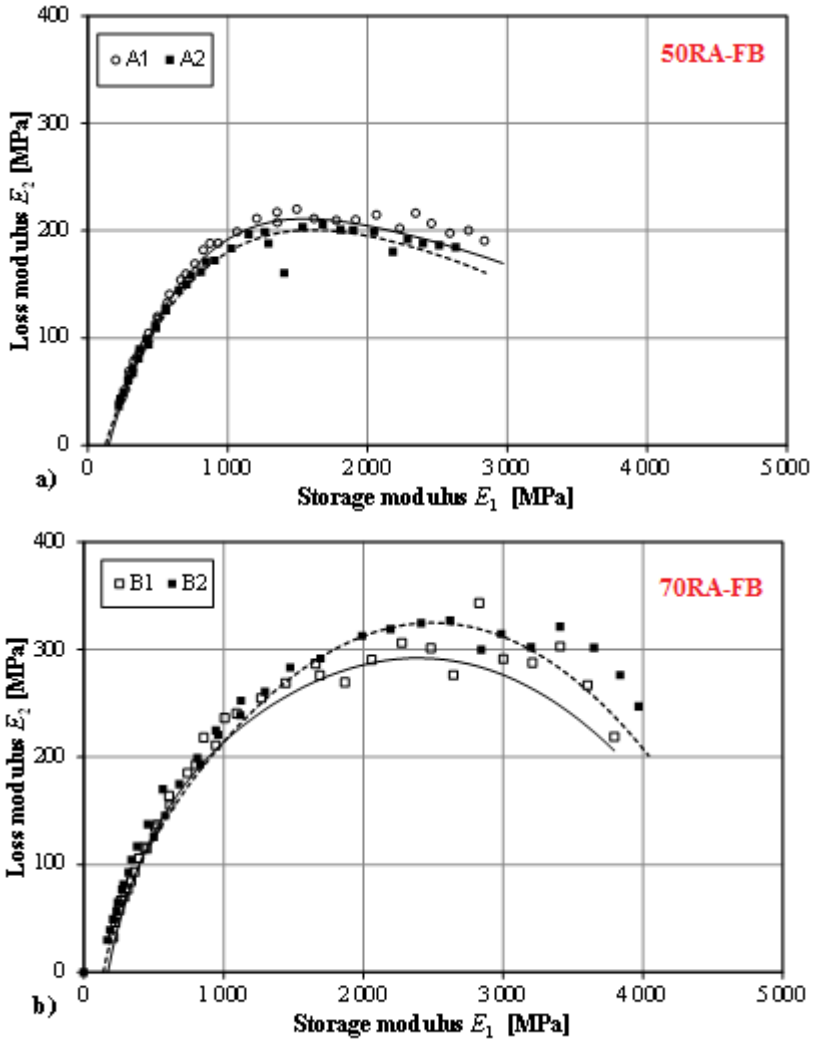
A1
A2
50RA-FB
Loss modulus $E_2$ [MPa]
Storage modulus $E_1$ [MPa]
a)
B1
B2
70RA-FB
Loss modulus $E_2$ [MPa]
Storage modulus $E_1$ [MPa]
b)

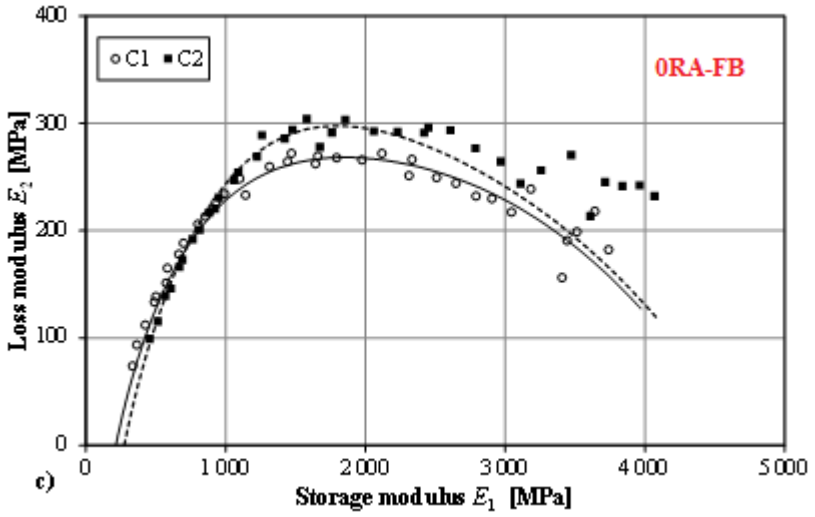


**Figure 11. 18** Cole-Cole plots for the complex modulus; a) Mixture A (50RA-FB; FB=3%; C = 1.5%), b) Mixture B (70RA-FB; FB=3%; C = 1.5%), c) Mixture C (0RA-FB; FB=3%; C = 1.5%).

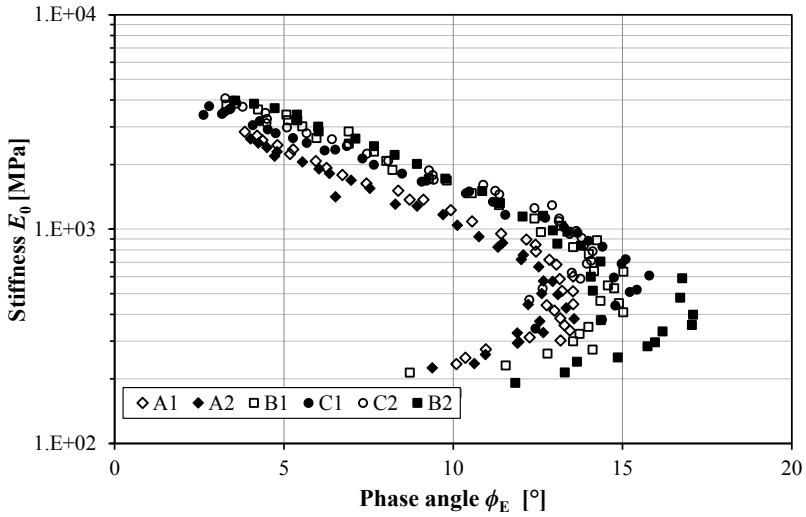


**Figure 11. 19** Black diagram for the complex modulus of mixtures A, B and C (50RA-FB, 70RA-FB and 0RA-FB).

## 11.4.3 Advanced rheological modelling

For each specimen, the measured $E^*$ values were fitted using the Huet-Sayegh (H-S) rheological model [Sayegh, 1967] following the procedure already described in Section 5.2.3. In the present research the chosen reference temperature for the H-S model was $T_{REF}$ = 25 °C.

It is highlighted that, the actual (measured) test temperatures had small differences with respect to the nominal temperatures; for example, the actual test temperature corresponding to $T_{REF}$ = 25 °C was 26 °C. Therefore, in order to use a unique temperature reference, the following procedure was adopted. For each specimen, the H-S model was initially fitted choosing the actual test temperature $T'_{REF}$ = 26 °C. Next, the Williams-Landel-Ferry (WLF) model was used to fit the temperature dependency of the shift factors [Ferry, 1980]:

$$\log a_{T'_{REF}}(T) = \frac{-C'_1 \cdot (T - T'_{REF})}{-C'_2 \cdot (T - T'_{REF})} \tag{70}$$

where $C'_1$ and $C'_2$ are experimental coefficients that can be calculated using a linear regression on the experimental values of the shift factors [Emri, 2005]. Equation 70 has been rearranged by changing the reference temperature to the unique value $T_{REF}$ = 25 °C. This required new values for the regression coefficients that were calculated as follows [Chailleux et al., 2006]:

$$C_1^{25} = \frac{C'_1 \cdot C'_2}{C_2^{25}} \tag{71}$$

$$C_2^{25} = C'_2 + 25 - T'_{25} \tag{72}$$

The values of $C^{25}_1$ and $C^{25}_2$ were used to obtain the new shift factors $a_{25}(T)$ using Equation 70 and finally the new value of the characteristic time $\tau_{25}$ was calculated, according to Equation 22 (see Section 5.2.3).

Master curves of $E_0$ and $\phi$, at $T_{REF}$ = 25 °C, and the corresponding shift factors, are reported in **Figure 11. 20** and **Figure 11. 21**, respectively. The H-S and WLF model parameters are summarized in **Table 11. 6**.

As it can be observed, the RA content had a negligible impact on both the glassy and the equilibrium moduli ($E_g$, $E_e$). Since all the tested specimens were characterized by the same grading curve and volumetric properties, this result is consistent with the behaviour of HMA, where the upper and lower bounds of the $E_0$ master curve are related only to aggregate gradation and mixture volumetric [Pellinen et al., 2007]. Indeed, this also supports the indication of considering RA as a black rock, at least in asymptotic conditions.

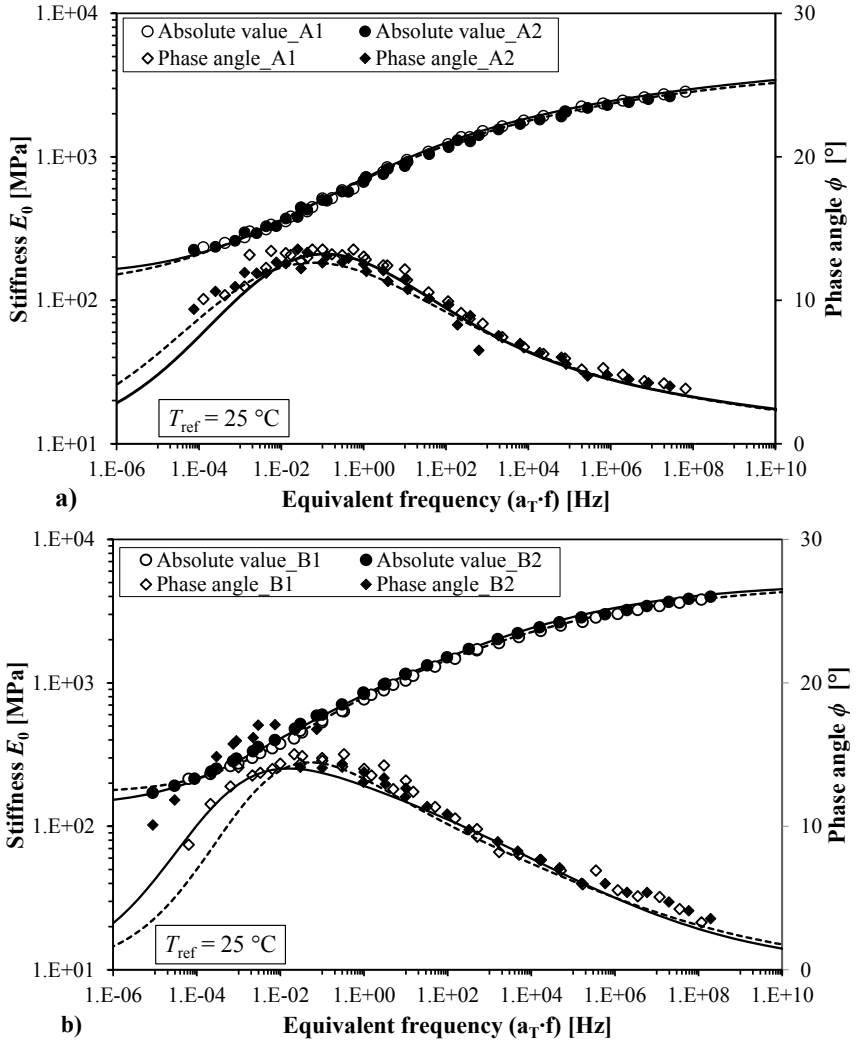
Absolute value_A1
Absolute value_A2
Phase angle_A1
Phase angle_A2
Stiffness $E_0$ [MPa]
Phase angle $\phi$ [°]
$T_{ref}$ = 25 °C
1.E+04
1.E+03
1.E+02
1.E+01
30
20
10
0
1.E-06
1.E-04
1.E-02
1.E+00
1.E+02
1.E+04
1.E+06
1.E+08
1.E+10
a)
Equivalent frequency ($a_T$·f) [Hz]
Absolute value_B1
Absolute value_B2
Phase angle_B1
Phase angle_B2
Stiffness $E_0$ [MPa]
Phase angle $\phi$ [°]
$T_{ref}$ = 25 °C
b)
Equivalent frequency ($a_T$·f) [Hz]

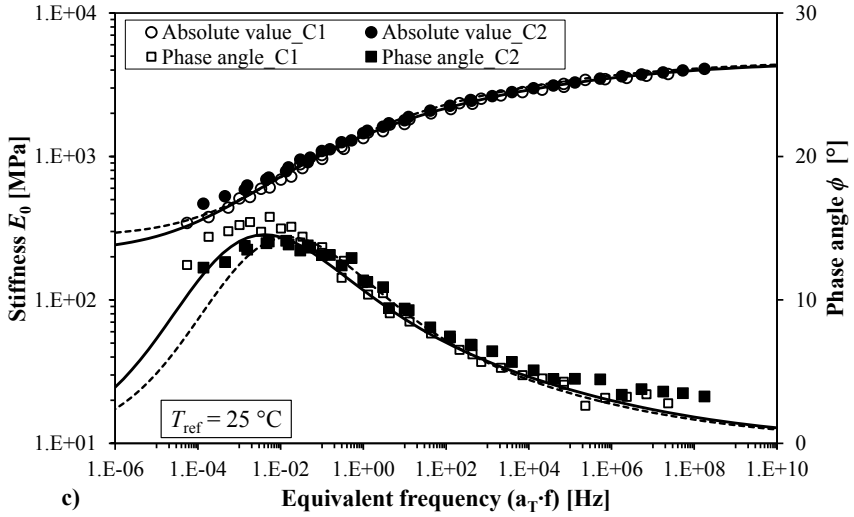


**Figure 11. 20** Master curves for $E_0$ , $\phi$; a) Mixture A (50RA-FB), b) Mixture B (70RA-FB), c) Mixture C (0RA-FB).

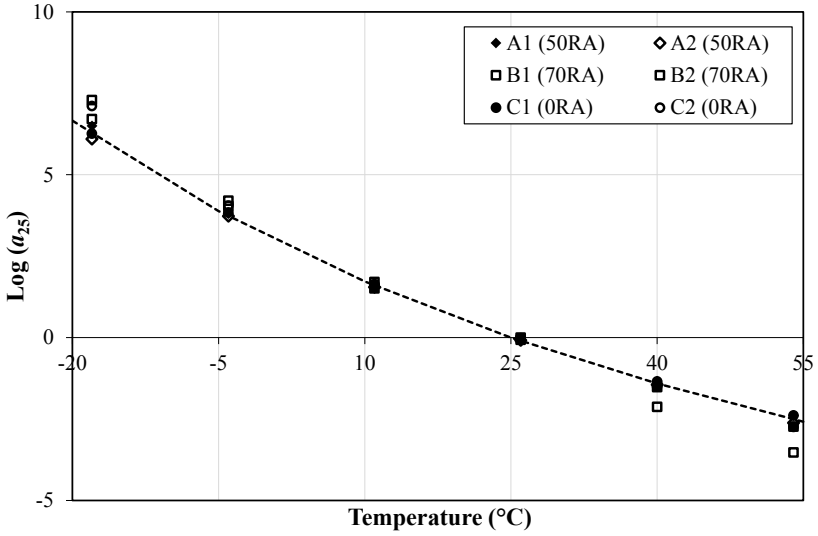


**Figure 11. 21** Shift factors at 25 °C for mixtures A (50RA-FB), B (70RA-FB) and C (0RA-FB).

| Specimen ID | Mixture ID | $E_g$ MPa | $E_e$ MPa | $k$ - | $h$ - | $\delta$ - | log $\tau_{25}$ - | $C^{25}{}_1$ - | $C^{25}{}_2$ °C |
|---|---|---|---|---|---|---|---|---|---|
| A1 | 50RA | 5076 | 158 | 0.091 | 0.302 | 2.613 | -2.91 | 13.0 | 130.2 |
| A2 | 50RA | 4850 | 168 | 0.095 | 0.311 | 2.817 | -2.68 | 17.8 | 168.7 |
| B1 | 70RA | 5295 | 112 | 0.099 | 0.245 | 1.150 | -3.65 | 16.8 | 149.8 |
| B2 | 70RA | 6025 | 115 | 0.075 | 0.239 | 1.210 | -3.85 | 17.1 | 147.3 |
| C1 | 0RA | 4231 | 215 | 0.161 | 0.453 | 3.512 | 0.36 | 19.4 | 175.3 |
| C2 | 0RA | 4384 | 351 | 0.164 | 0.532 | 3.593 | 0.15 | 11.9 | 114.9 |

**Table 11. 6** Huet-Sayet and WLF fitted model parameters for the tested specimens

The impact of RA content on the shape parameters of the H-S model is not straightforward (**Table 11. 6**). In fact, the values of $k$, $h$ and $\delta$ for mixture C (0RA-FB) lie between those of mixture A (50RA-FB) and B (70RA-FB). This can also be graphically observed by introducing the normalized complex modulus:

$$E^*_n(j\omega\tau) = \frac{E^*(j\omega\tau)-E_e}{E_g-E_e} \quad (73)$$

where $E^*(j\omega\tau)$ is the complex modulus expression given by the fitted H-S model. The Real and Imaginary components of $E^*_n$ for the six tested specimens are plotted in **Figure 11. 22** (normalized Cole-Cole diagram).

It has been shown [Olard et al., 2003; Mangiafico et al., 2013] that, for HMA mixtures, the values of $k$, $h$ and $\delta$, and consequently the shape of the $E^*_n$ curves, depend only on the properties of the bituminous binder. With this in mind, the different shape of the fitted models (**Figure 11. 22**) allegedly indicates that the LVE response of the tested mixtures is not related only to the thermo-rheological behaviour of the FB. Hence, the influence of RA content, but also the influence of cement dosage clearly needs further investigation.

Overall the present study showed that it is certainly possible to study the LVE response of cold recycled mixtures produced with foamed bitumen (i.e. CBTM-FB) using the same experimental and analytical approach commonly adopted for HMA mixtures. Treating RA as black rock proved to be a valid concept, at least when considering mixture volumetrics. However, in order to achieve an effective thermo-rheological characterization, the deformability of RA and its thermal dependence should be properly considered. This in no way supports the idea, commonly accepted for hot recycling, of finding some sort of quantitative equivalence between fresh binder and aged binder (the so called re-activated binder). Instead, it is the Author's opinion, that the impact of FB and RA should always be considered separately, at least from a mechanical point of view.

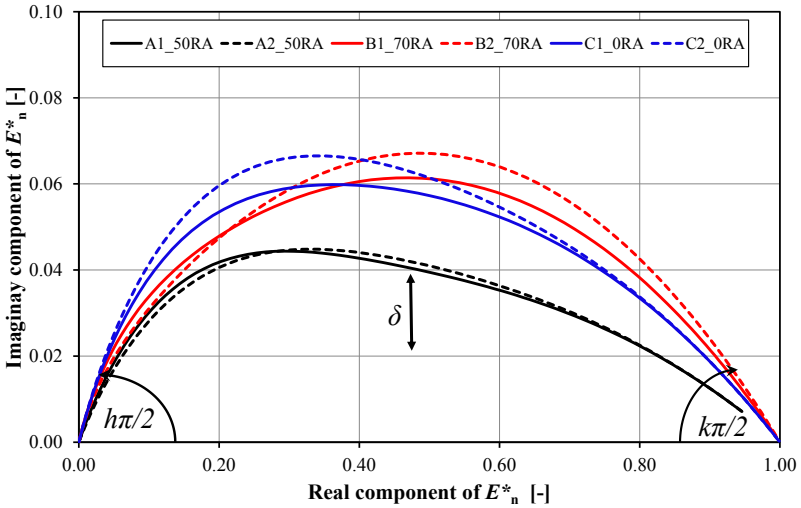


**Figure 11. 22** Normalized Cole-Cole diagram for the tested specimens.

# 11.5 Summary and comparison

## 11.5.1 CBTM-BE mixtures

In the present investigation, CBTM-BE mixtures were characterized by 2 % of cement and 3.0 % of bitumen emulsion (i.e. 1.8% of residual bitumen) and different RA contents (50%, 80% and 0%). The experimental results showed that an excessive compaction effort may cause free water to be squeezed out of the mixture together with a fraction of the dispersed fresh bitumen, modifying the initial composition of the mixtures. Therefore, the optimal water content ($W_{opt}$ =4 % for mixtures 50RA-BE and 80RA-BE, $W_{opt}$ = 5 % for mixture 0RA-BE) was selected to guarantee densification and prevent liquid loss, during the compaction process. Results also showed that, increasing reclaimed bitumen content, mixtures compactability improved, due to the shape and surface texture of the reclaimed aggregate.

The complex modulus values, highlighted that mixtures containing reclaimed asphalt exhibited an asphalt-like behavior (i.e. frequency-dependent and thermo-dependent), whereas the frequency- and thermo-dependence of the mixture containing only virgin aggregate was almost negligible.

For all reclaimed asphalt contents, validity of the time-temperature superposition principle was verified for the stiffness modulus but not for the phase angle.

Analysis of experimental results suggests that, in the mixture containing only virgin aggregate, the *cementitious mortar* (fine aggregate and cement) forms a rigid structure together with the coarse aggregate skeleton. This induces a mechanical behavior similar to that of cement treated materials. On the other hand, in mixtures containing reclaimed asphalt, the particles forming the coarse skeleton are almost totally coated with aged bitumen ("black rock"). This hinders the formation of stable bonds with the hydraulic mortar. In this case, the

mechanical behavior is controlled by the *bituminous mortar* (fine aggregate and fresh bitumen), bringing to a clear dependence on temperature and frequency.

## 11.5.2 CBTM-FB mixtures

In the present research, the LVE response of CBTM-FB mixtures was characterized by measuring and modelling the complex Young's modulus of three mixtures with different content of RA (50%, 70% and 0%). Before mechanical testing composition and compactability of the mixtures were analyzed in order to produce samples with the same FB content and similar volumetric properties.

The mixing water content was established based on the proctor compaction procedure. The optimum water content of the mixtures containing RA (4.5 %) was slightly lower with respect to that of the mixture containing only virgin aggregate (5.0 %) because of the lower internal friction related to the shape and surface texture of RA coated particles.

In order to analyze the volumetric properties of the mixtures, three parameters were defined and monitored during gyratory compaction: voids in the mixture $V_m$, voids in the mineral aggregate *VMA*, and voids filled with liquid *VFL*. For all FB contents, an increasing of the number of gyrations lead to a decreasing of the *VMA* and $V_m$, whereas the *VFL* increased. However, higher FB dosages resulted in a *VMA* increase, indicating a lower densification of the aggregate skeleton and suggesting that the chosen aggregate gradation was probably too dense and that additional void space was necessary to accommodate the water amount required to achieve a proper compactability.

Specimens for complex modulus testing were prepared with 3% FB and characterized by a close range of voids in the mixture (9.4 % to 10.5 %). Although the values of both the stiffness modulus $E_0$ and phase angle $\phi$ were well below those normally measured on HMA, the frequency and temperature variations clearly highlighted a typical asphalt-like behavior. In addition, the TTSP was verified for $E^*$ and therefore, regardless of the RA content, the FB mixture behavior could be considered thermo-rhelogically simple.

The Huet-Sayegh rheological model was successfully used to fit the experimental results. The RA content had a negligible impact on both the glassy and the equilibrium moduli. However, the fitted values of the shape parameters $\delta$, $k$, $h$ suggest that the overall LVE response of the tested mixtures depends on the thermo-rheological properties of the FB, the RA content and the cement dosage.

Overall the experimental results showed that it is possible to study the LVE response of CBTM-FB mixtures using the same experimental and analytical approach adopted for HMA mixtures. Although treating RA as black rock is useful, especially for the volumetric analysis of the mixtures, its deformation behavior and thermal dependence had a clear impact on the thermo-rheological characterization of the mixtures, and will be investigated in future studies.

## 11.5.3 CBTM-BE vs CBTM-FB mixtures

Considering the volumetric point of view, CBTM-BE and CBTM-FB mixture characterized by similar RA contents exhibited a common behavior in terms of volumetric properties.

Mixtures with higher RA content showed improved compactability and consequently, these materials required lower water content. This can be explained by the rounded shape and smooth surface texture of the reclaimed aggregate particles.
Additional considerations are not possible because, the evolution of volumetric properties for CBTM-BE mixtures was investigated varying the amount of water content while, with CBTM-FB mixtures, different amounts of foamed bitumen are considered at fixed water content.
In order to compare the rheological behavior of CBTM-BE and CBTM-FB mixtures, the master curve obtained for CBTM-BE mixture at reference temperature $T_{REF}$= 30 °C (**Figure 11. 13**) was shifted at the same $T_{REF}$ used for CBTM-FB, $T_{REF}$= 25 °C.
This required new values for the regression coefficients were calculated using the procedure suggested by Chailleux et al. (2016), already adopted during the CBTM-FB rheological modelling. In this case, $T'_{REF}$= 30 °C.
In **Figure 11. 23**, both master curves of CBTM-BE and CBTM-FB mixtures, in terms of $E_0$, are reported at $T_{REF}$= 25 °C. Master curves of $\varphi$ was not considered because the TTSP principle was only partially validated for CBTM-BE mixture.

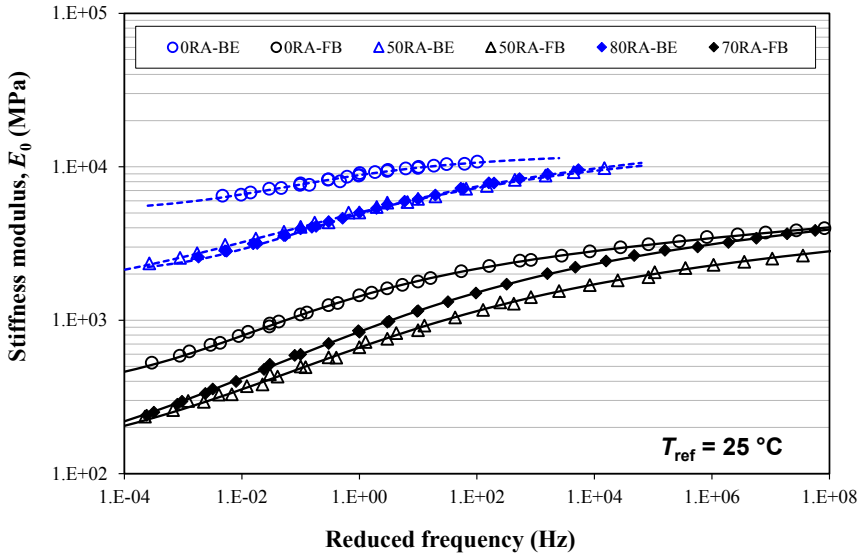


**Figure 11. 23** Master curves based on Huet-Sayegh model of $E_0$ for CBTM-BE and CBTM-FB mixtures are reported at $T_{REF}$= 25 °C.

In addition, it is important to highlight that the start goal to produce both CBTM-BE and CBTM-FB mixtures at the same bitumen/cement ratio is failed because, from the CBTM-FB mix-design resulted a foamed bitumen content equal to 3% by dry aggregate weight. Consequently, the studied B/C ratios were about 1 and 2 for CBTM-BE (B=1.8% and C=2%) and CBTM-FB (B=3% and C=1.5%), respectively.

For this reason, additional studies are necessary if the influence of production technique, i.e. with bitumen emulsion or foamed bitumen, on rheological behaviour of CTMB mixtures should be characterized.
On the basis of the comparison reported in **Figure 11. 23**, the following conclusions can be drawn:

- The influence of RA contents is limited to CBTM-FB mixtures;
- Rheological modelling usually adopted with HMA mixtures can also be adopted to study the LVE response of both CBTM-BE and CBTM-FB mixtures;
- Analyzing different types of CBTM mixtures characterized by similar RA contents, it is possible to observed that master curves are parallel to each other but CBTM-BE master curves are shifted versus higher values in stiffness modulus. This difference is due to the lower B/C ratio (equal to 1) used in the production of CBTM-BE mixture and as a consequence, to the higher cement content adopted (cement-like behavior). In fact CBTM_FB with B/C ratio of 2 exhibited an higher asphalt-like behavior (i.e. more time-temperature dependence).
- The selected B/C ratio equal to 1 caused an increasing in stiffness modulus of one order of magnitude for all CBTM-BE mixtures.

# CHAPTER 12.

# Three-dimensional linear viscoelastic response of cold recycled mixtures

This Chapter is focused on the characterization of the three-dimensional linear viscoelastic response of cold recycled mixtures (CRMs). The topic is a quite new subject for this material and for this reason, no similar data are available for comparison in literature.
Results of an experimental investigation aimed at the simultaneous measurement of $E^*$ and $\nu^*$, are presented. The mixture is the CBTM-SITE already adopted during the experimental test section located on The A14 Motorway near to the city of Ancona, Italy (see Chapter 8).The cement-bitumen treated material is a CRM fabricated using sement, bitumen emulsion and 100% of reclaimed aggregate.

## 12.1 Overview

The analysis of three-dimensional (3D) stress-strain fields produced by vehicular loads and temperature variations inside road pavements, even in the simple case of isotropic linear elasticity, requires pavement materials to be characterized by at least two material properties, for example the axial (or Young's) modulus $E$ and the Poisson's ratio (PR) $\nu$.
As far as bituminous mixtures are concerned, the mechanical characterization at small strains is based on the linear viscoelasticity (LVE) theory and, for the isotropic case, the measurement of two independent response functions, for example the complex Young's modulus $E^*$ and the complex Poisson's ratio $\nu^*$, is required [Tschoegl, 1989; Sauzeat and Di Benedetto, 2015].
The measurement of $E^*$ of bituminous mixtures has been a central topic in pavement engineering since its very beginning [Papazian, 1962; Huet 1963] and nowadays, after more than 40 years of experimental research [Di Benedetto et al., 2001; Witczak et al. 2002], various standard testing methods are available [EN 12697-26, AASHTO T342]. On the other hand, although measurement and modeling of $\nu^*$ of bituminous mixtures in the LVE domain is not a new research issue [Papazian, 1962; Sayegh, 1967], the topic has been overlooked for many years. In fact, in most practical applications, the PR is assumed to be time and temperature independent, e.g. $\nu = 0.35$, or its value is correlated to the value of the time and temperature dependent Young's modulus [NCHRP, 2004]. In both cases it is clear that, for the sake of simplicity, a fundamental aspect of the material stress-strain behavior, i.e. the response in transverse direction, is disregarded.
In the last 10 years, numerous experimental studies have shown that $\nu^*$ bituminous mixtures is actually a complex number, i.e. its phase angle is small (generally less than 10°) but not null and is characterized by a typical time and temperature dependence [Di Benedetto et al., 2007; Nguyen H.M. et al., 2009; Di Benedetto et al., 2009; Pouget et al., 2010; Graziani et al., 2014, Bocci et al., 2015]. Recently, the RILEM Technical Committee 237-SIB "Testing

and characterization of sustainable innovative bituminous materials and systems" organized a round robin test focused on the simultaneous measurement of $E^*$ and $\nu^*$ of bituminous mixtures. The results confirmed that the phase angle of $\nu^*$ is not null and that the upper limit of its absolute value (norm) is not necessarily 0.5. Moreover, the validity of the time-temperature superposition principle (TTSP) for $\nu^*$ was validated, at least if pure bitumen is used [Perraton et al., 2016; Graziani et al., 2016c]. As a result of the RILEM TC activities, a recommendation on the simultaneous measurement of $E^*$ and $\nu^*$ by means of axial testing on cylindrical specimens was also prepared [Graziani et al., 2016b].

## 12.2 Measurement of Poisson's ratio of bituminous materials

A cyclic (sinusoidal) axial test on a cylindrical specimen is considered (**Figure 12. 1**). Linearity implies that both axial and transverse stress-strain have the same fundamental period ($T$), whereas isotropy implies that the transverse response is the same in all directions. Using complex exponentials, stress and strain can be written as follows:

$$\sigma_1(t) = \sigma_{1,0} \sin(\omega t + \delta_1) \rightarrow \sigma_1^*(\omega) = \sigma_{1,0} \exp[\mathrm{j}(\omega t + \delta_1)] \quad (74a)$$

$$\varepsilon_1(t) = \varepsilon_{1,0} \sin(\omega t) \rightarrow \varepsilon_1^*(\omega) = \varepsilon_{1,0} \exp[\mathrm{j}(\omega t)] \quad (74b)$$

$$\varepsilon_3(t) = \varepsilon_2(t) = \varepsilon_{2,0} \sin(\omega t - \delta_2) \rightarrow \varepsilon_2^*(\omega) = \varepsilon_{2,0} \exp[\mathrm{j}(\omega t - \delta_2)] \quad (74c)$$

where $\sigma_{1,0}$, $\varepsilon_{1,0}$ and $\varepsilon_{2,0}$ are the steady-state amplitudes of the sinusoidal signals, $\omega = 2\pi f$ is the angular frequency, $f = 1/T$ is the testing frequency, $\delta_1$, $\delta_2$ are the phase angles, with respect to the axial strain to which a zero phase is assigned and j is the imaginary unit ($\mathrm{j}^2 = -1$).

The sign of $\delta_1$ and $\delta_2$ in Equations 74 is selected according to the convention customarily adopted in the Signals & Systems theory [Oppenheim et al., 1996] whereby the phase angle is added to indicate a lead and subtracted to indicate a lag. Therefore, Equation 74a assumes that axial stress leads axial strain, whereas Equation 74c assumes that transverse strain lags axial strain. It is important to note that, while the first assumption follows from the LVE theory, the second is a heuristic hypothesis [Tschoegl, 1989; Tschoegl et al., 2002]. According to such an hypothesis, the maximum transverse contraction (or expansion) lags the maximum axial expansion (or contraction) and hence implies $\delta_2 > \pi$, as outlined in **Figure 12. 1**b.

The complex exponentials described by Equations 74 are represented in **Figure 12. 2** (complex plane) as phase vectors (or phasors). In particular, the condition $\delta_2 > \pi$, is depicted in **Figure 12. 2**a, whereas the condition $\delta_2 < \pi$, is depicted in **Figure 12. 2**b.

According to the previous notations, the complex Young's modulus and the complex Poisson's ratio are defined as follows:

$$E^*(\omega) = \frac{\sigma_1^*}{\varepsilon_1^*} = \frac{\sigma_{1,0}}{\varepsilon_{1,0}} \exp[\mathrm{j}\delta_1] = E_0 \exp[\mathrm{j}\delta_E] \quad (75)$$

$$\nu^*(\omega) = -\frac{\varepsilon_2^*}{\varepsilon_1^*} = -\frac{\varepsilon_{2,0}}{\varepsilon_{1,0}}\exp[-\mathrm{j}\delta_2] = \nu_0 \exp[-\mathrm{j}\delta_\nu] \tag{76}$$

where $E_0 = \sigma_{1,0}/\varepsilon_{1,0}$, $\nu_0 = \varepsilon_{2,0}/\varepsilon_{1,0}$ are the absolute values (or norms), $\delta_\mathrm{E} = \delta_1$ and $\delta_\nu = \delta_2 - \pi$ are the phase angles of $E^*$ and $\nu^*$, respectively (**Figure 12. 2**). It is worth noting that in Equation 76, the minus "−" sign was converted to a π rotation of $\nu^*$.

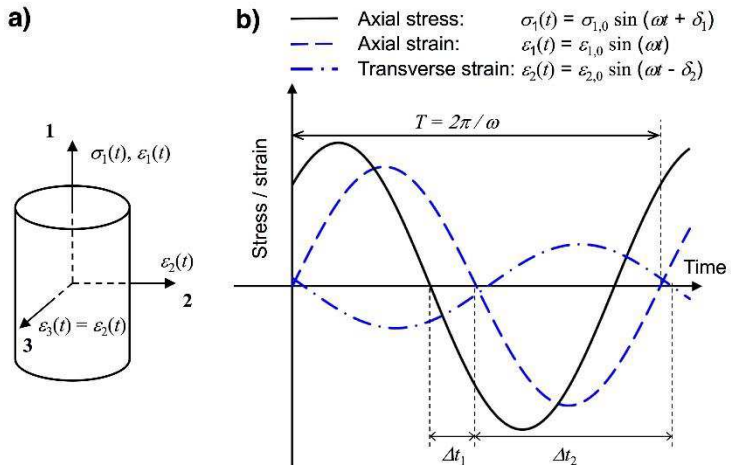


**Figure 12. 1** Stress and strain signals during an axial test on an isotropic specimen, ($\delta_2 > \pi$).

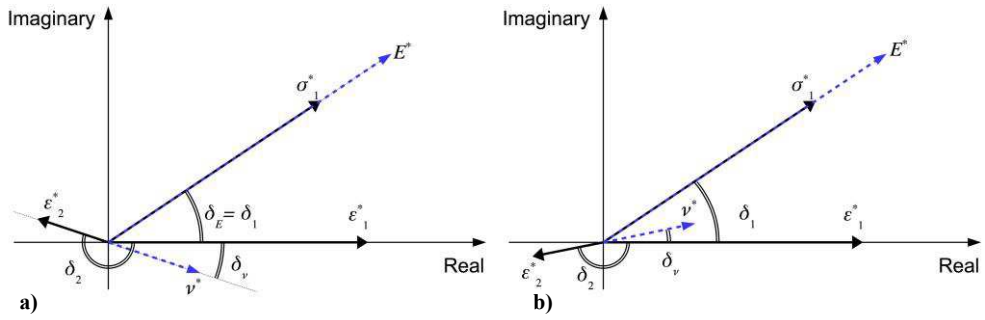


**Figure 12. 2** Complex plane representations of stress-strain phasors and response functions $E^*$ and $\nu^*$: a) $\delta_2 > \pi$; b) $\delta_2 < \pi$.

# 12.3 Experimental program

## 12.3.1 Materials and mixtures

The two sources of RA and the RAg were sampled from a jobsite located on the A14 Motorway near the city of Ancona, Italy (**Figure 12. 3**). The RA was obtained from the milling of the binder and base courses (both were originally produced using PMB), whereas the RAg was obtained from the milling of the underlying cement-treated layer. All aggregates were characterized in terms of gradation, particle density, water absorption and bitumen content (only RA), results are summarized in **Table 8. 1**.

**Figure 12. 3** Recycled aggregate blend sampled from the jobsite.

An over-stabilized cationic bitumen emulsion C 60 B 10 (EN 13808) (**Table 6. 1**) and a Pozzolanic cement type IV/A (P) with strength class 42.5R (EN 197-1), were selected to fabricate the CBTM mixture.
The CBTM mixture was composed of 50% RA and 50% RAg, 3% of bitumen emulsion, corresponding to 1.8% of fresh bitumen and 2% of cement (both binders were dosed by dry aggregate mass). The composition was the same adopted during the laboratory validation of CBTM mixtures produced in field during the construction of the experimental pavement section (Chapter 8).
The gradation of the recycled aggregate blend is reported in **Figure 8. 3**.

## 12.3.2 Sample preparation

The CBTM mixture was prepared in the laboratory using a total water content equal to 5% (by dry aggregate mass), including water from bitumen emulsion and pre-wetting water [Grilli et al., 2012; Cardone et al., 2015]. After water addition, cement and bitumen emulsion were added to the blend and samples were mixed with a mechanical mixer, at room temperature, for the time required to guarantee good particle coating. Immediately after mixing, cylindrical specimens were compacted in a 150 mm diameter mold by means of a gyratory compactor [EN 12697-31]. After compaction, CBTM specimens were cured for 14 days at 40 °C in order to achieve stable stiffness properties.

Before mechanical testing, CBTM specimens were cored to the nominal diameter of 100 mm (**Figure 12. 4**a).

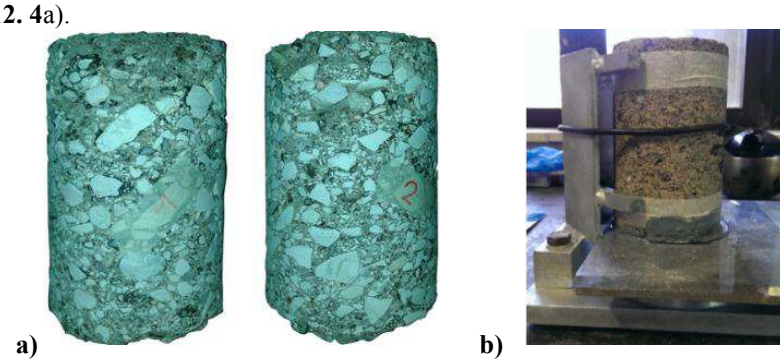


**Figure 12. 4** CBTM testing specimens: a) after coring bur before sawing and capping; b) during capping with two-component polymer resin.

Afterwards, the upper and the lower parts of the specimens were sawed and capped using a two-component polymer resin and then polished with a mechanical device, in order to obtain a perfectly smooth surface (**Figure 12. 4**b). The final height of the specimens and their air voids content are (150.5±1.5) mm and 12.4% [EN 12697-5], respectively.

## 12.3.2 Test setup and data acquisition

The Complex Young's modulus and the complex PR were measured performing uniaxial compression tests on cylindrical specimens, using a servo-hydraulic press associated with a temperature-controlled chamber. A haversine compression load was applied in the axial direction, in control stress mode and a friction reducer (vaseline grease) was used to limit the confining action of the loading platens that alters the uniaxial stress-strain state.
Axial and transverse strains were measured using two couples of strain gauges (SG), glued on opposite sides of each specimen at mid-height (**Figure 12. 5**).

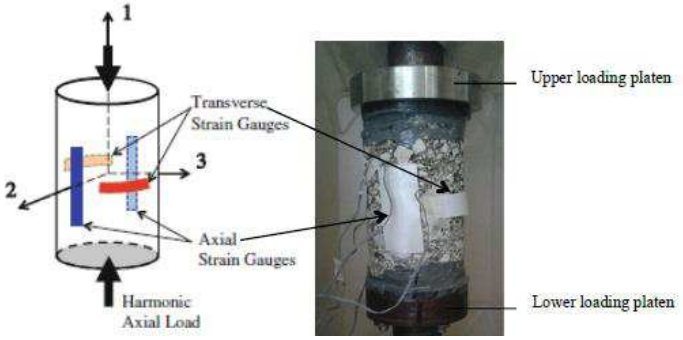


**Figure 12. 5** Test setup: axial and transverse strain gauges configuration.

Conventional bonded-wire SG with polyester resin backing (TML P60) were employed, with length of 60 mm and nominal resistance of 120 Ω (**Figure 12. 6**). An one-component cyanoacrylate adhesive (TML CN-E) was used to glue the SG (**Figure 12. 7**a and b). Moisture and physical protection was obtained with a butyl rubber covering tape (TML SB tape) (**Figure 12. 7**c).

**Figure 12. 6** Bonded-wire SG with polyester resin backing (TML P60).


**Figure 12. 7** Strain gauges setting: a) application of one-component cyanoacrylate adhesive; b) Axial and transverse stain gauges glued; c) application of butyl rubber covering tape.

Two separate Wheatstone half-bridge circuits were employed to measure axial and transverse strains (**Figure 12. 8**). Compensation of temperature effects was obtained with a dummy specimen positioned close to the test specimen inside the thermal chamber (**Figure 12. 9**). Signal conditioning, bridge compensation and A/D conversion were carried out using a portable HBM Spider8 unit. The sampling frequency ($f_s$) was adapted to the test frequency ($f_t$) in order to obtain 100 samples per cycle ($f_s = 100\ f_t$). This allowed an effortless data analysis since the same numerical algorithm could be used for all test frequencies.

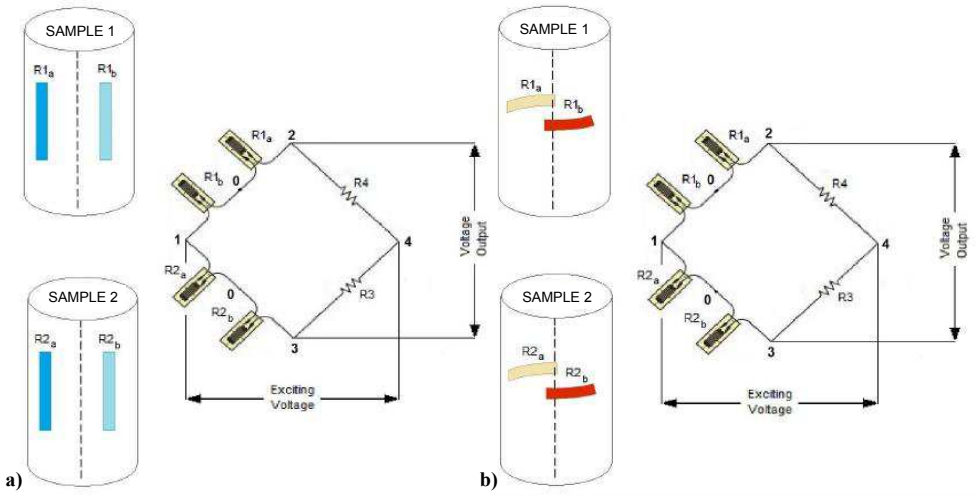


**Figure 12. 8** Wheatstone half-bridge circuits: a) axial and b) transverse strain measurements.

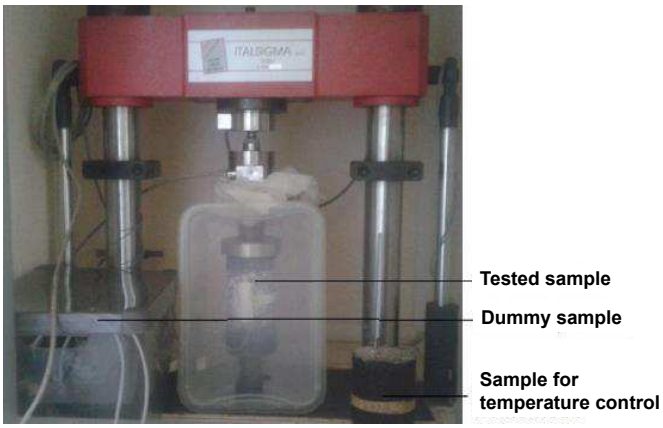


**Figure 12. 9** Compensation of temperature effects.

## 12.3.3 Laboratory testing: test program and analysis of time histories

The experimental program was based on cyclic compression tests performed on cylindrical specimens, where both the axial and the diametral (transverse) strain are simultaneously measured. The main objective is to verify the applicability of the 3D testing protocol that was previously developed for HMA, on CBTM materials. Moreover, the 3D stress-strain response of a CBTM mixture is reported for the first time.

The testing program consisted of frequency sweeps (12, 4, 1, 0.25 and 0.1 Hz) carried out over six different temperatures (0, 10, 20, 30, 40 and 50 °C). One strain amplitude was

investigated for CBTM specimens (30 "με" ). Testing started from the lower temperature and the higher frequency. Frequency sweeps (20 cycles per frequency) at the same temperature were carried out in the same day and at least 300 s of rest were allowed between two successive frequencies. The testing program is summarized in **Figure 12. 10**.

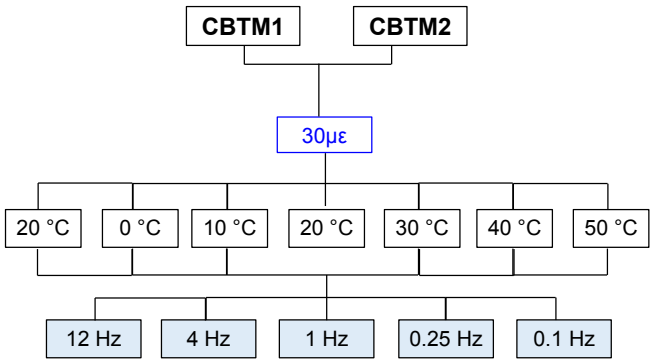


**Figure 12. 10** Testing program.

*Analysis of time histories*

In order to calculate the viscoelastic material functions $E^*$ and $\nu^*$ (Equations 75 and 76), only the sinusoidal components of the measured stress and strain signals (time-histories), at the testing frequency, shall be considered.

In practice, since testing was carried out in cyclic compression, the stress wave was actually the sum of a constant compression (creep component) and a sinusoidal wave. Moreover, since the stress wave was generated using a closed-loop control systems, it contained inherent imperfections due to performance of the testing equipment; such imperfections result in a higher-frequency components superposed to the stress signal. As a consequence, the strain signals also contained a non-periodic component, plus additional higher-frequency components which may also originate from nonlinearity in the material response.

The separation of the non-periodic (creep) component from the periodic component of the measured signals, was obtained with the application of a simple moving average filter:

$$y_{\mathrm{ma}}[n] = \frac{1}{N} \sum_{i=-N/2+1}^{i=N/2} y[n+i] \tag{77}$$

where $y[\cdot]$ is the acquired discrete-time signal (either stress or strains) and $y_{\mathrm{ma}}[\cdot]$ is its moving average over a period ($N$ = 100). The periodic component $y_{\mathrm{p}}[n]$ is calculated as follows:

$$y_{\mathrm{p}}[n] = y[n] - y_{\mathrm{ma}}[n] \tag{78}$$

Then, the sinusoidal components were computed using Fourier analysis. In particular, the third order Fourier polynomial approximation was calculated:

$$y_{\mathrm{p}}[n] = \sum_{k=1}^{3}\left[a_{\mathrm{k}}\sin\left(\frac{2\pi k}{N}n\right) + b_{\mathrm{k}}\cos\left(\frac{2\pi k}{N}n\right)\right] \tag{79}$$

where $a_{\mathrm{k}}$ and $b_{\mathrm{k}}$ are the Fourier coefficients that were estimated using a least squares linear regression analysis. Finally, amplitude and phase angle of each sinusoidal component was calculated as follows:

$$c_{\mathrm{k}} = \sqrt{a_{\mathrm{k}}^2 + b_{\mathrm{k}}^2} \tag{80a}$$

$$\delta_{\mathrm{k}} = \arctan\frac{b_{\mathrm{k}}}{a_{\mathrm{k}}} \tag{80b}$$

In the present research, only the first harmonic component ($k = 1$) was considered in order to calculate $E^*$ and $\nu^*$ by means the Equations 75 and 76. The statistical software R-project [R Development Core Team, 2016] was used to perform the least squares linear regression analysis according to the procedure described by Cowpertwait and Metcalfe (2009). An example of the results of the data processing algorithm is reported in **Figure 12. 11** where the evolution of complex Young's modulus and complex PR for specimen CBTM1 tested at 0.25 Hz and 40 °C, is shown.

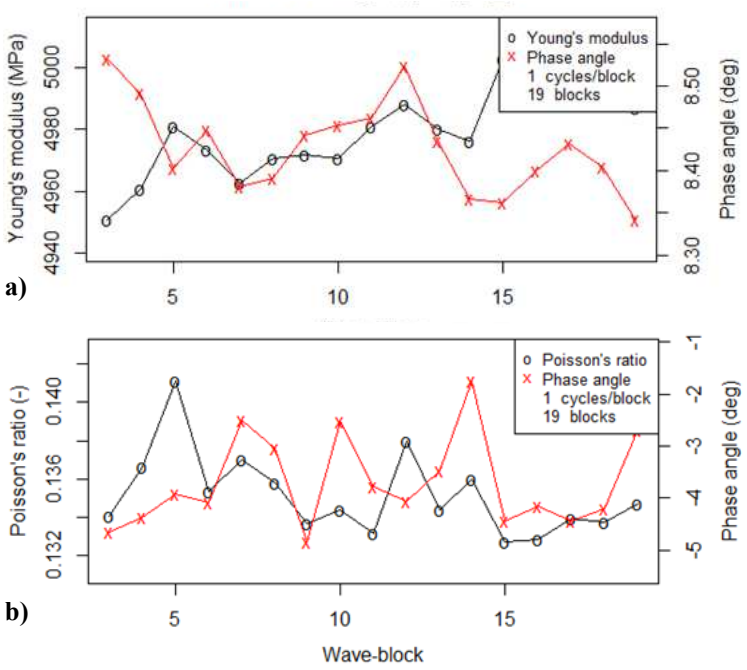


**Figure 12. 11** Analysis of time histories for specimen CBTM1 at 0.25 Hz and 40 °C: a) evolution of complex Young's modulus; b) evolution of complex Poisson's ratio.

# 12.4 Experimental findings

## 12.4.1 Analysis of complex Young's modulus

In **Figure 12. 12**, the absolute value $E_0$ and phase angle $\delta_E$ of the complex Young's modulus measured at the strain level 30 με on specimens CBTM1 are reported.
As expected, for CBTM mixture, the dependency on frequency and temperature was present, but not so marked. Specifically, for specimen CBTM1 and CBTM2 actual measurements of $E_0$ ranged from 3151 to 10519 MPa and from 2596 to 8900 MPa, respectively. It is observed that this range of variability is less than one order of magnitude. The values of $\delta_E$ for specimen CBTM1 and CBTM2 ranged from 12.1° to 3.0° and from 11.1° to 2.7°, respectively; they decreased if temperature increased and frequency decreased. In addition, at low temperature (0 °C), both $E_0$ and $\delta_E$ were almost constant, varying the test frequency.

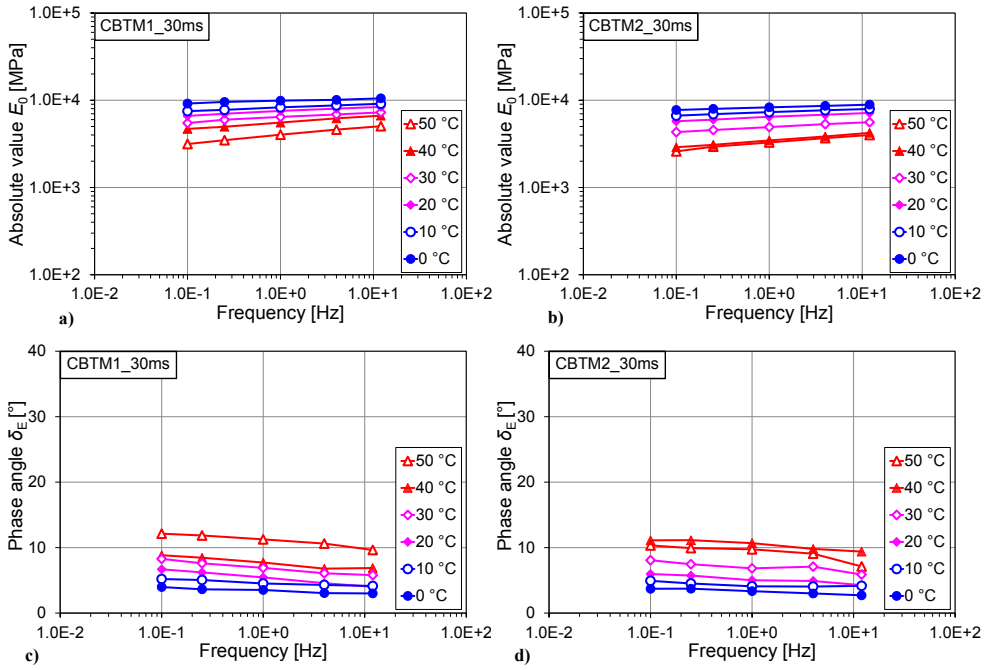


**Figure 12. 12** Measured values of complex Young's modulus for CBTM1 specimens (strain level = 30 με): a) and b) specimens CBTM1 and CBTM2, absolute value ($E_0$); c) and d) specimens CBTM1 and CBTM2, phase angle ($\delta_E$).

In **Figure 12. 13**, $E_0$ is represented as a function of $\delta_E$ (Black space) for both mixtures and strain levels; the previously observed dependency on frequency and temperature is confirmed. As regards the CBTM, the two specimens gave comparable results in terms of both $E_0$ and $\delta_E$, thus confirming that the LVE response of this kind of cold-recycled mixture

can be effectively characterized using the same approach normally used for HMA. Overall, the thermo-rheological behavior appeared to be similar to that usually detected with HMA [Di Benedetto et al., 2007; Graziani et al., 2014; Graziani et al., 2016b; Perraton et al., 2016], but the variability of both $E_0$ and $\delta_E$ across the tested temperature and frequency range was very limited. It is worth noting that the maximum value of the stiffness $E_0$ is very small, possibly because of the high air void content and the low bitumen dosage (emulsified bitumen) of the CBTM mixture.

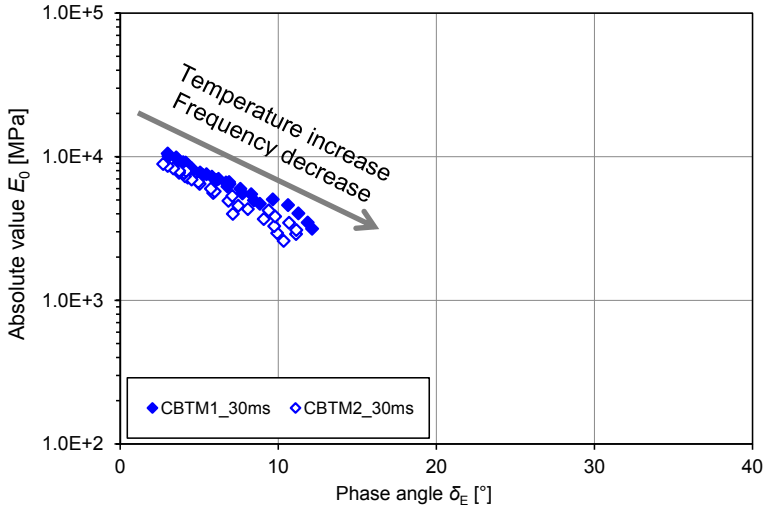


**Figure 12. 13** Measured values of $E_0$ and $\delta_E$ represented in the Black space for CBTM specimens.

In **Figure 12. 13** it can also be observed that unique curves appear to identify the thermo-rheological behavior of CBTM mixtures, suggesting the validity of the TTSP. Consequently, the measured $E^*$ values were fitted using the Huet-Sayegh (H-S) rheological model [Sayegh, 1967]. The procedure adopted is described in Section 5.2.3.
The model parameters and the temperature shift factors were calculated using a numerical fitting procedure (nonlinear least squares) and are reported in **Table 12. 1** and **Table 12. 2**, respectively.

| **Specimen ID** | **Strain level [με]** | $E_g$ **[MPa]** | $E_e$ **[MPa]** | $k$ | $h$ | $\delta$ | Log $\tau_{ref}$ |
|---|---|---|---|---|---|---|---|
| CBTM1 | 30 | 14900 | 1800 | 0.118 | 0.430 | 2.600 | 2.10 |
| CBTM2 | 30 | 11100 | 1800 | 0.110 | 0.240 | 1.100 | 2.10 |

**Table 12. 1** Parameters of the fitted Huet-Sayegh model for E*.

| Specimen ID | Strain level [με] | *a(50)* | *a(40)* | *a(30)* | *a(20)* | *a(10)* | *a(0)* |
|---|---|---|---|---|---|---|---|
| CBTM1 | 30 | -4.00 | -2.11 | -1.15 | 0 | 1.20 | 3.55 |
| CBTM2 | 30 | -4.50 | -4.20 | -2.10 | 0 | 1.19 | 3.05 |

**Table 12. 2** Temperature shift factors for $E^*$.

In **Figure 12. 14**, master curves of $E_0$ and $\delta_E$, at the reference temperature of 20 °C, are reported. As it can be observed, at high reduced frequencies (low temperatures) whereas at low reduced frequencies (high temperatures), the stiffness of CTBM is almost the same. The low thermo-rheological sensitivity of the CBTM mixture is due to both the presence of cement and the low fresh bitumen content in the mixture. This observation is in accordance with two previous investigations carried out on CBTM prepared with bitumen emulsion or foamed bitumen, and reported in Chapter 11.
As regards the parameters $k$, $h$ and $\delta$, similar values were calculated for specimens obtained from the same mixture.

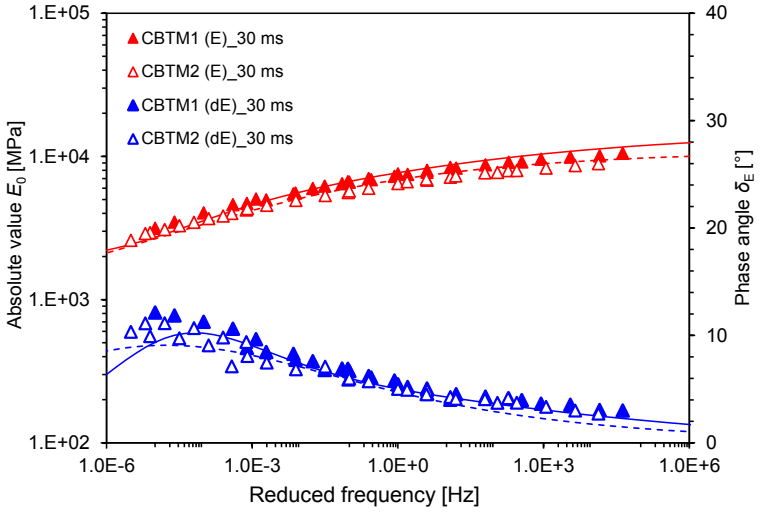


**Figure 12. 14** Young's modulus master curves and Huet-Sayegh fitted models ($T_{ref}$= 20 °C): absolute value $E_0$ and phase angle $\delta_E$.

## 12.4.2 Analysis of complex Poisson's ratio

In **Figure 12. 15**, the absolute value $\nu_0$ and phase angle $\delta_\nu$ of the complex PR measured at the strain level 30 με on specimens CBTM1 and CBTM2 are reported.
For specimens CBTM1 and CBTM2, $\nu_0$ was almost independent of temperature and frequency (**Figure 12. 15**a). The maximum value $\nu_0 = 0.169$ was measured at 0 °C and 0.25 Hz, whereas the minimum value $\nu_0 = 0.130$ was measured at 40 °C and 0.1 Hz.
On the other hand, for specimen CBTM2, the same conclusion can be drawn observing $\nu_0$ (**Figure 12. 15**b). The maximum value $\nu_0 = 0.151$ was measured at 10 °C and 12 Hz, whereas the minimum value $\nu_0 = 0.108$ was measured at 50 °C and 0.1 Hz.

As regards the phase angle (**Figure 12. 15**c and d), for both CBTM1 and CBTM2 specimens, the values of $\delta_\nu$ were also very small but mostly negative, with some positive values measured at lower temperatures and higher frequencies.
It is worth noting that, the dispersion of the measured $\delta_\nu$ was comparable with the magnitude $\delta_\nu$. This was due to the fact that the magnitude of the transverse strain is very small and thus precision of the measurement system becomes very important. In fact, considering a $\nu_0 = 0.15$ and an amplitude of the axial strain $\varepsilon_{1,0} = 30$ με, one obtains an amplitude of the transverse strain $\varepsilon_{2,0} = 4.5$ με, is very close to the precision limit of the adopted measuring chain ($\pm 1.0$ με).

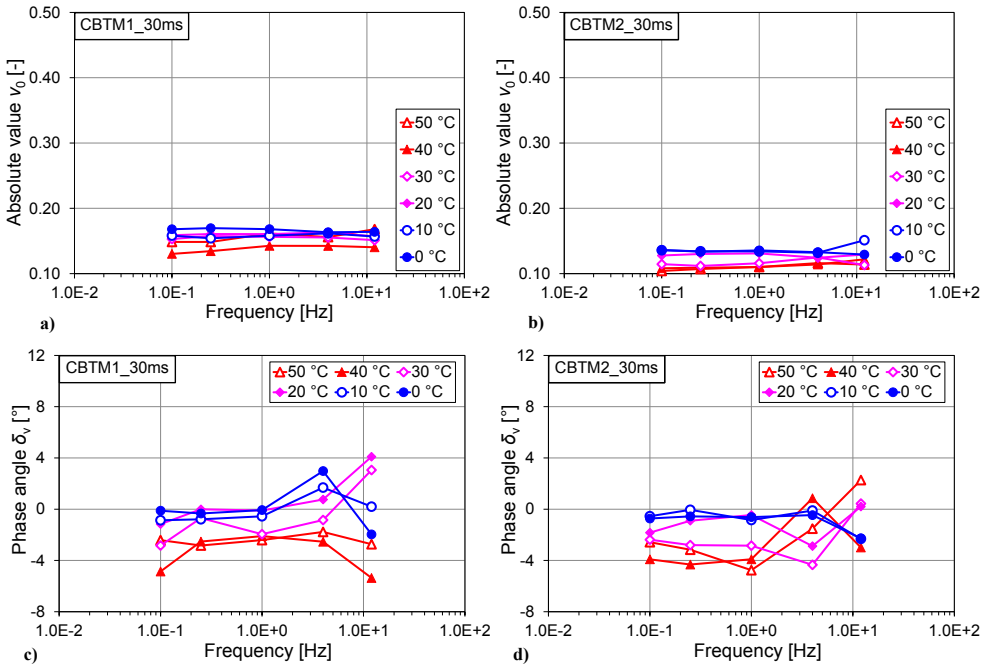


**Figure 12. 15** Measured values of complex PR for CBTM1and CBTM2 specimens (strain amplitude = 30 με): a) and b) specimens CBTM1 and CBTM2, absolute value ($\nu_0$); c) and d) specimens CBTM1 and CBTM2, phase angle ($\delta_\nu$).

In **Figure 12. 16**, $\nu_0$ and $\delta_\nu$ measured on specimens CBTM1 and CBTM2 (strain amplitude 30 με), are reported in the Black space. As it can be observed, the thermo-rheological response of CBTM mixtures was completely different from that of HMA mixtures, in particular, $\nu_0$ was almost constant and $\delta_\nu$ ranged between about -5.8° and 3°. Since the three-dimensional characterization of this type of cold-recycled mixtures, i.e. fabricated using bitumen emulsion and cement, is quite a new subject, there are no similar data available for comparison in the literature. As previously observed for $E^*$, certainly cement had a critical role in the response of CBTM mixture in limiting the thermo-rheological susceptibility of the material. Indeed, a constant value $\nu$ =0.15 is normally assumed for cement concrete and

cement-treated materials [Huang, 2004] and therefore it can be concluded that the studied CBTM showed a typical cement-like behavior.

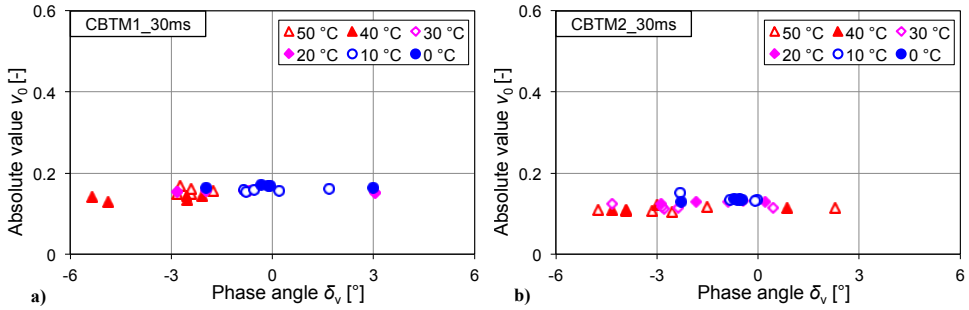


**Figure 12. 16** Measured values of $v_0$ and $\delta_v$ (Black space) for CBTM mixture: a) CBTM1 (30 με); b) CBTM2 (30 με).

## 12.5 Summary

This experimental investigation presents the results of an experimental study aimed at the 3D LVE characterization of a cold-recycled mixture: a cold-recycled CBTM mixture fabricated using bitumen emulsion and cement, containing 50% RA and 50% RAg.

Analyzing the experimental results, the following conclusions can be drawn:

- The thermo-rheological response in terms of $E^*$ is similar to that usually detected with HMA, in that the time-temperature superposition principle is valid and the Huet-Sayegh model can be used to simulate the frequency-temperature dependence;
- Considering the $E_0$ master curves, it is observed that at high reduced frequencies (low temperatures), the stiffness of CBTM is lower probably due to the higher voids content that characterized the investigated specimens. On the other hand, at low reduced frequencies (high temperatures), the stiffer behavior of CBTM is related to the presence of cement in the mixture.
- The thermo-rheological response in terms of $v^*$ is very different to that usually detected with HMA, in that $v_0$ is almost constant and very close to 0.15. Therefore, it can be concluded that the studied CBTM shows a typical cement-like behavior.
- These results are in accordance with those obtained in Chapter 6 where the mechanical behavior of different CRMs fabricated during the construction of the experimental pavement section, were analyzed. In addition, the assumption of Poisson's ratio equal to 0.15 for subbase layers, in the back-calculation process moduli, was also verified.

# Part 3
# Mortar-scale analysis: Laboratory characterization of Cold bituminous mortars

# CHAPTER 13.

# Introduction

The third part of this thesis is focused on the laboratory characterization of cold bituminous mortar (CBM), produced with bitumen emulsion (*Task 3*). In particular, both volumetric and mechanical properties of CBMs were analyzed during a wide program of experimental activities.
In detail, the main objective of this task is to explore the mechanical behavior of cold mixtures considering their complex multiphase structure at the intermediate level: mortar-scale level.
CBM consists in a composite of fine aggregate particles, bitumen emulsion and mineral addition. In this context, starting from the composition of a typical cold mixture, three different CBMs were analyzed taking into account relative proportions of each constituent. Particular care was taken in order to recreate the same CBM composition that fill the voids in a cold mixture (CM).
The planned experimental activities provided an overall knowledge about factors as curing time and conditions, types of mineral addition may influence the physical and mechanical behavior of CBMs.

## 13.1 General overview

As previously described, CBMs consists of bitumen (in form of foam or emulsion), filler-sized particles (mineral additions), fine aggregate particles and air, and it exists in the interstitial spaces between the coarse aggregate particles of CM. In fact, cold mixture similar to hot mix asphalt may be schematized as a composite where the bitumen disperses mainly amongst the finest particles, resulting in a bitumen-rich mortar binding the coarse particles. CBM is important because it is a single characteristic size scale smaller than CM and is therefore closer in characteristic size of the damage that occurs within the CM [Kim, 2003]. Experiments with bituminous mortar have been used to study fatigue damage, moisture damage and healing in asphalt concrete, with the argument that the phenomena occur largely between the coarsest aggregate particles and so tests with bituminous mortar should provide direct indications of how they will affect the whole mixture [Kim, 2003; Underwood and Kim, 2013].
CBM materials are characteristically similar to CMs with the primary difference being that the maximum aggregate size is generally smaller than 4 mm. Therefore, test samples can be created at smaller geometries and still meet representative volume element, RVE, requirements [Hashin, 1983]. Maintaining the RVE requirements ensures that measured properties are not functions of the test geometry (*scale effect*) and for this reason they can represent the fundamental characteristics of the material.
One shortcoming in the available literature is the detailed understanding of the fundamental characteristics of CBM as a function of volumetric composition changes.

For example, the composition can be standardized by defining the proportions of all constituents and by using the aggregate with exact properties, particle size distribution, and origin [Miljković and Radenberg, 2015]. Thus, the variability in the aggregate properties was eliminated, and only the contribution of the considered constituent can be evaluated.
This lack of understanding makes it difficult to view the literature as a coherent set of information since most researchers utilize their own techniques to define and produce CBMs. Aside from volumetric composition, compaction of the CBM is also an issue and Izadi et al. found that gyratory compaction replicated the microstructure of CBM as it exists in its corresponding mixture [Kim, 2003; Izadi et al., 2011]. Obviously, there is no firm consensus on how the CBM exists in the mixture and how to replicate this in the laboratory.
In addition, CBM is characterized by an evolutive behavior as the whole CM that contains it. In fact, the physical and mechanical behavior of these materials can be evaluated in the early-age of curing (fresh state) or at the long-term curing (cured state). It is important to highlight that, at the early-age of curing, the water membrane in the interface between bitumen emulsion and aggregate represents the weak point of the material at the considered curing level. As the curing time increases, the continuous bitumen membrane is formed in the interface between aggregates with cement hydration and bitumen emulsion demulsification, which causes the bonding strength exceeding the cohesive strengths of CBM mortar [Lin et al., 2015].
In road construction industries, CBM produced with cement as mineral addition is vastly used in the slab track railroad system, which is one of the key technologies in high-speed railways (HSR) [Kong et al., 2014]. Experiments conducted by Li et al. (1998) on the mechanical properties of a CBM indicated that it combined many characteristics of cement and bitumen, such as low temperature sensitivity of cement concretes and higher toughness of asphalt concretes. The incorporation of bitumen emulsion into cement-based materials generally reduces both strength and the stiffness [Pouliot et al., 2003; Song, 2006] but improves the deformability [Pouliot et al., 2003]. Moreover, the interaction between cement and bitumen emulsion was studied in the past few years. Bitumen emulsion was proved to have retarding effect on cement hydration. This retarding effect is relevant to bitumen emulsion type, emulsion dosage, and emulsifier type [Nadia et al., 2003; Tan et al., 2013].
Obviously, the mechanical properties of such cement-bitumen composites and their temperature susceptibility depend mainly on the binder which basically consists of two phases, namely hardened cement paste and a solidified bitumen phase.

Tests on bituminous mortars can be used for a multiscale evaluation of the corresponding mixture [Izadi et al., 2011; Schüler, 2013]. The structural similarity between CBM to CM materials enables the measured values to represent the fundamental material properties [Underwood and Kim, 2013].

# CHAPTER 14.

# Laboratory characterization of Cold bituminous mortar

## 14.1 Experimental program

This experimental investigation aims at characterizing the mechanical response of cold bituminous mortars (CBMs) produced with three different types of mineral addition (calcium carbonate, cement and hydrate lime), bitumen emulsion, sand and water. The influence of experimental variables such as curing conditions (time and relative humidity) and types of mineral addition was investigates evaluating both volumetric and mechanical properties of CBMs produced in laboratory.
The whole experimental program (**Figure 14. 1**) can be divided in two phases:

- First preliminary phase focused on the development of the compaction and mixing protocol and on the evaluation of the effect of the mineral addition on the workability of the cold bituminous mortars. The objective was to determine the mixing water content, $W_{des}$ and the compaction energy $N_{des}$, that guarantee similar volumetric properties, avoiding any material loss during compaction.
- Laboratory testing, where each CBM was characterized in terms of Indirect tensile stiffness modulus (ITSM); indirect tensile strength (ITS) and resistance to crack propagation.

The composition of each CBM was standardized fixing a unique source of both fine aggregate (fluvial sand) and bitumen emulsion in order to focus the analysis on the influence of the type of mineral addition.
The proportion between residual bitumen (obtained from bitumen emulsion) and mineral addition was calculated by volume with the aim to recreate the exact composition of bituminous mortar that fills voids in a cold mixture (CM). The resulted bitumen-mineral addition ($B/M_A$) ratio was equal to 1, typical ratio that characterizes the composition of cement-bitumen treated materials (CBTMs).

The three types of CBMs were coded according to the type of mineral addition added in the mortar:

- CEM, CBM produced with cement;
- CC, CBM produced with calcium carbonate;
- HL, CBM produced with hydrated lime.

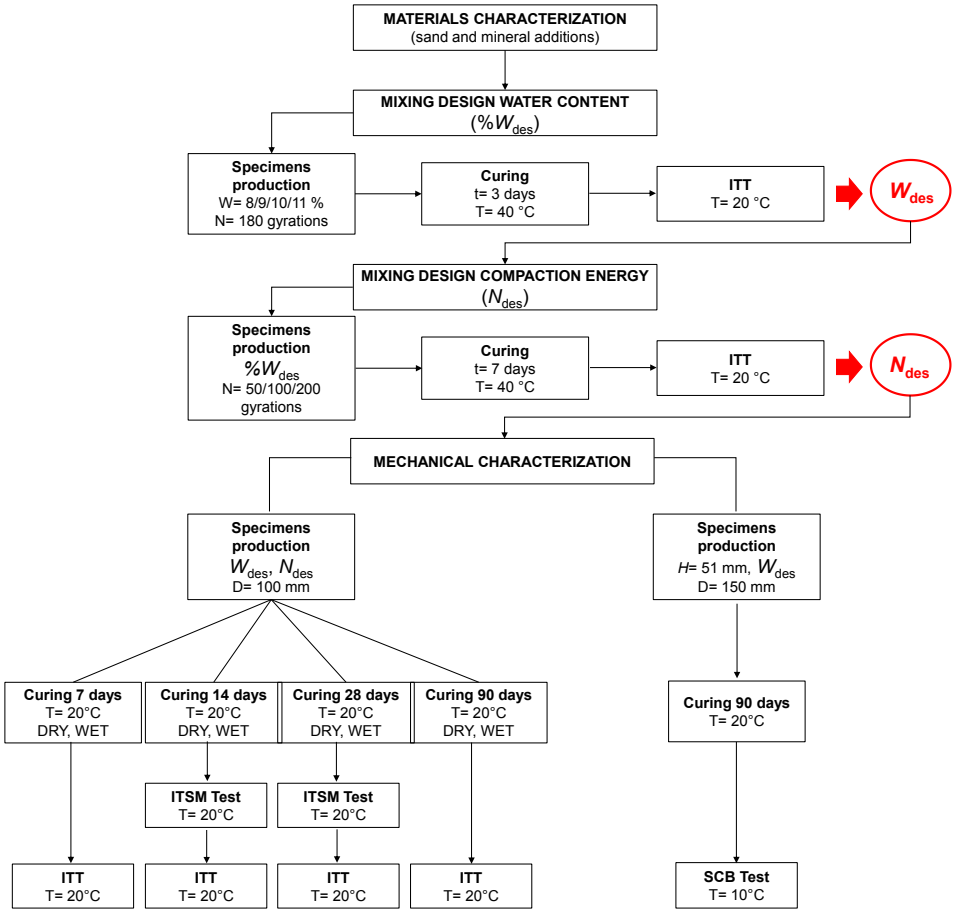


**Figure 14. 1** Experimental program.

### 14.1.1 Preliminary phase1: mixing design water content, $W_{des}$

As previously described, the aim of the first part of preliminary phase is to determine the mixing design water content $W_{des}$ in order to improve as much as possible the workability of the mortar avoiding any material loss, during the compaction phase.
Four total water contents $w_{tot}$ were selected: 8%, 9%, 10% and 11% by dry aggregate weight. A total of 24 CBM specimens, two replicate specimens for each total water content and type of mortar (CEM, CC and HL) were compacted by means of SGC compactor using 100 mm diameter mold and 180 gyrations. 800 g of loose wet CBM were used for each 100 mm diameter specimen.
Immediately after mixing, CBM specimens were cured for 3 days at the temperature of 40 °C and 50% of relative humidity in a controlled climatic chamber.
The temperature of 40 °C was selected to achieve accelerate curing conditions.

At the end of curing time, CBM specimens were conditioned at 20°C for 4 hours and then the indirect tensile strength was measured at the temperature of 20 °C. Analyzing ITS results, the $W_{des}$ for each studied CBM was selected.

### 14.1.2 Preliminary phase2: mixing design compaction energy, $N_{des}$

The second part of preliminary phase is focused on the evaluation of the mixing design compaction energy $N_{des}$ in order to produce CBM mortars with comparable volumetric properties, at the end of the compaction phase.

Three levels of compaction energy $N$ were selected: 50, 100 and 200 gyrations.
800 g of loose wet CBM were produced using $W_{des}$ and compacted by means of SGC compactor using 100 mm diameter mold.
A total of 18 CBM specimens, two replicate specimens for each compaction level and type of mortar (CEM, CC and HL) were manufactured.
Immediately after mixing, CBM specimens were cured for 7 days at the temperature of 40 °C and 50% of relative humidity in a controlled climatic chamber.
The temperature of 40 °C was selected to achieve accelerate curing conditions.
At the end of curing time, CBM specimens were conditioned at 20°C for 4 hours and then the indirect tensile strength was measured at the temperature of 20 °C . Analyzing ITS results, the $N_{des}$ for each studied CBM was selected.

### 14.1.3 Mechanical testing

After the preliminary phase, ITS and ITSM were measured on CBM specimens with 100 mm diameter, produced at total water content equal to $W_{des}$ and compacted by means of SCG compactor at $N_{des}$ gyrations.
Differently, CBM specimens for semi-circular bending test were compacted in a 150 mm diameter mold and the weight of wet CBM mortar was adjusted (1850 g) in order to obtain specimens 50 mm height and characterized by the same density previously achieved with 100 mm diameter specimens, compacted at $N_{des}$.
CBM specimens were cured in a controlled climatic chamber, at different times and curing conditions (relative humidity, DRY or WET). A unique curing temperature of 20 °C was selected.
The moisture loss was monitored by carefully weighting each CBM specimen, before mechanical testing.
Experimental program phases and the corresponding compaction and curing procedures are summarized in **Table 14. 1**.

| **Experimental program phase** [-] | **SCG mold** [mm] | **Total water content, *W*** [%] | **Number of gyrations** [-] | **Curing conditions** [-] | **Curing time** | **Test** |
|---|---|---|---|---|---|---|
| Preliminary phase: CBMs workability ($W_{des}$%) | 100 | 8, 9, 10, 11% | 180 | 40 °C DRY (R.U.=50%) | 3 days | ITT |
| Preliminary phase: Compaction energy ($N_{des}$) | 100 | $W_{des}$ | 50, 100, 200 | 40 °C DRY (R.U.=50%) | 7 days | ITT |

| | | | | | | |
|---|---|---|---|---|---|---|
| Mechanical testing: | 100 | $W_{des}$ | $N_{des}$ | 20 °C<br>DRY (R.U.=50%)<br>WET (R.U.>90%) | 14 and<br>28 days | ITSM |
| Mechanical testing: | 100 | $W_{des}$ | $N_{des}$ | 20 °C<br>DRY (R.U.=50%)<br>WET (R.U.>90%) | 7, 14, 28,<br>90 days | ITT |
| Mechanical testing: | 150 | $W_{des}$ | H=50 mm | 20 °C<br>DRY (R.U.=50%) | 90 days | SCB |

**Table 14. 1** Experimental program phases: compaction and curing procedures.

## 14.2 Materials and mortars

A fluvial sand with maximum dimension of 0.5 mm, particle density 2.71 Mg/m$^3$ and absorption 1 % [EN 1097-6], was adopted to prepare the CBM. The aggregate gradation [EN 933-2] is reported in **Figure 14. 2**.

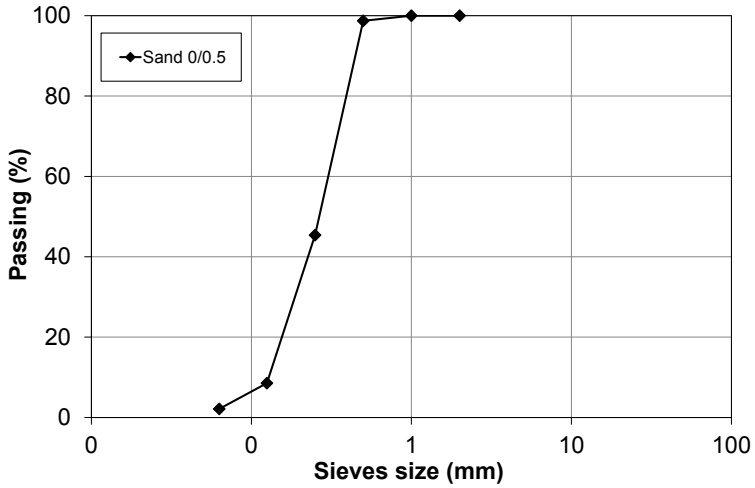


**Figure 14. 2** Sand aggregate gradation [EN 933-2].

A cationic slow-setting bituminous emulsion designated as C 60 B 10 [EN 13808] was selected in this research and its formulation guarantee high workability during the mixing and compaction phase. The bitumen emulsion properties are listed in **Table 6. 1**.
Three mineral additions were selected (**Figure 14. 3**):

- Portland limestone cement II A/LL, strength class 42.5 R [UNI EN 197-1];
- Calcium carbonate, finely ground, $CaCO_3$;
- Hydrated lime obtained by the turn off of quicklime, $Ca(OH)_2$.

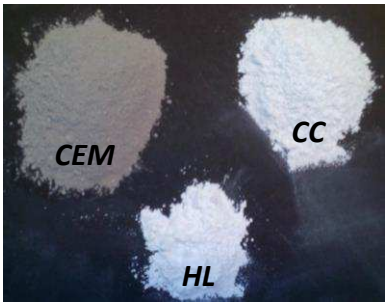


**Figure 14. 3** Mineral additions: cement (CEM), calcium carbonate (CC) and hydrate lime (HL).

Portland cement, calcium carbonate and hydrated lime were characterized determining the Rigden voids and the fineness (specific surface) using the Blaine method (**Table 14. 2**).

| Parameter | | Cement | Calcium carbonate | Hydrated lime |
|---|---|---|---|---|
| Rigden voids [%] | UNI EN 1097-4 | 40.18 | 31.14 | 53.87 |
| Specific Surface [$m^2/g$] | UNI EN 196-6 | 0.41 | 0.51 | 0.345 |

**Table 14. 2** Characterization of mineral additions.

The adopted dosage of bitumen emulsion was calculated comparing the specific surface of the mortars produced with sand and that of a typical CBTM mixture with a maximum dimension of 20 mm. The objective is to recreate a comparable coating rate of bitumen of aggregate particles, in CBM and cold mixture using the concept of film thickness. Bearing in mind that the film thickness is inversely proportional to surface area and decreases as the surface area of aggregate increases; small particles have a greater specific surface than large particles. In existing model specific surface area is calculated assuming that the aggregate is spherical or cube shaped. The surface area calculations are not exact but mostly approximate [Attia et al., 2009].
The calculation of surface area per unit mass for aggregate blend was carried out using the Edward-Hveem method outlined in the asphalt Institute's MS-2 [Asphalt Institute, 1997]. The surface area (SA) is calculated by summing the product of the surface area factor and the percent material passing each sieve, as reported in Equation 81. The surface area factors used by Hveem are presented in **Table 14. 3**.

$$SA = \sum SF_i \times P_i \tag{81}$$

where $SA$ is the surface area [$m^2/kg$]. $SF_i$ is the surface area factor for sieve $i$ and $P_i$ is the percent passing sieve $i$, expressed in decimal form.

| Sieve | #4 | #8 | #16 | #30 | #50 | #100 | #200 |
|---|---|---|---|---|---|---|---|
| **Sieve size [mm]** | 4.75 | 2.36 | 1.18 | 0.60 | 0.30 | 0.15 | 0.075 |
| **Surface area factors** | 0.41 | 0.82 | 1.64 | 2.87 | 6.14 | 12.29 | 32.77 |

**Table 14. 3** Surface area factors, used by Hveem [Asphalt Institute, 1997].

As previously described in Chapter 2, CBTM mixtures are usually characterized by a bitumen emulsion content of 3% by dry aggregate weight (corresponding to 1.8% of residual bitumen). The total surface area of CBTM (D= 20 mm) is 6.59 $m^2$/kg as reported in **Table 14. 4**.

| Sieve size [mm] | $P_i$ [%] | $S \cdot F_i$ [$m^2$/kg] | $S \cdot F_i \times P_i$ [$m^2$/kg] |
|---|---|---|---|
| 19.5 | 100 | 0 | 0 |
| 12.7 | 82.45 | 0 | 0 |
| 9.51 | 72.39 | 0 | 0 |
| 4.76 | 53.02 | 0.41 | 0.2174 |
| 2.36 | 38.66 | 0.82 | 0.3170 |
| 1.18 | 28.30 | 1.64 | 0.4641 |
| 0.6 | 20.88 | 2.87 | 0.5993 |
| 0.3 | 15.28 | 6.14 | 0.9382 |
| 0.15 | 11.18 | 12.29 | 1.3740 |
| 0.075 | 8.19 | 32.77 | 2.6839 |
| | | | **Total = 6.5939** |

**Table 14. 4** Total surface area calculated for a CBTM mixture with nominal maximum dimension of 20 mm.

Considering the nominal maximum dimension of CBM (D=0.5 mm), its calculated surface area is 6.06 $m^2$/kg while the remain part of CBTM mixture (excluding particles smaller than 0.5 mm) is characterized by a surface area of 0.53 $m^2$/kg.

Within the CBTM mixture, the amount of bitumen that covers the aggregate particles with dimension lower than 0.5 mm is equal to 1.65%. It's important to highlight that this bitumen distribution is related to a CBTM mixture composed by 80% of coarse aggregate (D>0.5 mm) and 20% of fine aggregate (D<0.5 mm).
In this context, the corresponding bitumen content that characterized the CBM (D=0.5 mm) is about 8.3% by dry aggregate weight (1.65%/20%).
Following the same procedure, the dosage of cement was evaluated obtaining a CBM characterized by a cement content of 10% by dry aggregate weight.
In order to replicate the CBM within a typical CBTM with bitumen/cement (B/C) ratio equal to 1, both bitumen and mineral addition (cement, calcium carbonate and hydrated lime) content were fixed equal to 10% (corresponding to 16.67% of bitumen emulsion).

### 14.2.1 Samples production and curing procedure

Concerning the production of CBM sample, the same procedure adopted for CBTM mixture was considered.

The design water content $W_{des}$, evaluated in the preliminary phase of the experimental program, is the total water content $w_{tot}$ used during samples preparation. It was composed of the water from the emulsion ($w_{em}$) and additional water ($w_{add}$), which is added in two parts. The first part, related to the water absorption ($w_{add\_1} = w_{abs}$) of the constituent aggregates, was added to the dry aggregates blend the day before mixing. Then, the wet mixture (aggregate containing $w_{add\_1}$) was stored in a sealed plastic bag for 12 hours at room temperature, in order to ensure a homogeneous moisture condition and to allow absorption by the aggregates. Subsequently, the aggregate blend was thoroughly mixed, gradually adding the remaining part of the mixing water ($w_{add\_2}$), mineral addition and emulsion in sequence. Samples were mixed by hand at room temperature for at least two minutes, time required to achieve a homogeneous particle coating (visual observation) (**Figure 14. 4**).


**Figure 14. 4** Sample production: a) wet mortar stored in a plastic bag; b) dosage of mineral addition; c) dosage of bitumen emulsion; d) mixing.

Immediately after mixing, CBM specimens were compacted by means of SGC compactor [EN 12697-31] (see section 7.2.1).

## 14.3 Laboratory equipment, test methods and data analysis

### 14.3.1 Indirect tensile stiffness modulus

The indirect tensile stiffness modulus (ITSM) were measured on cured CBM specimens (**Table 14. 1**) at 20 °C according to UNI EN 12697-26-Annex; details of the test procedure are reported in Section 7.2.2.

### 14.3.2 Indirect tensile strength

The indirect tensile strenght ITS was measured on cured CBM specimens (**Table 14. 1**) at 20 °C, with constant rate of deformation of 50 ± 2 mm/min, according to UNI EN 12697-23. The standard test configuration (reported in Section 7.2.3) was modified adding two inductive displacement trasducers in order to measure the horizontal deformation (**Figure 14. 5**). The scheme of the indirect tensile test setup with the relevant stresses and displacements indicated is shown in **Figure 14. 6**.

This updated configuration was introduced to better understand the failure behavior that can not be analyzed evaluating only the indirect tensile strength. In fact, various parameters related to bitumen emulsion or adopted mineral addition may induce the fracture to be more ductile or brittle.

**Figure 14. 5** Indirect tensile test equipped with two inductive displacement trasducers.

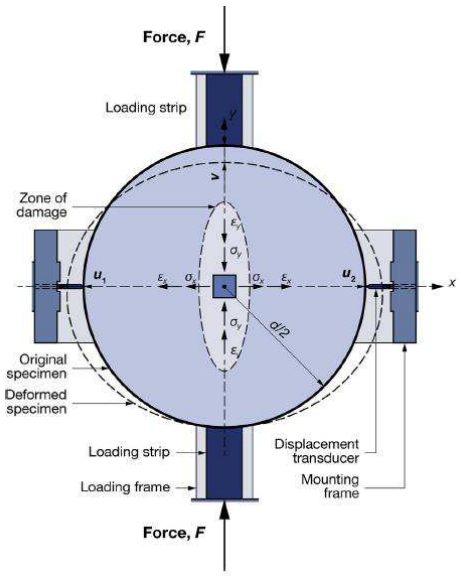


**Figure 14. 6** Illustration of the indirect tensile test setup with the relevant parameters of stress and displacement [Miljković and Radenberg, 2014].

Therefore, to quantitatively characterize the mode of fracture, it is necessary to take additional energy-based mechanical properties [Wen, 2013] of the specimens into account. In this regard, the fracture work and the deformation energy of the specimens were calculated

based on the force-displacement diagrams obtained by the indirect tensile testing. **Figure 14. 7** shows typical force versus vertical and force versus horizontal displacement diagrams obtained by the testing.

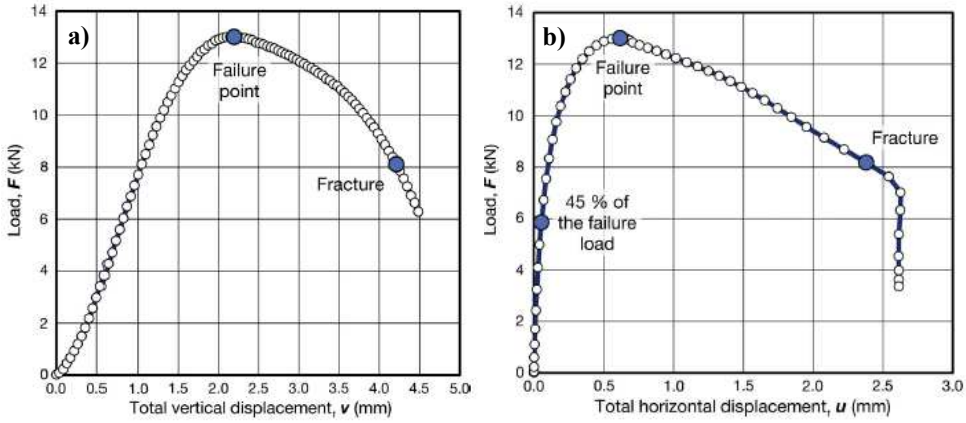


**Figure 14. 7** Indirect tensile test: a) Example of a typical diagram of a dependency of the loading force on the vertical displacements; b) Example of a typical diagram of a dependency of the loading force on the horizontal lateral displacements.

By integrating the differential work of the vertical load, the expression for the fracture work becomes

$$W\ (t) = \int_v\ F(v)\mathrm{d}v = I_v \tag{82}$$

where $W$ is the fracture work, v is the measured vertical displacement of the upper loading strip, and $F(v)$ is the dependency of the load from the vertical displacement.
The value of the fracture work calculated by the above equation is dependent on the specimen size. By dividing the fracture work by the volume of the cylindrical specimen, the following expression for the specific fracture work is obtained:

$$W^* = \frac{4}{\pi d^2 h} \cdot \int_v\ F(v)\mathrm{d}v = \frac{4}{\pi d^2 h} \cdot I_v \tag{83}$$

where $W^*$ is the specific fracture work which takes into account the specimen size, $d$ is the specimen diameter, and $h$ is the specimen height.
Similarly like for the fracture work, by integrating the differential deformation energy of the horizontal stress in the centre of the specimen

$$\mathrm{d}U = \sigma_x \mathrm{d}\varepsilon_x \tag{84}$$

along the abscissa, and having regard that the horizontal tensile stress and the corresponding strain in the centre of the specimens are, respectively

$$\sigma_x(u) = \frac{2F(u)}{\pi \mathrm{d} h} \tag{85}$$

and

$$\varepsilon_x(u) = \frac{2u}{d} \cdot \frac{1+3v}{4+\pi v-\pi} \tag{86}$$

where $F(u)$ is the dependency of the load from the horizontal (lateral) displacement, and ν is Poisson's ratio, the expression for the deformation energy becomes

$$U^* = \frac{4}{\pi d^2 h} \cdot \frac{1+3v}{4+\pi v-\pi} \cdot \int_u F(u)\mathrm{d}u = \frac{4}{\pi d^2 h} \cdot \frac{1+3v}{4+\pi v-\pi} \cdot I_u \tag{87}$$

The deformation energy is based on the stress and strain in the centre of the specimen and is independent from the specimen size. The designations $I_v$ and $I_u$ are adopted for the corresponding integrals to simplify the equations and the calculation.
Examples for the integrals $I_v$ and $I_u$ calculated for the force-displacement diagrams in **Figure 14. 7** is shown in **Figure 14. 8**.

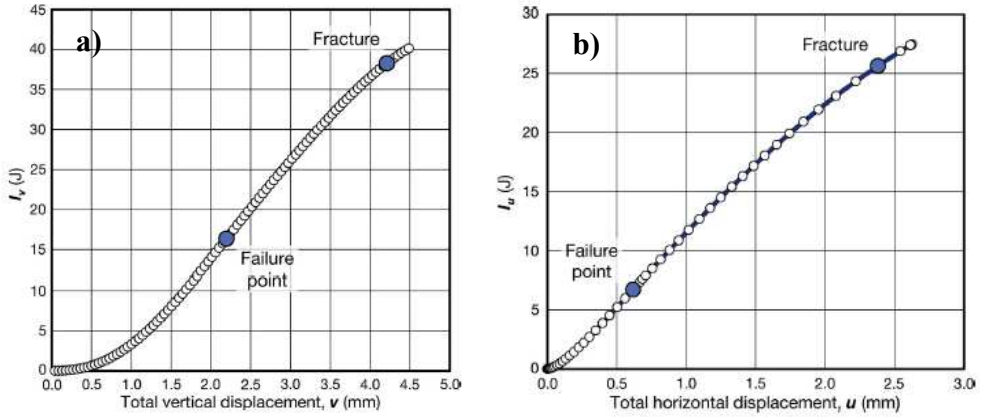


**Figure 14. 8** a) Dependency of the integral $I_v$ which is proportional to the specific fracture work $W^*$ from the total vertical displacement; b) Dependency of the integral $I_u$ which is proportional to the deformation energy $U^*$ from the total vertical displacement.

To obtain an insight into the relation of these values calculated for the point of failure and fracture and to additionally characterize the fracture, the following ratios were calculated:

$$\frac{W^*}{W_t^*} \cdot 100\% \tag{88}$$

and

$$\frac{U^*}{U_t^*} \cdot 100\% \tag{89}$$

where $W^*$ and U* are the values calculated for the point of failure, and $W_t^*$ and $U_t^*$ are the values calculated for the total failure, i.e. the fracture.

To determine an actual point of fracture could be a controversial topic, especially for the dependency of the load from the vertical displacement (**Figure 14. 7**). However, from the diagram of the differential deformation energy, $F(u)\,\Delta u$, shown in **Figure 14. 9**, two points with a sudden drop in the differential deformation energy could be clearly distinguished. As it is designated in the graph, these two points indicate the failure and the fracture of the specimens, as well as the development of the damage in the meanwhile. This damage initiation is followed by the phase of the fairly constant rate of damage by micro cracking. The second sudden drop represents the fracture, which is, for the case of this mixture concept, mostly not explicitly distinguished from the $F(v)$-diagram. Therefore, thus determined point of fracture was used to determine the limits of integration for both the total fracture work, $W_t^*$ , and the total deformation energy, $U_t^*$ .
It is important to point out that a discontinuity in the specimen structure occurs in the centre of the specimen by the damage at the point of failure. This causes a change in the stress state, too, and therefore, the above provided equations for stress and strain in the centre of the specimen are not valid anymore. In this regard, the deformation energy should be calculated up to the point of failure only. However, the fracture work was calculated for both the failure and the fracture of the specimen because it relates to the overall resistance of the specimen regardless of the stress state. Relation between these two values of the fracture work indicates how much of the energy was left after the failure. This could also indicate the contribution of the adhesive properties of the bitumen emulsion to the mechanical performance, and show whether more brittle or more ductile fracture of the mixture is dominant [Miljković and Radenberg, 2014].

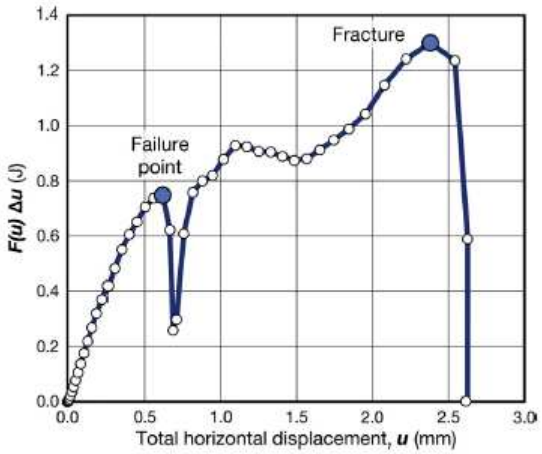


**Figure 14. 9** Diagram of the differential deformation energy depending from the horizontal displacement.

## 14.3.3 Semi Circular Bending

Traffic load on pavement surfaces produces tensile stress at the bottom of the layer that, as the traffic continues, leads to fatigue cracks. Once cracks have been formed, they start to spread and became visible; the crack growth proceeds until there is the possibility of crack

propagation through the stressed body. Thus, the capability of mixtures to resist cracking propagation represents an important property to ensure durability of the pavement layer.
Semi Circular Bending (SCB) test had been found to be a valid method to characterize the fracture properties of bituminous mixtures and the crack propagation potential in relation to the presence of recycled material [Arabani et al., 2009]. The SCB test was carried out according to EN 12697-44 at 10°C; semi circular samples (**Figure 14. 10** and **Figure 14. 11**) were cut from specimens compacted with the SGC with a diameter of 150 mm. The test consists in a half cylindrical specimen (diameter = (150±1) mm, thickness = (50±3) mm, height = (75±1) mm) with a central artificial notch (thickness = (3.5 ± 0.10) mm; height = (10 ± 1) mm) loaded in three-point bending in such way that the middle base of the specimen is subjected to a tensile stress.
The test is conducted at a constant vertical deformation rate equal to 5 mm/min; the load and the vertical deformation are recorded in continuous. Results are expressed in terms of fracture toughness, strain at the maximum force and fracture energy [Biligiri et al., 2012; Li and Marasteanu, 2004; Li and Marasteanu, 2010].
As shown in **Figure 14. 11**, during the test, the crack starts to propagate from the tip of the artificial notch where the concentration of the stresses is highest; then the crack tends to propagate in the direction of the applied load. In order to consider the test acceptable, the fracture must be comprised within a pre-defined area, not larger than ±15 mm from the central vertical axis of the half cylindrical specimen (**Figure 14. 11**). Such limit is defined in order to have lower dispersion of the test data.
The fracture toughness K of the material is directly related to the maximum horizontal stress $\sigma_{max}$, as defined in the following equation:

$$\sigma_{max} = \frac{4.263 * F_{max}}{D * t} \quad [N/mm^2] \tag{91}$$

where $F_{max}$ is the maximum force (N), $D$ is the diameter (mm) and $t$ is the thickness (mm) of the specimen.

According to EN 12697-44, the fracture toughness is calculated as follows:

$$K = \sigma_{max} * f\left(\frac{a}{W}\right) \quad [N/mm^{1.5}] \tag{92}$$

where $\sigma_{max}$ is the stress at failure (N/mm$^2$), $a$ is the notch depth (mm), $W$ is the specimen height (mm) and $f\left(\frac{a}{W}\right)$ is a geometric factor equal to 5.956 for a = 9 ÷ 11 mm and W = 70÷75 mm, or otherwise calculated with the following formula:

$$\mathrm{f}\left(\frac{\mathrm{a}}{\mathrm{W}}\right) = -4.9965 - 155.58\left(\frac{\mathrm{a}}{\mathrm{W}}\right) - 799.94\left(\frac{\mathrm{a}}{\mathrm{W}}\right)^2 - 2141.9\left(\frac{\mathrm{a}}{\mathrm{W}}\right)^3 - 2709.4\left(\frac{\mathrm{a}}{\mathrm{W}}\right)^4 + 1398.5\left(\frac{\mathrm{a}}{\mathrm{W}}\right)^5 \tag{93}$$

The strain at the maximum force, $\varepsilon_{max}$, is also determined as following defined:

$$\varepsilon_{max} = \frac{\Delta W}{W} * 100 \quad (94)$$

where $\Delta W$ is the vertical displacement at the maximum force (mm).

Low $\varepsilon_{max}$ values indicate a material with a brittle behavior, since it cannot accommodate deformations before failure.

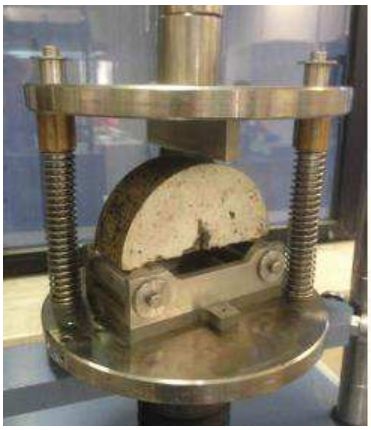

**Figure 14. 10** Semi-Circular Bending configuration

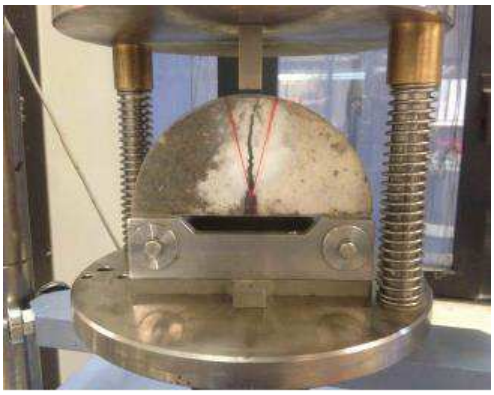

**Figure 14. 11** Fracture propagation

Moreover, the total fracture energy G was determined as the whole area under the load-displacement curve normalized with respect the area of ligament (**Figure 14. 12**). G represents the work required to increase the fractured surface until complete failure, and it is calculated as defined in Equation 95):

$$G = \frac{\int F\, ds}{t*(W-a)} \quad [kJ/m^2] \quad (95)$$

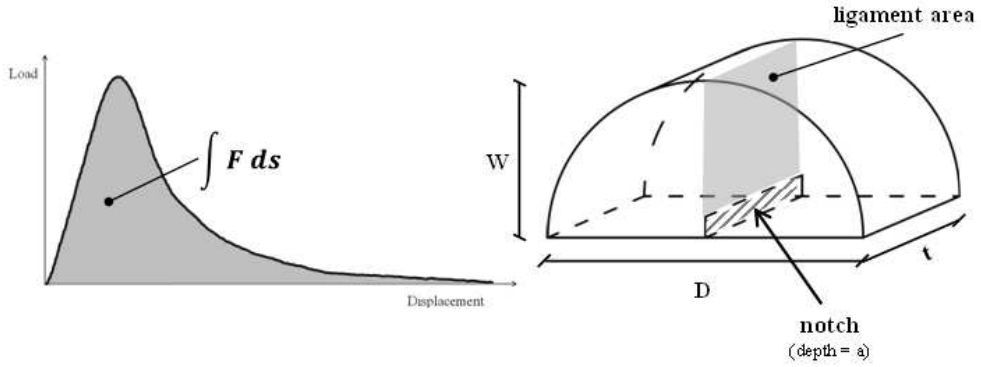


**Figure 14. 12** Fracture Energy

### 14.3.3 Scanning electron microscope

The scanning electron microscope (SEM) is one of the most versatile instruments available for the examination and analysis of the microstructural characteristics of solid objects. The primary reason for the SEM's usefulness is the high resolution that can be obtained when bulk objects are examined; values on the order of 2 to 5 nm (20-50 Å) are now usually quoted for commercial instruments, while advanced research instruments are available that have achieved resolutions of better than 1 nm (10Å).

The basic components of the SEM are the lens system, electron gun, electron collector, visual and recording cathode ray tubes (CRTs), and the electronics associated with them. In the SEM, a fine electron probe is produced which rapidly scans (rasters) across the area of interest. The signals generated in the latter case are detected and converted to CRT electronic signals, which are then fed to a cathode ray tube (CRT) (**Figure 14. 13**). The CRT and the scanning coils are linked through the same scan generator, so that the image appearing on the CRT corresponds spatially to the area of the sample scanned.

The interaction of the electron beam with the specimen produces a variety of signals that are used for imaging and spectroscopy. These signals are not generated at a point, but rather within a volume known as the interaction volume [Stokes, 2003; Goldstein et al., 2012].

The incident (primary) electrons lose energy as they penetrate the sample, giving rise to an X-ray continuum, which consists of all possible wavelengths corresponding to the range of energies of the incident beam. The high-energy primary electrons may penetrate some distance into the sample before being scattered outside of the sample again by the Coulombic repulsion of the electron clouds in the solid. It has been experimentally determined that a significant fraction of the incident electrons that strike a flat, bulk target placed normal to the probe subsequently escape through the same surface that they entered. The re-emergent beam electrons are called backscattered electrons (BSE). The strength of the scattering will depend on the atomic number of the scattering atom, so that backscattered electron images exhibit atomic number contrast. Backscattered electrons provide an extremely useful signal for imaging in scanning electron microscopy. Backscattered electrons respond to composition (atomic number or compositional contrast), crystallography (electron

channeling), and internal magnitude fields (magnetic contrast). Note that these backscattered electrons may be generated at greater depths than that indicated, in which case they may not possess enough energy to escape the sample. The primary or backscattered electrons may knock electrons out of the conduction band of the solid. These secondary electrons are relatively low in energy, and so can only escape from a region near the surface of the sample. This signal is thus often used for generating topographic information.
The electron probe and the CRT are linked through the same scan generator, so that both sample and screen are scanned in the same X-Y grid pattern. The intensity of the signal reaching the detector from a given point on the sample is used to adjust the brightness of the CRT at the corresponding point. The result is the construction of a map of the sample.

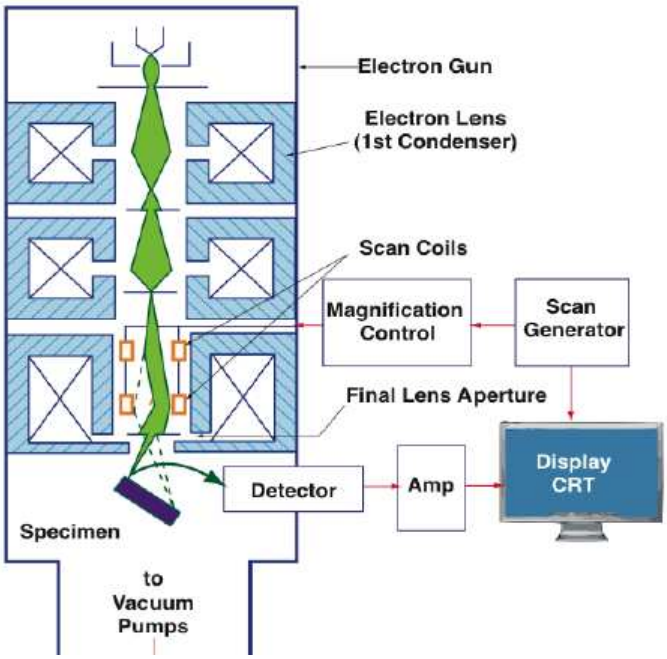


**Figure 14. 13** Schematization of scanning electron microscope (SEM).

*Interaction Volume*
The concept of interaction volume of the primary beam electrons and the sampling volume of the emitted secondary radiation are important both in interpretation of SEM images and in the proper application of quantitative Xray microanalysis. The image details and resolution in the SEM are determined not by the size of the electron probe by itself but rather by the size and characteristics of the interaction volume.
When the accelerated beam electrons strike a specimen they penetrate inside it to depths of about 1 μm and interact both elastically and inelastically with the solid, forming a limiting interaction volume from which various types of radiation emerge, including BSE, SE, characteristic and brehms strahlung x-rays, and cathode luminescence in some materials.

The combined effect of elastic and inelastic scattering controls the penetration of the electron beam into the solid. The resulting region over which the incident electrons interact with the sample is known as interaction volume. The interaction volume has several important characteristics, which determine the nature of imaging in the SEM.
The energy deposition rate varies rapidly throughout the interaction volume, being greatest near the beam impact point. The interaction volume has a distinct shape (**Figure 14. 14**). For low-atomic-number target it has distinct pear shape. For intermediate and high-atomic number materials the shape is in the form of hemi-sphere. The interaction volume increases with increasing incident beam energy and decreases with increasing average atomic number of the specimen. For secondary electrons the sampling depth is from 10 to 100 nm and diameter equals the diameter of the area emitting backscattered electrons. BSE are emitted from much larger depths compared to SE [Goldstein et al., 2012].
Ultimately the resolution in the SEM is controlled by the size of the interaction volume.

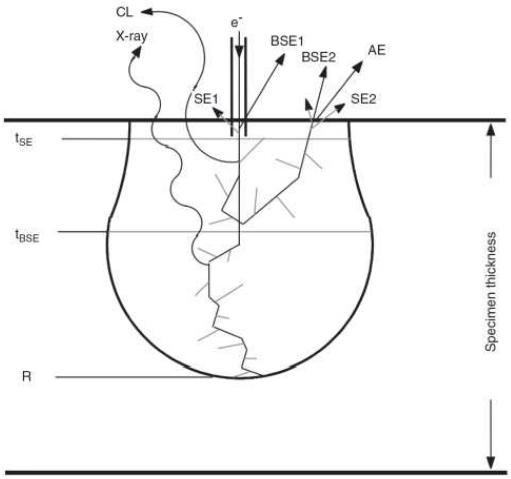


**Figure 14. 14** Scanning electron microscope: interaction volume.

*Image formation*
The SEM image is a 2D intensity map in the analog or digital domain. Each image pixel on the display corresponds to a point on the sample, which is proportional to the signal intensity captured by the detector at each specific point (**Figure 14. 15**). Unlike optical or transmission electron microscopes no true image exists in the SEM. It is not possible to place a film anywhere in the SEM and record an image. It does not exist.
The image is generated and displayed electronically. The images in the SEM are formed by electronic synthesis, no optical transformation takes place, and no real of virtual optical images are produced in the SEM. In an analog scanning system, the beam is moved continuously; with a rapid scan along the X-axis (line scan) supplemented by a stepwise slow scan along the Y-axis at predefined number of lines. The time for scanning a single line multiplied by the number of lines in a frame gives the frame time. In digital scanning systems, only discrete beam locations are allowed. The beam is positioned in a particular location

remains there for a fixed time, called dwell time, and then it is moved to the next point. When the beam is focused on the specimen an analog signal intensity is measured
by the detector. The voltage signal produced by the detector's amplifier is digitized and stored as discrete numerical value in the corresponding computer registry. Typically, the intensity is digitized into 8 bits (256 levels), 12 bits (4096) or 16 bits (65,536). The digital image is viewed by converting the numerical values stored in the computer memory into an analog signal for display on a monitor [Stokes, 2003].

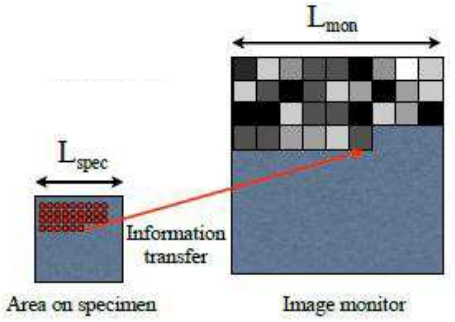


**Figure 14. 15** SEM image formation

*Sample requirements*
Since the SEM is operated under high vacuum the specimens that can be studied must be compatible with high vacuum (~ 10-5 mbar). This means that liquids and materials containing water and other volatile components cannot be studied directly. Also fine powder samples need to be fixed firmly to a specimen holder substrate so that they will not contaminate the SEM specimen chamber.
Non-conductive materials need to be attached to a conductive specimen holder and coated with a thin conductive film by sputtering or evaporation. Typical coating materials are *Au*, *Pt*, *Pd* and their alloys, as well as carbon [Goldstein et al., 2012].

## 14.4 Experimental findings: preliminary phase

The preliminary phase of the experimental program was focused on the development of the compaction and mixing protocol and on the evaluation of the effect of the mineral addition on the workability of the cold bituminous mortars. The objective was to determine the mixing water content, $W_{des}$ and the compaction energy $N_{des}$, that guarantee similar volumetric properties, avoiding any material loss during compaction.
The compactability of CBM mortars was evaluated observing the evolution of volumetric parameters as voids in mixture ($V_m$), voids in mineral aggregate (*VMA*) and voids filled with liquids (*VFL*) during compaction phase.
The same calculation of each volumetric parameter, already defined for cold mixture (see section 2.8), are adopted for cold bituminous mortar. It is also important to remark that *VFL* parameter is an indicator of the saturation level of the studied materials.

### 14.4.1 Mixing design water content

In **Figure 14. 17**, the SGC compaction curves obtained in order to select the mixing design water content $W_{des}$ are reported. In particular, the percentage variation of $V_m$, *VMA* and *VFL* are plotted as a function of the number of SGC gyrations. The results are obtained from the average of measurements on two replicate CBM specimens.
As it can be observed, for all water content (8%, 9%, 10% and 11% by dry aggregate weight) and mineral addition, three CBM mortars followed a unique trend: $V_m$ and *VMA* decreases and VFL increases. Moreover, for a fixed number of gyration, an increase of water content produces a Vm and VMA decrease, indicating a reduction of the volume occupied by air voids and water. This is due to the larger water films that develop around the aggregate particles, which make it easier for them to be moved and reoriented into a denser configuration.
This result is in accordance with that previously obtained with CBTM mixture produced with bitumen emulsion (Section 11.3.1) and can be related to the densification of the aggregate skeleton, promoted by increasing water content: air volume is reduced and progressively filled with water or bitumen, instead of air.
In addition, it can be noted that for all types of CBM mortar, VMA parameter exhibited the same trend of Vm parameter but it is shifted above it of a quantity equal to bitumen content (10% by dry aggregate weight) added in the mortars. This observation is constant during compaction phase highlighting that no bitumen losses occur.
Considering high water content, small quantities of material loss (water and fresh bitumen) may be squeezed out from the mold and obviously, these losses increase if higher water content are considered (**Figure 14. 17**). This phenomenon is related to the achievement of saturation condition (VFL close to 100%). If VFL parameter exceeds the value of 100%, no more voids are available to be filled by liquids (water or bitumen) and as a consequence, they flow out of the compaction mold.

**Figure 14. 16** Material loss during compaction phase.

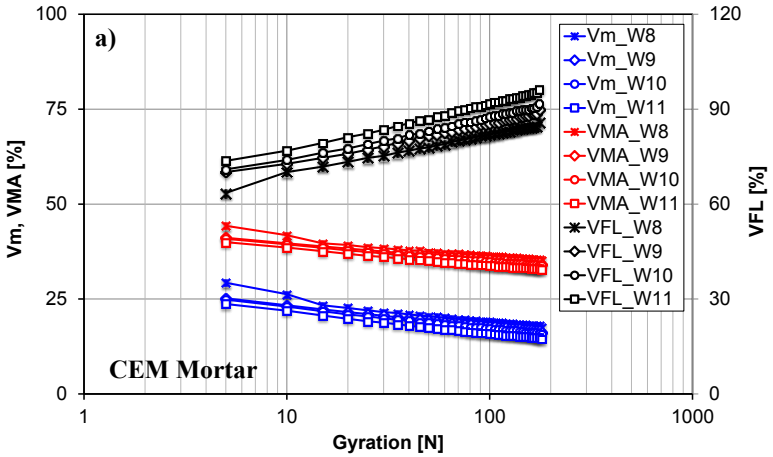
a)
CEM Mortar
Vm, VMA [%]
VFL [%]
Gyration [N]
Vm_W8
Vm_W9
Vm_W10
Vm_W11
VMA_W8
VMA_W9
VMA_W10
VMA_W11
VFL_W8
VFL_W9
VFL_W10
VFL_W11
100
75
50
25
0
120
90
60
30
0
1
10
100
1000

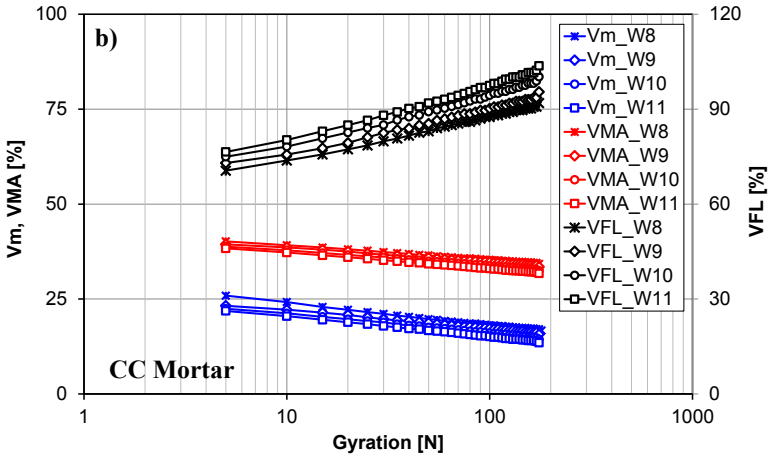
b)
CC Mortar
Vm, VMA [%]
VFL [%]
Gyration [N]
Vm_W8
Vm_W9
Vm_W10
Vm_W11
VMA_W8
VMA_W9
VMA_W10
VMA_W11
VFL_W8
VFL_W9
VFL_W10
VFL_W11
100
75
50
25
0
120
90
60
30
0
1
10
100
1000

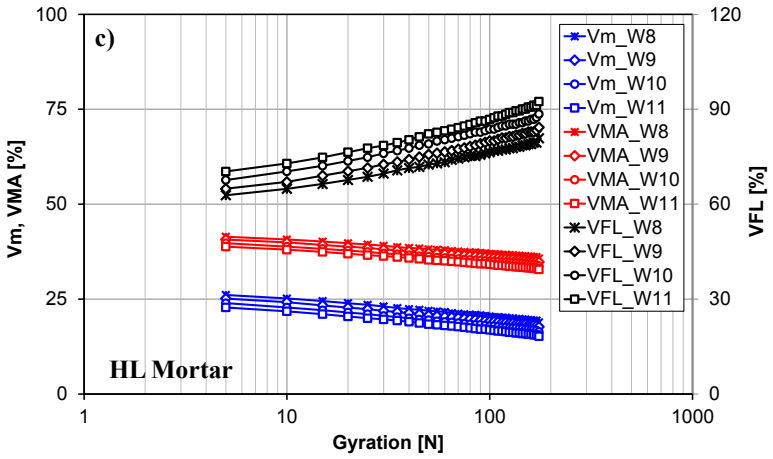


**Figure 14. 17** Evolution of volumetric parameters ($V_m$, *VMA* and *VFL*) as a function of SGC gyrations: a) CEM mortar; b) CC mortar and c) HL mortar.

Anyway, particular care should be taken in the volumetric parameters computation because these material loss may influence the initial CBM mortar composition.
In the present investigation, the saturation condition was fixed at VFL=90% (when liquids loss from the compaction mold are observed) (**Figure 14. 18**).

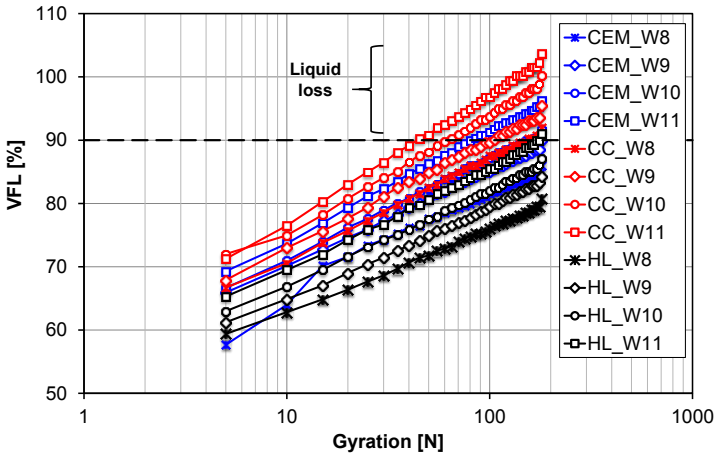


**Figure 14. 18** Saturation condition (VFL>90%) during SGC compaction.

The saturation condition was reached at water content of 9% for CEM and HL mortar and at 8% for CC mortar.

In addition, the final densification (*N*=180gyrations) of the studied CBM mortars is strongly influenced by the selection of mineral addition.
As can be noted from **Figure 14. 19**, mineral addition characterized by higher fineness (high specific surface) improved the compactability of the CBM mortar. Considering VMA parameter as indicator of the degree of packing of the aggregate skeleton, CC mortar achieved the lower value of VMA at the end of compaction (**Figure 14. 19**). In fact, CC mortar is produced using calcium carbonate as mineral addition that is characterized by the higher value of fineness (**Table 14. 2**). Differently, HL mortar exhibited the opposite behavior (**Figure 14. 19**).

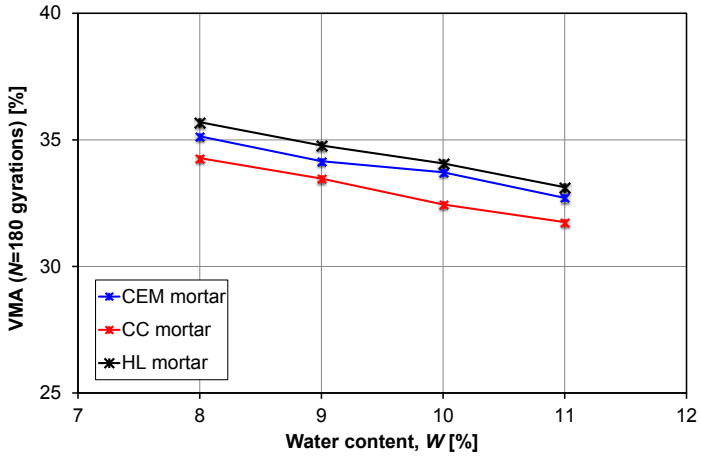


**Figure 14. 19** VMA (*N*=180 gyrations) as a function of water content.

After three days of curing at 40 °C, CBM specimens produced with different mineral addition and at different water content were characterized in terms of indirect tensile strength. Results are reported in **Figure 14. 20** and **Table 14. 5**.

| | ITS [MPa] | | | | | |
|---|---|---|---|---|---|---|
| $W_{tot}$ | **CEM mortar** | | **CC mortar** | | **HL mortar** | |
| [%] | #1 | #2 | #1 | #2 | #1 | #2 |
| 8 | **0.487** | **0.477** | **0.198** | **0.212** | 0.216 | 0.213 |
| 9 | 0.494 | 0.496 | 0.219 | 0.199 | **0.250** | **0.228** |
| 10 | 0.543 | 0.518 | 0.184 | 0.207 | 0.221 | 0.230 |
| 11 | 0.543 | 0.548 | 0.218 | 0.223 | 0.219 | 0.214 |

**Table 14. 5** Mixing design water content: ITS results.

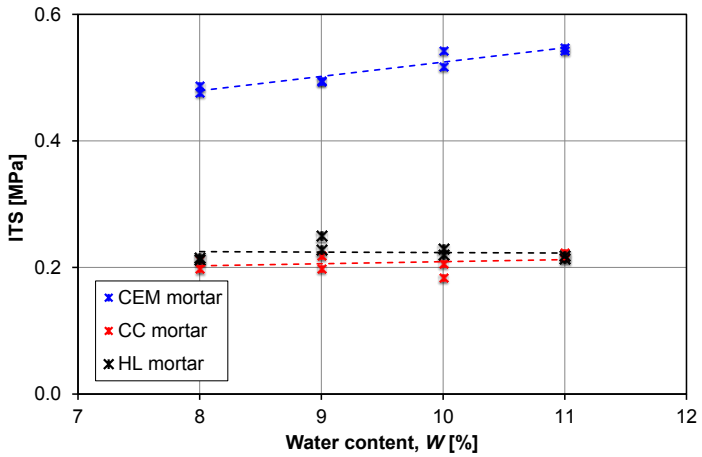


**Figure 14. 20** Evolution of ITS value for CEM, CC and HL mortars as a function of water content.

As it can be observed from **Figure 14. 20**, the maximum value of ITS was registered with CEM mortar and both CC and HL mortars exhibited constant value of ITS varying water content.
The higher strength that characterized CEM mortar is due to the development of cementitious products within the mortar (hydration process) and to the cohesion improved by the bituminous binder. Differently, the strength development for CC and HL mortars is exclusively related to the contribution of the bituminous fraction.
The mixing design water content $W_{des}$ was selected with the aim to achieve good degree of packing of the aggregate skeleton, minimize liquids loss during compaction and guarantee an adequate strength development.
Basing on experimental results and on the previous hypothesis, the mixing design water content $W_{des}$ is 8% for CEM and CC mortar and, 9% for HL mortar.

### 14.4.1 Mixing design compaction energy

The second part of preliminary phase is focused on the evaluation of the mixing design compaction energy $N_{des}$ in order to to produce CBM mortars with comparable volumetric properties, at the end of the compaction phase.

CEM, CC and HL mortars were produced at $W_{des}$ and compacted at three levels of compaction energy $N$: 50, 100 and 200 gyrations. Particular care was taken in avoiding material loss during compaction.
The percentage variation of $V_m$, *VMA* and *VFL* are plotted in **Figure 14. 21** as a function of the number of SGC gyrations, for each CBM mortar. In order to provide an overview of the whole compaction phase, 200 gyrations are considered.
Results are the averaged measurements on two replicate CBM specimens.

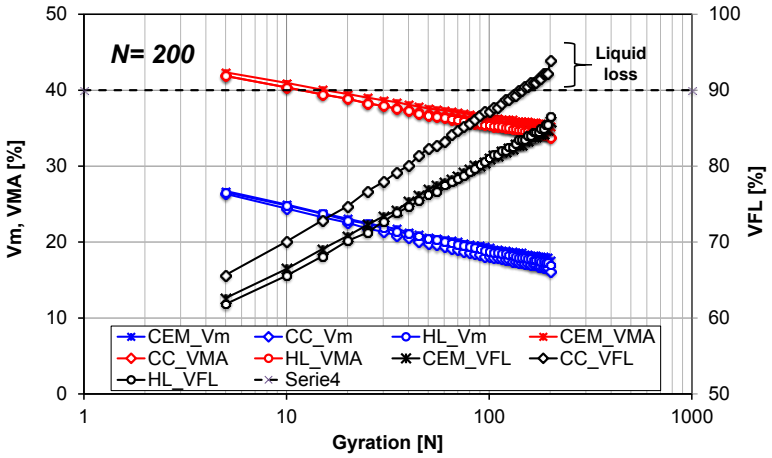


**Figure 14. 21** Evolution of volumetric parameters (Vm, VMA and VFL) as a function of SGC gyrations (N= 200) for CEM mortar, CC mortar and HL mortar.

As can be noted from **Figure 14. 21**, Vm and VMA parameters are not affected by the type of mineral addition. Otherwise, considering VFL parameter, CC mortar behaves in totally different manner from CEM and HL mortars. In addition, at the end of compaction, CC mortar achieved VFL>90% and liquids loss was observed at the end of compaction, i.e. after 200 SGC gyrations.
No liquids loss were observed at lower levels of compaction energy (50 and 100 gyrations), for all CBM mortars.
Results of the compaction process at three levels of compaction energy, for all CBM mortars, are reported in **Table 14. 6**.

| | **CEM mortar** | | | **CC mortar** | | | **HL mortar** | | |
|---|---|---|---|---|---|---|---|---|---|
| | $V_m$ | *VMA* | *VFL* | $V_m$ | *VMA* | *VFL* | $V_m$ | *VMA* | *VFL* |
| *N*=50 | 20.44 | 37.42 | 77.60 | **19.24** | **36.27** | **83.90** | 19.99 | 36.60 | 77.60 |
| *N*=100 | **18.88** | **36.19** | **82.00** | 17.50 | 34.90 | 89.34 | **18.29** | **35.25** | **82.51** |
| *N*=200 | 17.58 | 35.17 | 85.90 | 16.13 | 33.82 | 93.95 | 16.98 | 34.21 | 86.57 |

**Table 14. 6** Summary of volumetric properties.

After seven days of curing at 40 °C, CBM specimens produced with different mineral addition and compacted at different number of gyrations, were characterized in terms of indirect tensile strength. Results are reported in **Figure 14. 22** and **Table 14. 7**.

| | ITS [MPa] | | | | | |
|---|---|---|---|---|---|---|
| *N* | **CEM mortar** | | **CC mortar** | | **HL mortar** | |
| [-] | #1 | #2 | #1 | #2 | #1 | #2 |
| 50 | 0.640 | 0.568 | **0.237** | **0.234** | 0.182 | 0.196 |
| 100 | **0.704** | **0.652** | 0.302 | 0.290 | **0.235** | **0.255** |
| 200 | 0.851 | 0.793 | 0.336 | 0.342 | 0.305 | 0.288 |

**Table 14. 7** Mixing design compaction energy: ITS results.

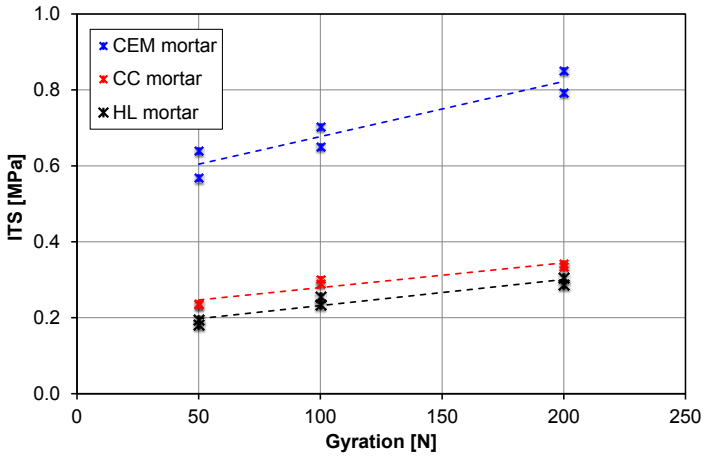


**Figure 14. 22** Evolution of ITS value for CEM, CC and HL mortars as a function of number of gyrations.

Results confirmed that CEM mortar are characterized by the higher ITS value at any compaction levels and ITS values achieved with both CC and HL mortars slightly increase at higher compaction levels.

The mixing design compaction energy $N_{des}$ was selected with the aim to achieve good degree of packing of the aggregate skeleton, minimize liquids loss during compaction, guarantee an adequate strength development and homogeneous volumetric properties for all the produced CBM mortars (**Table 14. 6**).
Bearing this hypothesis in mind, the mixing design compaction energy $N_{des}$ is 100 gyrations for CEM and HL mortars, and 50 gyrations form CC mortar.

In conclusion, CBM specimens for mechanical testing were produced following the parameters summarized in **Table 14. 8**.

| Mortar | Curing condition | Specimen Code | $W_{des}$ [%] | $N_{des}$ [Gyrations] |
|---|---|---|---|---|
| **CEM** | DRY<br>WET | CEM-DRY<br>CEM-WET | 8 | 100 |
| **CC** | DRY<br>WET | CC-DRY<br>CC-WET | 9 | 50 |
| **HL** | DRY<br>WET | HL-DRY<br>HL-WET | 8 | 100 |

**Table 14. 8** Final mix design parameters.

## 14.5 Experimental findings: mechanical testing

In this phase of the experimental program, CBM specimens were produced using the design parameters ($W_{des}$ and $N_{des}$) selected at the end of the preliminary phase.
At the end of each curing period (**Table 14. 1**), moisture loss. ITSM and ITS were measured on CBM specimens with 100 mm diameter.
Differently, CBM specimens with 150 mm diameter were subjected to semi-circular bending test after a curing period of 90 days at 20 °C, in DRY condition.

### 14.5.1 Indirect tensile stiffness modulus

**Figure 14. 23** shows the evolution of *ITSM* as a function of curing time, for CEM, CC and HL mortars and for both curing conditions (DRY and WET).
ITSM was measured after 14 and 28 days of curing and a unique curing temperature of 20 °C was selected.

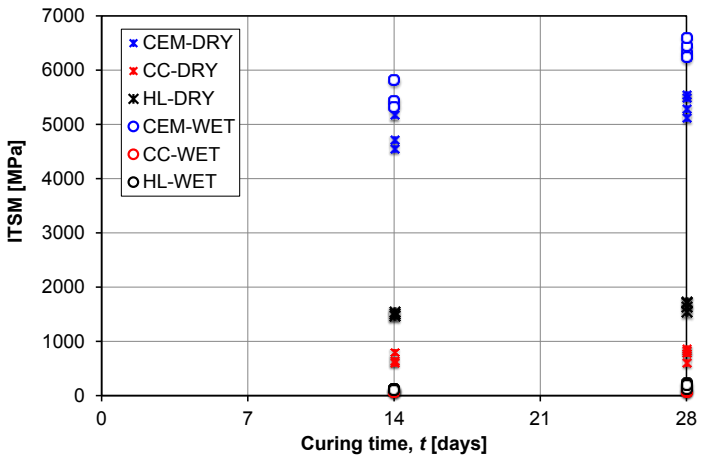


**Figure 14. 23** Evolution of ITSM at 20 °C with curing time for mortars CEM, HL and CC, DRY and WET curing conditions (14 and 28 days of curing).

As can be noted in **Figure 14. 23**, ITSM increases with curing time for all CBM mortars and both curing conditions; this evidence disappears when CC-WET and HL-WET mortars are considered.
CEM mortar exhibited the higher ITSM values at both curing conditions (DRY and WET) and curing times (14 and 28 days). In particular, CEM-WET mortar is characterized by the maximum ITSM value (6601.9 MPa at 28 days). This observation can be related to the contribution of cementitious products developed during the considered curing period. This phenomenon is more marked in WET condition because the wet mortar contains more water available for cement hydration that otherwise, in DRY curing condition might be lost by evaporation (cement-like behavior).
The stiffness development achieved with CC and HL mortars is exclusively due to the cohesion improved by the bitumen added in the mortar. ITSM recorded for HL-DRY mortar is higher with respect to that measured with CC-DRY mortar. Differently, WET curing condition corresponds to a strong ITSM decrease for both CC-WET and HL-WET mortars (asphalt-like behavior).

## 14.5.2 Indirect tensile strength

ITS values, measured at different curing times and conditions, are depicted in **Figure 14. 24**. Each value is the average of three replicates. In WET curing condition, both mortars HL and CC exhibited very low strength as compared with DRY curing conditions. In DRY conditions, for mortar CC, ITS increased from 0.23 MPa (7 days) to 0.4 MPa (14 days) stabilizing at longer curing periods. This behavior can be related to the evaporation process and water evaporation. In fact, the weight loss exhibited a similar trend and stopped after 14 days. For mortar HL, ITS showed a constant trend over the observed curing time and the ITS average value was 0.3 MPa. As it can be observed, ITS values measured for HL-DRY are lower with respect to CC-DRY. This result could be related to the higher Rigden voids obtained analyzing hydrated lime (**Table 14. 2**). In addition, the mortar HL was characterized by less compactability and this led to a reduction of ITS.
As expected, the adoption of cement resulted in higher ITS at any curing time and both DRY and WET curing conditions. This increase was the consequence of the additional contribution given by cement hydration. Until 28 days, mortar CEM-DRY showed higher ITS compared with that obtained for CEM-WET. This suggested that the evaporation process controls the early-stage of curing (curing of bituminous fraction).
At 100 days of curing, ITS was equal to 0.77 MPa and 0.92 MPa for CEM-DRY and CEM-WET respectively. For CEM-DRY, the evaporation and the ITS increasing stopped as previously observed for HL-DRY and CC-DRY. The ITS development continued for CEM-WET thanks for the water that was available in the environment. This highlights the contribution given by the complete development of hydration process [see Section 10.2.2].

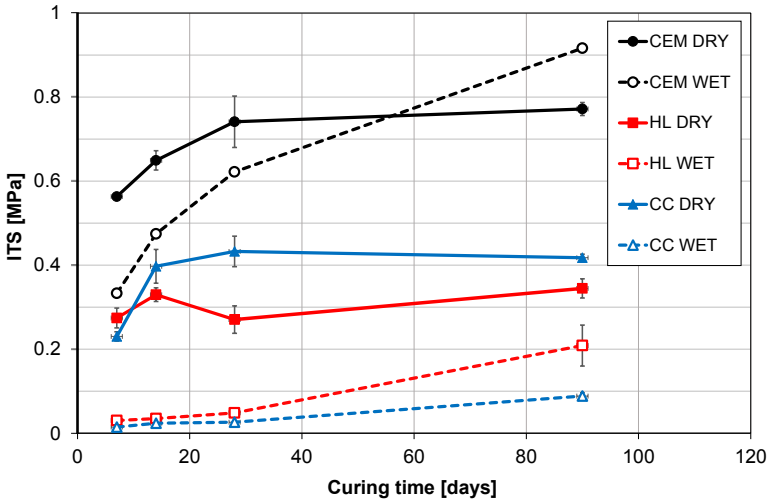


**Figure 14. 24** Evolution of ITS at 20 °C with curing time for mortars CEM, HL and CC, DRY and WET curing conditions (error bars represent the maximum and minimum values).

The obtained results are totally in accordance with those previously achieved with CBTM mixtures produced wit bitumen emulsion and characterized with bitumen-cement ratio equal to 1 (see Section 8.3.2 and 10.2.2).

*Fracture work*

After indirect tensile test was conducted, the fracture work related properties were calculated for 7, 14, 28, and 90 days of cuing.

The time dependencies of the specific fracture work ($W^*$), the total specific facture work ($W^*_t$), and the ratios of these two values ($W^*/ W^*_t$) of the investigated CBM mortars are shown from **Figure 14. 25** to **Figure 14. 27**.

The specific fracture work (**Figure 14. 25**), after 7 days of curing ranged approximately from 0.7 to 8.5 kJ/m$^3$. From 7 to 28 days, an averaged increase of about 25% was observed for both CEM-DRY and CEM-WET mortars. Differently. HL-WET and CC-WET mortars exhibited a constant $W^*$ trend and $W^*$ detected for CC-DRY mortar was up to times after 28 days of curing. In addition, a slight decrease in $W^*$ was detected for HL-DRY.

Considering long-term behavior (from 28 to 90 days), no general rule could be recognized for $W^*$. Anyway, it is very noticeable that the wet curing conditions induced an evident decrease of $W^*$ during the considered curing period.

In particular, the higher values of $W^*$ characterized CC-DRY mortar over time but in WET conditions, the specific fracture work was almost null.

It can be observed that the total specific fracture work $W^*_t$ (**Figure 14. 26**), mostly had the same flow of change over the considered time period.

Finally, the results of the $W^*$ and $W^*_t$ ratio (**Figure 14. 27**) indicated that the CEM-DRY and CEM-WET had the most brittle behavior with respect to other CBM mortars. In particular, CC-DRY exhibited the higher ductile behavior and the $W^*/ W^*_t$ values ranged from 36.5 to

42% and from 39 to 46.2%, after 7 days and at the end of curing period (after 90 days) respectively.

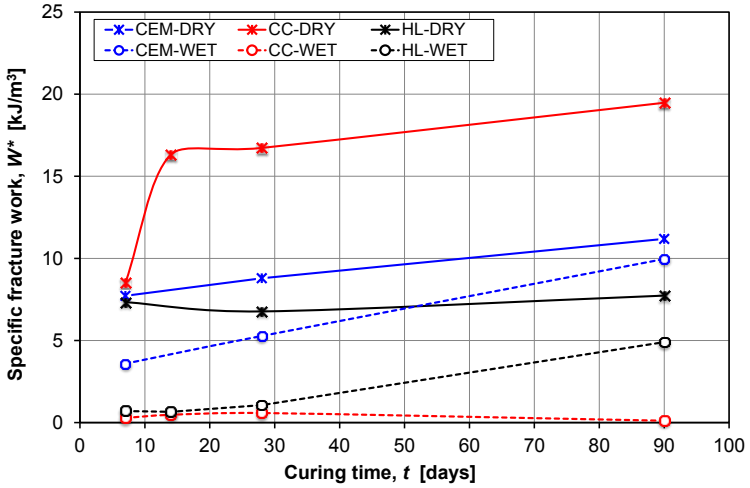


**Figure 14. 25** Development of the specific fracture work of the specimens over time.

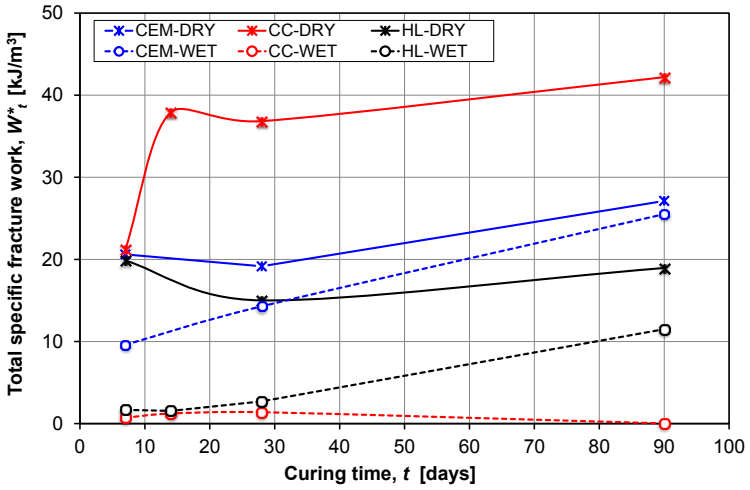


**Figure 14. 26** Development of the total specific fracture work of the specimens over time.

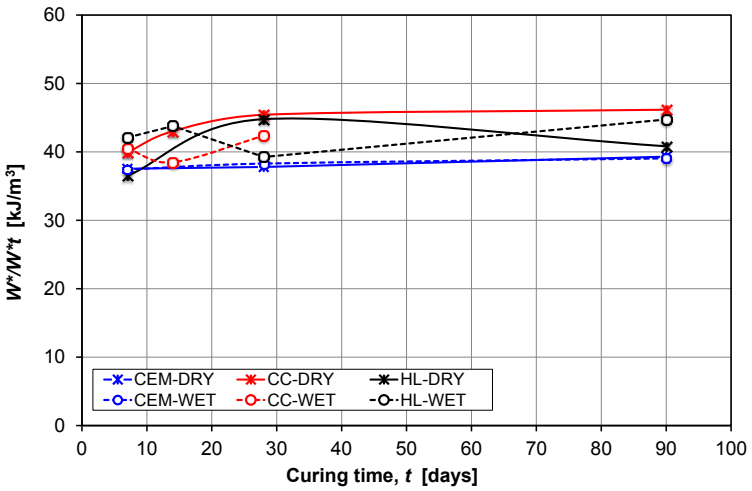


**Figure 14. 27** Development of the ratio between the specific and the total specific fracture work of the specimens over time.

*Deformation energy*

The time dependencies of the deformation energy ($U$*), the total deformation energy ($U_t$*), and the ratios of these two values ($U$*/ $U_t$*) of the considered mixtures are shown from **Figure 14. 28** to **Figure 14. 30**.

Considering DRY curing conditions, the specific deformation energy increased over time for CC-DRY while both HL-DRY and CC-DRY mortars exhibited a slow decreasing trend during the considered curing period. In WET conditions, $U$* increased over time for CEM-WET and HL-WET mortar and $U$* was constant for CC-WET mortar.

The total specific deformation energy ($U_t$*) (**Figure 14. 29**) had the maximum value after 14 days of curing with CC-DRY mortar and then $U_t$* increased continuously very slow; the overall tendency detected for other CBM mortars was a faster increase of the total specific deformation energy after 28 days of curing. The unique exception was CC-WET mortar, the observed $U_t$* was constant from 7 to 28 days (about 1.5 kJ/m$^3$) and then decreased reaching zero at the end of curing period.

Finally, the time dependency of the ratio of the deformation energy to the total deformation energy (**Figure 14. 30**) remarks the brittle fracture detected for CEM mortar cured in both curing conditions; in fact, the range of the values remained mostly the same during the entire curing period (from 16 to 13.7%).

In addition, HL mortar is characterized by a no clear behavior in terms of $U$*/ $U_t$* because it exhibited an opposite tendency, when DRY or WET curing conditions are analyzed at long curing period (from 28 to 90 days). This phenomenon can be related to the lower level of affinity between hydrate lime and bitumen emulsion. However, additional studies are required to better understand and characterized the fracture phenomenon of these materials.

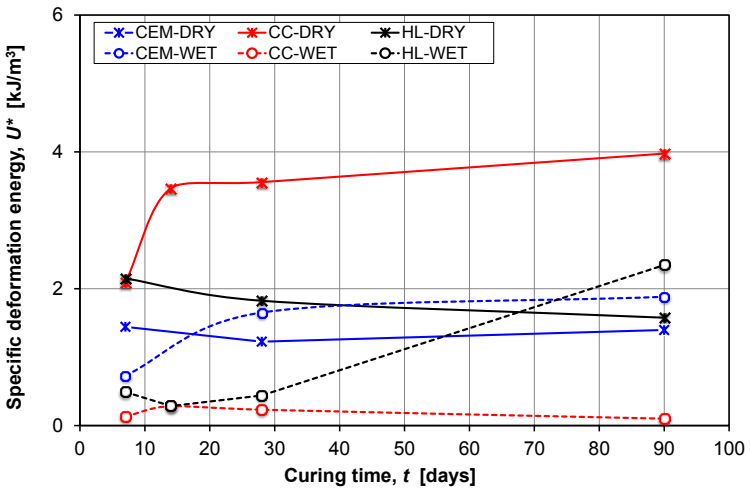


**Figure 14. 28** Development of the deformation energy of the specimens over time.

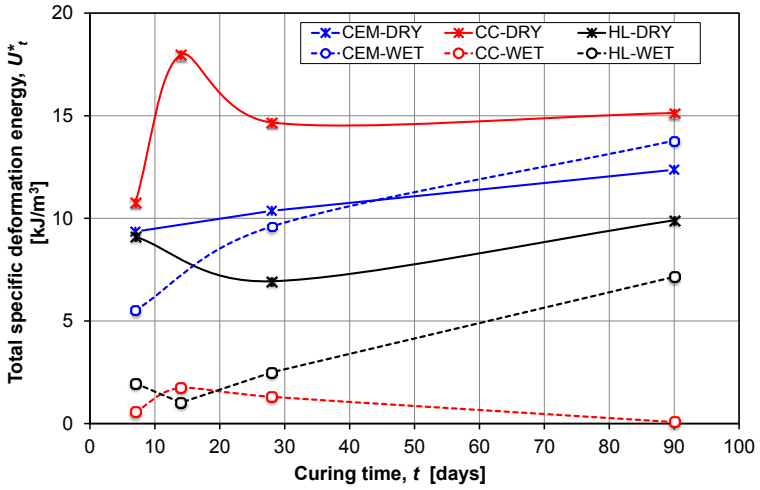


**Figure 14. 29** Development of the total deformation energy of the specimens over time.

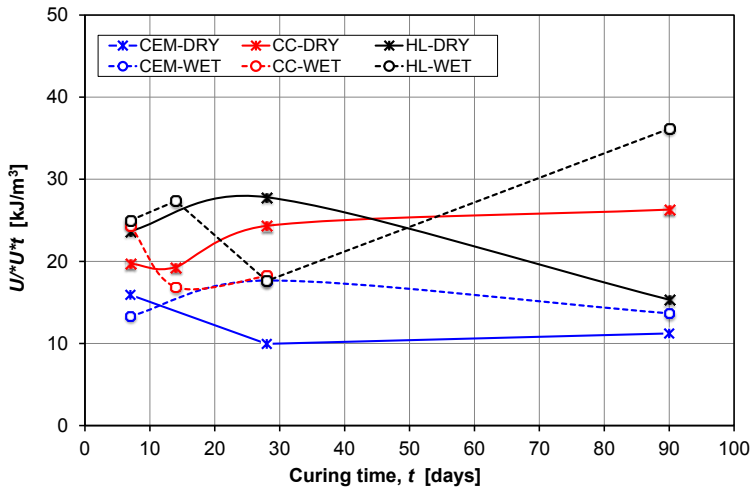


**Figure 14. 30** Development of the ratio between the deformation energy and the total deformation energy of the specimens over time.

### 14.5.3 Semi-circular bending test

SCB tests were carried out in order to evaluate the crack propagation aptitude in relation to the mineral addition adopted in the mortar. During the test, the crack starts to propagate from the tip of the artificial notch where the stress concentration is the highest; then the crack propa-gates [Frigio et al., 2013].

**Figure 14. 31** reports the typical load-deformation curves. As it can be observed, the relation-ship was non-linear and this response was more pronounced if hydrated lime or calcium carbonate were used in mortars. As expected, the mortar CEM-DRY had higher maximum load values with respect to HL-DRY and CC-DRY. Mortar CEM-DRY was characterized by a brittle behavior: low deformation at maximum load and a rapid decline. Otherwise, for HL-DRY and CC-DRY, a high deformation at maximum load and a slow decline after-wards was observed (typical plastic behavior).

Fracture toughness $K$ and the fracture energy were calculated according to EN 12697-44. The mean values are shown in **Figure 14. 32** along with the minimum and the maximum values (error bars). CEM-DRY showed high fracture toughness, k = 13.44 N/mm$^{3/2}$, but small fracture energy, e = 0.41 kJ/m$^2$ (cement-like behavior). Differently, mortar CC-DRY exhibited lower fracture toughness, k = 7.23 N/mm$^{3/2}$, and higher fracture energy, e = 1.24 kJ/m$^2$, with respect to CEM-DRY (asphalt-like behavior). Mortar HL-DRY was characterized by low mechanical performance in terms of both fracture toughness ($k$ = 4.96 N/mm$^{3/2}$) and fracture energy ($e$ = 0.42 kJ/m$^2$).

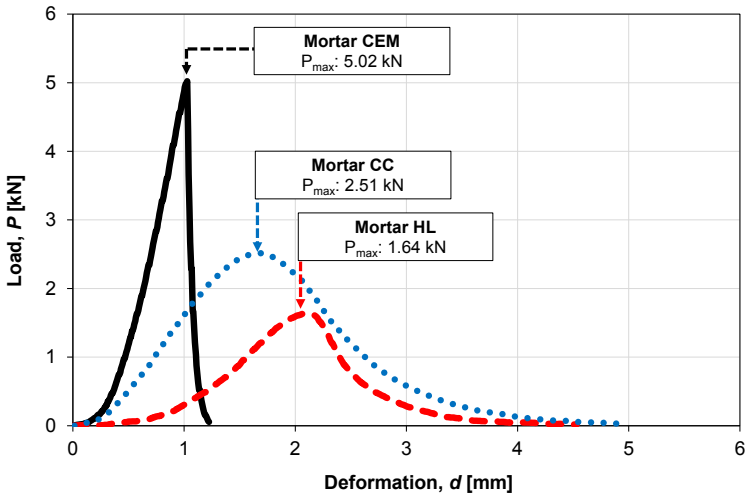


**Figure 14. 31** Results of SCB tests: typical load-deformation curves a for mortars CEM, HL and CC, in dry curing condition.

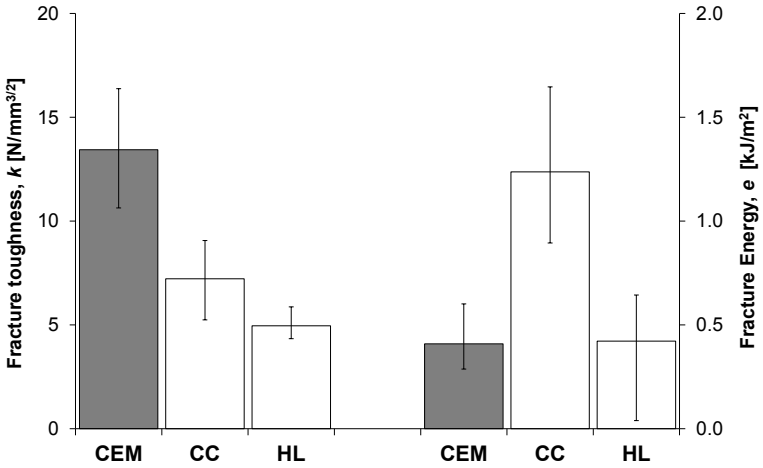


**Figure 14. 32** Results of SCB tests: average value of fracture toughness *k* and fracture energy *e* for mortars CEM, HL and CC, in dry curing condition.

## 14.4.2 Modelling of curing process

The moisture loss (*DW*) by evaporation (i.e. difference between the weight of specimen after compaction and the weight measured at the specific curing time), as function of curing time is reported in **Figure 14. 33** for CEM, CC and HL mortars.

Data available are referred to a curing time of 28 days, where CBM specimens were cured at 20 °C and both DRY and WET curing conditions. In addition, in order to avoid errors during *DW* analysis, the effective total water content ($W_{eff}$) was calculated weighting each CBM immediately after compaction.
As it can be observed, in DRY condition all CBM mortars exhibited an asymptotic behavior over time (*equilibrium* condition). In addition, HL-DRY and CEM-DRY are characterized by the higher and lower moisture loss, respectively.
For HL-DRY, *DW* was 6.56% and 6.74% after seven and 28 curing days, respectively.
Analogously, For CEM-DRY, *DW* was 4.36% and 4.56% after seven and 28 curing days, respectively. CC-DRY showed an intermediate behavior, *DW* was 5.98% and 6.25% after seven and 28 curing days, respectively.
*DW* measured in WET conditions are very small because the evaporation is not allowed and, for this reason, the data are not considered during the analysis.
A parametric evaluation of the *DW* evolution can be obtained considering the Michaelis-Meneten model, already adopted and validated for the analysis of CBTM curing process (section 10.2.2 and 8.3.2). In particular, the estimated value of $K_c$ can be used to evaluate the initial curing rate (i.e. the time required to reach one half of the asymptotic value),whereas the estimated value of $y_A$ can be used to estimate the long-term (asymptotic) behavior (i.e. *equilibrium* condition).
$K_c$ parameters were 0.24 days, 0.44 days and 0.43 days for CEM-DRY, CC-DRY and HL-DRY, respectively. Clearly, the use of cement as mineral addition has a marked effect on the *DW* evolution because the phenomenon is faster with respect to CC-DRY and HL-DRY.
Considering the long-term behavior, it can be observed that the asymptotic values of *DW* were 4.55%, 6.39% and 6.92% for CEM-DRY, CC-DRY and HL-DRY, respectively.
It is evident that cement addition affects the amount of evaporable water in the mortar that is necessary to develop the cementitious products during the hydration process.

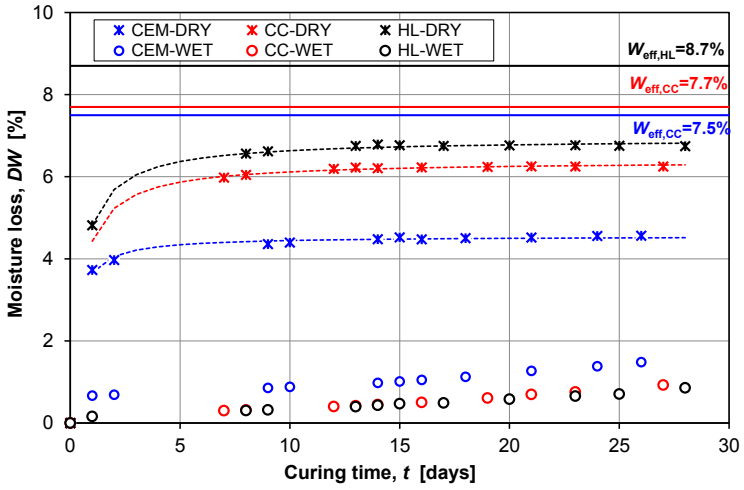


**Figure 14. 33** Evolution of moisture loss monitored over time for CEM, CC and HL mortars.

It can be concluded that the cement addition led to lower moisture loss with respect to other mineral additions.
For CEM-DRY, it should be considered that $W_{eff}$ contains the water required for the hydration of cement $w_{hydr}$ that is not available for evaporation. Part of $w_{hydr}$, about 23% of cement weight, is required to form the calcium-silicate-hydrate (C-S-H) gel, whereas another part, about 19% of cement weight, is absorbed by the nanoporosity of C-S-H gel and can be removed only at very low relative humidity [Mehta and Monteiro 1993]. Hence, the amount of water needed for the hydration process can be calculated using the Equation 57.
Assuming an average of the clinker content range $k$=0.87 and $\alpha$ = 0.90 at 28 days of curing [Mehta and Monteiro 1993], resulted a $w_{hydr}$ = 3.3%.
The comparison between the $y_A$ (moisture loss by evaporation, 4.55%) and $w_{hydr}$ (3.3%), with respect to the effective total water content $W_{eff}$ (7.5%), showed that the water available in CEM-DRY not evaporated is $\Delta W$= 7.5-4.55= 2.95% (< $w_{hydr}$ =3.3%). This small fraction of water is not enough to hydrate the entire cement added in the mortar: the cement percentage that reacted with water is 8.94% instead of 10%, the remain part is inert filler present in CEM-mortar and as a consequence, did not contribute to increase the mechanical properties of CEM-DRY mortar.
This result is in accordance with those previously achieved with CBTM mixtures produced wit bitumen emulsion (see Section 10.2.2).

## 14.4.6 Microstructure observation by scanning electron microscope

At the end of mechanical testing (after 90 days), small pieces (1 cmx1 cm x1 cm) were carefully sampled from CEM, CC and HL mortars, cured in both DRY and WET conditions and each surface morphology was investigated by the SEM Philips XL20.

Samples were treated with a thin layer of Au in order to improve its reactive properties during SEM observations.
Many researchers [Richardson, 1999; Rutherford, 2014; Liu, 2015] adopted the analysis of SEM microstructure images in order to evaluate the development of different microstructures in CBM mortars that contain cement or other mineral additions.
Considering CEM mortars, cement hydration products, such as such as calcium silicate hydrates (C–S–H) and ettringite (AFt), can be clearly identify in **Figure 14. 34** and **Figure 14. 35**. C–S–H is the main binding phase in all Portland cement-based materials. The strength of hardened Portland cement material depends in part on the ability of the C–S–H to bind effectively other products of hydration and aggregates [Richardson, 1999]. The hydration products can pierce the bitumen film, smooth areas (**Figure 14. 34**), and form bonds with other hydration products or sand surface. The cementitious phase in the CEM-mortars was dispersed within the bitumen binder. The cement hydration consumed a portion of the water that occupies the micro air void spaces between bitumen emulsion and sand, which had a stiffening effect on bitumen binder [Du, 2014].

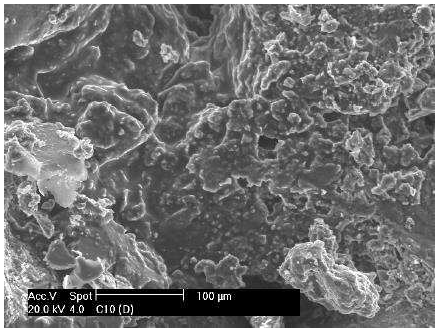


**Figure 14. 34** SEM images: CEM-DRY mortar.

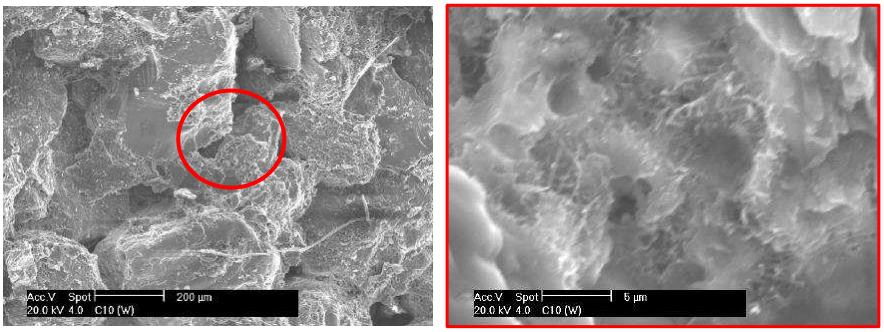


**Figure 14. 35** SEM images: CEM-WET mortar and ettringite formation.

However, AFt crystals grew well where the concentration of C-S-H products is lower (**Figure 14. 35**); in fact, the marked development of AFt is promoted by WET curing conditions (high level of relative humidity).
As it can be observed in Figure **Figure 14. 35**, AFt shows needle-like morphology and the needles interlocked with each other, which also contributed to the stiffening of the CEM-mortar. In addition, some areas are characterized by higher concentration of bitumen binder (dark color) that can hinder the formation of cementitious compounds. In fact, this indicates that the higher bitumen concentration may lead to formation of less cement hydration products [Tan et al., 2014]. Although the water phase in bitumen emulsion can react with cement particles, they could also be wrapped by bitumen film in CEM-mortar, preventing formation of more cement hydration products (anhydrous cement). It can be concluded that the stiffening and strengthening effect of cement particles is significantly decreased by the presence of bitumen binder.
**Figure 14. 36** and **Figure 14. 37** depict CC and HL mortars, within these materials no cement hydration products (i.e. C-S-H and AFt) can be observed. In both case, SEM observations highlighted the presence of aggregate particles differently coated by bitumen. In particular, analyzing the microstructure of HL mortar (**Figure 14. 36**), it is evident that the low affinity between hydrated lime and bitumen emulsion produced a limited dispersion of bitumen among aggregate particles. Otherwise, within CC-mortar, bitumen appears well dispersed:

aggregate particles are coated by bituminous mastic (**Figure 14. 37**). This result can be also confirmed by visual observations on CC and HL-mortar specimens. (**Figure 14. 38**).

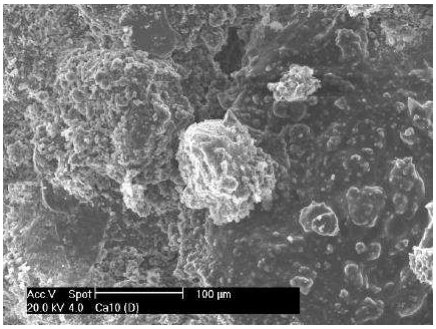


**Figure 14. 36** SEM images: CA-DRY mortar.

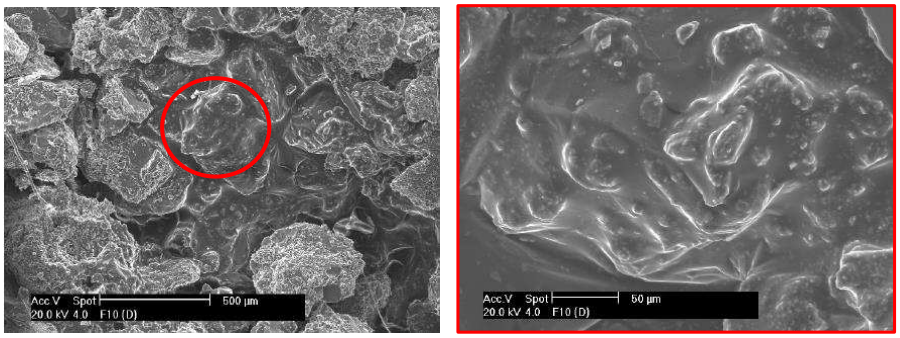


**Figure 14. 37** SEM images: CC-DRY mortar and bituminous mastic that coats aggregate particles.

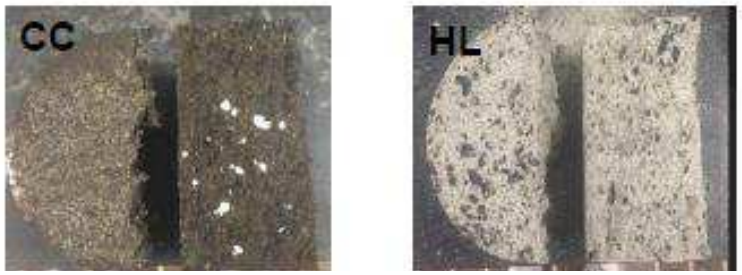


**Figure 14. 38** Specimens of CC and HL mortars characterized by a different level of bitumen dispersion.

## 14.5 Summary

In the present experimental study, the characterization of the mechanical response of cold bituminous mortars (CBMs) produced with three different types of mineral addition (calcium carbonate, cement and hydrate lime) was investigated. The influence of experimental variables such as curing conditions (time and relative humidity) and types of mineral addition was also analyzed from both volumetric and mechanical point of view.

Considering the preliminary phase, the mixing design water content and compaction energy were evaluated for all the studied CBM mortars. The selection of both mixing design parameters was carried out with the aim to achieve good degree of packing of the aggregate skeleton, minimize liquids loss during compaction and guarantee an adequate strength development.

Results showed that higher water contents and compaction energy correspond an increase in compaction level connected to a dramatic liquids loss (VFL>100). In addition, it was highlighted that the type of mineral addition affects the compactability of CBM mortars: mineral additions characterized by high surface area (calcium carbonate) contributed to achieve a better degree of packing of the mortar.

From the mechanical point of view, CBM mortars (CEM, CC, HL) cured in both curing conditions were characterized in terms of ITSM, ITS and resistance to crack propagation.

CEM mortars are characterized by higher ITSM values for both curing conditions, this observation is related to the stiffening contribution of cementitious products. Obviously, WET curing conditions led to an increase of ITSM values promoted by higher water content available for hydration process. CC-DRY and HL-DRY mortars are characterized by lower ITSM measurements. In fact, the stiffening contribution is exclusively related to the cohesion improved by the bitumen emulsion breaking . Differently, in WET conditions, the registered ITSM values are almost null because the evaporation was not allowed and, as consequence, bitumen emulsion breaking did not occur.

ITS values measured for CEM mortar increased over the considered curing period, with different rates depending on the curing conditions (DRY or WET). At the early stage, CEM-DRY had higher ITS with respect to CEM-WET. This indicates that the curing of bituminous component (emulsion breaking and evaporation) controls the curing process. Otherwise, at long term curing (90 days), CEM-WET had higher ITS with respect to CEM-DRY. This suggests that the curing of cementitious phase (cement hydration) prevails over the curing of bituminous component because, in dry condition, the water was almost completely evaporated. Both mortars HL-WET and CC-WET exhibited very low strength as compared with DRY curing conditions. This result was due to the absence of the resistance contribution related to the bituminous emulsion breaking and water evaporation. Otherwise, for mortars CC-DRY and HL-DRY, the ITS development was exclusively connected to these phenomena. The evaluation of energy parameters (fracture work and deformation energy) confirmed the observation obtained analyzing ITS results.

As expected, CEM mortars are characterized by higher stiffness and strength but also by a brittle behavior, typically detected for cement-based materials (cement-like behavior).

Differently, CC mortar cured in DRY conditions exhibited the most ductile behavior (asphalt-like behavior).

The evolution over time of both $W^*$ and $U^*$ is noticeable exclusively in WET curing conditions, for CEM mortars. For CC and HL mortars, WET curing conditions correspond to a dramatic decrease of both energy parameters.
Regarding to the resistance to crack propagation, results confirmed the observations carried out with ITS test. Mortar CEM-DRY showed high fracture toughness but small fracture energy (cement-like behavior). Differently mortars CC-DRY exhibited low fracture toughness and high fracture energy (asphalt-like behavior). Mortar HL-DRY was characterized by low mechanical performance in terms of fracture toughness and fracture energy.

SEM microstructure observations also confirmed the different mechanical behavior that can be achieved with different mineral additions. Cement additions led to the formation of cementitious products (C-S-H and Aft), mostly developed in WET curing conditions instead of DRY curing conditions where some particles of anhydrous cement can be observed.
In particular, analyzing the microstructure of HL mortar, SEM observations highlighted the presence of aggregate particles differently coated by bitumen. It is evident that the low affinity between hydrated lime and bitumen emulsion produced a limited dispersion of bitumen among aggregate particles. Otherwise, within CC-mortar, bitumen appears well dispersed: aggregate particles are coated by bituminous mastic that promotes a more ductile behavior
The moisture loss data, recorded for all CBM mortars, demonstrated the applicability of Michealis-Menten model to evaluate the curing process of these materials.
Considering DRY curing conditions, CBM mortars exhibited an asymptotic behavior over time. The type of mineral addition affects the amount of evaporable water; in fact, the main part of water content included in CEM mortars is dedicated to cement hydration: cement addition led to lower moisture loss with respect to other mineral additions.
Finally, results obtained from the modelling of curing process, are totally in accordance with those previously carried out on CBTM materials.

# Part 4
# Mastic-scale analysis: Rheological characterization of Cold bituminous mastics

# CHAPTER 15.

# Introduction

The fourth and last part of this thesis is focused on the rheological characterization of cold bituminous mastics (CBms), produced with bitumen emulsion (*Task 4*). In particular, the effect of both curing time and type of mineral addition was analyzed during a wide program of experimental activities.
Cold bituminous mastic is composed by bituminous binder (in form of emulsion or foam) and filler-sized aggregate particles (cement or other mineral additions) and establishes the connection between bituminous binder and mixture.
In detail, the main objective of this task is to investigate phenomena that occur at the interface between mastics [Huang and Di Benedetto, 2015] and coarse aggregates in a typical cold mixture. The mechanical behavior of this complex multiphase structure can be analyzed at small level of investigation: at mastic-scale level, where the overall mechanical properties of the mixture are decided. In addition, when cold bituminous mastic (CBm) rheology is considered, the role of mineral addition used (active or inactive fillers) as emulsion breaking regulator, material stiffener or filler, should be addressed.

## 15.1 General overview

The fact that the adoption of cold mixtures offers certain benefits over hot mixtures has been accepted from many years. Anyway, the use of bitumen emulsion as a binder in cold mixtures for structural layers has attracted relatively little attention mostly because of the problems associated with the time taken for full strength development after paving and the susceptibility to early life damage by rainfall. An efficient way of improving the mechanical properties of cold mixtures is the addition of Portland cement [Brown and Needham, 2000]. Even at small dosages (less than 1% by mass of dry aggregate), cement has important effects on the emulsion breaking and setting process and can improve the short-term performance of cold mixtures by increasing their stiffness, strength and moisture resistance [Asphalt Academy, 2009]. In general, although the simultaneous presence of bitumen and cement does not produce a new binder [Giuliani, 2001], the physical and mechanical properties of the mixtures (e.g. strength and stiffness) depend on the dosages and relative proportions of residual bitumen from emulsion and cement, i.e. on the bitumen/cement ratio (B/C). A distinctive feature of cold mixtures produced with emulsion is that their physical and mechanical properties evolve over time, because emulsion breaking and setting, moisture loss and hydration of cement are all time-dependent processes [Montepara and Giuliani, 2002; Cardone et al., 2015]. The study of this process, known as curing, is of the outmost practical importance because freshly mixed cold mixtures should be plastic and workable in order to allow laydown and compaction, whereas after construction the development of internal cohesion and suitable mechanical properties should be as fast as possible, in order to allow construction of the upper layers and opening to traffic [Graziani et al., 2016a].

Two main causes of bitumen emulsion breaking in contact with mineral aggregates were described by Lesueur and Potti (2004): the increase of bitumen droplets concentration and the disappearance of electrostatic repulsion between bitumen droplets. The use of cement in cold mixtures has an influence on both causes, because: a) cement hydration subtracts free water from the mixture [Garcia et al., 2013], thus contributing to coalescence of bitumen droplets and b) produces an increase of pH that can neutralize the stabilizing action of cationic emulsifiers [Wang et al., 2013]. In this regard, over-stabilized emulsions are specifically formulated to allow mixing of high cement dosages avoiding premature breaking. On the other hand, both cationic and anionic emulsifiers may have a retarding effect on cement hydration in the early age (i.e. cement setting) and also cause a loss in the long term content of cement hydrates [Weiss et al., 2008; Tan et al., 2014].

Similar to HMA, cold mixtures can be schematized as a two-phase composite where a fine aggregate matrix (cold bituminous mortar) incorporates coarser aggregate particles [Underwood and Kim, 2013]. At smaller scale, the cold bituminous mortar can further be considered a two-phase composite where fine aggregate particles are incorporated into a matrix composed of bitumen and filler-sized aggregate particles, i.e. the cold bituminous mastic (CBm) [Underwood, 2015; Lackner et al., 2006].

As long as fresh cold mixtures are concerned, the mastic phase also includes filler-sized particles (active or inactive filler). Experiments at the scale of the mastic are extremely important because they allow the physicochemical interactions that occur between emulsified bitumen, water, filler sized aggregates (as *inactive* filler) and cement (as *active* filler) to be emphasized [Zhang et al., 2012].

Immediately after mixing, CBm is concentrated multiphase dispersions consisting of both filler-sized aggregate grains and bitumen droplets (dispersed species) in water (continuum liquid phase) [Pal, 2000]. Their rheological properties, specifically their viscosity ($\eta$), depend on the forces acting between aggregate grains, bitumen droplets and water molecules and are strongly influenced by the volumetric concentration ($\phi$) of the dispersed species as well as by their particle size distribution [Tadros, 2011; Peng et al., 2014].

Considering both CBm at cured state (long-term behavior) and CBm characterized by high volumetric concentration of filler-sized aggregate particles, the CBm physical state evolves from a concentrated multiphase dispersion to an inverted dispersion where bitumen droplets and filler-sized particles are the continuous phase and the dispersed phase is the remain amount of water available.

It is well understood that the rheological behavior of fresh CBms depends on the volume fraction and on the type of dispersed solid phase (filler-sized aggregate, i.e. active or inactive fillers).

Differing from other inert suspension systems (inactive filler addition), cement hydration (active filler) in CBm brings forth noticeable complexity to the elucidation of the rheological behavior of the paste. The hydration process continuously alters the phase composition and microstructure of the mastic, so that the rheological properties of cement suspension constantly change over time and with temperature [Hanehara and Yamada, 1999]. In fact, as far as recent researches are concerned, the macroscopic rheological properties and mechanical behavior of CBm suspension are related to the microstructure evolution of the suspension during early-age of curing. In this context, test methodology and rheological property to be investigated should be selected according to the physical state of the

considered CBm (i.e. at different curing times or volumetric concentration of filler-sized aggregate grains).

**Figure 15. 1** presents a schematic illustration of the evolution of CBm physical state (from liquid, plastic or solid state) as a function of both increasing in curing time ($t$) or volumetric concentration ($\phi$) of filler-sized aggregate grains. In addition, material properties that can be analyzed according to the physical state of the material, are also reported in this illustration.

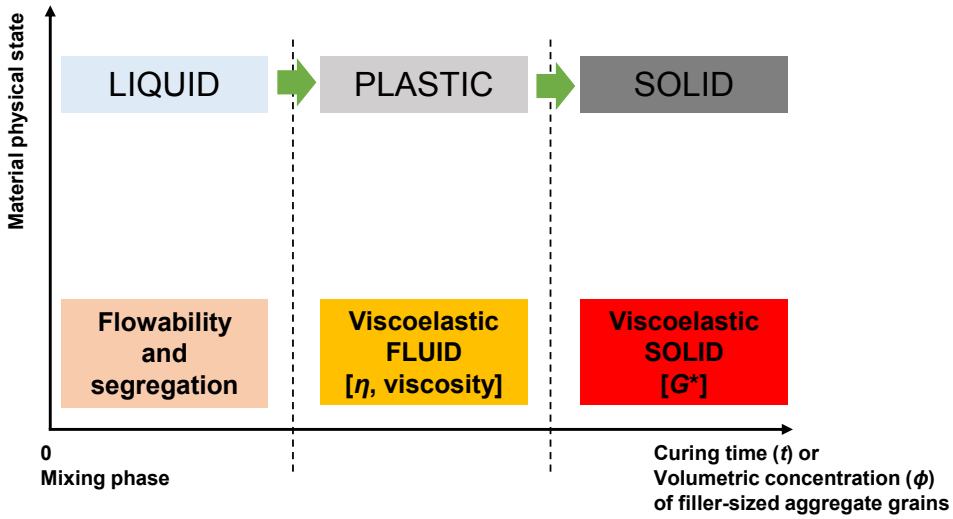


**Figure 15. 1** Evolution of physical state of CBms as a function of curing time ($t$) or volumetric concentration ($\phi$) of filler-sized aggregate grains.

# CHAPTER 16.

# Rheological characterization of Cold bituminous mastics

## 16.1 Experimental program

The experimental program is focused on the laboratory characterization of cold bituminous mastics (CBm) prepared with bituminous emulsion (unique source) and two different mineral additions at three volumetric concentration ratios (volume of mineral addition/volume of residual bitumen, $V_A/V_B$).
The experimental investigation considered cement and calcium carbonate as mineral additions in order to compare the influence of both active or inactive filler addition in the mechanical behavior of CBms.
CBms are characterized from the rheological point of view in terms of *complex modulus*. In addition, the influence of curing time on rheological properties of CBms was also investigated.
A unique curing temperature of 40 °C and three different curing times were selected:

- 15 hours (early-age of curing);
- One day;
- Three days (long-term curing).

CBms cured for 15 hours were tested exclusively using DSR equipment because the physical state of the specimen does not allowed specimens for Metravib testing to be produced.
The experimental program is summarized in **Figure 16. 1**.

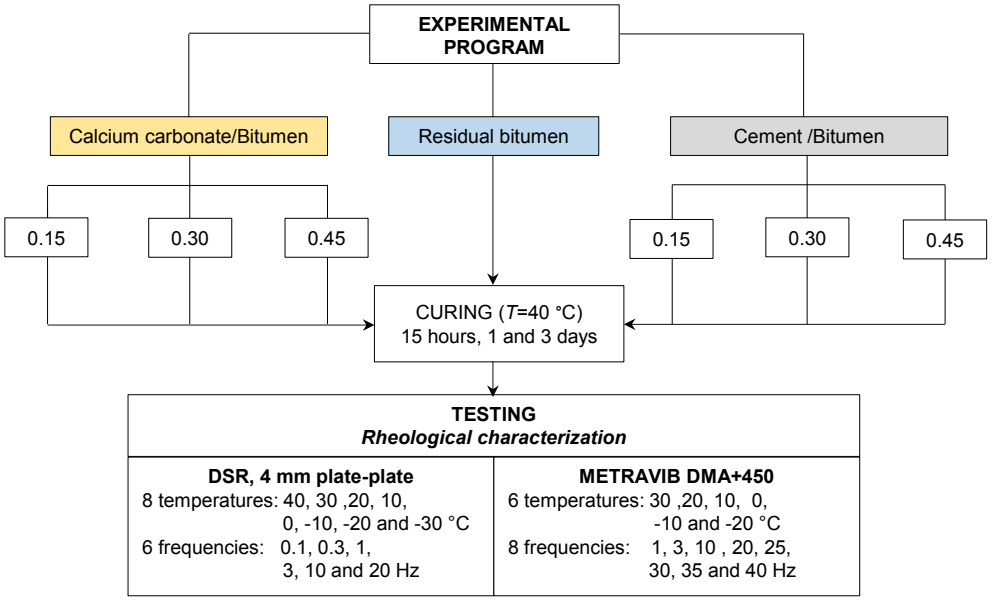


**Figure 16. 1** Experimental program.

A Dynamic Shear Rheometer (DSR) in plate-plate configuration was used to characterize the CBms in terms of complex shear modulus ($G^*$). Frequency sweep tests (plate diameter = 4 mm, gap = 1 mm) were performed by the application of sinusoidal load waves in the frequency range from 1 to 20 Hz (six frequencies: 0.1, 0.3, 1, 3, 10 and 20 Hz ) and in the temperature range from 40 to -30 °C (eight temperatures, 10 °C each step).
In addition, METRAVIB DMA+450 apparatus was adopted to measure the complex Young's modulus ($E^*$) of the studied CBms performing uniaxial cyclic tension-compression tests, in control strain mode. Mechanical tests were performed on CBm parallelepiped specimens applying a sinusoidal axial strain in the frequency range from 1 to 40 Hz (8 frequencies: 1, 3, 10, 20, 25, 30, 35 and 40 Hz) and in the temperature range from 30 to -20 °C (six temperatures, 10 °C each step).

Experimental activities were carried out *at Institut francais des Sciences et Technologies des Transports, de l' Amenagement et des Reseaux* - IFSTTAR (Nantes, France), during a visiting period of two months.

# 16.2 Materials and mastics

A cationic over-stabilized bitumen emulsion designated as C 60 B 10 [EN 13808] (**Table 6. 1**) was adopted to prepare cold bituminous mastics (CBms). Bitumen emulsion was stored in a climatic chamber at 40 °C during the experimental program in order to prevent premature breaking.
Two mineral additions (**Figure 16. 2**) were selected:

- Portland limestone cement II A/LL, strength class 42.5 R [UNI EN 197-1];
- Calcium carbonate, finely ground, $CaCO_3$.

Portland cement and calcium carbonate were the same mineral additions adopted for the production of cold bituminous mortars. Their physical properties in terms of Rigden voids and fineness (specific surface) are reported in **Table 14. 2**.
The selected mineral additions are extremely different considering the chemical point of view. Portland cement is a hydraulic binder and it reacts with water producing cementitious products that stiffen the material.
Nowadays, calcium carbonate filler and cement are also known as inactive and active fillers, respectively. The addition of the so-called "*active*" filler with the aim to improve the mechanical and durability properties to cold mixtures, is a common practice, especially during cold recycling operations (see Section 2.2 and 2.3)
However, if the breaking emulsion phenomenon is considered, both calcium carbonate filler and cement could be considered as active-filler because both promote the breaking of the bituminous emulsion (see Section 2.6.3).

**Figure 16. 2** Mineral additions: Portland cement and calcium carbonate.

Three different volumetric concertation ratios (volume of mineral addition over volume of bitumen) of mineral additions were considered for mastics preparation: 0.15, 0.30 and 0.45. These values were calculated starting from the mass concentration ratio (mass of mineral addition over mass of bitumen) and considering the particles densities of 1.02, 3.15 and 2.69 g/cm$^3$ for bitumen emulsion, cement and calcium carbonate, respectively.
The adopted volumetric concentration ratios aim to simulate the common composition of bituminous mastics that partially coat coarse aggregate in a cold bituminous mixture.
In addition, the residual bitumen (RB) obtained thought bitumen emulsion evaporation, was also tested using the same test procedures of CBms in order to achieve reference measurements. In fact, it represents the CBms at volumetric concentration ratio equal to zero.
CBms were coded using an alphanumeric code composed by letters referring to the types of mineral addition adopted (CEM or CC, for cement or calcium carbonate, respectively) and a number representing the concentration ratio (0.15, 0.30 or 0.45). Mastic composed only by the residual bitumen recovered from bitumen emulsion was coded as RB.
In addition, information regarding the curing time (15 hours, 1 day and three days) was also included into the CBms codification. For example, a CBm produced using cement at 0.15 of volumetric concentration ratio and cured for one day, is coded as CEM0.15-1d.
The list of CBms produced and tested during the experimental program is summarized in **Table 16. 1**.

| Mineral addition | Volumetric conc. ratio | Curing time [day] | Sample code [-] | Test performed |
|---|---|---|---|---|
| None | 0 | 15 h | RB-15h | DSR |
| | | 1 day | RB-1d | DSR+M |
| | | 3 days | RB-3d | DSR+M |
| Cement | 0.15 | 15 h | CEM0.15-15h | DSR |
| | | 1 day | CEM0.15-1d | DSR+M |
| | | 3 days | CEM0.15-3d | DSR+M |
| | 0.30 | 15 h | CEM0.30-15h | DSR |
| | | 1 day | CEM0.30-1d | DSR+M |
| | | 3 days | CEM0.30-3d | DSR+M |
| | 0.45 | 15 h | CEM0.45-15h | DSR |
| | | 1 day | CEM0.45-1d | DSR+M |
| | | 3 days | CEM0.45-3d | DSR+M |
| Calcium carbonate | 0.15 | 15 h | CC0.15-15h | DSR |
| | | 1 day | CC0.15-1d | DSR+M |
| | | 3 days | CC0.15-3d | DSR+M |
| | 0.30 | 15 h | CC0.30-15h | DSR |
| | | 1 day | CC0.30-1d | DSR+M |
| | | 3 days | CC0.30-3d | DSR+M |
| | 0.45 | 15 h | CC0.45-15h | DSR |
| | | 1 day | CC0.45-1d | DSR+M |
| | | 3 days | CC0.45-3d | DSR+M |

**Table 16. 1** Summary of CBm samples.

### 16.2.1 Production protocol of mastic samples

No standardized procedures are available in literature for the production of CBms. In the present experimental program, cement and calcium carbonate were dosed in a shallow container and firstly mixed by hand with bituminous emulsion and a little amount of water (about 25% of dry mineral addition weight) until obtaining an homogeneous compound without any lumps (**Figure 16. 3**).

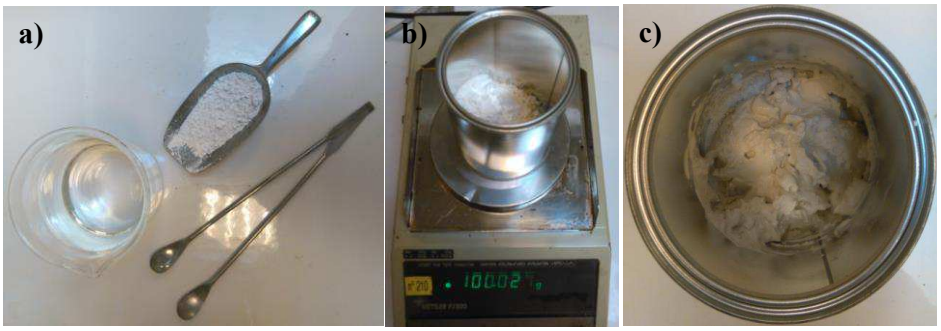


**Figure 16. 3** CBm sample production: a) and b) dosage of water and mineral addition (calcium carbonate); c) wet calcium carbonated mixed by hand.

Then a mechanical high-shear mixer was adopted for the second mixing phase. The lower rotation speed rate ranged from 191 to 222.3 rpm was selected in order to avoid the premature emulsion breaking during mixing (**Figure 16. 4**a).
CBms were mixed continuously for one hour using the mechanical mixer at room temperature and sampled at the end of mixing phase. Sedimentation phenomena were checked exclusively by visual observations.
After mixing, CBms were poured in silicone molds with different dimensions (**Figure 16. 4**b). In particular, samples should be characterized by flat surface in order to simplify the cutting phase during the production of specimens for Metravib tests (**Figure 16. 5**a). The decision to produce small size test samples has permitted to avoid separation between materials characterized by different densities and obtain homogenous specimens for rheological laboratory testing.

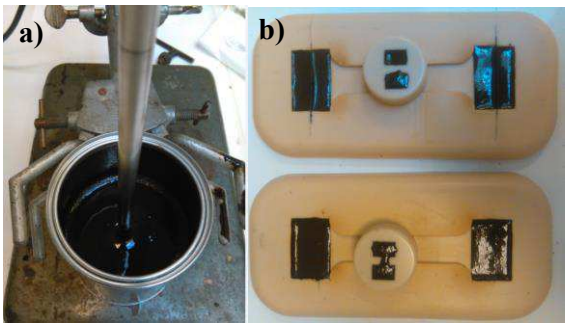


**Figure 16. 4** CBm sample production: a) mechanical mixing of CBm sample; b) Cbm sample poured in silicone mold immediately after mixing.

Then, produced CBm samples are cured in a controlled climatic chamber at 40 °C for different curing times (**Table 16. 1**), with the aim to allow evaporation of the water phase in bitumen emulsion. Immediately after the selected curing period, CBms are stored overnight in the freezer to facilitate the following cutting phase of CBm specimens.
The day after, small CBm pieces were cut off from the bigger cured CBm sample. For DSR testing, a definite shape of the cutted CBm specimens is not required (**Figure 16. 5**b). Differently, CBm specimens for Metravib testing were obtained cutting in accurate manner the bigger CBm samples. Small parallelepiped CBm specimens (**Figure 16. 5**c) are necessary to perform Metravib testing; particular attention should be taken to fix the proportions among the three parallelepiped dimensions in order to avoid any problems during data acquisition phase. CBm specimens for both DSR and Metravib testing were stored in freezer before rheological tests were performed. This procedure was necessary to block the curing phenomenon.

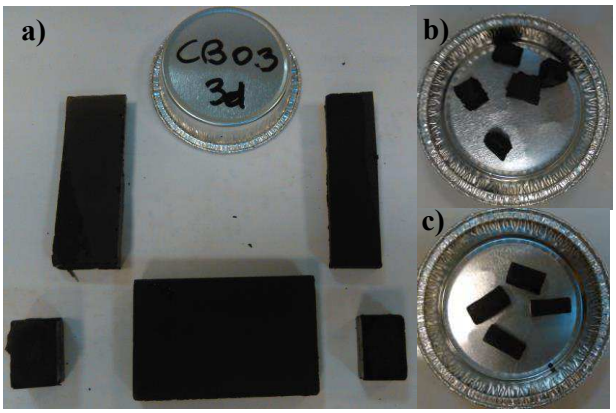


**Figure 16. 5** CBm sample production: a) cured CBm samples with flat surface; b) CBm specimens for DSR testing and c) Parallelepiped CBm specimens for Metravib testing.

## 16.3 Laboratory equipment, test methods and data analysis

The produced cold bituminous mastics are characterized in terms of rheological properties measuring the complex Young's modulus ($E^*$) and complex shear modulus ($G^*$) employing Dynamic shear rheometer device and Metravib apparatus, respectively.
Tests were carried out in *controlled strain* mode, reducing the strain level in order to perform measurements in linear viscoelastic (LVE) domain.

Both DSR device and Metravib apparatus systems are based on *Dynamic Mechanical Analysis* (DMA) that consists of applying a vibration of known amplitude and frequency on a specimen. Measurements of the applied displacement and the resulting force lead to a precise determination of LVE properties, such as $E^*$ and $G^*$, depending on the deformation mode considered.
DMA is a very widespread characterization technique employed to control mechanical performances and temperature influence on the mechanical properties of materials.
Measurements in LVE domain are carried out using DSR equipment in shear strain control mode and fixing the shear strain limit equal to 0.01 %.
Regarding Metravib tests, the strain control mode consists in fixing the applied deformation lower than 2 μm that corresponds to about 1 microstrain whether CBm specimens with an average height of 15 mm are tested.
Measurements of rheological properties were carried out on two replicates specimen for both DSR and Metravib testing.

### 16.3.1 Kinexus Pro+ dynamic shear rheometer

The Dynamic Shear Rheometer (DSR) can be used to determine and characterize rheological properties, in order to identify the viscous and elastic behavior of bituminous materials (see Section 2.10 "*Viscoelastic properties*").
In this research study, the Melvran Kinexus Pro$^+$ rheometer (**Figure 16. 6**) was used to perform many rheological investigations.

When used for testing bituminous materials, the DSR measures the rheological properties (e.g. complex shear modulus, phase angle) at low, intermediate and high temperatures. The test can be performed in control strain or control stress mode.
In particular, it allows the application of oscillatory or continuous shear sinusoidal loading stress or strain, characterized by a given amplitude and frequency.
In details, the sinusoidal loads should simulate the effect induced in the pavement by the intermittent passage of traffic. The different vehicles speed can be reproduced through the adoption of different loading frequencies. Usually, the frequency is set to 1.59 Hz (10 rad/s), since this value corresponds to a loading time of 0.1 s that represents a reference value in laboratory for all the tests aimed at simulating the effects caused by traffic on pavements [Christensen and Anderson, 1992].
Two main geometric configurations are usually employed: the plate-plate configuration or the cone-plate configuration depending on the type of measurements required. For the purposes of this study, only the plate-plate configuration was used to carry out oscillatory tests in control strain mode.
The distance between the plates is maintained constant and is referred as gap. The gap has to be appropriately determined according to the type of material to be tested; in general, it should be at least 5 times larger than the maximum size of the particles contained in the specimen, in order to avoid interferences between the system and the sample and in particular errors in measurement.


**Figure 16. 6** Melvran Kinexus Pro$^{+}$ rheometer: a) closed active hoods configuration and b) open active hoods configuration.

DSR Kinexus Pro+ is equipped with Peltier Plate Cartridge that ensures to achieve temperature control requirements. In addition, DSR device is also equipped with Active Hood Cartridge (**Figure 16. 6**) that allows to minimize thermal gradients for plate measuring systems. This is particularly suggested during the testing of highly thermally-sensitive samples, and for temperature-critical testing that means where the temperature range is significantly above or below ambient temperature.

*4mm plate-plate configuration system for frequency sweep test*
The principle used with DSR device is to apply sinusoidal, oscillatory stresses under shear-strain control mode, over a range of temperatures and loading frequencies, to a thin disc of CBm, which is sandwiched between a fixed plate and a moving plate that oscillates back and forth (**Figure 16. 7**). In this study, the measuring system configuration employed was 4mm plate-plate with a 1 mm of testing gap. The 4 mm plate-plate configuration is usually adopted to characterize materials at low temperatures range.

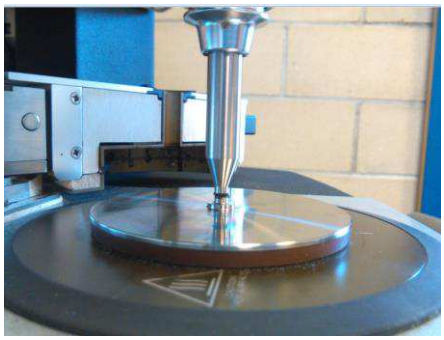

**Figure 16. 7** Measuring system configuration: 4 mm plate-plate.

*Specimens preparation*
The CBM specimens are little piece of CBm with a diameter equal to the oscillating plates and a height equal to the gap. They are prepared according to the procedure explained in Section 16.2.1. After the storage at low temperature, the material is left at ambient temperature for at least 5 minutes to warm up. Then, it is placed between the two DSR parallel plates to be tested (
**Figure 16. 8**). Prior to start the test, the trimming of the edge specimen through a spatulas is needed in order to remove the bitumen in excess and obtain a specimen with the required dimensions (**Figure 16. 7**).
The test configuration, the loading steps and the setting of the equipment can be controlled through the software RHEOPLUS associated to the DSR instrument. In particular, all the tests carried out with the DSR provided two fundamental steps:

- a conditioning phase of 10 minutes at the test temperature to allow the specimen to reach the desired temperature homogeneously. In this step, no loads are applied;
- a loading phase where the different loading conditions are applied, depending on the type of test performed.

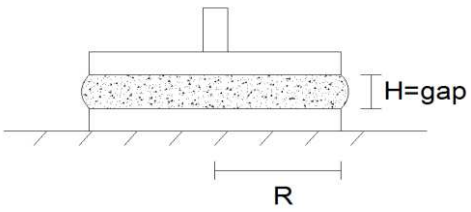

**Figure 16. 8** Schematic representation of the plate-plate configuration.

## 16.3.2 METRAVIB DMA+450

The Metravib DMA+450 (**Figure 16. 9**) may be used to characterize the LVE properties of different materials.
Metravib DMA+450 is composed by very rigid frames that exhibit high ranges of measurable stiffness and frequency.
Based on a wide range of specimen loading holders, DMA+450 can analyze a large variety of materials and specimen dimensions. Selecting the appropriate specimen-holder, it allows the instrument to be adapted to:

- different excitation modes (tension, compression, bending, shear);
- physical state of the material (solid, paste, liquid);
- different specimen dimensions (plates, cylinders, films, fibers, gels, foams, etc.);
- the expected state of the material during the analysis (glassy state, glass transition, rubbery state, hardening, fluidizing, melting, etc.).

In addition, DMA+450 include Metravib's software DYNATEST, which has been specifically developed to manage the instruments and perform data acquisition and processing.
Many test modes are available in order to analyze LVE material properties, taking into account their dependence from different parameters (temperature, excitation frequency, strain, force, time, mechanical or thermal history, etc.).


**Figure 16. 9** Metravib DMA+450 apparatus.

*Tension-Compression testing*

In this experimental study, Metravib DMA+450 was used to characterize the rheological response of cold bituminous mastics performing uniaxial cyclic tension-compression tests in control strain mode.

For each produced CBms, mechanical performances were evaluated on parallelepiped specimens (**Figure 16. 5**). The dimensions of each specimen are around 10, 5 and 4 mm for height, length and thickness, respectively. The parallelepiped specimen should be straight as much as possible because each small errors during specimens preparation can affect the goodness of the measurement. In addition, it is important to highlight that the size and the geometry of specimen are fundamental to avoid problems during the test. In fact, if the material to be tested is too stiff and the Metravib DMA+450 apparatus reaches its operating limit ($E^*$ = 3E+12 Pa), the specimen size should be reduced to decrease the stiffness of the material to be tested.

*Testing procedure*

Test settings with Metravib DMA+450 device comprised the following steps:

- Installation of the loading holders for tension-compression tests (**Figure 16. 10**a and b);
- Test setting parameters were added in the software DYNATEST: temperatures, commutation between air and nitrogen, frequencies, limit for the deformation control mode, sensor type and dimensions of the specimen to be tested. Temperature was controlled fixing a commutation air/nitrogen equal to 10/150 °C; it means that, with temperatures higher or equal to 10 °C, temperature stability was guaranteed using potassium solution while, with temperatures lower than 10 °C, temperature stability was obtained using an apparatus equipped with nitrogen liquid. The speed rate for the heating phase was equal to 0.5 °C/min, from 0 up to 30 °C, and for the cooling phase was equal to -0.2 °C/min, from 0 up to -20 °C. The conditioning time selected to reach the temperature stability was 15 minutes;
- The high frequencies (HF) sensor was adopted because more suitable for testing stiffer material such as CBm produced with cement addition.
- Each specimen was glued in both upper and lower edges using a cyanoacrylate glue. After this step, a careful check of the efficiency of the gluing should be done;
- The upper loading holder was approached slowly to the specimen until reaching contact. Then, frames should be blocked using two knobs (**Figure 16. 10**c and d);
- Thermal hood was placed in order to avoid any thermal gradients during the test (**Figure 16. 11**);
- Test can be run after verifying the thermal apparatus.

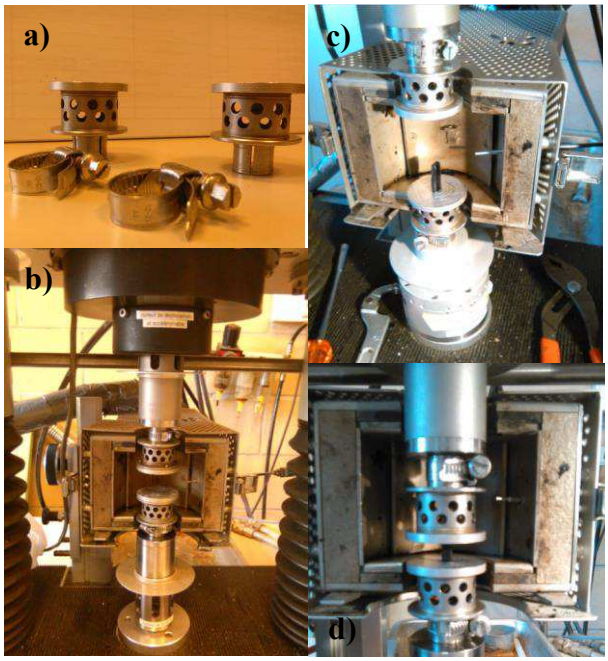


**Figure 16. 10** Metravib DMA+450 device, testing procedure: a) loading specimen-holders for tension-compression tests; b) installation of loading specimen-holders; c) specimen glued and approaching of loading specimen-holders and d) loading holders are in contact with specimen.


**Figure 16. 11** Metravib DMA+450 device, testing procedure: placing of thermal hood.

### 16.3.3 Rheological data analysis: DSR and Metravib measurements

Rheological properties of the produced CBms were evaluated in terms of complex Young's modulus ($E^*$) and complex shear modulus ($G^*$) performing DSR and Metravib testing, respectively.

Both *E** and *G** measurements were carried out on two CBm replicate specimens starting from the higher to the lower test temperatures in order to avoid specimen damage that can occur during tests at low temperatures.

*DSR rheological measurements*
As described above, the most typical geometric configuration used by the DSR is the plate-plate configuration where sample is sandwiched between two metal parallel plates. One is fixed, whereas the other one can rotate and is able to apply sinusoidal loading waves described as follows:

$$\tau = \tau_0 \cdot sin(\omega t) \tag{96}$$

where $\tau$ is the shear stress, $\tau_0$ is the amplitude of the stress, $\omega$ is the angular frequency and t is the time.

The material reacts to this loading action with a response that is sinusoidal itself and characterized by the same frequency of loading wave, but with a time lag equal to δ:

$$\gamma = \gamma_0 \cdot \mathrm{sen}(\omega t - \delta) \tag{97}$$

In this way, it is possible to characterize the material behavior through its stiffness properties. In particular, the complex shear modulus *G** can be determined according to the following relationship:

$$G^*(\omega) = \frac{\tau^*(t)}{\gamma^*(t)} \tag{98}$$

where
$$\tau^*(t) = \tau_0 \cdot [\cos(\omega t) + i \cdot \sin(\omega t)]$$
$$\gamma^*(t) = \gamma_0 \cdot [\cos(\omega t - \delta) + i \cdot \sin(\omega t - \delta)]$$

By substituting these expressions (periodic sinusoidal loads) in the previous equation, the following form can be obtained:

$$G^*(\omega) = \frac{\tau_0}{\gamma_0} e^{i\delta} \tag{99}$$

This equation represents a complex number with an absolute value equal to the ratio between the maximum amplitude ($|G^*|$ or $G_0$) of the applied stress and the maximum amplitude of the corresponding strain. Based on what introduced so far, it is worth noting that the complex modulus *G** is independent on the loading time, but is function of temperature, frequency and stress/strain level (if the linear viscoelastic limit of the material is exceeded).

The *frequency sweep test* is one of the most common test performed by means of the DSR and is used for determining the LVE properties of undamaged bituminous samples. The test procedure provides the application of a constant load over a range of loading frequency.
The test is carried out at various temperature values to ensure the application of the Time-Temperature Superposition Principle (TTSP). The application of TTSP was previously

described in Section 6.2.3, for the thermo-rheological characterization of cold mixtures where rheological properties are represented by complex Young's modulus ($E^*$).
Based on the TTSP, the data measured at each temperature are horizontally shifted and aligned to the data measured at the selected reference temperature (**Figure 16. 12**).

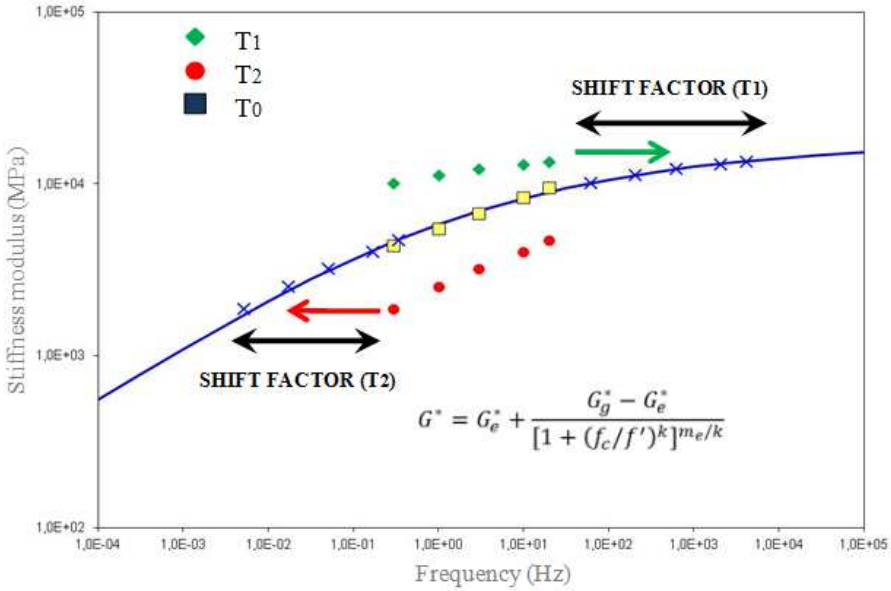


**Figure 16. 12** Time-Temperature Superposition principle: schematic representation

Thus, the obtained master curve describes the rheological behavior of a material at a specific temperature and represents the trend of a rheological property as a function of loading frequency.
Also in this case, the Williams-Landel-Ferry (WLF) equation [Williams et al., 1955] was assumed as variation law for the shift factors.
The following rheological model (**Figure 16. 13**) was used to represent the complex shear modulus $G^*$ as function of reduced frequency [Bahia et al., 2001]:

$$G^* = G_e^* + \frac{G_g^* - G_e^*}{\left[1+(f_c/f')^k\right]^{m_e/k}} \quad (100)$$

where:

$G_e^*$ = equilibrium complex modulus, measured for frequencies close to zero. It is equal to zero for bitumens;
$G_g^*$ = glassy complex modulus, measured for very high frequencies, it is assumed equal to 1 GPa for bitumens;
$f'$ = reduced frequency, function of temperature and strain [Hz];
$f_c$ = location parameter with dimensions of frequency;

$k, m_e$ = shape parameters, dimensionless.

Also the relationship between phase angle and reduced frequency can be modeled through the formulation proposed by Bahia et al (2001):

$$\delta = 90I - (90I - \delta_m)\left\{1 + \left[\frac{\log(f_d/f')}{R_d}\right]^2\right\}^{-m_d/2} \quad (101)$$

where:

$\delta_m$ = phase angle at $f_d$, the value at inflection;
$f'$ = reduced frequency;
$f_d$ = location parameter with dimensions of frequency;
$R_d, m_d$ = shape parameters;
$I$ = 0 if $f > f_d$
=1 if $f \leq f_d$

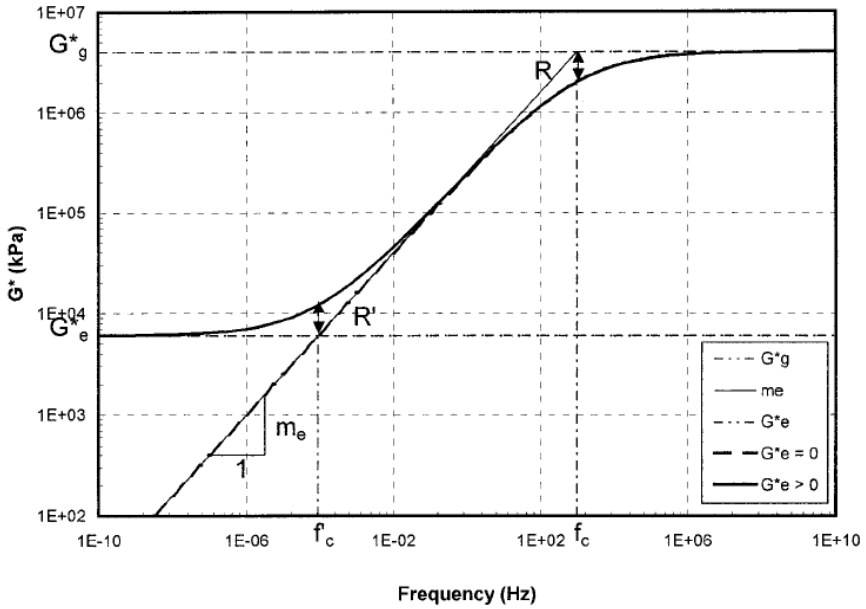


**Figure 16. 13** Complex modulus representation as a function of frequency [Bahia et al., 2001]

*Metravib rheological measurements*
Uniaxial cyclic compression tests were performed using the Metravib DMA+450 testing equipment, in control strain mode.
A sinusoidal (haversine) axial strain with 2 µm amplitude (peak-to-peak) was applied to CBm parallelepiped specimens characterized by controlled size.

According to the specimen size employed, Metravib apparatus adjusted the amplitude of the sinusoidal axial strain obtaining about 1 με as resulted amplitude (peak-to-peak).
A total of 10 load cycles were applied at each frequency in order to measure complex Young's modulus $E^*$.
Each $E^*$ measurement obtained at various temperatures was shifted at a selected reference temperature to verify the applicability of the Time-Temperature Superposition Principle (TTSP). The application of TTSP was previously described in Section 5.2.3.
Thus, the obtained master curve describes the rheological behavior of a material at a specific temperature and represents the trend of a rheological property as a function of loading frequency. Also in this case, the Williams-Landel-Ferry (WLF) equation [Williams et al., 1955] was assumed as variation law for the shift factors.
In order to compare the rheological modelling carried out on DRS results and Metravib results, the same rheological model of Bahia et al. (2001) was adopted during the analysis. Obviously, the rheological model was converted in terms of $E^*$ instead of $G^*$.

# 16.4 Experimental findings: complex shear modulus *G**

## 16.4.1 Effect of curing process

From **Figure 16. 14** to **Figure 16. 16**, the norm of the complex shear modulus ($|G^*|$) is represented as a function of $\delta_G$ (Black space) for residual bitumen (RB) and all CBms (CC0.15, CC0.3, CC0.45) cured for 15 hours, one day and three days.
As it can be observed from **Figure 16. 14**, the rheological behavior of RB was independent from curing time. Specifically, measurements ranged from 21 kPa to 368150 kPa and from 76° to 5.24 °C for $G_0$ and $\delta_G$, respectively. It is also important to highlight that the rheological behavior detected for RB was very close to that usually observed for plain bitumen.
For further analysis, results carried out on RB cured for one day are used as reference.

From **Figure 16. 15**a, it can be noted that CC0.15 at any curing times exhibited a mechanical behavior very close to that achieved with RB cured for one day. $|G^*|$ and $\delta_G$ ranged from 470450 kPa to 14 kPa and from 6° to 69° at low and high temperatures, respectively. Focusing in high temperatures range, it can also be observed that increasing curing time, phase angle slightly decreased and $|G^*|$ was almost constant.
Considering mastic CC0.3 (**Figure 16. 15**b), at low temperatures longer curing times caused an increasing in $|G^*|$, from 304300 kPa to 876600 kPa for CC0.3-15h and CC0.3-1d, respectively and phase angle was almost constant ($\delta_G = 7\,°$). Differently, at high temperatures, the increasing in curing time induced lower $\delta_G$ but $|G^*|$ almost constant: $\delta_G$ ranged from 69 ° to 60 ° for CC0.3-15h and CC0.3-1d, and $|G^*|$ of about 22 kPa. After three days of curing, $|G^*|$ was almost equal to that measured with CC0.3-1d but the phase angle detected at high temperature increased up to 71 °.
Analyzing the higher volumetric concentration ratio for CBms produced with calcium carbonate, CC0.45 cured at three different curing time, is characterized by two opposite trends (**Figure 16. 15**c). CC0.45-1d and CC0.45-3d mastics exhibited equal measurements in terms of $|G^*|$ that ranged from 848000 kPa to 83 kPa at low and high temperatures, respectively. Regarding the phase angle, the same observation can be drawn for CC0.45-1d and CC0.45-3d at low temperatures ($\delta_G = 7\,°$) while, at high temperatures the increasing in

curing time induced higher phase angle, from 66 ° to 72 ° for CC0.45-1d and CC0.45-3d, respectively.
Reducing the curing time at 15 hours, both $|G^*|$ and $\delta_G$ decreased at both low and high temperatures. CC0.45-15h is characterized by $|G^*|$ ranged from 98900 kPa to 47 kPa and phase angle ranged from 25 ° to 48 °.
In conclusion, considering CBms produced with calcium carbonate: at low volumetric concentration (0.15), the increasing in curing time induced a decreasing in phase angle and norm of complex shear modulus almost constant. At high volumetric concentration (0.45), the observed behavior was completely reversed.

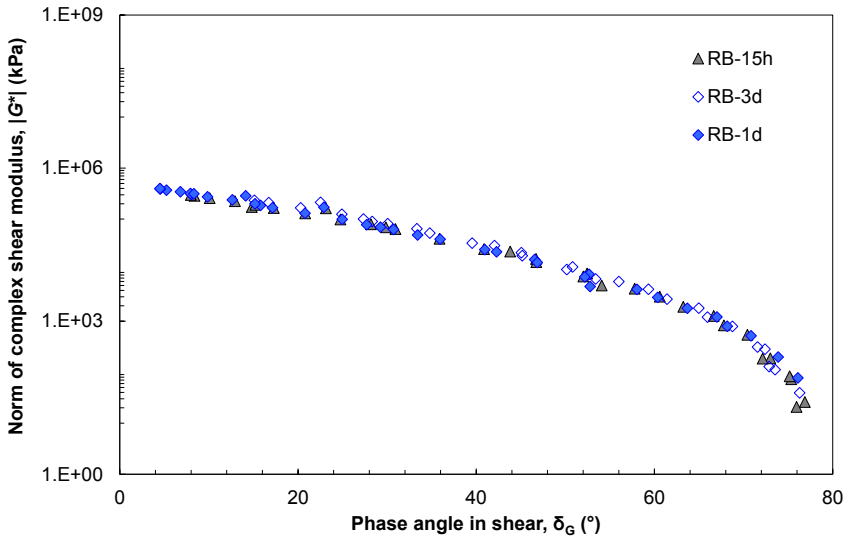


**Figure 16. 14** Measured values of $|G^*|$ and $\delta_G$ represented in the Black space for residual bitumen (RB) cured at 15 hours, one and three days.

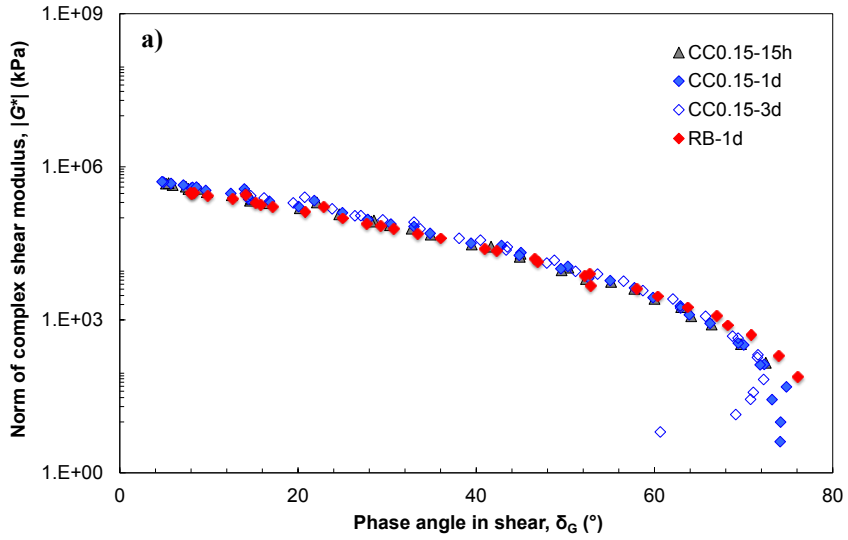
a)
CC0.15-15h
CC0.15-1d
CC0.15-3d
RB-1d
Norm of complex shear modulus, |G*| (kPa)
1.E+09
1.E+06
1.E+03
1.E+00
0
20
40
60
80
Phase angle in shear, δG (°)

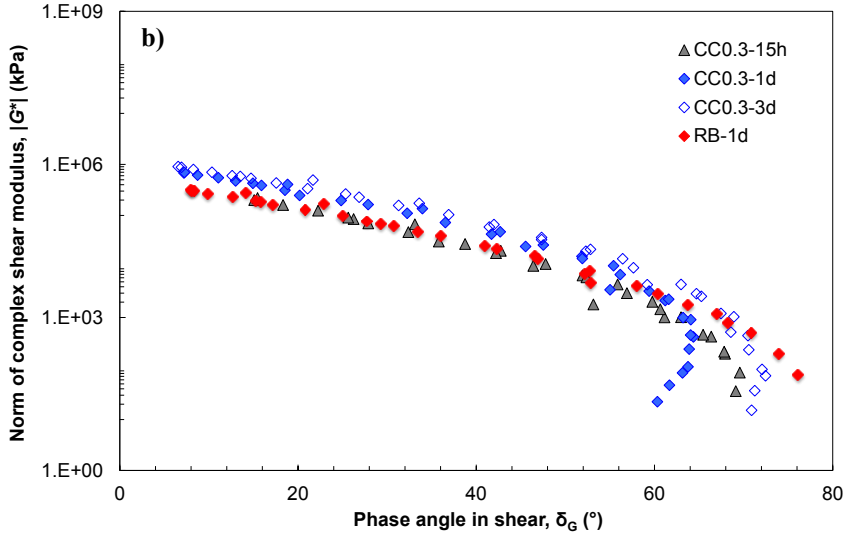
b)
CC0.3-15h
CC0.3-1d
CC0.3-3d
RB-1d
Norm of complex shear modulus, |G*| (kPa)
1.E+09
1.E+06
1.E+03
1.E+00
0
20
40
60
80
Phase angle in shear, δG (°)

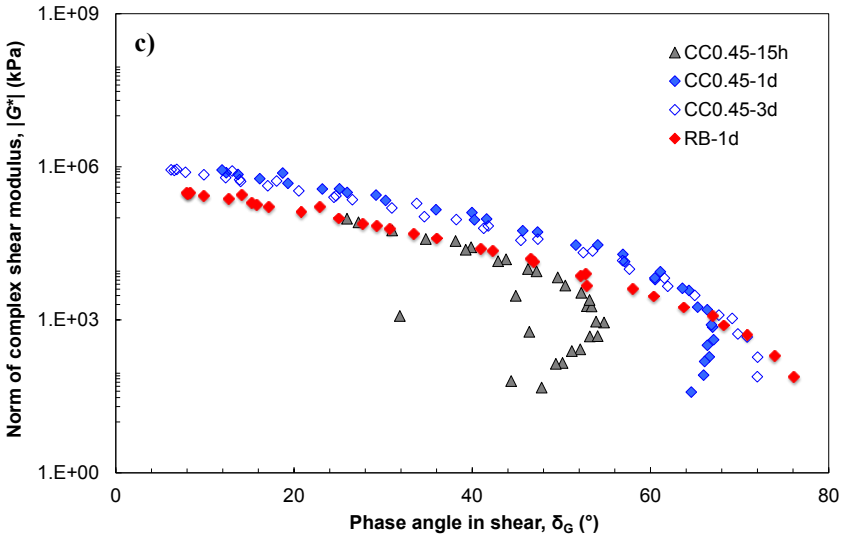


**Figure 16. 15** DSR measured values of $|G^*|$ and $\delta_G$ represented in the Black space for CBms cured at 15 hours, one and three days: a) CC0.15; b) CC0.3 and c) CC0.45.

In the same manner, $G^*$ measurements can be analyzed for CBms produced with cement as mineral addition.

From **Figure 16. 16**a, it can be noted that at low temperatures, CEM0.15 exhibited the same $G^*$ at any curing times; in fact $|G^*|$ and $\delta_G$ were 640450 kPa and 5 °, respectively. Focusing in high temperatures range, it can also be observed that increasing curing time, $|G^*|$ and $\delta_G$ slightly increased from 80 kPa to 124 kPa and from 40 ° to 44° for CEM0.15-15h and CEM0.15-3d, respectively.

Considering mastic CEM0.3 (**Figure 16. 16**b), at low temperatures curing time did not affect both $|G^*|$ and $\delta_G$ that were about 842600 kPa and 4 °. Differently, at high temperatures, the increasing in curing time induced lower $\delta_G$: it decreased from 40 ° to 27° for CEM0.3-15h and CEM0.3-3d, respectively and the measured $|G^*|$ was almost constant: it ranged from 1117 kPa to 1076 kPa for CEM0.3-15h and CEM0.3-3d, respectively.

Analyzing the higher volumetric concentration ratio for CBms produced with cement (Figure 16. **15**c), at low temperatures both $|G^*|$ and $\delta_G$ detected for CEM0.45 seemed to be independent from the curing time: $|G^*|$ was about 1000700 kPa and $\delta_G$ was about 4°. In addition, at high temperatures range, the increasing in curing time produced a shifting of phase angle towards higher values and a slightly decrease in $|G^*|$. In fact, phase angle increased from 12 ° to 24 ° and $|G^*|$ decreased from 10800 kPa to 3450 kPa for CEM0.45-15h and CEM0.45-3d, respectively.

In conclusion, considering CBms produced with cement: at low volumetric concentration (0.15), the increasing in curing time caused small increases in both norm of complex shear modulus and phase angle. At high volumetric concentration (0.45), the curing time did not

affect the rheological properties in low temperatures range but at high temperatures, the increasing in curing time produced lower $|G^*|$ and higher $\delta_G$ values.

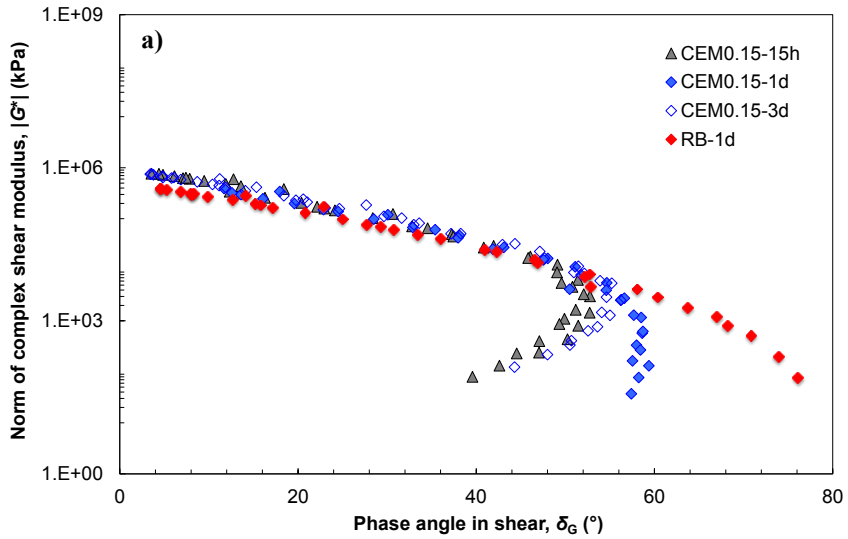


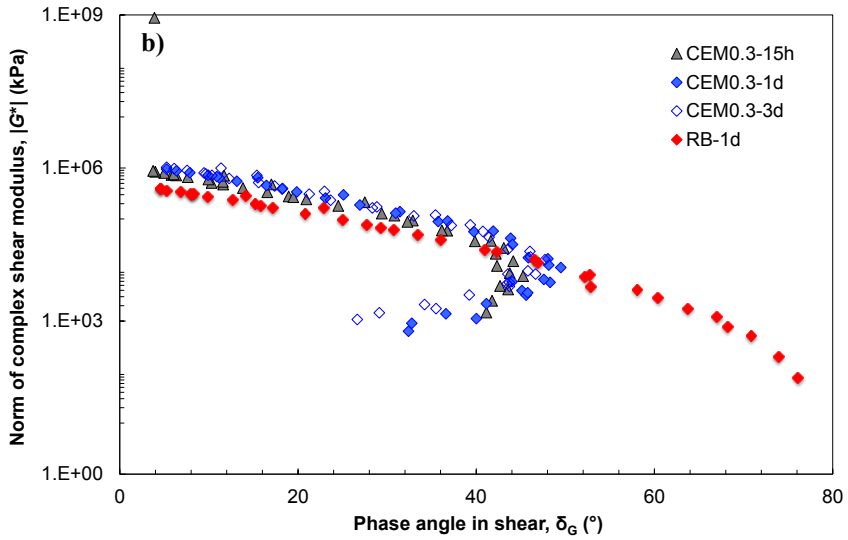

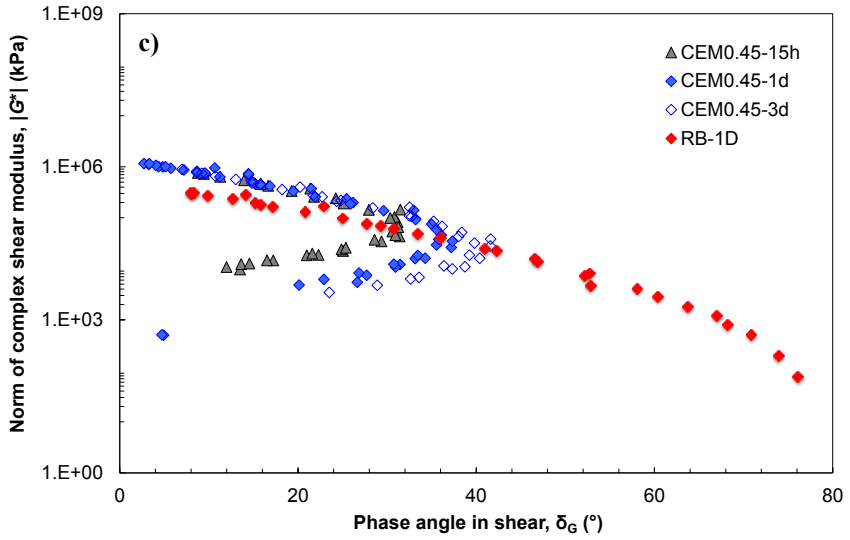


**Figure 16. 16** DSR measured values of $|G^*|$ and $\delta_G$ represented in the Black space for CBms cured at 15 hours, one and three days: a) CEM0.15; b) CEM 0.3 and c) CEM 0.45.

## 16.4.2 Effect of volumetric concentration ratio

In **Figure 16. 17**, CBms produced at different volumetric concentration ratios (0.15, 0.3 and 0.45) with calcium carbonate or cement and cured for 1 or 3 days are compared using Black space in order to analyze the effect of volumetric concentration ratio.
Results obtained on RB cured one day are added in the comparison as reference values.
Considering CBms produced with calcium carbonate, after one day of curing the increasing in volumetric concentration ratio induced a reduction in phase angle and a small increase in $|G^*|$ at high temperatures. At low temperatures, both $|G^*|$ and $\delta_G$ are almost constant (**Figure 16. 17**a). Differently, after three days of curing the effect of volumetric concentration ratio disappeared (**Figure 16. 17**b).
Analyzing CEM mastics, the effect of volumetric concentration ratio is marked at both selected curing times. At low temperatures, this variable seems not affect the rheological properties of the material at both curing times (**Figure 16. 17**c and d). Differently, at high temperatures and both curing times, an increasing in volumetric concentration ratio strongly influenced the mechanical behavior of CEM mastics: lower $\delta_G$ and higher $|G^*|$.
In particular, $|G^*|$ ranged from 37 kPa to 4800 kPa and $\delta_G$ ranged from 57 ° to 20 ° for CEM0.15-1d and CEM0.45-1d, respectively and after three days of curing, $|G^*|$ ranged from 124 kPa to 2795 kPa and $\delta_G$ ranged from 44 ° to 21 ° for CEM0.15-3d to CEM0.45-3d, respectively.

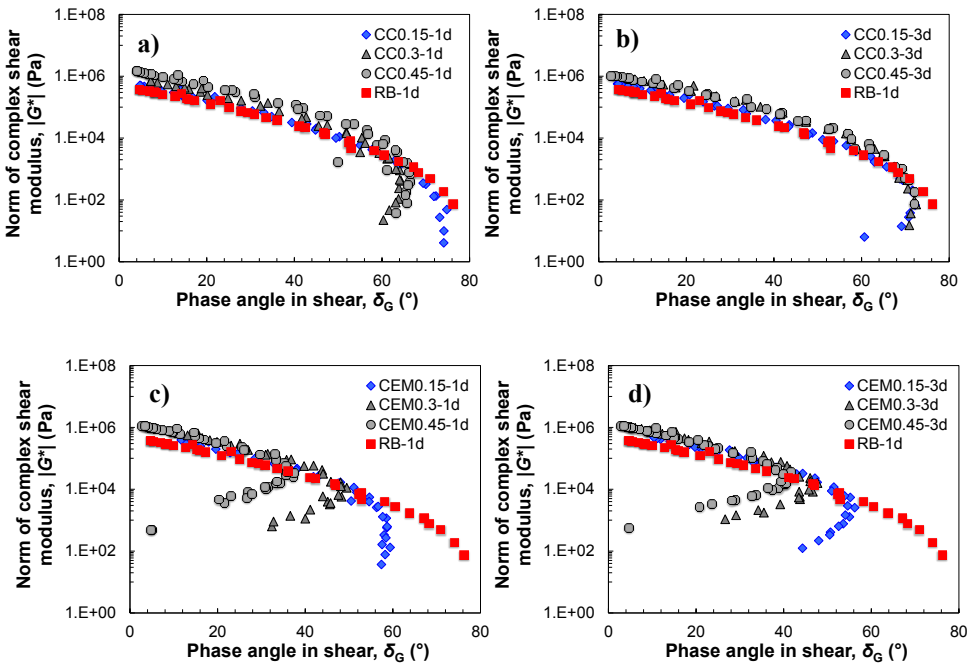


**Figure 16. 17** DSR measured values of $|G^*|$ and $\delta_G$ represented in the Black space for CBms produced at different volumetric concentration ratios (0.15, 0.3 and 0.45): a) CC cured one day; b) CC cured three days; c) CEM cured one day and d) CEM cured three days.

## 16.4.3 Effect of mineral addition type

In **Figure 16. 18**, CBms produced at fixed volumetric concentration ratio (0.3) with calcium carbonate or cement and cured for 1 and 3 days are compared using Black space with the aim to evaluate the effect of the type of mineral addition.

At low temperatures, no evident differences can be noted for all the considered CBms and curing times. Increasing temperature, at both curing times a transition of the mechanical behavior of the material were observed, when cement was used in CBms production. In fact, rheological properties are shifted from those usually detected testing a liquid-like material (viscous material, e.g. bitumen) i.e. reduced storage modulus ($G_1$) and higher loss modulus ($G_2$), to those achieved testing a solid-like material (elastic material, e.g. mixture) i.e. higher storage modulus ($G_1$) and reduced loss modulus ($G_2$).

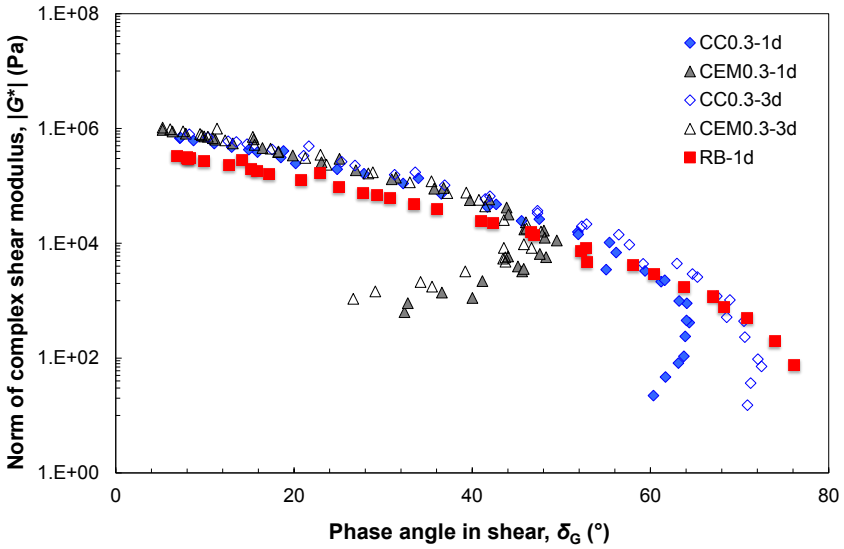


**Figure 16. 18** DSR measured values of $|G^*|$ and $\delta_G$ represented in the Black space for CC0.3 and CEM0.3 cured for one and three days.

# 16.5 Experimental findings: complex Young's modulus *E**

## 16.5.1 Effect of curing process

In **Figure 16. 19** and **Figure 16. 20**, the norm of the complex Young's modulus ($|E^*|$) is represented as a function of $\delta_E$ (Black space) for CBms (CC0.15, CC0.3, CC0.45) cured for one day and three days.

As described above, Metravib testing did not investigate 15 hours of curing time and RB mastic because for both, problems regarding the production of CBm parallelepiped specimens related to material physical state were detected.

From **Figure 16. 19**a, it can be noted that CC0.15 exhibited a mechanical behavior totally independent from the curing time, at low temperatures. $|E^*|$ and $\delta_E$were almost equal to 2025780 MPa and 7 °, respectively. Focusing in high temperatures range, it can also be observed that increasing curing time, both $|E^*|$ and $\delta_E$slightly increased: $|E^*|$ ranged from 3872 MPa to 6050 MPa and $\delta_E$ ranged from 60 ° to 65 ° for CC0.15-1d and CC0.15-3d, respectively.

Considering mastic CC0.3 (**Figure 16. 19**b), at both low and high temperatures, curing time did not affect $E^*$. $|E^*|$ ranged from 1041400 MPa to 602 MPa and $\delta_E$ ranged from 25 ° to 53 ° at low and high temperatures, respectively.

Analyzing the higher volumetric concentration ratio for CBms produced with calcium carbonate, CC0.45 cured at both curing times, were characterized by a constant behavior of both $|E^*|$ and $\delta_E$ at low temperatures (**Figure 16. 19**c). $|E^*|$ and $\delta_E$ were about 2211720 MPa and 13 °, respectively. Differently, at high temperatures the increasing in curing time

produced higher values of phase angle, from 64 ° to 67 ° for CC0.45-1d and CC0.45-3d, respectively and |*E**| almost constant over time (2014 MPa).
According to obtained results, it can be concluded that: at low volumetric concentration (0.15), curing time did not induce changings in rheological properties and at high volumetric concentration (0.45) and considering high temperatures range, after three days of curing a small increase in phase angle was observed.

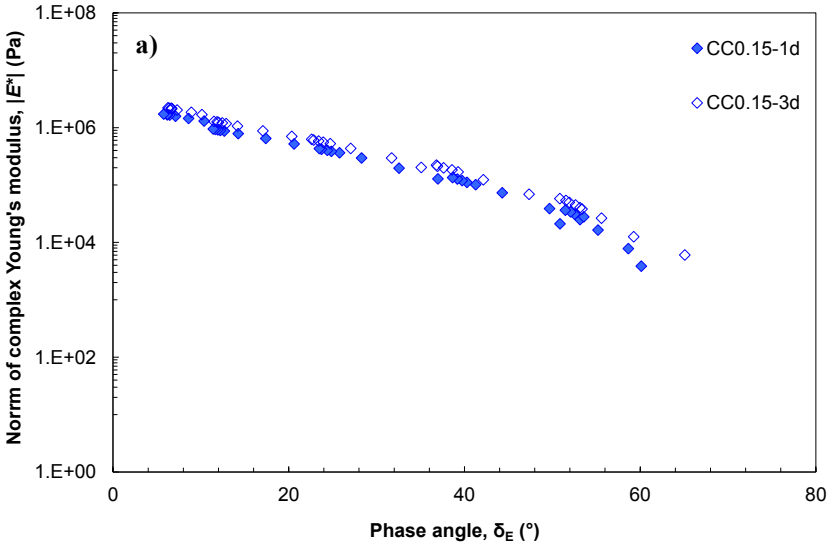


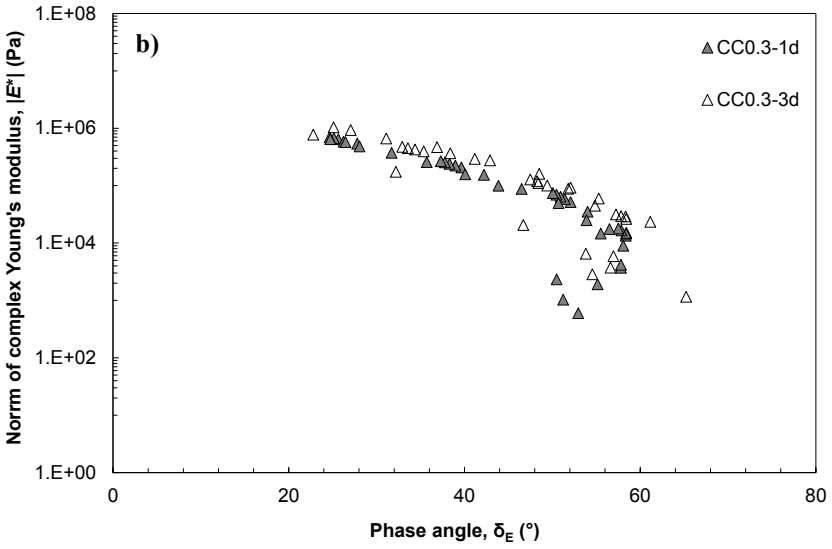

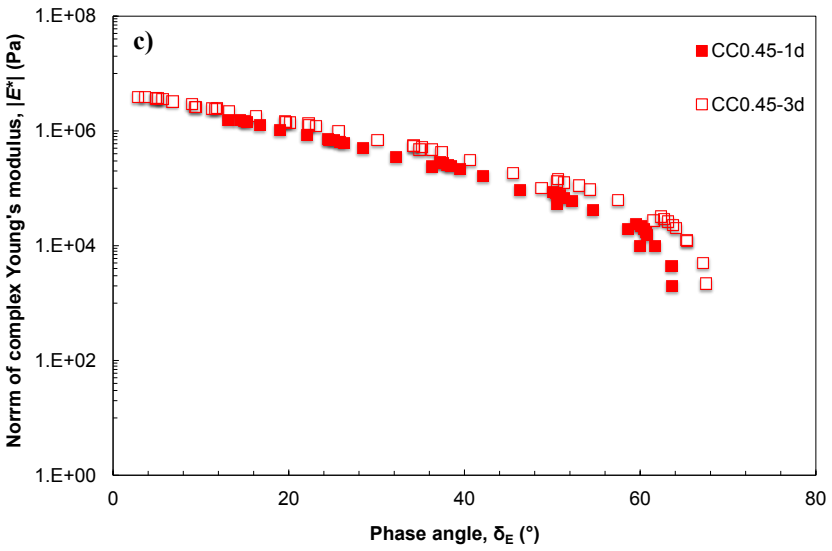


**Figure 16. 19** Metravib measured values of $|E^*|$ and $\delta_E$ represented in the Black space for CBms cured at one and three days: a) CC0.15; b) CC0.3 and c) CC0.45.

In the same manner, $E^*$ measurements can be analyzed for CBms produced with cement as mineral addition and cured for one and three days.

From **Figure 16. 20**a, it can be noted that at low temperatures, CEM0.15 exhibited the same $E^*$ at any curing times; in fact $|E^*|$ and $\delta_E$ were 3123800 MPa and 2 °, respectively. Focusing in high temperatures range, it can also be observed that increasing curing time, $|E^*|$ and $\delta_E$ slightly increased from 2747 MPa to 5400 MPa and from 58 ° to 60° for CEM0.15-1d and CEM0.15-3d, respectively.

Considering mastic CEM0.3 (**Figure 16. 20**b), at low temperatures curing time slightly affected both $|E^*|$ and $\delta_E$ that were about 2008150 MPa and 6 °, respectively. Differently, at high temperatures, the increasing in curing time induced marked effect on $\delta_E$: it ranged from 38 ° to 52 ° for CEM0.3-1d and CEM0.3-3d, respectively; $|E^*|$ was almost constant (24315 MPa).

Analyzing the higher volumetric concentration ratio for CBms produced with cement (**Figure 16. 20**c), at low temperatures both $|E^*|$ and $\delta_E$ detected for CEM0.45 seemed to be independent from the curing time: $|E^*|$ was about 205660 MPa and $\delta_E$ was about 13°. In addition, at high temperatures range, the increasing in curing time produced a shifting of phase angle towards higher values and a marked decrease in $|E^*|$. In fact, phase angle increased from 22 ° to 52 ° and $|E^*|$ decreased from 90385 MPa to 17962 MPa for CEM0.45-1d and CEM0.45-3d, respectively.

In conclusion, considering CBms produced with cement: at low volumetric concentration (0.15), the increasing in curing time caused small increases in both norm of complex Young's modulus and phase angle. At high volumetric concentration (0.45), the curing time did not affect the rheological properties in low temperatures range but at high temperatures, the increasing in curing time produced lower $|E^*|$ and higher $\delta_E$ values.

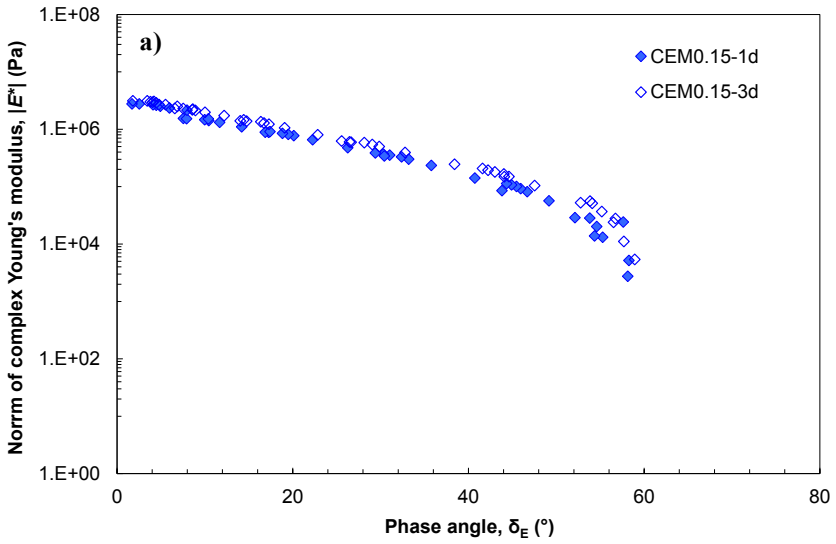
a)
CEM0.15-1d
CEM0.15-3d
Norrm of complex Young's modulus, |E*| (Pa)
1.E+08
1.E+06
1.E+04
1.E+02
1.E+00
0
20
40
60
80
Phase angle, δE (°)

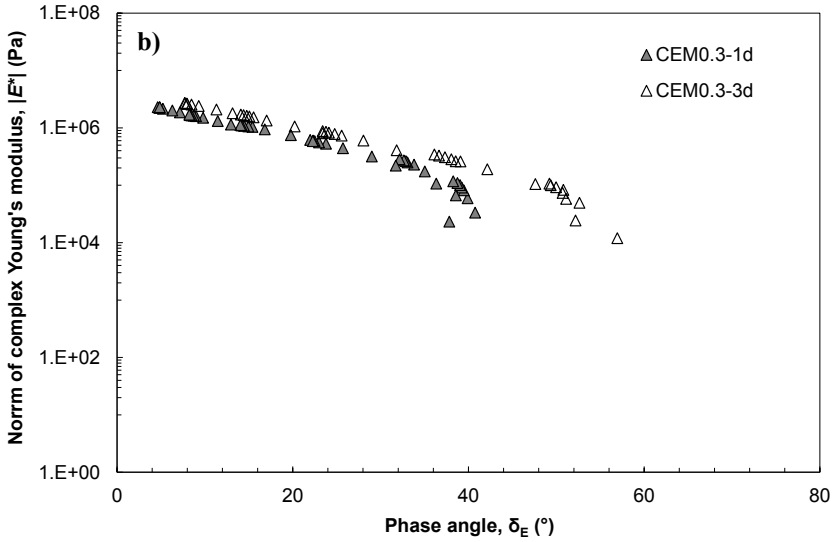
b)
CEM0.3-1d
CEM0.3-3d
Norrm of complex Young's modulus, |E*| (Pa)
1.E+08
1.E+06
1.E+04
1.E+02
1.E+00
0
20
40
60
80
Phase angle, δE (°)

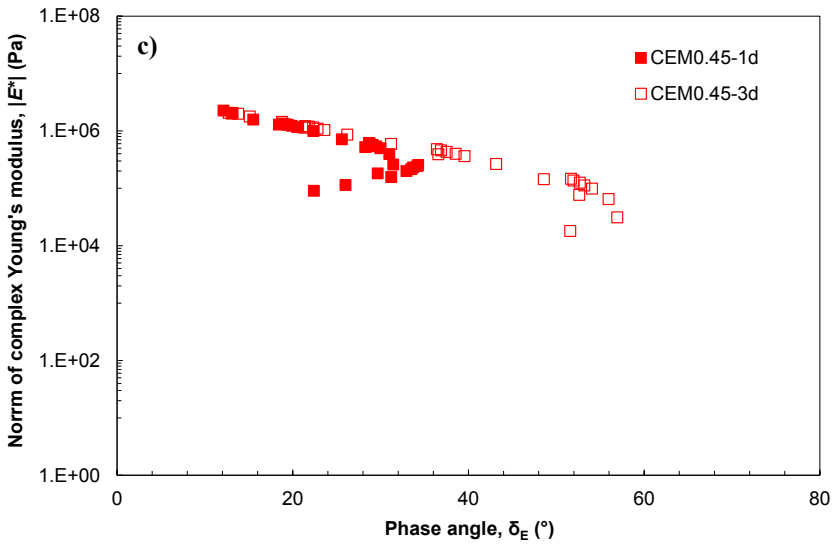


**Figure 16. 20** Metravib measured values of $|E^*|$ and $\delta_E$ represented in the Black space for CBms cured at one and three days: a) CEM0.15; b) CEM0.3 and c) CEM0.45.

## 16.5.2 Effect of volumetric concentration ratio

In **Figure 16. 21**, CBms produced at different volumetric concentration ratios (0.15, 0.3 and 0.45) with calcium carbonate or cement and cured for 1 or 3 days are compared using Black space in order to analyze the effect of volumetric concentration ratio.

Considering CBms produced with calcium carbonate at both curing times, the increasing in volumetric concentration ratio induced a small increase in both phase angle and $|E^*|$ at high temperatures. At low temperatures, no difference can be (Figure 16. **17**a and **Figure 16. 21**b). Analyzing CEM mastics cured one day (**Figure 16. 17**c), the effect of volumetric concentration ratio was negligible at low temperatures. Differently, at high temperatures the influence of volumetric concentration ratio was marked: $|E^*|$ increased from 2747 MPa to 90385 MPa and $\delta_E$ decreased from 58 ° to 22 ° for CEM0.15-1d and CEM0.15-3d, respectively. After three days of curing, the effect of volumetric concentration ratio disappeared at both low and high temperatures (**Figure 16. 17**d).

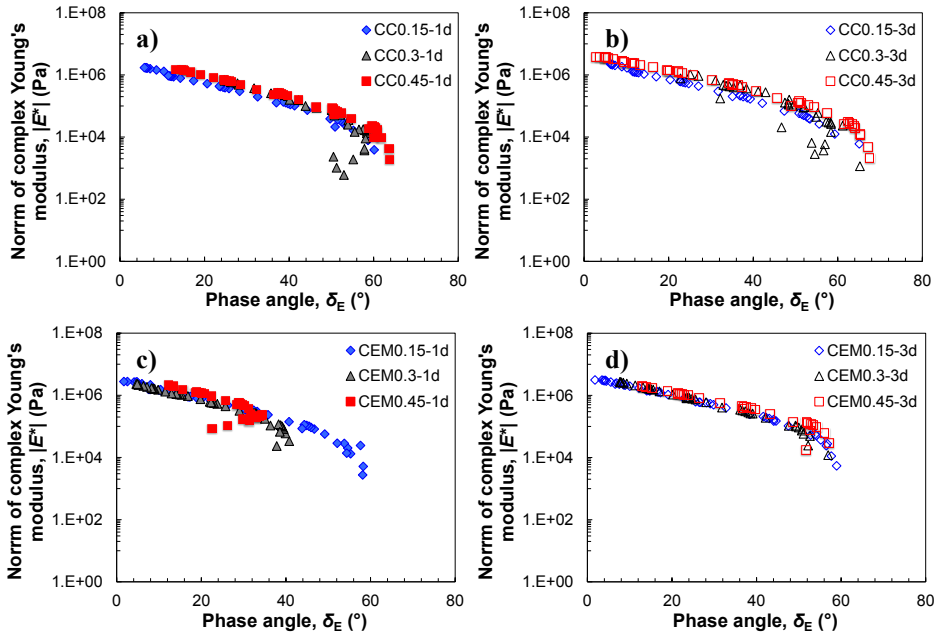


**Figure 16. 21** Metravib measured values of $|E^*|$ and $\delta_E$ represented in the Black space for CBms produced at different volumetric concentration ratios (0.15, 0.3 and 0.45): a) CC cured one day; b) CC cured three days; c) CEM cured one day and d) CEM cured three days.

## 16.5.3 Effect of mineral addition type

In **Figure 16. 22**, CBms produced at fixed volumetric concentration ratio (0.3) with calcium carbonate or cement and cured for 1 and 3 days are compared using Black space, with the aim to evaluate the effect of the type of mineral addition.

At low temperatures and both curing times, the use of cement instead of filler produced higher norm of complex Young's modulus and lower phase angles. After one day of curing, $|E^*|$ increased from 783040 MPa to 2398890 MPa (and from 1041400 MPa to 2153750 MPa, after three days of curing) and $\delta_E$ decreased from 24° to 9° ( and from 22° to 5° after three days of curing) for CC0.3-d1 and CEM0.3-1d, respectively.

The same trend can be detected at high temperatures but the effect on phase angle was less marked. In fact, after one day of curing, $|E^*|$ increased from 602 MPa to 23291 MPa (and from 1159 MPa to 11956 MPa, after three days of curing) and $\delta_E$ decreased from 53° to 38° ( and from 55° to 52° after three days of curing) for CC0.3-d1 and CEM0.3-1d, respectively. According to the adopted results, it can be conclude that the higher LVE response detected with CEM mastic can be related to a cementitious microstructure developed within the considered mastic.

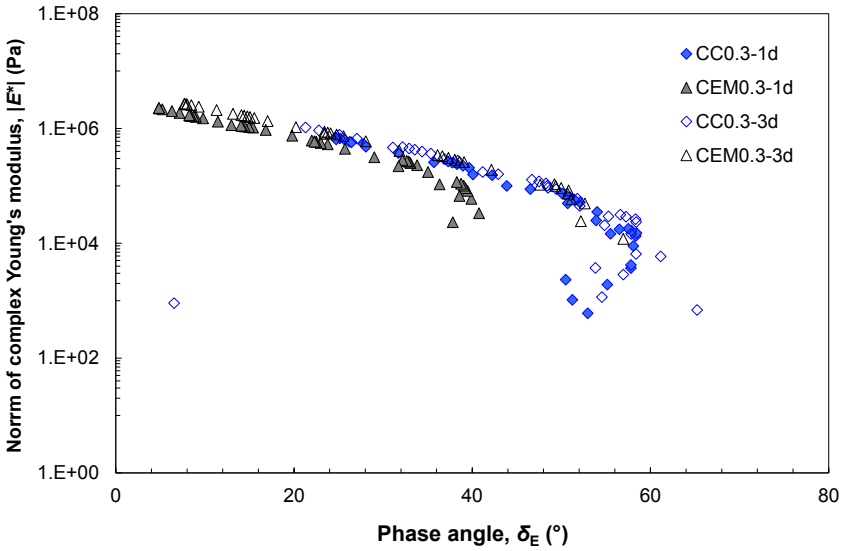


**Figure 16. 22** Metravib measured values of $|E^*|$ and $\delta_E$ represented in the Black space for CC0.3 and CEM0.3 cured for one and three days.

## 16.6 Rheological modeling

Analyzing $G^*$ and $E^*$ results (obtained with DSR device and Metravib apparatus, respectively) reported in Section 16.4 and 16.5, the validity of the time-temperature superposition principle (TTSP) can be checked. Unique curves appeared to identify the material response of all the investigated materials and curing times. Therefore, a thermo-rheologically simple behavior can be assumed, that is, the TTSP can be considered valid for $G^*$ and $E^*$ regardless: the type of mineral addition, volumetric concentration ratio, curing time. For each material, the measured $G^*$ and $E^*$ values were fitted using the Bahia et al. (2001) rheological model (see Section 16.3.3).

In the present research, the selected reference temperature for the rheological model was $T_{REF}$=20 °C.

The rheological modelling of $G^*$ measurements carried out on all CBms mastics and bitumen emulsion cured for 15 hours and 1 day, and $E^*$ measurements carried out on CBMs mastics cured for one day were presented in this section.

Master curves of $|G^*|$ and $\delta_G$, and of $|E^*|$ and $\delta_E$, at $T_{REF}$=20 °C are reported from **Figure 16. 23** to Figure 16. 25. The rheological and WLF fitted model parameters are summarized from **Table 16. 2** to **Table 16. 5**.

As it can be noted, the same observations can be obtained analyzing $G^*$ and $E^*$ measurements. The adoption of cement as mineral addition and the higher volumetric concentration ratios in both CC and CEM mastics induced a marked increase of both equilibrium and glassy moduli ($G_e$ and $E_e$, $G_g$ and $E_g$) and a reduction in phase angle ($\delta_G$ and

$\delta_E$). The influence of volumetric concentration ratio was less marked on glassy modulus and more evident on equilibrium modulus for CEM mastics with respect to CC mastics.
In particular, the increasing of volumetric concentration ratio with CEM mastics restricted the difference between $G_e$ (or $E_e$) and $G_g$ (or $E_g$ ) from five (CEM0.15) to two orders of magnitude (CEM0.45), highlighting the limited thermal susceptibility of this material.
In addition, considering $G^*$ measurements carried out on bitumen emulsion, the observed rheological behavior was comparable with that one typically detected with pure bitumen ($G_e$ =0). According to rheological model fitted parameters, a dependency of these calculated parameters from the type of mineral addition, volumetric concentration ratio and curing time cannot be clearly identified.
Although the selected rheological model [Bahia et al., 2001] seemed to be appropriate in the fitting of $G^*$ and $E^*$ measurements, further studies should be addressed to the development of a rheological model specifically dedicated to these type of materials (CBms), considered as reversed emulsion where the concentration of filler-sized particles plays a fundamental role in the rheological analysis.
Regarding the thermal susceptibility of the studied materials (**Table 16. 4** and **Table 16. 5**), we can assess that CBms produced with cement exhibited a limited thermo-dependency (*cement-like* behavior). The thermal susceptibility of CEM mastics was noticeable exclusively at high temperatures. Differently, CC mastics showed a typical *asphalt-like* thermo-dependency in the investigated range of the temperatures.

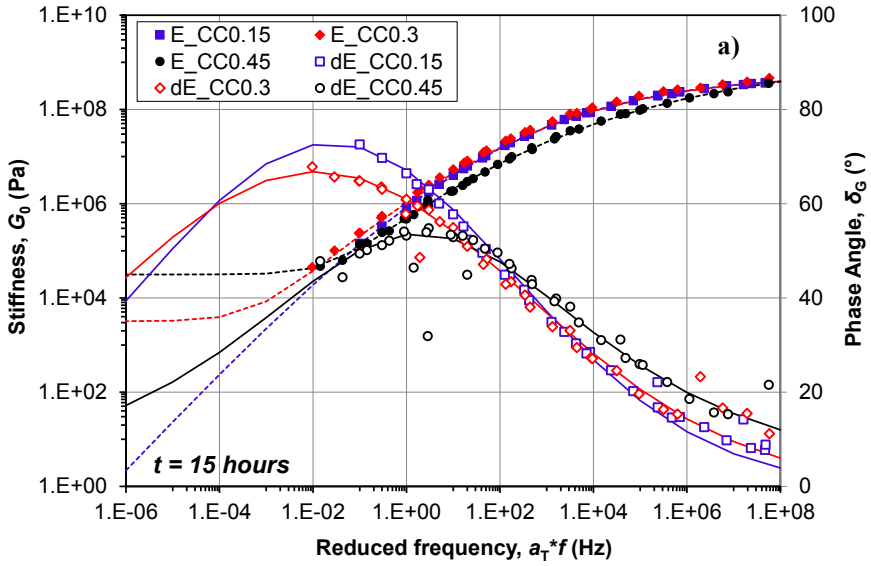

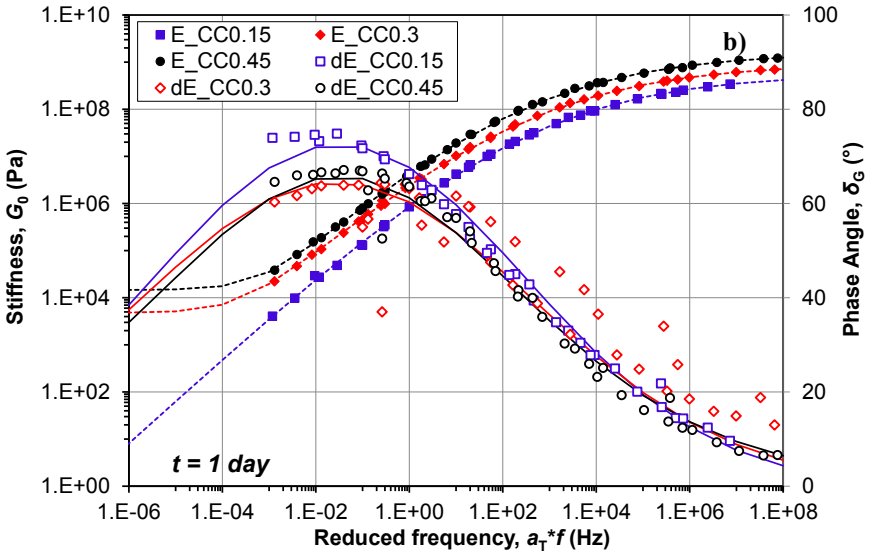


**Figure 16. 23** Master curves for $|G^*|$ and $\delta_G$ for: a) CC mastics cured for 15 hours and b) CC mastics cured for one day.

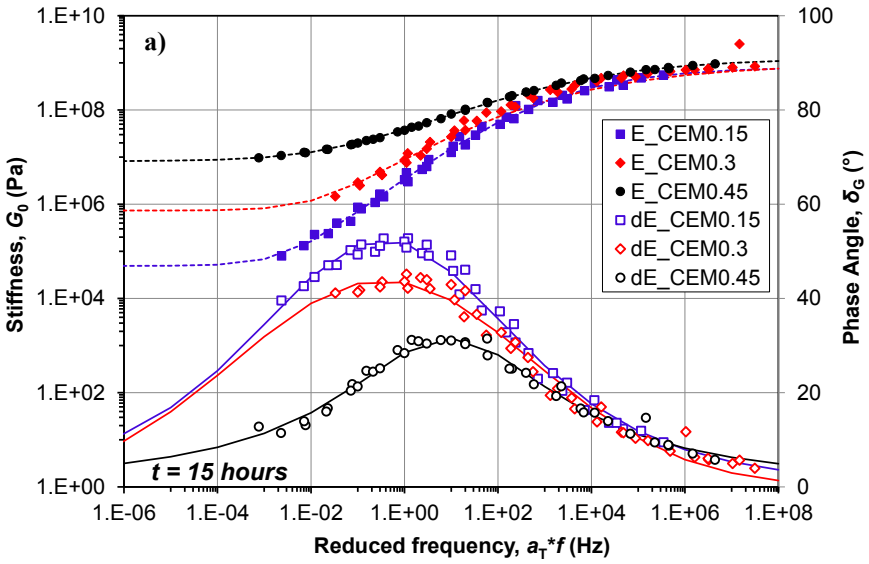

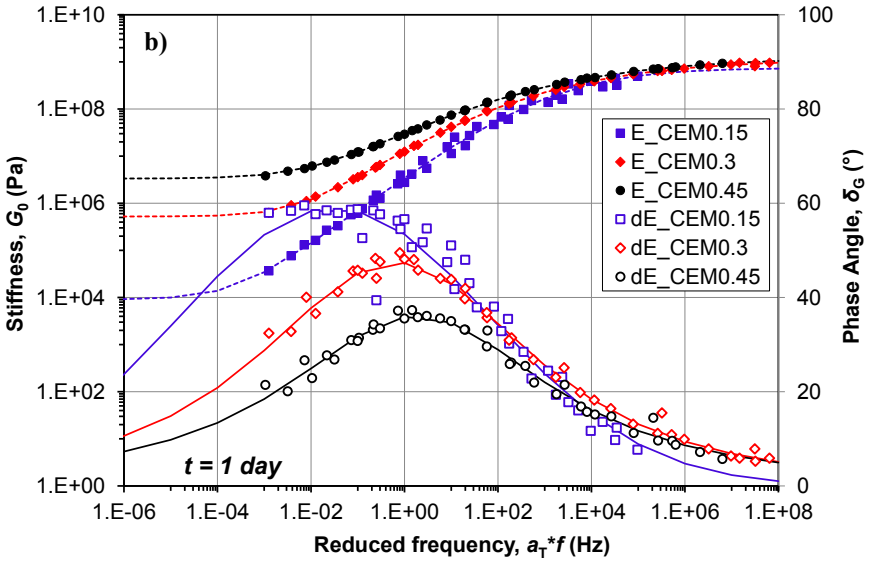


**Figure 16. 24** Master curves for $|G^*|$ and $\delta_G$ for: a) CEM mastics cured for 15 hours and b) CEM mastics cured for one day.

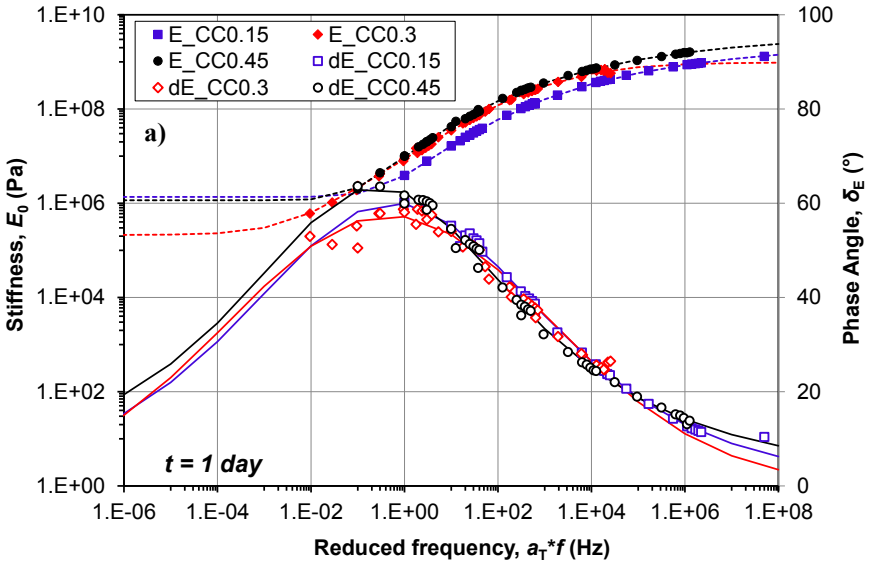

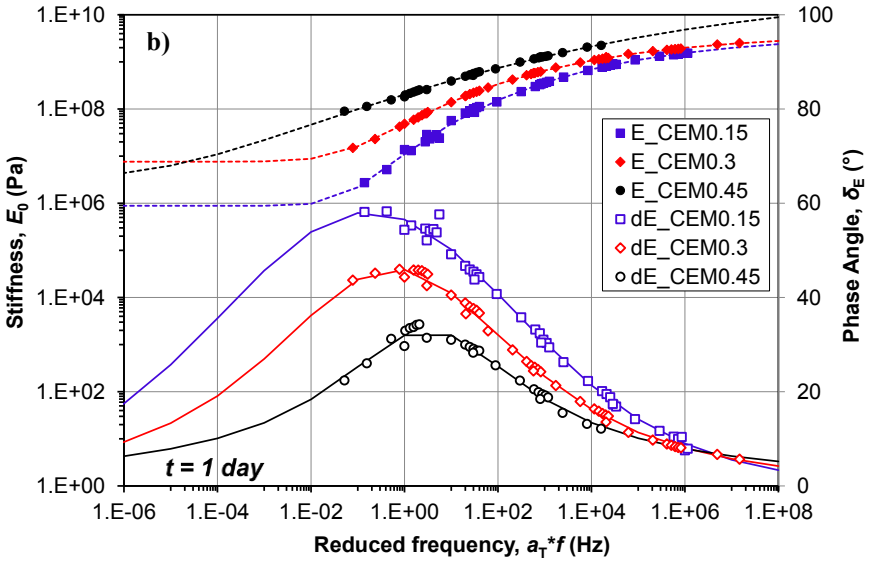


Figure 16. 25 Master curves for $|E^*|$ and $\delta_E$ for: a) CC mastics cured for 1 day and b) CEM mastics cured for one day.

| **CBms** | **$G_g$** | **$G_e$** | **$f_c$** | **k** | **$m_e$** | **$\delta_m$** | **$f_d^*$** | **$m_d$** | **$R_d$** |
|---|---|---|---|---|---|---|---|---|---|
| Code | [Pa] | [Pa] | [Hz] | - | - | - | [Hz] | - | - |
| **CC0.15-15h** | 5.60E+8 | 0 | 62.2 | 0.19 | 1.07 | 73 | 0.025 | 4814 | 275 |
| **CC0.3-15h** | 5.65E+8 | 3.2E+3 | 197.5 | 0.19 | 0.92 | 67 | 0.012 | 284.29 | 75.9 |
| **CC0.45-15h** | 14.51E+8 | 3.1E+4 | 0.03 | 0.11 | 1.72 | 54 | 1.96 | 3.08 | 6 |
| **CEM0.15-15h** | 8.18E+8 | 4.9E+4 | 563.7 | 0.29 | 0.8 | 53 | 0.362 | 4.61 | 5.71 |
| **CEM0.3-15h** | 9.70E+8 | 7.1E+5 | 48.8 | 0.19 | 0.81 | 44 | 0.22 | 7400 | 342.3 |
| **CEM0.45-15h** | 12.42E+8 | 8.2E+6 | 2052 | 24 | 0.45 | 32 | 9.14 | 1.89 | 2.83 |
| **CC0.15-1d** | 5.52E+8 | 0 | 430 | 0.22 | 0.9 | 73 | 0.032 | 6936 | 333 |
| **CC0.3-1d** | 9.21E+8 | 4.8E+3 | 386 | 0.22 | 0.87 | 65 | 0.028 | 88.4 | 33.94 |
| **CC0.45-1d** | 15.94E+8 | 14.6E+3 | 213 | 0.22 | 0.89 | 66 | 0.033 | 9.24 | 11.75 |
| **CEM0.15-1d** | 7.47E+8 | 9.1E+3 | 1345 | 0.36 | 0.73 | 60 | 0.032 | 7400 | 286.9 |
| **CEM0.3 -1d** | 11.54E+8 | 5.2E+5 | 46.1 | 0.21 | 0.81 | 48 | 0.65 | 3.07 | 4.53 |
| **CEM0.45-1d** | 12.62E+8 | 3.3E+6 | 49.8 | 0.2 | 0.66 | 36 | 1.93 | 2.46 | 3.85 |

**Table 16. 2** Bahia et al. fitted rheological model parameters for CBms characterized in terms of $G^*$.

| **CBms** | **$E_g$** | **$E_e$** | **$f_c$** | **k** | **$m_e$** | **$\delta_m$** | **$f_d^*$** | **$m_d$** | **$R_d$** |
|---|---|---|---|---|---|---|---|---|---|
| Code | [Pa] | [Pa] | [Hz] | - | - | - | [Hz] | - | - |
| **CC0.15-1d** | 24.57E+8 | 1.36E+5 | 0 | 0.14 | 5.56 | 60 | 0.596 | 5.03 | 6.80 |
| **CC0.3-1d** | 9.74E+8 | 0.21E+6 | 1007 | 0.41 | 0.67 | 57 | 0.49 | 104.8 | 35.33 |
| **CC0.45-1d** | 37.72E+8 | 1.15E+6 | 0 | 0.15 | 5.14 | 64 | 0.273 | 2.6 | 4.42 |
| **CEM0.15-1d** | 37.91E+8 | 8.82E+5 | 0 | 0.14 | 5.03 | 58 | 0.178 | 11.2 | 10.75 |
| **CEM0.3 -1d** | 39.47E+8 | 7.64E+6 | 0.00 | 0.15 | 2.84 | 48 | 0.602 | 3.2 | 4.37 |
| **CEM0.45-1d** | 32.28E+9 | 3.19E+6 | 481 | 0.09 | 0.48 | 33 | 3.194 | 1.50 | 2.29 |

**Table 16. 3** Bahia et al. fitted rheological model parameters for CBms characterized in terms of *E**.

| **CBms** | $a_{40}$ | $a_{30}$ | $a_{20}$ | $a_{10}$ | $a_0$ | $a_{-10}$ | $a_{-20}$ | $a_{-30}$ | $C_1$ | $C_2$ |
|---|---|---|---|---|---|---|---|---|---|---|
| Code | - | - | - | - | - | - | - | - | - | - |
| **CC0.15-15h** | - | - | 0 | 1.22 | 2.63 | 4.38 | 6.37 | 8.21 | 23.7 | 193 |
| **CC0.3-15h** | - | -1.02 | 0 | 1.24 | 2.65 | 4.49 | 7.29 | 12.3 | 7.90 | 82 |
| **CC0.45-15h** | - | -0.84 | 0 | 0.95 | 2.2 | 3.69 | 5.58 | 8.75 | 14.6 | 122 |
| **CEM0.15-15h** | -1.63 | -0.92 | 0 | 1.04 | 2.18 | 3.38 | 5.06 | 6.78 | 15.1 | 161 |
| **CEM0.3-15h** | - | -1.13 | 0 | 1.29 | 2.79 | 4.50 | 6.44 | 8.53 | 18.0 | 178 |
| **CEM0.45-15h** | -2.12 | -1.15 | 0 | 1.30 | 2.77 | 4.36 | 6.17 | 8.02 | 25.0 | 205 |
| **CC0.15-1d** | -1.93 | -1.02 | 0 | 1.27 | 2.66 | 4.40 | 6.39 | 8.35 | 18.8 | 161 |
| **CC0.3-1d** | -1.88 | -1.08 | 0 | 1.26 | 2.74 | 4.44 | 6.51 | 9.01 | 15.2 | 133 |
| **CC0.45-1d** | -1.88 | -1.06 | 0 | 1.34 | 2.85 | 4.54 | 6.58 | 8.68 | 18.7 | 156 |
| **CEM0.15-1d** | -1.90 | -1.14 | 0 | 0.92 | 2.07 | 3.24 | 4.51 | 5.23 | 104 | 111 |
| **CEM0.3 -1d** | -1.90 | -1.10 | 0 | 1.29 | 2.76 | 4.42 | 6.51 | - | 15.2 | 133 |
| **CEM0.45-1d** | -1.90 | -1.14 | 0 | 1.27 | 2.78 | 4.43 | 6.32 | 8.13 | 22.5 | 186 |

**Table 16. 4** WLF fitted model parameters for CBms characterized in terms of *G**.

| **CBms** | $a_{30}$ | $a_{20}$ | $a_{10}$ | $a_0$ | $a_{-10}$ | $a_{-20}$ | $C_1$ | $C_2$ |
|---|---|---|---|---|---|---|---|---|
| Code | - | - | - | - | - | - | - | - |
| **CC0.15-1d** | - | 0 | 1.19 | 2.80 | 4.75 | 7.70 | 9.5 | 89.2 |
| **CC0.3-1d** | -1.03 | 0 | 1.22 | 2.82 | 4.78 | - | 11.3 | 100.6 |
| **CC0.45-1d** | -1 | 0 | 1.10 | 2.50 | 4.50 | - | 9.1 | 91.0 |
| **CEM0.15-1d** | -0.86 | 0 | 1.50 | 2.93 | 4.46 | 7.42 | 10.8 | 98.7 |
| **CEM0.3 -1d** | -1.10 | 0 | 1.31 | 2.76 | 4.31 | 6.69 | 14.5 | 127.1 |
| **CEM0.45-1d** | -1.28 | 0 | 1.47 | 2.91 | - | - | 37.0 | 273.3 |

**Table 16. 5** WLF fitted model parameters for CBms characterized in terms of *E**.

In the context of linear viscoelastic isotropic materials, any elastic constant can be expressed as a function of two others (e.g. *E* and *G*). In particular, the various response function in terms

of material behavior can be interconverted as a function of the considered deformation mode [Tschoegl, 1989].
According to this, a correlation between the elastic part of both measured $G^*$ and $E^*$ can be developed in order to verified if a CRM and a CEM mastic with a cement-like rheological behavior may be characterized by the same Poisson's ratio ($\nu$). To accomplish this objective, the stiffness modulus $E_0$ was calculated as follow:

$$E_{0-CALC} = 2 \cdot (1 + \nu) \cdot G_0 \quad (102)$$

where $G_0$ is the norm of $G^*$ measurements carried out using DSR equipment and $\nu$ is the Poisson's ratio fixed equal to 0.15 as obtained in Section 12.4.2. Then, $E_{0\text{-CALC}}$ was compared with the norm of $E^*$ values carried out using Metravib apparatus ($E_{0\text{-METRAVIB}}$). To this aim, $E_{0\text{-CALC}}$ results were reported in a correlation plot as a function of $E_{0\text{-METRAVIB}}$, for a common range of temperatures and frequencies (from 30 °C to -10 °C and from 1 to 20 Hz) for CEM0.45-1d (**Figure 16. 26**).
As shown in **Figure 16. 26**, $E_{0\text{-METRAVIB}}$ measurements were slightly higher with respect to $E_{0\text{-CALC}}$. However, this variation can be considered not significant at the aim of this validation. According to these results, it can be concluded that CEM mastics at high volumetric concentration ratio that exhibited cement-like rheological behavior (i.e. limited time-temperature dependency), are characterized by a $\nu$ equal to 0.15 as well as cold bituminous mixtures with a bitumen/cement ratio about 1.

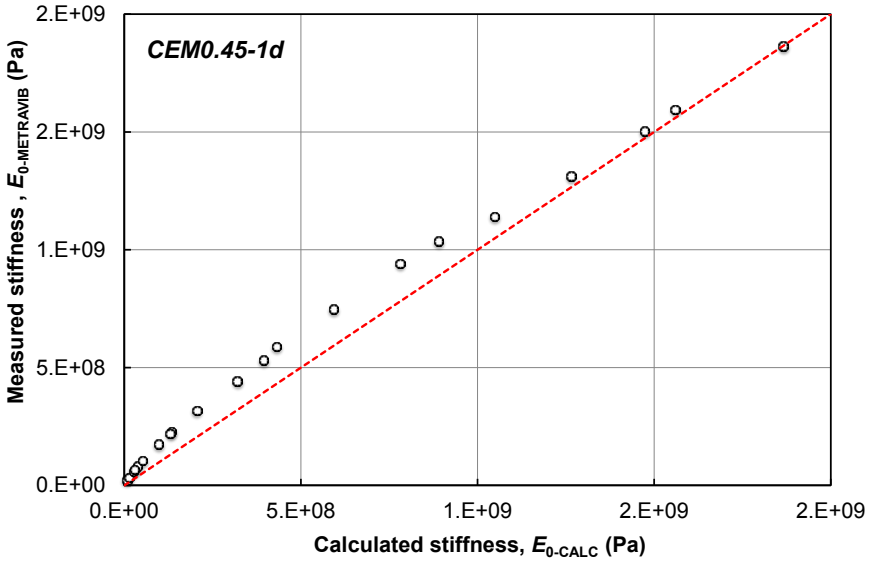


**Figure 16. 26** Correlation plot for $E_0$ measured versus calculated.

## 16.7 Summary

The experimental program of these research was focused on the laboratory characterization of cold bituminous mastics (CBm) prepared with bituminous emulsion (unique source) and two different mineral additions at three volumetric concentration ratios (volume of mineral addition/volume of residual bitumen, $M_A/B$).
The experimental investigation considered cement and calcium carbonate as mineral additions in order to compare the influence of both active or inactive filler addition in the mechanical behavior of CBms.
CBms are characterized from the rheological point of view in terms of *complex modulus*. In addition, the influence of curing time on rheological properties of CBms was also investigated.

According to the obtained results, the following considerations can be drawn:

- A standardized and reliable procedure for CBms production was developed;
- The analysis of the curing process performing mechanical test after 15 hours, one and three days of curing was not completely defined because the mechanisms of this phenomenon are more noticeable during the first hours of curing where the breaking of the emulsion occurs. A deeper study in the early age of curing (one or three hours after the CBm production) may be very decisive to obtain a full knowledge on the curing process and on the predominant mechanisms that characterized the early age of the CBms.
- Regarding the selected curing times, we can observed that both $G^*$ and $E^*$ measurements detected for CC mastics were lightly influenced by the curing time; in particular, the glassy modulus ($G_g$ or $E_g$) was almost the same for each investigated volumetric concentration ratio. Moreover, in low temperatures range, phase angle ($\delta_g$ and $\delta_e$) was almost constant and at each curing time and it slightly increased after 3 days. This finding can be explained analyzing the composition of CC mastics. In fact, considering longer curing times, water bubbles present within CC mastic have more time available to evaporate and consequently, evaporation process reduces water concentration in the mastic. The physical state of CC mastic evolves starting from an emulsion, where the bitumen droplets are dispersed in water to a reversed emulsion, where water bubbles are dispersed in bitumen (longer curing times, when the bituminous emulsion is already broken); bitumen and water become the continuous and discontinuous phase, respectively. Considering the CC mastic cured state, water bubbles are stiff and strongly connected each others; in addition, they behave as some little filler-sized particles (solid particles) that coat the bitumen fraction as a thin film. During the test, at low temperatures, this phenomenon was not noticeable because it was covered by the higher bitumen stiffness (solid-like behavior). Differently, at high temperatures, CC mastic was more viscous and its rheological behavior is shifted toward a liquid-like behavior: CC mastic flows and little water bubbles around the bitumen phase, act as a film.

Water bubbles were stiff and they produced the same effect detectable testing a CC mastic characterized by higher volumetric concentration ratio (reduced liquid-like behavior). In fact, after one day of curing, CC mastic still contained a lot of water bubbles and consequently, CC mastic was less viscous (lower phase angles). On the contrary, after three days of curing, the concentration of water bubbles decreased within CC mastic, the material was more viscous (higher phase angles).

- For CEM mastic, curing time did not affect the rheological behavior of the material. Phase angles were slightly lower than those obtained on CC mastic. In addition, at high frequencies, phase angle ($\delta_g$ and $\delta_e$) was almost constant and it decreased at lower frequencies and reduced curing times. In fact, the presence of water within CEM mastic was limited by both evaporation and hydration process. Basically, the opposite condition analyzed with CC mastic was obtained. Deeper studies should be addressed to better understand what kind of micro-chemical structure characterized each CBm over time (gel or dispersed solution).
- Regarding the influence of volumetric concentration ratio, the glassy modulus ($G_g$ or $E_g$) did not increase at high volumetric concentration ratio for all CBms mastics. Some negligible variations were noticed at higher temperatures, for both CC and CEM mastics. The reduction in phase was marked with CEM mastic, because its microstructure is characterized by strong cementitious bonds that inhibit the viscous component of the material.
- Fixing concentration ratio and curing time, the effect of the type of mineral addition can be observed. In terms of stiffness moduli, $G_g$ (or $E_g$) was almost constant but an opposite trend was detected at low frequencies. In fact, $G_e$ (or $E_e$) increased, moving from CC to CEM mastics.
- Bitumen emulsion tested using DSR device exhibited a rheological behavior typically detected with bituminous binder at all investigated curing times.
- The TTSP was verified for all CBms and, according to this result, both CC and CEM mastics can be classified as thermo-rheologically simple materials. In addition, the Bahia et al. (2001) rheological model was successfully adopted in the fitting of $G^*$ and $E^*$ measurements. Therefore, further studies are required in order to develop a rheological model specifically dedicated to analyze the rheological behavior of CBms that are characterized by an evolutive internal microstructure.

# Summary of the overall experimental study

# CHAPTER 17.

## Concluding remarks

The experimental study described in this dissertation was focused on the rheological and mechanical characterization of cold mixtures (CMs) as support layers for road pavements, material commonly used in Italian road infrastructures. In particular, the possibility to employ high contents of reclaimed aggregates in the production of cold-recycled mixture (CRMs), without penalizing the performance of road pavements, was also investigated.

Besides the traditional laboratory investigations, an original research methodology based on the multiscale analysis was applied in order to deeply understand each physical and chemical mechanisms that occur within these materials. Experimental activities were carried out involving advanced characterizations and targeting testing method at different investigation scales (*pavement*-, *mixture*-, *mortar*- and *mastic*-scale) where those mechanisms are most noticeable. Established that CMs are evolutive materials at each scale of investigation because its physical state evolves over time according to moisture loss, additional attention was taken during laboratory testing to characterize the material at each phase during its in-service life (early-life behavior and long-term behavior).

The main reason of adopting this research approach was the possibility to identify which and how mechanisms that derive from the smaller scale of investigation, may regulate and affect the in-service behavior of the material within the pavement structure.

First, the in-service performance (long-term behavior) of different CRMs was evaluated carrying out two experimental pavement section. The first section aimed at comparing different full-depth reclamation techniques, as well as different CMs totally produced using reclaimed aggregates, bitumen emulsion and cement. The mechanical response of the road pavement was monitored over time with repeated FWD surveys.

FWD surveys combined with additional laboratory testing, with the aim to correct field measurements from temperature effect, were reliable to draw a precise evaluation of the pavement performance. In particular, CRM produced using bitumen emulsion better preserves its mechanical properties over time if compared to CRMs produced with foamed bitumen or cement treated materials. On the contrary, CRM treated exclusively with cement (cement-treated material) exhibited the higher level in deterioration rate, over time.

The second experimental pavement section was carried out in order to characterize the in-situ curing process of CRMs, i.e. the development of strength and stiffness over time though moisture loss (evolutive behavior). Moisture loss was measured using time-domain reflectometer probes installed in the subbase layer. Subsequently, results obtained in field were compared with those obtained in laboratory and a marked disparity was detected in terms of moisture loss. This result was certainly related to field curing conditions (humidity and temperature) that are hard to simulate in laboratory. Additional studies are required to develop a laboratory procedure capable of better reproducing field curing conditions.

Concerning the curing process, this phenomenon is connected to the evolution of moisture loss that occurs over time promoted by evaporation during the early-age and to hydration process (at long-term), if cement is added to the material. It was observed that both results in moisture loss and mechanical properties evolved over time exhibiting an asymptotic trend that can be successfully fitted using the Michealis-Menten (MM) model. In addition, the

application of this model on both strength and stiffness results highlighted that the effect of cement hydration prevailed on that of emulsion breaking induced by moisture loss. This first task pointed out the importance to deeply investigate what factors affect the mechanical properties and curing process of CMs.
Laboratory experimental activities carried out on cement-bitumen treated materials in the second part of this research, confirmed the adequacy of the MM model in estimating the evolution of both physical (moisture loss) and mechanical properties (strength and stiffness) and in identifying the long-term behavior of these materials.
The influence of reclaimed asphalt (RA) on both volumetric and rheological properties of CBTM materials was also analyzed. Two different CBTM materials produced with cement and bitumen emulsion or foamed bitumen were considered. From the volumetric point of view, the use of RA did not lead disadvantages. On the contrary, higher RA content improved the workability of the mixture during compaction, because of the rounded shape and the smooth surface texture of RA particles. From the rheological point of view, at higher RA content corresponded a well-developed cement-like behavior and a limited thermo-dependency.
Differently, low RA contents promoted an asphalt-like behavior and an evident time-temperature dependency. In fact, the achievement of these two different rheological behaviors can be related to the nature of cold bituminous mortar (CBM) that partially coats coarse aggregates skeleton within the mixture (more cement-like or asphalt-like according to the relative proportion in which bitumen and cement are mixed). Bearing in mind these results, it can be concluded that the nature of CBM plays a fundamental role in strongly affecting the rheological behavior of the whole associated CM.
In addition, the validity of time-temperature superposition principle and the applicability of rheological model usually adopted with HMA were successfully proved.
In order to clarify this aspect, the third task of this thesis was addressed to characterize the overall properties of CBMs. In particular, this part demonstrated, on the basis of SEM observations, that the type of the microstructure developed within CBM, regardless the mineralogical origin of the filler-sized particles included in CBM and all the chemical and physical phenomena that can occur, are the unique responsible of the long-term behavior of CBM.
In this context, the rheological properties of cold bituminous mastics (CBms) were investigated to completely characterize the mechanical behavior of cold mixtures. In particular, the role of different mineral additions used as emulsion breaking regulator, material stiffer or filler was analyzed. During experimental activities, an evolution of both physical state and rheological behavior of CBm over time was observed. These phenomena were more evident if cement as mineral addition was adopted. In addition, the validity of time-temperature superposition principle and the applicability of rheological model usually adopted at mixture-level were successfully employed at mastic-level.
Optimum correlation was found between results collected from different levels of investigation (size and time-scales); hence demonstrating the scientific validity of the adopted research approach. In fact, results acquired through the experimental study hereby presented, demonstrated the significant importance of each one of the abovementioned levels of investigation, allowing an overall knowledge of the main mechanisms that affect the physical, mechanical and rheological behavior of cold mixtures.

Based on the overall findings, no elements discourage the use of cold mixture as support layers for pavement structures. Therefore, CM should be properly designed in terms of aggregate blend, water content and binding agents (type and dosage) before its adoption on site. Further efforts are needed to appropriately consider these aspects, along with accurate analysis for selecting adequate proportion between different binding agents to be adopted during materials production. Moreover, particular attention should be taken in respecting these suggested precautions during the construction operations of a subbase layer.
The obtained findings provide a valuable contribution to the achievement of standardized procedures regarding the analysis of curing process and the laboratory characterization of CMs, and an optimum reference point for further studies on each specific topic addressed. Finally, the work described in this thesis certainly represents a useful further step towards the "*paving*" of the actual gap between practice and theory and to a most widespread and conscious use of cold technologies in the construction and maintenance of road pavements.

# 3-years Ph.D. publications

1) Godenzoni C., Graziani A., and Bocci M. (2015). “Influence of reclaimed asphalt content on the complex modulus of cement bitumen treated materials”. Proc. 6th International Conference Bituminous Mixtures and Pavements, Thessaloniki, Greece, 589-596. Taylor & Francis Group, London, ISBN 978-1-138-02866-1. (Indexed Proceedings).
2) Godenzoni, C., Cardone, F., Graziani, A., & Bocci, M. (2016). The Effect of Curing on the Mechanical Behavior of Cement-Bitumen Treated Materials. In 8th RILEM International Symposium on Testing and Characterization of Sustainable and Innovative Bituminous Materials (pp. 879-890). Springer Netherlands.
3) Godenzoni, C., Graziani, A., & Perraton, D. (2016). Complex modulus characterisation of cold-recycled mixtures with foamed bitumen and different contents of reclaimed asphalt. Road Materials and Pavement Design.
4) Graziani, A., Godenzoni, C., Cardone, F., & Bocci, M. (2016). Effect of curing on the physical and mechanical properties of cold-recycled bituminous mixtures. Materials & Design, 95, 358-369.
5) Godenzoni, C., Graziani, A., & Corinaldesi, V. (2016). The Influence Mineral Additions on the Failure Properties of Bitumen Emulsion Mortars. In 8th RILEM International Conference on Mechanisms of Cracking and Debonding in Pavements (pp. 327-333). Springer Netherlands.
6) Garilli, E., Autelitano, F., Godenzoni, C., Graziani, A., & Giuliani, F. (2016). Early age evolution of rheological properties of over-stabilized bitumen emulsion-cement pastes. Construction and Building Materials, 125, 352-360.
7) Graziani, A., Godenzoni, C., Cardone, F., Bocci, E., & Bocci, M. (2016). An application of the Michaelis–Menten model to analyze the curing process of cold recycled bituminous mixtures. International Journal of Pavement Research and Technology.
8) Godenzoni, C., Graziani, A., Bocci, E., & Bocci, M. (2017). The evolution of the mechanical behaviour of cold recycled mixtures stabilised with cement and bitumen: field and laboratory study. Road Materials and Pavement Design, 1-22.
9) Godenzoni C., Bocci M. and Graziani A. “Rheological characterization of cold bituminous mastics produced with different mineral additions”. Accepted for International congress on Transport Infrastructure and Systems, TIS2017.
10) Godenzoni C,. Graziani A., Grilli A., Bocci E. and Bocci M. “Instrumented test section for analyzing the curing process of cold-recycled mixtures”. Accepted for BCRRA 2017, Tenth International Conference on the Bearing Capacity of Roads, Railways and Airfields.

# References

Abel, F., & Hines, C. R. (1979). Base Stabilization with foamed asphalt (No. FHWA-CO-RD-79-5 Intrm Rpt.).

Acott, S. M., & Myburgh, P. A. (1983). Design and performance study of sand bases treated with foamed asphalt (No. N908).

Asphalt Emulsion Manufacturers Association. (2008). A Basic Asphalt Emulsion Manual, fourth edition. AEMA.

Arabani, M., & Ferdowsi, B. (2009). Evaluating the semi-circular bending test for HMA mixtures. International Journal of Engineering A: Basics, 22(1), 47-58.

ARRA Asphalt Academy Asphalt Recycling and Reclaiming Association, (2001). Basic asphalt recycling manual [online]. Available from: http://www.mdt.mt.gov/publications/docs/brochures/research/toolbox/ARRA/BARM%20-%20B/1-124-BARM1.pdf.

Asi, I. M., Qasrawi, H. Y., & Shalabi, F. I. (2007). Use of steel slag aggregate in asphalt concrete mixes. Canadian Journal of Civil Engineering, 34(8), 902-911.

Asphalt Academy, The design and use of foamed bitumen treated materials. Interim Technical Guideline No. 2, Pretoria, South Africa, 2002

Asphalt Academy. (2009). Technical guideline (TG2): Bitumen stabilized materials (2nd ed.) CSIR Built Environment, South Africa, Pretoria:

Asphalt Institute (1997). Mix Design Methods for Asphalt Concrete and Other Hot-Mix Types. Manual Series, (2).

Attia, M. I., Abdelrahman, M. A., Molakatalla, U., & Salem, H. M. (2009). Field evaluation of asphalt film thickness as a design parameter in Superpave mix design. International Journal of Pavement Research and Technology, 2(5), 205.

Autostrade per l'Italia SpA, (2008). Construction specifications for stabilization with foamed bitumen (in Italian).

AzkoNobel, Bitumen emulsion, Technical Bulletin (2000) 3294.

Bahia, H. U., Hanson, D. I., Zeng, M., Zhai, H., Khatri, M. A., & Anderson, R. M. (2001). Characterization of modified asphalt binders in superpave mix design (No. Project 9-10 FY'96).

Biligiri, K. P., Said, S., & Hakim, H. (2012). Asphalt Mixtures. International Journal of Pavement Research and Technology, 5(4), 209-217.

Bissada, A.F. (1987). Structural response of foamed-asphalt-sand mixtures in hot environments. In: Asphalt materials and mixtures. Washington, DC: Transportation Research Board. (Transportation Research Record, 1115), pp 134-149.

Bocci, E., Graziani, A. and Canestrari, F., (2015). Mechanical 3D characterization of epoxy asphalt concrete for pavement layers of orthotropic steel decks, Construction and Building Materials, 79 (2015), pp. 145-152

Bocci, M., Canestrari, F., Grilli, A., Pasquini, E., & Lioi, D. (2010). Recycling techniques and environmental issues relating to the widening of an high traffic volume Italian motorway. International Journal of Pavement Research and Technology, 3(4), 171-177.

Bocci, M., Grilli, A., Cardone, F., & Graziani, A. (2011). A study on the mechanical behaviour of cement–bitumen treated materials. Construction and building materials, 25(2), 773-778.

Bocci, M., Grilli, A., Cardone, F., & Ferrotti, G. (2014). Full-depth reclamation for the rehabilitation of local roads: a case study. International Journal of Pavement Engineering, 15(3), 191-201.

Boussad, N., & Martin, T. (1996). Emulsifier content in water phase and particle size distribution: Two key-parameters for the management of bituminous emulsion performance. In EURASPHALT & EUROBITUME CONGRESS, STRASBOURG, 7-10 MAY 1996. VOLUME 3. PAPER E&E. 6.159.

Bourrel, M., & Verzaro, F. (1998). Controlling asphalt emulsion breaking for road paving. Revue Generale des Routes, (761).

Bowering, R. H. (1970). Upgrading marginal road-building materials with foamed bitumen. Highway Engineering in Australia, Mobil Oil Australia, Melbourne South.

Bowering, R. H., & Martin, C. L. (1976). Foamed bitumen production and application of mixtures evaluation and performance of pavements. In Association of Asphalt Paving Technologists Proc (Vol. 45).

Brayton, T. E., Lee, K. W., Gress, D. L., & Harrington, J. (2001). Development of performance-based mix design for Cold in-Place Recycling of asphalt mixtures. In Transportation Research Board Annual Meeting.

Brennen, M., Tia, M., Altschaefl, A., & Wood, L. E. (1983). Laboratory Investigation of the Use of Foamed Bitumen for Recycled Bituminous Pavement.

Brosseaud, Y., Gramsammer, J. C., Kerzreho, J. P., Goacolou, H., & Le Bourlot, F. (1997). Experimentation (première partie) de la Grave-Mousse® sur le manège de fatigue. Revue général des routes, (752).

Brown, S. F., & Snaith, M. S. (1974). The permanent deformation characteristics of a dense bitumen macadam subjected to repeated loading. In Association of Asphalt Paving Technologists Proc (Vol. 43).

Brown, S., & Needham, D. (2000). A study of cement modified bitumen emulsion mixtures. Asphalt Paving Technology, 69, 92-121.

Bruntland G. (1987). Report of the World Commission on Environment and Development: Our Common Future. UN Documents: Gathering a Body of Global Agreements compiled by the NGO Committee on Education.

Campbell Scientific (2012). CS616 & CS625 Water content reflectometry user guide.

Cardone, F., Grilli, A., Bocci, M., & Graziani, A. (2015). Curing and temperature sensitivity of cement–bitumen treated materials. International Journal of Pavement Engineering, 16(10), 868-880.

Castedo-Franco, L. H., Beaudoin, C. C., Wood, E. L., & Altschaeffl, A. G. (1984). Durability characteristics of foamed asphalt mixtures. In Proceedings of the 29th Annual Canadian Technical Asphalt Association Conference, held in Montreal, Canada.

Chailleux, E., Ramond, G., Such, C., & de La Roche, C. (2006). A mathematical-based master-curve construction method applied to complex modulus of bituminous materials. Road Materials and Pavement Design, 7(sup1), 75-92.

Chang TJ, Chen JS, Pan W (2000). Technologies for waste glass-recycling programs. Taiwan: National Taipei Technology University, p. 1–49.

Chambers, J. M., & Hastie, T. J. (1991). Statistical models in S. CRC Press, Inc..

Chen, D. H., Bilyeu, J., Lin, H. H., & Murphy, M. (2000). Temperature correction on falling weight deflectometer measurements. Transportation Research Record: Journal of the Transportation Research Board, (1716), 30-39.

Christensen, D. W., & Anderson, D. A. (1992). Interpretation of dynamic mechanical test data for paving grade asphalt cements (with discussion). Journal of the Association of Asphalt Paving Technologists, 61.

Cooley, L. A., Stroup-Gardinder, M., Brown, E. R., Hanson, D. I., & Fletcher, M. O. (1998). Characterization of asphalt-filler mortars with superpave binder tests. Journal of the Association of Asphalt Paving Technologists, 67.

Collings, D., Lindsay, R. and Shunmugam, R., (2004). LTPP exercise on a foamed bitumen treated base – evaluation of almost 10 years of heavy trafficking on mr 504 in Kwazulu-Natal. Proceedings of the 8th conference on asphalt pavements for Southern Africa, CAPSA, Sun City, 16–18 September, South Africa.

Cominsky, R. J., Huber, G. A., Kennedy, T. W., & Anderson, M. (1994). The superpave mix design manual for new construction and overlays (No. SHRP-A-407). Washington, DC: Strategic Highway Research Program.

COMMUNICATION FROM THE COMMISSION TO THE EUROPEAN PARLIAMENT AND THE COUNCIL. Construction 2020 - Strategy for the sustainable competitiveness of the construction sector and its enterprises. Brussels, 31.7.2012 COM (2012) 433 FINAL.

Cowpertwait, P. S., & Metcalfe, A. V. (2009). Introductory time series with R. Springer Science & Business Media

CROW 1998. Deflection profile – not a pitfall anymore (1998). Edited by C.A.P.M.. Van 590 Gurp, Record 17. Ede The Netherlands.

CSIR transportek, (1998). Foamed asphalt, mix design. Website: http:\\foamasph.csir.co.za:81/chap4.htm.

Dalgaard, P. (2002). "Introductory Statistics with R". Springer-Verlag, New York.

De La Roche, C., Van de Ven, M., Planche, J. P., Van den Bergh, W., Grenfell, J., Gabet, T., ... & Ruot, C. (2013). Hot recycling of bituminous mixtures. In Advances in Interlaboratory Testing and Evaluation of Bituminous Materials (pp. 361-428). Springer Netherlands.

Deneuvillers, C., and J. Samanos (1999). Relationship between Characteristics and Properties of Cationic Bitumen Emulsions. Proc., 1st International Symposium on Asphalt Emulsion Technology, Washington, D.C., Nov. 11–14, pp. 104–112.

Department of Transport, TRH 7: The use of bitumen emulsion in construction and maintenance of roads. Pretoria, South Africa, 1972

Di Benedetto H., De La Roche, C. (1998). State of the art on stiffness modulus and fatigue of bituminous mixtures. In: Francken L (ed) Bituminous binders and mixtures: state of the art and interlaboratory tests on mechanical behavior and mix design. E & FN Spon, London, pp 137–180.

Di Benedetto, H., Partl, M. N., Francken, L., & Saint André, C. D. L. R. (2001). Stiffness testing for bituminous mixtures. Materials and Structures, 34(2), 66-70.

Di Benedetto, H., Olard, F., Sauzéat, C., & Delaporte, B. (2004). Linear viscoelastic behaviour of bituminous materials: From binders to mixes. Road Materials and Pavement Design, 5(sup1), 163-202.

Di Benedetto, H., Delaporte, B. and Sauzeat, C., (2007). Three dimensional linear behavior of bituminous materials: experiments and modeling. International Journal of Geomechanics. 7, 149-157

Di Benedetto, H., Sauzeat, C., and Sohm, J. (2009). Stiffness of Bituminous Mixtures Using Ultrasonic Wave Propagation. Road Materials and Pavement Design, 10 (4), 789-814.

Di Benedetto, H., Sauzeat, C., Bilodeau, K., Buannic, M., Mangiafico, S., Nguyen, Q. T., & Van Rompu, J. (2011). General overview of the time-temperature superposition principle validity for materials containing bituminous binder. International Journal of Roads and Airports, 1(1), 35-52.

Du S (2014) Interaction mechanism of cement and asphalt emulsion in asphalt emulsion mixtures. Mater Struct 47: 1149-1159. doi:10.1617/s1 1527-013-0118-1.

Eckmann, E., Potti, J. J., Bourrel, M., Verlhac, P., Such, C., Leal Calderon, F., & Sanchez Polo, J. (2001). Cold mix technology: the contribution from the Optel project. Revue Générale des Routes et des Aerodromes, 792, 6-15.

Eller, A. and Olson, R., (2009). Recycled pavements using foamed asphalt in Minnesota, Report No. MN/RC 2009-09. Office of Materials & Road Research Minnesota, Department of Transportation, Saint Paul, Minnesota, USA.

Environmental Protection Agency (EPA), (2014). Introduction to Eco-Labels and Standards. U.S. Environmental Protection Agency, Washington, DC. (Web Link).

European Asphalt Pavement Association (EAPA), (2008). Arguments to stimulate the government to promote asphalt reuse and recycling. Position Paper. Brussels, Belgium, May 2008 [Online]. Available from: http://www.eapa.org/default_ news.htm

European Asphalt Pavement Association (EAPA), (2014). Asphalt in Figures [Online]. The Netherlands, Breukelen: European Asphalt Pavement Association. Available from: http://www.asefma.es/wpcontent/uploads/2015/12/AIF_eapa_2014.pdf.

European Commission (EC), (2011). Buying Green! A Handbook on Green Public Procurement. 2nd Edition. Publications Office of the European Union, Luxembourg.

Fang X, Garcia A, Winnefeld F, Partl MN, Lura P. (2015) Impact of rapid hardening cements on mechanical properties of cement bitumen emulsion asphalt. Mater Struct pp 1–12, DOI 10.1617/s11527-014-0512-3

Farrand, B., & Emery, J. (1995). Recent improvements in quality of steel slag aggregate. Transportation research record, 1468, 137-141.

Ferry, J. D. (1980). Viscoelastic properties of polymers (3rd ed.). New York, NY: John Wiley.

Fisher, C. Old Asphalt, New Foundation - Recycling Roads, Constructioneer, (2008) [Online]. Available: http://www.allbusiness.com/construction/heavy-civil-construction-road-bridge/11797187-1.html.

Frigio, F., Pasquini, E., Ferrotti, G., & Canestrari, F. (2013). Improved durability of recycled porous asphalt. Construction and Building Materials, 48, 755-763.

Fu, P. and Harvey, J.T., (2007). Temperature sensitivity of foamed asphalt mix stiffness: field and lab study. International Journal of Pavement Engineering, 8 (2), 137–145.

Fuller, W. B. and S. E. Thompson. (1907). The laws of proportioning concrete. ASCE Transactions 59: 67–143.

Furlong, S., James, A., Kalinowski, E., & Thompson, M. (1999). Water enclosed within the droplets of bitumen emulsions and its relation to viscosity changes during storage. Colloids and Surfaces A: Physicochemical and Engineering Aspects, 152(1), 147-153.

Gao, L., Ni, F., Charmot, S., & Li, Q. (2014). High-temperature performance of multilayer pavement with cold in-place recycling mixtures. Road Materials and Pavement Design, 15(4), 804–819. doi:10.1080/14680629.2014.924427

Garcia A, Lura P, Partl MN, Jerjen I. (2013) Influence of cement content and environmental humidity on asphalt emulsion and cement composites performance. Mater Struct 46:1275–1289, DOI 10.1617/s11527-012-9971-6

Giuliani, F. (2001, October). X-ray diffraction method for studying cement-modified bitumen-emulsion mixtures in asphalt pavement cold recycling. In International Symposium on Subgrade Stabilisation and In Situ Pavement Recycling Using Cement, 1st, 2001, Salamanca, Spain.

Godenzoni, C., Cardone, F., Graziani, A., & Bocci, M. (2016). The effect of curing on the mechanical behavior of cement–bitumen treated materials. Rilem Bookseries on Sustainable and Innovative Bituminous Materials, vol. 11, pp. 879-890.

Goldstein, J., Newbury, D. E., Echlin, P., Joy, D. C., Romig Jr, A. D., Lyman, C. E., ... & Lifshin, E. (2012). Scanning electron microscopy and X-ray microanalysis: a text for biologists, materials scientists, and geologists. Springer Science & Business Media.

Graziani, A., Virgili, A., & Belogi, L. (2011, June). Instrumented test section for the evaluation of geogrids in asphalt pavements. In Proceedings of the 5th international conference on bituminous mixtures and pavements, Thessaloniki (pp. 1107-1117).

Graziani, A., Bocci, M., Canestrari, F. (2014). Complex Poisson's ratio of bituminous mixtures: measurement and modeling. Materials and structures, 47(7), 1131-114

Graziani, A., Godenzoni, C., Cardone, F., & Bocci, M. (2016a). Effect of curing on the physical and mechanical properties of cold-recycled bituminous mixtures. Materials and Design, vol. 95, pp. 358-369.

Graziani, A., Di Benedetto, H., Perraton, D., Sauzéat, C., Hofko, B., Poulikakos, L.D., Pouget, S. (2016b). Recommendation of RILEM TC 237-SIB on complex Poisson's ratio characterization of bituminous mixtures. Materials & Structures. In publication, [DOI 10.1617/s11527-016-0923-4]

Graziani, A., Di Benedetto, H., Perraton, D., Sauzéat, C. et al, (2016c). Three-dimensional characterisation of linear viscoelastic properties of bituminous mixtures, RILEM State Of the Art Report, Springer (2016c, in publication)

Grilli, A., Graziani, A., and Bocci, M. (2012). Compactability and thermal sensitivity of cement–bitumen treated materials. Road Materials and Pavement Design, 13 (4), 599–617.

Grilli, A., Bocci, E., & Graziani, A. (2013a). Influence of reclaimed asphalt content on the mechanical behaviour of cement-treated mixtures. Road Materials and Pavement Design, 14(3), 666-678.

Grilli, A., Bocci, M., & Tarantino, A. M. (2013). Experimental investigation on fibre-reinforced cement-treated materials using reclaimed asphalt. Construction and Building Materials, 38, 491-496.

Grilli, A., Graziani, A., Bocci, E., & Bocci, M. (2016). Volumetric properties and influence of water content on the compactability of cold recycled mixtures. Materials and Structures, 1-14.

Gupta, S., Kang, D. H., & Ranaivoson, A. (2009). Hydraulic and mechanical properties of recycled materials.

Guinée, J. B. (2012). "Life Cycle Assessment: Past, Present and Future." International Symposium on Life Cycle Assessment and Construction. July 10-12, Nantes, France. Keynote Address. RILEM Publications, France.

Guthrie, W. S., Sebesta, S., & Scullion, T. (2002). Selecting optimum cement contents for stabilizing aggregate base materials (No. FHWA/TX-05/7-4920-2,). Texas Transportation Institute, Texas A & M University System.

Hanehara, S., & Yamada, K. (1999). Interaction between cement and chemical admixture from the point of cement hydration, absorption behaviour of admixture, and paste rheology. Cement and Concrete Research, 29(8), 1159-1165.

Hayhoe, G. F. (2002). LEAF: A new layered elastic computational program for FAA pavement design and evaluation procedures (pp. 1-15). Federal Aviation Administration.

Hashin, Z. (1983). Analysis of composite materials—a survey. Journal of Applied Mechanics, 50(3), 481-505.

Hoffman, M. S., & Thompson, M. R. (1982). Backcalculating nonlinear resilient moduli from deflection data (No. 852).

Holleran, G., Hicks, R. G., & Reed, J. R. (2002). Emulsion particle size and particle size distribution effects in microsurfacing emulsion performance. Paper 4F-044, Proc. In 3 rd World Congress on Emulsions, Lyon, France.

Huang, Y.H., (2004). Pavement Analysis and Design, 2nd Ed., Prentice Hall, Upper Saddle River, NJ.

Huang, Y., Bird, R. N., & Heidrich, O. (2007). A review of the use of recycled solid waste materials in asphalt pavements. Resources, Conservation and Recycling, 52(1), 58-73.

Huang, S. C., & Di Benedetto, H. (Eds.). (2015). Advances in Asphalt Materials: Road and Pave-ment Construction, Chapter 13 "*Paving with asphalt emulsion*". Woodhead Publishing.

Huet, C., (1963). Etude par une methode d'impedance du comportement viscoélastique des materiaux hydrocarbons, Thèse de Docteur Ingénieur, Faculté des Sciences de l'Université de Paris

Hunt, R. and W. Franklin. (1996). "LCA – How it Came About, Personal Reflections on the Origin and the Development of LCA in the USA." International Journal of Life Cycle Assessment. Vol. 1, No. 1. Ecomed Publishers, Landsberg, Germany.

Israelachvili, J. N. (2011). Intermolecular and surface forces: revised third edition. Academic press.

Izadi, A., Bhasin, A., & Motamed, A. (2011). Designing Fine Aggregate Mixtures to Evaluate Fatigue Crack Growth in Asphalt Mixtures (No. SWUTC/11/161022-1). Southwest Region University Transportation Center, Center for Transportation Research, University of Texas at Austin.

James A. (2006), Overview of Asphalt Emulsion. Transportation Research Circular EC102. Asphalt Technology, Transportation Research Board (TRB), Washington D.C.

Jenkins, K. J., Van de Ven, M. F. C., & De Groot, J. L. A. (1999). Characterisation of foamed bitumen. In 7th Conference on asphalt pavements for Southern Africa (pp. 1-18).

Jenkins, K. J. (2000). Mix design considerations for cold and half-warm bituminous mixes with emphasis of foamed bitumen (Doctoral dissertation, Stellenbosch: Stellenbosch University)

Jenkins, K.J., Long, F.M., & Ebels, L.J. (2007). Foamed bitumen mixes = shear performance? International Journal of Pavement Engineering, 8(2), 85–98.

Jenkins, K.J. and Moloto, P.K. (2008). Updating bituminous stabilized materials guidelines:mix design report. Phase II – Curing protocol: Improvement. Technical memorandum task 7.

Kalin Z. (1991). Canada targets C & D debris. Biocycle 1991;32(1):35–6.

Kandhal, P. and Mallick, R. (1997), "Pavement Recycling Guidelines for State and Local Governments", National Center for Asphalt Technology, Report FHWA-SA-98-042.

Kearney, E. (1997). Cold mix recycling: State-of-the-practice (with discussion). Journal of the Association of Asphalt Paving Technologists, 66, 760–784.

Kendall, A. (2012). Life Cycle Assessment for Pavement: Introduction. Presentation in Minutes, FHWA Sustainable Pavement Technical Working Group Meeting, April 25-26, 2012, Davis, CA.

Khosravifar, S., Schwartz, C. W., & Goulias, D. G. (2015). Mechanistic structural properties of foamed asphalt stabilised base materials. International Journal of Pavement Engineering, 16(1), 27–38.

Kim, Y. R. (2003). Mechanistic fatigue characterization and damage modeling of asphalt mixtures.

Kong, X. M., Liu, Y. L., Zhang, Y. R., Zhang, Z. L., Yan, P. Y., & Bai, Y. (2014). Influences of temperature on mechanical properties of cement asphalt mortars. Materials and Structures, 47(1-2), 285-292.

Kuna K, Airey G, Thom N (2014) A laboratory mix design procedure for foamed bitumen mixtures (FBM). Transport Res Rec 2444:1–10, DOI 10.3141/2444-01

Lambe, W and R. V. Whitman (1969). Soil Mechanics. John Wiley.

Lackner, R., Blab, R., Eberhardsteiner, J., & Mang, H. A. (2006). Characterization and multiscale modeling of asphalt-Recent developments in upscaling of viscous and strength properties. In III European Conference on Computational Mechanics (pp. 26-26). Springer Netherlands.

Lee, D. Y. (1980). Treating Iowa's Marginal Aggregates and Soils by Foamix Process (No. HR-212).

Lesueur, D., Coupé, C., & Ezzarougui, M. (2001). Skin formation during the drying of a bitumen emulsion. Road Materials and Pavement Design, 2(2), 161-179.

Lesueur, D., & Potti, J. J. (2004). Cold mix design: a rational approach based on the current understanding of the breaking of bituminous emulsions. Road Materials and Pavement Design, 5(sup1), 65-87.

Lewis, A.J.N. and Collings, D.C., (1999). Cold in place recycling: a relevant process for road rehabilitation and upgrading. Proceedings of 7th Conference on Asphalt Pavements for Southern Africa, CAPSA, Cape Town, South Africa.

Li, X., & Marasteanu, M. (2004). Evaluation of the low temperature fracture resistance of asphalt mixtures using the semi circular bend test (with discussion). Journal of the Association of Asphalt Paving Technologists, 73.

Li G, Zhao Y, Pang SS et al (1998) Experimental study of cement-asphalt emulsion composite. Cem Concr Res 28(5):635–641

Lin, J., Wei, T., Hong, J., Zhao, Y., & Liu, J. (2015). Research on development mechanism of early-stage strength for cold recycled asphalt mixture using emulsion asphalt. Construction and Building Materials, 99, 137-142.

Little, D. N., Button, J. W., & Epps, J. A. (1983). Structural properties of laboratory mixtures containing foamed asphalt and marginal aggregates. Transportation Research Record, (911).

Little, D. N., & Petersen, J. C. (2005). Unique effects of hydrated lime filler on the performance-related properties of asphalt cements: physical and chemical interactions revisited. Journal of Materials in Civil Engineering, 17(2), 207-218.

Liu, J., Zheng, X., Li, S., Ding, R., Zeng, Z., Weng, Z., & Yang, D. (2015). Effect of the stabilizer on bubble stability and homogeneity of cement emulsified asphalt mortar in slab ballastless track. Construction and Building Materials, 96, 135-146.

Loizos, A. (2007). In-situ characterization of foamed bitumen treated layer mixes for heavy-duty pavements. International Journal of Pavement Engineering, 8(2), 123-135.

Loizos, A., Papavasiliou, V., & Plati, C. (2012). Investigating in situ stress-dependent behaviour of foamed asphalt-treated pavement materials. Road Materials and Pavement Design, 13(4), 678-690.

Lytton, R. L. (1989). Backcalculation of layer moduli, state of the art. NDT of pavements and backcalculation of moduli, AJ Bush and GY Baladi, Eds, 1, 7-38.

Maccarrone, S., Holleran, G. & Ky, A. (1995). Cold Asphalt Systems as an Alternative to Hot Mix. In: 9th AAPA International Asphalt Conference.

Mallick, R. B., & El-Korchi, T. (2013). Pavement engineering: principles and practice. CRC Press.

Mangiafico, S., Di Benedetto, H., Sauzéat, C., Olard, F., Pouget, S., & Planque, L. (2013). Influence of reclaimed asphalt pavement content on complex modulus of asphalt binder blends and corresponding mixes: experimental results and modelling. Road Materials and Pavement Design, 14(sup1), 132-148.

Marrani, A., & Lancieri, F. (2008). Performance of cement stabilized recycled crushed concrete. In First International Conference on Transport Infrastructure ICTI, Beijing, China.

Marsey, W., & Arze, J. M. (2001). Analysis of nondestructive test data on flexible pavements acquired at the National Airport Pavement Test Facility.

McDaniel, R., Soleymani, H., & Shah, A. (2002). Use of reclaimed asphalt pavement (RAP) under Superpave specifications: A regional pooled fund project.

Mehta PK, Monteiro PJM (1993) Concrete: Structure, Properties, and Materials (2nd Ed). Prentice-Hall, Englewood Cliffs, NJ, USA.

Michaelis, L., & Menten, M. L. (1913). Die kinetik der invertinwirkung. Biochem. z, 49(333-369), 352.

Miljković, M., & Radenberg, M. (2014). Fracture behaviour of bitumen emulsion mortar mixtures. Construction and Building Materials, 62, 126-134.

Miljković, M., & Radenberg, M. (2015). Characterising the influence of bitumen emulsion on asphalt mixture performance. Materials and Structures, 48(7), 2195-2210.

Miljković, M., & Radenberg, M. (2016). Effect of compaction energy on physical and mechanical performance of bitumen emulsion mortar. Materials and Structures, 49(1-2), 193-205.

Molenaar, A. A., Xuan, D., Houben, L. J., & Shui, Z. (2011, September). Prediction of the mechanical characteristics of cement treated demolition waste for road bases and subbases. In Conference on Asphalt Pavements for Southern Africa [CAPSA11], 10th, 2011, KwaZulu-Natal, South Africa.

Montepara, A., & Giuliani, F. (2002). A study on design and performance of recycled pavements cold stabilized with cement and bituminous emulsion. Proceedings of the 4th European Symposium on Performance of Bituminous and Hydraulic Materials in Pavements, Nottingham, United Kingdom.

Montgomery, D.C., & Runger, G.C. (2003). Applied Statistics and Probability for Engineers, third edition, John Wiley & Sons, Inc.

Muthen, K. M. (1998). Foamed asphalt mixes-mix design procedure. Transportation Research Record, 898, 290-296.

Nadia P, Jacques M, Pigeon M (2003) Hydration mechanisms, microstructure, and mechanical properties of mortars prepared with mixed binder cement slurry-asphalt emulsion. J Mater Civil Eng 15(1):54–59

National Cooperative Highway Research Program (NCHRP) (2004). Guide for mechanistic–empirical design of new and rehabilitated pavement structures. National Cooperative Highway Research Program 1-37 A. Washington, DC: Transportation Research Board. Available from: http://trb.org/mepdg

Needham, D. (1996). Developments in bitumen emulsion mixtures for roads (Doctoral dissertation, University of Nottingham).

Nguyen, H.M., Pouget, S., Di Benedetto, H., and Sauzeat, C. (2009). Time-temperature super- position principle for bituminous mixtures. European Journal of Environmental and Civil Engineering, 13 (9), 1095-1107.

Oke, O. O. (2011). A study on the development of guidelines for the production of bitumen emulsion stabilised RAPs for roads in the tropics (Doctoral dissertation, University of Nottingham).

Olard, F., Di Benedetto, H., Eckmann, B., & Triquigneaux, J. P. (2003). Linear viscoelastic properties of bituminous binders and mixtures at low and intermediate temperatures. Road materials and pavement design, 4(1), 77-107.

Oppenheim AV, Willsky AS, Nawab SH (1996). Signals and systems, 2nd ed. Prentice Hall, Upper Saddle River

Overby, C., Johansen, R. and Mataka, M., (2004). Bitumen foaming: an innovative technique used on a large scale for pavement rehabilitation in Africa. Case study: Same-Himo monitored pilot project. Proceedings of the 8th conference on asphalt pavements for Southern Africa, CAPSA, Sun City, 16–18 September, South Africa.

Pal, R. (2000). Linear viscoelastic behavior of multiphase dispersions. Journal of colloid and interface science, 232(1), 50-63.

Papazian, H.S., (1962). The response of linear viscoelastic materials in the frequency domain with emphasis on asphalt concrete. Proceedings of 1st International Conference on the Structural Design of Asphalt Pavements, Ann Arbor, Michigan, 453–464

Partl, M. N., Pasquini, E., Canestrari, F., & Virgili, A. (2010). Analysis of water and thermal sensitivity of open graded asphalt rubber mixtures. Construction and Building Materials, 24(3), 283-291.

Paige-Green, P., & Ware, C. (2006). Some material and construction aspects regarding in situ recycling of road pavements inb South Africa. Road Materials and Pavement Design, Poirier, J. E., Durand, G., Koenders, B., & Morizur, M. F. (2000). Maitrise de la viscosite des emulsions de bitume: la granulometrie ne peut seule tout expliquer. In Proc., 2nd Eurasphalt & Eurobitume Congress (CD-ROM), Barcelona, Spain.

Pellinen, T., Zofka, A., Marasteanu, M., & Funk, N. (2007). Asphalt Mixture Stiffness Predictive Models (With Discussion). Journal of the Association of Asphalt Paving Technologists, 76.

Peng, J., Deng, D., Liu, Z., Yuan, Q., & Ye, T. (2014). Rheological models for fresh cement asphalt paste. Construction and Building Materials, 71, 254-262.

Perraton, D. Di Benedetto H., Sauzéat C., Hofko B., Graziani A., Nguyen Q.T., Pouget S., Poulikakos L.D., Tapsoba N., Grenfell J., (2016). 3Dim experimental investigation of linear viscoelastic properties of bituminous mixtures, Materials & Structures, [DOI 10.1617/s11527-016-0827-3], published on line March 2016

Pouget, S., Sauzeat, C., Di Benedetto, H., and Olard, F. (2010). From the Behavior of Constituent Materials to the Calculation and Design of Orthotropic Bridge Structures [Special Issue: EA T A 2010]. Road Materials and Pavement Design, 11, 111-144

Pouliot n, Marchand JD, Pigeon M. (2003). Hydration mechanisms, microstructure and mechanical properties of mortars prepared with mixed binder cement slurry-asphalt emulsion. J Mater Civ Eng, vol. 15(1), pp. 54-59.

Plati, C., Loizos, A., Papavasiliou, V., & Kaltsounis, A. (2010). Investigating in situ properties of recycled asphalt pavement with foamed asphalt as base stabilizer. Advances in Civil Engineering, 2010.

Presti, D. L. (2013). Recycled tyre rubber modified bitumens for road asphalt mixtures: a literature review. Construction and Building Materials, 49, 863-881.

R Developement Core Team (2016). R: A language and environment for statistical computing. URL http://www.R-project.org/. Visited 2016-08-02

Raaijmakers, J. GW. (1987). "Statistical analysis of the Michaelis-Menten equation." Biometrics: 793-803.

Rabiot, D., B. G. Koenders, and M. Andre (1999). A Quality Concept for Emulsion Grade Bitumens. Proc., 1st International Symposium on Asphalt Emulsion Technology, Washington.

Ramzi Taha, A.M., Al-Harthy, A., Al-Shamsi, K., & Al-Zubeidi, M. (2002). Cement stabilization of reclaimed asphalt pavement aggregate for road bases and subbases. Journal of Materials in Civil Engineering, 14, 239–246.

Richardson, I. G. (1999). The nature of CSH in hardened cements. cement and concrete research, 29(8), 1131-1147.

Ritz, C., & Streibig, J. C. (2008). Nonlinear regression with R. Springer Science & Business Media.

Roberts, F. L., Kandhal, P. S., Brown, E. R., Lee, D. Y., & Kennedy, T. W. (1996). Hot mix asphalt materials, mixture design and construction. 2nd ed. NAPA, Lanham, Maryland.

Rodrıguez-Valverde, M. A., Cabrerizo-Vılchez, M. A., Paez-Duenas, A., & Hidalgo-Alvarez, R. (2003). Stability of highly charged particles: bitumen-in-water dispersions. Colloids and Surfaces A: Physicochemical and Engineering Aspects, 222(1), 233-251.

Ruckel, P. J., Acott, S. M., & Bowering, R. H. (1983). Foamed-asphalt paving mixtures: preparation of design mixes and treatment of test specimens. Transportation Research Record, 911, 88-95.

Rupnow, T. D. (2002). Subgrade stabilization using recycled asphalt pavement and fly ash mixtures. Midwest Transportation Consortium, Iowa State University, Ames (IA).

Rutherford, T., Wang, Z., Shu, X., Huang, B., & Clarke, D. (2014). Laboratory investigation into mechanical properties of cement emulsified asphalt mortar. Construction and Building Materials, 65, 76-83.

SABITA. Manual 14: GEMS – The design and use of granular emulsion mixes. Roggebaai, South Africa, 1993.

SABITA. Manual 21: ETB – The design and use of emulsion-treated bases. Roggebaai, South Africa, 1999

Sakr, H.A. & Manke, P.G. (1985). Innovations in Oklahoma foamix design procedures. In: Asphalt materials, mixes, construction and quality. Washingtong, DC: Transportation Research Board. (Transportation Research Record;1034), pp 26-34.

Santagata, E., & Chiappinelli, G. (2003). Experimental evaluation of cold-recycled bituminous mixtures used for major rehabilitation works. Proceedings of the 3rd international symposium on maintenance and rehabilitation of pavements and technological control (MAIREPAV3), Guimarães, Portugal.

Santagata, E., & Chiappinelli, G. (2004). Improvement in the mix design of cold-recycled bituminous mixtures. Proceedings of Euroasphalt&Eurobitume conference, Wien.

Santagata, F. A., Bocci, M., Grilli, A., & Cardone, F. (2009). Rehabilitation of an Italian highway by cold in-place recycling techniques Vol. 2 (pp. 1113–1122). Proceedings of the 7th international RILEM symposium on advanced testing and characterization of bituminous materials, Rhodes, Greece.

Sauzeat, C. and Di Benedetto, H. (2015). Tridimensional linear viscoelastic behavior of bituminous materials. In: Advances in Asphalt Materials: Road and Pavement Construction & Di Benedetto Eds. Woodhead Publishing

Sayegh, G. (1967, January). Viscoelastic properties of bituminous mixtures. In Intl Conf Struct Design Asphalt Pvmts.

Schramm, L. L. (1994). Foams: fundamentals and applications in the petroleum industry (Vol. 242). An American Chemical Society Publication.

SFERB (1991), "Emulsions – general information applications", pp. 174-196.

SFERB (2002), Symposium of World Road Bitumen Emulsion Producers, Lyon, France, p. 59.

Shackel, B., Makiuchi, K., & Derbyshire, J. R. (1974). The response of a foamed bitumen stabilised soil to repeated triaxial loading. In Australian Road Research Board (ARRB) Conference, 7th, 1974, Adelaide (Vol. 7, No. 7).

Shahin, M. Y. (2005). Pavement management for airports, roads, and parking lots (Vol. 501). New York: Springer.

Schüler, T., Manke, R., Jänicke, R., Radenberg, M., & Steeb, H. (2013). Multi-scale modelling of elastic/viscoelastic compounds. ZAMM-Journal of Applied Mathematics and Mechanics/Zeitschrift für Angewandte Mathematik und Mechanik, 93(2-3), 126-137.

Siripun, K., Jitsangiam, P., & Nikraz, H. (2009). Characterization analysis and design of hydrated cement treated crushed rock base as a road base material in western Australia. International Journal of Pavement Research and Technology, 2(6), 257.

Smith, W., (1999). Foamed bitumen stabilisation project – Warwick, QLD, Joint Transport South Australia/AustStab Seminar.

Soleymani, H. R., McDaniel, R., Abdelrahman, M., & Anderson, M. (2000). Investigation of the black rock issue for recycled asphalt mixtures. ASPHALT PAVING TECHNOLOGY, 69, 366-390.

Song H, Do J, Soh Y (2006) Feasibility of asphalt-modified mortars using asphalt emulsion. Constr Build Mater 20(5): 332–337

Spencer R. (1989). Recycling opportunities for demolition debris. Biocycle 1989;30(11):42–4.

Stimilli A, Ferrotti G, Graziani A, Canestrari F. (2013) Performance evaluation of cold recycled mixture containing high percentage of reclaimed asphalt. Road Mater Pavement 14:149–161, DOI 10.1080/14680629.2013.774752.

Stokes, D. J. (2003). Recent advances in electron imaging, image interpretation and applications: environmental scanning electron microscopy. Philosophical Transactions of the Royal Society of London A: Mathematical, Physical and Engineering Sciences, 361(1813), 2771-2787.

Straube, E., & Jansen, D. (2009, June). Temperature Correction of Falling-Weight-Deflectometer Measurements. In Bearing Capacity of Roads, Railways and Airfields, Two Volume Set: Proceedings of the 8th International Conference (BCR2A'09), June 29-July 2 2009, University of Illinois at Urbana-Champaign, Champaign, Illinois, USA (p. 789). CRC Press.

Stroup-Gardiner, M. (2011). Recycling and reclamation of Asphalt pavements using in-place methods (No. Project 20-05 (Topic 40-13)).

Su, N., & Chen, J. S. (2002). Engineering properties of asphalt concrete made with recycled glass. Resources, Conservation and Recycling, 35(4), 259-274.

Tadros, T. F. (2011). Rheology of dispersions: principles and applications. John Wiley & Sons.

Taha, R., Al-Harthy, A., Al-Shamsi, K., & Al-Zubeidi, M. (2002). Cement stabilization of reclaimed asphalt pavement aggregate for road bases and subbases. Journal of Materials in Civil Engineering, 14(3), 239-245.

Takamura, K., Chow, R. S., & Tse, D. L. (1987). The Prediction of Electrophoretic Mobilities and the Coagulation Behavior of Bitumen-in-Water Emulsions in Aqueous NaCl and CaCl2 Solutions Using Ionizable Surface-Group Model. Flocculation in Biotechnology and Separation Systems, 565-577.

Tan Y, Ouyang J, Lv J et al (2013) Effect of emulsifier on cement hydration in cement asphalt mortar. Constr Build Mater 47:159–164.

Tan, Y., Ouyang, J., & Li, Y. (2014). Factors influencing rheological properties of fresh cement asphalt emulsion paste. Construction and Building Materials, 68, 611-617.

Tebaldi G, Dave E, Marsac P, Muraya P, Hugener M, Pasetto M, Graziani A, Grilli A, Bocci M, amd L Wendling AM, Gaudefroy V, Jenkins K, Loizos A, Canestrari F (2014) Synthesis of standards and procedures for specimen preparation and in-field evaluation of cold-recycled asphalt mixtures. Road Mater Pavement 5(2):272–299, DOI 10.1080/14680629.2013.866707

Terrel RL, Wang CK. (1971). Early curing behavior of cement modified asphalt emulsion mixtures. Proceedings of Association of Asphalt Paving Technologists, 40, 108-125.

Texas Department of Transportation (2011). “Pavement Design Guide”, <http://onlinemanuals.txdot.gov/txdotmanuals/pdm/manual_notice.htm > (January 01, 2011)].

Thomas, M. D., Folliard, K. J., Fournier, B., Drimalas, T., & Garber, S. I. (2013). Methods for preventing ASR in new construction: Results of field exposure sites (No. FHWA-HIF-14-004).

Thompson, M.R., Garcia, L., and Carpenter, S.H., (2009). Cold in place recycling and full-depth recycling with asphalt products. Report no. FHWA-ICT-09-036. Rantoul, IL: Illinois Center for Transportation.

Tia, M., & Wood, L. E. (1983). Use of asphalt emulsion and foamed asphalt in cold-recycled asphalt paving mixtures (No. N908).

Timm, D. H., Priest, A. L., & McEwen, T. V. (2004). Design and instrumentation of the structural pavement experiment at the NCAT test track. National Center for Asphalt Technology, Auburn University.

Timm, D. H. (2009). Design, Construction and Instrumentation of the 2006 Test Track Structural Study. National Center for Asphalt Technology: NCAT Report, 09-01.

Topp, G. C., Davis, J. L., & Annan, A. P. (1980). Electromagnetic determination of soil water content: Measurements in coaxial transmission lines. Water resources research, 16(3), 574-582.

Tschoegl, N.W. (1989) The phenomenological theory of linear viscoelastic behavior: an introduction. Springer Science & Business Media

Tschoegl, N.W., Knauss, W., Emri. I. (2002) Poisson's ratio in linear viscoelasticity—a critical review. Mechanics of Time-Dependent Materials. 6:3-51

Underwood, B. S., & Kim, Y. R. (2011). Experimental investigation into the multiscale behaviour of asphalt concrete. International Journal of Pavement Engineering, 12(4), 357-370.

Underwood, B. S., & Kim, Y. R. (2013). Effect of volumetric factors on the mechanical behavior of asphalt fine aggregate matrix and the relationship to asphalt mixture properties. Construction and Building Materials, 49, 672-681.

Underwood, B. (2015, April). Multiscale modeling approach for asphalt concrete and its implications on oxidative aging. In Elsevier Inc..

Uzan, J. (1994). Advanced backcalculation techniques. In Nondestructive Testing of Pavements and Backcalculation of Moduli: Second Volume. ASTM International.

Valentin, J., Suda, J., Formanová, Z., Mollenhauer, K., Engels, M., Batista, F., & McNally, C. (2014, April). Introduction to European COREPASOL project on harmonizing cold recycling pavement techniques. In Transport Research Arena (TRA) 5th Conference: Transport Solutions from Research to Deployment.

Van de Yen, M. F. C. (2003). The spatial approach of hot mix asphalt. In PRO 28: 6th International RILEM Symposium on Performance Testing and Evaluation of Bituminous Materials (PTEBM'03) (Vol. 28, p. 264). RILEM Publications.

Vennapusa, P. K. R., White, D. J., Siekmeier, J., & Embacher, R. A. (2012). In situ mechanistic characterisations of granular pavement foundation layers. International Journal of Pavement Engineering, 13(1), 52-67.

Verlhac, P., F. Verzaro, F. Leal Calderon., J. J. Potti, and B. Eckmann (2002). Characterisation of Bituminous Emulsions: Particle Size Distribution and Amount of Residual Emulsifier. Paper 1C-172, Proc., 3rd World Congress on Emulsions, Lyon, France.

Walter, J., and D. Day (2002). Coalescence of Quick Set Surface Dressing PMB Emulsions. Paper 4F-011, Proc., 3rd World Congress on Emulsions, Lyon, France.

Wang F., Liu Y., Hu S. (2013). Effect of early cement hydration on the chemical stability of asphalt emulsion. Construction and Building Materials, 42:146-151

Weiss WJ, Lura P, Rajabipour F, Sant G., (2008). Performance of shrinkage reducing

admixtures at different humidities and at early ages. ACI Mater J, vol. 105(5), pp. 478-486.

Wen, H. (2013). Use of fracture work density obtained from indirect tensile testing for the mix design and development of a fatigue model. International Journal of Pavement Engineering, 14(6), 561-568.

White, G., & Gnanendran, C. (2002). The characterization of cementitious insitu stabilized avement materials: the past, the present and the future. Road and Transport Research, 11(4), 56–69.

White†, G. W., & Gnanendran, C. T. (2005). The influence of compaction method and density on the strength and modulus of cementitiously stabilised pavement materials. International Journal of Pavement Engineering, 6(2), 97-110.

Wirtgen Cold Recycling Technology (3rd ed.). (2010). Windhagen: Wirtgen GmbH.

Witczak, M.W., et al., (2002). Simple performance test for Superpave mix design. National Cooperative Highway Research Program Report 465. Washington, DC: Transportation Research Board.

Xuan, D. X., Houben, L. J. M., Molenaar, A. A. A., & Shui, Z. H. (2012). Mixture optimization of cement treated demolition waste with recycled masonry and concrete. Materials and structures, 45(1-2), 143-151.

Yuan, D., Nazarian, S., Hoyos, L., & Puppala, A. (2011). Evaluation and mix design of cement-treated base materials with high content of reclaimed asphalt pavement. Transportation Research Record: Journal of the Transportation Research Board, (2212), 110-119.

Zhang, Y., Kong, X., Hou, S., Liu, Y., & Han, S. (2012). Study on the rheological properties of fresh cement asphalt paste. Construction and Building Materials, 27(1), 534-544.